NUREG–0675
Supplement No. 34

Safety Evaluation Report

related to the operation of
Diablo Canyon Nuclear Power Plant,
Units 1 and 2

Docket Nos. 50–275 and 50–323

Pacific Gas and Electric Company

(148-

U.S. Nuclear Regulatory Commission

Office of Nuclear Reactor Regulation

June 1991



AVAILABILITY NOTICE

Availability of Reference Materials Cited in NRC Publications

Most documents cited in NRC publications will be available from one of the following sources:

1. The NRC Public Document Room, 2120 L Street, NW, Lower Level, Washington, DC 20555
2. The Superintendent of Documents, U.S. Government Printing Office, P.O. Box 37082, Washington, DC 20013-7082
3. The National Technical Information Service, Springfield, VA 22161

Although the listing that follows represents the majority of documents cited in NRC publications, it is not intended to be exhaustive.

Referenced documents available for inspection and copying for a fee from the NRC Public Document Room include NRC correspondence and internal NRC memoranda; NRC Office of Inspection and Enforcement bulletins, circulars, information notices, inspection and investigation notices; Licensee Event Reports; vendor reports and correspondence; Commission papers; and applicant and licensee documents and correspondence.

The following documents in the NUREG series are available for purchase from the GPO Sales Program: formal NRC staff and contractor reports, NRC-sponsored conference proceedings, and NRC booklets and brochures. Also available are Regulatory Guides, NRC regulations in the Code of Federal Regulations, and Nuclear Regulatory Commission Issuances.

Documents available from the National Technical Information Service include NUREG series reports and technical reports prepared by other federal agencies and reports prepared by the Atomic Energy Commission, forerunner agency to the Nuclear Regulatory Commission.

Documents available from public and special technical libraries include all open literature items, such as books, journal and periodical articles, and transactions. Federal Register notices, federal and state legislation, and congressional reports can usually be obtained from these libraries.

Documents such as theses, dissertations, foreign reports and translations, and non-NRC conference proceedings are available for purchase from the organization sponsoring the publication cited.

Single copies of NRC draft reports are available free, to the extent of supply, upon written request to the Office of Information Resources Management, Distribution Section, U.S. Nuclear Regulatory Commission, Washington, DC 20555.

Copies of industry codes and standards used in a substantive manner in the NRC regulatory process are maintained at the NRC Library, 7920 Norfolk Avenue, Bethesda, Maryland, and are available there for reference use by the public. Codes and standards are usually copyrighted and may be purchased from the originating organization or, if they are American National Standards, from the American National Standards Institute, 1430 Broadway, New York, NY 10018.

NUREG–0675
Supplement No. 34

Safety Evaluation Report

related to the operation of
Diablo Canyon Nuclear Power Plant,
Units 1 and 2

Docket Nos. 50–275 and 50–323

Pacific Gas and Electric Company

U.S. Nuclear Regulatory Commission

Office of Nuclear Reactor Regulation

June 1991



ABSTRACT

Supplement 34 to the Safety Evaluation Report for the application by Pacific Gas and Electric Company (PG&E) for licenses to operate Diablo Canyon Nuclear Power Plant, Unit Nos. 1 and 2 (Docket Nos. 50-275 and 50-323, respectively) has been prepared by the Office of Nuclear Reactor Regulation of the U.S. Nuclear Regulatory Commission. This supplement documents the NRC staff review of the Long-Term Seismic Program conducted by PG&E in response to License Condition 2.C.(7) of Facility Operating License DPR-80, the Diablo Canyon Unit 1 operating license.

TABLE OF CONTENTS

		Page
ABSTRACT		iii
1 INTRODUCTION AND SUMMARY		1-1
1.1	Background	1-1
1.2	The License Condition	1-3
1.3	Summary of NRC Staff Review of the LTSP	1-4
1.3.1	Element 1 of the License Condition	1-4
1.3.2	Element 2 of the License Condition	1-5
1.3.3	Element 3 of the License Condition	1-5
1.3.4	Element 4 of the License Condition	1-6
1.4	Summary of Staff Conclusions	1-7
1.5	NRC Staff Consultants	1-8
1.6	NRC Staff Contributors	1-9
2 SITE CHARACTERISTICS		2-1
2.5	Geology, Seismology and Foundation Engineering	2-1
2.5.1	Geology	2-1
2.5.1.1	Regional Geology and Tectonics	2-4
2.5.1.2	Site Region and Site Area Geology	2-8
2.5.1.2.1	San Simeon Fault Zone	2-8
2.5.1.2.2	Cambria Stepover Basin	2-9
2.5.1.2.3	Piedras Blancas Anticlinorium	2-10
2.5.1.2.4	Hosgri Fault Zone	2-11
2.5.1.2.5	San Luis-Pismo Structural Block	2-22
2.5.2	Seismology	2-31
2.5.2.1	Seismicity	2-32
2.5.2.2	Maximum Earthquake Potential	2-35
2.5.2.3	Reevaluation of Earthquake Ground Motions	2-39
2.5.2.4	Seismology Conclusions	2-49
2.5.3	Surface Faulting	2-49

TABLE OF CONTENTS (Contd.)

	Page
3 DESIGN CRITERIA - STRUCTURES, COMPONENTS, EQUIPMENT, AND SYSTEMS ..	3-1
3.7 Seismic Design	3-1
3.7.1 Seismic Design Parameters	3-1
3.7.1.1 Ground-Motion Input	3-1
3.7.1.2 Conclusions--Seismic Design Parameters	3-2
3.7.2 Soil-Structure Interaction Analysis	3-2
3.7.2.1 SSI Analysis Methodology	3-3
3.7.2.1.1 The CLASSI and SASSI Codes	3-3
3.7.2.1.2 Audit of the CLASSI and SASSI Codes	3-4
3.7.2.2 Modeling of Structures and Rock Foundation ..	3-6
3.7.2.2.1 Structural Modeling and Ground-Motion Wave Effects	3-6
3.7.2.2.2 Site Rock Profile and Properties	3-7
3.7.2.3 Parametric Studies of SSI Effects	3-9
3.7.2.4 Soil-Structure Interaction Studies	3-10
3.7.2.4.1 Coherent Ground Motions	3-10
3.7.2.4.2 Ground-Motion Incoherence	3-11
3.7.2.4.3 Effects of Basemat Uplift on Responses	3-11
3.7.2.5 Independent Check of SSI Analysis	3-14
3.7.2.6 Conclusions--SSI Analysis	3-16
3.8 Design of Category I Structures	3-16
3.8.1 Deterministic Evaluation of Structures and Equipment	3-16
3.8.1.1 Ground-Motion Input for Deterministic Evaluation	3-17
3.8.1.2 Procedure Used To Determine Plant Responses .	3-19
3.8.1.3 Conversion of SSI Analysis Results Into Plant Responses	3-19
3.8.1.4 Comparison of LTSP and Seismic-Qualification-Basis Response Spectra	3-21
3.8.1.4.1 Comparison of Free Field and Basemat Response Spectra	3-21
3.8.1.4.2 Comparison of In-Structure Response Spectra	3-23

TABLE OF CONTENTS (Contd.)

	Page
3.8.1.5 Margin Evaluation Using Fragility Analysis Method	3-25
3.8.1.6 Additional Deterministic Margin Evaluations	3-26
3.8.1.6.1 Procedure Used To Calculate Plant Response Loads (Demands)	3-28
3.8.1.6.2 Comparison of LTSP Seismic Base Shear and Overturning Moments With Previous Analyses	3-28
3.8.1.6.3 Deterministic Evaluation Based on CDFM Method	3-29
3.8.1.7 Comparison of Seismic Demand With CDFM Capacity	3-32
3.8.1.7.1 Containment Building	3-32
3.8.1.7.2 Auxiliary Building	3-33
3.8.1.7.3 Turbine Building	3-33
3.8.1.7.4 Fuel Handling Building Crane	3-35
3.8.1.7.5 CDFM Evaluation of Selected Equipment	3-36
3.8.1.7.6 Audit of CDFM Evaluations	3-38
3.8.1.7.7 Masonry Walls	3-38
3.8.1.8 Conclusions--Deterministic Evaluation	3-42
23 PROBABILISTIC RISK ASSESSMENT	23-1
23.1 Introduction	23-1
23.1.1 Background	23-1
23.1.2 Relationship to Other Elements of the License Condition	23-1
23.1.3 Objectives and Scope of the Review	23-3
23.1.4 Review Process	23-3
23.1.4.1 Description	23-3
23.1.4.2 Interactive Phase of the Review	23-4
23.2 Overview of PRA Approach and Results	23-4
23.2.1 Significant Plant Features	23-4
23.2.2 Overall PRA Approach	23-5
23.2.2.1 Scope, Assumptions, and Limitations	23-5
23.2.2.2 PRA Methodology	23-6
23.2.3 Summary of PRA Results	23-7
23.3 Review of Internal Events	23-12

TABLE OF CONTENTS (Contd.)

		Page
23.3.1	The Review Process	23-12
23.3.2	Initiating Events	23-15
	23.3.2.1 PRA Approach	23-15
	23.3.2.2 Review and Evaluation	23-18
	23.3.2.2.1 Completeness	23-18
	23.3.2.2.2 Initiating Event Frequencies	23-18
23.3.3	Success Criteria	23-22
23.3.4	Event Sequence Model	23-22
23.3.5	System Modeling	23-24
	23.3.5.1 Event Trees	23-24
	23.3.5.2 Fault Trees	23-25
23.3.6	Failure Data Analysis	23-28
23.3.7	Human Reliability Analysis Methodology	23-29
	23.3.7.1 Scope of the Review	23-29
	23.3.7.2 Overview of the HRA	23-29
	23.3.7.3 Summary of Review Findings	23-30
23.3.8	Accident Sequence Quantification	23-30
	23.3.8.1 Approach Used in the PRA	23-30
	23.3.8.2 Internal Event Sequence Characteristics and Results of the Staff Quantification	23-32
23.3.9	Summary and Conclusions of Internal Events Review	23-49
23.4	Review of Seismic Events	23-52
23.4.1	PRA Approach	23-53
23.4.2	Detailed Description of Review Approach	23-54
23.4.3	Seismic Hazard Analysis	23-55
	23.4.3.1 Methodology	23-56
	23.4.3.2 Seismicity Assessment	23-58
	23.4.3.3 Ground-Motion Studies	23-58
	23.4.3.4 Conclusion	23-59
23.4.4	Seismic Hazard/Fragility Interface	23-59
23.4.5	Fragility and Building Response Analysis	23-60
	23.4.5.1 Methodology	23-60
	23.4.5.2 Review Approach	23-60
	23.4.5.3 Structure Response and Fragility Review	23-63

TABLE OF CONTENTS (Contd.)

		Page
23.4.5.4	Equipment Fragility Review	23-65
23.4.5.5	Summary Evaluation of Fragilities	23-68
23.4.6	System Modeling	23-69
23.4.7	Accident Sequence Quantification	23-70
23.4.7.1	Evaluation of the Mean Point Estimate	23-70
23.4.7.2	Uncertainty Analysis	23-71
23.4.8	Characteristics of Seismic Sequences	23-76
23.4.9	Sensitivity Studies	23-76
23.4.10	Summary and Conclusions	23-82
23.5	Review of Non-Seismic External Events	23-83
23.5.1	Non-Seismic/Non-Fire External Events	23-83
23.5.2	Fire Analysis	23-84
23.6	Summary and Conclusions	23-88
23.6.1	Summary of Findings	23-88
23.6.2	Conclusions	23-89
23.6.2.1	General	23-89
23.6.2.2	Internal Events Analysis	23-91
23.6.2.3	Seismic Events Analysis	23-92
23.6.2.4	Fire Events Analysis	23-93
23.6.2.5	Overall Conclusion	23-93

APPENDICES

A CHRONOLOGY OF LTSP REVIEW

B BIBLIOGRAPHY

C TECHNICAL EVALUATION REPORT, U.S. GEOLOGICAL SURVEY: "REVIEW OF GEOPHYSICAL INTERPRETATIONS CONTAINED IN PG&E FINAL REPORT OF THE DIABLO CANYON LTSP FOR THE DIABLO CANYON POWER PLANT

D TECHNICAL EVALUATION REPORT, UNIVERSITY OF NEVADA, RENO: "INDEPENDENT ASSESSMENT OF THE EARTHQUAKE POTENTIAL AT THE DIABLO CANYON POWER PLANT, SAN LUIS OBISPO COUNTY, CA"

E GLOSSARY OF ABBREVIATIONS AND TECHNICAL TERMS

TABLE OF CONTENTS (Contd.)

Page

FIGURES

2.1 San Gregorio-Hosgri fault system 2-2
2.2 The Los Osos/Santa Maria Valley Domain 2-6
2.3 Structural elements associated with the San Luis-Pismo structual block 2-25
2.4 Horizontal acceleration response spectra 2-44
2.5 Vertical acceleration response spectra 2-45

3.1 Comparison of the 1988 LTSP site-specific median and 84th percentile horizontal response spectra with the 1977 Hosgri evaluation (Newmark) response spectrum 3-18
3.2 Comparison of scaled soil-structure interaction input with 84-percent probability of nonexceedance site-specific spectrum 3-20
3.3 Overall process of developing plant responses 3-22
3.4 Comparison of floor-response spectra for equipment qualification for the containment building, interior structure, El 140 ft, north/south response 3-24
3.5 Comparison of floor-response spectra for equipment qualification for the containment building, interior structure, El 140 ft, east/west response 3-24

23.1 Relationship between PRA and other LTSP programs 23-2
23.2 Contribution of each earthquake range to the seismic CDF 23-13
23.3 Plant fragility curve, including random and nonseismic failures 23-13
23.4 The four-part event sequence model 23-23
23.5 Total aggregate hazard curves 23-57
23.6 Simplified logic block diagram 23-72
23.7 Contribution of each earthquake range to the seismic CDF 23-78
23.8 Plant total mean fragility curve 23-78
23.9 Sensitivity study on 230-kV fragility median 23-82
23.10 Other probabilistic risk assessments 23-90

TABLES

3.1 LTSP demand vs. Hosgri demand--containment building 3-28
3.2 LTSP demands vs. Hosgri capacities--containment building 3-29
3.3 Summary of conservative deterministic failure margin approach 3-31
3.4 Demand vs. CDFM capacity for LTSP analysis--containment building . 3-33
3.5 Demand vs. CDFM capacity for LTSP analysis--auxiliary building ... 3-34
3.6 Demand vs. CDFM capacity for LTSP analysis--turbine building 3-34
3.7 CDFM evaluation of modified masonry walls 3-41

23.1 Diablo Canyon PRA summary statistics 23-7
23.2 Internal initiating event contribution to CDF 23-8
23.3 Functional internal events scenarios contributing to core damage 23-9
23.4 Seismic failures of components contributing to core damage 23-11

Page

TABLES (Contd.)

23.5 Initiating event categories selected for quantification of the Diablo Canyon risk model 23-16
23.6 Initiating events and their mean frequencies per year in the reduced model 23-19
23.7 Initiating event contributions to non-seismic CDF dominant sequence model 23-34
23.8 Initiating event contributions to non-seismic CDF initiating events not included in the DSM 23-35
23.9 Event scenarios ranked according to non-seismic CDF contribution of dominant sequence model 23-37
23.10 Special issues importance summary 23-42
23.11 Fussel-Vesely importance of the special failure categories 23-43
23.12 Fussel-Vesely importance for the leading top events 23-44
23.13 System/operator action importance for non-seismic CDF ranking according to system/operator action importances 23-45
23.14 Major elements of alternative review quantification 23-50
23.15 Comparison of internal event contributions to CDF 23-51
23.16 Overall internal event CDF estimates for various assumptions .. 23-52
23.17 PRA seismic fragilities 23-61
23.18 Logical blocks as described by PG&E 23-73
23.19 Comparison of PRA seismic CDF percentiles with Monte Carlo results 23-77
23.20 Ranking of block model accident sequences from Monte Carlo uncertainty analysis 23-77
23.21 Component risk reduction potentials as given in the PRA (PG&E) and as computed by Monte Carlo approach (SNL) 23-79
23.22 Impact of pipe conditional failure fraction 23-80
23.23 Fire scenario CDF 23-88
23.24 Overall mean CDF estimates based on the staff review 23-88

1 INTRODUCTION AND SUMMARY

1.1 Background

The two nuclear units at the Diablo Canyon Nuclear Power Plant (Diablo Canyon) are substantially identical pressurized-water reactors. Each unit consists of a Westinghouse-designed nuclear steam supply system (NSSS) in a four-loop reactor coolant system, with a turbine generator, auxiliary equipment, and associated controls and instrumentation. The NSSS for each unit is contained within a steel-lined, reinforced-concrete structure that is capable of withstanding the pressure that might be developed as a result of the most severe design-basis loss-of-coolant accident. Units 1 and 2 are licensed to produce 3338 and 3411 thermal megawatts, respectively. These power levels result in net electrical outputs of 1084 and 1106 MWe, respectively. The units are owned and operated by the Pacific Gas and Electric Company (PG&E).

The Diablo Canyon plant is located on a 750-acre site on the central California coast in San Luis Obispo County, approximately 12 miles west-southwest of the city of San Luis Obispo, California. The site is roughly equidistant from San Francisco and Los Angeles, California.

The Nuclear Regulatory Commission's predecessor agency, the Atomic Energy Commission (AEC), issued a construction permit (CP) for Diablo Canyon Unit 1 on April 23, 1968, and for Unit 2 on December 9, 1970. In 1975, the regulatory functions of the AEC were assumed by the Nuclear Regulatory Commission (the Commission, or the NRC). After construction was complete, the NRC issued operating licenses (OLs) for the Diablo Canyon units. The NRC issued a full-power OL for Unit 1 on November 2, 1984, and for Unit 2 on August 25, 1985. The two units have been in operation since their OLs were issued. Unit 1 recently completed its fourth refueling outage and is back on line. Unit 2 is scheduled to be shut down for its fourth refueling outage in September 1991.

Because California is an area of relatively high seismic activity, geological and seismic issues have played a major role in the design and licensing of Diablo Canyon. Before NRC issued the Diablo Canyon construction permits, PG&E conducted geological and seismic investigations to validate the acceptability of the site. These investigations included regional studies and detailed onshore site investigations consisting of trenching, core drilling, and geological mapping in the vicinity of the site. During the time of the Diablo Canyon CP review, the NRC regulation that currently governs seismic design (Appendix A to 10 CFR Part 100) was in the early stages of development, and the concepts of the safe shutdown earthquake (SSE) and operating basis earthquake (OBE) were still being developed.

At the time the CP was issued, PG&E concluded, and the AEC concurred, that the earthquake design bases for Diablo Canyon would be a peak horizontal ground acceleration (PGA) of 0.4g for safety-related structures and a PGA of 0.2g for operational-related structures. These seismic design criteria were based on consideration of two design-basis earthquakes: a magnitude 7-1/4 earthquake on

the Nacimiento fault 20 miles from the site, and a magnitude 6-3/4 aftershock at the site associated with a large earthquake on the San Andreas fault. It was also concluded at that time that there was no surface displacement hazard (capable fault) in the site vicinity. This conclusion was based on the absence of any displacement of the 80,000-year-old and 105,000-year-old marine terraces underlying the site area.

Later, while geological investigations in support of the Diablo Canyon OL applications were under way, oil company geoscientists discovered that a major zone of faulting existed a few miles off shore from the plant site. This proprietary offshore geophysical information was made public in 1971 (Hoskins and Griffith, 1971). When the Diablo Canyon Final Safety Analysis Report (FSAR) was initially submitted for NRC review in 1973, it briefly described the offshore fault zone, calling it the East Boundary Fault Zone.

During the next few years, in response to NRC staff requests for additional information, PG&E investigated this fault zone. In addition, the U.S. Geological Survey (USGS), with NRC funding, conducted numerous offshore investigations of the fault zone. The zone was later re-named the Hosgri fault after its discoverers, Hoskins and Griffith (Wagner, 1974). Based on the results of these studies, recommendations by the USGS, and the issuance of Appendix A to Part 100 (1973), the NRC required that the SSE for Diablo Canyon be established as a horizontal PGA of 0.75g based on a postulated magnitude 7.5 earthquake on the Hosgri fault 5 km (3 mi) from the Diablo Canyon site [Supplemental Safety Evaluation Report (SSER) 4, May 1976]. This is usually called the Hosgri ground motion. Subsequently, PG&E reanalyzed and upgraded the plant to accommodate the new (Hosgri) seismic design basis.

The seismic design basis for Diablo Canyon was reviewed and approved by the Commission's Advisory Committee on Reactor Safeguards (ACRS). The ACRS letter approving the seismic design of the plant was issued on July 14, 1978, and included the statement that ultimately resulted in the Long-Term Seismic Program (LTSP): "The Committee recommends that the seismic design of Diablo Canyon be reevaluated in about ten years taking into account applicable new information."

After public hearings before the Commission's Atomic Safety and Licensing Board (ASLB) and Atomic Safety and Licensing Appeal Board (ASLAB), and meetings with the Commission, OLs were issued for both Diablo Canyon units. As stated above, full-power Facility Operating License DPR-80 for Unit 1 was issued on November 2, 1984, and full-power Facility Operating License DPR-82 for Unit 2 was issued on August 25, 1985. The Unit 1 full-power OL was conditioned to require that PG&E update the geological, seismological, and ground-motion information, reevaluate the magnitude of the earthquake used to determine the Diablo Canyon seismic design basis, reevaluate ground motion expected at the site, reassess engineering and equipment response, and perform a seismic probabilistic risk assessment (PRA) and deterministic studies, as necessary. The license condition was imposed because of (1) the substantial amount of offshore exploration for hydrocarbons, (2) significant advances in geology, seismology, and geophysics that had occurred since the beginning of the site review, and (3) the ACRS recommendation quoted above.

1.2 The License Condition

The license condition that led to the LTSP and the submittal of the LTSP Final Report was included in the Diablo Canyon Unit 1 full-power license, DPR-80, as License Condition 2.C.(7), which reads as follows:

> (7) Seismic Design Bases Reevaluation Program (SSER 27 Section IV.5)
>
> PG&E shall develop and implement a program to reevaluate the seismic design bases used for the Diablo Canyon Nuclear Power Plant.
>
> The program shall include the following Elements:
>
> (1) PG&E shall identify, examine, and evaluate all relevant geologic and seismic data, information, and interpretations that have become available since the 1979 ASLB hearing in order to update the geology, seismology and tectonics in the region of the Diablo Canyon Nuclear Power Plant. If needed to define the earthquake potential of the region as it affects the Diablo Canyon Plant, PG&E will also reevaluate the earlier information and acquire additional new data.
>
> (2) PG&E shall reevaluate the magnitude of the earthquake used to determine the seismic basis of the Diablo Canyon Nuclear Plant using the information from Element 1.
>
> (3) PG&E shall reevaluate the ground motion at the site based on the results obtained from Element 2 with full consideration of site and other relevant effects.
>
> (4) PG&E shall assess the significance of conclusions drawn from the seismic reevaluation studies in Elements 1, 2 and 3, utilizing a probabilistic risk analysis and deterministic studies, as necessary, to assure adequacy of seismic margins.
>
> PG&E shall submit for NRC staff review and approval a proposed program plan and proposed schedule for implementation by January 30, 1985. The program shall be completed and a final report submitted to the NRC three years following the approval of the program by the NRC staff.
>
> PG&E shall keep the staff informed on the progress of the reevaluation program as necessary, but as a minimum will submit quarterly progress reports and arrange for semi-annual meetings with the staff. PG&E will also keep the ACRS informed on the progress of the reevaluation program as necessary, but not less frequently than once a year.

PG&E responded to the license condition by submitting a program plan for the seismic design-basis reevaluation (the Long-Term Seismic Program, or LTSP) on

January 30, 1985. The staff reviewed the plan, and, after the plan was reviewed by the ACRS, the staff approved a modified version of the plan by letter dated July 31, 1985. PG&E then conducted the program as described in the program plan, issuing progress reports to the NRC staff in accordance with the requirements of the license condition. On July 31, 1988, PG&E submitted its final report on the Diablo Canyon LTSP (Brand, 1988). Since then, the NRC staff has met a number of times with PG&E, has made a number of requests for additional information, and has received submittals from PG&E in response (see Appendix A of this SSER, "Chronology of LTSP Review"). As a result of its review, conducted with the assistance of a number of expert consultants, the NRC staff has concluded that, subject to satisfactory analytical substantiation of the confirmatory item discussed below, PG&E has met all aspects of License Condition 2.C.(7) of Facility Operating License DPR-80.

1.3 Summary of NRC Staff Review of the LTSP

1.3.1 Element 1 of the License Condition

With regard to element 1 of the license condition, the NRC staff has reviewed submittals by PG&E and concludes that PG&E has identified, examined, and evaluated all relevant geologic and seismic data and interpretations since the 1979 ASLB hearing. Further, PG&E has updated the geology, seismology, and tectonic characteristics of the Diablo Canyon region. In addition, PG&E has reevaluated selected earlier information and acquired new data relating to the earthquake potential in the region as it affects the Diablo Canyon plant.

Specifically, PG&E has conducted a program over several years, including the following:

(1) acquisition and reprocessing of numerous oil industry seismic reflection profiles, including proprietary data

(2) acquisition of new seismic reflection data, principally off shore, but also on shore, to fill in the gaps between existing data

(3) analysis of deep-crust-penetrating seismic reflection and refraction lines

(4) analysis and interpretation of well-drilling logs

(5) investigations of onshore faults and their offshore extensions, including the San Simeon, Los Osos, Wilmar Avenue, Edna, San Miguelito, San Luis Bay, Olson, and Rattlesnake faults (these faults were investigated by geological mapping, trenching, borings, geomorphic studies, age dating, and mapping of marine and fluvial terraces)

(6) analysis of bathymetry, sea-floor sampling, and diver exploration

(7) installation of seismic and strong-motion networks and seismicity analysis

(8) tsunami and seismic analyses to relocate the 1927 Lompoc earthquake and reevaluate its magnitude

(9) empirical attenuation studies and numerical modeling to develop ground-motion estimates for the site

(10) probabilistic seismic hazards analysis

In summary, the NRC staff finds that the geological, seismological, and geophysical investigations and analyses conducted by PG&E and its consultants for the LTSP are the most extensive, thorough, and complete ever conducted for a nuclear facility in the United States, and have advanced the state of knowledge in these disciplines significantly. On this basis, the NRC staff finds that PG&E has complied with element 1 of the license condition in an acceptable manner.

1.3.2 Element 2 of the License Condition

Element 2 of the license condition requires that PG&E reevaluate the magnitude of the earthquake used to determine the seismic design basis at Diablo Canyon using the information developed for element 1. The NRC staff has reviewed the information submitted by PG&E and finds that the conclusion reached during the staff's review of the Diablo Canyon OL application, that the Hosgri fault is the seismic source that could cause the maximum vibratory ground motion at the Diablo Canyon site, is still valid. The maximum credible earthquakes that could occur on any other fault or fault zone in the site vicinity would produce smaller ground motions at the site. PG&E concludes that the maximum earthquake associated with the Hosgri fault zone has a magnitude of 7.2 and could be located on the strand of the Hosgri that is nearest the site (the closest epicentral distance from the Diablo Canyon site is 4.5 km). The NRC staff has reviewed the PG&E conclusion and finds it acceptable. On this basis, the staff finds that PG&E has met element 2 of the license condition.

1.3.3 Element 3 of the License Condition

Element 3 of the license condition requires that PG&E reevaluate the ground motion at the site with full consideration of site and other relevant effects. In order to determine the ground motion at the site, one necessary piece of data is an estimate of the style of faulting on the controlling fault. This is important because regression analyses of the empirical ground-motion database show that reverse-slip motion on the Hosgri fault would produce higher ground motion at the site than strike-slip motion, for the same earthquake magnitude. In the LTSP Final Report, PG&E concluded that earthquake motion on the Hosgri fault is best characterized as 65-percent strike-slip, 30-percent oblique-slip (midway between strike-slip and reverse-slip), and 5-percent thrust-slip (reverse-slip with a low dip angle). On the basis of its review and the advice of its consultants, the staff finds that the style of faulting on the Hosgri fault is predominantly right-lateral strike-slip, with a subordinate but substantial reverse (vertical) component. Specifically, the staff concludes that ground motion at the site should be evaluated for an earthquake on the Hosgri fault that is 2/3 strike-slip and 1/3 reverse-slip. Thus, the staff conclusion gives greater weight to the reverse-slip component of motion.

To determine ground motion at the plant site, it is also necessary to determine the attenuation of ground motion as it propagates from the earthquake hypocenter to the site. The staff has reviewed PG&E's empirical ground-motion attenuation model and numerical modeling studies and has performed an independent attenuation study to estimate ground motion at the Diablo Canyon

site. The staff's analysis was based on the staff's estimate (described above) of the ratio of strike-slip to reverse-slip motion expected from an earthquake on the Hosgri fault. The resulting independently estimated ground-motion spectra at the plant site have been compared to the spectra developed by PG&E for the LTSP.

As is discussed in Section 2.5.2.3 of this SSER, the results show that the staff's estimates of both the 50th and 84th percentile horizontal ground-motion spectra at the site is equal to or less than the PG&E spectra at frequencies above 1 Hz, but exceeds the PG&E spectra at frequencies at and below 1 Hz. For vertical ground motion, the staff's 84th percentile vertical spectra exceed the PG&E vertical spectra over the frequency range from 1 to 10 Hz (Figures 2.4 and 2.5). While PG&E has met the requirements of element 3 of the license condition by its reevaluation of ground motion at the site, to fully satisfy element 4 of the license condition, PG&E must demonstrate that the plant structures can withstand these exceedances.

1.3.4 Element 4 of the License Condition

Element 4 of the license condition requires PG&E to assess the significance of the conclusions drawn from elements 1, 2, and 3 using probabilistic and deterministic methods, as necessary, to assess seismic margin adequacy. PG&E has performed a deterministic analysis as well as a PRA and has concluded that the plant seismic margins are adequate.

PG&E performed detailed soil-structure interaction (SSI) analyses to determine the effects of dynamic interaction between the plant structures and the foundation rock underlying the plant on the seismic response of plant structures. The analyses showed that the effects of ground-motion incoherence and embedment of structures (lumped into the "tau effect" in previous studies) reduce the seismic response of some plant structures, but not others. Specifically, incoherence reduces response about 15 percent for the auxiliary building and about 20 percent for the turbine building, but is minimal for the containment shell and internal structures. The NRC staff found, based on its review of PG&E analyses and on analyses conducted by staff consultants, that the PG&E SSI analyses were comprehensive, thorough, and acceptable.

The Diablo Canyon PRA analysis conducted by PG&E included both internal and external events. The objectives of the PRA were to (1) assess the importance of various structures and items of equipment to seismic risk and (2) put the seismic risk in perspective by comparing it to the risk from other external and internal initiators. Risk in this context refers primarily to the estimated core damage frequency (CDF). The PG&E PRA results indicate that the mean overall CDF for Diablo Canyon is estimated to be 2.0E-4/yr (the staff estimate is 4.0E-4/yr), which is similar to that of other nuclear plants. The PG&E PRA shows that internal events contribute 63 percent of the total CDF, with seismic events contributing 18 percent and other external events contributing 19 percent. The NRC staff estimates of these values are: internal, 70 percent; seismic, 10 percent; and other external events, 20 percent. A component importance study indicated that the single greatest contributor to seismic risk is failure of the turbine building shear wall (30% of the total seismic CDF), followed by

loss of 230-kV offsite power (24% of the seismic CDF), and failure of the diesel generator control panel (10% of the seismic CDF).

PG&E performed deterministic comparisons using its LTSP ground-motion estimates and showed that the major plant structures at Diablo Canyon have adequate seismic margins. As a result of a separate reevaluation by the NRC staff of the adequacy of the seismic resistance of masonry walls, PG&E plans to modify all the safety-related masonry walls. The modifications will be determined on the basis of analysis using the Hosgri ground-motion. Selected walls will be evaluated against the LTSP spectra to ensure acceptable margins. The staff has reviewed and approved the modification criteria and the results of PG&E's evaluation of the deterministic margins of selected masonry walls.

As is discussed under element 3, above, the staff's estimates of the horizontal and vertical ground-motion spectra exceed PG&E's estimates by about 15 percent or less over part of the frequency range. PG&E has concluded (Shiffer, 1991i and k) that the plant seismic margins are adequate to accommodate the horizontal and vertical spectral exceedances that result from use of the staff's estimates of horizontal and vertical spectra. The staff has reviewed PG&E's evaluation of the vertical and horizontal exceedances and finds it acceptable, but will require PG&E to perform analyses to confirm its conclusion. Subject to satisfactory completion of analyses confirming that the seismic margins are adequate to accommodate the staff's spectral estimates, the staff concludes that PG&E has met element 4 of the license condition.

In summary, the staff has reviewed PG&E's PRA and deterministic analyses of selected structures and equipment and finds them acceptable. Therefore, subject to satisfactory completion of the analyses necessary to confirm that the spectral exceedances, discussed above can be accommodated by plant seismic margins, the staff concludes that PG&E has met element 4 of the license condition.

1.4 Summary of Staff Conclusions

In summary, the staff has reviewed the PG&E submittals relating to the LTSP and, subject to confirmation by PG&E that the plant seismic margins are adequate to accommodate the spectral exceedances discussed under element 4 above, the staff finds that License Condition 2.C.(7) of DPR-80 has been met.

The staff notes that the seismic qualification basis for Diablo Canyon will continue to be the original design basis plus the Hosgri evaluation basis, along with the associated analytical methods, initial conditions, etc. The LTSP has served as a useful check on the adequacy of the seismic margins and has generally confirmed that the margins are acceptable. For future plant design modifications, the staff concludes that LTSP spectra, increased to envelope the exceedances in the vertical and horizontal spectra discussed in Section 2.5.2.3 of this SSER, should be used to verify that the plant high confidence of low probability of failure (HCLPF) values remain acceptable (Section 3.8 of this SSER). PG&E has agreed (Shiffer, 1991l) to review future plant modifications in the light of the findings of the LTSP, and is currently developing an implementation procedure for that purpose.

1.5 NRC Staff Consultants

In conducting its review of the LTSP, the NRC staff engaged a number of consultants. In several instances, the consultants performed independent investigations and analyses. The following is a list of the consultants, their organizational affiliations, the areas they reviewed, and the independent work they performed.

(1) Keiiti Aki, University of Southern California, reviewed the numerical modeling ground-motion studies.

(2) Ralph J. Archuleta, University of California, Santa Barbara, reviewed the numerical modeling ground motion studies.

(3) Michael Bohn, Sandia National Laboratory, reviewed the PRA.

(4) Robert Brown, Thomas Brocher, Jerry Eaton, Steve Lewis, David McCulloch, and David Schwartz, U.S. Geologic Survey (USGS), reviewed geology, geophysics, and tectonics studies (see Appendix C of this SSER) and conducted independent interpretations of the seismic reflection data covering the offshore Santa Maria Basin.

(5) Kenneth W. Campbell, Dames & Moore (formerly with USGS), reviewed PG&E's empirical ground-motion attenuation studies and conducted independent empirical ground-motion studies.

(6) Carl J. Costantino, College of the City of New York, reviewed the soil-structure interaction analyses.

(7) Steven M. Day, San Diego State University, reviewed numerical modeling ground-motion studies.

(8) George Bozoki, Robert Fitzpatrick, P. Kohut, and M. Sabek, Brookhaven National Laboratory, reviewed the PRA analyses, did independent studies of several systems, and performed importance and sensitivity studies using a reduced plant model.

(9) James Johnson and M.K. Ravindra, EQE, Inc., reviewed the PRA.

(10) David B. Slemmons, Douglas Clark, Steve Nitchman, Katheryn Killeen, Barbara Matz, Xiaoyi Zhang, Eutizio Vittori, Richard Schweickert, and Kirk Swanson, University of Nevada, Reno, reviewed PG&E's geology, geophysics, and tectonics characterization studies (see Appendix D of this SSER). These consultants also conducted independent studies, including (1) geological field reconnaissance of the San Simeon area, (2) geological mapping of the Morro Bay, Los Osos, and Edna fault areas, (3) mapping of marine and fluvial terraces of the San Luis-Pismo structural block, (4) mapping, determination of capability, and determination of sense and magnitude of displacement on the Los Osos and Wilmar Avenue faults, (5) mapping and determination of the nature of displacement on the Foxen Canyon fault, (6) determination of the nature of regional tectonic stresses in the Diablo Canyon region, (7) conducting a remote sensing analysis of the Diablo Canyon region, and (8) determination of the cause

and amount of late Quaternary uplift on the Casmalia-Orcutt structural block.

(11) Anestis S. Veletsos, Rice University, reviewed soil-structure interaction analyses and conducted an independent soil-structure interaction study using a simplified analytical model of the Diablo Canyon power-block structures.

1.6 NRC Staff Contributors

The following members of the NRC staff contributed to the staff review discussed in this SSER:

G. Bagchi
A. Buslik
N. Chokshi
A. Lee
R. McMullen
R. Pichumani
H. Rood
R. Rothman
T. Ryan
P. Sobel

2 SITE CHARACTERISTICS

2.5 Geology, Seismology and Foundation Engineering

2.5.1 Geology

In conducting its Long Term Seismic Program (LTSP), PG&E identified, examined, and evaluated all relevant geological, seismic, and tectonic information that had become available since the 1979 ASLB hearing, and also earlier information as needed. As part of this effort, PG&E acquired a substantial amount of formerly proprietary seismic reflection and oil well data and additional new geological, seismic, and seismic reflection data. The major investigations characterized the Hosgri, Los Osos, and Southwest Boundary Zone fault zones.

Previously, the staff concluded that displacement on the Hosgri fault zone is essentially all strike-slip. The staff now concludes that displacement on the Hosgri is predominantly strike-slip with a substantial reverse-slip component. The strike-slip displacement on the San Simeon fault is transferred to the Hosgri fault zone through the Cambria pull-apart basin.

The Los Osos fault and the Southwest Boundary Zone are the northeast and southwest boundaries of the San Luis-Pismo block, the crustal block on which the Diablo Canyon plant is located. Since 1985, University of Nevada, Reno (UNR) researchers discovered that the Los Osos fault and the Wilmar Avenue fault (part of the Southwest Boundary Zone) are capable. Mapping of marine and fluvial terraces around the site vicinity by PG&E and the UNR demonstrated that the San Luis-Pismo block is not being internally deformed, but is being uplifted at a rate of about 0.1 to 0.2 mm/yr.

For the purpose of defining maximum credible earthquakes (see Section 2.5.2.2 of this SSER), PG&E developed logic trees to account for uncertainty in characterizing important faults. This approach is based on assessments of various fault characteristics, including rupture length, that were evaluated during the LTSP review.

The following is a summary of the staff's geology conclusions, based on PG&E's investigations and analyses and advice from the USGS and the UNR.

(1) Hosgri Fault Zone

The Hosgri and the San Simeon faults are capable faults and are components of the much larger San Gregorio-Hosgri fault system (Figure 2.1). Strain is transferred between them by means of a 3-km to 5-km wide by 10-km long, rightstep, pull-apart basin, the Cambria Basin. The Hosgri fault zone, which is about 110 km long, varies in character along its extent. Among the characteristics are (a) a single straight segment, (b) two or more splays, (c) a multicomponent system consisting of one or more low-angle thrust faults and folds (except for a 15-km section west of Cambria and northern Estero Bay), and (d) one or more high-angle components. The downdip geometry of the Hosgri

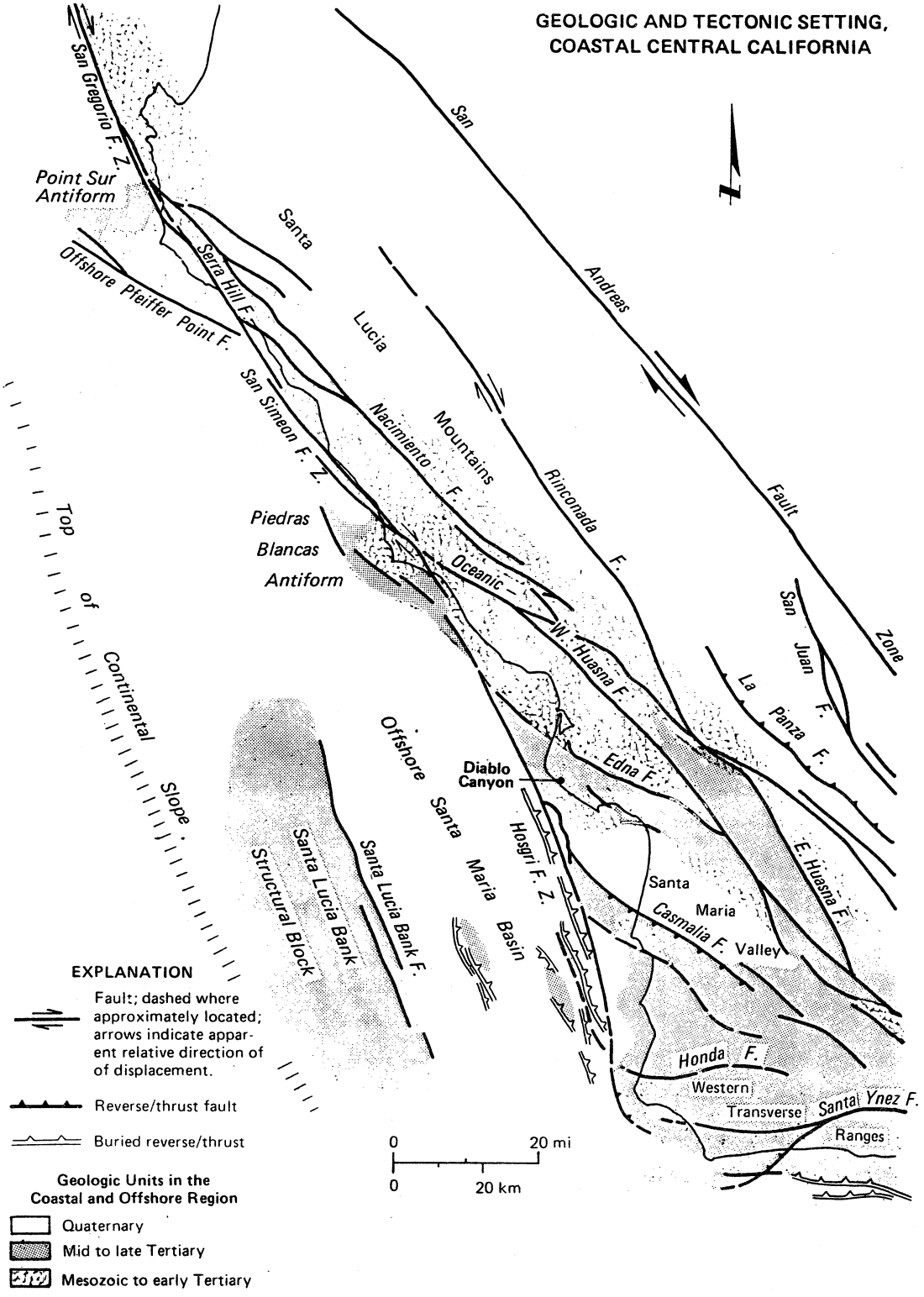


Figure 2.1
San Gregorio-Hosgri fault system (Figure 1 in LTSP Report on NRC/PG&E Geology/Seismology/Geophysics Workshop Held on October 21 and 22, 1986, San Francisco, California)

fault zone and the relationship among low- and high-angle faults is not resolved, but on the basis of the weight of the geological, geophysical, and seismological data, the staff concludes that displacement in the seismogenic zone (5-km to 12-km deep) is predominantly strike-slip with a substantial reverse-slip component.

The maximum length of rupture during a single earthquake could be as much as 70 km, but a more likely maximum rupture length during a single earthquake is 45 to 50 km. The horizontal slip rate is 1 to 3 mm/yr with a ratio of horizontal to vertical components of 2:1.

(2) San Luis-Pismo Structural Block

The Diablo Canyon plant is located on the San Luis-Pismo structural block. The San Luis-Pismo block is not undergoing internal deformation, and faults within the block (such as the San Miguelito and Edna) are not active. Instead, the block is being uplifted 0.10 to 0.20 mm/yr along the bordering reverse faults that dip beneath it. Therefore, the NRC staff concludes that there is no potential for surface faulting at the Diablo Canyon site.

(3) Los Osos Fault

The Los Osos fault, the northeast boundary of the San Luis-Pismo block, is approximately 57 km long, from its intersection with the Hosgri fault to its intersection with the West Huasna fault. The Los Osos fault is a reverse fault that dips approximately 60° to the southwest. Its slip rate, although not well constrained, is 0.25 to 0.8 mm/yr.

The staff finds PG&E's segmentation assessment of the Los Osos fault to be reasonable. That assessment resulted in the conclusion that a segment length of 19 km could rupture during a single maximum event, with a maximum displacement of 2.1 m.

(4) Southwest Boundary Zone

The Southwest Boundary Zone, the southwest boundary of the San Luis-Pismo block, is a diffuse zone of northeast-dipping reverse faults. It is generally 3 to 4-km wide but reaches a width up to 8 km. The San Luis-Pismo structural block to the northeast is being uplifted relative to the Santa Maria Valley block to the southwest. Faults of this zone include the San Luis Bay, Olson, Wilmar Avenue, Pecho, and Oceano. These Southwest Boundary Zone reverse faults dip at a high angle (60/70°) to the northeast. At that angle of dip they probably do not merge at depths shallower than 7 or 8 km.

The San Luis Bay fault is a capable fault. The closest mapped trace off shore is about 5 km from Diablo Canyon. The estimated slip rate is 0.02 to 0.12 mm/yr. The Olson fault, which is the closest active fault to the site (the nearest mapped trace off shore is about 3 km from Diablo Canyon), is considered to be a separate fault and not linked at the near surface with the San Luis Bay fault, but the two faults may merge at depth within the seismogenic crust. Possible offshore projections of both faults could be closer to Diablo Canyon than the nearest mapped locations.

The Wilmar Avenue fault is considered not to connect with the San Luis Bay fault at the surface, but may merge at depth. At the southwest end of the Irish Hills subblock, where the two faults approach one another, they are likely segmented and should not be considered to rupture simultaneously.

The Pecho and Oceano faults are likely to be capable faults, but because of their distances from the site, relative sizes, and low slip rate they are considered to be less of a hazard to the Diablo Canyon plant than the Hosgri fault zone.

Although the presence of an undetected coastal fault cannot be completely ruled out, investigations and analyses by PG&E indicate that the probability of such a fault is very low.

2.5.1.1 Regional Geology and Tectonics

Diablo Canyon is located along the south-central California coast. Coastal central California lies within the North American-Pacific plate boundary, which is a broad heterogeneous zone of translational and compressional deformation extending from the Great Basin (Dickinson and Snyder, 1979) to the continental slope (McCulloch, 1987). The relative motion between the two plates is determined by marine magnetic anomalies, hot spot tracks, transform azimuths, earthquake slip vectors, and geological observations and geodetic measurements along the San Andreas and other faults within the plate boundary (Brand, 1988).

The current seismotectonic characteristics of the Diablo Canyon region are largely the result of the influence of the late Cenozoic Era [2 to 24 million years before present (mybp)] development of the San Andreas transform fault system which lies in the approximate center of this broad plate boundary. Mesozoic and Tertiary subduction (approximately 200 mybp to 30 mybp) in this region were gradually replaced in the Miocene epoch (5 mybp to 24 mybp) by a broad zone of right-lateral shear between the plates (Atwater, 1970) and centered along the San Andreas fault. This activity caused a prominent northwest structural grain, right-lateral strike-slip fault systems, en-echelon folds, and pull-apart basins (Blake and others, 1978; Page, 1981). Crustal blocks with different rock types and geological histories were juxtaposed across the San Andreas fault and to a lesser extent across other faults such as the Rinconada and San Gregorio-Hosgri, because of the late Cenozoic right-lateral translations (Hill and Dibblee, 1953; Dibblee, 1976; Graham and Dickinson, 1978). A popular current theory is that these large crustal blocks within this boundary zone shift around relative to one another, such as the clockwise rotation of the western Transverse Ranges (Hornafius and others, 1986) and the extension within the Basin and Range.

During the late Cenozoic Era, some divergence of crustal blocks occurred within the predominantly strike-slip system (transtension) and was accompanied by basin formation and marine deposition. This transtension was replaced by convergence of crustal blocks within the strike-slip regime (transpression) in the Pliocene epoch (5 to 2 mybp) (Jahns, 1973; Blake and others, 1978) brought about by a clockwise rotation in the direction of movement of the Pacific plate that began 3.4 to 3.9 million years ago and continues to the present time (Cox and Engebretsen, 1985; Harbert and Cox, 1989). This caused the post-Miocene compression that is so much in evidence in coastal central California in the

form of intense folding, reverse/thrust (low-angle reverse faults) faulting, and range uplift. This compression culminated in the late Pliocene epoch and Quaternary period (3 mybp to 1 mybp) Coast-Range Orogeny (Reed, 1933; Taliaferro, 1943; Page, 1966 and 1981).

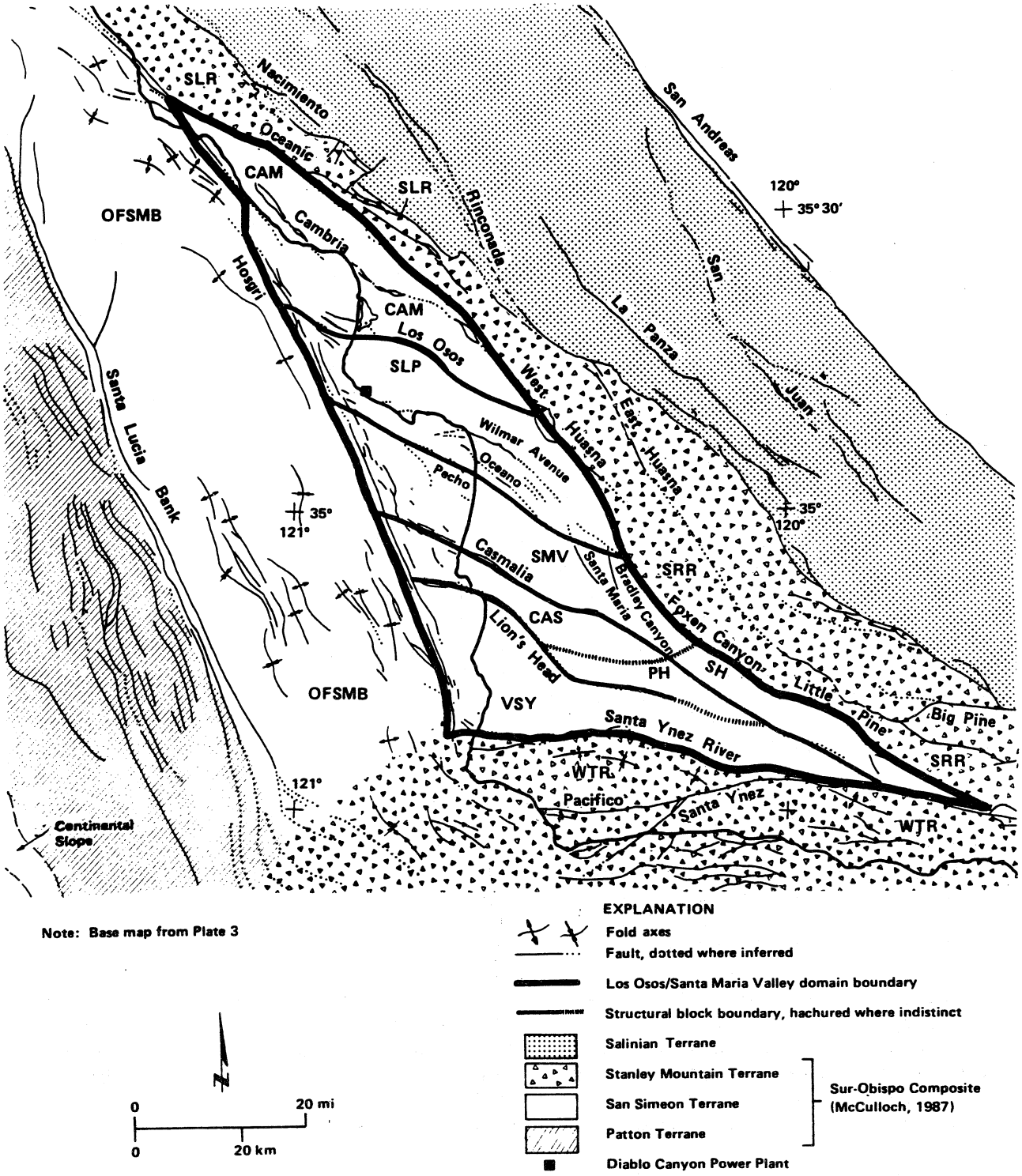
The San Andreas fault system is the main locus of differential motion between the North American and Pacific plates. Much of the motion is also accommodated by right-lateral strike-slip displacement on faults east and west of the San Andreas fault such as the San Gregorio-Hosgri fault system and by contraction in the Transverse Ranges and the Southern Coast Ranges (Minster and Jordan, 1978, 1984, and 1987; Weldon and Humphreys, 1986).

There is a deficit of several millimeters per year (mm/yr) between the estimated magnitude of relative plate motion and geological and geodetic evidence. This deficit is believed to be explained by errors in calculating plate motion, the existence of unquantified displacement within the Basin and Range, folding and thrusting, and the accommodation of some displacement along strike-slip faults other than the San Andreas within the plate boundary zone, such as the San Gregorio-Hosgri fault system.

Recent geodetic measurements (Feigl and others, 1990) indicate the integrated rate of deformation across the Santa Maria fold and thrust belt is 7 ± 2 mm/yr at N 03° W ± 13°. This vector can be broken down into 6 ± 2 mm/yr of crustal shortening along the structural trend of N 30° E plus 3 ± 1 mm/yr of right-lateral shear across this trend. These estimates are consistent with structural orientations, earthquake focal mechanisms, geologic cross-sections, and kinematic models of this region. The estimates account for a large part of the apparent discrepancy between relative plate motion and measured deformation along the San Andreas fault.

PG&E, in the LTSP Final Report (Brand, 1988), has divided the central coastal California region into four general geologic terrains or domains (Figure 2.2). The Diablo Canyon site is located within the Los Osos/Santa Maria Valley domain. Slemmons and Clark and others (Appendix D of this SSER) divided the same region into five structurally and physiographically distinct seismotectonic domains characterized by distinctive patterns of Quaternary or late Quaternary, or both, tectonic deformation and seismicity. In this characterization, the site is within the Santa Maria-San Luis Range domain. The two characterizations are similar, with the Hosgri fault zone being the western boundary and the Santa Ynez River being the southern boundary of both, but the northeast boundaries are different. PG&E's northeast boundary is the Oceanic-West Huasna-Foxen Canyon-Little Pine fault system, while the northeastern boundary of Slemmons' and Clark's Santa Maria-San Luis Range domain is the Los Osos-West Huasna-Foxen Canyon-Little Pine fault system.

The folding and faulting expressed in the upper rocks within the Los Osos-Santa Maria Valley domain are explained by PG&E as being the result of clockwise rotation of the western Transverse Range structural block and the domain's impingement to the north on the Salinian block (Brand, 1988). The Hosgri fault zone is interpreted by PG&E as a predominantly strike-slip fault that serves as a tectonic boundary between northeast-southwest directed compression on its eastern side and the east-west-oriented tectonic stress regime on its western side.



Map of the Los Osos/Santa Maria Valley Domain illustrating the general distribution of major basement terranes. CAM = Cambria block, SLP = San Luis/Pismo block, SMV = Santa Maria Valley block, CAS = Casmalia block, VSY = Vandenburg/Santa Ynez Valley block, WTR = Western Tranverse Ranges, SRR = San Rafael Range, SLR = Santa Lucia Range, OFSMB = Offshore Santa Maria Basin, PH = Purisma Hills block, SH = Solomon Hills block.

Figure 2.2
Los Osos/Santa Maria Valley Domain (Figure 2-8 in LTSP Final Report)

Other tectonic models have interpreted the Hosgri fault as a compressional feature. According to Crouch and others (1984), the region is characterized entirely by compression with little or no strike-slip motion on the Hosgri fault. They state that the area consists primarily of thrust faults (low-angle reverse faults) with associated folds dipping both to the east and to the west. Namson and Davis (1990) postulate faults ramping upward from a decollement resulting in fault bend folds, fault propagation folds, liftoff folds, and tectonic uplift. They do not consider the Hosgri fault to be important in current tectonics.

Another tectonic model for the Hosgri region is strain partitioning, which was raised by UNR advisor, Dr. Slemmons. In this model, oblique slip at depth is translated to a component of reverse and a component of strike-slip faulting in the upper crust. PG&E acknowledged that strain partitioning may be occurring in the Piedras Blancas anticlinorium area and along the southern reaches of the Hosgri fault zone. Although inconclusive, the staff finds that this model appears to best explain the late Tertiary (15 to 2 mybp) and Quaternary (2 mybp to Present) tectonic features and the current state of stress.

The site region is underlain by Jurassic (210 to 140 mybp) Franciscan formation basement which is a melange derived from subduction of the Pacific plate beneath the North American plate in the Jurassic period. Overlying the basement are predominantly middle to late Cenozoic marine sedimentary and volcanic rocks formed during the period of transtension described above. Bedrock directly beneath the Diablo Canyon plant is early middle Miocene (16 to 11 mybp) Obispo formation volcanic tuff. Also prevalent in the site area is sandstone of the upper middle Miocene (15 to 11 mybp) Monterey formation. Quaternary wave-cut benches were cut into these and younger rocks by the ocean when sea level was at higher elevations relative to the land and are preserved as relics at various levels on the coastal landscape. Colluvial and alluvial deposits overlie these terraces. Likewise, offshore wave-cut platforms created at times when sea level was lower relative to land are also preserved. These marine terraces, especially those on shore, have been invaluable tools used during the LTSP investigations in estimating uplift, age of tectonic deformation, and slip rate on faults.

San Gregorio-Hosgri Fault System

The San Gregorio-Hosgri (SGH) fault system (Figure 2.1) extends from its juncture with the San Andreas fault off shore just south of Bolinas Bay, southward to the Transverse Ranges, forming the structural boundary that separates the California onshore region of general uplift from the basins and other features that underlie the adjoining narrow continental shelf. Hamilton (1984) described the SGH fault system, which has had a long and varied tectonic history. The principal faults of the SGH system include from north to south the San Gregorio, Serra Hill-Sur, San Simeon, and Hosgri fault zones. The entire system is more than 400 km long and the principal faults are active as indicated by late Quaternary deformation and current seismicity. Senses of slip of faults within the system are characterized by right-lateral, right-oblique, and reverse displacements. The SGH fault system is entirely off shore, except where it crosses the coastline for short distances at Año Nuevo, Point Sur, and San Simeon. There is a profound structural contrast across the fault system as revealed by gravity and magnetic data across its southern part.

Nearly pure right-lateral strike-slip typifies the system north of Ragged Point. Compressional structures intersect the principal faults of the system at an angle from Monterey Bay to the Point Sal area. It is not clear whether the high-angle faults of the SGH offset these compressional features or the compressional features offset the faults, because the data resolution is poor at the depth where this happens. PG&E interpreted the high-angle strike-slip of the Hosgri fault zone, the southern element of the SGH fault system, to offset the compressional features because the Hosgri fault can be seen in the seismic reflection data to offset younger sediments, while the compressional features do not.

The San Gregorio fault extends from its intersection with the San Andreas fault to southwest Monterey Bay where it splays into several faults, the most significant of which is the Sur fault. On the basis of the observed offset of similar crystalline rocks (one at Point Reyes northwest of the fault and the other at Lopez Point southeast of the fault), about 190 km of right-lateral, strike-slip displacement is estimated to have occurred along the San Gregorio fault since early Eocene time. The Sur fault extends from Monterey Bay to Lopez Point where there is a stepover to the San Simeon fault. The two faults form the eastern boundary of the actively subsiding Sur Basin off shore. The northern part of the San Simeon fault has 2 km of topographic relief across it with Franciscan formation forming the Santa Lucia Mountains to the east and Franciscan and ophiolites within the basin to the west. It also exhibits a classic strike-slip, rift valley form in the area north of Cape San Martin. An offshore canyon is right-laterally offset 2 km. On shore to the south, the San Simeon fault leaves the Santa Lucia Mountain front and trends down Arroyo Laguna Creek, going off shore south of Point San Simeon. The west side of the fault is up along Arroyo Laguna Creek and in the offshore area south of Point San Simeon. There is a stepover from the San Simeon fault via the Cambria Basin to the Hosgri fault which extends southward to Point Pedernales.

Most of the observed strike-slip displacement on the SGH fault system took place in early Cenozoic time. This was followed by a transtensional environment between late Miocene and early Pliocene time (11 to 3 mybp), during which time the faults served as basin boundaries. With the onset of a change in the direction of plate motion in the Pliocene epoch (about 3 to 5 million years ago), the principal motion along the SGH fault system became right-lateral strike-slip and the staff considers this to be the principal style of motion at the present time.

2.5.1.2 Site Region and Site Area Geology

2.5.1.2.1 San Simeon Fault Zone

The San Simeon and Hosgri faults are the southern members of the SGH fault system. Both are offshore basin boundary faults, but the San Simeon fault trends on shore at Ragged Point, extends for 19 km on shore, and returns off shore at Point San Simeon.

The San Simeon fault, in addition to being a basin border fault south of Cape San Martin, is also partly a frontal fault to the Santa Lucia Mountain Range, where there is as much as 7,000 ft of vertical separation between the crest of the mountain range and the bottom of the basin (Hamilton, 1984). As part

of the SGH fault system, the San Simeon fault has a strong component of strike-slip displacement. At Ragged Point, where it comes ashore, the San Simeon fault zone consists of several splays. South of Ragged Point, apparently, the vertical component of slip trends slightly in a more easterly direction and follows the Santa Lucia mountain front as the Oceanic and West Huasna faults. The predominantly strike-slip component continues south-southeast along strike to Point San Simeon and is reflected in the topography as a rift valley with laterally displaced drainage and an east-facing escarpment.

Because of similarities between the San Simeon and Hosgri faults and the presence of a portion of the San Simeon fault on shore, detailed paleoseismic investigations were conducted on the onshore section of the San Simeon fault. These included geological mapping (including mapping, age dating, and determining cross-cutting relations of marine terraces); geomorphic studies; excavating, logging, and analyzing trenches across the fault; age-dating soils; and mapping the sea cliffs. The southern offshore extension of the fault zone was investigated by divers, sea floor sampling and analysis, and seismic reflection profiling. On the basis of the straight coastline in the vicinity of Cambria, the San Simeon fault is interpreted to extend to just north of Point Estero (the reach or section where strain is transferred across the pull-apart basin to the Hosgri fault) but not into Estero Bay. The San Simeon fault is seismically active, and focal mechanisms of earthquakes range from pure strike-slip to reverse-oblique.

On the basis of investigations and analyses of the San Simeon fault (particularly the onshore marine terrace studies, the offset drainages, and the analysis of trench logs), the staff agrees with PG&E's findings regarding the slip characteristics of the San Simeon fault:

- The sense of displacement is predominantly strike-slip.
- The rate of slip varies from 1 to 3 mm/yr.
- Horizontal displacement per earthquake is on the order of 1 m maximum.

2.5.1.2.2 Cambria Stepover Basin

The Cambria stepover, or pull-apart, basin, was interpreted by PG&E to be a Quaternary halfgraben that is 3-km to 5-km wide, 10-km long, and 28-m deep at its northwest end adjacent to the Hosgri fault. The basin lies between the southern termination of the San Simeon fault and the northern end of the Hosgri fault and 1 to 3 mm/yr of right-lateral strike-slip displacement is transferred across it between the two fault zones. Many seismic reflection lines crossing the basin and one line along the longitudinal extent of the basin are used as a basis for this interpretation (most notably seismic reflection lines CM-45, CM-47, and CGI-19; response to Question 43). Profiles crossing the northern part of the basin show the San Simeon image strongly, but the Hosgri fault is not seen. The seismic reflection lines crossing the middle section of the basin show the presence of the Hosgri and San Simeon faults. Seismic reflection lines crossing the southern portion of the basin show a strong Hosgri fault signature, but the San Simeon fault is not present.

The basin is bordered on the western side by north-northwest-striking normal faults. North-northwest-striking normal faults are also present within the basin. PG&E constructed a structural contour map of the basin (base of the

Pliocene time-structure) and an isopach map of the Pliocene epoch. The distribution of post-Wisconsinan sediment indicates late Holocene subsidence of the basin. Seismic reflections from the rocks beneath and adjacent to the basin show evidence of substantial compression. However, this deformation appears to be confined to Miocene sedimentary rocks and is interpreted to be related to compressional deformation during that time (more than 5 mybp).

Characteristics used by PG&E to analyze strain transfer between the two faults across the Cambria Basin include: (a) 5-km separation between the faults, (b) 10 km of overlap, (c) an amount of crustal shortening equal to the amount of subsidence in the basin, and (d) the depth of the basin. The rate of horizontal slip calculated using these values is 1 to 4 mm/yr, which compares closely with the slip rate of 1 to 3 mm/yr calculated from the trench and marine terrace studies at San Simeon.

PG&E compared the Cambria Basin with other pull-apart basins worldwide, such as the Niksar pull-apart basin between segments of the North Anatolian fault in Turkey, the basin associated with the Hope fault in New Zealand, the pull-apart basin associated with the Dead Sea fault, and the Cholame Valley pull-apart basin within the San Andreas fault zone. Pull-apart basins are not uncommon throughout the world in similar tectonic environments.

The staff concludes that the data support the presence of a Quaternary basin between the extremities of the San Simeon and Hosgri fault zones and that transfer of strain from one zone to the other is a reasonable interpretation. The staff further finds that the estimated 1 to 3 mm/yr horizontal right slip that characterizes the southern San Simeon fault is transferred via the basin to the northern Hosgri fault zone.

2.5.1.2.3 Piedras Blancas Anticlinorium

A concern during this review was that some of the strike-slip displacements of the SGH fault system may be transferred to the Hosgri fault via the Piedras Blancas anticlinorium. Thus, simply assuming the transfer of only the displacement estimate for the San Simeon fault to the Hosgri via the Cambria pull-apart basin would cause an underestimation of the total ongoing strike-slip displacement on the Hosgri. Investigations and analyses by PG&E adequately demonstrate that deformation within the anticlinorium (a series of folds so structurally arranged to form a broad arch) is consistent with PG&E's conclusion that right-lateral displacement along the San Simeon fault is being transferred to the Hosgri and that there is no additional significant right-lateral displacement transferred through the Piedras Blancas anticlinorium.

The Piedras Blancas anticlinorium is described by Hamilton (1984) as a major northwest trending and plunging structural high that is located to the west of the San Simeon fault. It is expressed on shore as a broadly arched area of marine terraces between Ragged Point and San Simeon Point. It is expressed off shore in the marine platform above the 100-m bathymetric contour north of Point Piedras Blancas, and south in the slope between the 100-m and 200-m contours along the coast north of Estero Bay. On shore, reverse faults splay northwestward across the eastern flank of the anticlinorium from the west side of the San Simeon fault north of San Simeon Bay. One of these faults, the

Arroyo del Oso fault, displaces the base of the lowest marine terrace sequence along the coastline (Hall, 1975).

The core of the Piedras Blancas anticlinorium is basement rock, which is overlain and surrounded by Miocene-lower Pliocene strata. The lack of thinning of the Miocene-lower Pliocene section, and the fact that it is onlapped by the upper Pliocene-Pleistocene section, indicates that the anticlinorium developed after Miocene-Pliocene times. Deformation of Quaternary deposits and seismicity indicate that the Piedras Blancas anticlinorium is still tectonically active.

Within the anticlinorium are many southwest vergent anticlines with axes that dip northeast and northeast vergent anticlines with axes that dip southwest. These folds are assumed to be underlain by thrust faults. PG&E calculated the rates of crustal shortening caused by these folds and faults using the Miocene unconformity as a reference and assuming a minimum age of 2.8 million years. PG&E appears to have a basis for at least that age from dating the Squire Member of the Pismo formation on shore and age-dating ocean-bottom samples from the flanks of the anticlinorium. The calculated rate of shortening is 0.4 mm/yr perpendicular to the San Simeon fault and 1 to 3 mm/yr parallel to the San Simeon fault. These rates are consistent with rates calculated by other methods.

Many of the structural characteristics of the Piedras Blancas anticlinorium can be explained by the concept of strain partitioning (as presented by the UNR at the June 12, 1989, workshop) applied to the northern portion of the Hosgri fault and the southern portion of the San Simeon fault. That is, oblique displacement at depth (at the base of the seismogenic crust--greater than about 12-km depth) is being translated to strike-slip displacement on the Hosgri and San Simeon faults and reverse displacement on adjoining and branching blind thrust faults associated with the folds in the Piedras Blancas anticlinorium. The staff agrees with its advisor, the UNR, and PG&E, that strain partitioning is occurring in the Piedras Blancas region.

2.5.1.2.4 Hosgri Fault Zone

As described in an earlier part of this section of the SSER, much of the knowledge about late Quaternary behavior of the Hosgri fault zone was derived from onshore investigations of the San Simeon fault zone by field mapping, mapping by borings of buried marine platforms, mapping marine terrace strand lines relative to the fault, studying the fault's linearity and other geomorphic effects, analyzing the attitude of slickensides, developing soil profiles, and age-dating the fault. The characteristics derived from these studies and used by PG&E to assess the Hosgri fault are: (1) a predominantly right-lateral sense of slip, (2) the rate of horizontal slip of 1 to 3 mm/yr, and (3) the ratio of lateral slip to vertical slip that ranges from 2.3:1 to 30:1.

The Hosgri fault zone is a boundary between (1) folds and thrust faults that approach it from the east at a high angle and (2) features to the west in the offshore Santa Maria Basin that are nearly parallel to the Hosgri fault. The origin of the compressive features west of the Hosgri fault is interpreted to correspond with the opening of the Gulf of California 5 mybp, as geological and

geophysical evidence indicates compression began between 6.0 and 5.2 mybp and apparently ended by 3.0 to 2.8 mybp (Brand, 1988).

PG&E has divided the Hosgri fault zone into five sections or reaches. This approach, which is equivalent to the segmentation hypothesis used in its seismic source characterization hypothesis, is used below in describing the Hosgri fault. The staff agrees with some, but not all, of PG&E's segmentation characterization.

° Northern Reach of the Hosgri Fault Zone

The southwestern flank of the Piedras Blancas anticlinorium is characterized by a series of west-northwest trending folds that appear not to be offset by high-angle faulting, which indicates that the Hosgri fault does not continue through or around the anticlinorium. The Hosgri fault is first observed as the west boundary of the Cambria pull-apart basin. A low-angle thrust component is present in this area. This component may structurally control the scarp on the low-sea-level stand terrace that occurred 18,000 years ago, thus indicating recent activity.

South of Point Estero the Hosgri fault zone is a single trace striking N 40° W and dipping at an angle of 80° or greater in the upper 2 km beneath the sea floor. Extending south from about the latitude of Morro Rock another trace (west trace) is observed close to the east trace which continues south. The northern reach extends from the Cambria pull-apart basin approximately 20 km to its intersection with the Los Osos fault and the San Luis-Pismo structural block. At this intersection, the Hosgri fault zone makes an 11° bend to the west, and the width of the zone increases abruptly to the south. The number of fault traces increases from two to several. Local compression at the Hosgri-Los Osos intersection is indicated by the presence of a local uplifted bathymetric feature, referred to as 59 Meter Ridge. Tertiary folds and faults present in the San Luis-Pismo block east of the Hosgri fault zone are truncated and do not exist west of the fault. Vertical uplift east of the fault increases substantially south of this intersection. A cluster of seismicity occurs near the intersection of the Los Osos and Hosgri faults. PG&E concluded that the Los Osos intersection is a rupture-segmentation point. On the basis of the changes in complexity of the Hosgri fault zone from north to south, and the location of the Los Osos deformation in Estero Bay, the staff concludes that this intersection is a strong segmentation point.

° San Luis-Pismo Reach of the Hosgri Fault Zone

In this reach, the Hosgri fault zone is the boundary between the highly deformed San Luis-Pismo block and the offshore Santa Maria Basin for about 20 km. This section of the Hosgri fault zone is the one nearest to the Diablo Canyon site (as close as 4.5 km). It strikes N 20° W and is composed of two discontinuous high-angle faults (east and west strands) that are less than 2 km apart and a buried low-angle thrust fault to the west. The low-angle fault apparently merges with the western strand below the depth of resolution of the seismic reflection data. The western strand is nearly vertical in the shallow depths but its dip decreases to

65/70° NE at 3-km to 4-km depth. The eastern strand dips 70/80° to the northeast. Both fault strands are expressed as discontinuous sea floor scarps and offset the late Wisconsinan [17,000 years before the present (ybp)] unconformity. The low-angle thrust fault dips 35/45° NE at shallow depths and about 60° at depths of 2 to 3 km and apparently merges with the western strand. The low-angle fault does not appear to affect the Pliocene/Miocene unconformity at a 1-km depth, indicating that its last displacement predated that feature. However, it is difficult to detect a fault in relatively soft sediment, and the age of the horizon referred to as the Pliocene/Miocene unconformity varies, and may be much younger west of the Hosgri fault zone than further east where its age is relatively well known. This reach ends at the intersection between the Hosgri and Pecho faults. The Pecho fault is a member of the southwest boundary of the San Luis-Pismo structural block. There is also a slight bend at this intersection and a marked decrease in the number of folds and faults south of the Pecho fault and east of the Hosgri fault zone.

PG&E makes a case for the intersection of the Pecho fault being a segmentation point in that there is likely to be a reduction in vertical uplift east of the Hosgri from that intersection south due to the end of the San Luis-Pismo block and the beginning of the Santa Maria Basin. Additionally, the Hosgri fault has a slight change in trend, and there is a pronounced decrease in mapped folds and faults on the east side of the Hosgri south of the Pecho intersection. However, the staff agrees with its advisor, the UNR, that if the Southwest Boundary Zone is a broad (3 to 5-km wide) diffuse zone as described by PG&E, the intersection of that zone is likely to also be diffuse and, therefore, may not be a strong segmentation point.

° San Luis Obispo Bay Reach of the Hosgri Fault Zone

South of its intersection with the Pecho fault, and continuing for 23 km to its intersection with the Casmalia fault zone, the Hosgri fault zone strikes N 15° W. The zone in this reach is characterized by a continuous west trace and several discontinuous east traces, all within a zone 2 to 3-km wide. The west trace is nearly vertical in the shallow depths but the dip is reduced to 60/75° NE at a depth of 4 km. The late Wisconsinan unconformity is offset by the west strand and locally by several strands of the eastern trace. The low angle of dip is prominent throughout this reach of the Hosgri fault zone. In the north it dips 40° NE and flattens to the south. Seismic reflection line JEBCO-126 indicates at least two low-angle faults that continue to the south. Neither fault offsets the Miocene/Pliocene unconformity.

This reach is the most controversial with respect to the interpretation of current tectonics. Crouch and others (1984) identified major low-angle reflectors which they interpret to be thrust faults that are listric to an aseismic detachment zone at depth. This interpretation is used to support their position that this region is undergoing pure compression with little or no strike-slip displacement along the Hosgri fault zone. At several LTSP workshop meetings, McCulloch and Lewis, USGS, presented their unpublished interpretation of several seismic reflection lines in this region that lead them to a similar conclusion. PG&E

identified many of the same low-angle reflectors but interpreted them to be subordinate to the high-angle, strike-slip components of the Hosgri fault zone. The relationship of the low-angle reflectors to the high-angle faults cannot be resolved from the seismic reflection data because the intersection of most of the reflectors occurs at depths greater than 1 to 3 km, which is below the depth of good resolution. Many of these low-angle reflectors were likely formed during an earlier episode of compression.

PG&E performed retrodeformable analyses (a procedure wherein geological cross-sections are readjusted to project their configuration at various times in the past) (Suppe, 1983 and 1985) to test Crouch and others (1984) interpretation of seismic reflection lines SM-1 and SM-4 (NEKTON 202 and NEKTON 233, respectively). PG&E found in using this method that the predicted folds that would be produced by thrusting on the interpreted faults would have been significantly larger and tighter than the folds observed in the data.

In trying to resolve the dilemma caused by poor resolution at depth, the staff has relied on other lines of evidence and concludes that there is a substantial amount of right-lateral displacement on relatively high-angle components along this segment as well as other segments of the Hosgri fault zone. Those lines of evidence include: (1) in the shallower depths (1 to 2 km), the high-angle components deform late Quaternary deposits and the sea floor, whereas the low-angle features do not appear to deform post-Pliocene sediments; (2) microearthquakes recorded on the Hosgri fault at the intersection of the Los Osos and Hosgri faults and the intersection of the Pecho and Hosgri faults at depths up to 7 km have largely strike-slip fault mechanisms; (3) the 1980 Point Sal earthquake and aftershock sequence suggest the Hosgri is a high-angle fault zone (see below); and (4) seismic reflection lines S-29 and S-31, which cross the San Gregorio fault, a well-documented, high-angle, strike-slip fault, south of its intersection with the San Andreas fault, show low-angle reflectors analogous to those adjacent to the Hosgri fault. The intersection of the Hosgri fault with the Casmalia fault is considered by the staff to be a strongly expressed segment point, as noted in the next section of this SSER.

- Point Sal Reach of the Hosgri Fault Zone

This section of the Hosgri fault zone is 14 to 18-km long and lies between the Casmalia fault to the north and Lions Head fault to the south. The area east of the Hosgri fault zone is characterized by vertical uplift and is referred to as the Point Sal high. On the basis of the mapping of marine terraces, the UNR determined that the Casmalia Range, which lies within the Point Sal high, has been uplifted at the rate of 0.14 to 0.17 mm/yr during the late Quaternary period.

The Hosgri fault zone in this area consists of two parallel high-angle faults; the western one is continuous, and the eastern one is only about 6-km long. The eastern strand is truncated by a west-northwest trending syncline associated with the Casmalia fault zone to the north and by the Lions Head fault to the south. The western strand dips 70 to 90° east to

a depth greater than 2 km, and the eastern strand dips at a high angle to the northeast, based on PG&E's interpretation. A series of low-angle, west-verging faults splay from the western strand near the southern end of this reach and are interpreted as a flower structure by PG&E to support its conclusion that the Hosgri is predominantly a strike-slip fault within this segment.

On the basis of abrupt changes in style of deformation at the Casmalia fault intersection, not only along the Hosgri fault zone, but both east and west of the Hosgri, PG&E defined this intersection as a rupture segmentation point. There is a cluster of microearthquakes at the intersection of the Hosgri and Casmalia faults. In addition to the uplifted Casmalia block to the east, extreme deformation is present west of the Hosgri fault zone within the Purisima and Lompoc structures. The staff agrees with PG&E and the UNR that the Casmalia-Hosgri intersection is a strong rupture-segmentation point. PG&E also described the intersection of the Lions Head fault as another segmentation point, primarily because it is the southern boundary of the uplifted Casmalia block, and also because to the south the Hosgri becomes a more well-defined boundary between strain regimes to the east and to the west. The UNR concluded that because of the low degree of late Quaternary activity on the Lions Head fault (less than 0.012 to 0.017 mm/yr), the intersection is not a strong point of segmentation. The staff concludes that because of the low level of Quaternary activity on the Lions Head fault as determined by the UNR (Clark, 1990), the Lions Head-Hosgri intersection should not be considered a potential rupture-segmentation point.

The staff agrees with PG&E that both this portion of the Hosgri fault zone and the southern reach are undergoing strain partitioning. Oblique-slip below the seismogenic crust is being manifested as strike-slip displacement along the high-angle strands of the Hosgri and as thrust displacement along thrust faults and folds within the Queenie, Lompoc, and Purisima structures west of the Hosgri. Thrust components of strain partitioning may also be occurring east of the Hosgri within the Casmalia block. In addition to strain partitioning associated with the Hosgri fault zone, the region is further complicated by northward rotation of the Transverse Ranges (Brand, 1988; Luyendyk and others, 1980) and north-south compression within that region.

° Southern Reach of the Hosgri Fault Zone

The southern reach of the Hosgri extends for 24 to 26 km from just south of the Lions Head fault to about 4 km northwest of Pedernales Point where it splays into short en-echelon traces and dies out. The northern part of the southern reach, which lies about 5.5 km west of Purisima Point, strikes N 20° W. It is not continuous with the Point Sal Reach, but lies 1/2 to 2 km west of and en-echelon with it. About halfway between Purisima and Pedernales Points, the trend changes strike to N 5° W. The Hosgri fault zone in this reach forms the western flank of a series of gravity lows that parallel the coast between the Santa Maria and Santa Ynez Rivers. Those gravity signatures are similar to those that characterize the thick sediments within the offshore Santa Maria Basin.

Gravity, magnetic, and seismic reflection data indicate that basement is high west of the Hosgri fault zone within this reach.

The Hosgri fault in this area is characterized by two high-angle strands, but neither is sufficiently well defined to be considered the eastern boundary of the offshore Santa Maria Basin. The Hosgri fault zone, however, still forms the boundary between east-west striking folds and faults to the east and northwest-southeast striking features (parallel to the Hosgri) to the west. South of Point Arguello, east-west to northwest-southeast trending structures appear to cut across any southern projection of the Hosgri fault zone, thus supporting its termination or mergence with Transverse Range structures in that area. The precise termination is not defined, but it is near the intersection of the Honda fault.

° 1989 Loma Prieta Earthquake Findings and Impact on the Hosgri Fault Analysis

Several issues arose in the LTSP review following the magnitude 7.1 earthquake on October 17, 1989, at Loma Prieta, California. Those issues were:

- Does the lack of tectonic surface rupture associated with this earthquake invalidate trenching investigations such as those carried out by PG&E along the southern reach of the San Simeon fault?

- What is the relevance of observations away from the rupture segment in determining sense of displacement such as strike-slip versus oblique-slip?

- What is the relevance of surface observations in predicting subsurface geometry?

- Would it have been possible to have anticipated the location, style, and size of the earthquake based on paleoseismic investigations several tens of kilometers from the epicenter?

- Did strain partitioning play a part in this event?

- Did segmentation play an important part in this earthquake and what does that indicate regarding segmentation of the Hosgri fault?

- What was the depth, extent, and magnitude of the earthquake?

In May 1990, PG&E addressed these issues and presented its responses to the staff. At that time, PG&E and the staff conducted field reconnaissance in the region of this earthquake. On the basis of these responses, published reports on the earthquake, and the field trip, the staff concludes that:

- The Loma Prieta earthquake occurred on or near the San Andreas fault about 10 miles east-northeast of the city of Santa Cruz with rupture at depths of 5 to 18 km and had a rupture length of 39 km and a magnitude of 7.1. The rupture did not propagate to the surface.

- In spite of the lack of surface rupture, other historical and paleoseismic indicators (such as sag pond strata and liquefaction over a broad zone of deformation, vertical deformation and many other features) can provide information on timing, recurrence intervals, and estimates of the levels of ground motions experienced. However, other important information, such as amount of offset per event, cannot be estimated without surface rupture.

- Observations made in a trench 65 km north of the epicenter indicated pure strike-slip displacement on the San Andreas fault. However, the focal mechanism of the earthquake as calculated from seismograms was oblique-slip. This raised questions about the validity of concluding that the Hosgri maximum earthquake would be generated by displacement on a strike-slip fault based on observations in trenches across the San Simeon fault. PG&E found that the presence of a restraining bend at an angle greater than 10° on the San Andreas fault should have been a clue that oblique-slip was possible along that segment, even though displacement on segments to the north and south were strike-slip. The staff concludes that, in part, because of the oblique sense of displacement during the Loma Prieta earthquake, consideration should be given to the possibility of a similar offset on the Hosgri.

- There is a lack of surface rupture directly related to the seismogenic fault, but there are indications of potential oblique-slip on relatively high-angle faults (a double restraining bend greater than 10°, an interplay with the Sargent fault, and evidence for partitioning of strain). Such evidence is present in the Piedras Blancas region at the north end of the Hosgri fault and in the Purisima, Lompoc, and Queenie structures near the southern part of the Hosgri fault. On the basis of this information and other data, a significant component of reverse motion which would result in oblique displacement should be considered likely on the Hosgri fault zone.

- Observations at the surface, such as the presence, locations, and interrelationships of double restraining bends, intersecting faults, paleoseismic evidence, and seismic gaps, make it possible to estimate, to some extent, the location, size, and style of the potential earthquake.

- Strain partitioning could have played a part in this earthquake; for example, oblique slip at depth could have been converted to reverse displacement (vertical component) on the Sargent fault or some other as yet unnamed fault and strike-slip displacement (horizontal component) on the San Andreas fault.

- Segmentation, both vertical and horizontal, appears to have constrained this earthquake. This could also occur on the Hosgri fault zone.

Evaluation and Conclusions--Hosgri Fault Zone

(1) Fault Length--Hosgri Fault Zone

The UNR (Appendix D of this SSER) found that the SGH fault system extends from Bolinas, where it intersects the San Andreas fault, to the south at least to Point Pedernales (410 km). It could extend to the Santa Barbara Channel (Appendix D of this SSER), which would make it 450 km long. The UNR favored a total length of the SGH fault system of 410 km because recent geodetic work (Feigl and others, 1990) indicated that a geodetic station near Point Arguello may be located on the Pacific plate, which suggests that the Hosgri fault zone does not extend to that area.

The USGS (Appendix C of this SSER) concluded that the 2-km to 4-km wide, relatively high-angle fault zone (referred to by PG&E as the Hosgri fault zone) that offsets material within the upper 1/2-km depth to the sea floor extends from off the Cambria coast to Point Pedernales (approximately 110 km). However, the USGS concluded that this fault zone is part of a larger fold and thrust belt that is up to 12-km wide.

The staff concludes that the Hosgri fault zone is the 110-km long southern part of the 410-km long SGH fault system. Over its entire length, the Hosgri is the eastern boundary of the offshore Santa Maria Basin. It is also a tectonic boundary between two major compressional stress systems. That is, it separates the stress regime to the east, which has a maximum compression oriented in a northeast-southwest direction, from the stress regime to the west, which has a maximum compression oriented in an east-west direction. Strain is currently being transferred between the Hosgri fault zone and another member of the SGH fault system, the San Simeon fault, by means of the Cambria stepover, a 5-km wide by 10-km long Quaternary pull-apart basin.

(2) Focal Mechanisms--Hosgri Fault Zone

In general, the San Simeon fault is characterized by diffuse seismicity. To the south, microearthquakes are aligned along the Hosgri fault, and seismicity clusters occur at the Hosgri-Los Osos and Hosgri-Casmalia intersections and at the southern end of the Hosgri off shore of Point Arguello. Focal mechanisms along the SGH fault zone are both strike-slip and reverse. The mechanisms on the Hosgri generally change from strike-slip to reverse-oblique-slip from north to south. There is little or no seismicity west of the Hosgri fault in the zone where the low-angle thrust faults have been mapped, except in the vicinity of the Piedras Blancas anticlinorium to the north and the Queenie, Purisima, and Lompoc structures to the south; focal mechanisms in these areas are predominantly thrust. These observations suggest that there is agreement between focal mechanisms and the geological structures.

The hypocenters of the 1980, magnitude 5.1, Point Sal earthquake and its aftershock sequence were at depths of 8 to 10 km, had reverse focal mechanisms, and had strike and dip consistent with the Casmalia fault. These characteristics of the Point Sal earthquake indicate that the Casmalia fault is in the hanging wall (the east side) of the Hosgri. These hypocentral locations support the premise that the Hosgri is a high-angle fault and are not consistent with a low-angle, thrust fault. If the Hosgri dips to the northeast at

60° or less, it would cut off the Casmalia fault above the earthquake hypocenter. Additionally, recent microearthquakes recorded by PG&E near the Hosgri fault zone have pure strike-slip mechanisms to depths as great as 7 km, well within the seismogenic zone.

(3) Fault Geometry--Hosgri Fault Zone

The downdip geometry of the Hosgri fault zone below a depth of 1 to 2 km is not well constrained because of the poor resolution of the seismic reflection data. However, on the basis of the weight of the geological, seismological, and geophysical data, the staff concludes that the Hosgri fault at depth dips between 60° and 90° over most of its length through the seismogenic zone. This conclusion is based on:

- The nature of the Hosgri as a major crustal strain boundary, as indicated by the nature of late Tertiary and Quaternary tectonic structures and seismicity on both sides of the fault zone.

- Focal mechanisms and depths of earthquakes occurring on the Hosgri fault and those of the 1980 Point Sal earthquakes described above which constrain the dip of the Hosgri at 8 to 10-km depth.

- Seismic reflection data which indicate that the most recently active components of the Hosgri fault zone are high-angle faults within the upper 2 km.

(4) Sense of Slip--Hosgri Fault Zone

The preponderance of the geological and seismological data leads the staff to conclude that the Hosgri fault zone is experiencing predominantly right-lateral, strike-slip displacement with a subordinate, though substantial, component of reverse displacement. The staff concludes that the following evidence supports the dominance of strike-slip offset on the Hosgri:

- The linearity of the Hosgri fault zone and its tectonic relationship and approximate alignment with the San Gregorio and San Simeon faults, which are well documented, strike-slip faults (Weber and Lajoie, 1979; Weber, 1983; Brand, 1988).

- The observation that, although basement and Tertiary rocks are generally upthrown on the northeast side of the fault, several seismic reflection lines, such as PG&E-3, GSI-112c, GSI-115, and possibly GSI-118 and CSLC-D-29, indicate that these rocks are downdropped on the northeast side. This apparent variation from side to side of the fault of upthrown and downdropped strata is a relatively common characteristic of strike-slip faults.

- The late Quaternary horizontal slip, based on paleoseismic investigations conducted by PG&E along the San Simeon fault, is greater than late Quaternary vertical displacement on the Hosgri fault.

- The focal mechanisms of microearthquakes occurring at depths of up to 7 km and aligning with the Hosgri fault zone are predominantly strike-slip, with some oblique-slip mechanisms.

- Paleoseismic studies along the San Simeon fault, which the staff considers to be an onshore analogue to the Hosgri fault, identified horizontally offset geomorphic features and subhorizontally oriented slickensides, which are characteristic of strike-slip faults.

- The existence of a large strike-slip component is required on the Hosgri fault zone because the San Simeon fault terminates north of Estero Bay and it is highly unlikely that its considerable strike-slip dies out in that reach. Instead, that right-slip is transferred to the Hosgri fault across the Cambria pull-apart basin. This is a means of transferring horizontal motion from one fault to another that characterizes most large strike-slip faults worldwide.

- The concept of strain partitioning as described above appears to best explain the complex array (in plan and in section) of faults and folds associated with the Hosgri fault zone. This concept requires the presence of subparallel strike-slip and reverse-slip faults and is consistent with strike-slip displacement on the Hosgri fault. The staff agrees with PG&E (response to Question GSG-2) that oblique-slip at depth is being partitioned into horizontal and vertical components at shallower depths. The horizontal component is expressed as right-lateral, strike-slip displacement on the southern San Simeon fault and the extreme northern end of the Hosgri fault. The vertical component is expressed as compressional faulting and folding within the Piedras Blancas anticlinorium. A shortening due to the Santa Lucia Banks fold and thrust belt may also be influencing this region. A similar condition is occurring within the San Luis Bay, Point Sal, and southern reaches of the Hosgri fault zone, where the horizontal component of oblique-slip displacement below the seismogenic zone is being translated to right-lateral slip along the Hosgri fault zone and the vertical component is being manifested by compressional deformation (thrust faulting and folding) within the Queenie, Purisima, and Lompoc structures west of the Hosgri fault zone and possibly the Casmalia-Orcutt structure east of the Hosgri fault zone. The tectonics of this region is further complicated by the north-south compression and possible clockwise rotation of the Transverse Range structural block. The northern reach of the Hosgri fault zone opposite Cambria and northern Estero Bay exhibits no evidence of the compressional folding and thrust faulting that is seen to its immediate west (seismic reflection lines W-500, W-16A and J-113). Farther south and continuing on to the first indications of the Purisima and Lompoc structures, folds and thrust faults are present west of the Hosgri but they apparently do not deform the mid-Pliocene unconformity. Additional evidence for strike-slip displacement through these reaches is presented in the LTSP Final Report and also supports the staff's conclusion.

- Seismic reflection profiles taken across the offshore San Gregorio fault zone, a well documented strike-slip fault, indicate features very similar to those observed in profiles across the Hosgri, including associated compressional features such as low-angle thrust faults, folds, and flower structures.

- The analysis of the 1980 Point Sal earthquakes leads to the conclusion that the Hosgri fault dips at a high angle at depths of 8 to 10 km, which supports the strike-slip nature of the Hosgri fault in that region.

(5) Slip Rate--Hosgri Fault Zone

PG&E concluded, on the basis of its investigations of the onshore part of the San Simeon fault, that right-lateral, strike-slip displacement is occurring along the Hosgri fault at the rate of 1 to 3 mm per year. PG&E analyzed the rate of uplift east of the Hosgri fault zone and concluded that vertical slip is occurring at the rate of 0.1 to 0.44 mm/yr. The staff agrees with this rate of vertical slip.

The UNR concluded (Appendix D of this SSER) that the predominant sense of slip on the Hosgri fault zone is right-lateral strike-slip with a significant but subordinate reverse-slip component. The UNR further concluded, and the staff agrees, that right-lateral strike-slip is occurring at a rate of 2 to 3 mm/yr.

The USGS concluded (Appendix C of this SSER) that strike-slip displacement of 1 to 3 mm/yr measured by PG&E in trenches across the San Simeon fault several kilometers north of Point San Simeon is likely transferred to the Hosgri fault zone. However, there is evidence for greater vertical offset than is acknowledged by PG&E. That evidence consists of stratigraphic correlations across the fault such as the juxtaposition of Franciscan bedrock to the northeast against Neogene rocks to the southwest, the youngest of which is the upper Pliocene Carreaga formation. This evidence extends from Point San Simeon for a distance of 37 km to the southeast. Farther to the south there are elevation differences between basement across the Hosgri fault zone ranging from 1 to 2 km. There is also evidence of more recent or ongoing uplift in the form of thicker Quaternary deposits west of the Hosgri fault zone and the sparsity or absence of these deposits east of the Hosgri fault zone.

PG&E's estimate of ongoing vertical slip is based to a large extent on the apparent lack of deformation of a horizon that is interpreted to be the middle Pliocene unconformity. The age of this unconformity is estimated by comparing seismic velocities of the soils overlying it with similar velocities in soils of demonstrated age in the Point Arguello oil field many tens of kilometers to the south. Therefore, the age of these soils in this part of the Santa Maria Basin is in doubt and could be less than estimated by PG&E.

Because of uncertainties in the ratio of horizontal to vertical slip, the staff has conservatively assumed for purposes of ground motion analysis (see Section 2.5.2 of this SSER) that displacement on the Hosgri fault zone is predominantly strike-slip with a substantial component of reverse-slip.

(6) Segmentation and Rupture Lengths--Hosgri Fault Zone

The staff considers the Hosgri fault zone to be segmented, but not precisely as proposed by PG&E. The staff considers the Cambria pull-apart basin, the intersections of the Los Osos fault and the Casmalia fault with the Hosgri, and the southern termination of the Hosgri fault zone to be valid points of fault segmentation. The intersections of the Pecho and Lions Head faults are not considered to be strong segmentation points. Therefore, in calculating earth-

quake magnitude on the basis of the rupture length, the greatest weight should be given to a length of 45 km to 50 km, which is the approximate distance from the Los Osos fault intersection to the Casmalia fault intersection. Slightly less weight should be given to a 20-km rupture. Recognizing that larger earthquakes often rupture through relatively strong segmentation features, some weight should be given to a 70-km rupture. The highest weight rupture length (45 to 50 km) is similar to that which has occurred historically on the Imperial fault during the magnitude 7.1 El Centro earthquake that occurred in 1940. The Imperial fault is a subsidiary fault of the San Andreas fault system analogous to the San Gregorio-Hosgri. The staff's preferred rupture lengths were used in the UNR analysis (see Appendix D of this SSER).

2.5.1.2.5 San Luis-Pismo Structural Block

The San Luis-Pismo block, along with the Santa Maria Basin to the south, occupies a zone of transition between the Coast Ranges represented by the Santa Lucia Mountains to the northeast and the Transverse Ranges represented by the Santa Ynez Mountains to the south. The Hosgri fault zone is the western boundary of the block. The internal structure of the San Luis-Pismo-Santa Maria region is dominated by west-northwest-trending antiformal and synformal folds. A series of west-northwest-striking, northeast-dipping, reverse or thrust faults forming a zone of deformation 3 to 4-km wide separates the San Luis-Pismo block from the Santa Maria block. This zone is called the Southwest Boundary Zone and is described below.

The San Luis-Pismo block derives its name from the late Tertiary Pismo syncline which forms the core of the San Luis Mountains (or Irish Hills). On the basis of studies of the fluvial terraces along antecedent streams crossing the San Luis-Pismo block and marine terraces around it, the Pismo syncline is no longer deforming internally (Killeen and others, 1987; Brand, 1988). It is instead being uplifted as a rigid block at the rate of 0.10 to 0.20 mm/yr or an average rate of 0.14 to 0.16 mm/yr along N 60°-70° W striking reverse faults bounding it. The northeast margin is the southwest-dipping Los Osos fault. On the basis of paleoseismic studies done by PG&E, the Irish Hills segment of this fault has undergone multiple late Quaternary displacements at a slip rate of 0.2 to 0.4 mm/yr of pure reverse displacement.

The southwest boundary of the San Luis-Pismo block, as stated above, is a 3 to 4-km wide zone of west-northwest-striking, northeast-dipping, reverse faults, including the San Luis Bay, Olson, Wilmar Avenue, Pecho and Oceano faults. These faults will be described in this section of the SSER. Because there is no folding or tilting of the San Luis-Pismo block, the late Quaternary slip rate distributed among these faults is equal to that on the Los Osos fault.

Faults within the San Luis-Pismo block, such as the San Miguelito and Edna faults, were investigated in detail by PG&E and found to be noncapable in the meaning of Appendix A to 10 CFR Part 100. These results, along with the mapping by the UNR of fluvial terraces along antecedent streams that crossed the block (Killeen and others, 1987) demonstrated the absence of late Quaternary near-surface deformation within the San Luis-Pismo block.

Studies by the UNR (Appendix D to this SSER) showed that northeast-southwest directed, maximum horizontal-compressive stress (1) has characterized this

region for several million years, (2) is consistent with the most recent style of deformation on mapped tectonic structures, and (3) still characterizes the current stress regime as indicated by earthquake fault plane solutions.

(1) Los Osos Fault

The Los Osos fault is the northeast boundary of the San Luis-Pismo structural block. It is a southwest-dipping, reverse fault expressed at the surface by a series of discontinuous fault scarps, closed depressions, lines of springs, tonal lineaments, and deflected drainages along the southwest side of the Los Osos Valley. The scarps are younger than 10,000 years, thus demonstrating that the Los Osos fault is a capable fault. The Los Osos fault intersects the Hosgri fault to the northwest in the mouth of Estero Bay and probably merges with the West Huasna fault at the front of the Santa Lucia Mountains to the southeast.

The Los Osos fault is a 57-km long, southwest-dipping zone of subparallel and en-echelon faults that is up to 2-km wide and is 10 km from the Diablo Canyon site at its closest approach. It is a pure dip-slip feature as demonstrated by the orientation of slickensides within the fault and supported by its orientation with respect to the N 32° E direction of principal horizontal compression (Appendix D to this SSER). UNR researchers first identified the capability of the Los Osos fault and PG&E later conducted a detailed investigation of it, consisting of trenching and logging, geological mapping, geomorphic studies, soil studies, age dating, borings, and mapping of marine and fluvial terraces.

Primarily on the basis of topography, PG&E divided the Los Osos fault zone into four segments: Estero Bay--13-km long, Irish Hills--19-km long, Lopez Reservoir--17-km long, and Newsome Ridge--8-km long. The Irish Hills is the most active and best documented segment, supported by (1) subsidence of the Morro Bay area northeast of the fault, (2) accumulation of ponded alluvium behind the fault, (3) the elevation of a flight of marine terraces near Montano de Oro (which are continuous to the Los Osos fault where they are abruptly terminated and show an uplift rate of 0.22 to 0.24 mm/yr), (4) location of the fault relative to the Irish Hills range front, and (5) a difference of tectonic behavior and a 1 to 2-km right step between the Irish Hills and Lopez Reservoir segments. PG&E interpreted the Los Osos fault, like the San Miguelito fault, as originally being a high-angle, strike-slip fault, which is behaving as a reverse fault in the current compressional stress regime. At the surface, the fault dip measured in the Ingley trench is in the range of 9° to 29°. The fault dip increases at depth to between 30° and 60°. PG&E prefers the 60° dip based on analysis of the log of an oil exploratory well drilled in the northeast Irish Hills which PG&E interpreted to suggest that the Los Osos fault does not truncate the Pismo syncline above seismogenic depths. Deformation and apparent repeat of sections recorded in the well log could also be interpreted as related to a more-shallow-dipping Los Osos fault. The staff, however, accepts the steeper dip based on (1) the hypocentral location of a recent earthquake beneath Point San Luis, which would fall on a 60° dipping Los Osos fault, (2) the similarity of a steeper-dipping fault with other known relatively high-angle reverse faults such as the Casmalia fault (based on the depth of the 1980 Point Sal earthquake) and the San Luis Bay fault, and (3) the

presence in the area of inactive, high-angle, strike-slip faults, such as the San Miguelito fault, which document the existence of an earlier transcurrent stress regime.

In its logic tree analysis (see Section 2.5.2.2 of this SSER), PG&E assumed rupture segment lengths of 19 and 36 km (with 19 km being preferred), a maximum displacement per event of 2.1 m, and a slip rate of 0.25 to 0.8 mm/yr, and calculated a mean maximum earthquake magnitude of 6.8. The staff agrees with PG&E that the slip rate, though not well constrained, the 19-km segment length, and the 60° dip are reasonable, and the PG&E value of about 2-m maximum displacement per event is conservative.

(2) Southwest Boundary Zone

The Southwest Boundary Zone is a diffuse zone of discontinuous, en-echelon, northeast-dipping, reverse faults that is generally 3 to 4-km but up to 8-km wide. Individual faults in this zone are the San Luis Bay, Olson, Wilmar Avenue, Pecho, and Oceano. Collectively, they truncate and elevate the San Luis-Pismo block and separate it from the subsiding Santa Maria Valley block. The San Luis Bay, Olson, and Wilmar Avenue faults have been demonstrated to be capable faults and the Pecho and Oceano faults are also assumed to be capable. A low slip rate is indicated by the degree to which the range front (San Luis Mountains or Irish Hills) has been backwasted to the east away from the faults. A study of the marine terraces by PG&E and the UNR indicates stepdowns in shoreline angle elevations and associated uplift that translate to a late Quaternary uplift rate of 0.2 mm/yr on the Irish Hills section of the San Luis-Pismo block and no uplift of the Santa Maria Valley block.

PG&E interpreted the distances between the faults (2 to 5 km), the mapped traces of the faults, the observed maximum dips of the onshore faults, and the broad distribution of smaller earthquakes with reverse mechanisms which indicate the style of deformation, to indicate that the faults do not merge or intersect above the seismogenic zone (i.e., above a depth of 5 km) nor above depths of 7 to 8 km. On the basis of that interpretation, PG&E characterized each fault individually, segmenting each fault to estimate maximum potential earthquakes.

The UNR (Appendix D of this SSER) presented an alternative model that suggests that the Olson and San Luis Bay faults and the possible extension of the Wilmar Avenue fault should also be considered as an integrated earthquake source. This idea is based on the relatively uniform uplift of the San Luis-Pismo structural block with little or no tilting or internal deformation. Deformation beneath the seismogenic zone may be resulting in a mirror-image effect with the northeast boundary (Los Osos fault). This fault zone is considered to be segmented by subblocks (see Figure 2.3) similar to the segmentation of the Los Osos fault (i.e., Irish Hills, Lopez Reservoir (Edna), and Newsome Ridge subblocks). This source zone is considered to be about 1 to 2-km wide and about 13-km long across the strike of the Irish Hills subblock and is accommodating approximately 2/3 of the total deformation of the Southwest Boundary Zone. The Pecho fault is considered by the UNR to be a separate source.

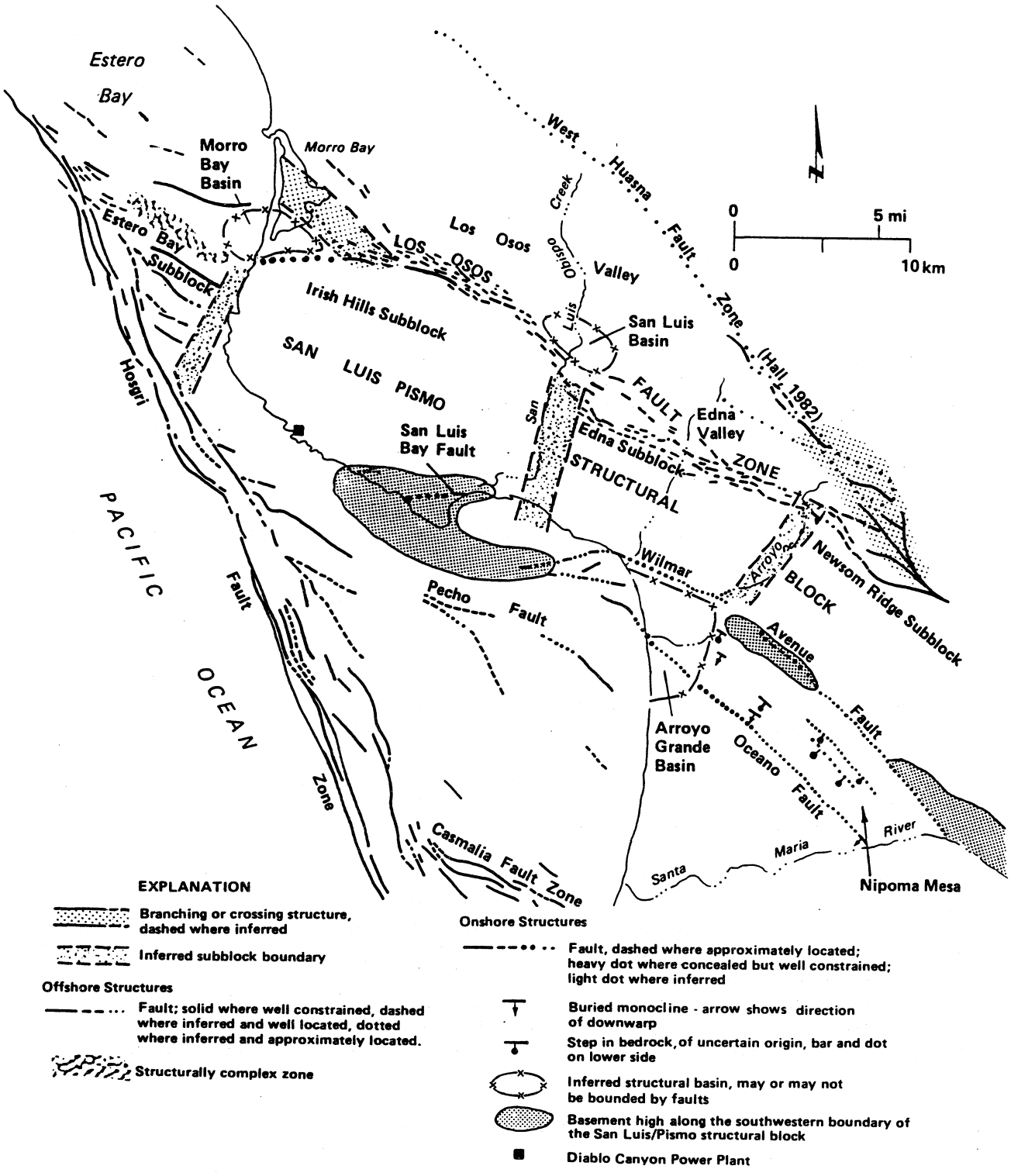


Figure 2.3
Structural elements associated with the San Luis-Pismo structural block
(Figure 2-15 in LTSP Final Report)

In responses SSC-5 and GSG-16 to NRC questions, PG&E presented geological, paleoseismic, and geophysical evidence to support the absence of direct connections between faults of the Southwest Boundary Zone. On the basis of this evidence, the staff concludes that the faults that make up the zone should be considered individual seismic sources. This conclusion is based primarily on evidence that indicates the faults of the Southwest Boundary Zone have undergone relatively uniform and independent displacement during the late Quaternary period. However, the possibility that the Olson and San Luis Bay faults may become a single fault at depth or that both faults may rupture during a single event cannot be ruled out. The following are descriptions of each fault within the Southwest Boundary Zone.

(a) San Luis Bay Fault. The San Luis Bay fault is a capable fault exposed at Avila Beach. The most convincing geological evidence for the presence of a fault is found along the segment between Avila Beach and the coastline west of Rattlesnake Canyon. This is the basis for PG&E's preferred rupture length of 6 km. At Avila Beach, the fault offsets the 5e (120,000-year-old) marine terrace 4 to 8 m vertically. It strikes west-northwest and has a dip, measured within the outcrop, in the range of 15° to 46° to the northeast. PG&E estimated its slip rate to be 0.02 to 0.12 mm/yr. The shallower dips occur in the upper part of the exposure and become progressively steeper with depth (thrust fault to reverse fault). The fault is mapped to the northwest through the topographic saddle between San Luis Hill and the Irish Hills, and across the coastline near Rattlesnake Canyon. Although the fault is not exposed at Rattlesnake Canyon, there is a 5 to 8-m stepdown of the 5e marine terrace. On the basis of observations by divers, sea floor samples, bathymetric data, and seismic reflection lines, PG&E mapped the offshore extension of the San Luis Bay fault as taking a more westwardly trend for at least 1 km (expressed as discordance of bedding) based on its coincidence with a stratigraphic onlap. This westernmost mapped extent is about 5 km from the site. Seismic reflection data allow for, but don't require, projection farther west to a fault adjacent to the Hosgri fault zone. The San Luis Bay fault extends from Avila Beach southeastward into San Luis Bay, and, according to PG&E, either dies out or is truncated by the east-west striking Avila fault.

The UNR (Appendix D of this SSER) inferred, on the basis of continuity of deformation, that the San Luis Bay fault is connected at depth to the Olson fault. Because of these possibilities, the UNR suggested that a longer rupture segment (13 km) should be used in determining the maximum magnitude for the San Luis Bay (and Olson) fault. Furthermore, the USGS suggested that (1) the San Luis Bay and other faults of the Southwest Boundary Zone may extend further offshore than currently mapped, and (2) the Southwest Boundary Zone may converge with a larger trend of faults, thus increasing its seismic potential.

(b) Olson Fault. Hall and others (1979) mapped a thrust fault where the Franciscan melange contacts the Cretaceous sandstone at the coastline, approximately 6.4 km northwest of Point San Luis. PG&E (Brand, 1988) identified down-to-the-south steps in the 5a (80,000-year-old) and 5e (120,000-year-old) wave-cut marine platforms that translate into a slip rate of about 0.02-0.06 mm/yr. Extension of this fault to the east is difficult because erosion and deposition has occurred faster than the relatively slow rate of slip along the Olson fault. Investigations by PG&E along Deer Canyon and Irish Canyon, which cut across an eastward projection of the Olson fault along the coast, allowed for possible

extensions of the Olson fault, a more northerly trace that would merge with the San Miguelito fault, and a more southerly trace that trends toward the San Luis Bay fault. In the latter case, PG&E contended that the Olson fault dies out before reaching the San Luis Bay fault, based on calculated uplift rates from marine terrace elevations east of Rattlesnake Canyon.

PG&E investigated the offshore extension of the Olson fault by diver observation, sea-floor sampling, mapping sea-floor topography, and interpreting seismic reflection data. Like the onshore extension, the low slip rate is outstripped by erosion of the sea floor. The fault was traced westward for 2 km off shore as a discordant contact between the Franciscan melange and the Squire Member, and for part of that distance as a south-facing scarp on the sea floor, which is interpreted as a fault-line scarp. The offshore mapped extent is approximately 3 km from the site. Folds and northeast-dipping thrust faults in Miocene rocks near the eastern trace of the Hosgri fault zone 7 and 8 km west and northwest of Olson Hill could be interpreted to be seaward extensions of the Olson fault. Poor resolution of reflection data, because of shallow water and the steeply dipping strata just below the sea floor, do not permit for definition of the fault in that area.

On the basis of its investigations and analyses, PG&E used rupture lengths of 2, 5, and 8 km and rupture widths of 8 and 12 km to estimate the earthquake hazard of the Olson fault.

(c) Wilmar Avenue Fault. During its independent investigations (Nitchman and Slemmons, 1987), the UNR identified a capable subsidiary fault of the Wilmar Avenue fault zone exposed in the sea cliff near Wilmar Avenue at Pismo Beach. It is also exposed for 2 km along strike to the southeast in the "Farmboy" quarry. Vertical offsets at these sites range from 4.0 to 6.4 m down to the southwest (reverse slip) as determined by displacement of the 5e terrace (120,000 years old). These offsets translate into a slip rate that ranges from 0.03 to 0.07 mm/yr. The fault is mapped as about 30-km long from its offshore reach in San Luis Bay to the Santa Maria River. The Wilmar Avenue fault strikes predominantly northwest-southeast with minor trend changes ranging from east-west to N 64° W and dips 45° to 60° northeast. Surface expression of the fault is poor because of its low slip rate and because it has been obscured by cultural development (i.e., road and housing construction). However, it can be traced to Arroyo Grande by terrace mapping and well logs along the northeast margin of the Nipomo mesa to the northern Santa Maria Valley.

PG&E divided the 30-km-long fault into four segments: the Birdrock segment which extends off shore from the Pismo Beach outcrop for 5.2 km along a west-southwest strike and dies out in San Luis Bay; the Pismo Beach segment, which extends from its sea cliff exposure through the Farmboy quarry 2.3 km to the east-southeast to Arroyo Grande for a distance of 7 km; the Picacho segment, 7.5-km long; and the Nipomo segment, 10-km long.

The segments of the Wilmar Avenue fault proposed by PG&E were not well supported by behavioral or geometric evidence. The UNR (Appendix D of this SSER) concluded that faults of the Southwest Boundary Zone should be segmented like the Los Osos fault, which bounds the northeast margin of the San Luis-Pismo structural block. The UNR further proposed that the fault is segmented by subblocks of the San Luis-Pismo block. The San Luis Bay fault

bounds the Irish Hills subblock to the southwest. The UNR suggested that the San Luis Bay and Wilmar Avenue faults are segmented at the boundary between the Irish Hills and Lopez Reservoir subblocks. As the Wilmar Avenue fault forms the boundary of the Lopez Reservoir (Edna) subblock and the Newsome Ridge subblock, segmentation of the Wilmar Avenue fault at the boundary between the Lopez Reservoir and Newsome Ridge subblocks was also suggested. An important observation, however, is that marine terraces on both sides of the Wilmar Avenue fault have been uplifted, indicating that this fault is not the primary fault separating the San Luis-Pismo block from the Santa Maria Basin. The highest slip rates estimated along the Wilmar Avenue fault by PG&E were 0.04 to 0.08 mm/yr on the Pismo Beach segment. The staff concludes that these are reasonable estimates based on the ages of offset marine terraces, amounts of displacements, and dips of the fault.

(d) Oceano Fault. The Oceano fault extends east-southeast from about 3.3 km off shore in San Luis Obispo Bay across the coastline west of the town of Oceano on a strike of N 45° to 50° W, across the Nipomo mesa to the Santa Maria River for a total minimum length of about 15 km. The fault probably connects with the Santa Maria River fault (Hall, 1982) at its southeastern extremity. The Oceano fault is poorly expressed at the surface due to its low slip rate, extensive erosion, and burial beneath dune sand and alluvium. The fault trace lies near the base of a flight of marine terraces indicating that vertical displacement along it is contributing to uplift of the San Luis-Pismo structural block and/or subsidence of the Santa Maria block.

The Oceano fault, identified during the LTSP by onshore and offshore seismic reflection data, coincides or projects to faults on shore previously mapped by the California Department of Water Resources, and to faults off shore that can be seen in geophysical data about 1.8 km from the coastline. Offshore geophysical data suggest displacement of probable Pleistocene sediment overlying a probable Pliocene unconformity. The 18,000-year Wisconsinan unconformity is not offset, however. Slip rates calculated by PG&E are 0.01 and 0.03 mm/yr in San Luis Obispo Bay, 0.01 and 0.05 mm/yr near the coastline, and 0.04 and 0.13 mm/yr in the center of the Nipomo mesa. The staff has reviewed the bases for these offsets and concludes that they are reasonable.

(e) Pecho Fault. The Pecho fault probably merges with the Hosgri fault zone a little north of the latitude of Point San Luis, due west of where Pecho Creek crosses the coastline and about 4 km south of the Diablo Canyon site. It is the southwesternmost fault of the Southwest Boundary Zone. The Pecho fault trends southeast as a discontinuous line of southwest facing sea floor scarps for about 5 km. Along this trend, south of Point San Luis and beyond a 4.5-km gap, the fault is expressed as two branches, a northern trace and a southern trace. Both branches die out in San Luis Obispo Bay. The total length of the fault, including the gap and northern trace is 22 km; the total length, including the southern trace, is 19 km. It is characterized by PG&E as a high-angle, reverse, northeast-dipping, northeast-side-up fault.

Seventeen meters of vertical offset of early Pleistocene sedimentary rocks is indicated in seismic reflection data near the southeast end of the northern trace of Pecho fault. Near its junction with the southern trace, the late Wisconsinan unconformity (18,000 years old) has been uplifted 6 m on the northeast side. These displacements translate to a slip rate of 0.01 to 0.02 mm/yr.

PG&E inferred that the intersection between the Hosgri and Pecho faults is a segmentation point. However, the staff concludes that because of its relatively subdued geomorphic expression and low slip rate, the Pecho fault is not a primary structure within the Southwest Boundary Zone, and therefore, not a valid segmentation point. This lengthens the potential segment to about 40 km.

(f) Undetected Coast-Parallel Fault. The UNR raised an issue concerning the possible presence of an unknown fault immediately adjacent to the coastline. This issue is based on the deficit in slip between the northeast boundary (Los Osos fault zone) of the San Luis-Pismo structural block (which is untilted and lacks internal Quaternary definition, based on the mapping of fluvial terraces along San Luis Obispo Creek and marine terraces from Montano de Oro to Mallagh Landing by PG&E and the UNR) and the Southwest Boundary Zone. It is also based on the linear nature of the coastline in this area and the presence of lineaments and escarpments that parallel the coast.

At meetings and in its response to NRC Questions 43e and GSG-16, PG&E presented evidence supporting its conclusion that there is no undetected fault paralleling the coast in the zone from the shore out to a distance of 1 to 2 km, where shallow water precludes obtaining seismic reflection profiles. This evidence consisted of seismic reflection data that covered the area off shore of the shallow water zone, and seismic reflection lines CM-21 and CM-23, which would cross any projection of a coast-parallel fault to the north into Estero Bay. Additionally, the offshore investigation of a possible seaward extension of the Olson fault indicated that the fault extended at least 2 km off shore and would cut across a coast-parallel fault. No evidence for a coast-parallel fault was found in these data. However, recognizing the difficulties of identifying faults in shallow water in an acoustic basement characterized by steeply dipping structure, as is found in this area, PG&E relied heavily on other lines of evidence, mainly bathymetric data in the near shore from Morro Bay to Point San Luis. The prominent escarpment that can be traced from Point Buchon to Deer Creek was interpreted to be a series of closely spaced shoreline features formed during a previous low-sea-level condition. Although the general trend of this series of escarpments appeared to cut obliquely across bathymetric contours, each individual slope break is subparallel to the contours and is sinuous and irregular, indicating that the breaks in slope are not tectonically controlled. Similar features (i.e., escarpments or breaks in slope) in the bathymetry wrap around Point Buchon and are also observed in the vicinity of Point San Luis, further indicating that they are related to stillstands of sea level and not tectonics. The linear, narrow, inner-shelf zone and shoreline from Point Buchon to Deer Creek is underlain by highly resistant Obispo volcanic rocks and Monterey rocks, whereas the areas to the north and northeast and south are underlain by less-resistant rocks. Therefore, the coastline and the sea-floor features are bedrock-controlled and were to some extent shaped by wave directions during storms.

Terrace mapping on shore shows that the coastline straightness is temporary, recent, and has not been in existence throughout the Quaternary period. Because of the more-resistant bedrock between Deer Creek and Point Buchon, the terraces are narrow in this area and fan out to become wider both north and south of this stretch of the coast. PG&E also stated that the rock comprising sea stacks, which lie as much as 1 km off shore, can be correlated to similar

rocks on shore. Although the slip deficit across the San Luis-Pismo structural block is unresolved, the staff concludes that the evidence provided by PG&E supports the absence of a coast-parallel fault, although the presence of such a fault cannot be completely ruled out. The slip deficit, although unresolved, could be explained by additional undetected slip on the faults of the Southwest Boundary Zone, i.e., the Pecho fault, since the late Quaternary displacement of this fault is not well defined.

Evaluation and Conclusions - San Luis-Pismo Block

The San Luis-Pismo structural block extends from the Hosgri fault in Estero Bay east-southeast to the Santa Lucia-San Raphael Mountains. It is bounded on the northeast by the capable Los Osos fault, on the west by the Hosgri fault, and on the southwest by a zone of discontinuous, capable faults, collectively called the Southwest Boundary Zone. The block is being uniformly uplifted along these boundary faults at the rate of 0.10 to 0.20 mm/yr. No internal deformation has occurred during the late Quaternary period.

(1) Los Osos Fault

The Los Osos fault is approximately 57-km long from its intersection with the Hosgri fault to the northwest to its intersection with the West Huasna fault to the southeast. The Los Osos fault is a reverse fault that dips approximately 60° to the southwest. Its slip rate, although not well constrained, is 0.25 to 0.8 mm/yr.

The staff finds that PG&E's assessment of segmentation on the Los Osos fault is reasonable. That assessment resulted in the conclusion that the 19-km segment bounding the Irish Hills subblock could rupture during a single event with a maximum displacement of 2 m.

(2) Southwest Boundary Zone

The Southwest Boundary Zone is a northwest-trending diffuse zone of northeast-dipping reverse faults generally 3 to 4-km but up to 8-km wide. Along the Southwest Boundary Zone, the San Luis-Pismo structural block to the northeast is being uplifted and thrust over the Santa Maria Valley block to the southwest. Faults of this zone include the San Luis Bay, Olson, Wilmar Avenue, Pecho, and Oceano. Slip rates within this zone, although distributed among the member faults, are probably equivalent to that measured on the Los Osos fault. This characteristic leads the UNR to conclude that the Southwest Boundary Zone should also be considered as an integrated seismic source. The UNR further suggested that this fault is segmented along boundaries between subblocks of the San Luis-Pismo block, leading to a possible rupture length of about 13 km. The USGS suggested that the faults of the Southwest Boundary Zone, although representing a smaller seismic hazard than the Hosgri fault zone, could extend off shore or merge into a northwest-trending structure. The staff, based on the weight of the data, concludes that the faults of the Southwest Boundary Zone dip at a high angle (60° to 70°) to the northeast and are not likely to merge at depths above 7 or 8 km. However, recognizing the uncertainties and in the interest of conservatism, the staff accepts the recommendation of the UNR and concludes that a rupture length of 13 km should be used in determining the maximum earthquake on the nearest approach of the Southwest Boundary Zone. The

staff has evaluated the significance of this alternative hypothesis to the Diablo Canyon site in Section 2.5.2.2 of this SSER.

(a) San Luis Bay Fault. PG&E's consideration of rupture lengths of 6, 9, and 12 km and rupture widths of 8 and 12 km during single events on the San Luis Bay fault is reasonable based on surface geology and geomorphology for the model it proposes. The late Pleistocene slip rate is estimated to be 0.02 to 0.12 mm/yr with reverse sense of displacement.

(b) Olson Fault. The Olson fault, which is the closest active fault to the site, is considered not to be linked at the near surface with the San Luis Bay fault, but the two faults may merge within the seismogenic crust. PG&E's use of rupture lengths of 2, 5, and 8 km and rupture widths of 8 and 12 km is reasonable. The late Pleistocene slip rate is approximately 0.02 to 0.06 mm/yr of reverse slip.

(c) Wilmar Avenue Fault. The Wilmar Avenue fault appears not to connect with the San Luis Bay fault in the near surface beneath the sea floor. Even if the two faults coalesce at depth, the staff agrees with the UNR that because they approach one another at the southwest end of the Irish Hills subblock, they are likely segmented and should not be considered to rupture simultaneously. The highest reverse-slip rate is 0.04 to 0.08 mm/yr on the Pismo Beach segment.

(d) Pecho Fault. Although the Pecho fault is clearly identifiable in bathymetric and seismic reflection data, it is not regarded as a major contributor to current deformation within the Southwest Boundary Zone. The reverse slip rate is estimated to be on the order of 0.01 to 0.02 mm/yr.

(e) Oceano Fault. The Oceano fault is a capable fault which probably projects to a fault beneath the Santa Maria River and, therefore, is probably longer than is shown on Figure 2.3. However, it is farther from the Diablo Canyon site. Maximum reverse slip, which is measured at the central part of the Nipomo mesa segment, is 0.04 to 0.13 mm/yr.

(f) Unknown Coastal Fault. The presence of a fault within the offshore area near the coast between Point Buchon and Point San Luis is very unlikely based on seismic reflection, bathymetry, and diver reconnaissance investigations performed by PG&E.

2.5.2 Seismology

The seismology issues addressed during the LTSP were (1) the maximum credible earthquakes associated with the significant faults, including the Hosgri, Los Osos, and Southwest Boundary Zone fault zones, and (2) estimated ground motions at the Diablo Canyon site from maximum credible earthquakes on these sources. Further reanalysis of the 1927 Lompoc earthquake, the largest historical earthquake in the region, led to a revised surface-wave magnitude of 7.0. Although PG&E presented strong evidence that the Lompoc earthquake is not associated with the Hosgri fault zone, the staff assumes the 1927 earthquake occurred on a structure related to the Hosgri and an earthquake of similar magnitude can occur on the Hosgri fault zone. Both the deterministic and probabilistic studies confirmed the earlier conclusion reached during the operating license

(OL) review that the Hosgri fault zone is the most significant source of expected ground motion at the Diablo Canyon site. Updated ground-motion studies have reassessed the expected ground motion at the Diablo Canyon site from the maximum credible earthquake on the Hosgri fault zone. The worldwide database of strong ground-motion recordings was enlarged. Both empirical and numerical modeling approaches were used to estimate site-specific horizontal and vertical response spectra at the site.

The staff's seismology conclusions are:

(1) The maximum earthquake associated with the Hosgri fault zone is a magnitude 7.2 event. A maximum earthquake of magnitude 7.2 on the Hosgri fault zone at an epicentral distance of 4.5 km to the Diablo Canyon site is the controlling earthquake for reevaluating the earthquake ground motions.

(2) For the Los Osos fault, a maximum earthquake of magnitude 6.8 is assumed to occur 10 km from the site.

(3) The maximum earthquake associated with the Southwest Boundary Zone faults is a magnitude 6 to 6-1/2 event.

(4) The PG&E LTSP 50th and 84th percentile horizontal spectra are appropriate for design evaluation above 1 Hz. Since the staff's weighted spectra derived from the Campbell (1990 and 1991b) spectra exceed the LTSP spectra at and below 1 Hz, higher ground motions should be considered at and below 1 Hz.

(5) The PG&E reanalysis of the vertical spectra and Campbell's (1990) spectra suggest exceedances of the LTSP 84th percentile spectrum between 1 and 10 Hz. Higher ground motions should be considered in that frequency range.

Items 4 and 5 are discussed further in Section 3.8 of this SSER.

2.5.2.1 Seismicity

Earthquake detection within the coastal region near the Diablo Canyon site improved significantly with the installation of the USGS network of seismic stations in 1978 and 1979. In addition, since 1986, PG&E has operated the 18-station Central Coast Seismic Network in the site region from Ragged Point south to Point Sal. This network supplements seismic stations in the region to provide better resolution of hypocentral locations and focal mechanisms. Hundreds of microearthquakes were recorded by PG&E near or within the network. This section of the SSER summarizes the recent seismicity data and historical earthquakes for the significant faults near the Diablo Canyon site.

Hosgri Fault Zone

The Diablo Canyon plant is located on the San Luis-Pismo structural block, which is bounded on the west by the Hosgri fault zone. Seismic activity is low west of the Hosgri fault zone and is scattered within the San Luis-Pismo structural block east of the Hosgri. The Hosgri fault zone as observed over the last 20 years is a seismic and strain boundary over most of its length be-

tween seismicity in the offshore and onshore area to the east and the offshore Santa Maria Basin to the west where there is relatively little seismicity.

Microearthquakes align along the Hosgri fault and clusters occur at the Hosgri-Los Osos and Hosgri-Casmalia fault intersections and off Point Arguello where the southern reach of the Hosgri dies out. In the vicinity of the Hosgri, as in other areas of coastal California, seismicity occurs to depths of about 12 km (the base of the seismogenic zone) (Dehlinger and Bolt, 1987). Along the section of the fault zone opposite the Diablo Canyon site, epicenters of several microearthquakes having nearly pure, strike-slip focal mechanisms are located along the fault. These earthquakes were as deep as 7 km, indicating the Hosgri fault zone in this area is nearly vertical to at least mid-crustal depths (response to Questions SSC-2 and LP-13). However, the hypocenters are diffuse and do not clearly define a fault plane. As discussed in Section 2.5.1 of this SSER, the Hosgri fault zone at seismogenic depths is assumed to have predominantly right-lateral strike-slip with a substantial component of reverse slip.

No historical earthquakes with magnitude greater than 5, except possibly the November 4, 1927, magnitude 7.0 Lompoc earthquake, have been associated with the Hosgri fault zone. The December 31, 1948, magnitude 4.6, earthquake and the January 2, 1960, magnitude 4.9, earthquake occurred in the vicinity of the Hosgri fault zone (Dehlinger and Bolt, 1987).

The location and structural association of the 1927 Lompoc earthquake has been an issue because it is the largest historical event to have occurred in the region and it provides a lower bound for the maximum credible earthquake for the associated structure. The 1927 Lompoc earthquake occurred off shore and coverage by seismic stations was sparse. Prior to the LTSP review, the USGS estimated the magnitude of the 1927 Lompoc earthquake to be magnitude 7.3 [OL SSER 4 (USNRC, 1976a)]. PG&E reevaluated the magnitude using the California Institute of Technology database and found that the average surface-wave magnitude (Ms) was 7.0. The staff agrees with the PG&E position that the Ms of the Lompoc earthquake was 7.0. As will be discussed in the next section of this SSER, the reduction in the magnitude value of the 1927 Lompoc earthquake leads to a reduction from the staff's previous estimated maximum magnitude associated with the Hosgri fault zone.

PG&E has studied the 1927 earthquake extensively to determine its location. The analyses undertaken include: (1) comparisons of teleseismic data from DeBilt, Netherlands, for the 1927 earthquake and two modern thrust events--the 1969 Santa Lucia Banks and the 1983 Coalinga earthquakes, (2) modeling of the DeBilt seismograms and regional seismograms of the 1927 event from the University of California's Lick Observatory in Berkeley and the U.S. Coast and Geodetic Survey's observatory in Tucson, (3) location analysis using teleseismic (DeBilt) and regional (Santa Barbara and Pasadena, California, and Tucson, Arizona) data, (4) analysis of tsunami data from the 1927 event recorded at La Jolla and Fort Point (San Francisco), California, and Hilo, Hawaii, (5) evaluation of intensity data from the 1927 event, and (6) analyses of seismic reflection data in the epicentral region. Some of these analyses were undertaken following publication of the LTSP Final Report (Brand, 1988). These further analyses of the 1927 earthquake epicenter resulted in a location about 10 km south of the LTSP Final Report location (response to Questions GSG

5, 8 and 9). The current PG&E epicenter is about 35 km southwest of Point Arguello at about 34.35° N, 120.90° W and the focal depth is between 3 and 16 km. The focal mechanism was reverse-slip on a plane striking N 20° W and dipping either northeast or southwest. On the basis of these studies, the PG&E position is that the 1927 Lompoc earthquake occurred west of the Hosgri fault zone on structures that are interpreted to be a southeastern extension of the Santa Lucia Bank fault zone. The epicenter is in a compressive tectonic domain of northwest-striking faults and folds.

The USGS (Appendix C of this SSER) preferred an epicenter located closer to the Hosgri fault. The USGS compared intensity patterns for the magnitude 7.1, October 17, 1989, Loma Prieta earthquake and the 1927 Lompoc earthquake and concluded the 1927 event had a more northerly location and was associated with the broader, more complex Hosgri fault system.

The staff finds the PG&E evaluation of the epicenter of the 1927 Lompoc earthquake was thorough and agrees with PG&E that the 1927 earthquake did not occur on the Hosgri fault zone. Because of its offshore location and epicentral uncertainty, it is difficult to associate the 1927 epicenter with a specific geological structure. However, several northeast-dipping reverse faults have been observed on seismic lines in the vicinity of the epicenter; the trend and sense of slip on these faults agree with the fault plane solution. Because the 1927 epicenter may have occurred on the Santa Lucia Bank fault, which may merge with the San Gregorio fault to the north, or on another structure in the Santa Maria Basin subparallel to the Hosgri, the staff assumed an earthquake of similar magnitude can occur on the Hosgri.

San Simeon Fault Zone

The San Simeon fault zone, north of the Hosgri fault zone, is a member of the San Gregorio-Hosgri fault system. The San Simeon fault strikes in the same direction as the Hosgri and is separated by about 5 km from the Hosgri by the Cambria stepover, or pull-apart, basin. The San Simeon fault is characterized by moderate-level diffuse seismicity to depths of 10 to 12 km. Epicenters of these earthquakes are a few kilometers northeast of the mapped surface trace of the fault, but their fault planes, projected to the surface from focal mechanism analyses, fall along the mapped trace of the fault, suggesting a fault plane with a northeast dip of 55°. Focal mechanisms along the San Simeon fault zone are both right-lateral strike-slip and reverse. The largest historical earthquakes associated with the San Simeon fault zone are the estimated magnitude 5 events in 1852 and 1853 and a magnitude 5.2 earthquake on August 29, 1983.

The February 4, 1991, magnitude 4.3, Lopez Point earthquake occurred east of the San Simeon fault at a depth of about 6 to 7 km. It had a reverse focal mechanism with a more westerly strike than the San Simeon fault. PG&E interpreted the earthquake to be associated with the boundary between the Salina structural block granites to the northeast and basement rocks to the southwest and not with the San Simeon fault.

Los Osos Fault

The Los Osos fault, a reverse fault, is the northeast boundary of the San Luis-Pismo structural block. The fault trends northwest and dips southwest. At its closest approach, it is 10 km from the site. The interior of the San Luis-Pismo block and the Los Osos fault are characterized by scattered microearthquakes. A cluster of seismicity occurs near the intersection of the Los Osos and Hosgri faults. Focal mechanisms for two recent small earthquakes at depths of 8 to 10 km below the fault indicate thrust solutions. PG&E found the microearthquake data suggest the Los Osos fault extends to depths of 12 km and the fault dips between 60° and 70°. No historical earthquakes with magnitude greater than 5 have been associated with the Los Osos fault. Earthquakes of about magnitude 5 in 1913 and 1916 may have been located on the fault.

Southwest Boundary Zone

The southwest boundary of the San Luis-Pismo block is a zone of northwest-trending, northeast-dipping, reverse faults, including the San Luis Bay, Olson, Wilmar Avenue, Pecho and Oceano faults. Recent seismicity is low level and diffuse near these faults. The largest historical earthquakes associated with the Southwest Boundary Zone are the October 20, 1913, Arroyo Grande earthquake of estimated magnitude 5 or greater and the December 1, 1916, and November 18, 1927, earthquakes of estimated magnitude 5. Focal mechanisms for two recent small earthquakes near the fault yield reverse fault mechanisms.

Nacimiento Fault

The Nacimiento fault is about 30 km northeast of the Diablo Canyon site. The fault occurs along the east side of a wide band of small to moderate-level earthquakes. Focal mechanisms are both strike-slip and reverse. The largest historical earthquake associated with the Nacimiento fault is the November 22, 1952, Bryson earthquake of magnitude 6.2.

2.5.2.2 Maximum Earthquake Potential

The staff finds that for the purposes of defining the maximum credible earthquakes to be used in the reanalysis under the LTSP, an evaluation of the Hosgri fault zone, the San Simeon fault zone, the Los Osos fault, the Southwest Boundary Zone, and the Nacimiento fault must be considered. This section of the SSER describes the maximum credible earthquakes; the geological arguments are discussed in more detail in Section 2.5.1 of this SSER.

Logic-Tree Approach

To account for uncertainty in characterizing important faults (especially the lack of historical earthquakes), PG&E designed a logic-tree approach to derive maximum magnitudes for the important faults. Logic trees are composed of nodes and branches. Each element in the logic tree has a set of nodes representing an uncertain state of nature. Each branch represents discrete possible values for that state. Probabilities are assigned to each branch using subjective assessments.

Each path through the logic tree defines a scenario associated with a maximum magnitude. The relative weight of each magnitude estimate is the product of the probabilities assigned to each parameter on the logic tree. End branch probabilities are calculated as the product of all the intermediate branch probabilities. By calculating a maximum magnitude for each logic-tree path, a probability distribution of maximum magnitudes for each fault was obtained. The distribution has a mean magnitude value and a standard deviation. The maximum magnitude distributions are used in the seismic hazard analysis part of the probabilistic risk assessment.

The logic-tree approach assigns weights, using scientific judgment, to the following variables: sense of slip, dip angle, depth of seismogenic zone, length of fault, maximum rupture length, maximum and average displacement per event, largest historical earthquake associated with the fault, and techniques for magnitude assessment (empirical relations between magnitude and rupture length, rupture area, total fault length, maximum displacement per event, and seismic moment). Maximum rupture length is based on an assessment of segmentation of each fault. The alternative hypotheses and weights on the logic trees are based on the geoscience data in the LTSP Final Report as interpreted by a panel of 16 PG&E consultants.

Hosgri Fault Zone

Until the OL review for the Diablo Canyon site, the nearest major fault considered to be seismically active was the Nacimiento fault. However, during the OL review, studies of the geological structure off shore revealed the Hosgri fault zone, passing within about 5 miles of Diablo Canyon. The staff's advisor, the United States Geological Survey (USGS), concluded, "the occurrence of an earthquake as large as events characteristic of subparallel strike slip faults, which bound basins, such as the Santa Maria" could not be precluded. An earthquake similar to the 1927 Lompoc event occurring on the Hosgri or the Santa Lucia Bank fault zones represents the maximum earthquake likely to occur near the site. The USGS considered that the 1927 earthquake is associated with the Santa Lucia Bank fault and the structural properties of the Santa Lucia Bank and Hosgri faults suggest these two faults have similar seismic potential. Furthermore, northwest-trending fault zones such as the Hosgri, both off shore and on shore, have been considered to be part of a system of faults with right-lateral movement.

In the current review, PG&E derived a maximum earthquake magnitude of 7.2 for the Hosgri fault zone. By calculating a maximum magnitude for each logic-tree path, a probability distribution of maximum magnitudes for the Hosgri fault was obtained. The distribution has a mean value of magnitude 6.96 and a standard deviation of 0.27 magnitude units. PG&E chose to use a maximum magnitude of 7.2 on the Hosgri for analysis of the plant structures, systems and equipment. The mean estimate was similar for different types of faulting (strike-slip, oblique, or thrust). The largest magnitudes resulted from the longest rupture lengths and largest rupture widths (associated with shallow-dipping thrust faults).

In its report to the staff, the USGS (Appendix C of this SSER) suggested that the parameters in the logic tree were biased to favor strike-slip faulting (weight of 0.65) although the offshore seismicity data, focal mechanisms on the

San Simeon fault, and the focal mechanism of the 1927 Lompoc earthquake support oblique and thrust-slip models. The USGS also suggested that the logic tree is biased toward short (20 km) rupture lengths for thrust and oblique-slip faults. The use of more oblique-slip and thrust mechanisms and earthquakes that rupture through segmentation points would raise the mean magnitude value. However, the USGS agreed with PG&E that it is reasonable to associate a maximum earthquake magnitude of 7.2 with the Hosgri fault. Furthermore, a PG&E sensitivity study to assess the impact of the type of slip on mean seismic hazard curves (response to Question LP8) showed little effect.

Professor Slemmons of the UNR, consultant to the staff, also reviewed the Hosgri logic trees (Appendix D of this SSER). He agreed with PG&E that the Hosgri fault behavior is predominantly strike-slip, but with a significant reverse-slip component. His preferred rupture lengths are longer (50 and 70 km) because earthquakes of magnitude greater than 7 rupture in multiple segments. Dr. Slemmons favored a slip rate of 2 to 3 mm/yr, which is within the PG&E preferred range of 1 to 3 mm/yr. His independent analysis determined a maximum magnitude of 7.2 for the Hosgri fault.

The staff concludes that the 1927 magnitude 7.0 offshore Lompoc earthquake did not occur on the Hosgri fault zone, but may have occurred on a structure related to the Hosgri and thus, an earthquake of similar magnitude can occur on the Hosgri. The staff agrees with PG&E and the staff consultants that the maximum earthquake on the Hosgri fault zone to be used in the LTSP seismic reevaluation is magnitude 7.2. This earthquake is assumed to occur at the closest approach of the Hosgri fault to the Diablo Canyon site (4.5 km).

San Simeon Fault Zone

The San Simeon fault zone is north of the Hosgri fault zone and at its closest approach is at least 30 km from the Diablo Canyon site. Both geological investigations and earthquake focal mechanisms suggest strike-slip and reverse behavior. The maximum earthquake associated with the San Simeon fault zone is similar to the maximum earthquake associated with the Hosgri fault zone.

Los Osos Fault

The Los Osos fault, a reverse fault, is the northeast boundary of the San Luis-Pismo structural block and trends northwest. It is 10 km from the Diablo Canyon site at its closest approach. The staff finds the fault to be capable, based on geological evidence and possible spatially associated seismicity.

PG&E used the logic-tree approach to calculate a mean maximum magnitude value of 6.8 for the Los Osos fault. PG&E had identified four fault segments on the Los Osos fault, based on differences in physical characteristics. The segment closest to the Diablo Canyon site, the Irish Hills segment, is 19-km long.

The USGS found it difficult to accept the segmentation model used to estimate rupture lengths because no historical earthquakes have been associated with the Los Osos fault. The USGS found the rupture lengths (19 and 36 km) and earthquake displacement (2.1 m) in the logic tree were not conservative. The USGS-preferred dip is 20° or less; the dip considered by PG&E for the fault

(60°) is too steep. However, the USGS concluded that a maximum magnitude 6.8 event is reasonable, since it is larger than the 1971, magnitude 6.6, San Fernando earthquake, whose associated fault was longer than the Los Osos fault. Dr. Slemmons generally agreed with the PG&E logic-tree values, and his independent analysis found the maximum magnitude to be 6.5 to 6.8. On the basis of the advice of its consultants, the staff concludes that the applicant's proposed maximum magnitude of 6.8 for the Los Osos fault is reasonable.

Southwest Boundary Zone

The southwest boundary of the San Luis-Pismo block is a zone of northwest-trending reverse faults, dipping to the northeast, that includes the San Luis Bay, Olson, Wilmar Avenue, Pecho, and Oceano faults. Geological information indicates that these faults are active. The zone of faulting is more than 60-km long, but the extent of the faults off shore is unclear. The closest capable faults to the Diablo Canyon site are the San Luis Bay fault (5 km from the site to the nearest mapped trace) and the Olson fault (about 3 km from the site to the closest mapped trace). Possible offshore projections of both faults could be closer to the site than the mapped traces.

PG&E has characterized each fault individually, including segmenting each fault, and used a logic-tree approach to estimate maximum magnitudes. In the LTSP Final Report, the San Luis Bay and Olson faults were treated as a single fault zone, with rupture lengths of 6, 8, and 12 km; the mean maximum magnitude value for the San Luis Bay fault was 6.15. In response to Question SSC-5, PG&E documented its revised characterization of the two faults as separate sources and reassessed the maximum magnitudes for these faults. The maximum magnitudes for the San Luis Bay fault were 5.6 to 6.2 and for the Olson fault, magnitudes were 5.0 to 6.0.

The USGS found the earthquake hazard from the Southwest Boundary Zone faults is probably much less than the Los Osos or Hosgri. The faults could, however, extend off shore or merge into a northwest-trending structure.

Dr. Slemmons suggested that the Los Osos fault and the Southwest Boundary Zone faults are mirror images and the Olson and San Luis Bay faults integrate at seismogenic depth. He considered these faults to be a single fault zone, but segmented along boundaries between topographic subblocks of the San Luis-Pismo block. This model leads to a longer rupture length (13 km) than the PG&E model. His analysis computed a maximum earthquake magnitude of 6.5, similar to that for the 1971 San Fernando earthquake.

On the basis of the PG&E and UNR analyses, the staff has adopted a maximum credible earthquake of magnitude 6 to 6-1/2 on the Olson and San Luis Bay faults, the closest of the Southwest Boundary Zone faults to the site. Uplift of the San Luis-Pismo block along the Southwest Boundary Zone is accommodated by multiple faults in a 3 to 4-km-wide zone of deformation. If several of these faults coalesce to form a single fault zone at depth, as suggested by Dr. Slemmons, the faults at shallow depths (less than 5 km) are not considered to be potential sources of the larger magnitude earthquakes. Furthermore, since slip rates and seismic activity associated with the Olson and San Luis Bay faults indicate a low degree of activity of these faults compared to the Hosgri

fault zone, the ground-motion effects at the Diablo Canyon site from the Hosgri fault zone are more significant.

Nacimiento Fault

The Nacimiento fault is about 30 km northeast of the Diablo Canyon site. Although Quaternary fault movements have not been recognized along the Nacimiento fault, it is assumed to be capable because of a low to moderate level of seismic activity associated with it. The largest historical earthquake associated with the Nacimiento fault is magnitude 6.2. In the construction permit (CP) safety evaluation report (SER) (USAEC, 1968) a maximum magnitude of 7-1/4 was associated with the Nacimiento fault; the staff continues to find this maximum magnitude reasonable.

2.5.2.3 Reevaluation of Earthquake Ground Motions

In the CP SER, the design peak ground acceleration of 0.20g was based on the occurrence of a magnitude 7-1/4 earthquake on the Nacimiento fault 20 miles from the site and a magnitude 6-3/4 aftershock at the site associated with a large earthquake on the San Andreas fault. For long periods, the response spectrum for the Nacimiento earthquake was larger, and for short periods, the response spectrum for the aftershock was larger. For design purposes, an envelope of the two response spectra was used. The same spectral shape and twice the peak ground acceleration value, 0.40g, was used for safe shutdown conditions. At that time, the nearest seismically active fault was considered to be the Nacimiento fault.

During the OL review, the offshore Hosgri fault zone was investigated. The Hosgri reanalysis peak ground acceleration was 0.75g, based on the occurrence of a magnitude 7.5 earthquake on the Hosgri fault (USNRC, 1975, 1976a and b, 1978). This acceleration was used as a high-frequency asymptote for the spectrum used in reevaluating the plant's seismic design.

As part of the seismic license condition, PG&E updated the ground-motion information. The next section of this SSER describes the staff review of the updated ground-motion information. Dr. Kenneth Campbell assisted the staff in the empirical ground-motion review by evaluating the PG&E studies and independently conducting studies to estimate empirical ground motion for the Diablo Canyon site. The staff was assisted in its numerical ground-motion modeling review by its advisors Drs. Keiiti Aki, Ralph Archuleta, and Steven Day.

The maximum magnitude of the 1927 Lompoc earthquake was reanalyzed during the LTSP program and found to be magnitude 7.0; this led to a reduction in the maximum credible earthquake associated with the Hosgri fault zone to magnitude 7.2. In assessing recent new information, the staff considered the ground-motion estimates at the site from a maximum earthquake of magnitude 7.2 associated with the Hosgri fault zone at a distance of 4.5 km to the site. The Hosgri fault zone at earthquake depths is assumed by the staff to have predominantly right-lateral strike-slip with a substantial component of reverse slip (see Section 2.5.1 of this SSER). The Hosgri fault zone is the dominant seismic source in the region. All other capable faults are farther from the site and/or not as significant a source of earthquakes (including the Santa Lucia Bank fault, hypothesized blind thrust faults, the Los Osos fault, and the

Southwest Boundary Zone faults). Because of uncertainties in the ratio of horizontal to vertical slip on the Hosgri fault zone and because ground motion from reverse-slip displacements are estimated to be higher than from strike-slip, the staff has analyzed the ground-motion effects at the Diablo Canyon site assuming 2/3 strike-slip and 1/3 reverse-slip displacement on the Hosgri.

PG&E conducted empirical investigations using strong-motion recordings and a numerical modeling study to estimate ground-motion response spectra. These studies are described in this section of the SSER. The October 17, 1989, magnitude 7.1, Loma Prieta, California, earthquake occurred during the review of the PG&E studies and strong-ground-motion data from the Loma Prieta earthquake were compared with the LTSP data (response to Workshop Question 2).

Empirical Investigations

PG&E established an updated worldwide strong-motion database to calculate site-specific horizontal and vertical response spectra. PG&E classified the Diablo Canyon site as a rock site and chose strong-motion records from rock and rock-like sites. The inclusion of hard-rock recordings significantly enlarged the data set of rock recordings and provided additional close-in recordings. Records from soil sites were used to augment the database for special studies, such as the effects of magnitude scaling and style of faulting. Since the potential seismogenic zones near the site are confined to the upper crust, down to a depth of 12 km, records were selected from shallow crustal earthquakes.

PG&E assessed the ground motion at the Diablo Canyon site from the Hosgri fault zone for a magnitude 7.2 earthquake at a distance of 4.5 km to the fault trace. The ground-motion estimates may be affected by the dip and source mechanism for the Hosgri fault at depths of 4 to 10 km, where most of the seismic energy would originate. Ground-motion values for a vertical strike-slip fault are generally smaller than for thrust-slip faults. In response to Question LP-9 and Workshop Question 5, PG&E provided geometries associated with the strike-slip, oblique, and thrust models of the Hosgri fault zone. These models show reasonable geometries and source-to-site distances for each fault type. PG&E's adoption of 4.5 km as the distance to the Hosgri fault rupture surface for strike-slip faults is conservative because it assumes rupture to the surface along the mapped trace of the Hosgri fault. Recent PG&E studies refined the distance to 4.5 km for an oblique-slip displacement on a steeply dipping fault and 5.8 km for thrust-slip displacement on a shallow-dipping fault.

To determine the characteristics of site response, local small-earthquake recordings at the Diablo Canyon site were compared to recordings from nearby stations. The spectra of these recordings are similar, which suggests the Diablo Canyon site has similar spectral amplification and there is no unusual site amplification. Finite difference modeling studies, finite element analyses, and ground motions recorded at the Diablo Canyon site also demonstrated the lack of topographic effects on ground motion.

PG&E used two empirical approaches to estimate the ground motion. In the first empirical approach, the statistical approach, 18 strong-motion records were selected at near-source distances (within 20 km) and from large earthquakes

(magnitude $\geq$ 6.3). Because the database for rock sites was small and included mostly thrust-slip events, five recordings on soil sites from strike-slip events were included. Each record was assigned a weighting factor that reflected differences in tectonic setting, unusual topographic or subsurface condition, or unusual site geometry (strong directivity effect). Then the records were modified to conform to a record at a rock site 4.5 km from a magnitude 7.2 earthquake. Because ground motions are higher for thrust than strike-slip faults, the records were also modified for style of faulting. The adjustments for magnitude, distance, rock site conditions, and style of faulting were based on empirical studies, including the LTSP deterministic studies and numerical modeling results. Then the spectra were combined to obtain median and 84th percentile levels of horizontal site-specific response spectra using weights proportional to the probabilities of occurrence of the three potential styles of faulting (65% strike-slip, 30% oblique, or 5% thrust) (LTSP Final Report, Figure 4-17).

The staff questioned the selection of ground-motion recordings used in the database and the adjustments for magnitude, distance, rock site conditions, and style of faulting, and the weighting factors for tectonic setting and site geometry. PG&E also augmented its database with the Loma Prieta strong-motion data. The responses to staff questions and the inclusion of the 1989 Loma Prieta records produced similar acceleration results.

In a second empirical approach, PG&E used the updated strong-motion database to develop attenuation relationships for peak ground acceleration and response spectral accelerations by regression analysis. Then these attenuation relationships were used to develop site-specific response spectra for the maximum Hosgri event. To develop response spectra, a spectral shape was developed for a reference magnitude of 6.5, because there is a larger database for this magnitude. Then the strong-motion database was used to develop peak ground attenuation relationships to scale this spectral shape to other magnitudes and recording distances. As part of the numerical modeling studies, PG&E found peak ground acceleration and spectral accelerations for oblique-slip events are halfway between accelerations for strike-slip and thrust-slip events. Response spectra for the three styles of faulting were combined with weights proportional to their probability of occurrence to give the horizontal and vertical, site-specific, response spectra (LTSP Final Report, Figures 4-22 and 4-23).

Both the empirical and numerical modeling studies suggest that at a distance of 1 km and for magnitudes above 6.5, the computed peak acceleration values are nearly saturated (response to Question 11). Also variability of ground motion was found to decrease with increasing magnitude (response to Ground Motion Question 6). These results were incorporated by both PG&E and the staff's consultant, Dr. Kenneth Campbell, in their ground-motion attenuation relationships.

Dr. Kenneth Campbell has assessed the PG&E empirical ground-motion studies (Campbell, 1990, 1991a and b). He reached the following conclusions:

(1) The crustal velocity model of the Diablo Canyon site and ground motions recorded at the site indicate that the site is a soft-rock (sedimentary rock) rather than hard-rock (crystalline rock) site. Recordings on soft-rock sites are not significantly different from soil sites. However,

recordings on hard-rock sites and shallow-soil sites should be excluded because they have different frequency content and amplitude than soft-rock sites. Seismic velocity profiles near the Diablo Canyon site were used to infer a depth to basement rock of 4 km. Campbell's depth-to-basement-rock parameter in his attenuation relationship affects response-spectral estimates for frequencies less than about 1 Hz. PG&E did not include a sediment-depth parameter in its analysis because it concluded that the Diablo Canyon site was a rock site. However, PG&E concluded that the differences between the soft-rock and hard-rock recordings are enveloped by the PG&E LTSP site-specific spectrum at frequencies above 2 Hz (response to Workshop Question 6).

(2) There are no unusual site conditions which would cause amplification of ground motion.

(3) PG&E did not address the effects of building size. Recordings greater than two stories in height have smaller peak accelerations and short-period response spectra and larger long-period response spectra than recordings from small buildings and free-field sites. However, recordings from embedded structures make up a small percentage of the total number of recordings used by PG&E and probably had little impact.

(4) The recordings used in the statistical analysis and attenuation regression analysis should not be weighted for tectonic regime, topography, directivity, and such. The only adjustment should be for the magnitude and source-to-site distance. The weighting factors are subjective and lead to a biased statistical estimate of ground motion. [PG&E presented sensitivity studies in which it concluded that the effect of the weighting factors is not significant (responses to Ground Motion Question 2 and Workshop Question 2 and Shiffer, 1991d).]

(5) Dr. Campbell found the reverse-oblique faulting scenario should be assigned the same style of faulting factor as the reverse faulting scenario because of uncertainty in the fault-slip parameter and the limited number of oblique-slip recordings in the database.

(6) The statistical approach has too few recordings and is thus not statistically reliable. The statistical approach should only be used to check the results obtained from the regression analysis.

(7) The vertical response spectra should be developed independently and not developed by scaling the horizontal spectra by a frequency-dependent, vertical-to-horizontal ratio. This is because the ratio has been shown to be dependent on magnitude and source-to-site distance. The PG&E reanalysis of the vertical spectra using an independent regression analysis indicates the reanalyzed 84th percentile spectrum exceeds the LTSP spectrum at frequencies from 2.5 to 10 Hz.

Dr. Campbell (1990 and 1991b) also developed independent attenuation relationships for near-source ground motion near the Diablo Canyon site. His database included soil and soft-rock recordings since he concluded there is no statistically significant difference between them. The resultant attenuation relationship includes parameters representing the style of faulting, sediment depth (depth to basement rock), and building effects (height and embedment).

Campbell's results confirm that peak ground-motion parameters and short-period response spectra saturate (become independent of magnitude) at small distances for large-magnitude earthquakes. Campbell also agreed with PG&E that the standard error of estimate decreases with increasing magnitude.

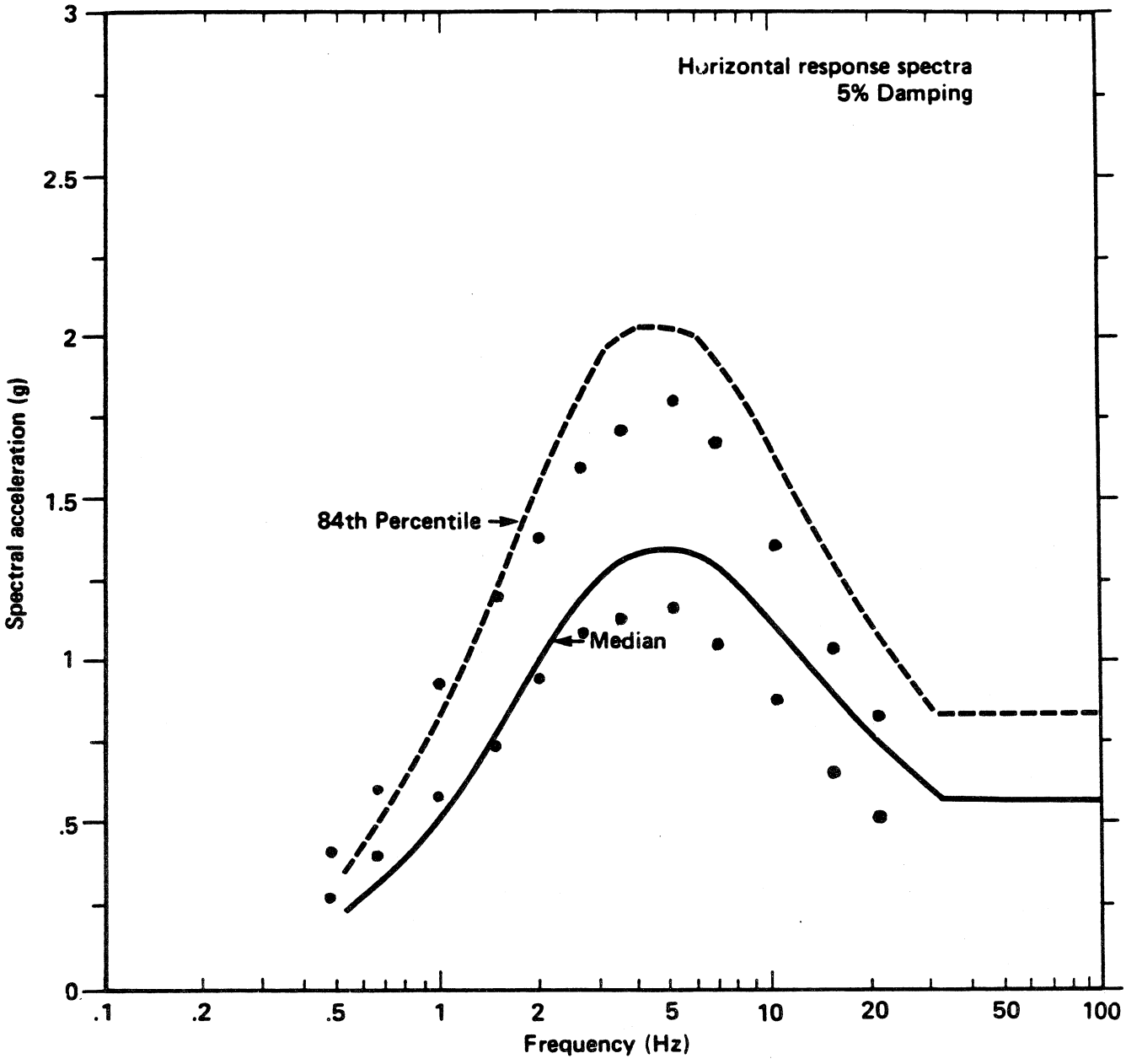
Campbell used his attenuation relationships to develop site-specific response spectra for a magnitude 7.2 earthquake on the Hosgri fault 4.5 km off shore. Seismogenic distances were 4.9 km for a strike-slip fault, 4.7 km for a reverse-oblique-slip event and 5.1 km for a thrust-slip event. The seismogenic distance is the shortest distance between the site and the assumed zone of seismogenic rupture. This distance is based on spatial distribution of aftershocks, earthquake modeling studies, regional crustal velocity studies, geodetic and geologic data, and the fact that for past events, faulting within the sediments and very shallow crust does not contribute significantly to recorded strong ground motions at frequencies of engineering interest. Similar to the PG&E results, ground motions from reverse-displacement events were larger than from strike-slip events.

PG&E used both empirical and numerical modeling studies to show that spectra for oblique-slip and thrust-slip hypotheses only slightly exceed the site-specific response spectra in the LTSP Final Report (response to Ground Motion Question 5 and Figure LP Q9-2). These exceedances are not significant.

The staff prefers the response spectral attenuation relationships developed by regression analysis to predict ground motion because these relationships reflect the frequency content of ground motion from a larger set of recordings than the statistical approach, which used only a small set of near-source records. The staff assumed the Hosgri fault zone at seismogenic depths has 2/3 strike-slip and 1/3 reverse-slip displacement. Since few spectra have been recorded for oblique-slip events, the staff compared weighted spectra derived from Campbell's (1990 and 1991b) results for 2/3 strike-slip and 1/3 reverse-slip to the LTSP spectra (Figure 2.4). The staff's 50th and 84th percentile weighted horizontal spectra derived from Campbell's (1991b) empirical predictions are at or below the LTSP horizontal spectra above 1 Hz, but exceed the LTSP spectra at and below 1 Hz. The exceedances appear to be due to the fact that Campbell's database excluded hard-rock recordings, which have lower amplitudes at low frequencies (responses to Question 17b and Workshop Question 6).

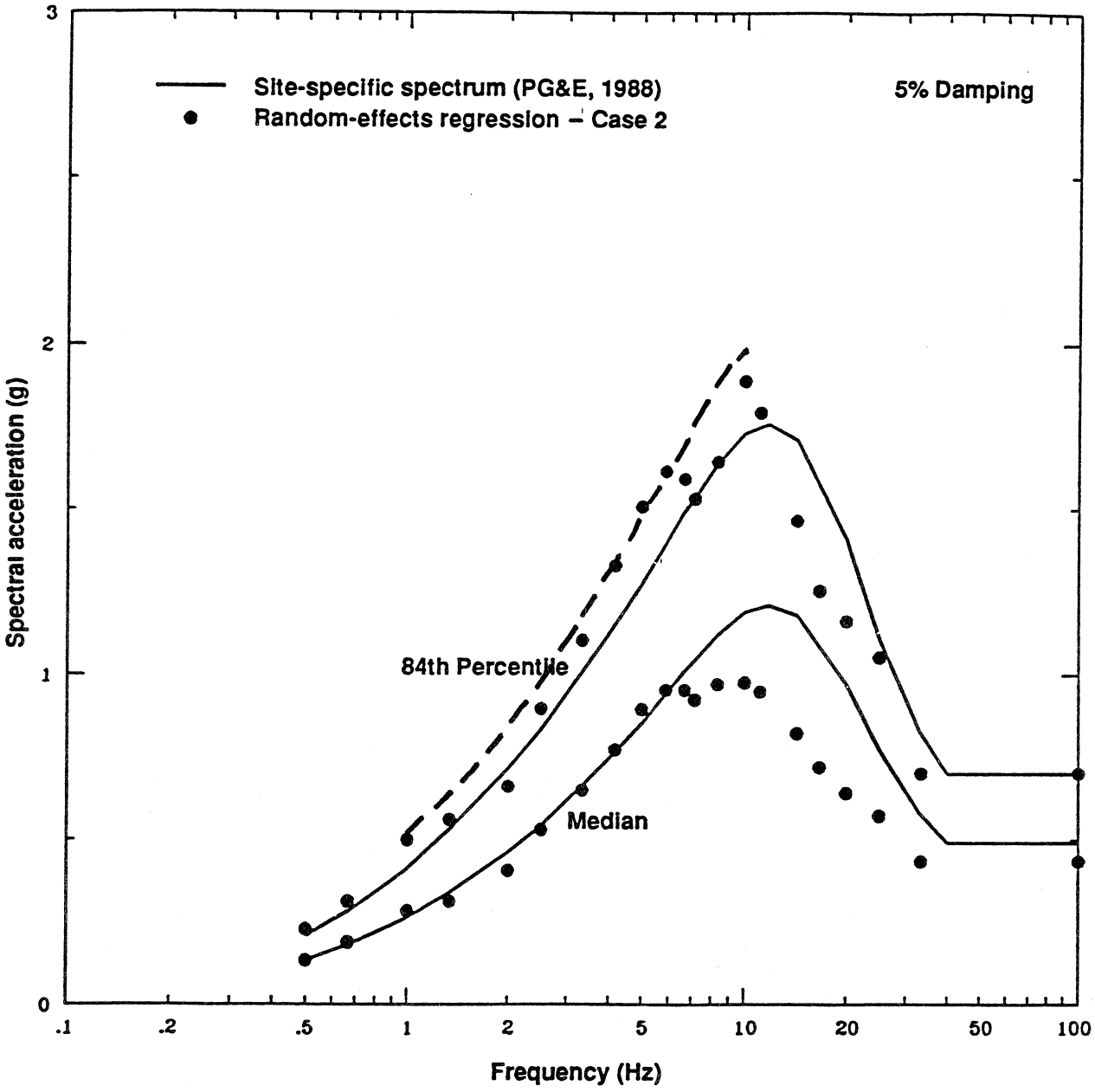
The staff concludes that the PG&E LTSP horizontal spectra are appropriate for design evaluation above 1 Hz. However, since the staff's weighted spectra derived from Campbell's regression analysis exceed the LTSP horizontal spectra at and below 1 Hz, the staff's weighted spectra should be used at and below 1 Hz. For example, the staff's 84th percentile spectrum is 10 to 20 percent higher than the LTSP spectrum at 0.5 to 1 Hz. The engineering implications of this exceedance are discussed further in Section 3.8 of this SSER.

To estimate the vertical spectra, PG&E originally developed a frequency-dependent ratio of vertical to horizontal components of ground motion and then applied this ratio to the horizontal results to estimate the vertical site-specific response spectra. In response to staff questions, PG&E recalculated the vertical response spectra using a regression-based model (Figure 2.5). Although Campbell's (1990) spectra exceeded the PG&E results, PG&E found that



LTSP (lines) and staff's estimate based on Campbell (1990 and 1991b) (dots) median and 84th percentile horizontal acceleration response spectra for a magnitude 7.2 earthquake at 4.5 km.

Figure 2.4
Horizontal acceleration response spectra



LTSP (lines and PG&E random-effects regression model (dots) median and 84th percentile vertical acceleration response spectra for a magnitude 7.2 earthquake at 4.5 km. Dashed line represents 15 percent above LTSP from 1 to 10 Hz.

Figure 2.5
Vertical acceleration response spectra

the differences could be reduced by adding recordings (including the Loma Prieta data) and applying the random-effects regression model to the Campbell database. Dr. Campbell is confirming PG&E's analysis of his data. In comparing the random-effects regression-based spectra and weighted (2/3 strike-slip and 1/3 reverse-slip) Campbell's (1990) spectra to the LTSP response spectra, the staff found that the PG&E 50th and 84th percentile LTSP spectra are exceeded between 1 and 10 Hz. Even the 84th percentile PG&E regression-based spectrum is about 20 percent higher than the LTSP spectrum at 1 Hz and 15 percent higher than the LTSP spectrum at 4 to 6 Hz. PG&E (Shiffer, 1991g) found that the ratio method used to develop the LTSP vertical spectra is a well-accepted procedure and questions still exist regarding the appropriateness of the regression analyses; therefore, the most appropriate vertical response spectra are those obtained by the ratio method. However, the staff concludes that 15 percent higher vertical ground motions should be considered in the frequency range 1 to 10 Hz for the 84th percentile spectrum (Figure 2.5). This issue is discussed further in Section 3.8 of this SSER.

Numerical Modeling Studies

Because the seismic hazard at the Diablo Canyon site is dominated by large, near-source earthquakes and only a few recordings are available for these site conditions, numerical modeling studies were used to estimate ground motions and supplement the empirical investigations. The numerical modeling studies also estimated the sensitivity of ground motions to variations in fault parameters.

PG&E developed a ground-motion simulation procedure in which the simulated accelerogram is the sum of responses from small fault ruptures on the rupture surface. The roughness of the rupture process was represented using an asperity model in which slip varied across the fault surface. Actual recordings of small earthquakes are used as source functions. Since the empirical source functions include the effects of propagation from the source to the recording instrument, the source function is corrected for its propagation term. Then the source function is convolved with a Green's function, which accounts for the site-specific effects of wave propagation. The ground-motion contributions for each subfault are then time-lagged and summed in accordance with a prescribed geometry of rupture evolution. A correction is also made for the differences in receiver functions between the receiver structure of the empirical source functions and the velocity structure at the Diablo Canyon site. This approach allows for modeling the fault rupture and site-specific propagation effects on ground motion.

A set of 116 simulations was generated to develop 50th and 84th percentile site-specific response spectra. The simulations varied the type of faulting, rupture mode (bilateral or unilateral), the rupture location with respect to the site, the asperity model, and source functions. Response spectra for each fault type (strike-slip, oblique, and reverse) were calculated and then the spectra were combined using weights proportional to their probability of occurrence to calculate the site specific response spectra (LTSP Final Report, Figure 4-24).

For the 1988 LTSP Final Report, recordings of an aftershock of the 1979 Imperial Valley earthquake and an aftershock of the 1983 Coalinga earthquake were used as source functions. In 1990, PG&E replaced the Coalinga aftershock

recording as an empirical source function with a 1987 Whittier Narrows, California, aftershock recording because the Coalinga aftershock had complex source characteristics that were difficult to use in the simulation procedure and produced overestimates of the recorded ground-motion data sets in the validation study (response to Workshop Question 1). The new 84th percentile spectrum is broader than the results in the LTSP Final Report, but is still lower than the spectrum from the regression attenuation relationships (response to Workshop Question 1, Figure WQ1-14).

The ground-motion simulation procedure was validated using strong-motion recordings from the 1979, magnitude 6.5, Imperial Valley earthquake; the 1987, magnitude 6.0, Whittier Narrows earthquake; the 1983, magnitude 6.4, Coalinga earthquake; the 1985, magnitude 6.9, Nahanni earthquake; and the 1989, magnitude 7.1, Loma Prieta earthquake. Simulated ground motions were compared with recorded ground motions.

The following are PG&E's conclusions:

(1) The response spectra obtained from the numerical modeling studies agree with the empirical results above 2 Hz, but are lower than the empirical results for frequencies below 2 Hz because the method does not include surface wave contributions (responses to Question 15 and Ground Motion Question 11).

(2) Oblique-slip motions are halfway between strike-slip and reverse-slip motions for both horizontal and vertical motions (LTSP Final Report p. 4-33, response to Ground Motion Question 17).

(3) Sensitivity studies support the use of a fault element size of 4 by 3 km.

(4) A fault asperity model simulates recorded accelerations.

(5) The shallow part of the fault rupture contributes very little to the simulated motions (responses to Questions 13d and 14).

(6) The directivity effect on strong ground motions due to rupture propagation is most pronounced at periods of several seconds for sites on the strike of the fault rupture, but was not found to be significant for predictions of accelerations at the Diablo Canyon site (responses to Question 17a and Ground Motion Question 19).

(7) Fluctuations in the calculated response spectra are due to irregularities in the source spectra (response to Ground Motion Question 4).

(8) The numerical modeling procedure was not valid for vertical ground motions because the simulation procedure underestimates the vertical component (response to Question LP-9).

The staff's ground-motion consultants questioned the details of the numerical modeling procedure. For example, Dr. Keiiti Aki noted that the simulated motions in the frequency range near the peak frequency (3 to 5 Hz) are similar to the empirical results. However, on either side of the peak, when compared to

empirical results, the simulation is underestimating, which is interpreted as the effect of the choices of recording site effects, empirical source functions, and subevent size on the rupture surface. Dr. Steven Day questioned the ability of the fault plane at shallow depth to generate seismic energy. Dr. Ralph Archuleta questioned the use of empirical sources which originate at 10 to 13 km, which is deep for California earthquakes; these deeper sources may produce smaller recorded ground motions than for shallow sources.

The staff concludes the numerical modeling studies provided a check on the attenuation relationship results, although the numerical modeling results appear to underpredict ground motion outside the peak frequency range of 3 to 5 Hz. The sensitivity studies were useful to the staff in assessing ground motion as a function of slip type and the effect of directivity on ground motions.

Integration of Empirical and Numerical Modeling Results

Figures 4-25 and 4-26 of the LTSP Final Report and Figure WQ1-14 compare the 50th and 84th percentile, horizontal, site-specific, response spectra from the two empirical approaches and the numerical modeling approach. All three approaches suggest a spectral acceleration of about 2.0g at 4 to 5 Hz. Since the results from the empirical attenuation relationships envelope the other results, PG&E selected both the horizontal and vertical site-specific response spectra derived from the attenuation relationships for use in the engineering evaluations of the plant structures, systems, and components for both the deterministic seismic-margin studies and the probabilistic risk assessment studies. Attenuation relationships were developed for spectral acceleration at 14 frequencies from 1 to 14 Hz and average spectral accelerations over two frequency ranges: 3 to 8.5 Hz and 5 to 14 Hz. The average spectral acceleration in the frequency range of 3 to 8.5 Hz was selected for use in the probabilistic risk assessment because this is the highest portion of the horizontal, site-specific, response spectra and it was found to exhibit the least variability with respect to ranges of earthquake magnitudes.

A suite of acceleration time histories were provided as input for the seismic-fragility evaluation. The time histories were developed from empirical data and from numerically simulated time histories. The empirical records were adjusted for source-to-site distance, site response, or magnitude, as needed. The time histories represented three styles of faulting (strike-slip, oblique, and thrust faulting). The simulated time histories increased the data set and provided a more balanced representation in the styles of faulting and other source parameters. A total of 24 empirical horizontal components and 14 simulated acceleration time histories were used to provide a measure of the spectral shape and the associated dispersion.

Three acceleration time histories were selected and modified to match the site-specific spectra for the soil-structure interaction analyses. These time histories have durations ranging from about 10 to 20 seconds and are acceptable for a source on the Hosgri fault zone.

The staff concludes that the PG&E LTSP horizontal spectra calculated from the attenuation relationships are appropriate for deterministic reevaluation of structures, systems, and components above 1 Hz. However, since the staff's weighted spectra derived from Campbell's spectra exceed the LTSP horizontal

spectra at and below 1 Hz, higher ground motions should be considered at and below 1 Hz.

In comparing the PG&E random-effects, regression-based, vertical spectra and weighted Campbell (1990) spectra to the LTSP response spectra, the staff concludes that the PG&E LTSP 84th percentile, regression-based vertical spectra are exceeded between 1 Hz and 10 Hz. For example, the PG&E 84th percentile regression-based spectrum is about 20 percent higher than the LTSP spectrum at 1 Hz and 15 percent higher than the LTSP spectrum at 4 to 6 Hz. Vertical ground motions 15 percent higher than the LTSP 84th percentile spectrum should be considered in the frequency range of 1 to 10 Hz.

2.5.2.4 Seismology Conclusions

The Diablo Canyon plant is located on the San Luis-Pismo structural block, which is bounded on the west by the Hosgri fault zone, the predominant source of expected ground motion at the site. The staff assumed that predominantly strike-slip with a substantial amount of reverse-slip is occurring on the Hosgri in the seismogenic zone. An earthquake similar in size to the 1927 magnitude 7.0 Lompoc earthquake occurring on the Hosgri fault zone represents the maximum earthquake likely to occur near the site. A maximum credible earthquake of magnitude 7.2 is assumed to occur at the closest approach of the Hosgri fault zone to the Diablo Canyon site (4.5 km).

PG&E employed empirical and numerical modeling investigations to estimate ground motion at the Diablo Canyon site for the Hosgri maximum credible earthquake. The staff concludes that the PG&E LTSP horizontal 50th and 84th percentile spectra are appropriate for design evaluation above 1 Hz; however, higher ground motions should be considered at and below 1 Hz. Higher ground motions should also be considered for the 84th percentile vertical spectra between 1 and 10 Hz. See Section 3.8 of this SSER for additional discussion of this issue.

PG&E made the following commitments at the public meeting on March 15, 1991, and in a letter from PG&E to the NRC (Shiffer, 1991f): (1) to continue to maintain a strong geosciences and engineering staff to keep abreast of new geological, seismic, and seismic engineering information and evaluate it with respect to its significance to Diablo Canyon, and (2) to continue to operate a strong-motion accelerometer array and the coastal seismic network, although likely with fewer stations than are currently operating. Since some issues (i.e., slip type of the Hosgri, the characterization of the Southwest Boundary Zone, and ground-motion estimates for oblique-slip earthquakes) are controversial because of the lack of definitive evidence, future geoscience discoveries may allow a more robust conclusion for these issues.

2.5.3 Surface Faulting

The nearest capable faults to the site are the Hosgri fault zone, 4.5 km from the site and the northeasternmost faults of the Southwest Boundary Zone, the San Luis Bay fault, and the Olson fault (the closest approach of the onshore locations of these faults are about 8 km and 4 km, respectively, from the site). Detailed mapping of marine terraces from Montano de Oro to Mallagh Landing by PG&E (Brand, 1988) and Killeen and others (1987), mapping of fluvial terraces along antecedent streams that cut across the San Luis-Pismo structural

block (Killeen and others, 1987) on which the Diablo Canyon plant is located, and the analysis of trenches by PG&E (Brand, 1988) excavated across mapped faults within the block such as the Edna and San Miguelito faults demonstrate that the San Luis-Pismo structural block has not been internally deformed during the late Quaternary period. On the basis of the information and analyses presented in Section 2.5.1.2 of this SSER on these faults, there is no potential for surface faulting at the site.

3 DESIGN CRITERIA--STRUCTURES, COMPONENTS, EQUIPMENT, AND SYSTEMS

3.7 Seismic Design

Element 4 of the license condition required PG&E to assess the significance of the conclusions drawn from the seismic reevaluation studies performed in elements 1, 2, and 3 by utilizing a probabilistic risk analysis (PRA) and deterministic studies, as necessary, to ensure adequacy of plant seismic margins. In order to satisfy this requirement, PG&E performed detailed soil-structure interaction (SSI) studies to determine the effects of the dynamic interaction between the plant structures and the supporting rock medium on the seismic response of the structures, and to generate the plant structure responses needed for the PRA and deterministic evaluations of the structures, systems, and components. This section of the SSER deals with the specification of the earthquake ground motion that is exerted on the system.

3.7.1 Seismic Design Parameters

3.7.1.1 Ground-Motion Input

The ground-motion studies discussed in Section 2.5.2.3 of this SSER provided the seismic ground-motion input for SSI analysis. The input data consisted of the median and 84th percentile, horizontal and vertical, site-specific earthquake, acceleration response spectra for the plant site. As shown in the LTSP Final Report (Brand, 1988) both the median and the 84th percentile spectra, normalized with respect to peak ground acceleration (PGA) values, have almost the same spectral shapes. Therefore, responses evaluated for one level of ground-motion spectra can be converted readily and with good accuracy to a different level.

The LTSP ground-motion study provided, for SSI analysis purposes, three sets of three-component actual earthquake ground-motion time histories associated with the site-specific response spectra. However, the SSI analyses were actually performed using the following two sets of ground-motion records after adjustments: (1) the Tabas records of the 1978 earthquake in Tabas, Iran, and (2) the Pacoima Dam records of the 1971 San Fernando earthquake.

Before they were used in the SSI analyses, these ground-motion time-history records were first adjusted for magnitude, distance from source to site, and local site conditions, and they were then further modified so that the resulting response spectra for systems with 5 percent of critical damping matched closely the corresponding median response spectrum used in the deterministic assessment of seismic margins. This was accomplished by modifying the Fourier amplitudes of the ground-motion records and keeping their phase angles the same. The absolute maximum pseudo-acceleration of the median spectrum is 1.4g, and its average value in the frequency range from 4.8 Hz to 14.7 Hz is 1.25g. The frequency range was chosen considering the fragility evaluations described in Section 23.4.5 of this SSER.

The modified ground-motion histories obtained in this manner were subsequently scaled up by a factor of 1.6 to correspond to the reference level of ground shaking used in the plant fragility evaluations. The maximum value of the corresponding 5-percent damped response spectrum is thus 2.2g and its average value in the frequency range from 4.8 Hz to 14.7 Hz is 2.0g. The latter spectrum and the associated ground motions are somewhat larger than the site-specific, 84th percentile level of the reanalysis response spectrum. The absolute maximum pseudo-acceleration for the latter spectrum is slightly less than 2.0g. The maximum peak ground acceleration for each of the two horizontal components of the modified Tabas and Pacoima records obtained in this manner range from 0.96g to 1.01g.

Although not specifically stated above, the ground-motion input is specified at the ground level as required by Section 3.7.1 of the Standard Review Plan (SRP) (NUREG-0800) (USNRC, 1981).

3.7.1.2 Conclusions--Seismic Design Parameters

After reviewing the information provided by PG&E in the LTSP Final Report, the staff concludes that PG&E has considered the maximum earthquake on the Hosgri fault for developing the median and 84th percentile horizontal and vertical LTSP response spectra. These spectra were used in the SSI analysis, and in the engineering deterministic evaluations, of Category I structures and equipment for the LTSP. As discussed in Section 2.5.2.3 of this SSER, the staff has accepted these LTSP site-specific spectra as appropriate for the Diablo Canyon plant site except for frequencies at or below 1 Hz in the horizontal spectra and for frequencies between 1 and 10 Hz in the vertical spectra.

3.7.2 Soil-Structure Interaction Analysis

The scope of the SSI analysis performed by PG&E consisted of the following tasks: PG&E (1) determined the site rock profiles and properties; (2) developed suitable analytical models for the power block structures; (3) validated two SSI analysis computer programs, CLASSI and SASSI; (4) conducted parametric studies to assess sensitivity of structural responses to the assumptions made, and identify significant parameters; and then (5) performed SSI analyses to obtain the responses of the power block structures subjected to coherent, vertically propagating plane, seismic wave inputs consistent with the site-specific earthquake response spectra. In addition to these basic tasks, PG&E also developed necessary computer tools for analyzing the effects of spatial incoherence of ground motions to obtain the spatial incoherence adjustment factors, and performed nonlinear SSI analysis to consider the non-linear base-uplifting response behavior of the containment base.

The results of the SSI analyses were reported in the LTSP Final Report (Brand, 1988) which was reviewed by the NRC staff and its consultants contracted through Brookhaven National Laboratory (BNL). As listed in Appendix A of this SSER, several technical information exchange meetings, workshops, and audits were held between PG&E staff and NRC staff and their respective consultants both before and after the LTSP Final Report was submitted. Additional information was provided by PG&E in response to the questions and concerns raised by the NRC staff and its consultants. After reviewing the SSI aspects of the LTSP Final Report and the additional information provided by PG&E, the two BNL

consultants, Dr. C. Costantino and Dr. A. S. Veletsos, have furnished their technical evaluation reports (Reich, 1991a and b).

3.7.2.1 SSI Analysis Methodology

PG&E has reevaluated the SSI effects on the Diablo Canyon power block structures using state-of-the-art analysis techniques. The SSI studies included the following major elements: (1) development of suitable three-dimensional dynamic models for the power block structures, (2) characterization of site rock profile and properties, and (3) parametric studies to evaluate the sensitivities of SSI response and to identify important SSI parameters to be considered in the final response analysis. In this connection, PG&E undertook an extensive effort to develop appropriate analytical tools for the SSI analysis. This effort included (1) the implementation and validation of the CLASSI and SASSI computer programs for three-dimensional analysis, (2) the development and validation of analysis methods and computer programs for SSI analysis incorporating the spatial incoherence of seismic ground motions, and (3) the modification and validation of the SSI analysis method and computer program for analyzing the nonlinear dynamic response of the containment building to base-uplifting.

3.7.2.1.1 The CLASSI and SASSI Codes

The SSI analyses were implemented with the aid of extended versions of two large computer programs CLASSI and SASSI (Bechtel, 1988a and b). In addition to the responses of arbitrarily shaped foundations supported on a layered half-space, these programs can be used to evaluate the harmonic and transient responses of structures supported on such foundations. They can also be used to evaluate the responses of groups of structures and the associated effects of structure-to-structure interaction. These programs utilize three-dimensional linear methods of analysis.

The inputs in these programs are represented by plane wave fields of arbitrary angles of incidence. The supporting medium is modeled as a half-space composed of a series of uniform, horizontal layers of elastic or visco-elastic material, and the foundation basemat itself is represented by finite elements. The CLASSI program is applicable only to surface-supported rigid foundations, whereas the SASSI program may also be used to account for the effects of foundation embedment and basemat flexibility.

The SASSI program uses the output from the SHAKE program (Schnabel and others, 1976) to obtain the strain-dependent properties of the foundation medium (soil or rock) for use in the SSI analysis of the power block structures. Once these properties are determined in the beginning of the dynamic SSI analysis, they are not changed during the subsequent time-steps of the dynamic analysis. This is a limitation of the SASSI code as it is currently coded and used in the LTSP. This is in contrast to the FLUSH code or similar computer programs which iterate on the properties of the foundation materials during each time-step of the dynamic analysis. Another limitation of the SASSI program, as it is coded now, is that the strains and the stresses in the supporting foundation medium cannot be determined by the SSI analysis using this program. However, these limitations do not affect the usefulness of the SASSI program for the SSI studies in the LTSP because of the particular nature of the foundation rock

material at the Diablo Canyon site, which does not exhibit significant reduction in stiffness due to increased strain, as discussed later in Section 3.7.2.2.2 of this SSER.

3.7.2.1.2 Audit of the CLASSI and SASSI Codes

In June 1987, the NRC staff and its consultant, Dr. Costantino, audited PG&E's calculation program using the CLASSI and SASSI computer programs. The purpose and scope of the audit are discussed in detail in Reich (1991a). Briefly, the audit team examined the following three types of calculations performed by PG&E to validate the two computer codes:

(1) calculations for given structure/half-space configurations for which analytic solutions are available for comparison purposes

(2) calculations for specific configurations using both computer codes for mutual comparison

(3) calculations using either computer code for configurations applicable for the Diablo Canyon site

The objective of the first set of calculations was to ensure that the codes are generating results which are compatible with known analytic solutions. The second category of calculations showed that both the SASSI and CLASSI codes yield the same response results for the same configuration, while the third set of calculations generated SSI response results applicable to the Diablo Canyon site. The specific objectives of the audit team were to

(1) Ascertain and evaluate the applicability of the analytic bases and formulations of both the CLASSI and SASSI codes.

(2) Perform a detailed audit of the modifications made to the programs and the calculations made by PG&E.

(3) Quantify the specific ranges of applicability of the codes by determining ranges of numerical stabilities and computational sensitivities.

(4) Audit the numerical output generated for both the generic structure/half-space configurations and the specific configurations of interest at the Diablo Canyon site.

Table 1 in Reich (1991a) lists the test problems used in the validation phase of the LTSP to test the various phases of each solution algorithm.

The CLASSI code treats the response of arbitrarily shaped rigid foundations resting on the surface of an elastic layered half-space. It does not treat either flexible or embedded foundations. It has the capability to generate frequency-dependent impedance functions and scattering matrices for the case of non-vertically propagating body waves. The version of CLASSI implemented by PG&E has been modified to include (1) new algorithms for computing and inverting Green's functions, (2) capability to determine forced vibration response of structures, and (3) capability to treat multiple foundations to allow for the study of structure-to-structure interaction. PG&E benchmarked

the updated CLASSI code by comparing results generated by CLASSI with available solutions for 16 test cases. These test problems were selected specifically to allow for the separate evaluation of the principal sections of the code, namely, the impedance, scattering, and forced response calculational details of the computation.

As was just mentioned, the formulation of the CLASSI program used in the LTSP cannot treat two important aspects of interest in the Diablo Canyon seismic evaluation, namely, foundation flexibility and embedment effects. To overcome these restrictions, the SASSI code was also used by PG&E. The SASSI code is restricted to treat the elastic, horizontally layered, rock/soil site, but uses a finite element formulation for the foundation model to allow for inclusion of both the embedment and foundation flexibility effects. Again, PG&E undertook a detailed effort to check the validity of the code. Modifications were made to expand the capability of the code as well as to enhance input/output options. The SASSI code was benchmarked by using a set of 20 test problems. The audit team reviewed in detail 6 of these 20 test problems which related to the three primary aspects of the SSI problem mentioned earlier.

In addition to the comparison problems discussed above, specific calculations for foundation configurations appropriate to the Diablo Canyon site were reviewed. These calculations were made using both the CLASSI and SASSI codes. The foundation was discretized into a three-layer rock system overlying an elastic half-space, with the foundation mat placed at El 91 ft. The shear wave velocity of the rock varied from 2600 feet per second (fps) to 4800 fps and corresponded to the best estimate properties of the site developed during the evaluations performed in the earlier phase of LTSP. The input to these calculations was an artificial time history fitted to the original Hosgri seismic response spectrum.

Calculations were made for both the reactor containment building and the auxiliary building, using appropriate stick models developed for these facilities. The stick model used for the reactor containment building was a simplified two-stick model, one stick representing the outer containment shell and the other the internal structure. For the auxiliary building, a single-stick model was used for these sensitivity studies, including appropriate eccentricity of mass at various elevations. The audit team examined plots of stiffness and damping characteristics as a function of frequency used for these stick models. The foundation slab for these evaluations was considered to be rigid. For those structural configurations run with both CLASSI and SASSI, response spectra were compared for the horizontal responses at the springline of the outer shell, the top of the internal structure and the base slab of the containment structure. Similar responses were calculated at the operating floor level and grade elevations of the auxiliary building.

The comparison of the CLASSI and SASSI results indicated excellent agreement over the entire range of frequencies considered in the computations. Both the structural frequencies, including SSI effects, and the peaks of the computed responses, agreed. These computations indicated that either the CLASSI or the SASSI code could be used with confidence, where appropriate, as they yield consistent results for the cases studied.

The results of the audit indicate that the validation by PG&E of both the CLASSI and SASSI computer codes was reasonable, based upon the comparison of

computed and available solutions for both the generic and the Diablo Canyon site-specific problems. PG&E has modified and tested the two computer programs and has demonstrated that these two codes, although based on different concepts, yield essentially the same results in the regions of their applicability. At the time of the audit (June 1987), recommendations were made to PG&E to ensure that the numerical results which were not yet generated for the plant structures would be complete and reliable. It was suggested that PG&E include in the LTSP Final Report a description of all those numerical criteria that are necessary when using either computer program to ensure numerical stability and accuracy of the computations.

Following the audit, PG&E submitted to the NRC four volumes describing the details of this computational program. These reports are complete and detailed enough to allow a reviewer to judge the applicability of the approach for the LTSP. At the time of the issuance of the LTSP Final Report, a question remained on the development of specific criteria to determine the frequency ranges over which the calculations were applicable (that is the frequency cutoffs above which the SSI calculations are considered inadequate). In response to questions (Shiffer, 1990e), PG&E has stated that the site-specific calculations are adequate up to a frequency of 25 Hz for the reactor containment building and the auxiliary building, and 20 Hz for the turbine building, and that these upper-bound frequencies are above the frequencies at which the PGA value is reached for the various structures of interest. On this basis, it can be concluded that the results using both the CLASSI and the SASSI codes to predict the Diablo Canyon site response are acceptable. However, in view of the importance of the foundation embedment and basemat flexibility for some of the power block structures, the majority of the final analyses were made using the SASSI code. The effects of ground-motion incoherence were evaluated using an extended version of the CLASSI code.

3.7.2.2 Modeling of Structures and Rock Foundation

3.7.2.2.1 Structural Modeling and Ground-Motion Wave Effects

For the final phase of the LTSP, three-dimensional structural models were developed for the reactor containment building, the auxiliary building, and the turbine building along with the turbine pedestal.

The model for the containment structure was a multi-stick model, one stick representing the outer containment shell and the other sticks representing the internal structures. The outer stick was similar to that used in previous evaluations of the plant during the independent design verification program (IDVP), and the sticks representing internal structures were suitably simplified from those originally developed. The foundation basemat was suitably discretized for input to the CLASSI/SASSI codes to satisfy the criteria developed during the code validation phase of the study.

The models used for the auxiliary and turbine buildings were developed from analyses of large finite element models of these structures, since these superstructures are large framed structures with some internal shear wall components. These models were developed originally during the IDVP evaluations and used to generate equivalent stick models of these structures for the LTSP. The sticks used in the LTSP evaluations were selected to yield the primary

modal properties (frequencies, mode shapes, and modal masses) of these structures.

In a parametric structural analysis program conducted to assess sensitivity of computed structural responses to the assumptions used in these models, simplified structural models were used with the CLASSI/SASSI computations to investigate SSI effects. Simplified models were generated for these power block structures to simplify the computational effort. For example, a two-stick model was used for the containment structure, while the stick model used for the auxiliary building was a single-stick model including three-dimensional eccentricities at various elevations. The foundation models used in the SASSI/CLASSI analyses were assumed to behave as rigid basemats.

Various problems were investigated, including fixed-base analyses, surface-supported structures, embedded structures, models of both the containment and auxiliary building together to assess building interaction effects, with the models located at both the surface and embedded. In addition, solutions were obtained for a variety of wave field inputs, including vertically propagating SV waves, inclined SV waves, and horizontally propagating SH waves. These analyses were performed to estimate inertial and kinematic interaction effects on the SSI response.

Independent evaluations of some of these effects were made by Dr. Veletsos, a staff consultant, in an effort to check the adequacy of the models being used by PG&E. In general, it was concluded from his evaluations that the approaches being used for modeling the power block structures were adequate and the results being obtained by PG&E were reasonable. For the containment structure (i.e., the shell and the internal structure), it was concluded that the responses could be reasonably evaluated by considering only the fundamental mode of response, and that the maximum values of critical structural responses were in good agreement with those obtained from single-degree-of-freedom models of the structure. For the containment structure, it was found that the SSI effects were dominated by inertial interaction effects and that kinematic interaction effects were relatively small. Results of the independent evaluations performed by Dr. Veletsos are more fully discussed later in this SSER and in Veletsos and Tang (1987).

In general, the structural models used by PG&E are capable of accounting for all important aspects of the seismic response of the plant structures, and are fully adequate for the LTSP studies.

3.7.2.2.2 Site Rock Profile and Properties

The primary site investigation data that were used to estimate rock properties were obtained from four deep boreholes made at the site in 1977. The data obtained from these holes consist of (1) downhole shear and compression wave velocity data, (2) cross-hole compression wave data, (3) Birdwell sonic logging data, and (4) some cyclic triaxial and resonant column test data to estimate the influence of shear strain on rock properties (shear modulus and effective hysteretic damping). The results of these data compared reasonably well with the original data obtained in 1968 for the upper 50 ft of the rock overburden. The resulting rock profile used in the SSI calculations for the site consisted of a shear wave velocity profile with a mean value of 2600 fps at the rock

surface near the plant grade and increasing in value to about 4800 fps at a depth of about 165 ft below the plant grade level at El +85 ft (Brand, 1988). The upper and lower bound limits selected for the site varied from ± 50 percent in the near surface rocks to ± 25 percent in the rocks located at El -80 ft and below. Most of the plant structures of interest are founded at elevations between +50 ft and +80 ft. These bounding ratios of shear moduli are less than the values recommended in Revision 2 of the SRP (NUREG-0800) for SSI calculations. However, variations in rock shear moduli are generally low and the bounding values of shear wave velocity used in the SSI calculations were found to envelope the low-strain velocities determined from the down-hole shear-wave data obtained during the 1977 field investigations. As described below, correlation of analytically computed and measured structural responses confirmed the adequacy of the low-strain shear-wave velocity data. On this basis, this range of variability is considered adequate.

Hysteretic damping ratios assumed for the rock throughout the depth of interest in the SSI calculations performed with the SASSI/CLASSI codes was 2 percent. This value was then compared with damping ratios obtained from resonant column and dynamic triaxial tests, which showed that measured damping ratios even at low-strain levels exceeded this assumed value. This was shown to be true for the case of measured damping ratios plotted either against depth or against test strain levels. This assumption of low hysteretic damping ratio is judged to be conservative, since it is expected that the results obtained by using higher damping values will lead to lower values of computed peak structural response in the SSI calculations.

It should be noted that the low level of damping used in the calculations refers to material damping only and is represented in the SASSI/CLASSI calculations by equivalent visco-elastic material behavior. However, in these SSI calculations, significant radiation damping levels are automatically included in the response evaluation since the complete three-dimensional aspects of the problem are incorporated into the solution. This radiation damping represents energy transfer away from the site from outgoing wave motion into the infinite field and represents an important aspect of the problem. In previous SSI analyses using lumped parameters, an arbitrary (usually low) limit of total damping including both material damping and radiation damping was imposed. No such limit on radiation damping is imposed in the present analyses because of the very nature of the solution procedure in CLASSI/SASSI codes. This will result in smoother response curves because large peaks at certain frequencies obtained in previous analyses have been eliminated.

One-dimensional, free-field deconvolution procedures were performed to determine compatible values of shear moduli as a function of strain level and depth in the rock, using the input ground motion specified at the ground surface. These degraded shear moduli were then used as input to the SASSI and CLASSI codes to define the elastic properties of the free-field rock materials. No further iteration of soil properties was done in these calculations since these codes, as currently written, are not capable of performing such iterations. The plot of shear modulus ratio (G/G_{max}) as a function of cyclic shear strain used in these deconvolution calculations was compared with the data obtained from the dynamic triaxial and resonant column tests on the rock material. The results of the comparison indicate that the shear modulus

degradation curve used in the SSI calculations is reasonable for these problems.

Additional calculations were made using higher values of input motion, scaling the time histories used to reach values of 1g peak acceleration. The purpose of this study was to attempt to bound the amount of degradation of rock properties with straining that could be anticipated for this site. At these higher levels of rock input motions, degraded shear moduli were calculated using the SHAKE computer code and were found to reach a value of about 85 percent of the low-strain shear moduli. Since SSI stiffness is proportional to the shear modulus, this change in shear modulus would correspond to a change in interaction frequency proportional to the square root of the shear modulus, or only about 8 percent. Thus, it can be concluded that the effect of strain degradation of the rock properties is small, even for these larger input motions.

Numerical studies were then performed with the CLASSI code using a stick model of the containment building. This study determined the sensitivity of the computed frequency to the variability in shear modulus from the lower-bound to the upper-bound values used in the calculations. These results showed that the computed frequency shifted from 3.3 Hz for the lower-bound rock model to 4.6 Hz for the upper-bound rock model. This result indicates that the variability of the rock properties agrees reasonably well with the spectral peak widening of ± 15 percent usually used in determining design floor response spectra.

A parametric study performed by PG&E indicated that the effects of variations in the Poisson's ratio and material damping within the ranges of values considered appropriate were found to be negligible. A constant Poisson's ratio was used in the SSI analysis.

Comparison of computational results with recorded site data obtained for a few small events agreed well with the analytically computed responses using the mean values of the site rock properties. The events considered were the Point Sal earthquake of May 28, 1980, the Coalinga earthquake of May 2, 1983, and the Santa Maria earthquake of June 20, 1984. Comparisons of responses both in the free field and in the structures of the power block were used to estimate the SSI frequency during these events. For example, the analytically determined SSI frequency for the containment building was calculated to be 4 Hz, while the measured frequency varied from 3.8 to 4.2 Hz, thus agreeing within ± 5 percent (Reich, 1991a). On this basis, the values of the data assumed for the free-field rock properties used in the SSI calculations are considered reasonable.

In summary, the characterizations of the rock profile and rock properties at the plant site are considered reasonable and proper for the conditions studied in the LTSP.

3.7.2.3 Parametric Studies of SSI Effects

PG&E performed a series of parametric studies to assess the SSI response sensitivities to various parameters and to identify those parameters that are important for the SSI modeling and analysis for the power block structures. The parameters that were studied are: (1) the foundation embedment effect, (2)

the structure-to-structure interaction effect, (3) the effect of non-vertically incident seismic wave inputs, (4) the basemat flexibility effect, (5) the sensitivity of results to the CLASSI/SASSI solution techniques, (6) the importance of strain-dependency of the site rock shear modulus under high-intensity earthquake conditions, and (7) the effects of variations in Poisson's ratio and material damping ratio for the foundation rock. The results of the studies for parameters 5, 6, and 7 have been discussed earlier in this SSER. A brief discussion of the effects of other parameters follows.

A comparison of the floor response spectra at El 140 ft of the auxiliary building for surface-founded versus sub-surface (embedded) founded conditions shows that the foundation embedment effect is relatively important. As shown in Figure 5-14 of the LTSP Final Report, the embedment effect reduces the peak spectral acceleration for frequencies greater than about 3 Hz.

The effects of structure-to-structure interaction were found to be relatively insignificant for the rock-supported primary structures, indicating that individual structures can be analyzed separately for obtaining the desired structural responses.

The results of the solutions obtained using inclined body waves indicate that the use of vertically propagating waves is a conservative assumption to use in the structural evaluations.

The effect of basemat flexibility was found to be relatively important for the auxiliary building, as shown in Figure 5-17 of the LTSP Final Report. Therefore, PG&E has concluded, and the staff agrees, that, for structures having basemats of large plan dimensions, the basemat flexibility should be considered in the SSI models.

As discussed earlier in this section of the SSER, the CLASSI and SASSI programs produce solutions that compare closely with each other. Therefore, the choice of either computer program can be based on the suitability of foundation model assumptions for the specific application.

3.7.2.4 Soil-Structure Interaction Studies

3.7.2.4.1 Coherent Ground Motions

The response of the power-block structures to the modified, spectrum-compatible Pacoima Dam and Tabas ground-motion time histories was first evaluated assuming vertically propagating coherent wave fields. Both rigid and flexible conditions of support were examined, and the differences in the responses obtained for the two conditions were used to assess the inertial component of SSI. In addition to the response of the structures themselves, floor response spectra were generated for selected points of the structure. Since they were made to be compatible with the same response spectrum, the two sets of ground motions and the corresponding maximum responses were, of course, quite similar.

The inertial interaction effects were found to be substantial for the relatively short, stiff, internal structure of the containment, as well as for the auxiliary building, but small for the taller and more flexible containment structure and turbine building. The results for the containment and internal

structures are consistent with those obtained in the BNL-Rice University studies summarized in Section 3.7.2.5 of this SSER.

3.7.2.4.2 Ground-Motion Incoherence

The ground-motion incoherence effects associated with the horizontal spatial variation of the free-field ground-shaking were evaluated by use of random vibration theory. The ground motions in this phase of the study were specified stochastically in terms of local power-spectral-density functions and incoherence functions; the latter define the interrelationship of the amplitudes and phase angles of the Fourier components of the motion at two neighboring points.

The incoherence functions used were determined from analyses of ground motion records obtained during the following low-intensity events:

(1) the aftershocks of the Imperial Valley earthquake
(2) recent earthquakes in the region of the Diablo Canyon plant
(3) dynamite explosions in boreholes at the Diablo Canyon site
(4) airgun shots fired in the region of the Diablo Canyon plant

As might be expected, the degree of incoherence was found to increase with increasing separation between points and increasing excitation frequency.

Although the applicability of the results deduced from the low-intensity events, particularly the airgun shots, to the strong ground motions that are of interest in the reanalysis of the plant has been questioned, the approach used in this phase of the program is at the forefront of the current state of knowledge, and it is as rational and refined as can be made at this time, as judged by the BNL consultant, Dr. Veletsos (Reich, 1991b).

The ground-motion incoherence analyses were implemented with the aid of an extended version of the CLASSI computer program, coupled with Bechtel's PROSPEC program (Brand, 1988). In addition to the responses of the plant structures, floor-response spectra were evaluated for selected locations of the structures, and the results were normalized with respect to those obtained for coherent free-field ground motions of the same maximum ground acceleration.

It was found that ground-motion incoherence generally reduces the maximum response of a structure, and that the reduction increases with increasing frequency of input excitation and the plan dimensions of the foundation. The reduction was found to be minimal for the containment shell and internal structure, of the order of 15 percent for the auxiliary building, and about 20 percent for the turbine building. Similar reductions were computed for the peak values of the associated floor-response spectra. These results are deemed to be reasonable and consistent with those found in the BNL-Rice University studies for the containment structure (Veletsos and Tang, 1987; Veletsos and others, 1988) and in other recent studies (Veletsos and Prasad, 1989).

3.7.2.4.3 Effects of Basemat Uplift on Responses

The issue of potential liftoff effects and their impact on SSI predictions for the Diablo Canyon plant structures was brought up during the licensing hearings

for Unit 1. The design input motions associated with the postulated Hosgri event were felt to be high enough that this issue should be evaluated as part of the LTSP. At the initiation of the LTSP, it was suggested that liftoff be addressed in the deterministic phase of the study, as well as in the PRA evaluations.

At a workshop to evaluate the progress of these evaluations, PG&E presented the result of calculations of structural responses for the containment structure, using three of the sets of ground motions obtained from the empirical ground-motion program. These indicated that liftoff could occur for these motions that may be considered appropriate for this site, although the magnitude of liftoff effects was considered small. After the initial review of these evaluations, it was felt that PG&E's method of analysis did not account for several items that may influence the computed response, for example, (1) loss of sidewall support due to compaction of the surrounding backfill during rocking motions; (2) impact effects on slapdown, after separation, which serve to couple vertical and horizontal motions and cause frequency shifts in the response; and (3) the effect of small modifications in the time phasing between horizontal and vertical input motions on the computed responses.

To assess the significance of these concerns, the details of the analysis of liftoff and the corresponding computer program UPLIFT used in the calculations were reviewed (Reich, 1991a). The results of this review indicated that the UPLIFT computer code used by PG&E for the liftoff calculations was operating as intended and developed reasonable estimates of response. The evaluations of the three concerns listed above are described in the following paragraphs.

Loss of Sidewall Support

The impact of the potential loss of sidewall support due to compaction of the surrounding backfill around the reactor containment building was addressed by considering structural responses using a reduced condition of sidewall support as compared to the original calculations. This is a reasonable engineering approach to evaluating the potential impact of the loss of sidewall support on the reactor containment building. The results indicate that even assuming full tension cutoff on one side throughout the rocking motion of the building leads to only a small change in calculated structural response spectra, while not severely overstressing the foundation bedrock through excessive bearing pressure (Reich, 1991a). The staff considers this assumption of full tension cutoff on one side to be conservative.

The computer output from the UPLIFT calculations was reviewed in detail to check these conclusions. The specific calculations reviewed made use of the Tabas north-south component as input to the stick model of the reactor containment building. The input motion was scaled to reach an average spectral acceleration of 2.25g in the 3 to 8.5-Hz frequency range. Data output for the full lateral sidewall support did not significantly affect the calculated spectral responses.

Slapdown Effects

In previous evaluations of liftoff effects on structures (Miller, 1986), it was found that significant amounts of effective damping had to be added to the

simplified computer models of the liftoff phenomenon to account for the effects of separation and slapdown of the base of the structure with the foundation soils. Slapdown effects influence two separate aspects of the structural response problem. Firstly, as slapdown occurs, the effective base area in contact with the soil changes rapidly and the change in the location of centroid and magnitude of the resulting bearing pressures causes a net additional overturning moment which serves to couple the rocking and vertical responses of the structure. Secondly, large effective slapdown damping, required to suitably model experimental results, causes significant shifts in interaction frequencies and broadening of the calculated response spectra. This effective damping was found to be significant when evaluating the importance of liftoff (Kennedy and others, 1976).

A review of the calculations performed by PG&E indicated that the neglect of the effects of slapdown damping yielded only small changes in calculated spectral responses for the configuration and amount of uplift computed for the reactor containment building. The staff thus concludes that the calculated responses neglecting these slapdown effects and using input motions at peak acceleration levels appropriate for the site are reasonable.

For the study of responses associated with higher spectral accelerations required for the hazards assessment program, the PG&E staff stated at the review meeting that the liftoff effects at higher acceleration levels would not be significant. This result was determined by using previously available data obtained for the evaluation of the high-temperature gas-cooled reactor (HTGR) containment (Kennedy and others, 1976). The building configuration in that calculation is similar to that of the Diablo Canyon reactor containment building and the effects of uplift were found to be scalable by using the ratio of the square of the peak ground acceleration (PGA). The application of these results to the Diablo Canyon reactor containment building indicates that such uplift effects even at the 3g level are small.

Time Phasing

The uplift calculations were performed using three sets of scaled, three-component, recorded, ground-motion input data sets, namely, the Pacoima Dam, Tabas, and El Centro No. 4 records. The uplift calculations were performed using the vertical component with each of the two horizontal records of the set, leading to a combination of six complete uplift calculations. A question was raised during the review about the potential impact of small perturbations in time phasing of strong shaking on the computed uplift effects. For such a nonlinear response problem, where horizontal and vertical motions couple through the uplift effects, time phasing can become important when determining maximum responses. The calculations should, therefore, cover the anticipated range of changes in the phasing of the vertical ground-motion component with the horizontal components. The PG&E staff presented comparisons of the time histories for these six input data sets which indicated that the time phasing of the strong motion shaking was different for the six record sets. For example, strong shaking occurs late in the strong-motion period for the Pacoima records, while it occurs early in the El Centro input sets and in the central portion for the Tabas set. In addition, the time interval between the peaks of the horizontal and vertical records for these sets is also different. Finally, uplift effects were found to be small, and not significantly different from

each calculation. On the basis of these results, the staff concludes that the time phasing concern has been adequately addressed.

Conclusions--Uplift Effects

On the basis of this assessment, the staff concludes that the potential effects of liftoff for the reactor containment building are small and do not lead to any significant changes in structural responses at important equipment support points.

3.7.2.5 Independent Check of SSI Analysis

Dr. A. S. Veletsos of Rice University (one of the consultants advising the NRC staff on the SSI analysis aspects of the LTSP) performed an independent study using a simplified analytical model of the power-block structures. (This study is referred to here as the BNL-Rice study, since Dr. Veletsos was working under a BNL contract with the NRC.)

The analyses were implemented on the following bases:

(1) without any soil-structure interaction, that is, considering the structures to be rigidly supported at the base

(2) with inertial interaction only, that is, providing for the dynamic coupling between the structure, foundation, and supporting rock medium, but disregarding the horizontal spatial variation of the free-field ground motion

(3) with total soil-structure interaction, that is, considering both the inertial and the kinematic interaction effects, which are associated with the spatial incoherence of the free-field ground motion

In the analyses of the rigidly supported systems, the containment shell and internal structure were modeled, as in the original studies, as stick-like systems with a total of nine and two concentrated point masses, respectively.

By contrast, in the analyses of the elastically supported systems, both the containment shell and the internal structure were presumed to vibrate in their fixed-base, fundamental natural modes as single-degree-of-freedom systems. This approximation was shown to be sufficiently accurate for the conditions considered.

Ground Motions Considered and Responses Evaluated for the BNL-Rice Study

The rigidly supported systems were analyzed for two sets of earthquake ground motions:

(1) an empirical set, composed of the 24 horizontal components of 12 strong ground-motion, near-source recordings

(2) a set of 28 horizontal components of 14 numerically generated ground motions

The elastically supported systems were analyzed for only three records from the empirical set. The foundation in the latter analysis was presumed to rest at the surface of a homogeneous, visco-elastic half-space with a shear wave velocity of 3300 fps and a material damping factor of 2 percent of critical damping.

The ground motions were presumed to be induced by vertically propagating coherent and incoherent wave fields. The horizontal variation of the ground motion for the incoherent wave fields was represented approximately by a phase-independent incoherence function, for which the amplitudes of the Fourier components at different points are exponentially decaying functions of the square of the exciting frequency and of the separation distance. The effects of the incoherent ground motions were evaluated by the approximate, semi-deterministic method of analysis described in Veletsos and Tang (1990).

The response quantities evaluated include the maximum values of the base shears and moments for the structures, the maximum displacements and accelerations at selected points, and response spectra for light equipment mounted at various points.

Findings of BNL-Rice Studies

The principal findings of these studies may be summarized as follows:

(1) The fixed-base dynamic characteristics (i.e., mode shapes and frequencies) of the containment and internal structures were identical to those computed by PG&E.

(2) Excellent approximations to the seismic responses of these structures were obtained by considering only the contributions of their fundamental modes of vibration. This finding justified the use of the simplified structural models in the analyses of the elastically supported, interacting systems.

(3) Under a broad range of conditions, reasonable approximations to the responses of the elastically supported containment and internal structures were obtained by neglecting their coupling through the foundation and analyzing each structure independently.

(4) For the ground motions considered, SSI was found to increase the maximum responses of the internal structure, and to either increase or decrease the corresponding responses of the containment structure. These changes, which ranged from a maximum increase of 40 percent to a maximum reduction of 18 percent, were due mainly to inertial interaction effects. The kinematic interaction effects were associated with a reduction in response and were generally small, especially for the relatively flexible containment shell.

(5) The variability in SSI effects referred to above was greater than that determined by PG&E. This is attributed in part to the fact that the ground motions used by PG&E had been adjusted to yield a smooth, design-type response spectrum, whereas those employed in the BNL-Rice studies were unadjusted records associated with highly irregular spectra.

(6) The variability in floor-response spectra due to the effects of SSI was generally substantially smaller than that due to the uncertainties involved in the definition of the free-field ground motion. This confirms the view that the proper definition of the design response spectrum is of far greater importance than the details of SSI analyses.

These findings are in general agreement with those of PG&E and the staff finds this to be a satisfactory resolution of the issues related to SSI effects.

3.7.2.6 Conclusions--SSI Analysis

On the basis of a review by the staff and its consultants of the LTSP Final Report and supplemental information related to the Diablo Canyon LTSP, the staff has reached the following conclusions: The analytical procedures developed and used by PG&E for performing the SSI analyses of the major power plant structures are comprehensive and thorough. These procedures utilize advanced state-of-the-art methodologies and large three-dimensional computer programs. During the course of the LTSP, PG&E has satisfactorily answered numerous questions by providing additional data and analytical results. These were related to the development and applicability of the computer codes, the adequacy of the properties of the foundation rock material used in the analyses, the development of suitable structural models to calculate the range of structural responses anticipated, and the evaluation of the potential effects of foundation base lifting and incoherence of ground motion on these responses. Therefore, the staff concludes that there are no outstanding issues related to the analytical methodology used in performing the SSI analyses, and the SSI analysis provides acceptable plant seismic responses.

3.8 Design of Category I Structures

3.8.1 Deterministic Evaluation of Structures and Equipment

Element 4 of the license condition required PG&E to assess the significance of the conclusions drawn from the seismic reevaluation studies performed in elements 1, 2, and 3 by utilizing a probabilistic risk analysis and deterministic studies, as necessary, to ensure the adequacy of plant seismic margins. The seismic margin for a given earthquake may be defined as the capacity of a specific plant structure, system, or component to withstand seismic motion, relative to the seismic demand, that is, the motion that will be produced by the given earthquake at the location of the plant structure, system, or component in question. Thus, if the capacity is greater than the demand, a positive margin results. In the probabilistic approach, the margin (and ultimately the risk) of a range of possible earthquakes is evaluated. In the deterministic approach, a single, "maximum" earthquake is postulated and the margin for plant structures and equipment is evaluated for that earthquake.

In order to comply with element 4 of the license condition, PG&E performed deterministic evaluations as well as PRA studies. In performing deterministic evaluations for the LTSP, PG&E obtained revised plant responses (the seismic demand) resulting from the LTSP maximum magnitude earthquake (the MME, a magnitude 7.2 earthquake at an epicentral distance from the plant of 4.5 km) and also determined plant capacities for key structures and equipment. These are designated "the LTSP" demand and capacity, and are to be distinguished from previous estimates, which are designated "the Hosgri" demand and capacity.

PG&E performed deterministic evaluations by (1) comparing the plant responses (demands) due to the LTSP MME with those used for the Hosgri evaluation, and (2) assessing the plant margin by comparing the LTSP capacities with the demands resulting from the LTSP MME. In addition, PG&E used two different methods to calculate the capacities of the plant structures and equipment. In the first, the fragility analysis (FA) method, PG&E derived the high confidence of low probability of failure (HCLPF) capacity of structures and equipment from the probabilistic fragility analysis results discussed in Section 23.4.5 of this SSER. In the second method, the conservative deterministic failure margin (CDFM) method (EPRI, 1988), less probabilistic concepts are used than in the first method to derive HCLPF values.

The objective in determining HCLPF values is to identify the highest level of ground motion for which the failure of a component is highly unlikely. In a mathematical sense, this value is the highest ground-motion level at which the probability of failure is less than 5 percent with a 95-percent confidence. The concept of HCLPF or seismic margin (Budnitz and others, 1985) was developed to assess the component capacity more realistically--using the best-estimate structural properties for seismic-margin evaluations rather than the code-based approach used for design. For example, in the seismic-margin assessments, the strength evaluation is partly based on the results of the available test data rather than the nominal code-specified values for the design. Seismic-margins methods have also been used in the Maine Yankee, Millstone 3, and Hatch seismic evaluations. The staff has previously used a similar approach in a less-formalized sense during reevaluation of the Diablo Canyon plant for the Hosgri earthquake. In both methods, the computed capacities of the structures, systems, and components are compared with the plant responses (demands) to assess the seismic margins.

The staff reviewed PG&E's deterministic evaluations and audited PG&E's calculations in December 1990 (Rood, 1991). The sections that follow summarize the results of the staff's review of the deterministic evaluations.

3.8.1.1 Ground-Motion Input for Deterministic Evaluation

The ground-motion input data used in the deterministic evaluation were the 84th percentile, 5-percent damped, horizontal and vertical, site-specific LTSP acceleration response spectra resulting from the MME. The LTSP site-specific, horizontal, ground-motion response spectra (SSRS) for 5-percent damping due to the MME and the 1977 Hosgri evaluation spectrum are compared in Figure 7-2 of the LTSP Final Report (reproduced here as Figure 3.1). It may be seen from this figure that the Hosgri evaluation spectrum is greater than the LTSP 50th percentile (median) spectrum at all frequencies, and is greater than the 84th percentile spectrum (called the "LTSP spectrum" in this section of the SSER) at all frequencies less than about 15 Hz. The magnitude of the exceedance at frequencies above 15 Hz is approximately 10 percent. On the basis of PG&E's margins evaluation discussed in Section 3.8.1.7 of this SSER, the staff concludes that these high-frequency spectral exceedances are not significant.

However, as discussed in Section 2.5.2.3 of this SSER, the NRC staff has concluded that the LTSP 84th percentile horizontal acceleration spectrum shown in Figure 3.1 underestimates the ground motions at frequencies at and below 1 Hz (see Figure 2.4). Also, the staff's estimate of the 84th percentile vertical

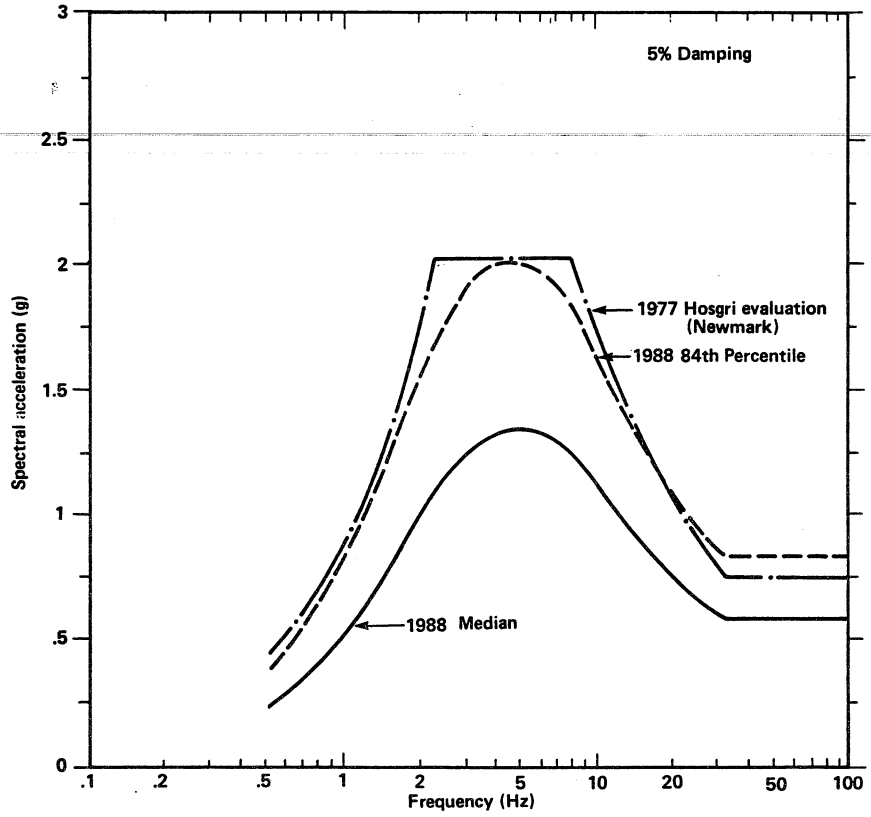


Figure 3.1
Comparison of the 1988 LTSP site-specific median and 84th percentile horizontal response spectra with the 1977 Hosgri evaluation (Newmark) response spectrum (Figure 7-2 in LTSP Final Report)

spectrum exceeds the LTSP spectrum over the frequency range from 1 to 10 Hz (see Figure 2.5). Both horizontal and vertical exceedances are on the order of 15 percent or less, as discussed in Section 2.5.2.3 of this SSER.

After determining that its estimates of the horizontal and vertical spectra exceeded the PG&E estimates, the staff requested that PG&E address the capability of plant structures and equipment to withstand the exceedances. In its response (Shiffer, 1991i and k), PG&E stated that it has evaluated the exceedances and has concluded that plant seismic margins are adequate to accommodate them.

PG&E noted that the horizontal exceedances only occur at low frequencies, and stated that no essential equipment or components at the plant have fundamental frequencies below 2.7 Hz. The plant structures that could be affected by the horizontal exceedances are made of structural steel, and include the pipeway structure, the fuel handling building superstructure, overhead cranes, tanks containing fluids, and the turbine building superstructure. PG&E has made a qualitative evaluation of each of these structures and has concluded that they all have sufficient seismic margin to accommodate the horizontal spectral exceedances postulated by the staff (Shiffer, 1991i). The staff has reviewed

PG&E's evaluation and finds it acceptable, but will require PG&E to perform an analysis of the plant structures that are subject to inelastic deformation, or that have had natural frequencies in the range of 1 Hz to confirm its conclusion that the seismic margins are adequate.

Similarly, PG&E has addressed the vertical spectral exceedances (Shiffer, 1991f) and concludes that the plant has adequate seismic margin to accommodate the vertical exceedances. PG&E states that the principal structures that could be affected by the vertical exceedances are roof and floor systems supported by structural steel beams and trusses, and some overhead cranes. PG&E notes that, for both the horizontal and vertical exceedances, the principally affected structures are steel, and have an inherent ability to resist high seismic loading without major structural failure, due to their inelastic energy absorption capability. In addition, components such as cranes are secured against liftoff, making them resistant to vertical forces. The staff has reviewed PG&E's evaluation of the vertical exceedances and finds it acceptable, but will require PG&E to perform an analysis of the plant structures that might be affected to confirm its conclusion that the seismic margins are adequate.

In summary, the staff finds PG&E's rationale for its conclusion that the sufficient seismic margins exist to accommodate the horizontal and vertical exceedances to be reasonable, and finds the conclusion acceptable. However, the staff will require that PG&E confirm its conclusion analytically.

3.8.1.2 Procedure Used To Determine Plant Responses

The horizontal seismic responses of the containment, auxiliary, and turbine buildings were computed using the SASSI code and the same three-dimensional dynamic models described in Section 3.7.2 of this SSER. The vertical responses of the structures to the 84th percentile LTSP ground motion were obtained by multiplying the vertical responses that were used for the Hosgri reevaluation by the ratio of the 5-percent damped 84th percentile, vertical ground-motion, LTSP spectrum to the 5-percent damped, Hosgri reevaluation, vertical ground-motion spectrum. The staff finds this method acceptable.

3.8.1.3 Conversion of SSI Analysis Results Into Plant Responses

The primary purpose of the SSI analyses was to determine the in-structure responses to the seismic ground motions. These responses were needed for the fragility analysis, the probabilistic risk assessment, and the deterministic evaluation. Because various parts of the LTSP were performed in parallel, the site-specific, ground-motion spectra were not in final form at the time results were needed for the fragility analysis. The SSI analyses were, therefore, performed using a "best estimate" spectrum, with a plan to adjust the SSI analysis results later on to be compatible with the site-specific ground spectra. The ground-motion spectral shape used in the SSI analyses was compared with the site-specific ground motion spectrum at the 84-percent level after the latter was tentatively completed before starting the deterministic evaluations. For this comparison, the ground-response spectrum used in the SSI analyses was scaled uniformly (using frequency-independent scaling) so that the average spectral acceleration between 3 and 8.5 Hz is the same as that of the 84th percentile site-specific ground-motion spectrum (1.94g). As seen from Figure 3.2, the site-specific, ground-motion spectrum matches the SSI analyses

input spectral shape reasonably well in the 3 to 8.5 Hz range. Since the SSI analyses were linear elastic, their results could be used with small adjustment factors to obtain plant responses to the finally selected site-specific ground motions.

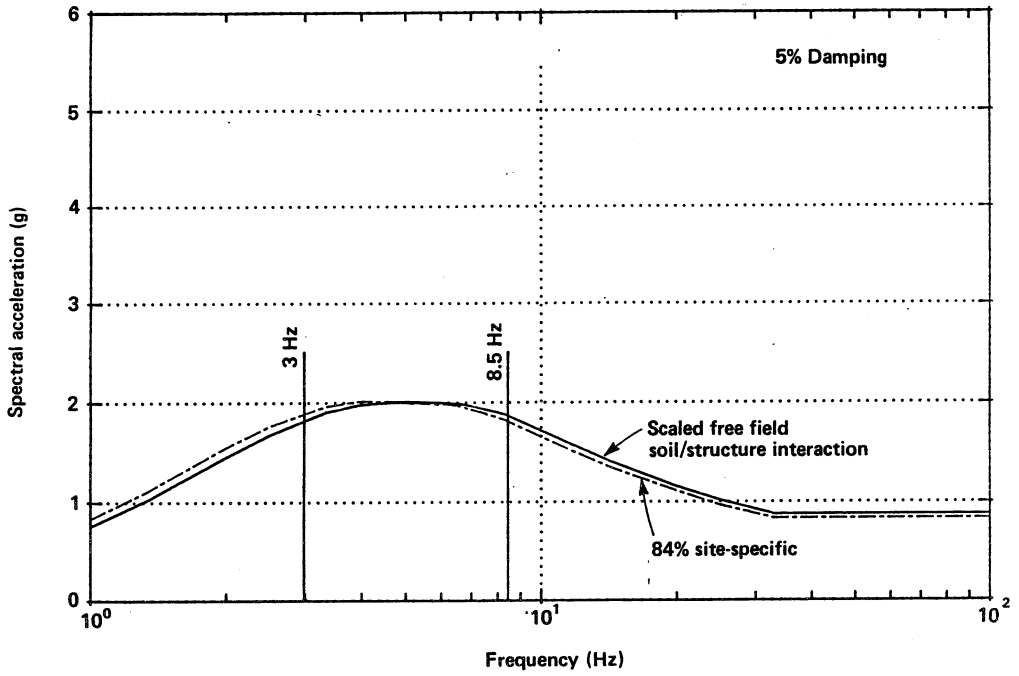


Figure 3.2 Comparison of scaled soil-structure interaction input with 84-percent probability of nonexceedance site-specific spectrum (Figure 7-3 in LTSP Final Report)

The following two adjustment factors were used to convert the SSI analysis results into the deterministic plant responses:

(1) a spectral shape factor (F_{ss}) to account for the minor variations between the site-specific, ground-motion spectrum and the SSI input spectrum

(2) a spatial incoherence factor (F_{gmi}) to account for the spatial variation of the ground motion

The spectral-shape factor is determined from the ratio of the response spectral ordinates of the free-field, site-specific, ground-motion spectrum (given in Figure 3.2) and the spectral ordinates of the SSI analysis smoothed input spectrum. This factor ranges from 0.86 to 1.0 for the 84-percent site-specific, ground-motion spectrum. These factors are applied to the SSI in-structure response spectra to obtain the plant responses at various floor levels due to coherent site-specific ground motions. By comparing plots of the site-specific, free-field, ground-motion spectrum with corresponding basemat response spectra at El 85 ft of the containment, auxiliary, and turbine buildings, PG&E has shown that, for frequencies above about 10 Hz, the SSI effect for coherent motion results in a reduction of the input motion to the basemat from the free-field motion. However, for frequencies lower than 10 Hz, the basemat

motion is slightly amplified. The effect of such amplification will be reflected in the plant responses (demands) that are determined for evaluating the plant seismic margins.

The development of the spatial incoherence factor, F_{gmi}, is described in Section 3.7.2 of this SSER. This factor is dependent on the plan area of the building foundation and the natural frequency of the building vibration, among other parameters. PG&E has shown that, for a specific site (i.e., Diablo Canyon), this factor generally reduces the building responses. The F_{gmi} factors are then applied to the response spectra developed for coherent, site-specific ground motions to obtain the composite effect of SSI. (A schematic of the above procedure is given in Figure 3.3.)

3.8.1.4 Comparison of LTSP and Seismic-Qualification-Basis Response Spectra

Originally, PG&E did not make a one-to-one comparison of the response spectra resulting from LTSP site-specific ground motions with the seismic-qualification-basis spectra (that were prepared at different times) from two other earthquakes, the double-design earthquake and the Hosgri earthquake. PG&E based this decision on the lack of direct comparability due to the differences between the LTSP assumptions and analysis methodology and those adopted for the Hosgri reevaluations. Although generally agreeing with PG&E's arguments in this area, during its review of the LTSP, the staff required PG&E to make this comparison to be able to judge the level of demand resulting from the LTSP ground motion. If the Hosgri responses were found to be greater than the LTSP responses, then no additional evaluation would be needed.

3.8.1.4.1 Comparison of Free Field and Basemat Response Spectra

PG&E has shown in Figure 3.1 that the 50-percent LTSP site-specific spectrum is enveloped by the 1977 Hosgri evaluation spectrum and that the 84-percent LTSP site-specific spectrum exceeds the Hosgri evaluation spectrum only at frequencies greater than about 15 Hz and only by about 10 percent. Using the LTSP ground-motion spectra as input, PG&E performed the SSI analyses and determined the response spectra at the top of the basemat. These response spectra include the effects of SSI, foundation embedment, and spatial incoherence of ground motions. PG&E then compared these responses to the corresponding Hosgri evaluation basemat (El 85 ft) response spectra that had been reduced from the free-field spectra to account for the tau effect (SSER 5) (USNRC, 1976). The tau effect in the Hosgri evaluation studies is generally analogous to the combined effects of SSI, embedment, and incoherent ground motion in the LTSP studies. However, unlike the LTSP studies in which variations in responses from point to point in the structure could be considered, in the Hosgri studies variations in the tau effect for different locations on the basemat could not be considered, because a "fixed base analysis" was performed and an average motion was assumed for all points on the foundation in the Hosgri evaluations. This is one of the reasons for the differences between the responses predicted by the LTSP and Hosgri studies at various structural frequencies.

A comparison of the results (i.e., spectra for basemat motions) shows that the responses to the 84th percentile, site-specific spectra exceed the response to the Hosgri evaluation spectra at various structural frequencies. The average values of these exceedances at frequencies of interest range from about 5

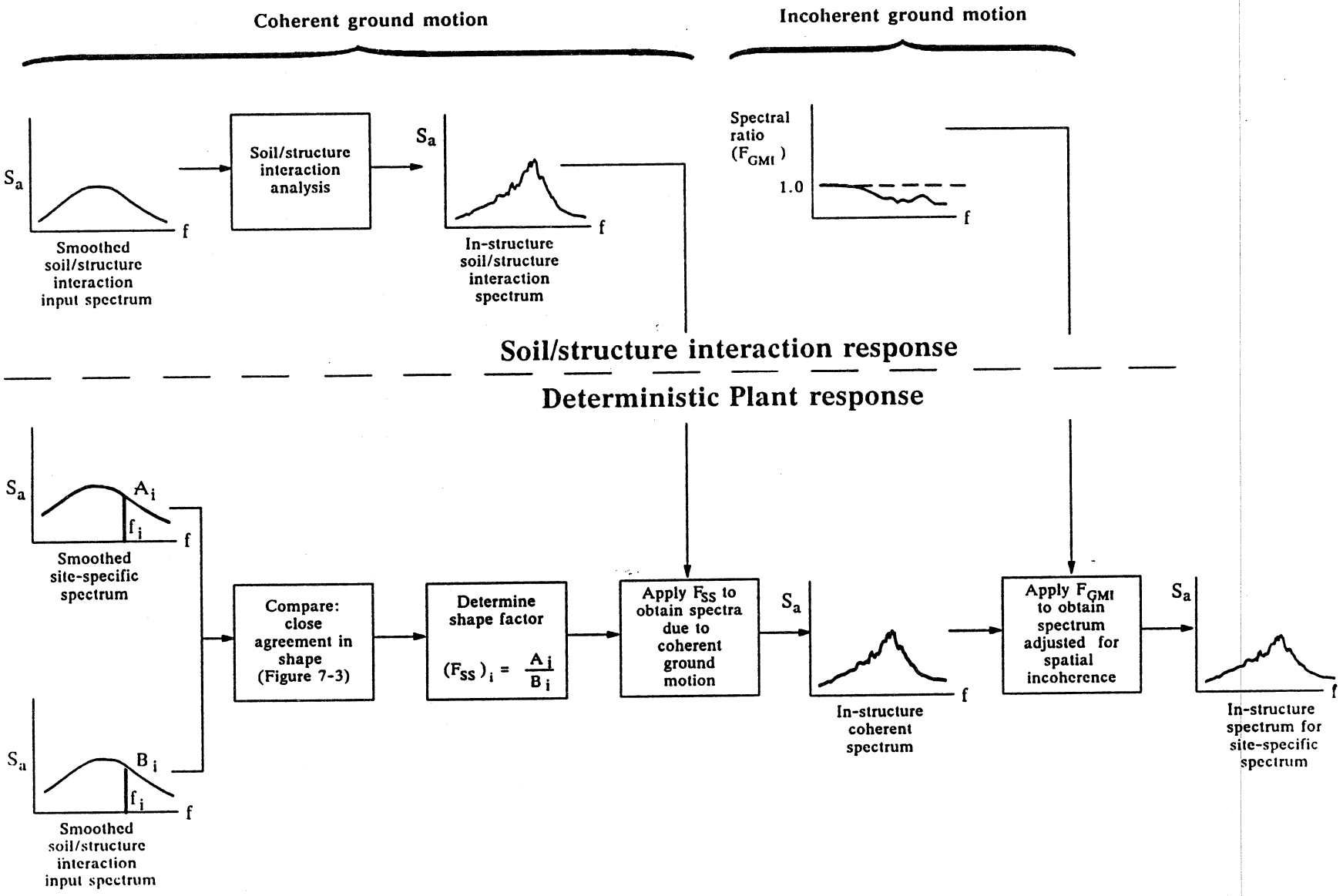


Figure 3.3 Overall process of developing plant responses (Figure 7-4 in LTSP Final Report)

percent for the containment building interior structure to about 10 percent for the auxiliary building. On the basis of PG&E's margins evaluation discussed in Section 3.8.1.7 of this SSER, the staff concludes that these high-frequency spectral exceedances are not significant.

3.8.1.4.2 Comparison of In-Structure Response Spectra

The primary purpose of comparing the in-structure response spectra predicted by the LTSP studies and the Hosgri studies is to assess the effect of the LTSP ground motions on seismic qualification of equipment. PG&E made the spectral comparisons for various locations that were selected on the basis of their importance in terms of structural design, or locations of critical safety-related components. The results of such comparisons indicate the following:

(1) For the operating floor at El 140 ft in the containment building interior structure, the seismic-qualification-basis spectra (which envelope the double-design earthquake (DDE) spectra and Hosgri spectra) exceed the LTSP in-structure response spectra in the 8 to 18 Hz range by a considerable margin as shown in Figures 3.4 and 3.5. Although not shown in these figures, PG&E has stated that the damping used for these two evaluations are different (Shiffer, 1989f). In spite of this difference in the damping (i.e., 5-percent damping for LTSP analysis, and 2-percent and 4-percent damping for the DDE and Hosgri analyses, respectively), the staff accepts PG&E's statement that, in the frequency range of 8 to 18 Hz, the qualification-basis spectra will exceed the LTSP in-structure response spectra because the difference in damping will not significantly alter the large differences in responses predicted by the two evaluations as seen in Figures 3.4 and 3.5. For other frequencies that are of interest to equipment qualification (5 to 8 Hz) the LTSP in-structure spectra generally exceed the qualification-basis spectra by about 15 percent, an exceedance that has been shown to be accommodated on the basis of PG&E's margin evaluations.

(2) In the case of the auxiliary building, the LTSP in-structure response spectra are exceeded by the qualification-basis spectra at all frequencies above about 8 Hz, while they slightly exceed the latter at frequencies between 3 and 8 Hz. In the frequency range of exceedance, the equipment is evaluated on the basis of fragility evaluations to determine seismic margins as discussed in Section 23.4.5 of this SSER.

(3) For the turbine building (El 119 ft), the LTSP in-structure spectra are generally enveloped by the qualification-basis spectra.

In summary, on the basis of its review and audit of selected equipment, the staff concludes that the existing seismic qualification of equipment continues to be acceptable, since the LTSP in-structure spectra are enveloped by the corresponding qualification-basis spectra. For certain essential equipment, the LTSP in-structure spectra exceed the qualification-basis spectra. Seismic margin assessments were made using CDFM and fragility evaluations to demonstrate that this equipment has adequate margin for the LTSP in-structure spectra.

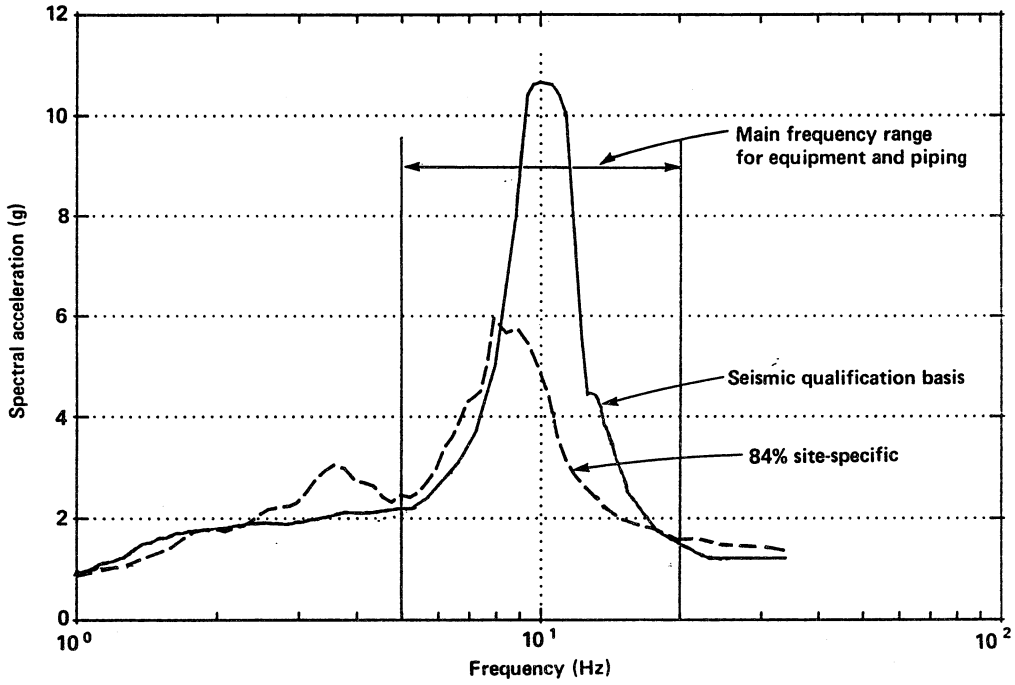


Figure 3.4 Comparison of floor-response spectra for equipment qualification for the containment building, interior structure, El 140 ft, north/south response (Figure 7-30 in LTSP Final Report)

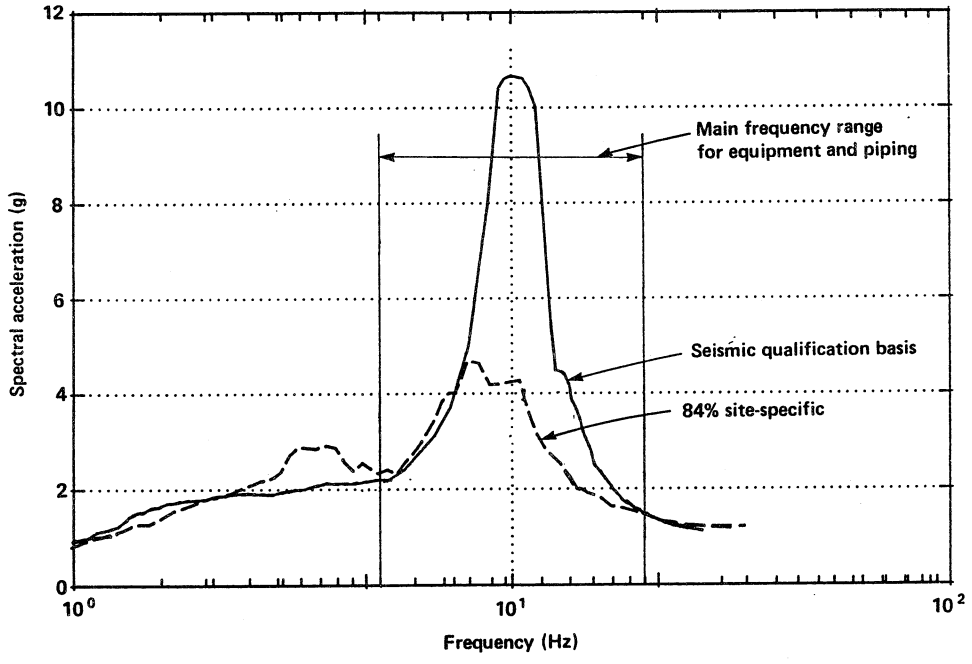


Figure 3.5 Comparison of floor-response spectra for equipment qualification for the containment building, interior structure, El 140 ft, east/west response (Figure 7-31 in LTSP Final Report)

3.8.1.5 Margin Evaluation Using Fragility Analysis Method

Capacities of Structures, Systems, and Components

In the LTSP Final Report, PG&E provided the results of a deterministic evaluation of the structures, systems, and components (SSC) performed using the high confidence of low probability of failure (HCLPF) capacities that were derived from the results of the fragility analysis used in the Diablo Canyon PRA studies (see Section 23.4.5 of this SSER). The concept of using the HCLPF seismic capacity estimates in seismic-margin evaluation of nuclear power plants has been accepted by the NRC as discussed in the beginning of this section of the SSER.

All fragility estimates used in the seismic PRA were expressed in terms of a free-field, ground-surface, control-motion response, spectral shape anchored to a 5-percent damped spectral acceleration, S_a, averaged over the 3.0 to 8.5 Hz frequency range. Therefore, the HCLPF capacities, derived from the fragility curves, are also expressed in terms of average spectral acceleration and the spectral shape. The HCLPF capacities in terms of average spectral acceleration can be compared directly to the average spectral acceleration of the site-specific, ground-motion spectra, since the fragility spectral shape is nearly identical to the site-specific ground-motion 84-percent spectral shape when both are anchored to the same 5-percent damped average spectral acceleration (see Figure 3.2).

In the LTSP Final Report, PG&E has cited the report by the NRC expert panel on quantification of seismic margins (Budnitz and others, 1985) in support of its claim that the HCLPF capacities represent a conservative estimate of seismic capacity. In simple terms, the HCLPF capacity corresponds to the earthquake level at which it can be stated with considerable confidence that the failure of the component is extremely unlikely. The HCLPF capacity values approximately correspond to a 95-percent confidence of not exceeding a 5-percent probability of failure. There is margin above the HCLPF capacity values, since the median capacity, which corresponds to the 50-percent probability of exceedance, is generally at least a factor of two greater than the HCLPF capacity. Therefore, it is unlikely that sudden failure will occur immediately beyond the HCLPF capacity. However, as a check on the results of the fragility analysis method, the staff has also required PG&E to determine the margins for a selected list of critical structures, systems, and components by the conservative deterministic failure margin (CDFM) method (see Section 3.8.1.6 of this SSER).

As explained in Section 23.4.5 of this SSER, and in the LTSP Final Report, the HCLPF capacity estimates may be directly computed from the fragility estimates. PG&E has determined the HCLPF capacities for the structures and equipment items which are included in the seismic PRA (see Table 23.17, Seismic Fragilities, in Section 23 of this SSER). These HCLPF capabilities, appropriate for comparison with both the 50-percent and 84-percent ground motion, are reported in terms of the 5-percent damped average spectral acceleration in the 3 to 8.5 Hz range in Chapter 7 of the LTSP Final Report. For example, as shown in Table 7-1 of the LTSP Final Report, the HCLPF capacities of the containment, auxiliary, and turbine buildings corresponding to the 84-percent ground motion are 4.01g, 3.19g, and 2.21g respectively. These values are to be compared to the 84-

percent site-specific, ground motion demand of 1.94g in the 3 to 8.5 Hz range. Similarly, Table 7-2 in the LTSP Final Report shows the HCLPF (structural) capacity of diesel generator control panel to be 2.69g, and the HCLPF (relay chatter) capacity of the 4-kV vital switchgear to be 1.57g as compared to the 84-percent site-specific ground-motion demand of 1.94g. However, as discussed in Section 23.4 of this SSER, because the relays have reset capability from the control room, the relay chatter failure mode does not significantly impact the estimate of core damage frequency.

In summary, as seen from Tables 7-1 and 7-2 in the LTSP Final Report, all structures and equipment items have sufficient seismic margins based on HCLPF capacities derived from fragility evaluations, except the 4-kV switchgear whose relay chatter mode has the lowest HCLPF capacity, 1.57g, which is about 80 percent of the 84-percent site-specific, 5-percent damped, average spectral acceleration of 1.94g. Section 23 of this SSER discusses relay chatter and how it affects the PRA studies.

The turbine building has the second-lowest HCLPF capacity, 2.21g, which shows a 14-percent margin over the 84-percent site-specific, average spectral acceleration of 1.94g. PG&E argues that, even if the demand were to reach the HCLPF capacity level, failure of the structure is unlikely because the median capacity is estimated to be about 2.65 times the HCLPF capacity. The turbine building margin is further evaluated using the CDFM method discussed in Section 3.8.1.6 of this SSER.

The diesel generator control panel has the third-lowest HCLPF capacity, 2.69 g, which shows a seismic margin of about 40 percent over the demand of 1.94g.

After reviewing the HCLPF capacities of all other SSC shown in Tables 7-1 and 7-2 of the LTSP Final Report, the staff generally agrees with the PG&E's statement that all components whose failure could lead to seismic risk to the plant have at least a margin of 40 percent when their HCLPF capacities are compared with the 84-percent, site-specific, ground-motion demand. Additional deterministic evaluations discussed in the next section of this SSER have shown that the HCLPF capacity of the turbine building, determined by the CDFM method, is 2.89g. This is equivalent to a 49-percent seismic margin for the turbine building.

3.8.1.6 Additional Deterministic Margin Evaluations

After reviewing the LTSP Final Report, the staff recognized that the deterministic evaluations of the seismic margins of the plant structures, systems, and components needed to be augmented by additional deterministic calculations (Rood, April 26, 1990). The purposes of the additional evaluations were to

- Compare the Hosgri-estimated structural response parameters such as base shear, overturning moment, and floor-response spectra with similar LTSP response parameters for all Category I structures.

- Compare the LTSP deterministic capacities with those predicted by the Hosgri analyses for selected structural elements and components.

PG&E was also asked to express the LTSP deterministic capacities in terms of

specific capacities such as base shear capacity and others, rather than in terms of acceleration levels.

The scope and criteria for such additional evaluations were discussed and agreed upon at a public meeting between the NRC staff and PG&E's staff in May 1990. In response to the decisions made at the meeting, PG&E has submitted additional deterministic evaluations for the following:

- containment building: global base shear and overturning moment, responses of the shell and interior structure
- auxiliary building: global base shear and overturning moment, responses of shear walls
- turbine building: responses of shear walls
- fuel handling building (FHB) crane: stability against lateral and vertical seismic forces
- containment fan cooler: anchorage failure modes
- diesel generator (DG) control panel: relay chatter and structural adequacy
- concrete masonry walls: top connection and wall flexure

In providing the above additional evaluations, PG&E has performed the following tasks:

- compared the shear forces and overturning/bending moments for the LTSP ground motion spectra with the corresponding responses determined for the Hosgri reevaluation
- compared the LTSP response with the Hosgri reevaluation capacity of the structural element for those cases in which the LTSP response exceeded the Hosgri response
- evaluated seismic margins using CDFM criteria and appropriate load combinations for those structural elements for which the LTSP responses using Hosgri load combinations exceeded the Hosgri capacities

The staff had asked PG&E to include some of the structural elements and components identified as "weak links" during the Hosgri reevaluation, when comparing the LTSP deterministic capacities with those predicted by the Hosgri analyses for selected structural elements and components. PG&E has reported that its selection of the structures and equipment for the seismic margin reassessment was based on the following criteria:

- structures or components identified by the seismic PRA studies to be the highest contributors to risk (e.g., the turbine building and diesel generator control cabinet)
- major structures important to plant safety
- governing capacity based on fragility studies described in the LTSP Final Report

- sensitivity to seismic vertical loadings
- sensitivity to anchorage failure mode
- equipment fragility based on results of a seismic testing program

The staff agrees with these selection criteria used for additional evaluations.

3.8.1.6.1 Procedure Used To Calculate Plant Response Loads (Demands)

The same procedure that is described in Chapter 5 of the LTSP Final Report was used to calculate the seismic responses of the major plant structures (i.e., the containment, auxiliary, and turbine buildings). The SSI analysis of these structures was performed using the SASSI computer program and the same three-dimensional dynamic models as described in LTSP Final Report. The seismic response quantities obtained for coherent ground motions were adjusted for spatial incoherency effects using the same adjustment factors as described in Section 3.8.1.3 of this SSER. As stated earlier in this section of the SSER, the vertical responses for the 84th percentile ground motion were scaled from the Hosgri reevaluation vertical responses based on the ratio of the 5-percent damped LTSP vertical ground spectrum to the 5-percent damped Hosgri reevaluation ground spectrum. The staff generally agrees with the procedures used by PG&E to obtain the plant responses (demands) described above.

3.8.1.6.2 Comparison of LTSP Seismic Base Shear and Overturning Moments With Previous Analyses

PG&E (Shiffer, 1990h) has compared the LTSP global seismic base shear and overturning moments for the structure and selected structural elements (in the containment and in auxiliary and turbine buildings) with corresponding seismic responses determined using the Hosgri reevaluation criteria.

The structural elements in the containment building selected for comparison are the exterior shell, and the concrete interior structure which includes the crane wall and the reactor shield wall. (These walls are the major lateral-force-resisting elements.) As illustrated in Table 3.1 below, the LTSP shear and moment demands for the containment building exceed the Hosgri demands.

Table 3.1 LTSP demand vs. Hosgri demand--containment building

Wall location	Elev. (ft)	Shear (kips x 10^3)		Moment (ft-kips x 10^3)	
		LTSP demand	Hosgri demand	LTSP demand	Hosgri demand
Shell	89	80.1	55.8	9800	7310
	172	62.1	45.4	4240	3400
Interior structure	91	37.6	24.1	1490	790

Similarly, PG&E has shown that, in general, the LTSP demands exceed the corresponding Hosgri demands for the auxiliary and turbine buildings, except that the global base shear and moments in the auxiliary building at El 85 ft due to MME are about 13 percent and 22 percent lower, respectively, than the corresponding Hosgri demands.

To compare the LTSP demands with the Hosgri capacities, PG&E derived the Hosgri capacities considering the loads to be the Hosgri seismic loads combined with other applicable loads. Containment structure capacities, for example, were determined considering the presence of a concurrent accident pressure due to a large-break loss-of-coolant-accident. As illustrated in Table 3.2 below, the Hosgri capacities of the containment shell and interior structure are considerably higher than the corresponding LTSP demands:

Table 3.2 LTSP demands vs. Hosgri capacities--containment building

Wall location	Elev. (ft)	Shear (kips x 10^3) LTSP demand	Shear (kips x 10^3) Hosgri capacity	Moment (ft-kips x 10^3) LTSP demand	Moment (ft-kips x 10^3) Hosgri capacity
Shell	89	80.1	120	9800	18000
	172	62.1	83	4240	10000
Interior structure	91	37.6	51	1490	2470

The comparison of LTSP demands with Hosgri capacities for the auxiliary building also shows the capacities to be greater than the demands, even though the margin is not as large as in the containment structure. In the case of the turbine building, the Hosgri moment capacities exceed the LTSP demands, while the LTSP base shear demands slightly exceed the corresponding Hosgri capacities at four out of five wall locations reported. The maximum exceedance of the base shear demand in these cases is about 8 percent (Table DE Q5-3 in Shiffer, 1990h).

It should be noted that there are differences in the objectives and methodologies of the Hosgri reevaluation and those of the LTSP evaluation, and that comparison of LTSP and Hosgri demands and capacities should not be a basis for determining the plant seismic margins. PG&E has, however, shown that any increased LTSP demands can be satisfied by the HCLPF capacities determined using the CDFM method discussed below. Since the median capacity is generally a factor of two greater than the CDFM HCLPF 84-percent capacity, the staff finds that the resistance of the walls of the turbine building to the base shear due to the LTSP ground motion is adequate.

3.8.1.6.3 Deterministic Evaluation Based on CDFM Method

The philosophy underlying the conservative deterministic failure margin (CDFM) methodology is described in an Electric Power Research Institute report (EPRI,

1988) and in a letter PG&E sent to the NRC (Shiffer, 1990h). The significant features of the CDFM method are briefly described below. A summary of the CDFM approach is given in Table 3.3.

Load Combinations

In the CDFM method recommended by EPRI, the seismic margin earthquake (SME) loadings are combined only with normal operating loads expected to occur concurrently with the SME. Load factors of unity are used for all loadings. In the case of the containment structure, EPRI has recommended combining an accident pressure with normal operating loads and the SME loads. In the Diablo Canyon deterministic evaluations, an accident pressure of 22 psi based on a postulated small-break loss-of-coolant-accident was used in the load combinations.

Structural Response (Demand)

In computing the structural response, the ground input response spectrum is specified in terms of an 84-percent site-specific SME response spectrum. EPRI has recommended that damping, structural modeling parameters, and the SSI evaluation should all be median-centered. In the Diablo Canyon deterministic evaluations, PG&E has used 7-percent damping for civil structures, and 5-percent damping for the bridge crane, fan coolers welded to floor, and electrical cabinets.

Structural Capacity

In arriving at the HCLPF capacity based on the CDFM method, each of the following parameters should be conservatively estimated: (1) material strength, (2) static capacity, and (3) inelastic energy absorption capability. For achieving the goal of specifying conservative material strength, the CDFM method recommends the use of either code-specified minimum strength or, when test data are available, 95-percent exceedance probability strength. Conservative static-capacity estimates should be based on the American Concrete Institute (ACI) code ultimate strength for concrete, the American Institute of Steel Construction (AISC) maximum strength for structural steel, and the American Society of Mechanical Engineers (ASME) Service Level D or functional limits for components. If test data are available to show excessive conservatism of code equations, then EPRI has recommended the use of 84-percent test data for capacity estimates.

For incorporating the inelastic energy absorption (IEA) capability into the CDFM capacity evaluation, EPRI has recommended the IEA factor, F_μ, to be 1.25 for ductile failure modes and linear analysis, and 1.0 for non-ductile failure modes and nonlinear analysis.

The CDFM capacities for components can also be evaluated using seismic test data. For this purpose, component-specific qualification or fragility test data may be used. Alternatively, a generic equipment ruggedness spectrum (GERS) may be used.

Table 3.3 Summary of conservative deterministic failure margin approach [Table 2-5 in EPRI NP-6041 (1988)]

Methodology/parameter	How determined in CDFM analysis evaluation
Load combination	Normal + SME
Ground response spectrum	Conservatively specified (84% non-exceedance probability)
Damping	Conservative estimate of median damping
Structural model	Best estimate (median) + uncertainty variation in frequency
Soil-structure interaction	Best estimate (median) + parameter variation
Material strength	Code specified minimum strength or 95% exceedance actual strength if test data are available
Static capacity equations	Code ultimate strength (ACI), maximum strength (AISC), Service Level D (ASME), or functional limits. If test data are available to demonstrate excessive conservatism of code equations, then use 84% exceedance of test data for capacity equation.
Inelastic energy absorption	For non-brittle failure modes and linear analysis, use 80% of computed seismic stress in capacity evaluation to account for ductility benefits, or perform nonlinear analysis and go to 95% exceedance ductility levels.
In-structure (floor) spectra generation	Use frequency shifting rather than peak broadening to account for uncertainty and use median damping.

Deterministic Seismic Margin

Conventionally, the seismic margin has been defined as the ratio of the capacity to the elastic computed demand;

$$\text{seismic margin} = (C-\Delta C_s)/(D_s + D_{NS}) \quad (1)$$

where C = CDFM capacity

D_s = Elastic computed demand following the CDFM guidance for the deterministic seismic spectra
D_{NS} = Concurrent non-seismic demand (loading) for all non-seismic loads in the load combination
ΔC_s = Reduction in the capacity due to concurrent seismic loadings.

Because of certain disadvantages in using equation 1, PG&E has used the following definition of seismic margin (which PG&E has called the scale factor, FS_i):

$$FS_i = (C - D_{NS})/(D_s + \Delta C_s)\, F_\mu \quad (2)$$

where Fμ is the CDFM inelastic energy absorption factor. The scale factor represents the amount by which the deterministic spectra can be scaled to produce a demand equal to the HCLPF capacity of a structure or component.

3.8.1.7 Comparison of Seismic Demand With CDFM Capacity

3.8.1.7.1 Containment Building

The shear and flexural capacities of the containment shell were evaluated at the building base (El 89 ft) where the seismic forces are the greatest and at El 172 ft where the inner curtain of diagonal reinforcing steel terminates. For calculating the shear capacity, the shell was treated as a thin-walled, reinforced-concrete cylinder whose shear resistance is provided by the concrete, the hoop reinforcing, and the diagonal bars. The CDFM ultimate shear capacity equations were used. A strength reduction factor, Φ, of 0.85 (needed to provide an 84-percent exceedance probability for the ultimate strength), was used in the ultimate shear capacity equation. The flexural capacity of the shell was evaluated using the ACI Code ultimate flexural strength equations.

The global shear capacity of the containment's interior structure was calculated by summing up the shear capacities of all the contributing walls at the base. The flexural capacity of the interior structures depends on the direction of the horizontal earthquake motion because of the configuration of the various walls, such as the fuel canal walls, the shield walls, and crane walls. In the controlling (north-south) direction, there is no shear wall interconnecting the shield and crane walls; therefore, they do not act as a composite system to resist overturning. The flexural capacities of the shield and crane walls were, therefore, evaluated separately.

A comparison of the LTSP demands with the corresponding capacities for the containment shell and the interior structures is shown in Table 3.4 along with the seismic margins in terms of scale factors FS_i.

In the tables that follow, shear is in units of kips and moment is in units of ft-kips.

Table 3.4 Demand vs. CDFM capacity for LTSP analysis--containment building

Wall location	Force component	LTSP demand ($X10^3$)	CDFM capacity ($X10^3$)	Scale factor (FS_i)
Shell at El 89 ft	Shear	80.1	115	1.80
	Moment	9800	22700	2.74
Shell at El 172 ft	Shear	62.1	103	2.01
	Moment	4240	15700	3.88
Crane wall at El 91 ft	Moment	1220	2030	1.94
Shield wall at El 91 ft	Moment	272	410	1.79
Interior structure, global, El 91 ft	Shear	37.6	66	2.18

3.8.1.7.2 Auxiliary Building

PG&E selected certain shear walls for deterministic evaluation because they were identified as "critical" walls either by the LTSP fragility analysis (Section 23 of this SSER) or by the Hosgri reevaluation. For illustration purposes, the LTSP demands on some of these walls are compared to the corresponding capacities in Table 3.5. This table also shows the seismic margins in terms of the scale factors.

In addition to determining the margins for individual shear walls as illustrated in this set of tables, PG&E has also computed the margins for the governing group of walls in the north-south and east-west directions. The margins for these groups of walls are generally somewhat higher than most of the individual walls that make up the group because of the capability of the building to redistribute forces by means of the building's lateral-force-resisting system consisting of floor diaphragm slabs connected to the shear walls.

3.8.1.7.3 Turbine Building

As in the auxiliary building, the shear walls in the turbine building were also selected for evaluation because they were identified for the controlling failure modes for the fragility analysis or as critical walls in the Hosgri reevaluation. Whereas an inelastic energy absorption factor, $F\mu$, of 1.25 was used in the auxiliary building, a value of 1.37 was used for the shear walls in the turbine

Table 3.5 Demand vs. CDFM capacity for LTSP analysis--auxiliary building

Wall location	Force component	LTSP demand ($X10^3$)	CDFM capacity ($X10^3$)	Scale factor (FS_i)
		North-south walls		
Wall H at El 85 ft	Shear	10.6	13.6	1.44
	Moment	335	567	1.51
Core west walls	Shear	40.9	73.8	1.81
		East-west walls		
Wall 15.7 or 20.3, El 85 ft	Shear	25.0	32.1	1.59
	Moment	851	1710	1.84
Main core walls	Shear	45.0	64.2	1.76

building; this higher Fμ value for the turbine building was computed at the 95-percent probability of exceedance level based upon the nonlinear time-history analyses conducted for the LTSP PRA studies.

The comparison of LTSP demands with corresponding CDFM capacities (along with scale factors) for a few walls in the turbine building is shown in Table 3.6.

Table 3.6 Demand vs. CDFM capacity for LTSP analysis--turbine building

Wall location	Force component	LTSP demand ($X10^3$)	CDFM capacity ($X10^3$)	Scale factor (FS_i)
Wall 17 (Unit 1), El 104 ft	Shear	9.1	11.4	1.70
	Moment	345	379	1.49
Wall G (Unit 1), El 85 ft	Shear	19.3	27.3	1.85
	Moment	738	941	1.70
Wall 19 (Unit 2), EL 104 ft	Shear	7.8	11.4	1.99
	Moment	295	380	1.73
Wall G (Unit 2), EL 85 ft	Shear	18.4	29.7	2.12
	Moment	703	1040	1.96

3.8.1.7.4 Fuel Handling Building Crane

The fuel handling building (FHB) crane has a rated lift capacity of 125 tons, and consists of two welded, box-type, steel, bridge girders spanning between runway girders and supported on the building's superstructure columns. A trolley is mounted on top of the bridge girders. Horizontal beams bolted to the building columns above the ends of the bridge prevent the bridge from moving vertically. Horizontal restraint bumpers are provided to transfer transverse loads from the crane bridge to the crane runway girders. Four brackets attached to the trolley that reach under the top flanges of the bridge girders prevent trolley derailment.

Two of the four governing failure modes of the FHB crane system relate to the crane bridge girders (i.e., bending of the girders and vertical movement) while the third relates to the trolley vertical restraints (to prevent crane uplift), and the fourth relates to the main hook cables (tension). Two load cases were considered: (1) crane loaded (250 kips hook load) for cables and bridge girder failure modes and (2) crane unloaded for vertical restraint (uplift) failure modes. The crane is considered to fail if (1) it uplifts enough to clear the lateral restraint and (2) it moves laterally a sufficient distance to fall from the crane runway. Crane bridge girder lift is resisted by gravity and by a hold-down beam.

The Hosgri reevaluation (both linear and nonlinear analyses) indicated that the bridge girder and the main hook cable were affected predominantly by vertical seismic loads. The LTSP analysis was performed, therefore, placing emphasis on the crane response to vertical loads. The linear elastic model analysis for the loaded case showed that the responses of the bridge girder and hoist cables were dominated by two modes, due primarily to the oscillation of the lifted mass and the bridge girder, with frequencies of 2.6 Hz and 9.8 Hz, respectively. The spectral acceleration of the system at the two dominant modes was determined by scaling the Hosgri vertical spectrum at the crane runway girder by the ratio of the LTSP to the Hosgri vertical spectral accelerations at the ground level. (It must be stated here that the site-specific vertical spectra suggested by the staff in Section 2.5.2.3 of this SSER will exceed the LTSP vertical spectra for frequencies below 10 Hz.)

A linear elastic analysis of the unloaded crane was performed using a single-degree-of-freedom system with a vertical frequency of 7.6 Hz. The LTSP forces were determined by scaling the Hosgri seismic demands by the ratio of the LTSP to the Hosgri vertical spectral accelerations at the ground level. These seismic demands were then combined with the effects of gravity loads.

A comparison of the LTSP demands (including gravity loads) with Hosgri reevaluation demands shows that the LTSP demands on the bridge girder and the hoist cables are less than the corresponding Hosgri demands. However, the LTSP demands (combined with gravity loads) for the bridge vertical restraint beams and trolley vertical restraints exceed the corresponding Hosgri demands by about 40 percent and 12 percent, respectively. Using an inelastic energy absorption factor of 1.25 for the bridge girder, and assuming that the wire rope cable has the minimum specified breaking strength, PG&E determined the CDFM capacities of the various elements of the FHB crane.

PG&E has compared the LTSP demands with the CDFM capacities of the cable and the bridge girder based on the linear analysis results and found that the controlling element of the crane was the bridge girder with a seismic margin of 55 percent expressed in terms of the scale factor, FS_1. This factor may be somewhat reduced if the LTSP vertical spectral shape is modified based on the current analysis on the vertical LTSP spectra by the NRC staff and its consultants.

PG&E found that the results of a linear analysis of the bridge and trolley restraints underestimated their seismic margins because the effects of trolley and bridge uplift were neglected. Therefore a nonlinear analysis was performed by considering the crane to fail when (1) it uplifts high enough to clear the lateral stop and (2) it moves a sufficient distance laterally to fall off the crane runway. Gravity and a hold-down beam resist the uplifting of the crane bridge girder. The staff finds acceptable the nonlinear analysis procedure involving an energy balance technique used by PG&E for determining a more realistic seismic margin. By comparing the CDFM capacities (i.e., the bridge resistance to global uplift and the trolley resistance to crane uplift) with the LTSP uplift demands, PG&E has determined that the scale factors (which represent the seismic margin) for the bridge and the trolley are adequate, that is, 3.2 and 2.4, respectively. For the FHB crane system at Diablo Canyon, the crane must uplift at least 7.25 in. before lateral restraint provided by the horizontal bumpers could be lost. Even then, the FHB structure must displace laterally more than 9 in. relative to the crane before the crane could fall off the runway girder. For calculating the CDFM capacity, PG&E used a lift of 4.75 in. As stated earlier, these factors may need to be reevaluated if the LTSP vertical ground spectrum is revised (see Section 2.5.3.2 of this SSER).

3.8.1.7.5 CDFM Evaluation of Selected Equipment

As part of the additional deterministic evaluations, PG&E selected the containment fan cooler (representing the class of equipment seismically qualified by analysis) and the diesel generator (DG) control panel (representing the class of equipment seismically qualified by dynamic testing). For this evaluation, the HCLPF acceleration capacity of the equipment was estimated using the CDFM method.

Containment Fan Cooler

The containment fan cooler, located at El 140 ft, has fundamental frequencies of 23 Hz in both horizontal directions, and is considered rigid in the vertical direction. For calculating the CDFM capacity of the system, four failure modes of the system (i.e., supply and outlet nozzles, backdraft damper, fan impeller deflection, and motor rotor deflection) and two structural failure modes (i.e., column-to-footplate weld and footplate-to-embedment weld) were considered. The controlling failure mode was determined to be the footplate-to-embedment weld which alone was used in the CDFM evaluation. Using the CDFM procedure for welded connections, the shear capacity of the controlling weldment was determined to be 39,200 psi (which is equal to 0.56 times the minimum code nominal tensile strength).

The LTSP demand loads in the horizontal direction were calculated using the in-structure floor response spectrum at El 140 ft resulting from the 84th

percentile ground motion. The demand load in the vertical direction was determined by scaling the Hosgri vertical floor response by the ratio of the LTSP to Hosgri vertical ground response at the floor slab frequency. However, the contribution from the vertical ground motion was found to be small and the weld stress was dominated by the horizontal seismic input plus the piping loads. From a finite element model analysis of the fan cooler, the fundamental frequencies of the containment fan cooler were found to be about 23 Hz in both horizontal directions and about 66 Hz in the vertical direction. Combining the variabilities due to frequency uncertainty in both the cooler and the structure by the square-root-of-the-sum-of-the-squares (SRSS) method, the spectral accelerations for obtaining the horizontal response were determined to be 1.83g in the north-south direction and 1.70g in the east-west direction. For these responses, the weld stresses were calculated by combining the stresses caused by deadweight, piping loads, and the three components of the earthquake motion. Thus, the demand shear stress in the weld (in psi) was determined to be 12,230 times the average spectral, horizontal, ground-motion acceleration, S_a (averaged over the 3-to-8.5 Hz frequency range) (Shiffer, 1990h). Including the effect of ground-motion incoherency, the final demand shear stress was reduced by about 4 percent. Thus, the demand shear stress is 11741 x S_a. Equating the CDFM capacity shear stress to the demand shear stress, the HCLPF capacity of the containment fan cooler was calculated to be 3.33g. The staff accepts this procedure to arrive at the margin represented by the HCLPF capacity determined by the CDFM procedure.

Diesel Generator Control Panel

The DG control panel, located at the turbine building basemat at El 85 ft, consists of a vertical cabinet and an attached horizontal "side cabinet." Two of the six failure modes analyzed for the CDFM evaluation were found to be the controlling modes. They were: (1) the Westinghouse ARD 440 relay chatter failure and (2) the generic structural failure.

Westinghouse ARD 440 Relay Chatter Failure Mode

The two important ARD 440 relays are located at heights of 22 in. and 31 in. above the base of the interior relay subpanel. These relays are primarily sensitive to front-to-back excitation of the panel on which they are mounted. The demand acceleration at the relay location was determined by analyzing a detailed model of the combined DG control panel using the longitudinal and transverse time histories corresponding to the 84-percent ground-response spectrum. A comparison of the resulting average 5-percent damped horizontal front-to-back response spectrum at relay location with the 5-percent damped, single-axis, broad-frequency, fragility test response spectrum (TRS) for the two relays shows that the ratio of the TRS to the required response spectrum (RRS) is lowest at 15 Hz (Shiffer, 1990h). Averaging the responses over a 20-percent bandwidth centered on 15 Hz, the average RRS is 5.6g and the average TRS is 12.5g. Including the effect of the ground-motion incoherence factor of 0.8 at El 85 ft, the CDFM demand horizontal spectral acceleration is determined to be 4.48g (0.8 x 5.6g). Using the procedure outlined in Attachment DE Q6-A to a PG&E letter to the NRC (Shiffer, 1990h), the corresponding CDFM capacity is found to be 9.62g. This analysis leads to a seismic margin scale factor

(FS_i) of 2.15. The CDFM HCLPF seismic margin earthquake level is then calculated as FS_i times the 84-percent average ground horizontal spectral acceleration from 3 to 8.5 Hz (which is 1.94g). This calculation gives an HCLPF of 2.15 x 1.94g, or 4.17g for the front-to-back response direction.

Generic Structural Failure Mode

This is the second controlling failure mode for the DG control panel and is based on the seismic qualification test.

The vertical panel being supported in the front-to-back direction, it essentially responds structurally to the side-to-side and vertical excitations. Also, the test response in the side-to-side direction represents the least overtest compared to the seismic demand. Therefore, the structural capacity of the cabinet was based on the side-to-side overtest. By considering the qualification test results and following a procedure recommended by Newmark and Hall (1978), PG&E has determined that the CDFM HCLPF capacity of the DG control panel is 2.62g.

3.8.1.7.6 Audit of CDFM Evaluations

The NRC staff audited PG&E's deterministic calculations on December 11-12, 1990 (Rood, 1991). The audit covered PG&E's additional deterministic calculations (based on the CDFM methodology) of the main power block structures, namely, the containment, auxiliary, and turbine buildings. In particular, the calculations pertaining to the global base shear and overturning moments of the containment and auxiliary buildings were examined by the staff. In addition, the calculations for shear walls in the major structures, and the calculations pertaining to the fuel handling building crane were also audited.

The staff was generally satisfied with both the methodology and the results obtained in the area of deterministic evaluations of the Diablo Canyon nuclear power plant structures. However, the staff requested that PG&E analyze additional failure modes of the containment shell in view of the difference between the connection details used in a containment test and those actually used in the Diablo Canyon containment. PG&E was asked to docket the CDFM reevaluation of the shell and interior structures of the containment if the results of such reevaluation alter the conclusions on the seismic margin. PG&E has performed the reevaluation considering additional shear modes of failure and confirmed the preliminary results that were reviewed during the audit. Therefore, this issue is considered closed.

3.8.1.7.7 Masonry Walls

Modifications--Strengthening of Masonry Walls

The staff had undertaken a reevaluation of its position on the adequacy of masonry walls at Diablo Canyon in the light of the appropriateness of the use of the energy balance technique (EBT) accepted by the staff in its previous positions and recent changes in industry codes and standards. The NRC staff and PG&E met several times to discuss two main issues, namely, (1) the adequacy of existing top connections between the masonry walls and the slabs or beams,

and (2) the use of the energy balance technique in conjunction with a displacement ductility ratio, U = 5, for qualifying the masonry walls at Diablo Canyon. The review by the staff and its consultant (Atkinson, 1990) raised two major concerns: (1) lack of ductility and redundancy at the wall top connections and (2) lack of an engineering similitude study regarding the data used in benchmarking the EBT for Diablo Canyon which were obtained from three proprietary wall tests.

PG&E responded to the NRC concerns in May 1990. PG&E and its consultants, and the NRC and its contractor, met on June 6, 1990, to discuss PG&E's responses to the NRC questions. In response to the meeting, PG&E submitted additional information in July 1990. After reviewing these submittals, the staff concluded that the masonry wall top connection details are not acceptable because they lack ductility and redundancy, and PG&E's method of calculating wall shear reactions at the clip angles may not be conservative.

Following additional meetings and discussions between the staff and PG&E on the masonry wall issue, PG&E proposed fixing all the safety-related masonry walls to satisfy the staff's concerns. In a letter to the NRC (Shiffer, 1990j), PG&E stated that it would modify the top connections to provide additional lateral load resistance. It also proposed a more conservative method (i.e., linear elastic analysis method) than the EBT to reevaluate the Diablo Canyon masonry walls and agreed to further modify those walls for flexure, if necessary. On January 31, 1991 the staff met with PG&E and its consultants to discuss several issues related to the analysis and modification of these walls. In response to this meeting, PG&E submitted a masonry wall reevaluation program in a letter to the NRC (Shiffer, 1991a). The program gave a schedule for implementing the engineering and modification work for different categories of walls in Units 1 and 2. According to this program, a linear elastic analysis coupled with the strength design method will be used to evaluate the walls for the Hosgri ground motion, and the walls will be evaluated to address the variability of material properties, workmanship, and construction tolerances by an inelastic analysis method. The results of these analyses will determine which walls need to be modified; however, PG&E expects that most of the masonry walls will need to be modified. The staff accepted the proposed analysis method (a linear elastic analysis coupled with the strength design), because the method reflects the state-of-art knowledge in masonry wall analysis and design. The staff also accepted PG&E's proposed schedule for wall modification, because this schedule calls for fixing all the walls in a reasonably short time.

Procedure Used in CDFM Evaluation of Masonry Walls

PG&E has performed deterministic evaluations of four safety-related masonry walls: two in the auxiliary building and two in the turbine building (Shiffer, 1991c and e). These evaluations are based on the conservative deterministic failure margin (CDFM) approach, and assume that necessary modifications, as discussed earlier in this section of the SSER, have been made to strengthen these walls. The CDFM criteria governing the masonry wall evaluations are briefly described below:

- The load combinations include the LTSP earthquake loading in addition to the normal loads.

- A damping value of 7 percent of critical damping is used for the supporting structures and the masonry walls.

- The masonry compressive strength is determined in accordance with ACI 531-79. For reinforcing steel, approximately 95th percentile strengths are used where test data are available.

- The nominal ultimate moment capacity is based on ultimate strength formulae with a Whitney stress distribution. A strength reduction factor of 0.90 is applied to obtain the CDFM moment capacity to account for potential equation error and rebar placement error.

- The CDFM permissible drift limit, set at about 95-percent confidence level from the results of applicable tests, is taken to be 4 percent of the wall height.

- The CDFM moment capacity is adjusted to account for the effect of the permissible drift. The adjusted moment capacity of the wall is expressed in terms of the spectral acceleration capacity, S_{AC}.

- A series of nonlinear time-history analyses were performed using wall models of varying lengths to obtain effective nonlinear demand. In these analyses, the walls were treated as pseudo-elastic members with an effective frequency equal to the secant frequency (Shiffer, 1991c) and an effective damping equal to 7 percent of critical damping. The reference floor-response spectrum was either frequency shifted or broadened by ± 15 percent for determining the effective nonlinear demand, S_{AD}.

It should be noted that the masonry walls are modified using the Hosgri reevaluation criteria. However, the CDFM capacity of the modified walls and the demand are determined using the LTSP site-specific ground motion to determine the seismic margins.

The walls were selected for evaluation based on the following considerations (Shiffer, 1991e):

- They are located in high seismic response areas.
- They represent variations in spans and modification schemes.
- They are judged likely to affect the PRA conclusions.

On the basis of PG&E's prioritization of the walls (which was discussed with the NRC staff), two walls from the auxiliary building and two from the turbine building were judged to be "high priority" walls for analysis and modification. The two walls selected in the auxiliary building are A-7A (a partition wall between cable spreading rooms) and A-5B (a partition wall for the battery room). The two walls selected in the turbine building are T-20B (a partition wall in the switchgear room) and T-14J (a partition wall in the diesel generator silencer room).

PG&E has provided details of tentative modification schemes (Shiffer, 1991e). It has further committed that any changes made in its proposed modification schemes will not reduce the seismic margins of the modified walls.

Seismic Margins of Modified Masonry Walls

PG&E has determined the seismic margins of the four masonry walls in terms of their CDFM capacities as shown in the following table (reproduced from Shiffer, 1991e). These CDFM capacities, expressed in terms of spectral accelerations, are to be compared with the LTSP ground motion of 1.94g in the 3 to 8.5-Hz frequency range. The CDFM capacities of the walls are determined as briefly described in Table 3.7, below (Shiffer, 1991e and h).

Table 3.7 CDFM evaluation of modified masonry walls

Wall	Elastic frequency (Hz)	Elastic demand (spectral acceleration)	Spectral acceleration capacity	Elastic scale factor	CDFM capacity (spectral acceleration)
A-7A	12 - 16.4	1.8g	3.6g	2.0	3.88g
A-5B	11.6 - 18.7	1.6g	2.4g	1.5	2.91g
T-20B	8.7 - 11.7	4.7g	6.9g	1.47	2.85g
T-14J	12.5 - 17.0	2.6g	3.8g	1.5	2.91g

At first, the spectral demand, S_{AD}, of the wall is obtained in terms of the spectral acceleration using proper earthquake component combination method (i.e., either the SRSS method or the 100-40-40 method). For this spectral demand, the maximum demand forces are calculated. Secondly, the flexural capacities (yield moments) are computed using pseudo-elastic techniques. An elastic scale factor is then obtained as the ratio of the capacity to the demand. The scale factor is determined for all possible failure modes of the masonry walls (e.g., wall flexure, wall shear, and expansion anchors at top and bottom connections). The lowest of these scale factors is taken as the scale factor for the masonry wall and used to multiply the spectral demand, S_{AD}, to obtain the spectral acceleration capacity, S_{AC}. The ratio S_{AC}/S_{AD} is the elastic scale factor which is then used to multiply the LTSP ground-motion demand of 1.94g in the 3 to 8.5-Hz frequency range to obtain the CDFM capacity of the walls.

The staff reviewed PG&E's calculations related to the CDFM evaluation of the modified masonry wall, T-14J, in the diesel generator silencer room, and concludes that the controlling scale factor was given by the expansion anchors at the bottom connection of this wall. This fact demonstrates the need for PG&E to devote utmost care in designing and installing the various connection elements for all the masonry walls.

The preceding table summarizes the results of the deterministic evaluations of the four masonry walls (Shiffer, 1991e). PG&E's analysis showed that the modified walls remain elastic under the seismic demand forces acting on them.

On the basis of the results of PG&E's deterministic evaluations of four of the most critical safety-related masonry walls in the plant, the staff concludes that these walls, when modified to meet the revised design-basis reevaluation criteria, will have adequate seismic margins for the LTSP earthquake.

3.8.1.8 Conclusions--Deterministic Evaluation

On the basis of a review of the LTSP Final Report and subsequent additional deterministic evaluations, and also on the basis of several meetings including an audit of the deterministic calculations, the staff finds that the major plant structures and equipment at Diablo Canyon have adequate seismic margins. This conclusion is subject to calculational confirmation as discussed in Section 3.8.1.1 of this SSER.

The objective of the LTSP deterministic evaluations is different from that of the Diablo Canyon qualification basis evaluations. (As discussed in Chapter 7 of the LTSP Final Report, the term "qualification basis" means the combination of the original design basis and the subsequent Hosgri evaluation basis.) The objective of the Diablo Canyon qualification-basis evaluations was to demonstrate that the capacity of the plant structures meet or exceed specified seismic criteria, rather than to quantify seismic margins. On the other hand, the objective of the LTSP was to evaluate plant seismic margins by comparing the capacity of the structures and equipment with the demand caused by site-specific LTSP ground motions. The LTSP deterministic, horizontal, ground-motion spectra were compared to the 1977 Hosgri evaluation spectra that were used as the licensing basis for the plant (LTSP Final Report Figure 7-2). The LTSP deterministic spectra were used to provide assurance that the plant HCLPF capacity estimates are at least equal to the seismic demand.

Thus, the LTSP results provide supplementary verification of, but do not replace, the qualification-basis criteria and methodology. In future plant design changes, the NRC staff concludes that safety-related structures, systems, and components should continue to be evaluated against the plant qualification basis, but the changes should also be evaluated to ensure that the LTSP HCLPF values for the plant remain acceptable. These HCLPF evaluations should be based on the LTSP horizontal and vertical spectra, increased to envelope the exceedances discussed in Section 2.5.2.3 of this SSER.

In summary, on the basis of its review of PG&E's deterministic evaluations, the staff concludes, subject to satisfactory completion of analyses confirming that plant seismic margins are adequate to accommodate the staff's spectral estimates, that PG&E has conducted deterministic studies to assure seismic margins in compliance with element 4 of the license condition.

23 PROBABILISTIC RISK ASSESSMENT

23.1 Introduction

23.1.1 Background

Element 4 of the license condition requires PG&E to assess the significance of conclusions drawn from the seismic studies in elements 1, 2, and 3, utilizing a probabilistic risk analysis and deterministic studies, as necessary, to assure adequacy of seismic margins. In order to address this element of the license condition, PG&E performed a Level 1 probabilistic risk assessment (PRA) including both internal and external events. The objectives of this PRA, as they relate to Element 4 of the license condition, are stated to be (Brand, 1988): (1) to assess the importance of various structures and items of equipment to seismic risk and (2) to put the seismic risk in perspective with the risk from other external and internal initiators. Risk in this context, primarily, refers to the estimates of core damage frequency (CDF).

As in the other parts of the Long-Term Seismic Program (LTSP), PG&E developed a program for the PRA consisting of three phases. Phase I was the development of a detailed program plan to address the license condition. This plan was submitted for NRC staff review on January 30, 1985. Phase II consisted of a scoping study to refine the scope of work for Phase III and associated schedules. A report describing Phase II activities and conclusions was submitted to the NRC staff on January 30, 1986. Phase III represented the actual detailed studies and the final report was submitted on July 31, 1988 (Brand, 1988). Chapter 6 of the LTSP Final Report summarizes the PRA results.

This section of the SSER summarizes the staff's evaluation of the PRA, and its findings and overall conclusions with respect to PG&E's compliance with element 4 of the license condition. References to "the PRA" in this section of the SSER refer to the Diablo Canyon PRA, a multi-volume document which was transmitted to the staff in a number of PG&E submittals, principally Brand, 1988; Shiffer, 1988a, b, c, and d; and Shiffer 1989a, b, and c.

23.1.2 Relationship to Other Elements of the License Condition

In order to understand the role of the PRA in the overall evaluation with respect to the license condition and the LTSP, the relationship between the PRA and other parts of the LTSP is detailed below.

Figure 23.1 is a schematic diagram of the major parts of the LTSP. This figure shows inputs that other parts of the LTSP provided to the PRA and the outputs from the PRA which were needed by these other parts of the LTSP. Because of scheduling constraints, most parts of the LTSP had to be conducted in parallel rather than in a natural, sequential order. For example, assumptions were made about the nature of the ground motion in order to proceed with the fragility calculations before the ground-motion studies could be completed. This perspective needs to be kept in mind in order to understand various assumptions and the presentations of results in the various parts and phases of the LTSP.

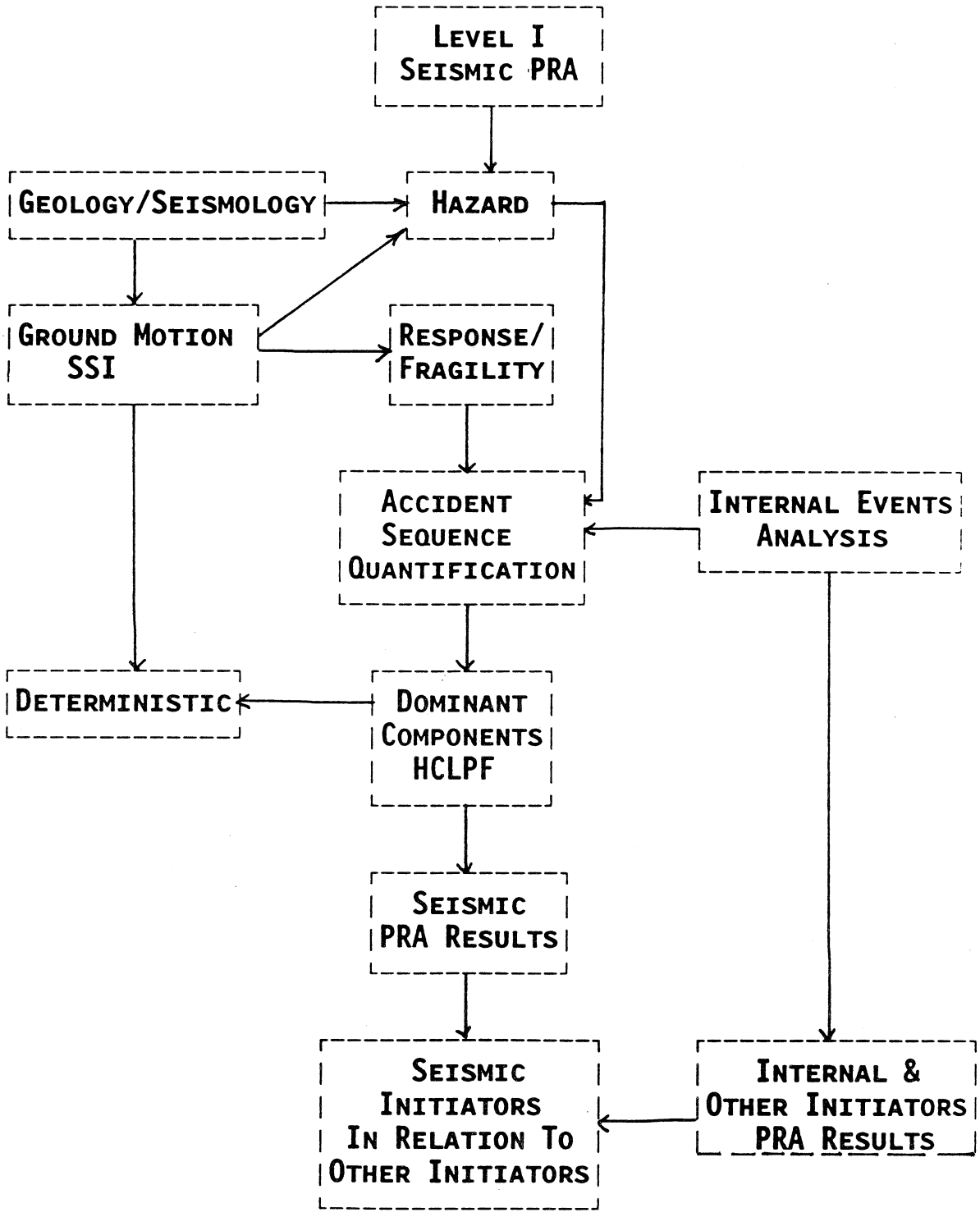


Figure 23.1 Relationship between PRA and other LTSP programs

23.1.3 Objectives and Scope of the Review

This review was performed to ensure that the PRA was sufficiently complete in scope, sufficiently accurate in modeling and data, and sufficiently detailed in its execution that it provides a sound basis for acceptance of the findings derived from it within the LTSP (and beyond).

Given that the driving force (from a regulatory perspective) for the PRA came from a license condition associated with the seismic concerns, the scope of the review was dominated by reviews of internal and seismic events. Other external events were also reviewed, but at a lower level of effort. Since fire initiators were also significant contributors to the overall results, they received additional scrutiny.

The review of internal events (Section 23.3 of this SSER) concentrated on the traditional major elements of a PRA (i.e., initiating events, event trees, fault trees, data analysis and reduction, human reliability analysis, and leading accident sequences, as well as independent sensitivity studies, importance analyses, and requantification).

The review of seismic events (Section 23.4 of this SSER) concentrated on fragilities, hazards, structural analyses, and uncertainty.

23.1.4 Review Process

23.1.4.1 Description

The staff selected the Brookhaven National Laboratory (BNL) as the primary contractor to perform the PRA review. BNL subcontracted with the Sandia National Laboratories (SNL) and EQE, Inc., to review the seismic portion of the PRA in detail. BNL concentrated its review on internal events and overall risk integration. Seismic hazard, human reliability analysis (methodology only), fire analysis, and other external events were reviewed primarily by the NRC staff. The detailed technical evaluation produced through the staff and contractor efforts appears in NUREG/CR-5726 (Bozoki and others, in process). This evaluation serves as the basis for safety findings given in this section of the SSER.

As with other elements of the LTSP, the review of the PRA was conducted in an interactive mode supplemented by a good deal of independent analysis, rather than by means of the traditional review process which does not begin until the final report is received. This interactive mode of review was chosen when the program was initiated. The staff, in consultation with the Advisory Committee on Reactor Safeguards (ACRS), reviewed the program plan submitted by PG&E, and after meetings and discussions, approved the program plan on July 31, 1985. Thus, the scope of the PRA required to address the license condition was established with NRC participation. The staff continued its review of the Phase II scoping study and provided further feedback for the Phase III detailed studies. This novel aspect of the review and its benefit to the staff and perceived benefit to PG&E are highlighted in Section 23.1.4.2 of this SSER.

In accordance with an ACRS recommendation, the staff not only reviewed the PRA and supporting reports but performed several independent assessments. The

staff met with PG&E a number of times and conducted a number of audits as documented in this SSER. Two plant walkdowns were conducted during the review.

23.1.4.2 Interactive Phase of the Review

The staff's overall assessment of the interactive review is that in the PRA review process, for the reasons described later, the review efforts were not significantly reduced when compared to a traditional review which begins after the receipt of a licensee's final report. However, several benefits, such as fewer areas of disagreement, were evident as the review unfolded. The staff perceives that PG&E benefited from these interactions by being able to analyze some staff concerns earlier in the review.

In the evaluation of internal events, the primary benefit accruing to the staff was in getting familiar with, among other things, the plant, PRA methodology and approach, plant operating and emergency procedures, and system layout and configurations. The staff was also able to provide some feedback on results of Phase II in review meetings. Much of the detailed review and independent assessment could not be started until the plant model and various data files became available.

In the area of seismic PRA, several meetings and audits were conducted to review Phase II, and some Phase III, building response and fragility calculations. As a result, in the final review, there were essentially no disagreements between the staff findings and the PG&E assessments. The staff began to prepare some studies as soon as time histories and building models used in the response analyses became available, instead of waiting for the advent of the final report.

Thus, interactive review definitely has some advantages and a potential for streamlining the review process; however, documentation and availability of data are vital to the success of this process from the staff's viewpoint.

23.2 Overview of PRA Approach and Results

23.2.1 Significant Plant Features

Diablo Canyon is a twin-unit plant located at a site on the California coast approximately midway between San Francisco and Los Angeles. Each unit employs a four-loop, pressurized-water reactor, nuclear steam supply system (NSSS) furnished by Westinghouse Electric Corporation. The NSSS for each unit is contained within a steel-lined, reinforced-concrete structure that is capable of withstanding the pressure that might be developed as a result of the most severe design-basis loss-of-coolant accident (LOCA).

The following paragraphs are extracted from the PRA (Brand, 1988) and they highlight some of the more important plant-specific features from the PRA perspective.

The vital 4-kV ac, 480-V ac, and dc systems are arranged to provide three redundancies, except for the instrument ac system which has four trains and six inverters. Emergency power for the two units is supplied by five diesel generators. One of these generators is a "swing" unit that is automatically

transferred to the unit with the first need. The diesel generators have self-contained automotive-style radiators that do not require plant cooling water. For long-term operation, the fuel to the day tanks is replenished by two redundant fuel oil transfer pump trains supplied from underground fuel oil storage tanks.

Two redundant auxiliary saltwater system pumps at the intake structure pump seawater to the component cooling water (CCW) heat exchangers. Three redundant CCW pumps are cross-tied to the two CCW heat exchangers which, in turn, feed three headers. The three headers provide CCW to the containment fan coolers, reactor coolant pump seals, charging pumps, and other systems requiring heat removal. The auxiliary saltwater system and CCW systems may be cross-tied between units if necessary.

The instrument air and nitrogen systems are classified as non-vital and for modeling purposes were assumed to fail; therefore, vital air-operated equipment that must function is furnished with backup air bottles. These systems were analyzed to determine for how long the operator could use the equipment before the backup air was exhausted. The recovery action modeled for these systems was manual operation of a valve or replenishment of the backup air.

The reactor charging system is important because it provides seal water to the reactor coolant pumps (RCPs). Loss of seal water will lead to failure of the seals and a resulting RCP seal LOCA. The charging system is dependent on CCW for pump cooling. However, the dependence on CCW may be mitigated by an emergency pump cooling system fed from the fire mains.

Simplified dependency tables of support systems to support systems and support systems to mainline (frontline) systems, are provided in the LTSP Final Report, and in NUREG/CR-5726 (Bozoki and others, in process).

23.2.2 Overall PRA Approach

23.2.2.1 Scope, Assumptions, and Limitations

As discussed earlier, the PRA is a full-scope (internal and external events), Level 1 PRA. Although, the PRA relates to Unit 1 only, it also models such interactions between the two units at the site as the possibility that the swing diesel generator may align to Unit 2 and the ability to cross-tie auxiliary saltwater cooling capability between units.

The PRA includes the analyses of accidents initiated during the full-power operations consistent with the traditional PRA practice. Neither accidents initiated during the low-power operations or during shutdown operations nor the results of accidents in the spent fuel pool are included in this investigation.

As is usual, this PRA utilizes a scenario-based approach to risk analysis. The scenarios represent the way the plant and its personnel respond to any initiating event that causes departure from the normal state of operation. The scenarios are chains of events leading to a variety of outcomes, including restabilization of the plant or various levels of plant damage up to and including core damage. The objective of the PRA was to determine the frequency of reactor core damage as a result of "all reasonably conceivable" accident-

initiating events, with an emphasis on seismically initiated scenarios. The assessment was developed over a number of years by a large team of PRA specialists from Pickard, Lowe and Garrick (PLG) with the extensive and active involvement of a number of PG&E personnel.

The PRA reflects the plant as it existed in the summer of 1988, including the changes in hardware and procedures that resulted from earlier phases of the LTSP. PG&E identified the following modifications in response to issues identified in earlier versions of the PRA. These modifications were included in the final PRA model submitted for review.

- Diesel Generator Fuel-Oil Transfer System. Constant recirculation paths were designed to eliminate multiple pump starts. Connections were also added for a backup portable fuel oil pump.

- Charging Pump Backup Cooling. Hose connections were added to allow use of the firewater system for emergency cooling in the event of a total loss of component cooling water. (Only one centrifugal charging pump can be connected at a time.)

- Substation Spare Parts. Dedicated spare parts are stored at the 230-kV substation to allow rapid recovery of offsite power in the event of a substation failure.

- Overcurrent Relay Remote Reset. The 4-kV overcurrent relays have a seal-in contact. It was originally believed that the relays had no remote reset capability. However, it was later determined that the ability to reset the relays from the control room did exist (Shiffer, 1991b)

- Valve Control Switch Replacement. The modification consisted of replacing three-position valve control switches with two-position valve control switches to prevent valve positions from changing in response to relay chatter during an earthquake.

23.2.2.2 PRA Methodology

The overall methodology of constructing the PRA model, that is, of describing the accident scenarios caused by various initiating events and rendering them amenable for quantification, is the "large event tree, small fault tree" approach. This methodology was introduced by PLG a decade ago, and has been substantially refined since that time. The refinements incorporate PLG's experience in preparing more than 20 PRAs during the 1980s. In addition, the PRA itself includes some other novel features in both internal and seismic events analyses. On the basis of its PRA review experience, the staff concludes that this PRA represents an advanced state of the art.

Advanced and novel features are discussed in NUREG/CR-5726 (Bozoki and others, in process) and elsewhere in this section of the SSER. Some of these features include: detailed analysis to identify initiating events with emphasis on common cause-initiating events; extensive application of event sequence diagrams; enhanced human actions analysis; relay chatter analysis for seismic events; and extensive nonlinear response analysis of the turbine building.

One of the most noteworthy features of this review was the extensive involvement of PG&E personnel in performing and maintaining the PRA. As the review progressed, the NRC staff and PG&E staff exchanged information during a number of meetings. It is apparent that PG&E intends this PRA to be a living assessment and to use it in plant operations. The findings of the PRA have already been used to demonstrate the viability of making some changes in the plant technical specifications.

23.2.3 Summary of PRA Results

Estimates of core damage frequency, as summarized in the LTSP Final Report [(Brand, 1988), with minor corrections suggested in the PG&E letter of February 19, 1991 (Shiffer, 1991b)], are reproduced in Table 23.1 (Table 6-54 of the PRA). The mean total CDF from all initiators is estimated to be 2.0E-4. Contributions from various categories of initiating events and the range of uncertainty associated with the core damage frequency are also listed in Table 23.1. Table 23.2 (Table 6-59 of the PRA) provides a breakdown by individual internal event initiators. Table 23.3 (Table 6-60 of the PRA) presents the leading functional scenarios of internal events that lead to core damage.

Table 23.1 Diablo Canyon PRA summary statistics
(Table 6-54 of the PRA as modified by Shiffer, 1991b)

	Core damage frequency			
Contributor	5th percentile	50th percentile	Mean	95th percentile
Seismic events	9.3×10^{-7}	6.2×10^{-6} (5%)	3.7×10^{-5} (18%)	1.1×10^{-4}
Internal events	5.2×10^{-5}	1.0×10^{-4} (82%)	1.3×10^{-4} (63%)	2.3×10^{-4}
Other external events	4.1×10^{-6}	1.5×10^{-5} (13%)	3.9×10^{-5} (19%)	1.0×10^{-4}
Total	7.7×10^{-5}	1.5×10^{-4} (100%)	2.0×10^{-4} (100%)	4.0×10^{-4}

Table 23.4 (Table 6-58 of the PRA) shows the results of a study of the importance of individual components to indicate how each contributes to the seismic core damage frequency. The single greatest contributor is the turbine building shear wall, followed by the loss of 230-kV offsite power. The dominant seismic scenarios were not discussed in detail in the PRA documentation. However, on the basis of additional information obtained from PG&E and the staff analysis [(discussed here in Sections 23.3 and 23.4 of this SSER, and in more detail in NUREG/CR-5726 (Bozoki and others, in process)], the dominant scenarios are as follows. The overall seismic CDF profile is dominated by accident sequences leading to station blackout (79%). These may be due to loss

Table 23.2 Internal initiating event contribution to CDF
(Table 6-59 of the PRA)

Initiating Event Category	Core Damage Frequency (Per Year)	Contribution (Percent)
1. Excessive LOCA	2.7-7	0.2
2. Large LOCA	2.5-6	2.0
3. Medium LOCA	5.8-6	4.6
4. Small LOCA, nonsolable	9.0-7	0.7
5. Small LOCA, isolable	1.7-6	1.4
6. Interfacing systems LOCAs		
6.a. At RHR pump suction	5.0-7	0.4
6.b. At RHR pump discharge	5.8-8	<0.1
7. Steam generator tube rupture	3.0-6	2.4
8. Reactor trip	1.6-5	12.5
9. Turbine trip	1.4-5	11.2
10. Loss of condenser vacuum	7.0-7	0.6
11. Closure of all MSIVs	2.4-7	0.2
12. Steamline break inside containment	2.3-6	1.8
13. Steamline break outside containment	2.7-6	2.2
14. Inadvertent safety injection	6.0-7	0.5
15. Main steam relief valve opening	5.0-8	<0.1
16. Total MFW loss	8.0-7	0.6
17. Partial MFW loss	1.1-5	8.8
18. Excessive feedwater	3.0-6	2.4
19. Closure of one main steam isolation valve	9.0-7	0.7
20. Core power excursion	3.0-7	0.2
21. Loss of primary flow	1.0-6	0.8
22. Loss of offsite power	4.1-5	32.4
23. Loss of one DC bus	9.2-6	7.3
24. Total loss of auxiliary saltwater	1.3-6	1.0
25. Total loss of CCW	3.0-6	2.4
26. Loss of 480V switchgear ventilation	1.5-6	1.2
27. Loss of control room ventilation	1.2-6	1.0
TOTAL	1.3-4	100

NOTE: Exponential notation is indicated in abbreviated form, i.e., 5.36-6 = 5.36×10^{-6}.

Table 23.3 Functional internal events scenarios contributing to core damage (Table 6-60 of the PRA)

Scenario	Frequency (Per Year)	Contribution (Percent)	Initiator	Direct Failures	Further Recovery Possible	Dependent Failures
1	5.36-6	3.1	RT	Failure to maintain hot standby	Yes	Unspecified Operator Errors
2	4.96-6	2.9	TT	Failure to maintain hot standby	Yes	Unspecified Operator Errors
3	3.53-6	2.0	PLMFW	Failure to maintain hot standby	Yes	Unspecified Operator Errors
4	2.28-6	1.3	MLOCA	Manual switchover to recirculation	No	Failure of Recirculation
5	2.13-6	1.2	LOCC	Fail to align backup cooling to charging pumps for RCP seal injection	No	Component Cooling Water, Charging SI Pumps, RCP Seal LOCA
6	1.72-6	1.0	LIDC	DC power train H, one AFW motor-driven pumps	Yes	Instrument Channels I2, I3, I4; 2 AFW Pumps; Bleed and Feed Cooling
7	1.71-6	1.0	MLOCA	Both RHR pump trains	No	Failure of Injection
8	1.70-6	1.0	LIDC	4-kV vital bus HH and one AFW motor-driven pumps	Yes	Instrument Channels I2, I4; 2 AFW Pumps; Bleed and Feed Cooling
9	1.40-6	0.8	EXFW	Failure to maintain hot standby	Yes	Unspecified Operator Errors
10	1.27-6	0.7	LLOCA	Accumulators	No	Failure of Injection
11	1.25-6	0.7	RT	Instrument channel I3, auxiliary feedwater, bleed and feed cooling	Yes	None
12	1.25-6	0.7	RT	Instrument channel I1, auxiliary feedwater, bleed and feed cooling	Yes	None
13	1.24-6	0.7	LOOP	Swing diesel goes to Unit 2, auxiliary feedwater, vessel integrity fails due to PTS	No	None
14	1.16-6	0.7	TT	Instrument channel I3, auxiliary feedwater, bleed and feed cooling	Yes	None

NOTE: Exponential notation is indicated in abbreviated form, i.e., 5.36-6 = 5.36 x 10^{-6}.

Table 23.3 (Contd.) Functional internal events scenarios contributing to core damage (Table 6-60 of the PRA)

Scenario	Frequency (Per Year)	Contribution (Percent)	Initiator	Direct Failures	Further Recovery Possible	Dependent Failures
15	1.16-6	0.7	TT	Instrument channel I1, auxiliary feedwater, bleed and feed cooling	Yes	None
16	1.16-6	0.7	RT	Auxiliary feedwater, bleed and feed cooling	Yes	None
17	1.14-6	0.7	TT	Auxiliary feedwater, bleed and feed cooling	Yes	None
18	1.13-6	0.7	LOOP	Diesel for bus HH, PORV sticks open and is not isolated, RHR pump train A fails, failure to recover AC before recirculation required	Yes	Failure of Recirculation

Table 23.4 Seismic failures of components contributing to core damage (Table 6-58 of the PRA)

Component	Does Failure Guarantee Core Damage?	Importance: Impact If Very Strong, that is, If Impervious to Earthquake — Core Damage Frequency	Importance: Impact If Very Strong, that is, If Impervious to Earthquake — Percent(1) Improvement in Mean Seismic Core Damage Frequency	Importance: Impact If Very Weak, that is, If Guaranteed to Fail — Core Damage Frequency	Importance: Impact If Very Weak, that is, If Guaranteed to Fail — Percent(1) Degredation in Mean Seismic Core Damage Frequency
Original core damage frequency	--	3.7-5	--	3.7-5	--
Turbine building sheerwall	Yes	2.6-5	30.5		
230-kV offsite power	No	2.8-5	24.4		
Vital DC	No				
Excessive LOCA	Yes				
Diesel generator control Panel	No	3.3-5	10.0		
4,160-kV/480V transformers	Yes	3.5-5	5.0		
Steam generators	Yes	3.5-5	3.4		
Relay chater (main control, diesel generator control, 4-kV switchgear)	No	3.6-5	2.4		
BOP piping and supports	No	3.6-5	2.2		
Pressurizer PORV	No	3.6-5	0.7	1.4-4	291
Strut for turbine building	No	3.7-5	0.4		
Small LOCA (PORV, RCPs, impulse lines, BOP piping and supports)	No			1.4-4	291
Human action to recovery relay chatter	No			1.0-4	173
Centrifugal charging pump	No			3.7-5	0.2

(1) Percentages have been carried to the indicated significant digits; core damage frequency has been rounded to two significant digits.

NOTE: Exponential notation is indicated in abbreviated form, that is, 3.67-5 = 3.67 x 10 $^{-5}$

of offsite power (LOOP) in conjunction with failures in the emergency diesel generator system, or due to failures of buildings (i.e., turbine building) or components (e.g., 4-kV switchgear or 4-kV/480-V transformers) which can lead to station blackout with or without LOOP.

Of these blackout sequences, 53 percent are those not directly failing the auxiliary feedwater (AFW) system, but leading to reactor coolant pump seal cooling failures, and, hence, small LOCAs. Direct failures of the AFW system account for 22 percent of the contributions from the station blackout sequence.

Figure 23.2 shows the contribution of each of several discrete earthquake ranges to the seismic CDF. As seen from this figure, the largest contribution comes from spectral accelerations between 2.0 and 3.0g.

Finally, Figure 23.3 (Figure 6-50 of the PRA) shows the plant-level fragility curves.

23.3 Review of Internal Events

This section of the SSER describes the overall approach used by the staff to review the internal events portion of the PRA as well as the major findings in each of the review areas. The format of this section closely follows that of the detailed technical evaluation contained in the assessment prepared for the staff (Bozoki and others, in process). Only technical findings and safety evaluations are highlighted here.

23.3.1 The Review Process

As discussed in Section 23.1.4 of this SSER, the review was divided into two phases. The review that took place after the submittal of the final PRA summary (Brand, 1988) is described next.

The review strategy called for a detailed review of selected portions of each of the major elements of the PRA. These elements essentially conform to the subsection headings of the remainder of Section 23.3 of this SSER. As the actual review progressed, some subjects received more attention than others, according to the perceived needs.

The staff developed the following seven-point plan as the overall basis for its review of the PRA:

(1) The logic for the primary event trees was reviewed to verify consistency and accuracy.

(2) For selected frontline and support systems, independent fault tree analysis was performed to verify the approach to unavailability modeling used in the PRA (the systems were selected according to perceived importance). This effort included requantification of an appropriate number of top event conditional split fractions.

(3) Selected failure probabilities and initiating event frequencies were reviewed (including the Bayesian updating process) to verify the PRA data

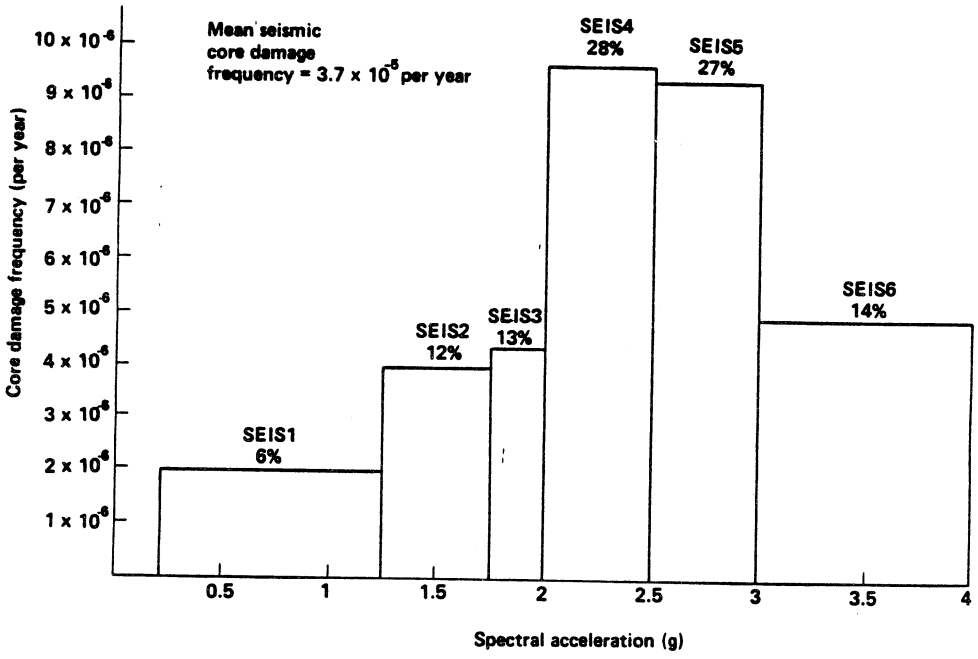


Figure 23.2 Contribution of each earthquake range to the seismic CDF (Figure 6-49 of the PRA)

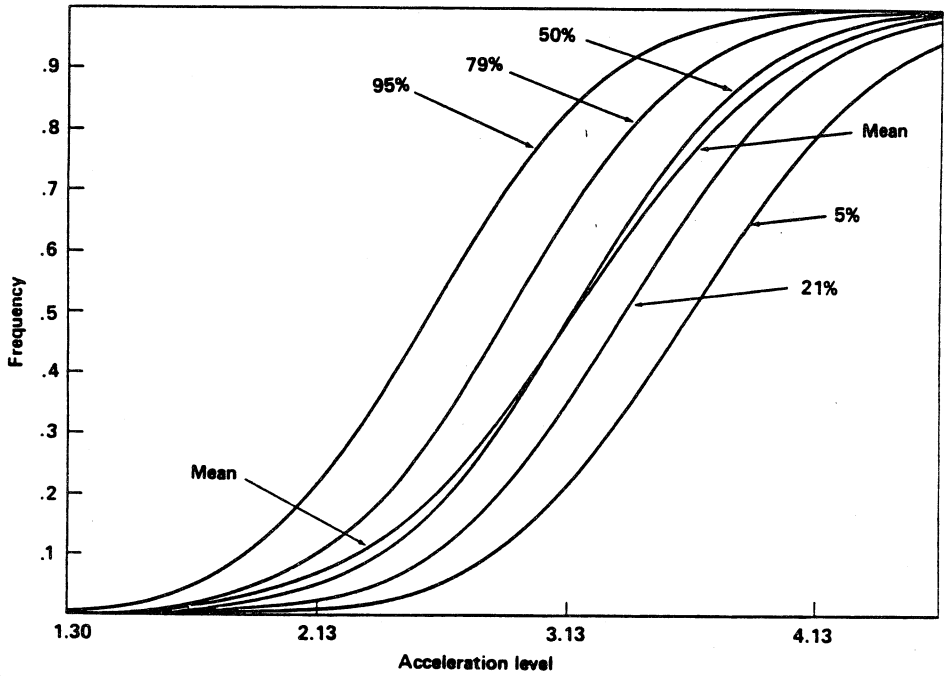


Figure 23.3 Plant fragility curve, including random and nonseismic failures (Figure 6-50 of the PRA)

analysis. Actual failure data selection was determined by the results of item 2 (above).

(4) An abbreviated fault model of the entire Diablo Canyon plant was obtained from PG&E which incorporated the leading accident sequences from the PRA. [Initially, the staff intended to develop such a model; however, PG&E developed a reduced model, called the dominant sequence model (DSM) described in Appendix D to NUREG/CR-5726 (Bozoki and others, in process) and gave it to the staff].

(5) Given the fault model from item 4 (above), investigations were undertaken on the impact of the findings from items 1, 2, and 3 (above) as well as the performance of such other analyses as importance measures, pair-importance, and sensitivity calculations.

(6) In addition to the overall review plan, two novel aspects of the PRA received special attention. These were: (a) the approach to human reliability analysis and (b) the relay chatter analysis. Novel aspects of the seismic analysis are described in Section 23.4 of this SSER.

(7) The seismic portion of the PRA review followed a similar overall methodological approach modified as necessary to account for the specifics of the seismic analysis.

The staff audited the relay chatter analysis mentioned in item 6 (above) in conjunction with a review meeting held with PG&E. PG&E performed the relay chatter analysis in a conservative fashion. The circuit of each relay that was determined to have the potential for chattering, was reviewed in detail. PG&E assumed the conservative position that all relays in a given circuit that could chatter would indeed chatter together in order to make or break the circuit. This assumption was uniformly applied even if it took six, seven, or more relays chattering in synchronism to accomplish the event. PG&E then looked at the consequences of the circuit failing or otherwise changing state and determined which circuits could lead to problems in the plant. At this point, the results of the relay chatter analysis were not simply input to the PRA model but rather those circuits identified as particularly vulnerable received hardware modifications in some cases to prevent the action.

The staff audit of the relay chatter analysis therefore focused on methodology, scope, and completeness. The staff audited a number of the systems (e.g., auxiliary saltwater, electrical power) and concluded that a rigorous and conservative electrical circuit analysis had been performed. The seismic PRA aspects of the review are addressed in Section 23.4 of this SSER.

The review process was very interactive in this phase of the review also. The staff documented results of its independent systems analyses in letter reports and forwarded them to PG&E. These reports contained additional questions and raised some areas of disagreement. These reports were discussed with PG&E in public meetings and written responses were obtained. Appendices A and B to NUREG/CR-5726 (Bozoki and others, in process) document all of the system analyses as well as results of the feedback process described. Audits were conducted to review selected data analyses and systems portions of the relay chatter analysis. Several meetings were held to discuss human reliability

analysis methods. Finally, the staff met with PG&E to discuss the results of the staff's importance and sensitivity analyses and overall core damage frequency results.

23.3.2 Initiating Events

23.3.2.1 PRA Approach

In order to make the list of initiating events as complete as possible, PG&E used three methods for initiating events identification. These were:

- master logic diagram (MLD)
- heat balance fault tree (HBFT)
- failure modes and effects analysis (FMEA)

The initiating event categories obtained as a result of these identifying/selecting methods were further compared and cross-checked with lists of initiators given or analyzed in several reports, such as, the Diablo Canyon FSAR, (for plant-specific factors) (PG&E, 1988), WASH-1400 (USNRC, 1975b), EPRI NP-2230 (McClymont and Poelilonan, 1982), the PRA Procedures Guide (Papazoglou and others, 1984), Indian Point Probabilistic Safety Study (PASNY/CECo, 1982), and Seabrook Station Probabilistic Safety Assessment (PLG, 1983).

The candidate initiating event categories were screened by the quantification process; that is, initiating events with low frequency of occurrence and with less relevance to challenge safety systems were omitted.

Using this procedure, the PRA lead to a rather comprehensive set of initiators consisting of 27 "internal" and 23 "external" initiating events. This set of initiating events is unusually large compared with that of previous PRAs.

The 7 LOCAs, 14 transients, 6 support system (common cause) failures, 14 fires, 3 flood/jet/sprays, and 6 levels of earthquake initiators and their code designators are listed in Table 23.5.

All the non-seismic initiators were analyzed and quantified in the context of the full PRA plant model and in this sense they were all considered in the core damage frequency analysis as "internal events."

The 27 internal initiating events (excluding internal fires and floods) of the PRA were divided into two groups for quantification. The first group comprises those initiators for which it was deemed that generic operating experience was applicable. The second group comprises initiators that were deemed to require plant-specific analysis. The quantification process for the first group entailed sophisticated Bayesian updating techniques which combined generic operating experience with plant-specific experience (4.7 years of operation). For the quantification of the second group, system unavailability calculations were used.

Table 23.5 Initiating event categories selected for quantification of the Diablo Canyon risk model (Table 6-26 of the PRA)

Group		Initiating Event Categories Selected for Separate Quantification	Code Designator
Loss of Coolant Inventory	1.	Excessive LOCA	ELOCA
	2.	Large LOCA	LLOCA
	3.	Medium LOCA	MLOCA
	4.	Small LOCA, nonisolable	SLOCN
	5.	Small LOCA, isolable	SLOCI
	6.	Interfacing systems LOCA	
	6a.	At RHR pump suction	VS
	6b.	At RHR pump discharge	VD
	7.	Steam generator tube rupture	SGTR
Transients	8.	Reactor trip	RT
	9.	Turbine trip	TT
	10.	Loss of condenser vacuum	LCV
	11.	Closure of all MSIVs	AMSIV
	12.	Steam line break inside containment	SLBI
	13.	Steam line break outside containment	SLBO
	14.	Inadvertent safety injection	ISI
	15.	Main steam relief valve opening	MSRV
	16.	Total main feedwater loss (includes feedwater line break)	TLMFW
	17.	Partial main feedwater loss	PLMFW
	18.	Excessive feedwater	EXFW
	19.	Closure of one main steam isolation valve (MSIV)	IMSIV
	20.	Core power excursion	CPEXC
	21.	Loss of primary flow	LOPF
Common Cause Initiating Events			
Support System Faults	22.	Loss of offsite power	LOSP
	23.	Loss of one DC bus	L1DC
	24.	Total loss of auxiliary saltwater	LOSW
	25.	Total loss of component cooling water	LOCC
	26.	Loss of 480-V switchgear ventilation	LOSWV
	27.	Loss of control room ventilation	LOCV
Seismic Events	28.	0.2 g to 1.25 g	SEIS1
	29.	1.25 g to 1.75 g	SEIS2
	30.	1.75 g to 2.0 g	SEIS3
	31.	2.0 g to 2.5 g	SEIS4
	32.	2.5 g to 3.0 g	SEIS5
	33.	3.0 g to 4.0 g	SEIS6

Table 23.5 (Cont'd.) Initiating event categories selected for quantification of the Diablo Canyon risk model (Table 6-26 of the PRA)

Group		Initiating Event Categories Selected for Separate Quantification	Code Designator
Fire and Smoke	34.	Loss of both motor-driven AFW pumps	FS1
	35.	Loss of all charging pumps and MSIV closure	FS2
	36.	Loss of component cooling	FS3
	37.	Loss of control ventilation	FS4
	38.	Loss of auxiliary saltwater	FS5
	39.	Loss of 4-kV buses HF and HG	FS6
	40.	Loss of 4-kV buses HG and HH	FS7
	41.	Loss of 4-kV buses HF, HG, and HH	FS8
	42.	Control room fire at vertical board VB-1	CR1
	43.	Control room fire at vertical board VB-2	CR2
	44.	Control room fire at the interface of vertical boards VB-2 and VB-3	CR3
	45.	Control room fire at vertical board VB-4	CR4
	46.	Cable spreading room fire one	CS1
	47.	Cable spreading room fire two	CS2
Flood, Jets, and Sprays (pipe breaks)	48.	Loss of all auxiliary feedwater	FS9
	49.	Loss of both motor-driven AFW pumps	FS10
	50.	Loss of auxiliary saltwater	FS11

Those initiators deemed significant contributors to the core damage frequency (i.e., those considered most important to CDF after truncating, merging, and correcting for scenarios with small CDF) were included in the reduced plant or dominant sequence model (DSM). These initiators are listed in Table 23.6. [(The DSM is described in detail in Appendix D: PRA Dominant Accident Sequence Model in Bozoki and others (in process)]. Within the DSM, the external initiating event "hazardous chemical release" was considered to be important enough that it was included (Table 23.6) and the control room and the cable spreading room CDF contributions were combined and were given a common designator: CRFIRE.

23.3.2.2 Review and Evaluation

23.3.2.2.1 Completeness

The initiating events list in the PRA was derived from applying three methods and a systematic comparison with other references. However, the staff noted that the screening process applied to the final list of initiators dismissed the following: (1) loss of two (or more) 120-V ac instrument buses; (2) loss of instrument air (in the PRA it was assumed that the instrument air system fails after each type of initiating event); and (3) loss of power to necessary plant systems (Category 37 of McClymont and Poelilonan, 1982). Omission of these initiating events is not expected to have significant impact on the core damage frequency; however, some important insights into plant dependencies and interactions might have been obtained by including them.

23.3.2.2.2 Initiating Event Frequencies

The staff's review of the initiating event frequencies did not include a recalculation of each initiator frequency. However, to determine potential outliers, all initiating event frequencies listed in Table 23.5 and those omitted were compared with those of other recent PRAs or other data sources. From those initiating frequencies which were determined in the PRA by system analysis (fault trees), two specific initiators were chosen for detailed audit/requantification. The two initiators were "loss of auxiliary saltwater (LOSW)" and "loss of component cooling water (LPCC or LOCC)."

The alternative initiating values used by the staff in a sensitivity analysis are summarized in Table 23.14.

Loss of Offsite Power, LOOP

After reviewing (1) the review of the electrical system model of Unit 1 [(discussed in detail in Appendix B2 to NUREG/CR-5726 (Bozoki and others, in process)], which considers the advantages offered by interconnections between the two units, but is tacit about LOOP events arising from non-LOOP transients at Unit 2 under any operational condition, and (2) a recent article (EPRI, 1989) and an information notice (USNRC, 1990) which call attention to the fact that solar magnetic storms represent a real threat to power grid integrity during the next 11 years, the staff requested that PG&G reevaluate LOOP initiator frequency and report its findings. In its response (Shiffer, 1990a), PG&E indicated that its reevaluation resulted in no changes. On the basis of the review of this information, the staff used the value listed in Table 23.14 in a sensitivity analysis.

Table 23.6 Initiating events and their mean frequencies per year in the reduced model

Initiating event designator	Mean frequency	Generic mean frequency
LOSWV	6.29E-05	---
L1DC	2.56E-02	3.35E-02
LOOP	9.10E-02	1.40E-01
SLOCN	5.26E-03	5.83E-03
FS1	2.94E-04	---
SLBO	5.53E-03	6.04E-03
RT	1.14E+00	1.53E+00
TT	1.05E+00	1.08E+00
FS8	6.18E-06	---
PLMFW	7.49E-01	1.13E+00
FS11	3.81E-04	---
LPCC	1.96E-04	---
MLOCA	4.63E-04	4.65E-04
FS9	1.35E-05	---
EXFW	2.79E-01	1.71E-01
LOSW	9.74E-05	---
LLOCA	2.02E-04	2.03E-04
SGTR	1.71E-02	2.88E-02
LOPF	1.21E-01	1.66E-01
SLBI	4.63E-04	4.65E-04
IMSIV	1.07E-01	8.43E-02
TLMFW	9.98E-02	1.64E-01
VSI	1.01E-06	---
SLOCI	1.61E-02	2.30E-02
LCV	8.73E-02	1.16E-01
LOCV	7.99E-02	---
ISI	7.39E-02	3.03E-02
FS6	2.41E-05	---
ELOCA	2.66E-07	2.66E-07
FS5	5.26E-05	---
FS10	1.40E-05	---
HAZCHM	4.39E-04	---
CRFIRE	3.17E-05	---

Reactor Trip (RT)

On the basis of comparisons with various PRAs (Millstone 3, Seabrook, and Midland) and studies related to the recent industry performance, the staff in its sensitivity analysis has assigned a frequency of 1.85 RT events/yr as compared to the PRA value of 1.14 RT events/yr. This increases the mean CDF by 6 percent.

Turbine Trip, TT

The mean generic prior frequency of the TT initiator, 1.08/yr, is also smaller compared with other data. Considering the review of PRAs cited earlier (McClymont and Poelilonan, 1982; Pelto and others, 1985), the staff used the value of 1.95 TT/yr compared to the value 1.05 TT/yr. The net increase in the mean CDF will be about 7 percent.

All Transient Categories

A similar trend (the prior and consequently the posterior mean frequencies used for a given transient are smaller than those of other PRAs) can be observed for practically each of the categories in the transient group of Table 23.5. The trend can be demonstrated by comparing the sums of the mean prior and posterior frequencies of the initiators of that initiator group with similar values of other PRAs. The sum of the mean prior frequencies of the group "transient" in Table 23.5 (i.e., RT+TT+LCV+...+LOPF) is: 4.53/yr. The sum of the mean posteriors (Diablo Canyon specific values) is: 3.79/yr (3.71/yr in the dominant sequence model). Seabrook's sum of posterior means is: 10.80/yr (the categories are the same as those of the PRA). Midland's sum of posterior means is: 8.98/yr (Midland categories are: RT, TT, EF, FW). The Millstone Unit 3 sum of the medians is: 7.71/yr and the sum of the means is: 10.57/yr (the Millstone values correspond to the categories of EPRI-NP-2230 (McClymont and Poelilonan, 1982), cross-referenced by using Tables C.1-6 of the PRA). Additional comparison with other sums of transient values obtained from PRAs on Westinghouse plants, shows the same discrepancy (e.g., USNRC, 1987).

On the basis of this review, the staff has used the combined value of 5.43 events/yr for all transient initiators minus RT and TT events compared to the value of 1.52/yr used by PG&E. The net increase in the mean CDF is about 34 percent.

Total Loss of Auxiliary Saltwater (AS), LOSW

The mean frequency of the LOSW initiator was derived in the PRA by an unavailability analysis (fault tree evaluation) of the AS system and not by reflecting appropriately screened industry experience. The analysis took into consideration the intertie to the parallel AS system of Unit 2. The staff performed a detailed review of the system analysis [(see Appendix B3 to NUREG/CR-5726 (Bozoki and others, in process)] and in addition conducted a data search and analysis to check whether the failure rates used in the quantification reflect the harsher environmental conditions that might be expected with a saltwater working fluid. The data search was directed also to obtain an industry-experience-based frequency for this initiator. The review showed that the

assumptions and failure values used in the PRA unavailability model to determine the frequency of LOSW were somewhat optimistic.

In response to the staff's initial findings, PG&E reevaluated initiator frequency and offered an updated value 44 percent higher than the original. This resulted in less than one percent increase in overall non-seismic mean CDF. In turn, in order to factor in an element of expert opinion and to provide an additional data point, the staff revised the value for this initiator as shown in Table 23.14; this resulted in a net increase of 8 percent in the overall internal (non-seismic) CDF.

Total Loss of Component Cooling Water System, LPCC

The staff did not requantify the unavailability model of the CCW system which serves as the basis for the determination of this initiator in the PRA. Instead a data search and analysis effort was carried out to provide an industry-experience-based frequency value [(see Appendix B4 to NUREG/CR-5726 (Bozoki and others, in process)]. As a result of the staff review, PG&E estimated a new mean initiating frequency to be: LPCC = 2.88E-04/yr. This was 47 percent higher than the original PRA value listed in Table 23.6.

The staff's revised value is shown in Table 23.14. This value will yield a 7-percent increase in the non-seismic mean CDF when substituted into the DSM.

LOCA Initiators

The categorization of LOCA events in the PRA is based on the analyses of generic Westinghouse plants. The LOCAs are:

- ELOCA - Excessive LOCA. Any LOCA more severe than the design-basis LOCA; i.e., beyond the capacity of the ECCS.
- LLOCA - Large LOCA. A LOCA resulting from a break in a pipe whose diameter exceeds 6 inches. An LLOCA is within the capacity of the ECCS.
- MLOCA - Medium LOCA. A LOCA resulting from a break in a pipe whose diameter exceeds 2 inches and is less than 6 inches.
- SLOCI, SLOCN - Small LOCA, Isolable and Nonisolable. A small LOCA results from a break in a pipe that is less than 2 inches in diameter. An SLOCI is isolable, for example, a leaking PORV. An SLOCN is nonisolable.
- SGTR - Steam Generator Tube Rupture.
- VDI, VSI - Interfacing Systems LOCA. A LOCA originating at an interface between the RCS and a low-pressure system. The release path for VDI and VSI bypasses containment. VDI is located on the discharge side of the RHR pump, and VSI is located on the suction side.

The staff considers this selection of LOCA initiators to be consistent with other PRAs. The review found that the mean frequencies of the majority of the LOCA categories were comparable with those used in PRAs for other Westinghouse reactors and are considered reasonable estimates.

23.3.3 Success Criteria

As part of the staff's system analysis reviews (three frontline and five support systems) discussed later [see Appendices A and B to NUREG/CR-5726 (Bozoki and others, in process) for details], all success criteria were reviewed to determine their validity. As part of this process, two specific success criteria were questioned. The first was associated with the ECCS low-pressure injection function provided by the residual heat removal (RHR) system. In some previous PRAs, the success criterion for a four-loop plant was taken to be injection to two of the three intact loops with no credit for the broken loop. The PRA success criterion for this scenario is only one-out-of-three (1/3) intact loops requires injection. In response to a staff question, PG&E referenced a study that demonstrated that 1/3 was sufficient for Diablo Canyon [Appendix A2 to NUREG/CR-5726 (Bozoki and others, in process)], thus resolving this issue.

The other success criterion that the staff questioned dealt with the ability of a single Unit 2 auxiliary saltwater pump to supply Unit 2 as well as Unit 1 given the loss of the Unit 1 ASW system. PG&E supplied the results of calculations that demonstrated a nearly equal split of the flow between the two units [Appendix B3 to NUREG/CR-5726 (Bozoki and others, in process)]. PG&E acknowledged that under certain circumstances one pump will not suffice. For these cases, PG&E performed a sensitivity study demonstrating the overall effect on the non-seismic CDF was negligible.

23.3.4 Event Sequence Model

The event sequence model is used to identify the many possible plant response sequences for each initiating event. The event sequence model of the PRA consists of four parts (event trees).

- electrical support system
- actuation and mechanical support system
- early-response frontline system
- long-term response frontline system

Figure 23.4 is a diagram of the event sequence model. This model served as a basis for evaluating the plant response to each of the 50 initiating categories. Depending on various combinations of plant equipment and operator response success or failure states, an event sequence either was terminated with no core damage (success) or led to core damage. Since the plant response to many of the initiating event categories is quite similar, common event tree modules were developed. They were quantified, however, with different boundary conditions and different system top event values specific to each initiator. Figure 23.4 indicates the essential modules of the event sequence model.

The electrical/actuation-mechanical modules are common to all initiating events. These modules represent different support system states, that is, combinations of support system top event successes and failures that affect the frontline systems in similar ways. The number of different support system states after a reduction/combination process became 178 distinct states.

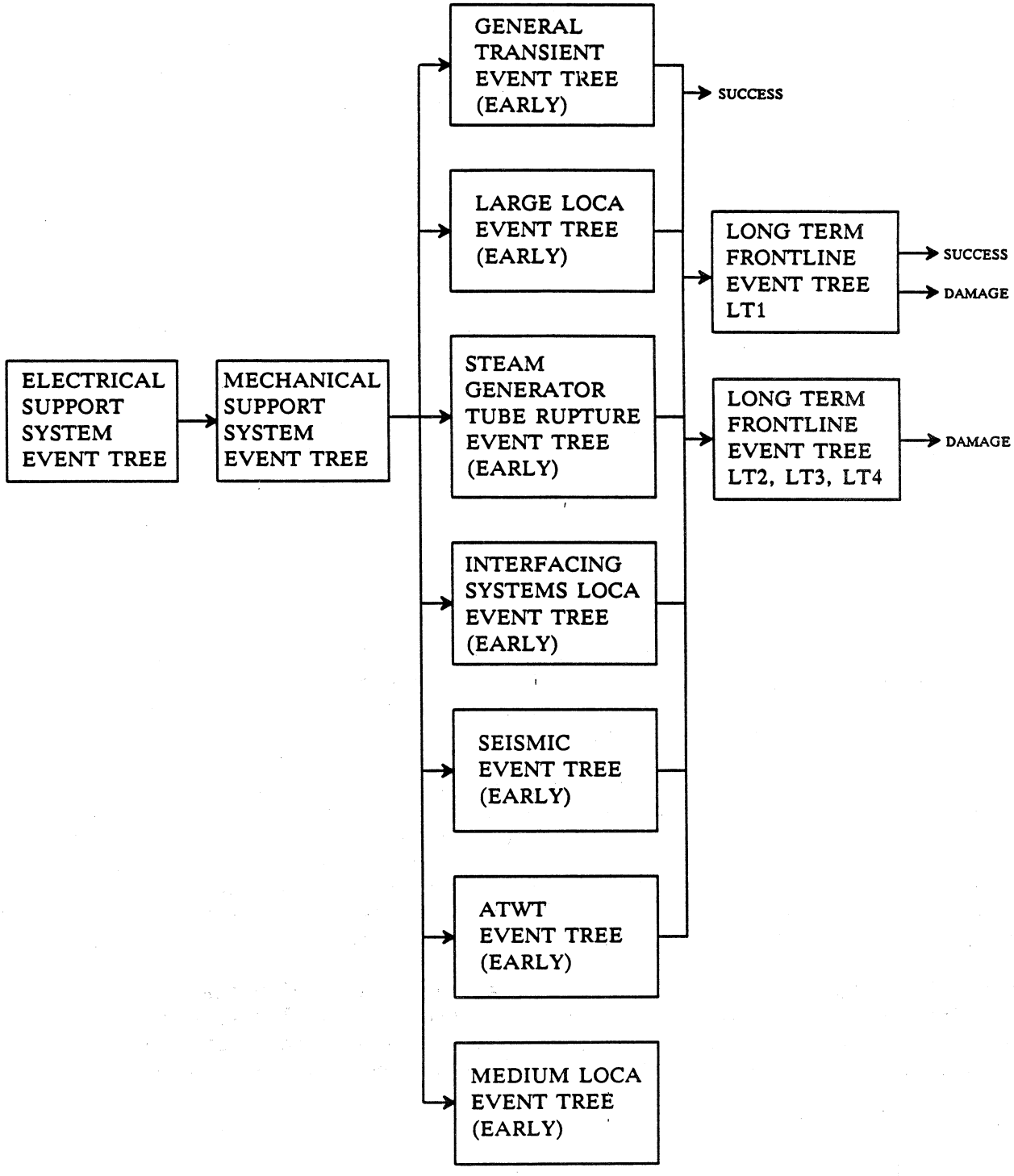


Figure 23.4 The four-part event sequence model (Figure 6-43 of the PRA)

Next are the seven early response frontline system event tree modules. These are:

- General Transient. For most initiating event categories that require active nuclear shutdown, heat removal or coolant injection.

- Large LOCA. For LOCAs resulting from breaks in the RCS boundary with diameter > 6 in. up to a full guillotine break of the cold-leg piping requiring high-capacity makeup.

- Steam Generator Tube Rupture. Similar to the general transient, with special requirements for operator actions to eliminate the flow of reactor coolant though the ruptured steam generator and thus bypassing containment.

- Interfacing Systems LOCA. For high-pressure/low-pressure boundary failures when reactor coolant can bypass containment, and equipment needed for control of the LOCA can also be damaged.

- Seismic Events. Similar to the general transient module; additional details added to account for earthquake-induced dependent failures and specially required human actions.

- Anticipated Transient Without Trip (ATWT). Covers all the initiating events that require trip if the trip was identified as failed in the support system model; considers potential ensuing overpressurizations and special actions to provide long-term shutdown of the nuclear reaction.

- Medium LOCA. For LOCAs resulting from breaks in the RCS boundary with diameters in the range from 2 inches to 6 inches. Similar to the general transient module with modified top event success criteria to reflect conditions imposed by the break flow.

If the event sequence has not reached a successful conclusion, sequences continue to one of the long-term event tree modules. Sequences requiring long-term cooling continue into LT1. The model for Diablo Canyon essentially ends here, since the PRA is a Level 1 PRA. Figure 23.4 shows the generic model as it relates to Level 2 of the PRA. In that case, sequences that have already reached core damage would branch to LT2, LT3, or LT4 to be classified into plant damage states depending on the status of the containment safeguards.

It should be emphasized that the event trees associated with the modules appearing in Figure 23.4 are essentially abstracted, simplified versions of the underlying event sequence diagram (ESD) models. They were quantified by using the appropriately selected top event split fractions discussed later.

23.3.5 System Modeling

23.3.5.1 Event Trees

The staff did not rigorously review the PRA event trees in detail as part of the overall PRA review process. The reason for this was that an extremely detailed and comprehensive methodology had been applied to the event tree

development and, therefore, the staff tried to concentrate its resources on other areas of the PRA.

The applied methodology utilized event sequence diagrams (ESDs) and stressed the involvement of both PRA analysts and plant operations personnel. The staff did check for any obvious errors in the event tree logic structure but found none.

23.3.5.2 Fault Trees

The fault tree review was conducted as part of the systems analyses documented in Appendices A and B to NUREG/CR-5726 (Bozoki and others, in process). This was a major effort which brought into single focus various aspects of PRA, such as validity of the fault trees, level of detail, success criteria, failure data, and requantification of at least a representative number of conditional split fractions. The system documentation associated with the PRA provided reliability block diagrams (as opposed to actual fault trees) containing supercomponents covering large portions of the system. After converting these diagrams into fault trees, the staff could display the leading cut sets for those top events so modeled. Such cut sets are not provided within the PRA.

PG&E quantified the supercomponents in equation form. For the staff requantification, the equation for each of the supercomponents had to be solved as well as broken down to identify/verify its constituent parts. Each equation represented an expression that combined all the failure modes of each of the elements of the supercomponents. The staff also checked the equation against the plant drawings, test and maintenance procedures, and Technical Specifications to verify that all major components, failure modes, and unavailabilities were included.

Then in order to verify the various split fractions associated with each fault tree, the staff set various items to one or zero to define each boundary condition and then solved that version of the fault tree four times to account for the different postulated sets of system alignment as discussed below. The methodology of systems analysis applied in the PRA requires that the top event split fraction (associated with a system under a given boundary condition) should reflect the notion that the system (or its portion) in question is in one of the following mutually exclusive alignments: normal alignment, testing alignment, maintenance alignment, or misalignment. Thus, the contribution to the system unavailability from a specific alignment is determined by the conditional system unavailability, given that the system is in that alignment multiplied by the fraction of time that the system spends in that alignment. The quantification/verification of the conditional split fractions in most cases agreed well with the PG&E results. The difference in the majority of the cases came from some modeling errors of minor significance and from the use of Monte Carlo techniques by PG&E and point estimates by the staff.

The following systems or functions were subjected to detailed review or requantification:

- high-pressure-injection function
- low-pressure-injection function
- auxiliary feedwater system

- diesel generator and diesel fuel transfer systems
- electrical power systems (ac and dc)
- auxiliary saltwater system
- component-cooling-water system
- solid-state protection/reactor protection systems

Frontline Systems

The staff reviewed the high-pressure-injection top event, logic diagrams and corresponding fault trees, along with supporting drawings and other information provided by PG&E. This information included the technical specifications, relevant operating and surveillance test procedures, and fluid-flow and actuation logic diagrams.

The PRA applied the simplifying assumption that the leak would always occur in cold-leg number one. The staff conducted an independent calculation that allowed the leak to occur in any of the four cold legs. The results of the analysis verified the validity of this assumption. The staff concludes that the HPI function system analysis in the PRA represents a fully adequate characterization.

The review of the staff's system analysis of the low-pressure-injection (LPI) function covered the same scope and depth as the HPI review discussed above, as well as an additional sensitivity analysis on the one-out-of-three (1/3) success criterion (flow to 1/3 of the intact loops) used in the PRA. The sensitivity analysis was performed to see the effect of using a 2/3 success criterion as had other previous PRAs. Later in the review, PG&E provided additional documentation to support the 1/3 criterion that was used. On the basis of the additional information, the staff concludes that the 1/3 criterion is adequate.

The PRA also used a simplifying assumption regarding break location for the low-pressure case. That is, it was again assumed that the break would always be in cold-leg number one. When the staff recalculated the split fractions assuming the break could occur in any of the four cold legs, the use of this assumption provided (on average) higher values. The difference in applicability of the same simplifying assumption between the HPI and LPI is the result of differences in the design features of the injection headers. In the case of the RHR system (LPI), each of two header systems feeds its own two branch lines. In the case of the charging and safety injection systems (HPI), one header feeds all four branch lines. In response to the staff review, PG&E requantified certain LPI function split fractions. In the end, the staff calculations agreed well with those presented by PG&E, and the alternative break location assumption produced a negligible increase in CDF when substituted into the DSM.

The staff's review of the system analysis of the auxiliary feedwater system included review of the top event logic diagrams and the corresponding fault trees related to the "low pressure" boundary conditions. The fault trees related to the "high pressure" boundary conditions were not reviewed as they pertained to the ATWT sequences which had no measurable impact on the CDF. During the review, the staff discovered an anomaly between split fractions AW5, AW7, and AW8. AW8 represents a more degraded set of boundary conditions and

yet it had a higher quantified availability than either AW5 or AW7. In the staff calculations, this anomaly did not appear. PG&E responded that this was the result of the way these split fractions went through the truncation process. When PG&E recalculated these split fractions on a point estimate basis, results agreed well with the staff results. When PG&E substituted the new values for these split fractions into its dominant sequence model, PG&E discovered the new values had a significant effect on the CDF. (The staff calculations showed a 38-percent increase in non-seismic mean CDF over PG&E's final results when the staff's values for AW5, AW7, and AW8 were used.) PG&E therefore decided to remove some of the modeling conservatisms present in the original calculations in attaining the final results. [This is discussed in detail in Appendix A3 to NUREG/CR-5726 (Bozoki and others, in process).] The remaining numerical differences between the PG&E and the staff calculations for the AW split fractions were attributed to the different approaches used by PG&E and the staff, Monte Carlo and mean value, respectively.

Support Systems

The results of the staff's detailed system analysis of the diesel generator and diesel fuel transfer systems can be found in Appendix B1 to NUREG/CR-5726 (Bozoki and others, in process). The review noted several inconsistencies and the omission of failures of diesel subsystems in the unavailability modeling of diesel generators in the PRA and the omission of the unavailability contribution from Unit 2 (and swing) diesel overhauls. The combined effect of these omissions may result in underestimation of the associated top event split fractions and through them the expected core damage frequency value of Unit 1. However, when the staff values for the conditional split fractions were substituted into the dominant sequence model, the overall unnormalized Fussel-Vesely importance of this class of events was 4.3E-05 (PG&E value) and 4.2E-05 (the staff value), respectively. This demonstrates excellent agreement between the staff and PG&E.

The results of the staff's detailed system analysis of the entire electrical power system (non-vital electric power, vital 125-V dc, vital ac, instrument ac, and Unit 2 vital ac and dc) can be found in Appendix B2 to NUREG/CR-5726 (Bozoki and others, in process). The staff review identified several inconsistencies and potential omissions in the unavailability modeling of the Diablo Canyon electrical power systems. The combined results of the identified omissions may result in a slight underestimation of the expected core damage frequency of Unit 1. However, the staff's independent calculations agreed closely with those in the PRA concerning the electrical power systems.

The results of the staff's detailed system analysis of the auxiliary saltwater (ASW) system can be found in Appendix B3 to NUREG/CR-5726 (Bozoki and others, in process). As a result of the staff's system analysis review of the ASW system, PG&E performed a number of additional calculations. One of the calculations demonstrated that under most circumstances (but not all as had originally been assumed) a single, Unit 2, ASW pump could supply both Unit 1 (via the cross-tie) and Unit 2 with sufficient ASW flow. This was one of the major concerns of the ASW review. PG&E then performed a sensitivity study to determine the impact of this finding on the overall results. PG&E determined that the change in non-seismic CDF was not appreciable and none of the conditional split fractions were changed as a result. The staff also performed an

independent analysis of the loss of auxiliary saltwater (LOSW) initiator frequency as discussed in Section 23.3 of this SSER.

The staff review of the component cooling water (CCW) system can be found in Appendix B4 to NUREG/CR-5726 (Bozoki and others, in process). This review was not as extensive as the previously described support system reviews. The review was more qualitative in nature in that none of the split fractions were requantified. The staff found some minor omissions and discrepancies, but none were believed to be significant with respect to the overall non-seismic CDF. The staff also performed an independent analysis of the loss of CCW (LOCC) initiator frequency as described in Section 23.3.2 of this SSER.

The staff found that the PRA predicted a lower solid-state protection system (SSPS) unreliability for both a single-channel failure and for system failure (both channels) than the predicted values presented by the Westinghouse Owners Group (WOG) in support of requests to change Technical Specifications. The staff's sensitivity analysis based on changing some split fractions [split fractions, SA (single-channel failures) and SB (second channel failing, given that the first had already failed)] increased the overall non-seismic mean CDF by approximately 19 percent. The comparative review of the RPS analysis with the WOG study/BNL review results showed reasonable agreement and no further review effort beyond that was considered necessary.

In summary, the staff quantification/verification of the conditional split fractions in most cases agreed well with the PG&E results. The difference in the majority of the cases came from the use of Monte Carlo techniques by PG&E and point estimates by the staff. There were a few notable exceptions, as discussed above; however, these were not caused by the fault tree/reliability block diagram structure or level of detail. The staff concludes that the fault trees/reliability block diagrams that were reviewed in detail, adequately represented the Diablo Canyon plant. Alternate split fractions used in the sensitivity analyses are listed later.

23.3.6 Failure Data Analysis

The PRA database was developed by updating the proprietary PLG database. The PLG database was first screened to exclude failure events that were believed clearly not applicable to the Diablo Canyon plant. This screened database then became the source of the "priors" for a Bayesian updating process. Diablo Canyon-specific data was used where available as the "experience" for updating and the resulting posterior distributions became the Diablo Canyon database used in the PRA. Appendix H (specifically Section H.2) of the PRA submitted by PG&E (Shiffer, 1989c) provides a comprehensive treatise on the complete data analysis approach that was used and is, therefore, not repeated here.

Appendix C to NUREG/CR-5726 (Bozoki and others, in process) presents the complete database as provided to the staff by PG&E and reflects its status as of July 8, 1988. Quantification of the conditional split fractions discussed above was based upon this database.

The staff limited its review in this area to a review of the overall methodology and then was specifically guided by the results of the systems analysis reviews. The staff finds acceptable the Bayesian updating approach used for

the PRA. Specific comments on individual failure probabilities are addressed as part of the systems analysis reviews. Specific comments on initiator quantification are in Section 23.3.2 of this SSER.

As a part of the systems analysis review of the auxiliary feedwater (AFW) system, the staff substituted generic failure probabilities into the AFW model to get an idea of how sensitive the results were to the Diablo Canyon-specific data used in the PRA. This analysis showed that the results were not very sensitive to an alternate database.

23.3.7 Human Reliability Analysis Methodology

23.3.7.1 Scope of the Review

The review of the human reliability analysis (HRA) methodology centered on Section 3.5 and Appendix G of the PRA (Shiffer, 1989b). Also reviewed were documents elaborating on the HRA prepared by PG&E and provided to the NRC in response to questions and solicitations arising from this review. These latter documents were included in Shiffer, 1989a and g.

No attempt was made to replicate any of the analyses performed by the PG&E HRA team. Rather, reasonableness of results was judged on the basis of the credibility of modeling, source data, and human factors assessment instruments employed. Therein, the review focused on data, methods, and comprehensiveness of analyses performed to assess involvement of humans as precursors, initiators, and mediators, including recovery, in each PRA accident sequence.

23.3.7.2 Overview of the HRA

The PRA HRA was performed by staff of PG&E and PLG, closely supported by Diablo Canyon plant personnel. The HRA segment of the PRA followed a sometimes iterative six-step process:

- First, event sequence diagrams (ESDs) were used as task analysis tools to identify pertinent human actions that would be analyzed as part of the event and fault trees.

- Second, human task actions identified as pertinent were categorized as skill-, rule-, or knowledge-based (Rasmusson's topology) using the Electric Power Research Institute's human cognitive reliability (HCR) criteria.

- Third, performance-shaping factors (PSFs) were identified by PG&E and PLG HRA team members by means of a nominal group technique, for each human task action selected for analysis.

- Fourth, some 21 equipment- and person-centered PSFs, identified as part of the previous step, were evaluated by the Diablo Canyon operators using a survey instrument developed and pre-tested by the HRA team.

- Fifth, error probability, recovery, and uncertainty estimates were calculated employing the NRC's success likelihood index method (SLIM) as the

quantification tool, and using Three Mile Island PRA human error data as bounding values.

- Sixth, HRA results documentation was guided by precedents established in earlier PRAs, especially Three Mile Island.

23.3.7.3 Summary of Review Findings

This review was conducted using the LTSP Final Report (Brand, 1988) and supplements described above. More specifics of the review and detailed findings are discussed in Section 3.8 of NUREG/CR-5726 (Bozoki and others, in process). On the basis of these documents, the staff concludes that the HRA team conducted a state-of-the-knowledge analysis, and introduced several innovations. These included stand-alone task analyses using ESDs, systematic scaling of PSFs using plant personnel, and applying real PSF data in quantification of human error using an otherwise expert-judgment SLIM approach. The quantitative results (point estimates and uncertainty bounds) emerging from this were reasonable when compared with data from other PRAs. In some instances, the main report failed to document completely and accurately the analyses performed, the techniques employed to gather data, and the manner in which quantification methods were used. Findings regarding lack of clarity and inadequacy of documentation, described in NUREG/CR-5726 (Bozoki and others, in process), while detracting from the HRA, do not compromise its overall acceptability.

23.3.8 Accident Sequence Quantification

23.3.8.1 Approach Used in the PRA

This section of the SSER provides information about some technical aspects of the internal event sequence quantification process. Its content was developed mainly as a result of the review effort because the originally submitted PRA documentation (Brand, 1988) was not sufficiently detailed to permit the staff to review this area.

Quantification of the Support State Modules

According to the PRA, the plant event sequence model was quantified for each initiating event and each support state. Since many of the internal (and seismic) event/support state combinations were extremely unlikely, the PRA grouped them into "other," "more likely," and "similar" groups. The review requested clarification about this procedure. The staff was concerned about the potential error in the plant response analysis if certain support states were neglected entirely. The response from PG&E is reproduced here to offer some detailed insight about the early phases of the event sequence quantification.

> In regards to frequency binning of support states, it should be noted that the PRA does not discard any support states; all support states are retained either explicitly or in a bin. Support states are binned, if low enough in frequency, to a support state with the worst possible impacts (on the frontline systems). The frequency of this support state is added directly

to the core damage frequency (it is not unused). The binning occurs in the following two steps:

The first step evaluates the combination frequency of the electric power event tree end states and the mechanical/actuation event tree end states without regard to impacts on frontline systems. If the combined frequency of an electric power state (i.e., first stage of the support model) and a mechanical/actuation state (i.e., second stage of the support model) for all initiators is low enough (5.0E-10) then this support state is mapped to the bin support state. This cutoff is primarily used to filter out the zero frequency states (i.e., those combinations which are logically impossible) although it is possible that some very low frequency support states are binned in this process.

The second step of binning occurs after the support states have been defined in terms of their impacts on the frontline systems. This binning also is done on the electric power/mechanical and actuation event tree end state combination frequency. Two different cutoffs were used; for the sum of all non-seismic events, the cutoff was 5.0E-09 and for the sum of all seismic events the cutoff was 1.0E-08. Again, all support states with frequencies below these cutoffs were mapped to a "bin" support state with the worst possible impacts.

Quantification of the Frontline System Modules

The support states of the support modules were linked with the sequences of the frontline modules by using a computer code, SQLINK, of the RISKMAN family of codes. From the vast number of sequences that result in core damage, SQLINK selected and retained the leading 1999 sequences. For practical purposes, PG&E developed a reduced dominant sequence model (DSM) by selecting the leading 420 sequences [the dominant sequence model is described in Appendix D to NUREG/CR-5726 (Bozoki and others, in process)].

The final values of the total non-seismic core damage frequencies were determined by multiplying a number of selected sequences by appropriate sequence recovery factors.

Quantification of the Long-Term Frontline System Module

The quantification of the long-term frontline system module LT1 was also performed by the code SQLINK. The reviewers noticed, however, that some of the sequences in the reduced model included top event split fractions associated with certain containment functions seemingly irrelevant to mitigate core damage (e.g., containment isolation). Their effect, at first, seemed simply to somewhat reduce the core damage frequency contribution of those sequences in which they appeared. Upon further review and discussions with PG&E, it was determined that the corollary sequences (i.e., those with the failure state) were also in the overall model, but were of too low a value to, in most cases, make the cutoff for the dominant sequence model. The basis for the inclusion of these top events was to facilitate the Level 2 PRA effort expected to follow.

Special Methods

Owing to their small core damage frequency, sequences belonging to eight of the initiating event categories are not represented in the DSM. In response to the staff's request for an explanation, PG&E supplied the following additional information. For three of the internal initiating events: (1) closure of all MSIVs, (2) main steam relief valve opening, and (3) core power excursion, PG&E calculated the core damage frequencies by the following special method:

> The conditional core damage frequency for these three initiators was assumed to be equal to the conditional core damage frequency for reactor trip initiating event after recovery; this assumption was based on the fact that the quantification of the event tree models for these initiating events are similar. The conditional core damage frequency for the reactor trip event was calculated by dividing the core damage frequency for reactor trip initiating event, by the reactor trip initiating event frequency. This conditional core damage frequency was then multiplied by the initiating event frequencies for "Closure of All MSIVs," "Main Steam Relief Valve Opening," and "Core Power Excursion" to calculate the corresponding core damage frequencies.

The core damage frequency resulting from interfacing systems LOCA (RHR pump discharge side) was estimated using a special interfacing LOCA event tree.

Uncertainty Analysis of the Total Internal Core Damage Frequency

The uncertainties of the core damage frequencies resulting from (strictly) internal events and resulting from the non-seismic external events (fires, floods, chemical hazards) included in the DSM were determined in the PRA by using Monte Carlo techniques.

23.3.8.2 Internal Event Sequence Characteristics and Results of the Staff Quantification

Initial documentation of the PRA and its results was limited to Chapter 6 of the LTSP Final Report (Brand, 1988). As such, a significant amount of information required for this review as well as insights that might be derived from the PRA were missing. This review has subsequently surfaced considerably more information and has sought to independently offer insights where feasible. To this end, the staff performed detailed initiator, system, and top event importance analyses for the whole model, both globally and also for each individual initiator/conditional split fraction based on the non-seismic dominant sequence model (DSM). The results of these review efforts are presented in the following sections of this SSER. As one would expect, several of the results will reiterate those of the original PRA; however, others provide some useful additional information.

Initiator Importance

The core damage frequency contributions for non-seismic initiators listed in Table 23.5 were calculated by using the DSM. Table 23.7 lists the ranked unnormalized and normalized Fussel-Vesely importance of the initiating events included in the DSM. Table 23.7 also includes the results of the Birnbaum importance analysis. Table 23.8 shows the core damage frequency contributions to the non-seismic core damage frequency due to initiating events not included in the DSM. Their total estimated contributions seems to be indeed negligible.

Using the data given in Table 23.7, one can make the following observations about the characteristics of the internal event sequences:

(1) The majority (73%) of the non-seismic core damage frequency results from internal events.

(2) The loss of offsite power (LOOP) initiator is by far the greatest contributor to the non-seismic core damage (24%), in magnitude and in number of leading sequences. About 3/4 of the LOOP-induced core damage is associated with extended unit blackout (for additional details see the Special Issues Importance Summary, Table 23.10).

(3) Initiators representing (common cause) support system failures other than LOOP [i.e., loss of one dc bus (L1DC), total loss of auxiliary saltwater (LOSW), total loss of component cooling water (LPCC), loss of 480-V switchgear ventilation (LOSWV), loss of control room ventilation (LOCV)] contribute about 9.6 percent to the non-seismic core damage frequency. Including LOOP, this initiator group is associated with 1/3 of the estimated core damage frequency, more than all the external initiators (fire, flood, etc.) combined. The plant mitigating capability against these initiators is varied (see the conditional core damage probabilities, i.e., Birnbaum importance); the worst is for the initiating event, loss of 480-V switchgear ventilation, LOSWV. This is followed by the loss of component cooling water, LPCC, and the loss of auxiliary saltwater, LOSW; then come LOOP, L1DC, and LOCV. (One should keep in mind that the ranking of the plant mitigating capability might be somewhat biased because many of the LOOP sequences were subjected to "sequence recovery" considerations, while others were not.) The average conditional core damage probability for this group of initiators is approximately 3.0E-04.

(4) Transients contribute to the non-seismic core damage frequency almost in the same proportion as the support system failures, i.e., 31 percent. Reactor trips, turbine trips, and feedwater losses are rather frequent initiating events. Their high frequency of occurrence represents a challenge to the plant's safety systems, but their nature seems to be mild. The average conditional core damage probability for this group is one order of magnitude smaller than that of the group associated with support system failures, i.e., 3.0E-05.

Table 23.7 Initiating event contributions to non-seismic CDF dominant sequence model

Initiating Event			Importance				
No. (i)	Designator	Category	Frequency, Ii (Per Year)	Unnormalized FUSS-VES	FUSS-VES (%)	BIRNBAUM	# of CD Sequences
1	LOOP	Loss of Offsite Power	9.10-02	4.18-05	23.57	4.59-04	183
2	CRFIRE	Control Room and Cable Spreading Room Fires		3.17-05	17.87		1
3	RT	Reactor Trip	1.14+00	1.62-05	9.13	1.42-05	34
4	TT	Turbine Trip	1.05+00	1.48-05	8.34	1.41-05	33
5	PLMFW	Partial Loss of Main Feedwater	7.49-01	1.08-05	6.09	1.45-05	26
6	L1DC	Loss of One DC Bus	2.56-02	9.50-06	5.36	3.71-04	34
7	FS8	Fire Scenario: Loss of 4.16kV Buses HF, HG and HH	6.88-06	6.48-06	3.65	1.00+00	2
8	FS11	Flood Scenario: Loss of Auxiliary Saltwater	3.81-04	6.20-06	3.50	1.63-02	4
9	MLOCA	Medium LOCA	4.63-04	5.97-06	3.37	1.29-02	7
10	SGTR	Steam Generator Tube Rupture	1.71-02	3.58-06	2.22	2.10-04	12
11	LPCC	Total Loss of Component Cooling Water	1.96-04	3.19-06	1.80	1.63-02	4
12	EXFW	Excessive Feedwater Flow	2.79-01	3.12-06	1.76	1.12-05	9
13	SLBO	Steam Line Break Outside Containment	5.53-03	2.80-06	1.58	5.06-04	24
14	LLOCA	Large LOCA	2.02-04	2.58-06	1.45	1.28-02	4
15	SLBI	Steam Line Break Inside Containment	4.63-04	2.38-06	1.34	5.15-03	8
16	SLOCI	Small LOCA; Isolable	1.61-02	1.81-06	1.02	1.12-04	6
17	LOSWV	Loss of 480V Switchgear Ventilation	6.29-05	1.61-06	.91	2.56-02	6
18	FS1	Fire Scenario: Loss of Both Motor-Driven AFW Pumps	2.94-04	1.47-06	.83	5.00-03	9
19	LOSW	Total Loss of Auxiliary Saltwater	9.74-05	1.45-06	.82	1.49-02	2
20	LOCV	Loss of Control Room Ventilation	7.99-02	1.24-06	.70	1.55-05	6
21	FS6	Fire Scenario: Loss of 4.16kV Buses HF and HG	2.42-05	1.10-06	.62	4.54-02	2
22	LOPF	Loss of Primary Flow	1.21-04	1.08-06	.61	8.89-06	5
23	IMSIV	Closure of One MSIV	1.07-01	9.51-07	.53	8.89-06	5
24	TLMFW	Total Loss of Main Feedwater	9.98-02	8.87-07	.50	8.89-06	5
25	SLOCN	Small LOCA; Non-Isolable	5.26-03	8.17-07	.46	1.55-04	4
26	LCV	Loss of Condenser Vacuum	8.73-02	7.76-07	.44	8.89-06	5
27	FS9	Flood Scenario: Loss of All AFW	1.35-05	6.87-07	.39	5.09-02	2
28	ISI	Inadvertent Safety Injection Signal	7.39-02	6.57-07	.37	8.89-06	5
29	FS5	Fire Scenario: Loss of Auxiliary Saltwater	5.26-05	5.71-07	.32	1.09-02	1
30	VSI(SS)	Interfacing LOCA (RHR Suction Side)	1.01-06	5.00-07	.28	4.95-01	1
31	HAZCHM	Chemical Hazard (e.g., chlorine/ammonia releases)	4.39-04	3.51-07	.20	7.99-04	1
32	ELOCA	Excessive LOCA	2.66-07	2.66-07	.15	1.00+00	1
33	FS10	Flood Scenario: Loss of Both Motor-Driven AFW Pumps	1.40-05	2.93-08	.02	2.10-03	1
		Total Internal		1.29-04	72.72		
		Total "External"		4.84-05	27.28		
		Total CDF (Dominant Sequence Model)		1.77-04			452

Table 23.8 Initiating event contributions to non-seismic CDF initiating events not included in the DSM

Initiating Event			Importance				
No. (i)	Designator	Category	Frequency, Ii (Per Year)	Unnormalized FUSS-VES+	FUSS-VES++ (%)	BIRNBAUM	# of C Sequences
34	CPEXC	Core Power Excursion	2.19-02	3.11-07	.18	1.42-05*	34
35	AMSIV	Closure of All MSIVs	1.74-02	2.47-07	.14	1.42-05*	34
36	VDI	Interfacing Systems LOCA (RHR Discharge Side)	3.86-06	5.80-08**	.03	1.50-02	1
37	MSRIV	Inadvertent Opening of Main Steam Relief Valve	3.59-03	5.10-08	.03	1.42-05*	34
		Total Internal CDF (Neglected by the Dominant Sequence Model)				6.67-07	

+Estimated by special methods.
++For normalization, the total CDF (Dominant Sequence Model) was used.
*Taken from Table 23.7 for RT initiator.
**Taken from Table 6-59 of the DCPRA.

Among the transients, the most sensitive initiating event is the steam-line break accident, particularly if the break is inside the containment. For each transient event, the conditional probability of failure to mitigate (Birnbaum importance) the transient was determined. In order of decreasing importance, the events belonging to this group rank as follows: SLBI, SLBO, PLMFW, RT, TT, EXFW, LOPF, IMSIV, TLMFW, LCV, and ISI.

(5) The total contribution of initiators belonging to the loss of coolant inventory group to the non-seismic core damage frequency is small, about 9 percent. Birnbaum importance ranking of the LOCAs is as follows: ELOCA, VSI (SS), LLOCA, MLOCA, SGTR, SLOCN, SLOCI.

In order to compare the Diablo Canyon plant responses for various types of internal event sequences with those of other PWRs, nine PRAs were selected, the majority of them representing Westinghouse plants. These were: Seabrook, Zion, Sequoyah, Surry, Millstone 3, Indian Point 2 and 3, Oconee, and Yankee Rowe PRAs. It must be noted that all of these PRAs were done on different bases for different utilities by different analysts. Therefore, the resulting insights yield an enhanced perspective of the Diablo Canyon plant and not a comprehensive and rigorous basis for direct numerical comparisons. These insights are discussed in NUREG/CR-5726 (Bozoki and others, in process).

Leading Non-Seismic Event Scenarios

Individual scenarios having core damage frequency $\geq$ 1.0E-06/yr selected from the dominant sequence model are listed in Part A of Table 23.9. The listing follows the ranking of the individual scenarios according to the contribution to the non-seismic core damage frequency. In addition to the individual ranking, the listing also gives information about the sequence ranking of appearance of the leading sequence of each given initiator.

In order to make the latter information more complete, Part B of Table 23.9 provides the ranking of the leading sequences associated with initiators not listed in Part A.

By examining the table one can make several observations:

(1) Except for the set of control room/cable spreading room fire sequences, CRFIRE, there is no scenario which contributes more than 3.5 percent to the non-seismic core damage frequency.

(2) In spite of the fact that the initiating event LOOP is the main contributor to the non-seismic core damage frequency, only two LOOP sequences appear among the leading 23 scenarios and the rank of the first one is 17th.

(3) External scenarios tend to have higher rank than internal scenarios.

(4) Transients (mainly RT, TT, PLMFW initiators) appear predominantly among the leading internal sequences as opposed to LOCAs.

(5) Among the initiators associated with support system failures, a loss of component cooling water (LPCC) sequence has the highest rank.

Table 23.9 Event scenarios ranked according to non-seismic CDF contribution of dominant sequence model

CDF Rank	CDF Contribution	Sequence	
Part A:	Leading Event Scenarios		
1	3.170-05	CRFIRE	
2	6.180-06	FS8	* IAF * AFF * AGF * AHF * CCF
3	5.377-06	RT	* IAF * HS1 * /RF4 * /CI1
4	4.953-06	TT	* IAF * HS1 * /RF4 * /CI1
5	4.136-06	FS11	* IAF * ASF * RP2 * SE1
6	3.533-06	PLMFW	* IAF * HS1 * /RF4 * /CI1
7	2.283-06	MLOCA	* IAF * RF3
8	2.128-06	LPCC	* IAF * ASF * RP2 * SE1
9	1.714-06	L1DC	* DGF * I2F * I3F * DH2 * I4F * AWA
10	1.705-06	MLOCA	* IAF * LB2 * LA3
11	1.699-06	L1DC	* DGF * I2F * I4F * AWA * AH4
12	1.524-06	FS11	* IAF * ASF * /RP2
13	1.398-06	EXFW	* IAF * HS1
14	1.267-06	LLOCA	* IAF * AC1
15	1.250-06	RT	* OB1 * I11 * AW5
16	1.280-06	RT	* OB1 * I31 * AW5
17	1.241-06	LOOP	* IAF * OGF * SW1 * AW3 * VI2
18	1.157-06	RT	* IAF * OB1 * AW1 * /RF4 * /CI1
19	1.152-06	TT	* OB1 * I11 * AW5
20	1.152-06	TT	* OB1 * I31 * AW5
21	1.134-06	LOOP	* IAF * OGF * LA1 * PRD * REAC06 * GH1
22	1.132-06	TT	* IAF * OB1 * AW1
23	1.057-06	LOSW	* IAF * ASF * RP2 * SE1
Part B:	Appearance of the First Event Scenario Associated with a Given Initiator Not Listed Above		
32	8.269-07	SGTR	* IAF * SL1 * MU1
49	6.889-07	FS6	* IAF * CC5 * AFF * AGF * RP2
58	6.334-07	SLBO	* IAF * LA1 * LB2 * MS2 * AWB
64	6.062-07	LOPF	* IAF * HS1
66	5.861-07	SLOCI	* IAF * LA1 * LB2 * PRN
67	5.823-07	FS1	* IAF * AW4 * OB1 * /RF4
68	5.710-07	FS5	* IAF * ASF * RP2 * SE1
74	5.360-07	IMSIV	* IAF * HS1
75	5.257-07	LOVC	* CVF * OSF * RT1
78	5.000-07	TLMFW	* IAF * HS1
79	4.999-07	VSI	* IAF * IT1 * ME1
81	4.816-07	SLBI	* MS2 * SA5 * SBE * OSF
84	4.767-07	LOSWV	* SVF * SA1
93	4.373-07	LCV	* IAF * HS1
105	3.901-07	FS9	* IAF * OB1
111	3.702-07	ISI	* IAF * HS1
119	3.507-07	HAZCHM	* ZHEHS5 * POINT1
144	2.913-07	SLOCN	* IAF * LA1 * LB2 * MU2 * /CI1
158	2.660-07	ELOCA	* IAF
356	2.933-08	FS10	* IAF * AW4 * OB1

Table 23.9 (Cont'd.) Event scenarios ranked according to non-seismic CDF contribution of dominant sequence model

Description of Top Events

HAZCHM	Designator for all chemical release sequences (in particular, chlorine and ammonia releases).
IAF	Global failure of instrument air system.
AFF,AGF,AHF	Guaranteed failure of vital 4.16kV ac buses: F, G, and H.
AH4	Failure of vital 4.16kV ac bus H, given failure of dc power train G (DG-F).
DFF,DGF,DHF	Global failure of vital 125V dc power train F, G or H.
DH2	Failure of vital 125V dc power train H, given available 480V ac bus 1H and top event DF failure and top event DG success (DF-F, DG-S).
OGF	Global failure of non-vital ac power from 230kV switchyard.
GH1	Failure of diesel generator 11, all support systems available.
SW1	Swing diesel is aligned to Unit 2.
I1F,I2F,I3F,I4F	Global failure of instrument ac channel I, II, II or IV.
I11,I21,I31,I41	Failure of instrument ac channel I, II, III or IV, with all support system or previous trains available.
RT1	Failure of reactor protection system; 1/2 trains, both SSPS signals generated.
SA1	Failure of signal generation (General Transient) by train A of the SSPS; all support available.
SA5	Failure of signal generation (SLBIC) by train A of the SSPS; all four instrument channels available.
SBE	Failure of signal generation (SLBIC) by train B, given failed train A; all four instrument channels available.
CVF	Global failure of control room ventilation system.

Table 23.9 (Cont'd.) Event scenarios ranked according to non-seismic CDF contribution of dominant sequence model

SVF	Global failure of 480V switchgear ventilation system.
ASF	Global failure of auxiliary saltwater system.
CCF	Global failure of component cooling water system.
CC4	Failure of component cooling water system, given loss of 4.16kV buses F and G.
	Failures of Auxiliary Feedwater System, Low Power
AW1	All support system available.
AW3	Support for one MDP unavailable.
AW4	Support for two MDPs unavailable.
AW5	Support for all 10% steam dump unavailable.
AWA	Support for all 10% steam dump, one MDP and TDP unavailable.
AWB	One SG depressurizes, all support systems available.
	Failures of ECCS, Low Pressure
AC1	Failures of accumulators and cold leg path.
LA1	Failure of RHR train A, all support available (SLOCA).
LA3	Failure of RHR train A, all support available (MLOCA).
LB2	Failure of RHR train B; given failed top event LA (SLOCA).
MU1	Failure of RHR suction from the hot leg or RWST makeup; power at ac buses G and H available.
MU2	Failure of makeup to RWST (via RFW pump); power available at ac buses G and H.
	Failures of Primary RCS Pressure Relief
PRD	1/2 PORVs or (1/3 SRVs) sticks open and is not isolated given LOSP/SGTR. No block valve available.
PRN	1/1 block valve closes, all support available.
OB1	Failure of feed and bleed (PORV opening and reclosure) given loss of instrument air.
MS2	Failure of main steamline isolation; given failed TT, all support available.

Table 23.9 (Cont'd.) Event scenarios ranked according to non-seismic CDF contribution of dominant sequence model

/CI1	Success of containment penetration isolation (inboard or outboard isolation valves for penetrations 50, 51, 52, and 45 are successful).
SE1	Failure to align backup cooling to charging pumps for RCP seal cooling; CCWS fails.
SL1	Failure of isolation of ruptured steam generator, all support available.
IT1	Failure of RHR piping integrity; VO successful (RHR pressure relief valves open).
ME1	RHR hole size >4 inches.
VI2	Failure of vessel integrity (due to pressurized thermal shock); loss of secondary heat sink.
Point1	Conditional probability of core damage in chemical sequences given that the CST was not initially replenished.
HS1	Failure of operator action to maintain hot standby (loss of control after an accident); all support systems are available.
REAC06	Failure to recover vital 4.16kV ac power before recirculation required.
OSF	Operator failure to actuate failed SSPS automatic actuation.
RP2	Operator failure to trip RCPs to prevent LOCA; given loss of CCW.
/RP2	Operator success to trip RCPs to prevent LOCA, given loss of CCW.
RF3	Failure of manual switchover to recirculation after LLOCA or MLOCA.
/RF4	Successful switchover to recirculation after core melt.
ZHEHS5	Operator failure to replenish the condensate storage tank.

(6) Among the system/component failures of the plant, loss of feed and bleed cooling (top event OB), loss of auxiliary feedwater system (top event AW), and occurrence of RCP seal LOCA (top event SE) are the most frequent.

The first observation implies that the present ranking of the leading sequences is not robust; that is, very small changes in the sequence variables (i.e., initiator frequency, top event split fractions, recovery actions) may change the ranking significantly. Change in the ranking is fairly conceivable because recovery actions were not applied to a great many of the internal event sequences and the PRA considers the potential for additional recovery actions for numerous scenarios where recovery actions already were applied.

The first observation has also a technical impact on the review process. The significance of changes or errors in the initiating event frequencies, top event split fractions, and such, cannot be estimated by simply changing several variables in a small group of leading sequences with high frequency as was the case in the majority of older PRAs. In the case of this PRA, where a relatively large number of sequences contribute almost uniformly to the core damage frequency, sensitivity calculations have to be carried out by performing more sophisticated importance analyses such as those done by the staff in this review.

Special Issues of Interest to PRA

This section of the SSER presents the results obtained by PG&E concerning several issues of special interest to PRAs that were identified in the PRA, but for various reasons were not presented in the LTSP Final Report. They were submitted to the staff as a consequence of the review effort. The nature of the issues involves both the non-seismic and seismic initiating events; therefore, the scope of the following presentation goes beyond the non-seismic scenario analysis. The presentation roughly follows the text of the PG&E submittal.

Six issues of special interest to PRAs are identified in the PRA:

- reactor coolant pump seal LOCA
- station blackout
- primary relief valves open and fail to reclose
- feed and bleed cooling
- PWR pressurized thermal shock (PTS)
- failure to trip the reactor (ATWT)

These issues are of interest because NRC has categorized them as unresolved safety issues or they are significant contributors to risk in other PRAs.

The core damage frequency and percent contribution to core damage frequency of each of these categories (i.e., unnormalized and normalized Fussel-Vesely importance) are presented in Table 23.10. These quantities are provided for both non-seismic and seismic initiators.

From the DSM, PG&E computed the contributions to core damage frequency associated with non-seismic initiators. PG&E sorted the scenarios in the DSM into special scenario groups indicated in the table and summed the frequencies of each group to determine contribution to each of the categories.

Table 23.10
Special issues importance summary

Special Scenario Group	Importances: Non-Seismic Unnormalized Fuss-Ves	Non-Seismic Fuss-Ves (%)	Seismic Unnormalized Fuss-Ves	Seismic Fuss-Ves (%)	Total Unnormalized Fuss-Ves	Total Fuss-Ves(%)
1. Station Blackout						
a. RCP Seal LOCA	2.3-05	13	1.8-05	53	4.1-05	19
b. Failure of Secondary Heat Removal	5.9-06	3	7.4-06	22	1.3-05	6
c. Primary Relief Valve Open and Fail to Reclose	2.2-06	1	1.4-06	4	3.6-06	2
d. Total	3.1-05	17	2.7-05	79	5.8-05	27
2. Failure of Reactor Trip (ATWT)						
a. Non-Station Blackout	1.4-06	.8	5.0-07	2	1.9-06	1
b. Station Blackout	0.0	0	3.2-06	9	3.2-06	2
c. Total	1.4-06	.8	3.7-06	11	5.1-06	3
3. RCP Seal LOCA (Non-Station Blackout)	3.0-05	17	1.8-06	5	3.2-05	15
4. Primary Relief Valve Open and Fail to Reclose	3.4-05	19	1.0-06	3	3.5-05	17
5. Bleed & Feed Cooling	2.0-05	11	0.0	0	2.0-05	9
6. Pressurized Thermal Shock	7.2-06	4	0.0	0	7.2-06	3

Notes to the table:
2a Seismic core damage sequences due to failure of reactor trip but not concurrent with station blackout.
2b Seismic core damage sequences due to failure of reactor trip with station blackout.
3 Non-station blackout scenarios; these scenarios result from loss of RCP seal injection and cooling.
4 Non-station blackout scenarios.
5 For seismic events, the contribution to core damage due to failure of operators to initiate bleed and feed cooling is negligible.
6 PTS events were not modelled for seismic initiators.

The scenarios associated with ATWT events in the DSM were supplemented with additional ATWT event sequences identified from a larger list of key sequences, including sequences that were too low in frequency to be included in the DSM.

To normalize the unnormalized non-seismic Fussel-Vesely importance, the total non-seismic core damage frequency (Table 23.7) was used.

For seismic initiators, PG&E obtained the contributions to core damage frequency from the PRA seismic key event sequence list, not the seismic uncertainty model. The key sequence list (the top 791 core damage sequences) accounts for approximately 82 percent of the total seismic core damage frequency. It was assumed that the remaining 18-percent contribution to the seismic core damage is distributed proportionally among each of the scenario groups of interest. The contributions from each of the scenario groups in the key event sequence list were therefore scaled up. The point estimate seismic core damage frequency from the key sequences is 3.4E-5/yr. This is the normalization value for the associated importances. The contributions from the scenario groups of interest shown in Table 23.10 are not mutually exclusive. Therefore, care must be taken when combining different scenario groups. For example, it would be incorrect to add the seismically initiated station blackout "ATWT" contribution to the "total" seismically initiated station blackout contribution since the "total" already contains the "ATWT" contribution. Notes to the table indicate the type of sequences that each of the groups contains.

From Table 23.10, one can obtain one of most important insights of the whole PRA: the vulnerability ranking of the Diablo Canyon plant for these special failure categories. This information is summarized in Table 23.11.

Table 23.11 Fussel-Vesely importance of the special failure categories

Special failure category	Fussel-Vesely importance (%)		
	Non-seismic	Seismic	Total
1. RCP seal LOCA (with and without station blackout)	31	58	35
2. Station blackout	18	79	28
3. Primary relief valves open and fail to reclose	20	3	17
4. Feed and bleed cooling	12	0	10
5. Pressurized thermal shock	4	0	3
6. Failure of reactor trip (ATWT)	0.8	11	3

It is noted here for completeness that the very low ATWT contribution reflects the fact that Diablo Canyon has made modifications to the reactor protection system in accordance with the NRC's ATWT (ATWS) rule.

Individual Split Fraction Importances

In order to gain insights into the importances of the individual top event split fractions, the staff performed a dedicated top event split fraction importance analysis. The detailed results of that analysis are presented in NUREG/CR-5726 (Bozoki and others, in process).

The overall ranking of the leading top event split fraction (CSF) importances is shown in Table 23.12.

Table 23.12 Fussel-Vesely importance for the leading top events

Top event		CSF	Normalized Fussel-Vesely importance (%)*
(1)	Operator inability to maintain hot standby (everything available)	HS1	11.5
(2)	Loss of primary pressure relief (loss of PORV operability for feed and bleed. No instrument air)	OB1	9.9
(3)	Loss of primary pressure relief (for LOOP/SGTR, failure of 1/2 PORVs or 1/3 SRVs)	PRD	9.1
(4)	Loss of DG13 (after loss of 4-kV bus HF).	GF1	8.6
(5)	Failure to trip RCP, after loss of CCWS to prevent seal LOCA.	RP2	6.8
(6)	Loss of DG12 (DG13 is successful).	GG1	6.3

*For normalization, the total non-seismic core damage frequency was used.

System Level/Operator Action Importances

In order to gain insights into the vulnerability of the Diablo Canyon plant with respect to system level failures, the staff performed a system level importance analysis using the dominant sequence model. The analysis included separate importance calculations for (1) support systems, (2) frontline systems, and (3) operator and recovery action failures. Each of these explicitly appear in the event sequences as top event split fractions. The analysis was global, in the sense that it did not distinguish between the various initiating events. In the analyses, each system/operator action importance was determined by calculating the importance of its associated top event or an aggregate of top events appearing in the DSM.

Table 23.13 presents the unnormalized Fussel-Vesely importances for both the overall systems safety functions as well as the constituent top events. Part A lists the support system, Part B the frontline system, and Part C the operator/recovery action importances. The system/operator action importances are given in ranked order.

Table 23.13 System/operator action importance for non-seismic CDF ranking according to system/operator action importances

A. Dominant Sequence Model, Support Systems

Support System	Associated Top Event(s)	Fussel-Vesely Importances: Unnormalized Top Event Importance	Fussel-Vesely Importances: System Importance	Fussel-Vesely Importances: Syst. Imp. (%)
Diesel Generator Systems			4.255-05	24.0
a. Unit 1 DGs	GF	1.517-05		
	GG	1.983-05		
	GH	2.139-05		
b. Unit 2 DGs	TG	7.387-06		
	TH	7.099-06		
c. Swing Diesel Alignment	SW	9.262-06		
d. Diesel Fuel Oil Transfer	FO	7.004-06		
Vital 125V DC Power, Unit 1			1.681-05	9.5
	DF	2.281-06		
	DG	3.926-06		
	DH	1.006-05		
Instrument AC Power			1.138-05	6.4
	I1	3.675-06		
	I2	1.771-06		
	I3	4.159-06		
	I4	1.771-06		
Component Cooling Water	CC	1.065-05	1.065-05	6.0
Vital AC Power, Unit 1			8.605-06	4.9
	AF	2.428-06		
	AG	6.722-07		
	AH	5.500-06		
	SF,SG,SH	---		
Solid State Protection System			5.153-06	2.9
	SA	4.000-06		
	SB	4.376-06		
480V Switchgear Ventilation	SV	4.411-06	4.411-06	2.5
Auxiliary Saltwater	AS	2.588-06	2.588-06	1.5
Control Room Ventilation	CV	2.583-06	2.583-06	1.5
Reactor Protection System	RT	1.558-06	1.558-06	0.9
Non-Vital Electric Power			1.309-06	0.7
	OG	1.309-06		
	NV	---		
Vital AC and DC Power, Unit 2			7.511-07	0.4
	BF	---		
	BG	5.402-07		
	BH	2.109-07		

Table 23.13 (Cont'd.) System/operator action importance for non-seismic CDF ranking according to system/operator action importances

B. Reduced Model, Frontline Systems

Frontline System	Associated Top Event(s)	Fussel-Vesely Importances Unnormalized Top Event Importance	Fussel-Vesely Importances Unnormalized System Importance	Fussel-Vesely Importances Syst. Imp. (%)
Auxiliary Feedwater System			4.586-05	25.9
	AW	4.586-05		
	TD	---		
Primary RCS Pressure Relief			3.717-05	21.0
	PR	1.689-05		
	PO	---		
	OB	2.028-05		
ECCS, Low Pressure			1.390-05	7.8
	LA	7.519-06		
	LB	7.149-06		
	LV	2.125-07		
	RW	2.072-07		
	VA	2.292-07		
	VB	7.663-07		
	AC	1.267-06		
	LI	---		
	MU	1.918-06		
ECCS, High Pressure			7.456-06	4.2
	CH	8.943-07		
	SI	7.268-07		
	HR	1.085-06		
	RC	---		
	RF(-RF4)	4.794-06		
Reactor Vessel Integrity After Pressurized Thermal Shock (PTS)	VI	7.175-06	7.175-06	4.0
Turbine Trip and Main Steam Isolation			5.984-06	3.4
	TT	---		
	MS	5.984-06		
Isolation of Ruptured SG	SL	1.940-06	1.940-06	1.1
Interfacing LOCA Tree Top Events			5.0-07	.3
	VO,VC,VR,SM	---		
	IT	5.0-07		
	LW	---		
	ME	5.0-07		
Containment Isolation			3.524-07	.2
	CI	3.524-07		
	CP,WL	---		
Containment Spray			2.982-08	.02
	CS	3.364-10		
	SR	2.949-08		

Table 23.13 (Cont'd.) System/operator action importance for non-seismic CDF ranking according to system/operator action importances

C. Reduced Model, Operator and Recovery Actions

Action	Associated Top Event(s)	Fussel-Vesely Importances: Unnormalized Top Event Importance	Fussel-Vesely Importances: Unnormalized Op. Action Importance	Fussel-Vesely Importances: Operator Action Imp. (%)
Maintain Control for Hot-Standby After an Accident	HS	1.960-05	1.960-05	11.0
Operator Trips RCPs After Loss of CCW to Prevent Seal LOCA	RP	1.215-05	1.215-05	6.8
Actions Needed to Maintain RCP Seal Cooling	SE	8.999-06	8.999-06	5.1
Electric Power Recovery Factors			5.958-06	3.4
	RESLC1	1.645-06		
	RESLC2	1.484-06		
	RESLC3	9.360-08		
	REAC06	2.733-06		
	REAC12	2.925-09		
Secure SI Per Operating Procedures Following SGTR	OP	1.643-06	1.643-06	0.9
Various Human Failures in Accident Recovery			1.136-06	0.6
	ZHESV3	2.874-07		
	ZHEHS5	3.508-07		
	ZHEAW4	8.748-08		
	ZHERP2	1.709-07		
	ZHESW1	2.236-08		
	ZHERE2	2.018-08		
	ZHEAW3	2.584-08		
	ZHEFO6	1.153-07		
	ZHEOB2	5.587-08		
Operator Actuation of SSPS Signal	OS	1.069-06	1.069-06	0.6

The most important support systems are: (1) the diesel generator systems and (2) the Unit 1 125-V dc power system. The most important frontline systems are: (1) auxiliary feedwater and (2) primary pressure relief. The most important operator action is maintaining hot-standby given a transient.

System Importances in Accident Sequences Induced by Various Initiators

Two questions posed frequently in connection with nuclear plant safety are: (1) Given an initiating event of a certain type, which are those safety systems/operator actions whose unavailabilities dominate the failure to mitigate the variety of event scenarios that may follow that initiator? (2) Given a safety system or operator action with its characteristic unavailability, which are those initiating events where this unavailability contributes most to the core damage frequency?

In order to give quantitative answers, the staff extended its system's importance analysis to individual initiating events. The staff analyzed each of the initiating events of the dominant sequence model by setting to zero all the initiating events in the DSM but the one of interest, and setting that event to a value of 1.0. Results of this analysis and insights derived are discussed in detail in NUREG/CR-5726 (Bozoki and others, in process).

Importances of System/Top Event Split Fraction Pairs

Individual system/top-event split fraction pair importances provide information that can be used to identify system/human action unavailabilities whose simultaneous occurrence is critical with regard to the core damage frequency. The identification of these pairs is more relevant for plant safety from an operational point of view; it guides the plant personnel to, for example, assess the advisability of permitting simultaneous activities (maintenances, tests) on two systems that may not be prohibited by the technical specifications.

The paired system importances represent a generalization of these concepts. They are determined by calculating the importances of the intersection between two aggregates of top-event split fractions, where each aggregate contains the top-event split fractions associated with a given system. The unnormalized Fussel-Vesely importances of support system pairs, as well as those of frontline system-support system pairs are tabulated in matrix form in detail in NUREG/CR-5726 (Bozoki and others, in process). Similar values in the tables express strongly correlated top events in the support system event tree module.

The overall ranking of the top five support system-support system pair importances is as follows:

(1) component cooling water - diesel generator systems
(2) component cooling water - vital 125-V dc systems
(3) diesel generator systems - vital 125-V dc systems
(4) control room ventilation - diesel generator systems
(5) 480-V switchgear ventilation - diesel generator systems

The overall ranking of the top five frontline system support system pair importances is as follows:

(1) primary RCS pressure relief - diesel generator systems
(2) auxiliary feedwater system - diesel generator systems
(3) primary RCS pressure relief - instrument ac power
(4) auxiliary feedwater system - instrument ac power
(5) auxiliary feedwater system - vital 125-V dc systems

The pair importances presented in this section of the SSER reflect aggregated split fractions and, in some cases, aggregated top events to represent the system/function level. Unnormalized Fussel-Vesely importances, as well as the associated Birnbaum importances, were also calculated for a variety of combinations of all top-event, individual split fractions of the DSM. These are listed in ranked form (according to the unnormalized Fussel-Vesely importance) in nine tables [Tables D2.1 through D2.9 of Appendix D2 to NUREG/CR-5726 (Bozoki and others, in process)]. Each of the tables provides some additional insight into plant safety. Among them, perhaps the most enlightening are those pair importances which describe support system-operator/recovery actions (Table D2.8), frontline system-operator/recovery actions (Table D2.6) and operator/recovery-operator/recovery actions (Table D2.9) top-event, split fraction pairs.

23.3.9 Summary and Conclusions of Internal Events Review

Alternative quantification has been offered throughout the report on a multitude of individual items/issues as a result of the internal events review. This section of the SSER collects these individual items and incorporates them into a set of integrated CDF calculations.

Table 23.14 lists each of the items within the PRA internal events review for which alternative quantification has been offered and any significant difference has been noted with the original/updated PRA. Table 23.14 also lists the original values provided by PG&E as well as the alternative values used by the staff in sensitivity estimates throughout the report.

Table 23.16 provides the results of a set of overall internal event CDF calculations in an attempt to place the internal events review results into an integrated and proper perspective. Case 1 in the table is simply the solution to the original DSM as described in Section 23.3.8 of this SSER (minus the external events). Case 2 represents Case 1 plus the three updated initiators provided by PG&E as a result of this review, and essentially represents the updated PRA internal event results. Case 3 represents Case 2 plus the substitution of the staff split fraction quantification from Table 23.14. Case 4 represents Case 3 plus the substitution of the staff value for LOOP. Case 5 represents Case 4 plus the staff values for LOSW, LPCC, and SLOCN. Case 6 represents the substitution of all alternative staff values from Table 23.14 into the DSM.

The staff concludes that Case 4 represents the most reasonable set of alternative quantification of those offered in Table 23.14. Case 2 is simply the updated PG&E results and Case 3 does not include the solar magnetic storm contribution identified by the staff for the LOOP initiator. Cases 5 and 6 are dominated by initiator frequencies that are heavily dependent on long-term industry-wide experience. On the basis of Diablo Canyon's demonstrated ability to avoid plant transients, as well as the industry trend to fewer transient events per year, the staff concludes that these cases are overly pessimistic.

Table 23.14 Major elements of alternative review quantification

Element Designator (DSM)	Description	PG&E DSM Value	BNL Review Value
Initiators:			
LOOP	Loss of Offsite Power	9.1E-2	1.08E-1
RT	Reactor Trip	1.14	1.85
TT	Turbine Trip	1.05	1.95
LOSW	Loss of Auxiliary Saltwater	9.74E-5	1.01E-3
	(PG&E updated Value)	(1.40E-4)	
LPCC	Loss of Component Cooling Water	1.96E-4	9.51E-4
	(PG&E updated value)	(2.88E-4)	
SLOCN	Small LOCA:Non Isolable	5.26E-3	1.33E-2
	(PG&E updated value)	(5.83E-3)	
LCV	Loss of Condenser Vacuum	8.73E-2	3.12E-1
SLBI	Steam Line Break Inside Containment	4.63E-4	1.66E-3
SLBO	Steam Line Break Outside Containment	5.53E-3	1.98E-2
ISI	Inadvertent Safety Injection Signal	7.39E-2	2.64E-1
TLMFW	Total Loss of Main Feedwater	9.98E-2	3.57E-1
PLMFW	Partial Loss of Main Feedwater	7.49E-1	2.68
EXFW	Excessive Feedwater Flow	2.79E-1	9.97E-1
IMSIV	Closure of One MSIV	1.07E-1	3.83E-1
LOPF	Loss of Primary Flow	1.21E-1	4.33E-1
Split Fractions:			
SA1		7.58E-3	3.79E-2
SA2		1.14E-2	5.70E-2
SA5		1.40E-2	7.00E-2
SB1	Solid State Protection System	7.48E-3	1.50E-2
SB2		2.40E-2	4.80E-2
SB6		8.44E-2	1.69E-1
SBC		1.34E-2	2.68E-2
SBE		7.43E-2	1.49E-1
AC1	Low Pressure Injection Function	6.27E-3	8.54E-3
AW5		3.30E-2	4.93E-3
AW7	Auxiliary Feedwater System	3.24E-4	7.01E-3
AW8		1.23E-3	2.38E-2
FO5	Diesel Fuel Oil System	5.08E-2	2.29E-2
AS3		1.22E-4	2.62E-4
AS4	Auxiliary Saltwater System	1.69E-2	2.94E-2
AS5		3.58E-4	4.97E-4
ASB		2.7E-2	1.0
RT1	Reactor Protection System	6.58E-6	2.90E-5
HS1	Operator Fails to Maintain Hot Shutdown	5.01E-6	0.0

Table 23.15 Comparison of internal event contributions to CDF

Updated DSM (PG&E) - Case 2			Case 4		
Initiator	Unnormalized Fussel-Vesely Importance	Fussel-Vesely Importance (%)	Initiator	Unnormalized Fussel-Vesely Importance	Fussel-Vesely Importance (%)
LOOP	4.180E-05	31.93	LOOP	1.089E-04	38.69
RT	1.615E-05	12.34	RT	3.383E-05	12.02
TT	1.477E-05	11.28	TT	3.105E-05	11.03
PLMFW	1.084E-05	8.28	PLMFW	2.245E-05	7.98
LIDC	9.496E-06	7.25	LIDC	1.966E-05	6.98
MLOCA	5.965E-06	4.56	MLOCA	9.975E-06	3.54
LPCC	4.684E-06	3.58	SLBI	7.642E-06	2.71
SGTR	3.582E-06	2.74	EXFW	6.245E-06	2.22
EXFW	3.116E-06	2.38	LLOCA	4.784E-06	1.70
SLBO	2.800E-06	2.14	LPCC	4.684E-06	1.66
LLOCA	2.576E-06	1.97	LOCV	4.270E-06	1.52
SLBI	2.383E-06	1.82	LOSWV	3.980E-06	1.41
LOSW	2.080E-06	1.59	SGTR	3.582E-06	1.27
SLOCI	1.805E-06	1.38	LOPF	2.958E-06	1.05
LOSWV	1.611E-06	1.23	SLBO	2.907E-06	1.03
LOCV	1.236E-06	0.94	IMSIV	2.615E-06	0.93
LOPF	1.076E-06	0.82	TLMFW	2.439E-06	0.87
IMSIV	9.511E-07	0.73	LCV	2.134E-06	0.76
SLOCN	9.049E-07	0.69	LOSW	2.080E-06	0.74
TLMFW	8.871E-07	0.68	ISI	1.806E-06	0.64
LCV	7.760E-07	0.59	SLOCI	1.805E-06	0.64
ISI	6.569E-07	0,50	SLOCN	9.049E-07	0.32
VSI	4.999E-07	0.38	VSI	4.999E-07	0.18
ELOCA	2.660E-07	0.20	ELOCA	2.660E-07	0.09
TOTALS	1.309E-04			2.815E-04	

It should also be noted that the staff's CSFs include the removal of HS1 (HS1 = 0.0) from the model because the staff concludes that HS1 is too conservative in the PRA. HS1 represents the complete failure of the operating staff to maintain the plant in a safe, hot-shutdown condition following a transient (predominantly RT and TT).

The breakdown of initiator importance for Case 4 can be found in Table 23.15. This table is equivalent to Table 23.7 which is based upon the original DSM input data minus the non-seismic external events. Case 2 is also included in Table 23.15 as this represents a more valid comparison between the updated PRA and the staff's alternative set of quantifications. (The updated input from PG&E came after the importance calculations on the DSM were completed and, therefore, those calculations were not repeated. The changes, however, do not represent a significantly different view of the Diablo Canyon core damage frequency profile.) These alternative results are offered as an additional set of sensitivity studies that may provide further insight to future users and reviewers.

Table 23.16 Overall internal event CDF estimates for various assumptions

Case		Point estimate CDF (/yr)
1.	Original PG&E input for the DSM	1.29E-4
2.	Case 1 + PG&E updated initiator frequencies (Table 3.10.1 of PRA; Table 23.14 of SSER 34)	1.31E-4
3.	Case 2 + BNL CSFs	2.65E-4
4.	Case 3 + BNL-LOOP	2.82E-4
5.	Case 4 + BNL values for LOSW, LPCC and SLOCN	3.06E-4
6.	All BNL values from Table 23.14	4.86E-4

In summary, the internal events Level 1 portion of the PRA represents a comprehensive and detailed effort. It has withstood detailed scrutiny and the staff finds it to be an acceptable and reasonable basis to address element 4 of the license condition.

23.4 Review of Seismic Events

This section of the SSER presents the results of a detailed review of the seismic portion of the PRA. Again, the format of this section of the SSER

closely follows that of NUREG/CR-5726 (Bozoki and others, in process). Pertinent technical findings and conclusions reached by the NRC staff are presented here.

23.4.1 PRA Approach

The seismic events analysis of the PRA is a natural extension of the internal events analysis. In this approach, a single initiating event is considered--the occurrence of the earthquake itself. The probability of exceeding a given level of ground motion is specified by a discrete family of hazard curves. Each curve is associated with a weight, normalized so that the summation of weights equals unity.

The response of the plant to this earthquake is then identified through a front line event tree which has the major structures and safety systems as top events (see the plant event sequence model, Figure 23.4). Each of the accident sequences identified on the front line tree are related to two support trees--one mechanical support tree and one electrical support tree. These support state trees are used to specify different combinations of successes or failures of the support systems for use in quantifying the accident sequences determined on the front line trees. Using the front line tree, a large number of accident sequences can be identified.

The accident sequences are expressed in terms of basic events or groups of basic events and include both random and seismically induced failures. The seismic probabilities of failure were derived from site-specific fragilities, all of which utilized average spectral ground acceleration as the independent variable. Detailed building response analyses were carried out for the auxiliary building and the turbine building to determine median responses and associated variabilities. Fragilities were developed for both buildings and for components.

For the components, both structural and functional failures were considered:

- For structural failures, the engineering factor of safety approach due to Kennedy and others (1980), was utilized. This approach was benchmarked, in a limited sense, with the detailed nonlinear analyses of the turbine building.

- For functional failures, seismic qualification test data were used with an assumed level of conservatism to determine the median failure probability.

Component and structural fragilities are reviewed later in this section of the SSER.

The accident sequences were quantified using mean values for each of the seismic component failure probabilities, and mean values for all random failure events, and then the dominant accident sequences were identified. Note that each different earthquake level yields a different accident sequence from the same branch on the event tree. From this initial point estimate quantification, a total of 791 accident sequences (seismic dominant sequence model) were identified and studied for the Diablo Canyon seismic PRA.

Finally, the 791 sequences were used to build a simplified block model for which an uncertainty analysis using the discrete probability distribution approach could be used to obtain mean core-melt frequencies and uncertainty bands about the distribution of core-melt frequency.

23.4.2 Detailed Description of Review Approach

The detailed review of the seismic PRA was performed by several different teams on the natural divisions of the PRA, namely,

- hazard curve development
- component and structures fragility development
- systems analysis (event and fault trees)
- accident sequence integration, quantification, and uncertainty analysis

As discussed earlier, Sandia National Laboratories and EQE, Inc., had primary responsibility to review the seismic portion as a subcontractor to BNL. NRC staff reviewed the hazard analysis. As with the internal events, emphasis was placed on independent analyses in selected areas. The scope and objectives of the reviews of each of these areas are described below.

(1) Review of the Hazard Curve

The family of hazard curves provided by PG&E was examined for the effect of any underlying assumptions as to "effective ground acceleration" or "upper ground acceleration limits" which PLG often applied after the basic hazard curves were developed.

In addition, the hazard curves developed were keyed to spectral acceleration, rather than to peak ground acceleration as has been done in the past. Implications of this new approach were examined.

(2) Review of Fragilities Development

Two separate aspects of the fragility development were considered--equipment fragility and building structural fragility. To perform this review, an initial two-day plant visit was required. In addition, copies of all supporting documentation (in particular, the engineering calculation sheets--usually handwritten) for all fragilities were made available. After preliminary review of the documentation, a meeting between the reviewers and the fragility development personnel was scheduled to allow discussion of the details of the fragility calculations.

(3) Review of Event Trees and Fault Trees

The event tree and the choice of initiating events were reviewed for completeness and appropriateness. In particular, proper inclusion of random failures and test/maintenance unavailabilities in the seismic sequences (which can be important at low earthquake levels) was examined. Assumptions underlying any credit taken for recovery were examined for appropriateness. Finally, any implicit assumptions as to correlation between seismically induced failures were identified and examined.

(4) Review of Accident Sequence Integration, Quantification, and Uncertainty Analysis

The assembly process resulting in the final seismic core melt frequencies was reviewed. Key results were independently calculated. Key assumptions driving the final result were identified, and limited sensitivity studies were performed to highlight the potential impact of alternative assumptions. Areas examined included the following:

- appropriateness of final sequences and method of screening used
- proper inclusion of seismically induced correlation
- completeness of evaluation of initiating events
- appropriateness of inclusions of seismically induced secondary failures (e.g., failure of interior block walls damaging nearby equipment)
- assumptions regarding correlation between modeling (as opposed to random) sources of uncertainties
- method of inclusion of relay chatter/breaker trip
- proper combination fragility failure modes
- development of plant-level fragility functions

The review of the seismic portion was conducted interactively over the course of 2-1/2 years. During the interactive phase, the review teams met with PG&E and its consultants to review individual pieces of input as they were developed. A number of meetings were held based on preliminary aspects of the PRA. One of the earliest major inputs completed was that of the development of the seismic fragilities. When this material was completed and documented, a detailed review was begun. Finally, an audit meeting was held to review detailed aspects of various parts of the fragility derivations.

Review of the entire seismic PRA began in mid-1988 after the receipt of the LTSP Final Report (Brand, 1988). On the basis of this document and subsequent meetings, a number of requests for further information were prepared. Basic data as to component failure probabilities at different levels and the multitude of accident sequences themselves were provided by PG&E on PC (personal computer) disk format. The review of the seismic PRA described here is based on the PRA and on the responses to the many questions formally submitted by the staff and PG&E's responses to them. As stated at the beginning of Section 23 of this SSER, references to "the PRA" refer to Brand, 1988; Shiffer 1988a through d; and Shiffer 1989a, b, and c.

23.4.3 Seismic Hazard Analysis

The objective of the seismic hazard analysis is to provide a probabilistic representation of the earthquake ground motion at the Diablo Canyon site for

the PRA. The seismic hazard analysis considers all the seismic sources that can affect ground-motion estimates at the site and compares the contribution of various earthquake source hypotheses. This approach allows the explicit incorporation of uncertainty. The seismic hazard estimate is then convolved with the plant fragility to arrive at the core-damage frequency assessment for the plant.

The seismic hazards analysis considers characteristics of seismic sources, maximum magnitude distribution, rate of earthquake occurrence, and attenuation of ground motion to develop a probabilistic representation of earthquake ground motions expected at the site. The results, probabilities of specified levels of ground motion being exceeded, are used as seismic input in the PRA.

23.4.3.1 Methodology

Uncertainties in defining risk are accounted for by the logic tree format and are represented by a family of hazard curves. Logic trees are composed of nodes and branches. Each element in the logic tree has a set of nodes representing an uncertain state of nature and each branch represents discrete possible values for that state. Probabilities are assigned to each branch using subjective assessments, and end-branch probabilities are calculated as the product of all the intermediate-branch probabilities. A seismic hazard analysis was performed for each end branch resulting in a single hazard curve. The hazard curves for all the branches in the logic tree are used to estimate seismic hazard at the site.

Logic trees present the following source characteristics of faults: sense of slip, dip angle, depth of seismogenic zone, length of fault, maximum magnitude, seismicity model, and rate of activity. Weights are assigned to each possible hypothesis for each characteristic. These weights were assigned by a panel of experts based on currently available data. Logic trees were developed for the Hosgri, Los Osos, San Luis Bay, Santa Lucia Banks, West Huasna, Lompoc, Rinconada, Nacimiento, and San Andreas faults. The maximum magnitude distributions calculated from the logic trees are discussed in Section 2.5.2.2 of this SSER and were found to be reasonable.

Earthquake recurrence relationships were selected for each seismic source. Because the historical seismicity record is limited, the rate of seismic activity was based on (1) seismic moment release inferred from estimated fault slip rates or (2) geologically estimated recurrence intervals for surface rupturing events [LTSP Final Report, Figure 3-13 (Brand, 1988)]. PG&E found the estimated recurrence rates to be conservative because the predicted recurrence rates for magnitude 5 and 6 earthquakes are higher than the historical seismicity observations in the region.

The logic trees used to calculate seismic hazard include the geological data used to calculate maximum magnitude distributions and the mean annual rate of potentially damaging earthquakes (magnitude $\geq$ 5) for each fault. The ground-motion attenuation relationships discussed in Section 2.5.2.3 of this SSER were used in the seismic hazard analysis. The results were summed over all faults which affect the site to calculate the seismic hazard curves (plots of the probability of exceeding various values of ground motion). This procedure takes into account randomness in the following variables: fault geometry,

location of rupture surface, magnitude, rupture size, closest distance from the site to the rupture, and ground-motion attenuation.

In the Diablo Canyon seismic hazard analysis, 20,700 end branches were calculated from the logic trees. These hazard curves were reduced to summary curves (fractile hazard curves) which show the distribution of hazard at each ground motion amplitude (spectral acceleration in the frequency range 3 to 8.5 Hz). To represent uncertainty in the hazard, the large number of hazard curves was aggregated into a limited number of aggregate hazard curves (eight curves) that maintain the character of the original curves while providing results appropriate for the PRA. The aggregate hazard curves represent 90 percent of the total variance of the original data set for all ground-motion amplitudes. These aggregate curves were used as input for the PRA. Figure 23.5 shows the hazard curves used in the seismic PRA.

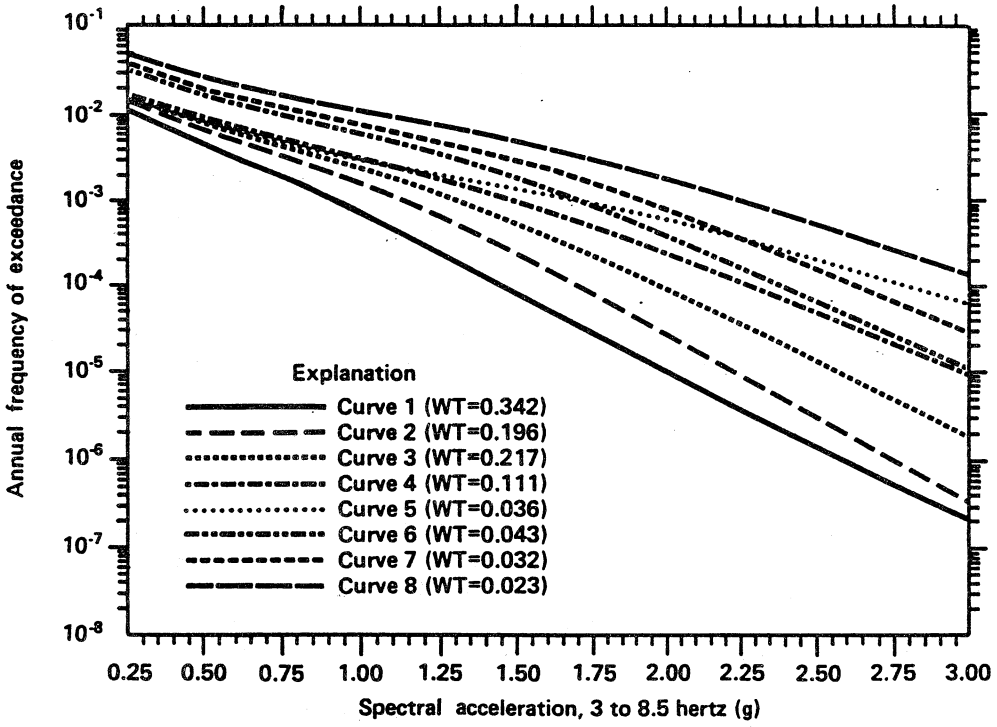


Figure 23.5 Total aggregate hazard curves (Figure 6-7 of the PRA)

Hazard analyses were performed in terms of response spectral accelerations to be consistent with plant fragility estimates. Estimates were made for 5-percent-damped accelerations at 2, 4, 8, 14, 25, and 33 Hz and for average spectral accelerations in the ranges of 3 to 8.5 Hz and 5 to 14 Hz. Hazard curves for different styles of faulting representing the frequency range of 3 to 8.5 Hz were selected for use in the PRA because this parameter provided the least variability between different earthquake magnitudes.

In addition, uniform hazard response spectra were also constructed over the frequency range of interest to plant structures and equipment [LTSP Final Report Figure 6-9 (Brand, 1988)]. Median uniform hazard spectra were calculated for 10E-3, 10E-4, and 10E-5 annual frequencies of exceedance. When compared to the LTSP median deterministic spectrum, the median LTSP deterministic spectrum is shown to have an annual probability of exceedance of about 10E-3/yr above 10 Hz and 10E-3 to 10E-4/yr for frequencies below 10 Hz. The 84th percentile LTSP deterministic spectrum is shown to have an annual probability of exceedance of about 10E-4/yr above 10 Hz and 10E-4 to 10E-5/yr for frequencies below 10 Hz.

23.4.3.2 Seismicity Assessment

In the seismic hazard analysis, those seismic sources that could affect the site were considered (the Hosgri, Los Osos, San Luis Bay, Santa Lucia Bank, West Huasna, Lompoc, Rinconada, Nacimiento, and San Andreas faults). The seismic hazards analysis found that the Hosgri fault zone dominates the seismic hazard at the site [LTSP Final Report Figure 6-6 (Brand, 1988)]. The Los Osos and San Luis Bay faults each contribute only a few percent to the total seismic hazard. Relative contributions to the total hazard from the other faults are insignificant. This agrees with the deterministic assessment of hazard. The possibility of a blind thrust fault under the San Luis-Pismo block was evaluated (response to Question GSG-11) and the hazard results were found to be similar to those from the San Luis Bay or Los Osos fault.

Hazard calculations were performed to assess the significance of key variables in the Hosgri logic tree and to assess the uncertainty in the hazard results. These results are summarized here for the range of spectral accelerations important to the plant (average spectral accelerations of 1.25g to 2.0g for the frequency range 3 to 8 Hz).

Since a significant effort was expended in determining the sense of slip on the Hosgri fault, the sensitivity of the seismic hazard to sense of slip on the Hosgri fault was assessed. The strike-slip assumption produced a higher hazard than oblique-slip, but overall there was little difference in the annual frequency of exceedance (see Figure LP8-1 of Shiffer, 1990f).

The sensitivity of the hazard to the activity rate on the Hosgri fault for a strike-slip fault showed up to an order of magnitude range in annual exceedance frequency for slip rates considered in the logic tree (0.5 to 6 mm/yr). The choice of the seismicity model (exponential or characteristic), the depth of the seismogenic zone (9, 12, or 15 km), and the dip angle of the fault showed little effect. The choice of maximum magnitudes for all slip types on the Hosgri fault showed up to an order of magnitude range in annual exceedance frequency for magnitudes varying from 6.25 to 7.75, but little hazard difference for maximum magnitude differences of 1/4-magnitude unit.

23.4.3.3 Ground-Motion Studies

The ground-motion attenuation relationships discussed in Section 2.5.2.3 of this SSER were used in the seismic hazard analysis. Three median ground-motion attenuation relationships were used (strike-slip, oblique-slip, and thrust-slip faulting). Both uncertainty in ground-motion amplitude and site conditions are used in estimating hazard. In Section 2.5.2.3 of this SSER, possible exceedances

of the horizontal LTSP spectra at frequencies below 2 Hz and exceedances of the vertical LTSP spectrum from 1 to 10 Hz are discussed. The impact of these exceedances on the seismic hazard analysis is discussed in Section 3.8.1 of this SSER.

A ground-motion sensitivity study was presented at the March 15, 1991, meeting with PG&E. The sensitivity to ±15 percent of the median attenuation equation was up to an order of magnitude, thus suggesting that ground-motion input is an important parameter.

23.4.3.4 Conclusions

The seismic hazard analysis provided a reasonable probabilistic representation of the earthquake ground motions at the site. The Hosgri fault zone was found to dominate the seismic hazard at the site. The Los Osos and San Luis Bay faults each contribute only a few percent to the total hazard. Relative contributions to the total hazard from the other faults are insignificant. Sensitivity studies showed the important parameters are slip rate, maximum magnitude, and ground-motion attenuation.

23.4.4 Seismic Hazard/Fragility Interface

In most previous PRAs, the peak ground acceleration (PGA) was used as the parameter. The variability in the spectral shape was estimated in the previous PRAs by taking the ratio of spectral acceleration at a specific frequency to the PGA. Since the logarithmic standard deviation of this ratio was found to vary over the frequency range of interest, it was conservatively assumed that this logarithmic standard deviation is independent of frequency and equal to 0.25 or more.

In the Diablo Canyon seismic PRA, the ratio of the spectral acceleration at any specific frequency to the average spectral acceleration (over the frequency range of 4.8 to 14.7 Hz) was found to have a constant logarithmic standard deviation of 0.18 for 5-percent damping. In addition, the randomness variability for earthquake directional effects alone was estimated to have an average value of about 0.12. Thus the use of average spectral acceleration was felt to provide lower uncertainty than the use of the PGA as well as preclude the possibility of "double counting" of uncertainty in the determination of fragilities and response analyses.

The independent parameter chosen for the PRA was the average of the ground-motion response spectra (5% damped) over the range of 3 to 8.5 Hz. $(Sa)_{3\text{-}8.5}$. The hazard and fragility curves were both expressed in terms of this independent parameter. The relation between the average spectral acceleration and the PGA is as follows:

$$(Sa)_{3\text{-}8.5} = 2.34 \times PGA$$

Although the use of average spectral acceleration as the fragility parameter avoids the double counting of variability introduced by attenuation and spectral shape factor, the reduction in the overall variability and the resulting reduction in the seismic CDF estimates are small. A PG&E study showed that the

increase in the seismic margin, as measured by the HCLPF capacity, may not be larger than 8 percent over that calculated using the PGA and the previous seismic PRA methods; the decrease in the seismic CDF estimate is even smaller.

23.4.5 Fragility and Building Response Analysis

23.4.5.1 Methodology

The fragility analysis method used in the Diablo Canyon LTSP has evolved over the last 10 years and has been applied in seismic PRAs of more than 25 nuclear power plants. So, in one sense, the methodology is mature. However, because of the high seismicity at the Diablo Canyon site, several aspects of the seismic PRA have been modified or performed in more detail than in previous applications. For example, the detailed probabilistic response calculations performed on the auxiliary building, the detailed nonlinear analyses of the turbine building, and the large number of equipment items for which specific fragility calculations were performed represent atypical applications of the methodology. In addition, the reference fragility parameter in the Diablo Canyon LTSP is the 5-percent-damped, average spectral acceleration of the horizontal ground motion averaged over the frequency range of 3.0 to 8.5 Hz. Table 23.17 presents the fragility values used in the PRA, with the median values expressed in terms of average spectral acceleration. The table also lists HCLPF values in terms of average spectral acceleration.

The use of median-centered reference horizontal floor spectra in the development of equipment fragilities has afforded a realistic representation of the seismic capacity and reduced the overall variability.

23.4.5.2 Review Approach

The review procedure consisted of the following:

(1) a plant walkdown of the Diablo Canyon plant, focusing on the seismic risk-important components and structures in March 1988

(2) review of calculations and reports submitted by PG&E

(3) independent calculations to verify various key aspects of the seismic PRA

(4) audit of calculations of selected components in June 1989

The review focused on methodology and its application in the response and fragility areas. In the response area, the auxiliary building and the turbine building were reviewed in detail. Independent response analyses and sensitivity studies were performed on the auxiliary building. The nonlinear analyses of the turbine building were reviewed in detail.

Regarding equipment fragility, the review focused on identification of failure modes; information sources for fragility evaluation, that is, loads, test response spectra, frequency calculations, and the like; methods used in the derivation of median capacity and variability estimates (β_R and β_U), assumptions made on anchorage adequacy, and reasonableness of the final fragility estimates.

Table 23.17 PRA seismic fragilities (Table 6.4-1 of the PRA)

Component/Structures	Median Acceleration	Beta R	Beta U	Beta C	HCLPF Value
1. Containment building	8.42	0.260	0.300	0.397	3.342
2. Concrete internal biostructure	6.91	0.200	0.310	0.369	2.979
3. Intake structure	8.55	0.280	0.310	0.418	3.230
4. Auxiliary building	5.79	0.210	0.260	0.334	2.666
5. Turbine building shear wall	4.87	0.260	0.330	0.420	1.840
6. Refueling water storage	9.92	0.290	0.360	0.462	3.394
7. Auxiliary saltwater piping	9.23	0.180	0.210	0.277	4.850
8. Reactor pressure vessel	8.71	0.250	0.330	0.414	3.345
9. Reactor internals	10.54	0.400	0.260	0.477	3.547
10. Steam generators	6.96	0.310	0.290	0.424	2.586
11. Power-operated relief valves	7.62	0.300	0.420	0.516	2.323
12. Reactor coolant pumps	8.82	0.370	0.320	0.489	2.825
13. RHR pumps	8.31	0.330	0.220	0.397	3.353
14. RHR heat exchangers	8.09	0.240	0.270	0.361	3.487
15. Safety injection accumulators	10.01	0.290	0.190	0.347	4.534
16. Boron injection tank	8.46	0.270	0.190	0.330	3.960
17. CCW pumps	8.53	0.290	0.210	0.358	3.738
18. CCW heat exchangers	6.31	0.270	0.280	0.389	2.546
19. CCW surge tank	7.22	0.330	0.220	0.397	2.913
20. Containment spray pmps	8.65	0.290	0.200	0.352	3.854
21. Spray additive tank	6.78	0.300	0.180	0.350	3.071
22. AFW pumps	7.71	0.290	0.210	0.358	3.379
23. Diesel generator fuel oil pumps/filter	8.33	0.270	0.230	0.355	3.650
24. Diesel generators	7.79	0.260	0.200	0.328	3.647
25. Diesel generator radiator/ water pump	8.78	0.290	0.240	0.376	3.662

Table 23.17 (Cont'd.) PRA seismic fragilities (Table 6.4-1 of the PRA)

Component/Structures	Median Acceleration	Beta R	Beta U	Beta C	HCLPF Value
26. Diesel generator excitation cubicle	7.40	0.290	0.350	0.455	2.574
27. Diesel generator control panel	4.55	0.300	0.130	0.327	2.238
28. Containment fan cooler	8.10	0.310	0.330	0.453	2.818
29. Supply fans	9.79	0.330	0.240	0.408	3.822
30. Supply/return fans	11.16	0.330	0.300	0.446	3.947
31. 4-kV switchgear	7.44	0.310	0.250	0.398	2.953
32. Bus G and H potential transformer	10.83	0.310	0.380	0.490	3.469
33. Safeguard relay panel	10.76	0.340	0.360	0.495	3.390
34. Bateries	6.04	0.300	0.180	0.350	2.736
35. Battery chargers	9.93	0.340	0.400	0.525	2.929
36. Switchgear/breaker panel	6.67	0.350	0.280	0.448	2.359
37. Inverters	6.82	0.310	0.240	0.392	2.752
38. 4,160V/480V transformers	5.34	0.280	0.200	0.344	2.419
39. Auxiliary relay panel	7.25	0.280	0.150	0.318	3.566
40. Main control boards	7.77	0.310	0.270	0.411	2.984
41. Hot shutdown panel	7.60	0.270	0.250	0.368	3.222
42. Process control and protection	10.78	0.390	0.280	0.480	3.569
43. Reactor trip switchgear	7.90	0.300	0.260	0.397	3.136
44. Pressure and ΔP transmitter	8.93	0.270	0.200	0.336	4.112
45. Impulse lines	7.09	0.280	0.320	0.425	2.634
46. Offsite power, 230 kV	1.69	0.240	0.200	0.312	0.818
47. Offsite power, 500 kV	0.81	0.240	0.200	0.312	0.392
48. BOP piping and supports	11.22	0.390	0.400	0.559	3.047
49. Penetrations/penetration boxes	7.38	0.310	0.270	0.411	2.834
50. HVAC ducting and supports	9.78	0.350	0.480	0.594	2.486
51. Switchgear/strut	7.07	0.310	0.250	0.398	2.806

Table 23.17 (Cont'd.) PRA seismic fragilities (Table 6.4-1 of the PRA)

Component/Structures	Median Acceleration	Beta R	Beta U	Beta C	HCLPF Value
52. Chatter, main control board	10.00	0.010	0.010	0.014	9.675
53. Chatter, DG control panel	7.77	0.250	0.140	0.287	4.083
54. Chatter, 4-kV switchgear	3.53	0.350	0.250	0.430	1.312
55. Chatter, safeguards relay panel	10.00	0.010	0.010	0.014	9.675
56. Strut for turbine building	6.71	0.250	0.320	0.406	2.620
57. Bus F potential transformer	5.85	0.310	0.380	0.490	1.874
58. Safeguard relay panel	5.81	0.340	0.360	0.495	1.830
59. Centrifugal charging pump	10.16	0.310	0.190	0.364	4.452

23.4.5.3 Structure Response and Fragility Review

A number of structures were considered in the seismic PRA as shown in Table 23.17, but only two played any significant role: the turbine building and the auxiliary building.

The development of fragilities for all structures (except for the turbine building) was based on the separation of variable approach. Details of this procedure and results of calculations are described in a report entitled "Seismic Fragilities of Civil Structures and Equipment Components at the Diablo Canyon Power Plant" (Kipp and others, 1988).

Because the turbine building is important, an alternate structural failure level was calculated as described in Kennedy and others (1988), submitted in response to a staff question. This calculation consisted of a multiple, non-linear, time-history analyses coupled with a story drift failure criteria. A fragility function was developed on the basis of these analyses. The turbine building calculations were also used to benchmark the separation of the variable approach.

Auxiliary Building Structural Response

This section of the SSER focuses on the review of the structural response variability study performed on the Diablo Canyon auxiliary building. PG&E utilized the study to benchmark a deterministically calculated median response with one generated by probabilistic response analysis techniques, and to calculate estimates of variability in floor-response spectral accelerations as a function of frequency and elevation in the structure due to variability in

ground motion, soil/rock properties, and structure dynamic characteristics. This study quantified the portion of the "structure response factor" attributed to ground-motion spectral shape, structural damping, structural frequency, structural mode combination, earthquake directional combination, and soil-structure interaction. The staff performed an independent evaluation to verify the simulation performed by PG&E and to identify parameters sensitive to the seismic PRA.

Details of the staff's independent verification and sensitivity analyses are presented in NUREG/CR-5726 (Bozoki and others, in process). These analyses, in general, verified the variability estimates used by PG&E for different parameters, and also has provided verification for deterministically calculated median response.

Turbine Building Fragility Review

Review of the turbine building fragility focused on the nonlinear dynamic analysis performed in a probabilistic manner and the probabilistic drift criterion used to derive the fragility functions for shear walls. A review of Brand (1988) and Kennedy and others (1988) along with meetings and discussions culminated in a series of questions to be addressed (Shiffer, 1989d and e, and 1990a). These questions focused on modeling assumptions and details of the analysis. All questions were addressed during the meeting of June 16-17, 1989 (Shiffer, 1989d) with the exception of the need to evaluate the assumption of impact occurring only at the center of the turbine pedestal whereas impact near the ends of the turbine pedestal would appear possible and have potentially more severe consequences on the capacities of controlling walls, walls 19 and 31 (Figure 6-26 of the PRA shows where these walls are located). As a result, additional studies were conducted by examining a limiting case of the effect of the turbine pedestal impacting the turbine deck very near to the wall connection. Shiffer (1989e) documented the results of these studies which indicate that the impact near these walls has minimal effect on the fragility function.

The methodology used for the nonlinear analysis was acceptable. The nonlinear analysis provided two important results. First, it provided a calculation of fragility that was independent of that provided by the separation of variables approach, and secondly, it substantiated the underlying assumptions regarding ductility and combination of uncertainties which are implicit in the separation-of-variables approach. Overall, the nonlinear analysis was felt to substantially contribute to the confidence level in the final seismic PRA results.

Masonry Wall Review

In the original PRA (Brand, 1988), seismic capacity of the masonry block walls was estimated to be high. However, an issue was identified outside the context of the PRA review regarding the adequacy of the masonry walls for the Hosgri reevaluation earthquake. The staff review of this concern and its resolution is described in Section 3.8.1.7.7 of this SSER. As a result of this activity, the masonry walls are being strengthened. The staff had requested that PG&E reexamine the fragility of masonry walls and assess impact of these revised fragilities on results of the seismic PRA. By letters dated April 12, 1991, and May 1, 1991 (Shiffer, 1991e and 1991j), PG&E informed the staff that the revised capacity of the masonry walls is sufficiently high that there is no

impact on the original PRA results. The margins of the masonry walls are discussed in Section 3.8.1.7.7 of this SSER.

23.4.5.4 Equipment Fragility Review

The fragility evaluation methodology was discussed in this section of the SSER. This section focuses on the equipment fragility review. In the PRA, the median capacities of equipment were estimated using site-specific and plant-specific information. Median-centered horizontal floor spectra were estimated for selected floors of the important civil structures as described earlier. This approach contrasts with many previous seismic PRAs wherein the design-basis floor spectra were used to establish equipment capacity through the use of structural response factors of safety estimated to account for conservatism or unconservatism in the generation of the design floor spectra. The approach followed in the LTSP gives a more realistic estimate of the median capacity with reduced uncertainty.

The randomness and uncertainty variabilities β_R and β_U are typically lower than those reported in previous PRAs. The reasons are the use of median-centered floor spectra and availability of analysis and test reports specific to Diablo Canyon equipment. In responding to a staff member's question, PG&E has provided the bases for most of the variability assignments, which rely rather heavily on expert judgments. However, seismic core damage or HCLPF estimates are not sensitive to small changes in uncertainty parameters. Overall, the variability estimates in the PRA are judged to be reasonable.

For each piece of equipment, a number of failure modes were examined in the LTSP. These included structural failure modes (e.g., buckling of tanks walls and component supports, anchor bolt failures, and pressure boundary failure of piping) and functional failures (e.g., chatter and trip in electrical components, excessive blade deflection in fans, and shaft seizure in pumps).

During the review and plant walkdown, the focus was on identifying potential failure modes. An example of the review is the identification of failure modes for the RHR heat exchanger. In Phase II, the heat exchanger support fragilities were calculated by extrapolating the Hosgri earthquake evaluation loads. For the Hosgri evaluation, the heat exchanger was modeled as fixed at the top and bottom and supported in the middle. It was pointed out in the review that the intermediate support would fail at higher accelerations and the anchor bolts would yield. Therefore, the horizontal frequency near failure level was evaluated by modeling the heat exchanger as a beam with the lower support treated as a pinned connection, the intermediate support not included, and the upper support treated as a pinned connection. This reduced the horizontal frequency from 29.6 Hz for the Hosgri evaluation to 11.9 Hz for the fragility evaluation.

In the PG&E calculations submitted in response to Question 32c, two failure modes were identified. These were failure of anchor bolts at the pedestal and at the upper N-S strut. For the upper support, the capacity was determined as the sum of tension in embedded studs and buckling load of longer strut. From the sketch supplied by PG&E, it appeared that the upper support could pull out of the concrete before the studs would yield. The embedded length for these studs (7/8-in. diameter) was shown as 4 in. If this failure mode was in fact

the governing one, the median strength factor would have been less than 50 percent of what was estimated. In the audit review of calculations, this failure mode was examined carefully. PG&E produced Drawing 439520 which showed that the actual embedded length of these studs is 8.75 in. Therefore, the studs would not be expected to pull out of the concrete before their tensile failure.

For the RHR heat exchanger, the two failure modes identified were estimated to have similar seismic capacities. The analysis correctly calculated the fragility of the component as the conditional probability that any one of the failure modes could occur.

Structural fragility of tested components was estimated by using a factor of 1.8 over the test response spectra for those cases in which no distress was noted during or subsequent to seismic qualification testing. Herein, the median factor of 1.2 represents the ratio of test response to onset of distress, and the median of 1.5 represents the ratio of response at the onset of distress to onset of failure. The composite variability in the first factor was estimated to be $\beta_R = 0.11$, whereas the uncertainty in the latter factor was estimated to be $\beta_U = 0.04$. Although these median and variability values were estimated using judgment, they appear to be reasonable, and the overall effect on the component fragility may have been conservatively estimated. In a few cases, the conservatism in the total median factor 1.8 has been demonstrated as discussed later in the case of the 4-kV switchgear.

PG&E identified relays that affect components necessary for safe shutdown using the circuit analyses as discussed in Section 23.3 of this SSER. Functional failure fragilities of relays were evaluated only for those relays considered to be chatter sensitive. The median strength factor for chatter mode was estimated using the generic equipment ruggedness spectrum, the cabinet amplification factor, and the floor spectral acceleration. The relay chatter failure mode fragilities were derived for diesel generator control panel, 4-kV switchgear, main control boards, and the hot shutdown panel. Except for the 4-kV switchgear, the chatter failure mode capacities were found to be sufficiently high so as not to contribute significantly to plant seismic risk. The 4-kV switchgear evaluation will be discussed later.

The anchorage failure modes investigated included some of the recent generic issues, such as edge distance, closer spacing, and cracked concrete. For example, the RHR heat exchanger is mounted on the pedestal with anchor bolts; the edge distance for anchor bolts appeared to be low. However, a closer examination revealed that the anchor bolts are of the j-type and are well inside the outer layer of reinforcement. There are a few items of equipment mounted on pedestals which may pose possible concern with small edge distance. However, the seismic fragilities for these components were developed using specific information; the review and walkdown generally focused on this issue. Therefore, the staff concludes that the anchor bolt failure modes are properly represented in the LTSP.

A question often raised in seismic PRAs is how the vertical ground motion and uncertainties are combined with the horizontal ground motion. Because of the nature of the vertical ground-motion estimates in the LTSP, this issue was of

more interest in this review. In Appendix D to Kipp and others (1988), provided as a response to a staff request, the procedure used in developing the median-centered, vertical, floor response spectra is described. By means of selected examples of the diesel generator control panel, 4-kV/480-V transformer, and 4-kV switchgear, it is shown that the fraction of the total critical response attributable to vertical excitation is generally small and is unimportant in terms of contribution to seismic CDF estimates. The staff finds the so-called "Hosgri factoring method" adequate for this purpose. Since reviewing Kipp and others (1988), the staff has identified some exceedances in amplitude when the staff spectrum is compared to the LTSP 84-percent site-specific, horizontal ground-motion spectrum in the range below 2.0 Hz. Some exceedances have also been identified in the vertical spectra in the frequency range of 1 to 10 Hz (see Section 2.5.3.2 of this SSER for a more detailed discussion). In letters from Shiffer (1991i and 1991k), PG&E has provided information to indicate that these exceedances will not have any significant effect on the seismic PRA results. As discussed in Section 3.8 of this SSER, the staff will require PG&E to submit analyses confirming the capability of plant structures to withstand the spectral exceedances.

In an audit meeting, the staff reviewed calculations for a number of components with the aid of equipment support drawings, qualification reports, and photographs of the equipment items. The staff focused on the equipment items for which PG&E had previously sent fragility calculations and had specifically addressed in response to NRC Question 32. The audit covered the following aspects:

- identification of failure modes
- information sources for fragility evaluation
- method for deriving median, β_R and β_U
- anchorage
- reasonableness of fragility estimates
- detailed information available for review

Among the components reviewed were: 4-kV switchgear, RHR heat exchanger, CCW heat exchanger, spray additive tank, DG control panel, pressurizer safety and relief valves, reactor coolant pump, control rod drive mechanism, main steam PORVs, containment fan cooler, 4-kV potential transformer, safeguard relay panel, 125-V dc batteries, battery racks, battery chargers, inverters, 480-V breaker panel, main control board and control console, reactor trip switchgear, and balance of plant piping. NUREG/CR-5726 (Bozoki and others, in process) details the review findings for each of these components. The following four items important to seismic CDF estimates are discussed here: (1) 4-kV switchgear, (2) loss of offsite power, (3) excessive LOCAs, and (4) all vital 125-V dc components.

4-kV Switchgear. PG&E identified two failure modes: functional failure (chatter) and structural failure. The fragility for the chatter failure mode was calculated using the generic equipment ruggedness spectra (GERS) obtained from tests and the median amplification factor. The relay is sensitive to the vertical seismic response and the vertical frequency of relays was estimated to

be from 19 to 21 Hz. The median spectral acceleration capacity in the chatter mode was estimated to be 3.53g and the HCLPF capacity was obtained as 1.31g. The relay chatter in this component is recoverable from the control room.

For the structural failure, it is customary to use the qualification test data; if there was no distress in the component in the qualification test, the median capacity in terms of acceleration is taken to be 1.8 times the ratio of TRS/RRS (test response spectra)/(required response spectra). It was found that this approach would give excessively conservative low capacity for this component. Instead, the structural failure mode was identified as the carriage guide rod bending. For this failure mode, the median capacity was calculated as 7.44g and the HCLPF capacity was obtained as 2.96g. This is a good example of evaluating the failure mode by analytical means.

Loss of Offsite Power. A key feature in the PRA is the treatment of the fragility for the 230-kV switchyard. The median average spectral acceleration capacity was estimated to be 1.69g (0.72g PGA) and the HCLPF was estimated to be 0.82g (0.35g PGA). These values were derived by segregating the recorded earthquake performance data on switchyards. During the staff audit, and on the basis of the preliminary information available to the staff on the performance of switchyard components during the Loma Prieta earthquake, the staff requested that PG&E reassess the 230-kV fragility. PG&E provided (Shiffer, 1990g) a detailed description of the performance of 230-kV switchyards on the PG&E system. In this response, the fragility was revised with the median capacity of 1.40g (0.6g PGA) and an HCLPF of 0.70g (0.3g PGA). The effect of this change on the mean CDF was minimal. The staff has conducted an additional sensitivity study (described later) and, in general, concurs with this finding.

Excessive LOCA. Excessive LOCAs were based on the probability of piping failure. The treatment of piping fragility in the LTSP is novel. The basis for the fragility of BOP piping is generic failure of the piping supports. The fragility is estimated for a piping segment containing approximately 20 supports. A piping system may contain a number of piping segments. The study calculated the piping system fragility by assuming the failure to occur if one or more segments fail. The number of piping segments in each system was estimated for use in the risk quantification. It also considered that probability of pipe break given the support failure for each piping segment. A sensitivity analysis is discussed in Section 23.4.9 of this SSER.

All Vital 125-V dc Components. Fragility estimates for components of this system (batteries, battery racks, chargers, and inverters) were reasonable and were mainly based on qualification tests. Table 23.17 lists the fragility values for these components.

23.4.5.5 Summary Evaluation of Fragilities

The fragility parameters for the structures and equipment were found to be reasonable. The documentation of fragility calculations and the supporting analysis and test data were examined in the audit and found to be acceptable. The sensitivity studies reported in Table 23.4 indicate the risk reduction if some of the components were further seismically upgraded. The conclusion is that there are no overwhelmingly weak links in the plant.

The level of effort in developing the seismic fragilities for equipment at Diablo Canyon is well beyond that expended on previous seismic PRAs because the high seismic motion at Diablo Canyon offers less scope for screening of components on the basis of earthquake experience data and generic qualification test data and results in specific evaluation being needed for most components.

Using the results of the seismic PRA, the component and plant seismic margins were derived in the LTSP Final Report (Brand, 1988); the margin against the 84-percent, site-specific ground motion was calculated. It is seen that all components whose failure will lead to seismic risk have at least 40-percent margin over the site-specific ground motion. The median capacities were shown to be much higher. This aspect is further discussed in Section 3.8 of this SSER.

23.4.6 System Modeling

The crux of the systems analysis for seismic events is contained in the seismic early frontline event tree (Figure 6-47 of the PRA), the electric power support event tree (Figure 6-44 of the PRA), the actuation and mechanical support event tree (Figure 6-45 of the PRA) and the seismic failure impacts table (Table 6-43 of the PRA). The frontline event tree defines the accident scenarios which follow the occurrence of an earthquake in terms of successes or failures of the top events identified as the tree. In keeping with the PLG methodology, the top events include support state flags, LOCA events, component failures (e.g., RWST, PORVs), and frontline systems (e.g., charging system, auxiliary feedwater system), and finally, human errors. In general, failures of these top events may be due to either seismic or random causes.

On the basis of the review of event trees associated with Westinghouse PWR reactors and other PRAs (e.g., those for Surry, Zion, and Indian Point) the top events included in the seismic early frontline tree are found to be a complete and logical set of systems and events which can be used to model accident sequences typical of commercial PWRs. In addition to the normal mitigating safety systems, instrumentation and relay chatter are explicitly included in a logical manner. Failure of the reactor protection system is not explicitly shown on this early frontline tree but it is explicitly considered (on a train level) in the mechanical support tree which is used to describe initial conditions for the sequences shown on the early frontline tree. Further, sequences normally associated with loss of offsite power (LOOP) and with station blackout (SBO) are not explicitly shown on this tree as they are explicitly contained in the various sequences in the electrical support tree which determines initial conditions for the early frontline tree. Thus, the staff finds that the sequence of scenarios and events which can be portrayed by the early frontline tree represents a reasonable and complete approach to modeling the Diablo Canyon seismic scenarios.

The early frontline tree represents a very large number of accident sequences. For these trees, approximately 3000 accident sequences were numerically evaluated, but only the dominant sequences were retained for further study, as discussed in Section 23.4.7 (below).

The impact of seismic failures on the top events of the early frontline event tree are given as the seismic failure impact table (Table 6-43 of the PRA).

For each top event, the various seismic component failures which contribute to the top event failure are identified in this table. It is assumed that the various contributors are independent of each other, and that their contributions can be combined using the logical "or" operator. Thus, in effect, this table gives Boolean expressions for each top event in terms of component failures. The Boolean expressions implied by this table were reviewed and found to be appropriate. In certain cases, the impacts of multiple redundant components were combined so as to conservatively estimate the failure probability of the top event, but this is not inappropriate provided undue conservatism does not skew the overall risk picture.

23.4.7 Accident Sequence Quantification

23.4.7.1 Evaluation of the Mean Point Estimate

As described earlier, the initial quantification consisted of a mean-point-estimate evaluation of the all-accident scenarios so as to identify the main contributors to core damage and to delete negligible scenarios from future consideration. The actual sequences themselves, in terms of basic events, are given in Appendix J to the PRA (Shiffer, 1988b). The split fractions for the basic events (conditional on the earthquake level) are given on Table 4-46 of the PRA, at six different ground-acceleration intervals.

In the numerical evaluation process, each sequence was evaluated for each of the six earthquake levels, and reported individually. This allowed an identification of which sequences dominated, as well as which earthquake levels contributed, for each accident sequence. A total of 791 individual sequences were identified.

As part of the review, the Boolean expressions for the 791 dominant sequences were obtained from PG&E, and were independently re-quantified using the split fractions of Table 6-46 of the PRA.

This independent evaluation allowed the staff to rank the sequences in terms of their contribution to the overall core damage frequency, and to identify the subset of accident sequences which dominated the CDF taking all earthquake levels into consideration. Where this was done, the staff found that the CDF was not dominated by a small set of sequences, but rather was spread out over at least 150 logical sequences to account for 90 percent of the total core damage frequency. The top 10 sequences only accounted for about 60 percent of the total.

This is partially accounted for by the fact that each of the 791 sequences corresponds to one specific earthquake level. That is, if a logical sequence were important at all six earthquake levels, there would be six separate accident sequences occurring in the 791 dominant sequence model. A second cause for the large number of sequences results from the use of two support trees and their relationship to the frontline tree. Although, this has no impact on the calculated CDF, it meant that a complicated review process was needed for developing the necessary insights (see Section 23.4.9 of this SSER). This aspect is described in detail in NUREG/CR-5726 (Bozoki and others, in process).

23.4.7.2 Uncertainty Analysis

As described earlier, a separate uncertainty analysis was performed following the mean-point-estimate calculation. As a first step, the dominant accident sequences identified in the mean-point-estimate calculation were used as the basis for constructing a simple block diagram model of core damage for the Diablo Canyon plant. This simplified block diagram, in effect, provides Boolean expressions which encompass the dominant failure scenarios, and which are simple enough so that the discrete probability distribution (DPD) approach to uncertainty analysis (developed by PLG) can be conveniently applied.

The logical block diagram was not reported in the PRA although the numerical results for total core damage frequency are listed in Table 6-54 of the PRA. At the staff's request, this block diagram was made available, and an uncertainty analysis was performed independently using an alternate approach, namely a full Monte Carlo analysis of the accident scenarios implied by the logical block diagram. As in the PRA evaluation, the random-failure/human-error basic events were fixed at their mean-point-estimate values, while lognormal fragility functions (as characterized by their random uncertainty β_R and modeling uncertainty β_U) as provided in Table 23.17 were used.

The seismic logical block diagram is shown in Figure 23.6. Circled numbers are seismic component numbers which correspond to the fragility descriptions in Table 23.17. The "+" denotes the logical "or" operator, while the "X" denotes the logical intersection operator. Twelve "boxed" blocks are shown, each corresponding to a functional accident scenario. Boxes containing a single (engineering notation) numerical value represent dominant groups of random failures of components. Each scenario block, as described by PG&E, is presented in Table 23.18.

The family of hazard curves used in the independent Monte Carlo uncertainty analysis was the identified set of eight discrete hazard curves whose non-exceedance probability ordinates (and associated weights) were given in Table 6-38 of the PRA and corrected later in a letter from PG&E (Shiffer, 1991b) (this correction was based on a review finding).

Table 23.19 compares the seismic core damage frequency percentiles (as given in Table 23.1) with those independently computed using a Monte Carlo process. This shows that the mean values of total core damage frequency were computed to be nearly the same by both discrete probability distribution (DPD) and Monte Carlo. The lower 5-percent values were also quite close, while the 95-percent value computed by Monte Carlo was 55 percent greater than that computed by the DPD method. This gives rise to a smaller error factor (17 vs. 26) being computed by the DPD method than by the Monte Carlo method. Overall, however, the results agree quite well between the two methods.

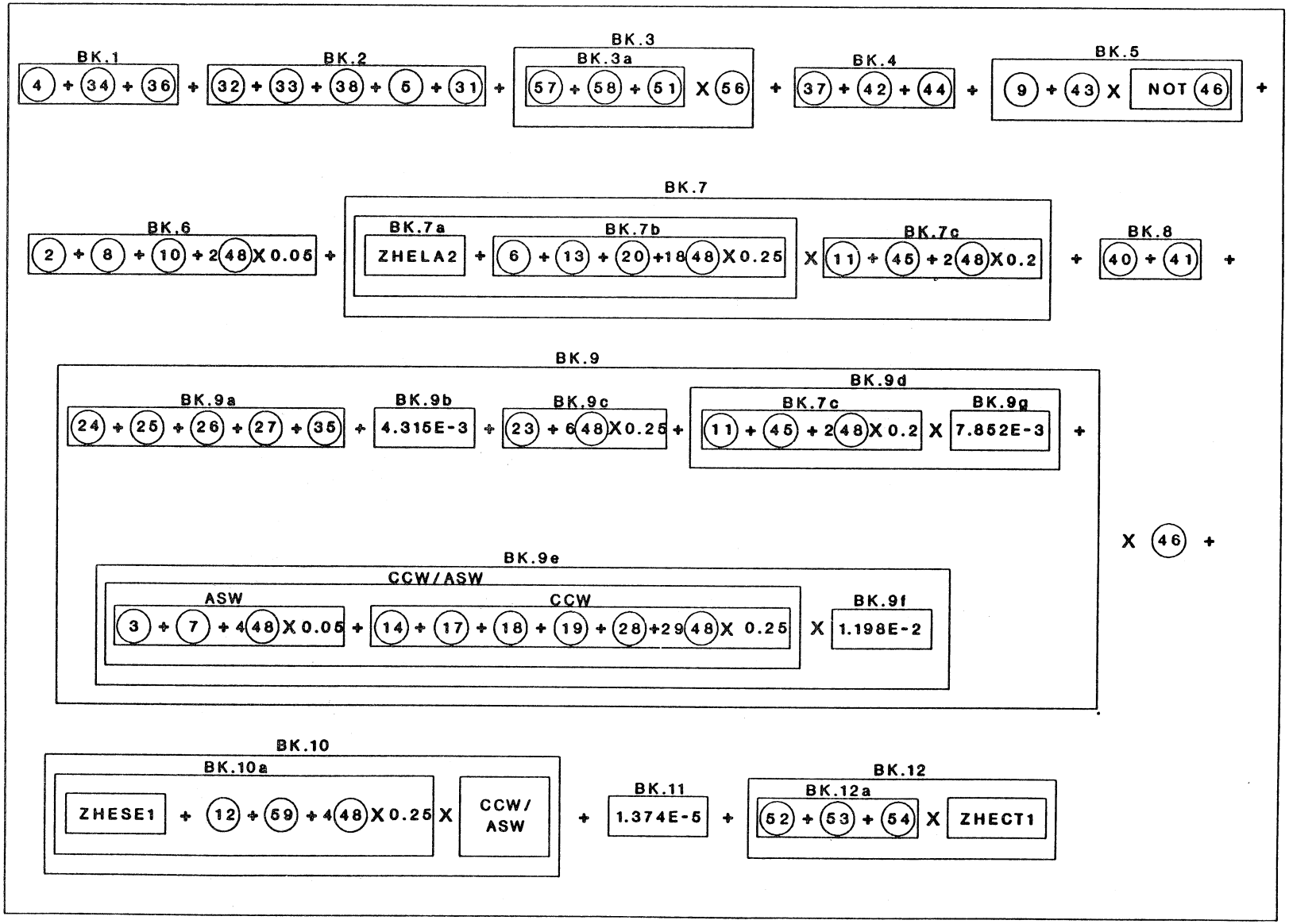


Figure 23.6 Simplified logic block diagram

Table 23.18 Logical blocks as described by PG&E

BLOCK 1

This Block includes the seismic fragilities assumed to result in a total loss of all 125V DC. The auxiliary building fragility was included among this group. All equipment in the auxiliary building and the control room is assumed lost if this fragility event fails. The total loss of all DC is used as a surrogate for this impact. Loss of 125V DC also implies loss of the associated train of AC power.

BLOCK 2

This Block includes the seismic fragilities which result in loss of all emergency AC power. Curve 32 of Table 6-40 in reference 1 is labeled "Buses G and H potential transformers." It is actually the fragility for the Bus F potential transformer. Although the corresponding potential transformers for Buses G and H are stronger than the one for Bus F, the seismic core damage model conservatively assumed that all three emergency buses fail if the weaker transformer fails.

BLOCK 3

Block 3 includes the fragilities that result in failure of all three trains of emergency AC power but which also involve failure of the strut for the turbine building. In the process of developing the fragilities, it was recognized that the turbine building strut failure would change the response of certain components in the turbine building. Separate fragility curves were therefore, developed for the Bus F potential transformer, the safeguard relay panel, and for the 4 kV switchgear for the conditions where the turbine building strut failure occurs. Curve 56 (i.e., that for the strut) is, therefore, combined with the three fragilities using a logical "AND" operation.

BLOCK 4

Block 4 includes just the fragility curves that, if failed, are modeled as a loss of all vital instrumentation. No credit was assumed for shutting down without instrumentation; consequently, core damage was conservatively assumed to occur.

BLOCK 5

Block 5 models the components that, if failed, could result in a failure to trip the reactor. For the reactor trip switchgear, it was recognized that failure of this component would not prevent reactor trip if offsite power was also lost. Consequently, Fragility 43 is combined with a logical "AND" with the complement of the loss of offsite power fragility.

BLOCK 6

Block 6 includes the component failure modes which are considered to lead to an excessive LOCA. One piping segment is modeled for each of the charging and

RHR system piping connections in their interface with the reactor coolant system boundary. The quantity 0.05 is the probability that a failure of the most stressed pipe support in these segments would lead to a complete severance of the pipe. In actuality, even if these pipes completely rupture, the resulting flow area is insufficient to result in an excessive LOCA; i.e., beyond the design basis of the ECCS. However, to simplify the model, this conservative assumption was made. Therefore, this failure mode of either of these two pipe segments is assumed to lead to core damage.

BLOCK 7

Block 7 models the seismic failures that result in a LOCA with failure of either RCS injection or recirculation from the containment support. The LOCA failure modes are included in Block 7C. Two pipe segments are modeled; i.e., charging and the RHR system connections. The factor 0.20 is the likelihood of a small break in the most stressed segment of these pipes given that the pipe support fails; this results in a LOCA from the RCS. Block 7B includes the failure modes that result in a failure of high head injection. Fragilities for the RHR and containment spray pumps are included here because the limiting seismic failure mode is a break in the pump boundary, which is assumed to drain the RWST, resulting in failure of RCS injection. A total of 18 pipe segments are also included. Again, failure of any one of these 18 segments is postulated to result in a draining of the RWST. The factor of 0.25 is the assumed probability of any size pipe break given failure of the most limiting pipe support in one of these segments. Block 7A models an operator error to align recirculation from the containment sump. Action ZHELA2 models the operator action to turn off the RHR pumps following an SI signal with the RCS at high pressure. Failure to turn off these pumps within about 4 hours is assumed to result in failure of the pumps due to overheating while operating on miniflow; this, subsequently, results in the failure of the ability to establish recirculation from the containment sump.

BLOCK 8

Block 8 considers seismic failure of the two sets of control panels; i.e., the main control boards and the hot shutdown panel. Rather than further considering the operator action to transfer control to the hot shutdown panel, given loss of the main control boards, the seismic model conservatively assumes that failure of either control station leads directly to core damage.

BLOCK 9

Block 9 considers the important system failure combinations (i.e., both seismic and non-seismic failures) that involve a loss of offsite power. Block 9A includes the different seismic failure modes of the diesel generators. The battery chargers (i.e., fragility curve 35) are also included in this assessment. It is assumed that their loss eventually leads to a loss of DC, which is needed for continued operation of the diesels. Block 9B is a constant which accounts for all the non-seismic failure combinations of the emergency diesel generators. Block 9C models the seismic failures of the

diesel generator fuel oil transfer system. Even a small break in any one of the six segments modeled is conservatively assumed to fail both trains of fuel oil. Block 9D consists of two terms. Block 7C is as described previously; i.e., it accounts for the seismic failure modes, which lead to a small LOCA. The constant in Block 9G accounts for the non-seismic failure modes that, together with a small LOCA, lead to core damage. Block 9E models the scenarios which involve failure of either component cooling water or auxiliary saltwater together with loss of power to the charging pumps. The Block labeled CCW/ASW, models the CCW and ASW seismic failure modes. It is assumed that a complete guillotine rupture of the ASW piping is required to cause loss of the ASW system. For the CCW system, even a small pipe break is assumed sufficient. The constant modeled by Block 9F accounts for the non-seismic failure combinations that, together with a loss of RCP seal cooling caused by a seismic failure of CCW or ASW, lead to core damage. These non-seismic failure combinations involve a loss of onsite emergency power to the charging pumps consequently resulting in a failure of seal injection and RCS makeup. Blocks 9F and 10A (to be discussed in the next section), together, model all the failure combination that prevent the operators from aligning the firewater system to the charging pumps in the event CCW or ASW failures occurs.

BLOCK 10

Block 10 accounts for scenarios that involve a seismic failure of either CCW or ASW. Block CCW/ASW is as described above when discussing Block 9E. The failures in Block 10A model all the important failure combinations which preclude the operators from aligning firewater to the charging pumps for continued rCP seal injection. The operator action itself is modeled by ZHESE1. This human error rate is modeled as being dependent on the seismic level; i.e., the human error rate increases as the earthquake level increases.

BLOCK 11

Block 11 accounts for all the non-seismic failure combinations, except those involving a loss of offsite power, which result in core damage. Examples of these sequences are failure of all vital AC and failure of all vital DC.

BLOCK 12

This Block accounts for the scenarios that result in core damage because of relay chatter. Block 12A models the three separate fragilities modeled for relay chatter. Any one of these events is modeled as leading to an initial loss of all AC. The relay chatter recovery action is ZHECT1; as with ZHESE1, the human action is dependent upon the seismic level. Given the occurrence of relay chatter and the failure to recover from it, the model assumes that core damage results.

23.4.8 Characteristics of Seismic Sequences

The following characteristics have been developed using the block model.

Table 23.20 shows the (unconditional) contributions of each of the 12 accident scenarios (blocks) on the simplified logic block diagram for different intervals on the hazard curve. Figure 23.7 compares the contributions at various earthquake intervals as computed by the DPD approach (as presented in Figure 6-49 of the PRA) versus the Monte Carlo approach. It can be seen that, because of the rather coarse interval on spectral acceleration used in the PRA, the contributions at the upper and lower intervals have been overestimated. However, both approaches show that most of the risk is due to earthquakes with average spectral accelerations in the 1.7 to 3.0g range. This can also be seen from the mean level plant fragility shown in Figure 23.8. This curve shows that the mean conditional probability of core damage is very small below 2.0g average spectral acceleration.

Finally, an evaluation of the risk reduction potential (RRP) for each of the components was made using the simplified logic block model. The risk reduction potential is defined as the percentage decrease in total core damage frequency which results if the probability of failure of that component is set equal to zero, and the total core damage frequency is reevaluated. Table 23.4 (Table 6-58 of the PRA) presented such values (denoted as "Impact if Very Strong, That Is, if Impervious to Earthquake"). Table 23.21 lists the RRP for all components in the block model, and compares them to those reported in Table 23.4. In general, for those components whose RRP values were listed in the PRA, the agreement is reasonably good. The RRP of the various diesel generator failure modes was found to be 16 percent although the PRA listed only 10 percent. The RRP of switchgear/breaker panels was found to be 6.6 percent, but was not listed in the PRA, although components with smaller values of RRP were listed. Finally, the RRP for BOP piping and supports was found to be 5.8 percent as contrasted to the PRA value of 2.2 percent. Overall, however, the agreement is quite good.

23.4.9 Sensitivity Studies

Using the uncertainty analysis block model, a number of sensitivity studies were performed to estimate the effect of certain assumptions in modeling techniques used in the seismic PRA. In each case, a mean point estimate calculation based on the block model was performed and changes in mean seismic core damage frequency were computed. Each study is reported separately and, in general, the changes in the seismic core damage frequency from the different sensitivity studies are not independent and are certainly not additive.

(1) Impact of Pipe Conditional Failure Fraction. In the modeling of pipe failures, different pipe segments were identified for the various safety systems and the probability of failure of each segment was estimated as the probability of the pipe support failure (generic fragility) multiplied by conditional fraction that failure of the pipe support would result in double-ended pipe fracture. In the uncertainty analysis block model, this conditional failure fraction varied between 0.05 to 0.25, depending on the system and type of piping being analyzed. The basis for the choice of

Table 23.19 Comparison of PRA seismic CDF percentiles with Monte Carlo results

	Total Core Damage Frequency Distribution				
	5%	50%	Mean	95%	EF
DCPRA	9.3E-7	6.2E-6	3.7E-5	1.1E-4	17
Monte Carlo	1.1E-6	6.5E-6	3.8E-5	1.7E-4	26

Table 23.20 Ranking of block model accident sequences from Monte Carlo uncertainty analysis

BLOCK ACC. Seq.		Ranking	Contribution
1	Loss of all 125V DC	No 3	12.4%
2	Loss of all AC power	No 1	38.7
3	Loss of 3 trains AC	No 12	0.4
4	Loss of vital instrumentation	No 6	2.9
5	RPS failure to trip	No 10	0.7
6	Excessive LOCA	No 4	5.8
7	LOCA w/o ECCS injection	No 9	1.5
8	Control Panels fail	No 8	2.0
9	Loss of offsite power	No 2	26.6
10	CCW or ASW systems fails	No 5	5.3
11	Random failures	No 11	0.6
12	Relay chatter fails AC power	No 7	2.9

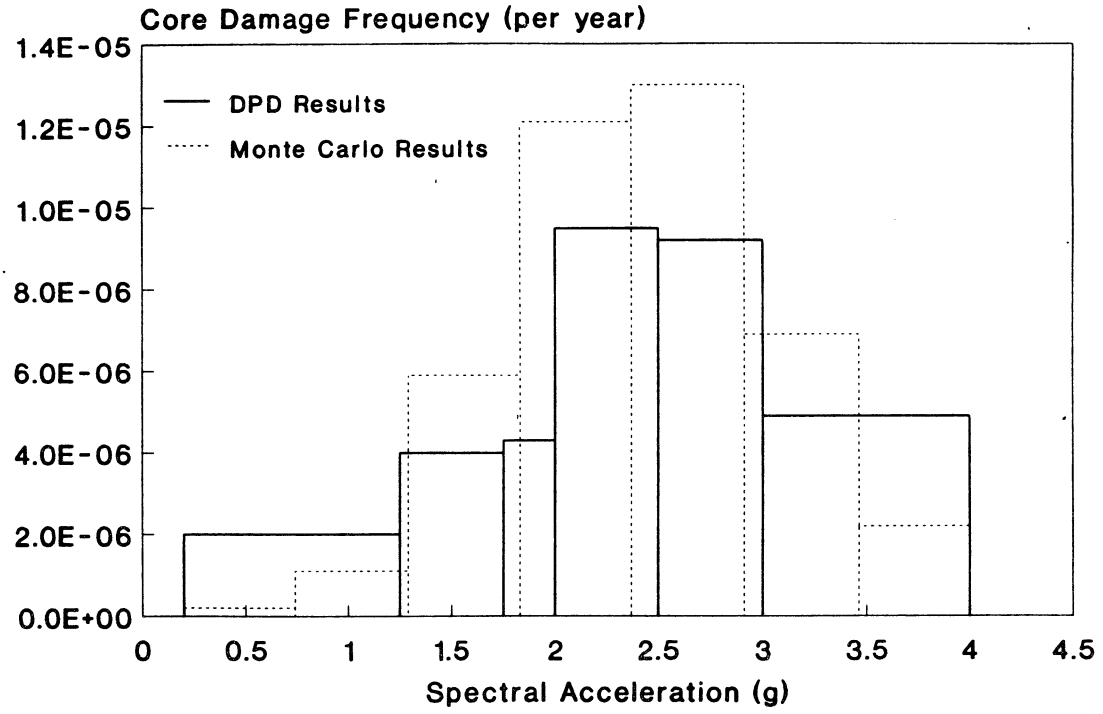


Figure 23.7 Contribution of each earthquake range to the seismic CDF (DPD vs. Monte Carlo)

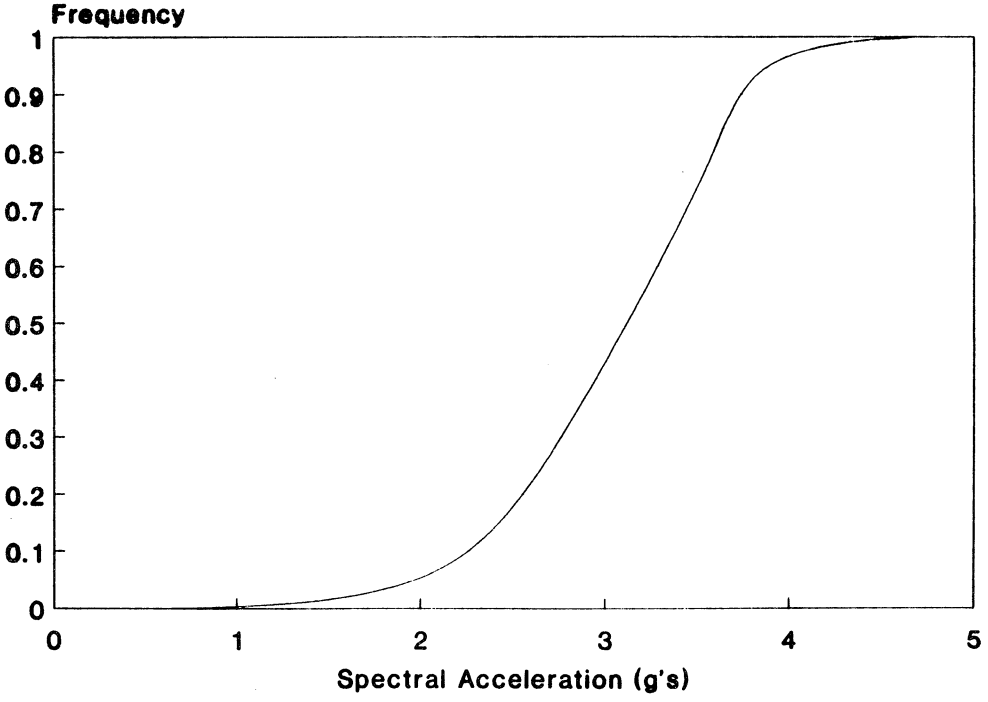


Figure 23.8 Plant total mean fragility curve

Table 23.21 Component risk reduction potentials as given in the PRA (PG&E) and as computed by Monte Carlo approach (SNL)

Component #	SNL %	PG&E %	Component Name
1	0		containment building
2	1.5		concrete internal biostructure
3	< 1		intake structure
4	2.9		auxiliary building
5	26.2	30.5	turbine building shear wall
6	< 1		refueling water storage
7	< 1		auxiliary saltwater piping
8	< 1		reactor pressure vessel
9	0		reactor internals
10	3.6	3.4	steam generators
11	< 1	0.7	power-operated relief valves
12	< 1		reactor coolant pumps
13	< 1		rhr pumps
14	< 1		rhr heat exchangers
15	0		safety injection accumulators
16	0		boron injection tank
17	< 1		ccw pumps
18	1.2		ccw heat exchangers
19	< 1		ccw surge tank
20	< 1		containment spray pumps
21	0		spray additive tank
22	0		afw pumps
23	< 1		diesel gen. fuel oil pumps/filter
24	< 1		diesel generators
25	< 1		diesel gen. radiator/water pump
26	3.1		diesel gen. excitation cubicle
27	11.7	10.0	diesel gen. control panel
28	< 1		containment fan cooler
29	0		supply fans
30	0		supply/return fans
31	1.2		4-kv switchgear
32	< 1		bus g & h potential transformer
33	< 1		safeguard relay panel
34	2.7		batteries
35	1.5		battery chargers
36	6.6		switchgear/breaker panel
37	2.4		inverters
38	5.3	5.0	4,160v/480v transformers
39	0		auxiliary relay panel
40	1.5		main control boards
41	< 1		hot shutdown panel
42	< 1		process control and protection

31.1 (components 2, 3, 4, 5)

15.6 (components 23, 24, 25, 26, 27)

Table 23.21 (Cont'd.) Component risk reduction potentials as given in the PRA (PG&E) and as computed by Monte Carlo approach (SNL)

Component #	SNL %	PG&E %	Component Name
43	< 1		reactor trip switchgear
44	< 1		pressure & del p transmitter
45	< 1		impulse lines
46	25.0	24.4	offsite power, 230 kv
47	0		offsite power, 500 kv
48	5.8	2.2	bop piping and supports
49	0		penetration(s) boxes
50	0		hvac ducting and supports
51	< 1		switchgear/strut
52	< 1		chatter, main control board
53	3.1 < 1	2.4	chatter, dg control panel
54	3.1		chatter, 4-kv switchgear
55	0		chatter, safeguards relay panel
56	< 1	0.4	strut for turbine building
57	< 1		bus f potential transformer
58	< 1		safeguard relay panel
59	< 1		centrifugal charging pump

these different fractions was not described. Hence, in this study, the conditional pipe break failure fraction was varied (the same for all systems) from a lower value of 0.0 to an upper value of 1.0 (that is, support failure equals pipe failure). The results of this study are summarized in Table 23.22.

Table 23.22 Impact of pipe conditional failure fraction

Conditional probability of pipe break	Probability of core damage	% difference
0.0	3.91E-5/yr	5% lower
0.05	3.96E-5/yr	4% lower
0.10	4.01E-5/yr	3% lower
0.20	4.12E-5/yr	0.2% lower
0.25	4.17E-5/yr	1% higher
0.40	4.33E-5/yr	5% higher
0.50	4.44E-5/yr	7% higher
1.00	4.96E-5/yr	20% higher

As can be seen from the values given in Table 23.22, the effect of varying the conditional pipe break failure fraction was relatively small. In fact, if the conditional failure fraction is taken as 1.0 (certainty), the result is only a 20-percent increase in the total core damage frequency. Thus, overall, the seismic total core damage frequency results are not particularly sensitive to the assumed failure fraction. This is not surprising since the overall generic fragility for the piping supports has a relatively high median value and, thus, is not expected to play a major role in the final core damage frequency results.

(2) Impact of Correlation on Uncertainty Analysis. As described earlier, correlation was incorporated somewhat differently in the point estimate model (in which the various support trains were considered explicitly) and in the final block model used for the uncertainty analysis (in which the failure of one train was assumed to imply the failure of all trains). Further, it was seen that the uncertainty analysis gave slightly higher mean core damage frequencies due to this more conservative assumption with respect to correlation. A sensitivity study was performed to estimate the impact of correlation on the block model uncertainty analysis. This was done by assuming that similar trains of the same support systems were identical (e.g., had the same random and seismic fragilities) and that the responses seen by these similar support trains were identical. It was assumed that the responses were fully correlated, but that there was no correlation between the fragility failure modes of the support systems. The uncertainty analysis block model was modified to incorporate these assumptions and the frequency of core damage was reevaluated. When this was done, the mean-point-estimate core damage frequency was reduced to 2.8E-5 per year, a reduction of 33 percent.

(3) Impact of Range of Integration. As described in the PRA, the seismic integration was performed up to an upper limit average spectral acceleration of 4.0g, and a total of 6 (unequal) intervals were used in the integration scheme. To verify that this range of integration was adequate, a mean-point-estimate calculation using the block model was performed in which the range of integration was increased to 5g and then to 6g average spectral acceleration. These two calculations showed increases in mean core damage frequency from the base-case value (4.1E-5) to 4.5E-5 and 4.6E-5, respectively. Thus it can be seen that the range of integration considered in the PRA was adequate, and if a greater range of integration were used, an increase of about 12 percent would be expected.

(4) Impact of Ceramic Insulator Fragility. A key feature in the results of the PRA results from the fact that the fragility taken for the 230-kV ceramic insulators in the switchyard was taken to have a median average spectral acceleration of 1.66g. Scaling to peak ground acceleration, this corresponds to a median peak ground acceleration value of 0.72g. This is at least twice as high as any ceramic insulator fragility median used in previous PRAs. The basis for this median value came from segregating the recorded earthquake performance data on ceramic insulators into several groups. It was found that the so-called "dead tank" type of ceramic insulator performed significantly better than other ceramic insulators typically used in commercial power plants. Further, it was verified that

the ceramic insulators in the 230-kV switchyard were of the dead tank variety and hence, it was appropriate to use a higher median value for their seismic fragility.

To examine the effect of the ceramic insulator fragility mean on the core damage frequency predicted for Diablo Canyon, a sensitivity study was performed in which the ceramic insulator fragility median was varied from 0.3g PGA to 0.72g PGA and the core damage frequency was recomputed. The results of this calculation are shown as a continuous curve on Figure 23.9. It can be seen that the mean core damage frequency increased from 4.15E-5 to a value of 6.25E-5 at the weaker limit. Thus, the effect of going from a median ceramic fragility value of 0.72g (PGA) down to a more usual value of 0.3g (PGA) is an increase in the mean core damage frequency of 50 percent. For a more realistic value of the median ceramic fragility, the impact on the calculated CDF is not appreciable, as discussed in Section 23.4.5.4 of this SSER.

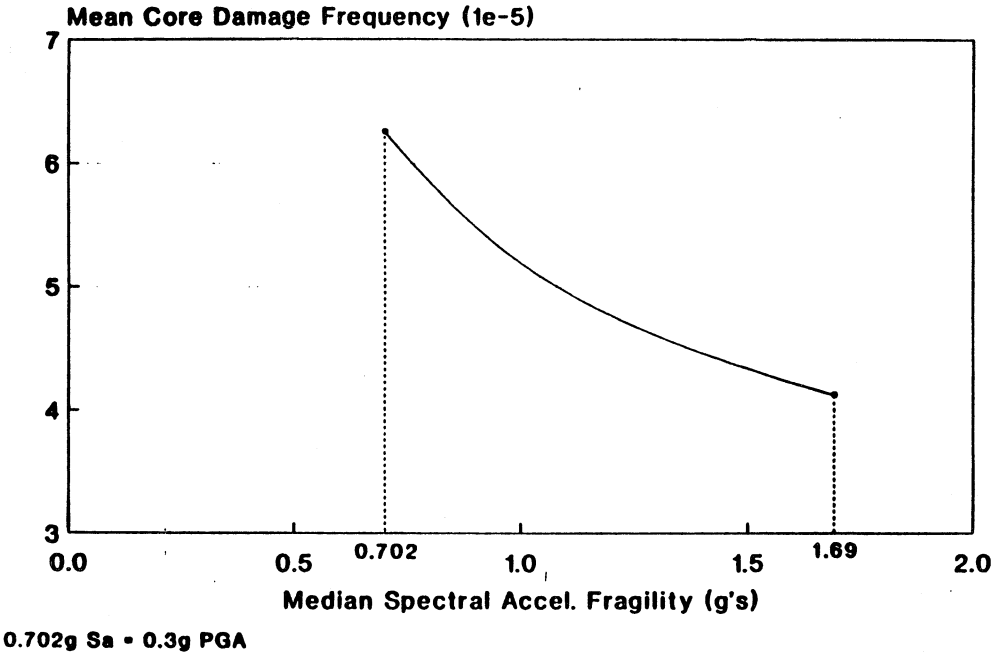


Figure 23.9 Sensitivity study on 230-kV fragility median

23.4.10 Summary and Conclusions

In general, the seismic portion of the PRA was found to be a defendable and detailed state-of-the-art seismic risk assessment. Due to the nature of the conservative assumptions made in modeling systems and including correlation on component failures, it is felt that the mean core damage frequency computed is somewhat conservative.

The PRA involved a number of relatively novel considerations. First of all, the examination and inclusion of relay chatter effects has advanced the state of the art. The detailed level to which circuits were examined for the potential impact of relay chatter and its documentation goes well beyond that performed in any previous seismic PRA. The detailed comparison of the non-linear response of the turbine building and comparison against drift limits against the engineering factor of safety approach provided a meaningful validation of the later more simplified method, which has been used in all the commercial seismic PRAs to date. This study provides considerable confidence in the use of the factor of safety approach for predicting failure levels of both structures and components. The use of average spectral acceleration as the independent seismic parameter (both for the seismic hazard curves and for the component fragilities) provided a consistent means of eliminating double counting in assigning uncertainties to both the hazard curve and the fragility. Overall, however, the use of average spectral acceleration versus peak ground acceleration was found to play little role in determining the overall magnitude of the core damage frequency at Diablo Canyon. This in itself is of interest because of the fact it substantiates the use of peak ground acceleration in all past seismic PRAs.

The PRA fragilities were found to have been derived by state-of-the-art and relatively mature methodology which has been applied to more than 25 power plants in the past. A review of the identified and analyzed modes found that the appropriate failure modes had been identified. A review of the anchor bolt failure modes showed that important recent generic issues (such as edge distance, bolt spacing, and concrete cracking effects) were properly included and taken into account. The methods and the basis for assigning the random and modeling uncertainties to the fragilities were found to be reasonable.

The procedure used for quantifying the risk of core damage was found to be acceptable and the quantification itself was found to be accurate. An independent evaluation of the block model used to perform the uncertainty analysis by a completely independent approach (Monte Carlo) was found to produce final distributions on core damage frequency that were reasonably close to those reported for the PRA. The main discrepancy was some difference in the 95th percentile core damage frequency values. The same dominant contributors to core damage frequency were found and the percentage contributions for these dominant contributors were found to be nearly the same.

23.5 Review of Non-Seismic External Events

This section of the SSER presents the results of a review of the core damage accidents initiated by external events other than the seismic events. As noted in Section 23.1 of this SSER, the staff has not performed a detailed review of these other external events except for some scrutiny of the fire events. Section 23.5.1 of this SSER describes the non-seismic/non-fire events and Section 23.5.2 describes results of the fire events review.

23.5.1 Non-Seismic/Non-Fire External Events

The quantification of the "external" initiating events involved a rather complex spatial interaction study (including fires, internal floods, and other spatially dependent events) and a detailed impact analysis on plant systems.

Flood scenarios were grouped into three initiating event categories: FS9, FS10, and FS11. Their initiator frequencies were determined individually and were fed into the plant model for core damage quantification (see Tables 23.5 and 23.6). Contribution to the CDF from internal flood events is estimated to be about 3 percent.

Seven truly "external" event initiators were also considered (i.e., aircraft impact, ship impact, external floods, hurricanes and tornadoes, hazardous chemical threat, turbine missiles, and external fires). The basic approach of analysis for all these events was to perform a conservative screening analysis in the area of initiator frequency as well as for the conditional likelihood of core damage. Except for the hazardous chemical initiator, these events were screened out in the PRA as rather insignificant contributors to the core damage frequency; thus, they were not considered further.

Those initiators deemed to be significant contributors to the core damage frequency (i.e., those considered to constitute the risk after truncating, merging, and correcting for scenarios with small core damage frequency) were included in the reduced plant model. These initiators are listed in Table 23.6. Only the hazardous chemical release (HAZCHM) appears as an initiating event in this table.

23.5.2 Fire Analysis

Since fire-initiated accidents were estimated to be one of the significant contributors to the core damage frequency, on the order of 16 percent, additional review was conducted in this area. The scope of the review was limited to a review of the methodology and the dominant fire core damage scenarios as reported in the PRA. Two of the control room fire scenarios were requantified, and a scenario initiated by a fire on the turbine operating deck was also requantified.

The methodology used for the fire analysis follows the scenario approach. First, a screening analysis was performed, in which it was conservatively assumed that a fire in any given fire area caused all equipment in that area to fail. Fire and smoke propagation through fire doors left open, and through other pathways, was included. For scenarios surviving the screening analysis, a more-detailed analysis, one which included operator recovery actions and uncertainties in the estimated core damage frequency, were performed. For scenarios requiring more detailed analysis, geometric factors and severity factors were estimated. The geometric factor gives the fraction of the fire area in which the fire must start in order to cause the target equipment to fail. The severity factor gives the fraction of the fire frequency for fires at least severe enough to cause the target equipment to fail. If the net result of a fire scenario was an initiating event with failures of mitigating systems at a frequency which was small compared to the frequency of the corresponding sequence from internal events, then the scenario was excluded from further analysis.

The geometric factors and severity factors were obtained by making use of the analyst's engineering judgment, and did not make use of calculations with fire propagation codes. However, an experienced fire analyst can make judgments concerning geometric and severity factors with adequate accuracy. The metho-

dology used in the fire portion of the PRA is acceptable, and judged capable of finding fire vulnerabilities in the plant, as well as ranking them in the order of importance.

Turbine Building Fire Scenarios

The dominant turbine building fire scenario in the PRA was sequence FS8 in Table 23.6. A fire starts on the operating deck of the turbine building, and smoke from this fire goes through vents to the safety-related 4-kV switchgear located one floor below, and causes all three safety-related trains of 4-kV (busses F, G, and H) to fail. A significant feature of the Diablo Canyon plant is the fact that the safety-related 4-kV switchgear are located in the turbine building. This means that a large fire in the turbine building has the potential for causing core damage.

The staff has requantified the fire sequence initiated by a fire on the turbine operating deck. In the fire database developed in NUREG/CR-4586 (Wheelis, 1986), there were 9 fires on the turbine operating deck in about 700 turbine-building years, which gives an estimate of 0.013 fire/yr as the initiating event frequency. The PRA used 2E-3/yr as the initiating event frequency. The PRA estimate was based on weighting the estimate of the frequency for all fires in turbine buildings by the area fraction for the turbine building operating deck. However, a disproportionate number of fires that occur in turbine buildings occur on the operating deck, and, since there are enough operating data to obtain an estimate from experience directly, that was done in the staff analysis. The PRA estimated that the fraction 2.5E-3 of the fires would result in smoke going through vents to the switchgear rooms (one floor below) and causing the switchgear to fail, leading to core damage. Using the same conditional probability of leading to core damage, the staff obtained 3.3E-5/yr as the estimate of core damage from a fire on the operating deck of the turbine building.

A review of international experience with fires beginning on operating decks of turbine buildings can also be used to help quantify this sequence. No systematic review was made, but there have been at least three such very serious fires in international experience: a fire at the Muehleberg nuclear power plant in Switzerland on July 28, 1971, a fire in Taiwan (Maanshan-1 nuclear power plant, July 7, 1985), and one in Spain (Vandellos-1 nuclear power plant, October 19, 1989). There are about 5600 reactor-years worldwide at the present time. Hence, the frequency of very severe fires on turbine operating decks is estimated at 5.4E-4/yr. If, for such a fire at Diablo Canyon, there is a 6-percent chance of the fire causing the failure of the 4-kV switchgear, either by smoke, by water damage through some unspecified path, or by the spreading of the fire through failure of a fire barrier, one obtains 3.2E-5/yr for the core damage frequency from this sequence, about the same as the previous estimate. Of course, there are considerable uncertainties in this estimate.

PG&E submitted clarifying information on the PRA fire risk analysis (Shiffer, 1990d). This analysis supports the PRA estimate of the conditional probability of core damage, given a fire on the turbine operating deck, but does not address how often such fires occur.

Control Room Fire Scenarios

Two control room fire scenarios were requantified. Each scenario involves loss of auxiliary saltwater (ASW) or component cooling water (CCW). On loss of CCW (either directly or indirectly through loss of ASW), the reactor coolant pumps (RCPs) must be tripped in a short time (about 10 minutes), or the bearings of the RCPs will fail, their shafts will vibrate, and their seals will fail, resulting in a small LOCA. These scenarios must be distinguished from another way of getting an RCP LOCA when CCW is lost. This other way involves loss of seal injection and CCW to the thermal barriers of the RCP seals, and results in a seal LOCA even for a tripped RCP, but in a much longer time frame, of about 1.5 hours. If a LOCA occurs, and the control room is evacuated, it is unlikely that the LOCA can be mitigated from the hot shutdown panel, since there are limited ECCS controls. This assumption is consistent with the PRA: in one of the dominant scenarios in Table 6-61 of the PRA, a cable spreading room fire in which a PORV sticks open, no credit is given for establishment of recirculation from outside the control room.

In a fire study for Surry, it is estimated that in 10 percent of all control room fires, heavy smoke will fill the control room within 5 to 10 minutes. For such fires, it is unlikely that the RCP pumps will be tripped before the control room was evacuated. If the pumps are not tripped from the control room, it is unlikely they will be tripped in time from outside the control room. First, the operators would have to recognize the need to trip the pumps, and, secondly, it is not possible to trip the pumps from the hot shutdown panel. It would be necessary to go to the non-safety-related 12-kV switchgear room, located five floors below the control room. No credit is given for re-initiation of ASW and CCW from the hot shutdown panel before the RCP seal LOCA, given that the RCP pumps are not tripped.

At a meeting with representatives of PG&E (April 3, 1990, in Rockville, Md.), it was learned that each control room panel has its own smoke alarm. Because of this, it was judged that fire suppression before control room evacuation was more likely to be successful at Diablo Canyon than at Surry, which does not have such smoke alarms. It was, therefore, assumed that in only 6 percent of the control room fires would heavy smoke fill the control room and force evacuation before the RCPs were tripped.

For fires that did create heavy smoke within 5 to 10 minutes, it was considered that the fire was sufficiently severe that a fire anywhere on a given control board would cause all equipment on that control board to fail.

The two control room scenarios that were requantified were scenarios CR1 and CR4 from the PRA (see Table 23.5). Scenario CR1 involves a fire on board VB-1 which causes the ASW/CCW control circuits to fail. Scenario CR4 involves a fire on board VB-4 which causes the 4-kV safety-related busses F, G, and H, and hence ASW/CCW, to fail, but leaves the non-safety-related reactor coolant pumps operating.

The CR1 scenario is quantified as follows:

Frequency of control room fires	5E-3/yr
Fraction of fires with heavy smoke	0.06
Probability fire is on board VB-1	94/2260
Core damage frequency from scenario	1.2E-5/yr

The probability the fire is on board VB-1 was the median estimate obtained in the PRA, and was obtained in the PRA as the ratio of the base area of VB-1 to the base area of all control panels in the control room.

The quantification of the CR4 sequence is the same, except that the probability the fire is on board VB-4 is 0.052 (taken from the PRA). (The PRA assumed that the fire had to be on 50 percent of the board to cause the 4-kV circuits to fail, but the staff is assuming that, for those fires creating heavy smoke the fire is sufficiently severe so that a fire anywhere on the board will cause these circuits to fail.) The core damage frequency from the CR4 scenario is 1.6E-5/yr.

In response to the staff's request for additional information, PG&E revised its analysis of the control room fire sequences (Shiffer, 1990b). In its revised analysis, PG&E obtained a frequency of 6.5E-6/yr for scenario CR1, and a frequency of 2.4E-6/yr for scenario CR4. The staff's analysis differs from PG&E's revised analysis primarily in assuming that in all fires so severe as to cause evacuation from the control room, all circuits on a board would fail (given that a fire initiated on the board), while PG&E assumed that the geometry/severity factor was independent of whether or not the control room would have to be evacuated. Additionally, for those sequences in which the control room had to be evacuated, the staff analysis gave no credit for operator action to trip the reactor coolant pumps, while PG&E gave some credit.

The instrumentation at the hot shutdown panel (HSDP) at Diablo Canyon is not independent of the instrumentation in the control room. As noted in the May 3, 1990, letter from PG&E (Shiffer, 1990b), if an instrumentation circuit should fail in the control room, the instrumentation at the HSDP will fail off scale. However, there is a dedicated shutdown panel (DSP), located elsewhere, in which some essential instrumentation is provided, including reactor coolant system temperature and pressure, pressurizer level, and steam generator level. For a fire in the control room to affect instrumentation there, coordination is required from two separate locations, which will increase the probability of human error. A rough estimate of the contribution to the CDF from these sequences indicates that they are not very important.

Additional evaluation of scenarios for fire in the cable spreading room is included in NUREG/CR-5726 (Bozoki and others, in process); however, these evaluations do not appreciably affect CDF estimates.

Results of the Fire Analysis Review

Table 23.23 gives the results obtained in the requantification of the fire scenarios, and compares them to the results obtained in the PRA, as revised by PG&E in a letter on May 3, 1990 (Shiffer, 1990b). The mean core damage frequency from all fire scenarios is estimated at 3.5E-5/yr in the PRA, and the review estimate is 8.0E-5/yr. The dominant fire scenarios initiated in the control room and in the cable spreading room are more or less typical of scenarios obtained in other fire PRAs. Although fires affecting electrical switchgear have also been important in other fire PRAs, one thing that is different about Diablo Canyon is the location of the safety-related switchgear in the turbine building, where it can possibly be damaged by a fire on the turbine operating deck. Uncertainties include uncertainties in the fire

initiator frequency, and the geometric/severity factors. In summary, the limited staff review finds that the fire analysis methodology is acceptable; however, in some area the evaluations are thought to be optimistic. The staff requantification roughly increases the fire-induced core damage frequency by a factor of two.

Table 23.23 Fire scenario CDF

Scenario	PRA frequencies	Review frequency
CS2 (cable spreading room fire)	1.2E-5/yr	1.2E-5/yr
CS1 (cable spreading room fire)	7.9E-6/yr	7.9E-6/yr
FS8 (turbine operating deck fire)	6.0E-6/yr	3.2E-5/yr
CR1 (control room fire on board VB-1)	6.5E-6/yr	1.2E-5/yr
CR4 (control room fire on board VB-4)	2.4E-6/yr	8.0E-5/yr
Sum, all fire scenarios	3.5E-5/yr	8.0E-5/yr

23.6 Summary and Conclusions

23.6.1 Summary of Findings

Using the alternative calculations discussed in Sections 23.3, 23.4, and 23.5 of this SSER, overall core damage frequency (CDF) results are summarized here. Table 23.24 lists the staff values as well as original PRA values for the mean CDF estimates for internal, seismic, and fire initiators. Two sets of staff values presented here are based on two representative internal events cases discussed in Section 23.3.9 of this SSER. The table also indicates percentage contributions to the mean CDF from these initiators.

Table 23.24 Overall mean CDF estimates based on the staff review

Event category	Initial PRA submittal	Updated PRA based on review	Staff review results
Internal events	1.29E-4 (65%)	1.31E-4 (62%)	2.8E-4 (70%)
Seismic events	3.7E-5 (19%)	3.7E-5 (18%)	3.7E-5 (9%)
Fire events	2.8E-5 (14%)	3.5E-5 (17%)	8.0E-5 (20%)
Other external events	6.9E-6 (3%)	6.9E-6 (3%)	6.9E-6 (2%)
Total	2.0E-4	2.1E-4	4.0E-4

As seen from Table 23.24, the staff has not proposed alternative results for the seismically induced CDF, because the staff agrees with the hazard and fragility estimates used by PG&E in the PRA. In seismic PRA reviews, alternate estimates of these two parameters have been generally the cause of different CDF estimates. Agreement between PG&E and the staff in the seismic PRA area is, in part, the result of the interactive mode in which this review was conducted. This mode identified several issues and sensitivity studies early in the review, and as a result, either the resolutions were incorporated in the final analysis or the issues were shown to be unimportant. However, the main reason for the small number of disagreements is the very rigorous and detailed plant/site-specific analyses performed for both the hazard and fragility estimates in this PRA. The staff performed sensitivity studies in the seismic analysis to verify PG&E's analysis and to gain additional insights.

The primary reason for the difference in the CDF estimates for internal events presented in Table 23.24 is the alternate conditional split fractions used by the staff for the auxiliary feedwater and auxiliary saltwater systems. The staff also revised the initiating event frequency for the LOOP event. In general, use of the staff's estimates does not change the order of importance of the initiating events that are the major contributors to the core damage frequency.

The reasons for the higher fire-induced CDF estimated by the staff are twofold: (1) the staff estimates a higher frequency of turbine deck fires and (2) the staff gives less credit to several operator actions used in the PRA to mitigate the fire scenarios.

The overall perspective, in the context of the license condition and the LTSP, is that the seismic events are not predominant contributors to the CDF estimates for the Diablo Canyon plant. Seismic contribution varies from 10 percent to 20 percent. Both the internal events and fire events contribute more to the CDF estimates than the seismic events. Figure 23.10, reproduced from the PRA, compares the results of the Diablo Canyon PRA with other Westinghouse PRAs (which included seismic events) performed by PLG. Both the original PRA estimate and the staff estimate (mean CDF only) are indicated on this figure. This figure indicates that the estimated CDFs for the Diablo Canyon plant are similar to those computed for other comparable PWRs. [A more detailed discussion on comparison with results of other PRAs is contained in NUREG/CR-5726 (Bozoki and others, in process).]

23.6.2 Conclusions

23.6.2.1 General

The following conclusions/observations are applicable to the entire PRA:

(1) The PRA methodology used represents state-of-the-art methodology, and in many cases has advanced the state of the art.

(2) Utility personnel were extensively involved in performing and maintaining the PRA.

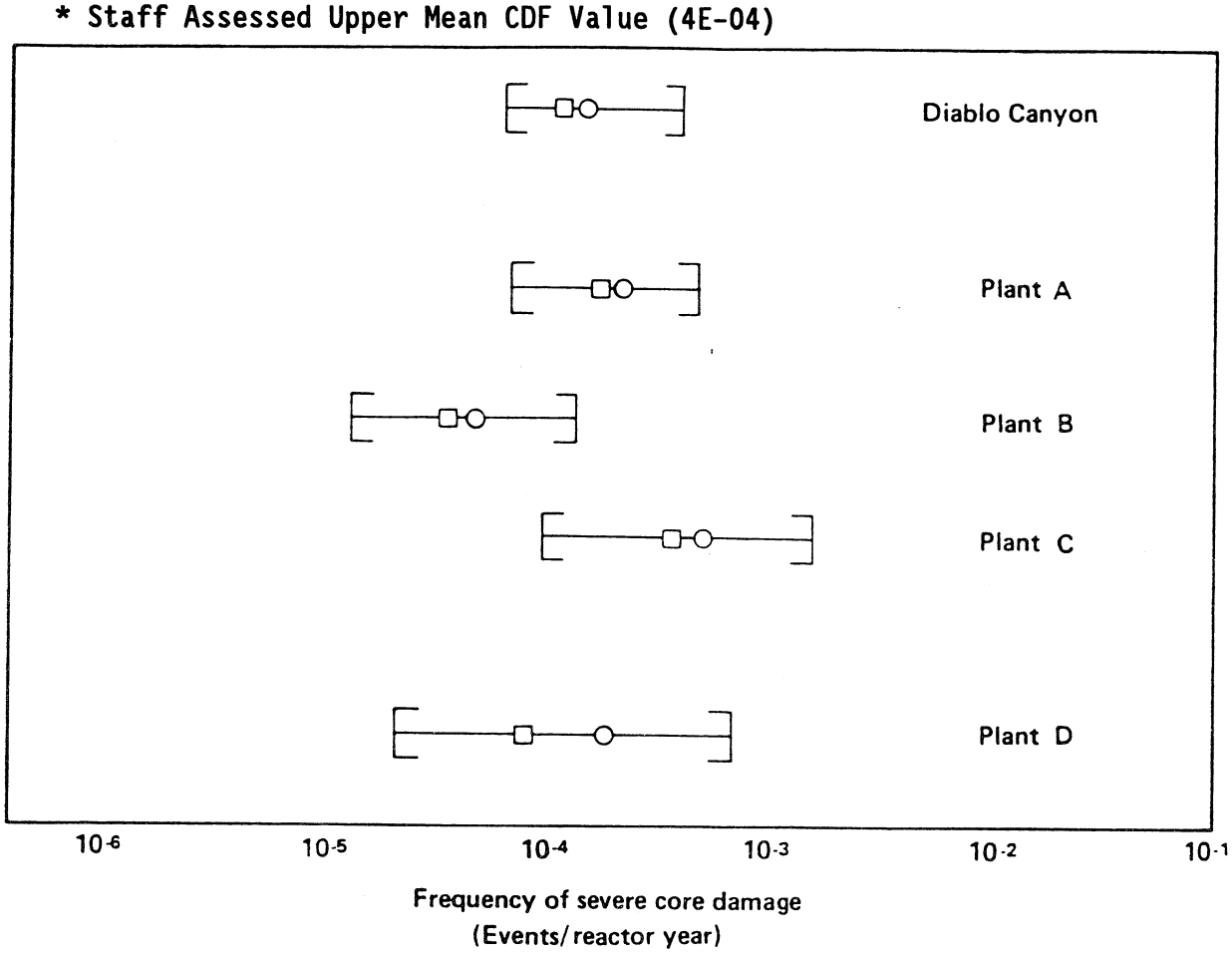


Figure 23.10 Other probabilistic risk assessments (Figure 51 of the PRA)

(3) Several modifications, based on the results of the early phases of the PRA study, have been made to the plant and have been incorporated in the PRA models.

(4) The review of the Diablo Canyon PRA was made difficult by the lack of adequate details in the original documentation (Brand, 1988) and the fact that the PRA uses a very complex plant model consisting of more than 2000 sequences for the internal events alone.

Specific conclusions with respect to the internal, seismic, and fire events are described in the following sections of this SSER, followed by an overall conclusions section.

23.6.2.2 Internal Events Analysis

(1) The internal events are the major contributors to the non-seismic core damage frequency (roughly 70%).

(2) The loss of offsite power (LOOP) initiator is by far the greatest contributor to the non-seismic core damage (roughly 1/3 to 1/4), in magnitude and in number of leading sequences. About 3/4 of the LOOP-induced core damage is associated with extended unit blackout (for additional details see the special issues importance summary, Table 23.9).

(3) Initiators representing (common cause) support system failures other than LOOP [i.e., loss of one dc bus (L1DC), total loss of auxiliary saltwater (LOSW), total loss of component cooling water (LPCC), loss of 480-V switchgear ventilation (LOSWV), loss of control room ventilation (LOCV)] contribute about 10 percent to the non-seismic core damage frequency. Including LOOP, this initiator group is associated with 1/3 of the estimated core damage frequency.

(4) Transients contribute to the non-seismic core damage frequency almost in the same proportion as the support system failures (including LOOP), roughly 1/3. Reactor trips, turbine trips, feedwater losses, and the like, are rather frequent initiating events.

(5) The total contribution of initiators belonging to the loss-of-coolant inventory group to the non-seismic core damage frequency is small, about 10 percent.

(6) By examining the leading sequences, the following observations are made regarding the leading individual sequences. No single internal event sequence contributes more than 3.5 percent of the total non-seismic CDF. Among the operational failures of the plant, loss of feed and bleed cooling, loss of auxiliary feedwater system, and occurrence of RCP seal LOCA are the most frequent.

(7) The special scenarios and their contribution to the non-seismic CDF are as follows: station blackout (18%); RCP seal LOCA, with and without station blackout (31%); primary relief valve opens and fails to reclose (12%); feed and bleed cooling (12%), and pressurized thermal shock (4%).

In summary, the internal events Level 1 portion of the PRA represents a comprehensive and detailed effort and is a firm and reasonable basis to address element 4 of the license condition.

23.6.2.3 Seismic Events Analysis

(1) The seismic core damage frequency generated by the PRA has withstood a detailed review, and was found to be a reasonable estimate taking into consideration the uncertainties inherent in such estimates.

(2) The overall seismic CDF profile is dominated by accident sequences leading to station blackout (79%). These may be due to (a) loss of offsite power (LOOP) in conjunction with failures in the emergency diesel generator system, (b) failure of buildings (i.e., turbine building), or (c) failure of components (e.g., 4-kV switchgear or 4-kV/480-V transformers) which can lead to station blackout with or without loss of offsite power.

Of these blackout sequences, 53 percent do not directly cause failure of the auxiliary feedwater system, but lead to reactor coolant pump seal cooling failure, and, hence, to small LOCAs. Direct failures of the AFW system account for 22 percent of the contributions to the station blackout sequence.

(3) The single greatest contributor is the failure of the turbine building, followed by the loss of 230-kV offsite power. There appear to be no weak links in the plant that dominate the plant CDF.

(4) The seismic hazard analysis provided a reasonable probabilistic representation of the earthquake ground motions at the site considering the information developed in elements 1 and 2 of the LTSP. The Hosgri fault zone was found to dominate the seismic hazard at the site. The Los Osos and San Luis Bay faults each contributed only a few percent to the total hazard. Relative contribution to the total hazard from the other faults was insignificant. Sensitivity studies showed the important parameters are slip rate, maximum magnitude, and ground-motion attenuation. The spectral shape and uncertainties used in the fragility analysis is thought to be a reasonable estimate, and consistent, in most part, with the detailed ground-motion studies carried out in the LTSP. However, as discussed in Section 23.4.6.4 of this SSER, the staff will require PG&E to submit analyses to confirm the capability of plant structures to withstand exceedances of the 84-percent LTSP-site-specific spectra. On the basis of PG&E's recent evaluations (Shiffer, 1991i and k), resolution of this confirmatory issue is not expected to have any significant effect on the seismic PRA results.

(5) The fragility parameters for the structures and equipment were found to be reasonable. The level of effort in developing the seismic fragilities for equipment is well beyond those expended on previous seismic PRAs. A review of the identified and analyzed modes found that the appropriate failure modes have been considered.

(6) On the basis of the systems review, the staff finds that the sequence of scenarios and events which can be portrayed by the early front-line tree

represents a reasonable and complete approach to modeling the Diablo Canyon seismic scenarios.

(7) Using the results of the seismic PRA, the component and plant seismic margins were derived, and the margin against the 84-percent site-specific ground motion was calculated. It is seen that all components whose failure will lead to seismic core damage have at least a 40-percent margin over the site-specific ground motion. The median capacities were shown to be much higher.

(8) The largest contribution to the seismically induced CDF comes from earthquakes with average spectral accelerations in the 2.0g to 3.0g range. This provides an important insight; that is, for high seismic hazard sites, the seismic CDF estimates appear to be governed by seismic levels at or near the HCLPF value.

In summary, the seismic portion of the PRA also represents a comprehensive and detailed effort. The staff finds it to be an adequate and reasonable basis to address element 4 of the license condition.

23.6.2.4 Fire Events Analysis

The limited staff review of the fire events finds that the methodology used is acceptable and incorporates a very exhaustive spatial interaction analysis to develop scenarios. The staff's alternative calculation has increased the fire-induced CDF by a factor of two. The staff finds the fire analysis is an adequate and reasonable basis to address element 4 of the license condition.

23.6.2.5 Overall Conclusion

Element 4 of the license condition called for an assessment of the significance of conclusions drawn from the seismic studies in element 1 (seismic/geologic studies), element 2 (evaluation of magnitudes of earthquakes), and element 3 (evaluation of ground motion at the site), utilizing a probabilistic risk assessment and deterministic studies, as necessary, to ensure seismic margins will be adequate.

The staff finds that the PRA performed by PG&E to address this element is a very comprehensive and detailed effort of sufficient scope using acceptable and, in some cases advanced, methodology. The seismic PRA has adequately accounted for the information developed in other parts of the LTSP.

The staff concludes that the seismic contribution to the mean CDF at the Diablo Canyon plant is on the order of 20 percent or less. Major contributors to the CDF are internal events and fire events. No single dominant seismic sequence has been identified, nor have any overwhelmingly weak components been identified. The computed seismic CDF is comparable to or less than those computed for nuclear power plants in the eastern part of the United States.

In summary, on the basis of its review of the Diablo Canyon PRA, the staff concludes that PG&E has met the probabilistic risk analysis part of element 4 of the license condition.

APPENDIX A

CHRONOLOGY OF LTSP REVIEW

July 6, 1978	219th Advisory Committee on Reactor Safeguards (ACRS) meeting. Discussion at meeting completes ACRS review of Pacific Gas and Electric Company's (PG&E's) application for operating licenses for Diablo Canyon Units 1 and 2.
July 14, 1978	ACRS letter on seismic issues, including recommendation that the seismic design of Diablo Canyon be reevaluated in about 10 years.
April 14, 1984	NRC issues Amendment 9 to Diablo Canyon Unit 1 operating license. Amendment includes license condition requiring PG&E to develop and implement a program to revalidate seismic design basis of the plant.
May 8, 1984	Meeting with PG&E regarding program to revalidate seismic design basis.
May 25, 1984	Meeting with ACRS subcommittees on Diablo Canyon and on extreme external phenomena regarding seismic reevaluation program.
June 14, 1984	290th ACRS meeting. Diablo Canyon seismic reevaluation program plan and schedule discussed. PG&E agrees to submit detailed program plan by January 30, 1985.
June 20, 1984	ACRS letter on seismic reevaluation program discussed at June 14, 1984, meeting.
July 15, 1984	NRC staff issues Supplemental Safety Evaluation Report (SSER) 27 addressing the seismic design-bases revalidation program.
October 4, 1984	Meeting with PG&E and U.S. Geological Survey (USGS) in Bethesda, Maryland, to discuss seismic reevaluation program and the license condition to be included in the full-power operating license for Diablo Canyon Unit 1.
November 2, 1984	NRC issues Facility Operating License DPR-80, the full-power operating license for Diablo Canyon Unit 1, including license condition 2.C.(7), which required PG&E to develop and implement a program to reevaluate the seismic design bases for the plant.

November 15, 1984	Meetings with PG&E in Bethesda, Maryland, to discuss elements 2, "earthquake magnitude", and 3, "ground motion," of License Condition 2.C.(7) requiring a seismic reevaluation program.
December 11, 1984	Meeting with PG&E in Bethesda, Maryland, to discuss probabilistic risk assessment (PRA) and deterministic studies for seismic reevaluation program.
January 10, 1985	Meeting with PG&E in Bethesda, Maryland, regarding seismic reevaluation program.
January 30, 1985	PG&E letter transmitting LTSP plan.
March 21, 1985	Meeting with ACRS subcommittee on Diablo Canyon in Culver City, California, to discuss LTSP plan.
May 9, 1985	NRC letter to PG&E transmitting NRC staff comments on LTSP plan.
May 17, 1985	NRC letter to PG&E transmitting comments of ACRS consultants regarding facility seismic reevaluation program, based on discussions at ACRS subcommittee meeting.
May 22, 1985	Meeting with PG&E and NRC staff consultants regarding NRC comments on seismic reevaluation program.
June 19, 1985	PG&E letter transmitting responses to NRC comments on LTSP plan.
July 10, 1985	Meeting with ACRS subcommittee on Diablo Canyon in Washington, D.C., to discuss LTSP plan.
July 11, 1985	303rd ACRS meeting. LTSP plan discussed.
July 31, 1985	NRC letter to PG&E approving amended LTSP plan.
October 21, 1985	Meeting with PG&E in Bethesda, Maryland, to discuss soil-structure interaction (SSI) aspects of the LTSP.
December 3, 1985	PG&E letter transmitting LTSP Quarterly Progress Report 1.
December 12, 1985	Meeting with PG&E and NRC consultants in San Francisco, California, regarding numerical modeling of strong ground motion for the LTSP.
January 30, 1986	PG&E letter transmitting results of LTSP Phase II scoping study.
March 4, 1986	PG&E letter transmitting LTSP Quarterly Progress Report 2.
March 11, 1986	Meeting with PG&E regarding overview of LTSP status and results of Phase II scoping study.

March 27, 1986	NRC letter to PG&E transmitting individual comments by NRC consultants on SSI.
April 14, 1986	Site visit and field trip to observe geological features in Diablo Canyon region.
April 15, 1986	Meeting with PG&E and NRC staff consultants to discuss SSI and ground motion.
May 28, 1986	Workshop meeting with PG&E in San Francisco, California, to discuss geology, seismology, and geophysics.
June 6, 1986	PG&E letter transmitting LTSP Quarterly Progress Report 3.
August 7, 1986	PG&E letter transmitting PRA background material.
August 15, 1986	Field trip to site to review geology, seismology, and geophysics.
August 20, 1986	Meeting with PG&E and Pickard, Lowe and Garrick in Newport Beach, California, regarding PRA.
September 5, 1986	PG&E letter transmitting LTSP Quarterly Progress Report 4.
October 21-24, 1986	Workshop meeting with PG&E in San Francisco, California, to review status of the LTSP, including geology, seismology, geophysics, and ground motion.
November 20, 1986	Meeting with ACRS subcommittee on extreme external phenomena at Diablo Canyon regarding the LTSP.
December 10, 1986	Meeting with PG&E regarding SSI for the LTSP.
December 16, 1986	Workshop meeting with PG&E in Bethesda, Maryland, to discuss ground-motion modeling estimates for the LTSP.
January 16, 1987	PG&E letter transmitting LTSP Quarterly Progress Report 5.
January 16, 1987	NRC letter to PG&E requesting additional information on PRA.
February 17, 1987	Workshop meeting with PG&E in Bethesda, Maryland, to discuss PRA, seismic hazards, and fragilities.
March 3, 1987	NRC letter to PG&E requesting detailed meeting summaries and methodology for deterministic evaluation.
March 11, 1987	PG&E letter transmitting report on geology, seismology, and geophysics workshop meeting held on October 21 and 22, 1986.
April 2, 1987	PG&E letter transmitting LTSP Quarterly Progress Report 6.

May 5, 1987	PG&E letter transmitting response to NRC request for PRA information.
May 5, 1987	Workshop meeting with PG&E in San Luis Obispo, California, to discuss geology, seismology, and geophysics.
May 6, 1987	PG&E letter transmitting report on fragilities analysis methodology.
May 12, 1987	PG&E letter transmitting report on ground-motion workshop held on October 23 and 24, 1986.
May 29, 1987	PG&E letter transmitting methodology for deterministic evaluation.
June 9-11, 1987	Audit by NRC staff and consultants of PG&E's SSI analysis and computer codes validation.
July 15-16, 1987	Workshop meeting with PG&E to discuss ground motion.
August 7, 1987	PG&E letter transmitting "Long-Term Seismic Program: Diablo Canyon PRA Draft Support Systems Analyses and Event Trees," Volumes 1 and 2.
September 30, 1987	NRC letter to PG&E requesting additional information to complete evaluation of PG&E database used in the empirical analysis of ground motion.
November 2-3, 1987	Workshop meeting in San Francisco, California, on fragility analysis.
November 4-6, 1987	Workshop meeting in San Francisco, California, on SSI.
November 30, 1987	PG&E letter transmitting proposed schedule for integrating ground-motion and engineering analyses. Schedule was requested by NRC letter to PG&E on October 15, 1987, forwarding comments from the July 15-16 ground-motion workshop meeting.
December 7, 1987	PG&E letter transmitting response to information requested for NRC LTSP auxiliary building probabilistic study.
December 22, 1987	PG&E letter transmitting PRA frontline systems analyses and top events.
January 14-15, 1988	Workshop meeting with PG&E on PRA.
February 7, 1988	PG&E letter transmitting information requested by NRC staff at the November 2-3, 1987, fragility evaluation workshop meeting, as identified in staff meeting summary dated November 16, 1987.
February 19, 1988	Meeting with PG&E in Rockville, Maryland, to discuss deterministic comparison for the LTSP.

February 23, 1988	Meeting of ACRS subcommittee on Diablo Canyon in San Francisco, California, regarding status of the LTSP.
February 25, 1988	Meeting with PG&E in San Francisco, California, to audit selected seismic fragility analyses.
March 14, 1988	PG&E letter transmitting information on PRA requested during the January 14-15, 1988, workshop meeting on PRA.
March 28-30, 1988	Plant walkdown to develop information to be used in the PRA evaluation.
May 9, 1988	NRC letter to PG&E transmitting comments from NRC consultants on facility seismic reevaluation program in preparation for meeting on ground motion.
May 20, 1988	PG&E letter transmitting information on deterministic evaluations being performed by PG&E for the LTSP.
July 31, 1988	PG&E letter transmitting "Final Report on the Diablo Canyon Long-Term Seismic Program."
September 12, 1988	Meeting with PG&E in Rockville, Maryland, regarding overview of PRA.
September 27, 1988	PG&E letter transmitting updated response to issues raised in JEBCO Seismic, Inc., letter regarding 1988 geophysical survey data.
October 5, 1988	Meeting with PG&E in Rockville, Maryland, to discuss PG&E's final report on the LTSP.
October 10, 1988	PG&E letter transmitting list of material to be provided to the NRC staff for PRA audit.
October 28, 1988	PG&E letter transmitting additional PRA analyses and methodology.
November 2, 1988	Meeting with PG&E in Rockville, Maryland, to discuss numerical modeling of ground motion.
November 29, 1988	PG&E letter transmitting additional PRA documentation on high- and low-pressure injection systems.
December 9, 1988	PG&E letter transmitting additional PRA documentation on auxiliary saltwater system.
December 10, 1988	Report transmitted to NRC by staff consultant A.S. Veletsos, "Studies of Earthquake Ground Motions and Soil-Structure Interaction at Diablo Canyon Nuclear Power Plant."
December 13, 1988	NRC letter to PG&E requesting additional information on the LTSP Final Report.

January 1, 1989	PG&E letter advising that response to Questions 16, 46, and 43 of NRC letter of December 13, 1988, will be delayed until February 28, 1989.
January 4, 1989	PG&E letter transmitting report on "Probabilistic Evaluation of Diablo Canyon Turbine Building Seismic Capacity Using Nonlinear Time History Analyses."
January 10, 1989	NRC letter to PG&E transmitting request for additional information relating to Brookhaven National Laboratory (BNL) review of the Diablo Canyon PRA.
January 16, 1989	PG&E letter transmitting response to Questions 34-38 of NRC letter of December 13, 1988, relating to the Diablo Canyon PRA.
January 30, 1989	PG&E letter transmitting response to Questions 1-3, 40-42, and parts of 43, 44, 45, and 47 of NRC letter of December 13, 1988.
January 31, 1989	PG&E letter transmitting report on "Diablo Canyon Long Term Seismic Program Response to Questions 1, 2a, and 2b."
February 6, 1989	PG&E letter transmitting responses to Questions 19, 21-33, 39, and 43j of NRC letter of December 13, 1988.
February 7, 1989	NRC letter to PG&E transmitting NRC staff consultant reports relating to the LTSP.
February 10, 1989	PG&E letter transmitting PG&E response to BNL comments and requests for additional information in NRC letter of January 10, 1989.
February 16, 1989	Meeting with PG&E in San Francisco, California, to discuss analysis by NRC consultants of selected systems important to PRA.
February 28, 1989	PG&E letter transmitting response to Questions 16, 43n, part 2 of 43z, 46, and Attachment Q43-5 (proprietary seismic records).
March 1-3, 1989	Meeting with PG&E in Rockville, Maryland, to discuss NRC questions and PG&E responses regarding seismic ground motion.
April 11, 1989	NRC letter to PG&E transmitting report by NRC staff consultant K.W. Campbell, "Preliminary Report on Empirical Analyses of Vertical Strong Motion for Diablo Canyon Site, California."
May 12, 1989	NRC letter to PG&E transmitting three reports by NRC staff consultants from BNL relating to PRA.
May 31, 1989	NRC letter to PG&E transmitting BNL letter report on PRA.

June 1, 1989	NRC letter to PG&E transmitting request for additional information relating to seismic ground motion.
June 2, 1989	PG&E letter providing additional documentation regarding PRA.
June 12-16, 1989	Meeting with PG&E in San Francisco, California, to discuss geology, seismology, geophysics, and tectonics.
June 12, 1989	PG&E letter transmitting responses to comments in three BNL reports transmitted to PG&E by NRC letter of May 12, 1989.
June 13-14, 1989	Meeting with PG&E in San Francisco, California, to discuss PRA.
June 16-17, 1989	Meeting with PG&E in San Francisco, California, to discuss fragility analysis topics regarding recent NRC questions.
July 18, 1989	PG&E letter transmitting additional information requested by the NRC staff in June 13-14, 1989, meeting on PRA.
August 1, 1989	NRC memorandum summarizing meeting with PG&E on June 12-16, 1989.
August 7, 1989	NRC memorandum summarizing meeting with PG&E on June 16-17, 1989.
August 8-10, 1989	Meeting with PG&E in Bethesda, Maryland, to discuss geology, seismology, and geophysics.
August 31, 1989	PG&E letter transmitting responses to PRA questions identified in BNL report transmitted to PG&E by NRC letter of May 31, 1989.
August 31, 1989	PG&E letter transmitting report on "Diablo Canyon Long-Term Seismic Program: Response to Questions 1, 2, 3, 4, 5, 7, 10, 11, 12, 13, 14, and 16."
September 8, 1989	PG&E letter transmitting response to NRC questions on seismic ground motion transmitted to PG&E by NRC letter of June 1, 1989.
September 29, 1989	NRC letter to PG&E transmitting two BNL letter reports regarding PRA, including comments and questions.
October 4, 1989	NRC letter to PG&E transmitting BNL report on PRA and request for additional information regarding PRA human factors and fire analyses.
October 13, 1989	NRC letter to PG&E transmitting three consultant reports and a request for additional information relating to seismic source characterization.

October 19, 1989	PG&E letter transmitting response to Questions 6, 8, 9, 15, 17, 18, and 19 on seismic ground motion transmitted to PG&E by NRC letter of June 1, 1989.
October 24, 1989	Meeting with PG&E in Rockville, Maryland, to discuss ground motion.
October 26, 1989	PG&E letter transmitting response to action items 1-5, 7-8, and 13 identified in NRC letter of August 7, 1989, summarizing the June 16-17, 1989, meeting on fragility analysis.
November 2-3, 1989	Meeting with PG&E in San Francisco, California, to discuss SSI.
November 13, 1989	PG&E letter transmitting list of attendees and presentation materials used in SSI meeting on November 2-3, 1989.
November 13, 1989	PG&E letter transmitting response to three PRA action items identified in NRC meeting summary of August 7, 1989.
November 15, 1989	Meeting with PG&E in Rockville, Maryland, to discuss human factors analysis for PRA for the LTSP.
November 30, 1989	PG&E letter responding to items 6 and 9-12 identified in NRC meeting summary of August 7, 1989, relating to the meeting on fragility analysis on June 16-17, 1989.
November 30, 1989	PG&E letter stating that responses to information requested by the NRC staff letters of August 1, 1989, and October 13, 1989, will be provided by March 31, 1990.
December 8, 1989	PG&E letter transmitting clarifying information on five items related to human actions analysis identified in NRC letter to PG&E of October 4, 1989.
January 10, 1990	Meeting with PG&E in Golden, Colorado, to review and discuss empirical ground-motion studies.
January 19, 1990	NRC letter to PG&E requesting additional information on PRA.
January 23, 1990	PG&E letter transmitting responses to questions identified in NRC letter of October 4, 1989, regarding PRA.
January 29-30, 1990	Meeting with PG&E in San Francisco, California, to review and discuss geophysical data and interpretations.
February 16, 1990	PG&E letter transmitting responses to PRA questions identified in NRC letter of January 19, 1990.
February 23, 1990	NRC letter to PG&E requesting additional information regarding geology, seismology, and geophysics.

March 14, 1990	NRC letter to PG&E requesting additional information regarding PRA.
March 19, 1990	Meeting with PG&E in Golden, Colorado, to review and discuss empirical ground-motion studies.
March 21, 1990	PG&E letter transmitting additional responses to PRA questions identified in NRC letter of January 19, 1990.
March 31, 1990	PG&E letter transmitting proprietary material consisting of Figures GSG 13-3 and GSG Q12-A.8 in response to NRC questions on geology, seismology, and geophysics.
April 2, 1990	PG&E letter transmitting response to NRC staff questions on geology, seismology, geophysics, and tectonics.
April 2-4, 1990	Meeting with PG&E in Rockville, Maryland, to discuss PRA.
April 12, 1990	NRC letter to PG&E requesting additional information relating to ground motion and forwarding consultant reports on ground motion.
April 13, 1990	PG&E letter transmitting responses to remaining questions and comments from NRC letters of August 1 and October 13, 1989, regarding (1) geology, seismology, and geophysics and (2) seismic source characterization.
April 16, 1990	Meeting with PG&E in Golden, Colorado, to review and discuss empirical ground-motion studies as part of the LTSP.
April 17-20, 1990	Meeting with PG&E in San Francisco, California, to discuss geology, seismology, and geophysics.
April 26, 1990	NRC letter to PG&E requesting additional information regarding NRC review of the LTSP.
April 27, 1990	NRC letter to PG&E requesting additional information regarding SSI based on questions raised during the SSI meeting held on November 2-3, 1989.
April 30, 1990	NRC letter to PG&E transmitting consultant reports and requesting additional information resulting from ground-motion meeting of April 30 and May 1, 1990.
April 30, 1990	Meeting with PG&E in San Francisco, California, to discuss ground motion.
May 3, 1990	PG&E letter transmitting response to NRC letter of March 14, 1990, requesting additional information on PRA.
May 8, 1990	Meeting with PG&E in Rockville, Maryland, to discuss deterministic evaluations for the LTSP.

May 29, 1990	PG&E letter transmitting summary of scope and criteria for additional deterministic evaluations to be performed by PG&E as part of the LTSP.
June 12, 1990	NRC letter to PG&E transmitting report regarding NRC review of the LTSP.
June 15, 1990	PG&E letter transmitting proprietary response to soil-structure analysis Question SSI-15 identified in NRC letter of April 27, 1990.
June 18, 1990	PG&E letter transmitting response to soil-structure analysis Questions SSI-1 through SSI-14 and SSI-16 identified in NRC letter of April 27, 1990.
June 18, 1990	PG&E letter clarifying fire risk analysis for PRA.
July 3, 1990	Meeting with PG&E in Golden, Colorado, to review and discuss empirical estimates of vertical ground motion.
July 17, 1990	PG&E letter transmitting material presented in LTSP meetings in San Francisco, California, during April and May 1990.
August 2, 1990	PG&E letter transmitting responses to Questions 2-8 and 10-13 identified in NRC letter to PG&E of February 23, 1990. Questions relate to LTSP geology, seismology, and geophysics issues.
August 10, 1990	PG&E letter transmitting reassessment of seismic capacity of the Diablo Canyon 230-kV switchyard as requested by NRC during staff audit of PG&E fragility calculations audit.
August 20, 1990	PG&E letter transmitting response to Questions LP-1 and LP-9 identified in NRC letter to PG&E of February 23, 1990. Also transmitted are responses to Questions 1-6 identified by the NRC staff at the NRC/PG&E workshop meeting of April 30, 1990.
September 18, 1990	PG&E letter transmitting report on "Additional Deterministic Evaluations Performed to Assess Seismic Margins of Diablo Canyon Units 1 and 2."
November 20, 1990	PG&E letter transmitting report on "Diablo Canyon Long-Term Seismic Program, Response to Ground Motion Workshop Question 7."
December 11, 1990	Audit by the NRC staff of PG&E calculations regarding deterministic comparisons for the LTSP.
December 12, 1990	Meeting with PG&E in Golden, Colorado, to discuss vertical ground motion and for the LTSP.

December 21, 1990	NRC letter to PG&E transmitting consultant report on ground motion.
February 13, 1991	PG&E letter transmitting addendum to the final report on the Diablo Canyon LTSP.
February 21, 1991	NRC memorandum summarizing audit of PG&E calculations on December 11-12, 1990.
February 21, 1991	NRC memorandum summarizing meeting with PG&E on seismic design of masonry walls at Diablo Canyon.
February 22, 1991	NRC letter to PG&E transmitting consultant report on ground motion.
March 5, 1991	PG&E letter transmitting information on deterministic evaluation of masonry walls for the LTSP.
March 15, 1991	Meeting with PG&E in Rockville, Maryland, to discuss the remaining open items associated with the staff review of seismicity, tectonics, and ground motion for the LTSP.
March 20, 1991	PG&E letter transmitting information on May 2, 1983, Coalinga earthquake.
April 4, 1991	PG&E letter stating that additional PG&E calculations confirm that seismic margins of containment shell and containment interior concrete structures are adequate.
April 12, 1991	PG&E letter transmitting a sensitivity study showing the effect of weighting factors and adjustment applied to certain records on the ground-motion attenuation equations.
April 12, 1991	PG&E letter transmitting an evaluation of selected safety-related masonry walls using the conservative deterministic failure margin (CDFM) criteria developed for the LTSP.
April 12, 1991	PG&E letter transmitting PG&E comments on the tectonic setting and seismogenic setting of the San Luis/Pismo block.
April 17, 1991	PG&E letter transmitting a summary of the benefits and insights gained as a result of the LTSP.
April 19, 1991	PG&E letter transmitting information supporting the use of vertical ground-motion spectra derived from the ratio method for the LTSP.
April 24, 1991	PG&E letter transmitting calculations on a selected safety-related masonry wall using the criteria developed for the LTSP.

April 30, 1991	PG&E letter transmitting a discussion of horizontal ground motion for the LTSP.
May 1, 1991	PG&E letter transmitting information on the structural response of the plant to seismic motion at frequencies below 2.5 Hz.
May 17, 1991	PG&E letter transmitting information on the adequacy of plant seismic margins assuming increased vertical ground motion in the frequency range from 2 to 10 Hz.
May 29, 1991	PG&E letter discussing use of the results of the LTSP in the implementation of future modifications at Diablo Canyon.

APPENDIX B

BIBLIOGRAPHY

Atkinson, 1990 — R.H. Atkinson, "Review of the SONGS-1 Masonry Test Program and Applicability to Diablo Canyon Masonry Walls," Atkinson-Noland and Associates, Inc., 1990.

Atwater, 1970 — T. Atwater, "Implications of Plate Tectonics for the Cenozoic Tectonic Evolution of Western North America," Geol. Soc. Amer. Bull., Vol. 81, pp. 3513-3536, 1970.

Bechtel, 1988a — Bechtel Power Corporation, "CLASSI" Computer Program: Theoretical Manual, User's Manual, and Validation Report, 1988.

Bechtel, 1988b — Bechtel Power Corporation, "SASSI" Computer Program: Theoretical Manual,User's Manual, and Validation Report, 1988.

Blake and others, 1978 — M.C. Blake, Jr., R.H. Campbell, T.W. Dibblee, Jr., D.G. Howell, T.H. Nilsen, W.R. Normark, J.C. Vedder, and E.A. Silver, "Neogene Basin Formation in Relation to Plate Tectonic Evolution of the San Andreas Fault System, California," Amer. Assoc. Petrol. Geol. Bull., Vol. 62, pp. 344-372, 1978.

Bozoki and others, in process — G. Bozoki, R. Fitzpatrick, M.P. Bohn, M.K. Ravindra, and J. Johnson, "Review of the Diablo Canyon Probabilistic Risk Assessment," NUREG/CR-5726, Brookhaven National Laboratory draft report in Public Document Room, Docket 50-275.

Brand, 1988 — D.A. Brand, PG&E Letter DCL-88-192 to USNRC, "Final Report of the Diablo Canyon Long Term Seismic Program," July 31, 1988.

Budnitz and others, 1985 — R.J. Budnitz, P.J. Amico, C.A. Cornell, W.J. Hall, R.P. Kennedy, J.W. Reed, and M. Shinozuko, "An Approach to the Quantification of Seismic Margins in Nuclear Power Plants," NUREG/CR-4334, Lawrence Livermore Laboratory, 1985.

Campbell, 1990 — K.W. Campbell, "Empirical Prediction of Near-Source Soil and Soft-Rock Ground Motion for the Diablo Canyon Power Plant Site, San Luis Obispo County, California," Dames & Moore, 1990.

Campbell, 1991a — K.W. Campbell, "A Review of the Diablo Canyon Long-Term Seismic Program: Empirical Ground-Motion Studies," Dames & Moore, 1991.

Campbell, 1991b — K.W. Campbell, "Revised Ground-Motion Estimates," Dames & Moore, May 22, 1991.

Clark, 1990 — D.G. Clark, "Late Quaternary Tectonic Deformation in the Casmalia Range, Coastal South Central California," in Neotectonics of South-Central Coastal California, W.R. Lettis, ed., Friends of the Pleistocene Pacific Cell Field Trip Guidebook, pp. 349-383, 1990 - see p. 2-27, line 11.

Cox and Engebretsen, 1985 — A. Cox and D. Engebretsen, "Change in Motion of Pacific Plate at 5 mybp," Nature, Vol. 313, pp. 472-474, 1985.

Crouch and others, 1984 — J.K. Crouch, S.B. Bachman, and J.T. Shay, "Post-Miocene Compressional Tectonics Along the Central California Margin," in Tectonics and Sedimentation Along the California Margin, J.K. Crouch and S.B. Bachman, eds., Soc. Econ. Paleon. Mineral., Pacific Section, Vol. 38, pp. 37-54, 1984.

Dehlinger and Bolt, 1987 — P. Dehlinger and B.A Bolt, "Earthquakes and Associated Tectonics in a Part of Coastal Central California," Bull. Seismol. Soc. Amer., Vol. 77, pp. 2056-2073, 1987.

Dibblee, 1976 — T.W. Dibblee, Jr., "The Rinconada and Related Faults in the Southern Coast Ranges, California, and Their Tectonic Significance," USGS Professional Paper 981, 55 pp, 1976.

Dickinson and Snyder, 1979 — W.R. Dickinson and W.S. Snyder, "Geometry of Triple Junctions Related to San Andreas Transform," J. Geophys. Res., Vol. 84, pp. 561-572, 1979.

EPRI, 1988 — Electric Power Research Institute, "A Methodology for Assessment of Nuclear Power Plant Seismic Margins," EPRI NP-6041, 1988.

EPRI, 1989 — Electric Power Research Institute, "A Storm From the Sun," Journal of the Electric Power Research Intitute, pp. 14-21, July/August 1989.

Feigl and others, 1990 — K.L. Feigl, R.W. King, and T.H. Jordan, "Geodetic Measurements of Tectonic Deformation in the Santa Maria Fold and Thrust Belt, California," J. Geophys. Res., Vol. 95, No. B3, pp. 2679-2699, 1990.

Graham and Dickinson, 1978 — S.A. Graham and W.R. Dickinson, "Apparent Offsets of On-land Geologic Features Across the San Gregorio-Hosgri Fault Trend," in San Gregorio-Hosgri Fault Zone, California, E.A. Silver and W.R. Normark, eds., California Div. of Mines and Geo. Special Report 137, pp. 13-23, 1978.

Hall, 1975 — C.A. Hall, Jr., "San Simeon-Hosgri Fault System, Coastal California: Economic and Environmental Implications," Science, Vol. 190, No. 4221, pp. 1291-1294, 1975.

Hall, 1982 — C.A. Hall, Jr., "Pre-Monterey Subcrop and Structure Contour Maps, South-central California," U.S. Geological Survey Map MF-384, 6 sheets, scale 1:62,500, 1982.

Hall and others, 1979 — C.A. Hall, Jr., W.G. Ernst, S.W. Prior, and J.W. Wiese, "Geologic Map of the San Luis Obispo-San Simeon Region, California," U.S. Geological Survey Map I - 1097, scale 1:48,000, 1979.

Hamilton, 1984 — D.H. Hamilton, "The Tectonic Boundary of Coastal Central California," Ph.D. thesis (unpublished), Stanford University, California, 290 pp., 1984.

Harbert and Cox, 1989 — W. Harbert and A. Cox, "Late Neogene Motion of the Pacific Plate," J. Geophys. Res., Vol. 94, pp. 3052-3064, 1989.

Hill and Dibblee, 1953 — M.L. Hill, and T.W. Dibblee, Jr., "San Andreas, Garlock, and Big Pine Faults, California--A Study of the Character, History, and Tectonic Significance of Their Displacements," Geol. Soc. Amer. Bull., Vol. 64, pp. 443-458, 1953.

Hornafius and others, 1986 — J.S. Hornafius, B.P. Luyendyk, R.R. Terres, and M.J. Kamerling, "Timing and Extent of Neogene Tectonic Rotation in the Western Transverse Ranges, California," Geol. Soc. Amer. Bull., Vol. 97, pp. 1476-1487, 1986.

Hoskins and Griffith, 1971 — E.G. Hoskins and J.R. Griffith, "Hydrocarbon Potential of Northern and Central California Offshore," in Future Petroleum Provinces of the United States--Their Geology and Potential," I.H. Cram, ed.: Amer. Assoc. Petrol. Geol. Memoir 15, pp. 212-218, 1971.

Jahns, 1973 — R.H. Jahns, "Tectonic Evolution of the Transverse Ranges Province as Related to the San Andreas Fault System," in Stanford University Publications in Geological Sciences, Vol. 13, pp. 149-170, 1973.

Kennedy and others, 1976 — R.P. Kennedy, S.A. Short, D.A. Wesley, and T.H. Lee, "Effect of Nonlinear Soil-Structure Interaction Due to Base Slab Uplift on the Seismic Response of a High Temperature Gas-Cooled Reactor (HTGR)", Nuclear Engineering and Design, Vol. 38, No. 2, pp. 323-355, 1976.

Kennedy and others, 1980 — R.P. Kennedy, C.A. Cornell, R.D. Campbell, S. Kaplan, and H.F. Perla, "Probabilistic Seismic Safety Study of an Existing Nuclear Power Plant," Nuclear Engineering and Design, Vol. 59, No. 2, pp. 315-318, 1980.

Kennedy and others, 1988 — R.P. Kennedy, D.A. Wesley, and W.H. Tong, "Probabilistic Evaluation of the Diablo Canyon Turbine Building Seismic Capacity Using Nonlinear Time-History Analyses," No. 1643-01, NTS Engineering, Prepared for PG&E, December 1988.

Killeen and others, 1987 — K.M. Killeen, D.B. Slemmons, and K.E. Swanson, "Timing of Folding and Uplift of the Pismo Syncline, San Luis Obispo County, California," Geol. Soc. Amer. Abstracts With Programs, Vol. 19, p. 394, 1987.

Kipp and others, 1988 — T.R. Kipp, D.A. Wesley, and D.K. Nakaki, "Seismic Fragilities of Civil Structures and Equipment Components at the Diablo Canyon Power Plant," No. 1643.02, NTS Engineering, Prepared for PG&E, September 1988.

Luyendyk and others, 1980 — B.P. Luyendyk, M.J. Kamerling, and R. Terres, "Geometric Model for Neogene Crustal Rotations in Southern California," Geol. Soc. Amer. Bull., Vol. 91, pp. 211-217, 1980.

McClymont and Poelilonan, 1982 — A.S. McClymont and B.W. Poelilonan, "ATWS: A Reappraisal - Part 3: Frequency of Anticipated Transient," EPRI NP-2230, Electric Power Research Institute, January 1982.

McCulloch, 1987 — D.S. McCulloch, "Regional Geology and Hydrocarbon Potential of Offshore Central California," in Geology and Resource Potential of the Continental Margin of Western North America and Adjacent Ocean Basins, Beaufort Sea to Baja California, D.W. Scholl, A. Gantz, and J. Vedder, eds., Amer. Assoc. Petrol. Geol. Circum-Pacific Earth Science, Vol. 6, pp. 353-401, 1987.

Miller, 1986 — C.A. Miller, "Soil-Structure Interaction: Influence of Lift-Off," NUREG/CR-4588, Vol. 2, Brookhaven National Laboratory, 1986.

Minster and Jordan, 1978 — T.B. Minster and T.H. Jordan, "Present-day Plate Motions," J. Geophys. Res., Vol. 83, No. B11, pp. 5331-5354, 1978.

Minster and Jordan, 1984 — T.B. Minster and T.H. Jordan, "Vector Constraints on Quaternary Deformation of the Western U.S. East and West of the San Andreas Fault," in Tectonics and Sedimentation Along the California Margin, J.K. Crouch and S.B. Bachman, eds., Soc. Econ. Paleon. Mineral. Pacific Section, Los Angeles, Vol. 38, pp. 1-16, 1984.

Minster and Jordan, 1987 — T.B. Minster and T.H. Jordan, "Vector Constraints on Western U.S. Deformation from Space Geodesy, Neotectonics and Plate Motions," J. Geophys. Res., Vol. 92, No. B6, pp. 4798-4808, 1987.

Namson and Davis, 1990 — J.S. Namson and T.L. Davis, "Late Cenozoic Fold and Thrust Belt of the Southern Coast Ranges and Santa Maria Basin, California," Amer. Assoc. Petrol. Geol. Bull., Vol. 74, pp. 467-492, 1990.

Newmark and Hall, 1978 — N.M. Newmark and W.J. Hall, "Development of Criteria for Seismic Review of Selected Nuclear Power Plants," NUREG/CR-0098, N.M. Newmark Consulting Engineering Services, 1978.

Nitchman, 1988 — S.P. Nitchman, "Tectonic Geomorphology and Neotectonics of the San Luis Range, San Luis Obispo County, California," Masters thesis (unpublished), University of Nevada, Reno, 120 pp., 1988.

Nitchman and Slemmons, 1987 — S.P. Nitchman and D.B. Slemmons, "Pleistocene Flexural Slip Faulting Possibly Triggered by Crustal Unloading, Pismo Beach, Central Coast California," Geol. Soc. Amer. Abstracts With Programs, Vol. 19, pp. 437, 1987.

Page, 1966 — B.M. Page, "Geology of the Coast Ranges of California," in Geology of Northern California, E.H. Bailey, ed., California Div. Mines and Geol. Bull. 1980, pp. 255-276, 1966.

Page, 1981 — B.M. Page, "The Southern Coast Ranges," in The Geotectonic Development of California, W.G. Ernst, ed., Prentice-Hall, Inc., Englewood Cliffs, N.J., pp. 329-417, 1981.

PASNY/CECo, 1982 — Power Authority of the State of New York and Consolidated Edison Company of New York, Inc., "Indian Point Probabilistic Safety Study," 1982.

Papazoglou and others, 1984 — I.A. Papazoglou, R.A. Bari, A.J. Buslik, R.E. Hall, D. Ilberg, P.K. Samanta, T. Teichman, R.W. Youngblood/BNL; A. El-Bassioni/USNRC; J. Fragola, E. Lofgren/SAI, Inc.; W. Veseley/BCL; "Probabilistic Safety Analysis Procedure Guide," NUREG/CR-2815, Brookhaven National Laboratory, January 1984.

Pelto and others, 1985 — P.J. Pelto, R.E. Rhoads, W.E. Veseley, and R.R. Fullwood, "Development of Transient Initiating Frequencies for Use in Probabilistic Risk Assessment," NUREG/CR-3682, Pacific Northwest Lab (Battelle), May 1985.

PG&E, 1973 — Pacific Gas and Electric Co., Final Safety Analysis Report, Units 1 and 2, Diablo Canyon Site, Section 2.5, "Geology and Seismology," 1973.

PG&E, 1988 — Pacific Gas and Electric Co., "Final Safety Analysis Report Update," December 1988.

PLG, 1983 — Pickard, Lowe and Garrick, Inc., "Seabrook Station Probabilistic Safety Assessment," prepared for Public Service Company of New Hampshire and Yankee Atomic Electric Company, PLG-0300, December 1983.

Reed, 1933 — R.D. Reed, Geology of California, Amer. Assoc. Petrol. Geol., Tulsa, Oklahoma, pp 355, 1933.

Reich, 1991a — M. Reich, BNL letter to R. Pichumani, NRC, "Technical Evaluation Report (TER) on Soil-Structure Interaction Analysis, Diablo Canyon LTSP, by C. Costantino," March 21, 1991.

Reich, 1991b — M. Reich, BNL letter to R. Pichumani, NRC, "TER on Soil-Structure Interaction Analysis, Diablo Canyon LTSP, by A.S. Veletsos," April 4, 1991.

Rood, 1990 — H. Rood, USNRC letter to J.D. Shiffer, PG&E, "Request for Additional Information Relating to NRC Staff Review of Diablo Canyon LTSP," April 26, 1990.

Rood, 1991 — H. Rood, USNRC memorandum to Distribution, "Summary of December 11-12, 1990, Audit of Calculations Related to Deterministic Comparisons for the Diablo Canyon Long Term Seismic Program," February 21, 1991.

Schnabel and others, 1976 — P. Schnabel, J. Lysmer, and H.B. Seed, "SHAKE-Computer Program for Earthquake Response Analysis of Horizontally Layered Sites," Earthquake Engineering Research Center (EERC) Report 72-12, 1976.

Shiffer, 1988a — J.D. Shiffer, PG&E Letter DCL-88-238 to USNRC, "Diablo Canyon Units 1 and 2--Long Term Seismic Program--Probabilistic Risk Assessment," October 10, 1988.

Shiffer, 1988b — J.D. Shiffer, PG&E Letter DCL-88-260 to USNRC, "Diablo Canyon Units 1 and 2--Long Term Seismic Program Probabilistic Risk Assessment," October 28, 1988.

Shiffer, 1988c — J.D. Shiffer, PG&E Letter DCL-88-285 to USNRC, "Diablo Canyon Units 1 and 2--Long Term Seismic Program - Probabilistic Risk Assessment," November 29, 1988.

Shiffer, 1988d — J.D. Shiffer, PG&E Letter DCL-88-297 to USNRC, "Diablo Canyon Units 1 and 2--Long Term Seismic Program - Probabilistic Risk Assessment," December 9, 1988.

Shiffer, 1989a — J.D. Shiffer, PG&E Letter DCL-89-010 to USNRC, "Diablo Canyon Units 1 and 2, Response to Questions 34-38 of NRC Letter of December 13, 1988," January 16, 1989.

Shiffer, 1989b — J.D. Shiffer, PG&E Letter DCL-89-152 to USNRC, "Diablo Canyon Units 1 and 2, Additional PRA Information," June 2, 1989.

Shiffer, 1989c — J.D. Shiffer, PG&E Letter DCL-89-191 to USNRC, "Diablo Canyon Units 1 and 2, PRA Information Requested by NRC Staff," July 18, 1989.

Shiffer, 1989d — J.D. Shiffer, PG&E Letter DCL-89-197 to USNRC, "Diablo Canyon Units 1 and 2, Long Term Seismic Program Meetings, Enclosure 3 Fragility Analysis Meeting, June 16-17, 1989," July 25, 1989.

Shiffer, 1989e — J.D. Shiffer, PG&E Letter DCL-89-269 to USNRC, "Diablo Canyon Units 1 and 2, Response to Action Items from the Long Term Seismic Program, Fragility Meeting, June 16-17, 1989," October 26, 1989.

Shiffer, 1989f — J.D. Shiffer, PG&E Letter DCL-89-282 to USNRC, "Diablo Canyon Units 1 and 2 - Long Term Seismic Program Soil-Structure Interaction Meeting," November 23, 1989.

Shiffer, 1989g — J.D. Shiffer, PG&E Letter DCL-89-313 to USNRC, "Diablo Canyon Units 1 and 2, PRA Human Actions Analysis," December 8, 1989.

Shiffer, 1990a — J.D. Shiffer, PG&E Letter DCL-90-046 to USNRC, "Long Term Seismic Program - Probabilistic Risk Assessment," February 16, 1990.

Shiffer, 1990b — J.D. Shiffer, PG&E Letter DCL-90-118 to USNRC, "Appendix F.3: Diablo Canyon Fire Risk Assessment," May 3, 1990.

Shiffer, 1990c — J.D., Shiffer, PG&E Letter DCL-90-137 to USNRC, "Diablo Canyon Units 1 & 2 Long Term Seismic Program-Deterministic Evaluations," May 29, 1990.

Shiffer, 1990d — J.D. Shiffer, PG&E Letter DCL-90-156 to USNRC, "Analysis of Turbine Building/Turbine Generator Fires," June 18, 1990.

Shiffer, 1990e — J.D. Shiffer, PG&E Letter DCL-90-157 to USNRC, "Diablo Canyon Units 1 and 2, Long Term Seismic Program--Soil/Structure Interaction, Response to SSI Questions 1-14 and 16," June 18, 1990.

Shiffer, 1990f — J.D. Shiffer, PG&E Letter DCL-90-201 to USNRC, "Diablo Canyon Long-Term Seismic Program, Responses to Questions 2-8 and 10-13," August 2, 1990.

Shiffer, 1990g — J.D. Shiffer, PG&E Letter DCL-90-205 to USNRC, "Diablo Canyon Units 1 and 2, LTSP - Seismic Capacity of 230-kV Switchyard," August 10, 1990.

Shiffer, 1990h — J.D. Shiffer, PG&E Letter DCL-90-226 to USNRC, "Additional Deterministic Evaluations Performed to Assess Seismic Margins of the Diablo Canyon Power Plant, Units 1 & 2," September 18, 1990.

Shiffer, 1990i — J.D. Shiffer, PG&E Letter DCL-90-278 to USNRC, "Diablo Canyon Long-Term Seismic Program, Responses to Ground Motion Workshop Question 7," November 20, 1990.

Shiffer, 1990j — J.D. Shiffer, PG&E Letter DCL-90-289 to USNRC, "Diablo Canyon Units 1 and 2, Reevaluation of Diablo Canyon Masonry Walls,"December 14, 1990.

Shiffer, 1991a — J.D. Shiffer, PG&E Letter DCL-91-026 to USNRC, "Diablo Canyon Units 1 and 2, Masonry Wall Reevaluation Program," February 12, 1991.

Shiffer, 1991b — J.D. Shiffer, PG&E Letter DCL-91-027 to USNRC, "Addendum to 1988 Final Report of the Diablo Canyon Long Term Seismic Program," February 19, 1991.

Shiffer, 1991c — J.D. Shiffer, PG&E Letter DCL-91-045 to USNRC, "Diablo Canyon Units 1 and 2 Long Term Seismic Program--Deterministic Evaluation of Masonry Walls," March 5, 1991.

Shiffer, 1991d — J.D. Shiffer, PG&E Letter DCL-91-084 to USNRC, "Long Term Seismic Program - Weighting of Ground Motion Records," April 12, 1991.

Shiffer, 1991e — J.D. Shiffer, PG&E Letter DCL-91-086 to USNRC, "Diablo Canyon Units 1 and 2 Long Term Seismic Program--Deterministic Evaluation of Masonry Walls," April 12, 1991.

Shiffer, 1991f — J.D. Shiffer, PG&E Letter DCL-91-091 to USNRC, "Benefits and Insights of the Long Term Seismic Program," April 17, 1991.

Shiffer, 1991g — J.D. Shiffer, PG&E Letter DCL-91-083 to USNRC, "Long Term Seismic Program - Vertical Ground Motions," April 19, 1991.

Shiffer, 1991h — J.D. Shiffer, PG&E Letter DCL-91-086 to USNRC, "Diablo Canyon Units 1 and 2 Long-Term Seismic Program--Deterministic Evaluation of Masonry Walls," April 24, 1991.

Shiffer, 1991i — J.D. Shiffer, PG&E Letter DCL-91-108 to USNRC, "LTSP - Low Frequency Ground Motions," May 1, 1991.

Shiffer, 1991j — J.D. Shiffer, PG&E Letter DCL-91-110 to USNRC, "LTSP - Probabilistic Risk Assessment," May 1, 1991.

Shiffer, 1991k — J.D. Shiffer, PG&E Letter DCL-91-131 to USNRC, "LTSP - Vertical Ground Motions," May 17, 1991.

Shiffer, 1991l — J.D. Shiffer, PG&E Letter DCL-91-143 to USNRC, "Long Term Seismic Program - Implementation of the Results of the Program," May 29, 1991.

Suppe, 1983 — J. Suppe, "Geometry and Kinematics of Fault-bend Folding," Amer. J. Sci., Vol. 283, pp. 648-671, 1983.

Suppe, 1985 — J. Suppe, Principles of Structural Geology, Prentice-Hall, Inc., Englewood Cliffs, N.J., 1985.

Taliaferro, 1943 — J.L. Taliaferro, "Geologic History and Structure of the Central Coast Ranges of California," Calif. Div. Mines and Geol. Bull. 118, pp. 119-163, 1943.

USAEC, 1968 — U.S. Atomic Energy Commission, "Safety Evaluation by the Division of Reactor Licensing, United States Atomic Energy Commission in the Matter of Pacific Gas and Electric Company Diablo Canyon Nuclear Power Plant, Docket No. 50-725," January 23, 1968.

USNRC, 1975a — U.S. Nuclear Regulatory Commission, "Supplement No. 1 to the Safety Evaluation of the Diablo Canyon Nuclear Power Station Units 1 and 2," January 31, 1975.

USNRC, 1975b — U.S. Nuclear Regulatory Commission, "Reactor Safety Study - An Assessment of Accident Risks in U.S. Commercial Nuclear Power Plant," WASH-1400 (NUREG-75/014), October 1975.

USNRC, 1976a — U.S. Nuclear Regulatory Commission, "Supplement No. 4 to the Safety Evaluation of the Diablo Canyon Nuclear Power Station Units 1 and 2, May 1976.

USNRC, 1976b — U.S. Nuclear Regulatory Commission, "Supplement No. 5 to the Safety Evaluation of the Diablo Canyon Nuclear Power Station Units 1 and 2," September 10, 1976.

USNRC, 1978 — U.S. Nuclear Regulatory Commission, "Supplement No. 7 to the Safety Evaluation of the Diablo Canyon Nuclear Power Station Units 1 and 2," May 26, 1978.

USNRC, 1981 — U.S. Nuclear Regulatory Commission, "Standard Review Plan for the Review of Safety Analysis Reports for Nuclear Power Plants," LWR Edition, NUREG-0800, July 1981.

USNRC, 1987 — U.S. Nuclear Regulatory Commission, "Reactor Risk Reference Document," NUREG-1150, Vol. 2, App. A-1, February 1987.

USNRC, 1990 — U.S. Nuclear Regulatory Commission, "Failure of Electrical Power Equipment Due to Solar Magnetic Disturbances," Information Notice 90-42, June 19, 1990.

Veletsos and Prasad, 1989 — A.S. Veletsos and A.M. Prasad, "Seismic Interaction of Structures and Soils: Stochastic Approach," J. Struct. Eng., Amer. Soc. Civ. Eng., Vol. 115, No. 4, 1989.

Veletsos and Tang, 1987 — A.S. Veletsos and Y. Tang, "SSI Studies for Containment Structure of Diablo Canyon Power Plant, Summary Report," Structural Analysis Division, Brookhaven National Laboratory, 1987.

Veletsos and Tang, 1990 — A.S. Veletsos and Y. Tang, "Deterministic Assessment of Effects of Ground-Motion Incoherence," J. Eng. Mech., Amer. Soc. Civ. Eng., Vol. 116, No. 5, 1990.

Veletsos and others, 1988 — A.S. Veletsos, Y. Tang, and A.M. Prasad, "Studies of Earthquake Ground Motions and Soil-Structure Interaction for Diablo Canyon Nuclear Power Plant," Structural Analysis Division, Brookhaven National Laboratory, 1988.

Wagner, 1974 — H.C. Wagner, "Marine Geology Between Cape San Martin and Point Sal, South-Central California Offshore," U.S. Geol. Surv. Open-File Report 74-252, 17 pp., 1974.

Weber, 1983 — G.E. Weber, "Geologic Investigation of the Marine Terraces of the San Simeon Region and Pleistocene Activity on the San Simeon Fault Zone, San Luis Obispo County, California," Technical Report to the U.S.G.S., Contract No. 14-08-001-18230, 66 pp., 1983.

Weber and Lajoie, 1979 — G.E. Weber and K.R. Lajoie, "Late Pleistocene Rates of Movement Along the San Gregorio Fault Zone, Determined From Offset of Marine Terrace Shoreline Angles," in Coastal Tectonics and Coastal Geologic Hazards in Santa Cruz and San Mateo Counties, California, G.E. Weber, K.R. Lajoie, and G.B. Griggs, eds., Geol. Soc. Amer., Cordilleran Section, 75th Annual Meeting, Field Guide, 1979.

Weldon and Humphreys, 1986 — R. Weldon and E. Humphreys, "A Kinematic Model of Southern California," Tectonics, Vol. 5, pp. 33-48, 1986.

Wheelis, 1986 — W.T. Wheelis, "Users Guide for a Personal-Computer-Based Nuclear Power Plant Fire Data Base, NUREG/CR-4586, Sandia National Laboratories, June 1986.

APPENDIX C

TECHNICAL EVALUATION REPORT

U. S. GEOLOGICAL SURVEY

REVIEW OF GEOLOGICAL AND GEOPHYSICAL INTERPRETATIONS

contained in

Pacific Gas And Electric Co. Final Report
of the
Diablo Canyon Long Term Seismic Program
for the
Diablo Canyon Power Plant

--A report to the staff of the U.S. Nuclear Regulatory Commission

by

U.S.Geological Survey staff
February, 1991

CONTENTS

Executive Summary 1

Introduction 4

Scope of LTSP Earth-science Investigation 4

LTSP Findings 6

Hosgri fault zone 6

Los Osos fault 7

Faults on the southwest side of the Pismo syncline 7

November 1927 earthquake 7

Working models 8

Logic tree 8

Review Comments 9

Hosgri Fault 9

Fault geometry 9

Activity of related structures 10

Regional geologic structure 11

Hosgri structural setting 12

Sea floor form and structure 12

Extent and thickness of post-Wisconsin deposits 13

Earthquake activity 13

Hosgri segmentation model 15

Slip rates and fault mechanism 16

Summary, Hosgri fault 18

Los Osos Fault 19

Los Osos down-dip geometry 20

Los Osos segmentation model 20

Olson, San Luis Bay, and Wilmar Avenue Faults 21

Logic Trees 22

References Cited 25

Table 1 . . . . . at end

Figure 1: location map . . . . . at end

Figure 2: geologic structures, offshore Santa Maria Basin . . . . . at end

Figure 3: Intensity and earthquake locations, 4 November 1927 earthquake . . . . at end

EXECUTIVE SUMMARY

The earth-science part of the Pacific Gas and Electric Company (PG&E) Long Term Seismic Program (LTSP) is perhaps the most comprehensive study yet of earthquake hazards at an operating power plant. Planned and implemented to evaluate controversial geologic issues that surfaced during construction of the Diablo Canyon plant, these investigations also disclosed previously unrecognized earthquake faults whose discovery required additional studies. The earth-science investigations have produced a large body of data that greatly improves our understanding of the earthquake hazard at the Diablo Canyon site. Yet some issues remain unresolved or controversial, chiefly because of the lack of definitive evidence.

The LTSP identified five active faults with significant earthquake capability near Diablo Canyon. Except for the Hosgri fault, all are newly recognized or newly determined to be active. They include the Los Osos fault on the northeast side of the Pismo syncline, and the Olson, San Luis, and Wilmar Avenue faults on its southwest side. The Hosgri fault, however, within 5 km of the plant and with an expected maximum magnitude of 7.2, still dominates the earthquake hazard as it is currently known. The Los Osos fault, somewhat more distant and with an expected earthquake magnitude of 6.8, is also a significant earthquake threat, exceeding that associated with faults southwest of the Pismo syncline.

This review by U.S. Geological Survey (USGS) staff generally confirms the identification of the faults considered as earthquake sources in the LTSP, and the magnitudes attributed to earthquakes expected along those faults. Reviewers, however, disagree with PG&E's interpretation of the Hosgri fault as a strike-slip fault with little or no vertical component of slip. The strike-slip interpretation is supported chiefly by surface and shallow trench investigations near San Simeon Point, which disclosed vertical faults and evidence for horizontal slip at a rate of 1 to 3 mm/yr. This evidence is not contested, but its relevance to the character of the Hosgri fault at depth must be weighed with other lines of evidence from geology, geophysics, and seismology.

Much of this other evidence shows that the Hosgri fault as mapped on the seafloor is part of a broader more complex structure, which for the purposes of this review is designated the Hosgri fault system. This system includes the set of seafloor faults mapped as the Hosgri fault zone by PG&E, the San Simeon fault, and fault and fold belts to the southwest of the Hosgri and San Simeon faults. The fault and fold belt is a set of southwestward-verging folds and reverse and thrust faults, some of which neither cut nor

deform the seafloor. Structures in this system are chiefly compressional, but they may also exhibit right-lateral strike-slip, as exemplified by the San Simeon fault. The Hosgri fault system dips northeastward beneath a coastal structural high characterized by exposed or near-surface basement rock of the Franciscan assemblage.

Strike-slip rates of 1 to 3 mm/yr, derived by PG&E from surface geologic evidence, probably represent only part of the potential seismogenic slip on the Hosgri fault. That additional components of compressional and vertical slip characterize the failure surface at depth is suggested by the amount of structural relief (>1 to 2 km) expressed across the structural high, the width of the deformed zone, strong contrasts in the geologic structures and processes on opposite sides of the fault zone, and oblique-slip and thrust earthquakes.

PG&E considers the Hosgri fault to be nearly vertical, but data for both the seafloor fault zone and the broader fault system suggests northeast dips of 50 to 70° at earthquake depths of 4 to 10 km. The evidence includes focal mechanisms for the Lompoc earthquake (M_S=7.0 to 7.5) and for earthquakes on the San Simeon fault, as well as seismic reflection profiles that show fault dips diminishing with depth.

Both the Los Osos fault and the set of faults on the southwest side of the Pismo syncline represent a lower degree of seismic hazard than the Hosgri fault system. The extent and surface geologic relations of these faults are well characterized by PG&E, but surface measurements of low dips on the Los Osos fault are largely discounted in PG&E's interpretations of fault character and in their tectonic model. Arguments for segmenting the Los Osos fault into discrete, independently rupturing, parts are also model-dependent and unconvincing. Despite these issues, the probabilistic magnitude of 6.8 derived for an earthquake on the Los Osos fault appears appropriate for the data available. The lower magnitudes and risk levels assigned by PG&E to faults on the southwest side of the Pismo syncline also appear appropriate, although other--and less likely--tectonic models could be chosen that would increase the level of seismic risk for these faults.

A logic tree for the Hosgri fault, designed by PG&E to characterize seismic sources probabilistically, contains several branches in which parameters derived from a strike-slip model are substituted for data. Model-based values, biased to favor strike-slip faulting, yield logic tree probability distribution functions for the Hosgri fault that are similarly biased. The consistent use of observed data would increase the weight for oblique slip and thrust earthquakes. Some questionable procedural steps in the logic tree also bias the number of outcomes in the same sense, producing more strike-slip outcomes. [PG&E's Hosgri logic tree (1988, p. 3-21) yields nearly 4,000 outcomes, 59 percent of them strike slip, 33 percent oblique slip, and 8 percent thrust mechanisms.] Greater reliance on LTSP

data in constructing the logic tree will tend to raise the mean magnitude value for the probabilistic earthquake and to alter the probability distribution in such a way as to change its standard deviation. Many of these points also apply to the seismic hazard analysis tree, used in the probabilistic risk assessment of the Diablo Canyon plant.

These review comments may be especially important to estimates of ground motion. The most significant differences with PG&E interpretations concern the dip and seismogenic-slip mechanism for the Hosgri fault at depths of 4 to 10 km, where earthquakes nucleate and where most seismic energy originates. If ground motions depend on fault characteristics other than earthquake magnitude, the ground motion values for a vertical strike-slip fault may underestimate those for oblique slip, reverse, or thrust faults.

INTRODUCTION

New earth-science information and analyses, revealed during the full-power licensing process for Diablo Canyon in 1978, prompted the Advisory Committee on Reactor Safety to recommend that the seismic design of the plant be re-evaluated in about 10 years. This re-evaluation became a condition of the operating license for Diablo Canyon, Unit 1, and thus a responsibility of the operator, PG&E. Planning for this effort was scheduled to begin in January 1985 and was to be completed within 3 years after approval of the work plan by the Nuclear Regulatory Commission (NRC). New information to be evaluated included geologic data related to active faults, earthquake magnitudes and mechanisms, earthquake-induced ground motions, the engineering response of the plant and its components, and a probabilistic risk assessment. This evaluation process, PG&E's Long Term Seismic Program (LTSP), produced a Final Report in June, 1988. Questions by NRC staff and their consultants regarding data and conclusions in the Final Report were answered by PG&E in separate documents that are important supplements to the Final Report.

The U.S. Geological Survey (USGS), through an interagency agreement, provided technical review services to NRC staff during the course of the LTSP. Robert Brown, USGS, Menlo Park, California, reviewed geology, geophysics, and seismology; he was regularly assisted by other USGS scientists (T. Brocher, J. Eaton, S. Lewis, D. McCulloch, and D. Schwartz) with special geographical or disciplinary knowledge. This report summarizes their findings and covers chiefly information presented in chapters 2 (Geology, Seismology, Geophysics, Tectonics Investigations) and 3 (Seismic Source Characterization) of the Final Report, LTSP (PG&E, 1988), and the Responses to Questions regarding those chapters.

SCOPE OF LTSP EARTH-SCIENCE INVESTIGATION

The Diablo Canyon plant (figure 1) draws cooling water from the ocean and is located within 200 m of the shoreline. This location, and the knowledge that the active Hosgri fault is less than 5 km offshore, underscored the need for acquiring and interpreting offshore data as well as that on land. Because different geological and geophysical methods must be used offshore, integrating onshore and offshore data can be difficult. But an equal or greater obstacle to understanding the geology is the difference in stratigraphy and structure on opposite sides of the Hosgri fault. In the following paragraphs onshore and offshore parts of the investigation are discussed separately, but they were designed and conducted as complementary parts of the LTSP. Some investigations, for example those

involving earthquake seismology, used essentially the same methods and categories of data for both onshore and offshore studies.

Onshore geologic studies for the LTSP were built upon modern geologic mapping by Hall and others (e.g., Hall and Corbató, 1967; Hall, 1973; Hall and others, 1979), earlier geologic studies to evaluate Diablo Canyon earthquake hazards, and a number of topical studies. PG&E's efforts addressed several issues: the potential for damaging earthquakes on suspected active faults; the magnitude and mechanism of earthquakes on those faults found to be active, or potentially active; and the most appropriate tectonic model(s) to account for observed structural geometries and strain in crustal rocks. Commonly used techniques included: large-scale geologic mapping of late Quaternary (the past 700,000 years, or 700 ka) and Holocene (the past 10 k.y.) deposits and landforms; drilling, trenching, or digging test pits to locate and map buried surfaces or deposits; standard and newly developed methods of dating geologic markers; and other field and office geologic methods.

Offshore geologic interpretation for the LTSP is based chiefly on reflection seismic data recorded by vessels sailing along parallel, chiefly west- to southwest-trending, track lines. Other geophysical methods and sea-floor mapping by diver geologists were used in some coastal areas. Most of the reflection seismic data acquired by PG&E came from existing public domain and proprietary records; these were supplemented by new surveys commissioned expressly for the LTSP. The reflection seismic records included both common-depth-point (CDP) and high-resolution lines. The CDP data were used chiefly to evaluate geologic relations down to depths of 3 to 5 km; the high-resolution data provided better detail for the seafloor and for the geology within about 100 m beneath it. Both sets of data were used to map and evaluate the earthquake capability of offshore faults, define fault geometry at depth, provide evidence of folding and faulting during the past 5 million years, and design tectonic models that are consistent with current geological and geophysical knowledge.

Earthquake seismology for the LTSP included a review and catalog of historical earthquake data near Diablo Canyon, installing and operating a local seismic network, and continued monitoring of both the network and strong-motion instruments, which are located at the site and triggered whenever earthquake ground motion exceeds some pre-selected threshold value. The seismological investigations were designed to identify map patterns of seismic activity, the depth of that activity, and earthquake focal mechanisms, which indicate the orientation and mode of fault slip at the earthquake source--commonly 4 to 10 km below the surface in this part of coastal California.

This brief summary of the LTSP only hints at the large amount of data acquired, and the number of new discoveries. The LTSP was planned and implemented to address a set of pre-defined geologic issues, but considerable flexibility was demonstrated in responding to such new and unexpected findings as the late Quaternary activity on the Los Osos and San Luis Bay faults. The broad range of earth-science methods used, the areal extent of the study, and the depth to which critical issues were probed mark this as an unusually comprehensive site study of earthquake hazards. Much of the credit for this effort belongs to the able and highly professional team assembled by PG&E management.

LTSP Findings

New evidence obtained by PG&E identifies major earthquake sources near Diablo Canyon and provides a basis for estimating earthquake magnitudes and source mechanisms. These estimates in turn become the basis for assumed ground motion spectral values, which enable engineers to model earthquake shaking of the plant and its components. As a prelude to USGS review comments, some of the major PG&E results are noted below.

Hosgri fault zone: The investigation confirms the importance of the Hosgri fault zone as the structure capable of producing both the largest (M_S=7.2) earthquake and the one closest (4.5 km) to the plant. PG&E defines the Hosgri fault zone as the 2-4 km-wide set of sea-floor faults that extends 110 km, from the latitude of Point Pedernales northwestward to the latitude of Cambria. (As noted elsewhere, this review also considers the Hosgri fault system, which includes a wider band of faulting and deformation.) Near Cambria, according to the PG&E interpretation, bedrock displacements that define the fault zone step 4 to 5 kilometers to the east and continue northwesterly as the San Simeon fault. Other interpretations of the northern part of the Hosgri fault and of its relation to the San Simeon fault are possible, but the continuity of faulting for at least 110 km north of Point Pedernales is clear. The Diablo Canyon power plant stands opposite the north-central part of this fault zone.

PG&E considers the Hosgri fault zone to be near-vertical (80-90°), and to be characterized by right-lateral strike slip with the block northeast of the fault moving, in a relative sense, horizontally and toward the southeast. The most convincing direct evidence for steep dip and strike slip come from onshore surface geology mapped and trenched along the San Simeon fault, 60 km northwest of the power plant. Here PG&E (1988, p. 2-122, 2-123) recognized 1 to 3 mm/yr of right-lateral strike-slip on a vertical fault. Many CDP lines that cross the Hosgri fault zone also confirm steep fault dips within a kilometer of the surface. The offshore Hosgri fault zone provides no unequivocal evidence of right-lateral separation of distinctive strata or structures, but some faults and fold axes that

approach the Hosgri fault from the east and southeast trend more northerly near the fault. Such changes in structural trend may accompany drag along a right-lateral strike-slip fault, but they may also occur in other ways. Arguments for strike-slip on the Hosgri fault are presented in the Final Report (PG&E, 1988, table 2-10) and in Responses to Questions.

Los Osos fault: The northwest-trending Los Osos fault zone is 10 km northeast of the power plant and parallels the axis of the Pismo syncline. It was determined to be active and capable of generating an earthquake of M_S=6.8. Trench exposures and geologic mapping of this fault are consistent with a low southwest (≤20°) dip, toward the plant site. PG&E interprets the dip to steepen with depth, and considers the Los Osos fault to be a high-angle reverse fault at seismogenic depths (about 4 to 10 km--where most earthquake energy is released). Net slip estimates for the Los Osos fault, derived from geologic evidence exposed in trenches (PG&E, 1988, p. 2-135), are about 0.5 mm/yr. The degree of activity established for this fault adds an important increment of seismic risk at the power plant; but because the Hosgri fault is closer to the plant and capable of producing larger earthquakes, it dominates the estimates of ground shaking.

Faults on the southwest side of the Pismo syncline: The LTSP also disclosed a third active fault zone on the southwest side of the Pismo syncline. This zone, defined by several faults that displace 120-ka marine-terrace platforms, includes from northwest to southeast the Olson, San Luis Bay, and Wilmar Avenue faults. The onshore trace of the Olson fault is less than 5 km from the power plant. Although these faults are well exposed in some places, they trend through the surf zone or near-shore areas where geologic and geophysical evidence are sparse or difficult to obtain, and their extent, map position, and dip are not well constrained. PG&E interprets the zone as a set of discontinuous, west- to northwest- trending, north- to northeast-dipping, high-angle reverse faults. Their slip rates, calculated from offset wave-cut platforms of known geologic age, are 0.1 mm/yr or less--much lower than the rates estimated for the Los Osos and Hosgri faults.

November, 1927, earthquake: The PG&E investigation also reexamined the offshore earthquake of 4 November, 1927. This earthquake, also known as the Lompoc earthquake, predated modern seismic networks in the western United States, and published estimates of its location and magnitude vary widely. PG&E relocated it using two ingenious techniques, one seismological and the other based on tsunami wave arrival times. The seismological method employs, as master events, the 2 May, 1983, earthquake (M_S=6.5) at Coalinga, California (100 km north-northeast of San Luis Obispo) and the 5 November, 1969, Santa Lucia Bank earthquake (M_L=5.6) on the continental shelf off the central California coast. The earthquakes in 1927, 1969, and 1983 were all recorded on the same seismograph at De Bilt, Netherlands, so that seismic wave arrival times from the better

located, more recent, earthquakes can be used to estimate the location of the one in 1927. From this analysis, PG&E (1988) placed the 1927 earthquake at lat 34.5° N, long 120.9° W, later revised (PG&E, 1990, Response to Question GSG 8) to lat 34.35° N, long 120.9° W. PG&E also confirmed the thrust nature of the 1927 earthquake and reestimated the magnitude as M_S=7.0 and the moment magnitude (M) as 6.6.

Tsunami arrival times at Hilo, Hawaii, and La Jolla, California (345 km southeast of Point Conception), were used together with estimated wave velocities derived from bathymetric data to locate the source region for the tsunami; this method placed the tsunami source (equivalent to the intersection of the fault with the seafloor) at lat 34.2° N, long 120.75° W. All of the PG&E locations lie south of those cited in other published reports.

Working models: Many of the findings in the Final Report depend on a number of working hypotheses, some of which are explicitly stated. One of these concerns the geologic history and the appropriate tectonic model for folding and faulting in the offshore Santa Maria basin. In part, this hypothesis holds (PG&E, 1988, p. 2-29 to 2-30) that the compressional episode that formed the offshore Queenie, Purisima, and Lompoc faulted anticlines ended at least 2.8 million years ago. Another working hypothesis assumes that a middle Pliocene unconformity (PG&E, 1989, Response to Question 42; 1990, Response to Question GSG-3), recognized in some offshore drill holes and on seismic reflection records, can be used as a time-stratigraphic marker for evaluating the vertical component of fault displacement. Other examples include the use of topography and structural geometry to define fault segments, of fault segmentation models to predict earthquake magnitudes, and of local deformation patterns to interpret contemporary regional tectonic models. Many of these working hypotheses are derived from recent earth-science publications or were developed independently by PG&E during the course of the LTSP.

Logic tree: Certainty is unlikely in conclusions drawn from any geologic investigation. To accommodate elements of uncertainty, the LTSP (PG&E, 1988, Chapter 3) employs a logic tree to evaluate seismic source character. This method allows for probabilistic weighting of competing interpretations at each stage in the evaluation of earthquake magnitude on a given fault. The end product, thousands of different solutions, are treated as a probability distribution from which mean values and other probabilistic measures can be drawn. The method displays clearly those decisions or weights that drive the final solution, thereby facilitating review of the most critical issues. Probabilistic magnitude values are determined from logic trees for the Hosgri, Los Osos, and San Luis Bay faults. A deterministic earthquake magnitude is provided only for the Hosgri fault zone, because that earthquake produces the greatest expected ground motions at the plant site.

REVIEW COMMENTS

An assessment of the earth-science findings reported in the Final Report and in the Responses to Questions is complicated by the sheer volume of information generated by the LTSP and by a sizeable and more diversified body of information found in published journals, books, and reports. Different interpretations sometimes make it difficult to separate trivial issues from those that significantly affect the seismic hazard. This review attempts to isolate and examine those geological, geophysical, and seismological issues that are now, or may someday be, critical to estimates of earthquake ground motion and seismic hazard analysis.

The possibility of future issues simply recognizes our incomplete knowledge of the tectonic setting and earthquake capability of the region surrounding Diablo Canyon. A similar caveat applies to levels of ground motion, which are estimated from a currently meager, but rapidly growing set of data. The chief topics discussed here are the Hosgri fault, the Los Osos fault, faults along the southwest side of the Pismo syncline, and the conclusions incorporated into the logic tree as part of the seismic source characterization.

Hosgri fault

Until the late 1970's most earth scientists probably viewed the Hosgri fault (figure 2) as a strike-slip fault, somewhat analogous to the San Andreas fault and other northwest-trending, strike-slip faults in the San Andreas fault system. Although geologic evidence (PG&E, 1988, p. 2-107 to 2-120) supports a strike slip component for the San Simeon fault, several investigators (Gawthrop, 1978; Crouch and others, 1984; Hamilton, 1984; and McCulloch, 1989) have presented evidence that compression, accompanied by reverse or thrust faulting, now controls slip on the Hosgri fault. PG&E employs data from the San Simeon fault as support for a strike-slip mechanism on the Hosgri fault zone, but other evidence along the Hosgri and San Simeon faults indicates recent compression and a significant component of vertical displacement.

Fault geometry: Faults that displace the seafloor, or strata within 0.5 km beneath it, define the 2- to 4-km-wide Hosgri fault zone, which can be mapped northwestward from near Point Pedernales to a point near Cambria. Within a kilometer or two of the seafloor seismic lines image these faults as vertical or dipping steeply (80° or more) northeastward. But many seismic reflection records that extend to depths of 3 or 4 km, show fault dips that diminish with depth. Dips of 60° to 75° (PG&E, 1988, plates 6 and 7; 1990, Response to Question GSG 1) characterize the lower part of these records. Indeed, some investigators (Crouch and others, 1984; McCulloch, 1989) interpret the faults as flattening into listric,

northeast-dipping failure surfaces at depths of 2 to 5 km.

Additional evidence on the subsurface geometry of the Hosgri fault zone comes from faults and folds (figure 2) paralleling the Hosgri fault zone and southwest of it. This fault-fold belt is as wide as 12 km, but is narrower in most places. Except for one 15-km gap opposite northern Estero Bay and Point Estero, the belt is evident for 150 km, from Point Pedernales to north of Point Piedras Blancas (PG&E, 1988, plate 5). Faults within this belt dip northeastward at 60° to 30° or less, converging downdip and to the northeast with the Hosgri fault zone. On interpreted seismic lines these faults join the seafloor Hosgri fault breaks at depths of 2 to 4 km; the junction on some lines occurs near an inflection point where the dip flattens with increasing depth. Fault-fold sets locally define thrust-fans that appear to be rooted in the Hosgri fault zone at depths of 3 km or more. Because they parallel the Hosgri fault zone and merge into it at depth, the thrust fans and the Hosgri fault zone are here considered together as the Hosgri fault system.

Activity of related structures: PG&E (1990, Response to Question GSG 1, p.3, 4) has recognized structures in the fault and fold belt as related to the Hosgri fault, but has not generally considered them as active members of the fault system. On most seismic lines neither these faults nor their associated folds deform a seismically defined, unconformity bounded, stratal unit that includes Quaternary (the past 1.65 m.y.) and presumed upper Pliocene (1.65 to 3.4 Ma) deposits. Thus it can be argued that the faults and folds southwest of the sea-floor Hosgri fault are older than the upper Pliocene and Quaternary strata, and therefore are irrelevant to the seismic capability of the Hosgri fault.

Some evidence conflicts with that interpretation. South of Point Sal, the Purisima and Lompoc faulted anticlines--parts of the fault-fold belt adjacent to the sea-floor Hosgri fault (figure 2)--are currently active, deforming strata in the upper Pliocene and Quaternary seismic unit; the Lompoc structure also deforms the seafloor. Map views (PG&E, 1988, plates 4 and 5) and seismic profiles (PG&E, 1990, Response to Question GSG-1, lines T-T' through FF-FF') show that, south of Point Sal, the tilting and faulting of upper Pliocene and Quaternary strata along the Hosgri fault shifts to the Purisima and Lompoc folds. The seafloor Hosgri fault and its parallel faults and folds may not be strictly contemporaneous everywhere, but clearly they are closely related parts of an active regional fault system.

The Purisima and Lompoc folds, well-documented compressional structures, parallel the Hosgri fault zone on the southwest (McCulloch, 1989) and lie within 40 km of it. This compressional domain extends southwest at least to the Santa Lucia Bank fault. Earthquakes have been reported (J. Eaton, oral communication, 22 February, 1990) on the Queenie structure (near lat 34°56' N, long 121°56' W), within the fault-fold belt near Point Piedras Blancas (Dehlinger and Bolt, 1987), and at other localities southwest of the Hosgri

fault zone. This seismic activity and the geologic evidence document the continuing deformation of the offshore compressional structures southwest of the Hosgri and San Simeon faults.

Regional geologic structure: Regional geologic maps (Jennings, 1958, 1959) and the seismic reflection data interpreted by PG&E show that the Hosgri fault system defines the southwest, seaward, flank of a coastal structural high. This crudely monoclinal structure trends north-northwest, parallel to the fault zone, and is best defined by the upper surface of the Franciscan assemblage. Franciscan rocks crop out along the coast and inland, from Point Sal to well north of Point Piedras Blancas. Seismic reflection profiles (PG&E, 1990, Response to Question GSG 1) and crustal velocity models (PG&E, 1988, figures 2-9, 4-13) confirm that offshore basement lies at shallower depths northeast of the Hosgri fault zone than it does to the southwest. Total structural relief on the top of basement in most places exceeds 1 km; south of Point San Luis it exceeds 2 km. South of Point Sal the axis of this structural high follows the Purisima and Lompoc structures and is therefore southwest of the Hosgri fault as mapped by PG&E (1988).

Late Neogene (middle Miocene and younger, or from about 15 m.y. to the present) strata also document the growth of the structural high bordering the Hosgri fault zone. Upper Pliocene and Quaternary strata, identified by their relatively low seismic velocity (1,770 m/s), onlap older rock along the southwest flank of the structural high, dip southwesterly away from the fault zone, and are folded along the Purisima and Lompoc structures. This late Neogene section is 1 to 2 km thick in the offshore Santa Maria basin (figure 1) west of the fault zone, but it thins or disappears along the Hosgri fault zone.

Northeast of the fault, onshore counterparts to the offshore upper Neogene deposits occupy a series of northwest- to nearly west-trending synclinal basins separated by exposed Franciscan basement rock. Nearly all of these onshore upper Neogene deposits are currently being eroded and many show evidence of Quaternary folding or faulting. Littoral or near-shore marine upper Pliocene and Quaternary strata are preserved onshore in only a few small areas; elsewhere the surface rocks are either older than upper Pliocene or are upper Pliocene and Quaternary non-marine alluvial fan deposits of the Paso Robles Formation. Such contrasts in sedimentary facies and age across the Hosgri fault zone confirm the continued growth of the structural high into Quaternary time and require a significant component of vertical slip on the Hosgri fault.

Hosgri fault structural setting: The Hosgri fault zone and the structural high separate two currently active tectonic subprovinces: one offshore with faults and fold axes trending N20-30° W, the other onshore with chiefly N60° W trends. Estimates of 1 to 2 km of

structural relief across the fault zone are minimal because the erosionally dissected surface northeast of the fault zone retains only small isolated remnants of supposed counterparts to the upper Pliocene and Quaternary marine strata of the offshore Santa Maria basin.

In separating the upper Neogene deposits of the offshore Santa Maria basin from a coastal Franciscan basement high, and an offshore depositional province from an onshore erosional province, the northeast-dipping Hosgri fault breaks define a major reverse or oblique-slip fault, along which the basement block to the northeast overrides the basinal block offshore. Other evidence supporting this interpretation includes the form and structure of the sea-floor, the extent and thickness of sediment deposited on a post-18 ka (late Wisconsin glacial stage) wave-cut platform, and historic seismicity.

Sea-floor form and structure: The seafloor off the California coast typically slopes seaward at a low angle (about 1.5°) from the surf zone out to water depths of 120 to 150 m; beyond those depths its slope increases to several degrees. This change in slope, the shelf break, is well defined in most places and is attributed to sea-level changes resulting from the growth and decline of continental ice sheets. The flat, shallow, near-shore part of the shelf has been inundated most recently in the last 12 k.y., as melting ice from Wisconsin glaciers caused sea level to rise. In some places, this landward part of the seafloor is a wave-cut platform on bedrock; in others it is the depositional surface of marine sediment whose age is less than 12 ka.

The seafloor between the Hosgri fault zone and the shoreline is both wave-cut and depositional (PG&E, 1988, plate 4; PG&E, 1989, Response to Question 43*l*). Remnants of wave-cut bedrock platforms, locally mantled by post-Wisconsin sediment, form the seafloor from northern San Luis Obispo Bay at least to Point Estero. Along this 45 km length of the fault zone many of these patches of sea-floor bedrock extend seaward to, but not beyond, the Hosgri fault zone (PG&E, 1988, plate 4). For much of this same distance, the shelf break also either follows the fault zone or closely parallels it (PG&E, 1990, Response to Question, figure GSG Q4-A.1).

These relations are consistent with a significant vertical component of post-Wisconsin slip at the fault zone: the rising block to the northeast of the fault, continuously exposed to marine erosion, typically exhibits a stripped wave-cut surface on rock; the sinking block to the southwest, consistently below the level of wave erosion, accumulates marine sediment. The rate of uplift is evidently sufficiently high locally to overcome the effects of sedimentation and maintain the position of the shelf break along the fault.

Another clue that the vertical component of faulting or uplift probably exceeds sedimentation rates along this part of the Hosgri fault zone is an unusual linear slump zone

(PG&E, 1988, plate 4; Niemi and others,1987, sheet 6) just seaward of the shelf break and about 2 km west of the Hosgri surface faults. This feature, about 30 km long and 1 km wide, appears in recently deposited sediment along an oversteepened southwest-facing slope. The slump, which parallels the Hosgri fault zone, is probably recent enough to be historic; it may well have been triggered by a nearby earthquake.

Extent and thickness of post-Wisconsin deposits: Post-Wisconsin sediment, deposited since the last rise in sea level began about 12 ka, mantles topographic irregularities formed by subaerial erosion during lower stands of the sea. Thus pre-existing topography largely defines the thickness and distribution of sediment at water depths less than about 120 m, the approximate level of the last glacial lowstand.

Locally, however, sediment thickness is structurally controlled. Seafloor outcrops of pre-Wisconsin rocks locally reveal the northwest-trending axial parts of the Purisima and Lompoc structures. Post-Wisconsin deposits thicken down dip from the fold axes, and a consistently thinner (8 to 20m) cover of post-Wisconsin sediment coincides with the Purisima fold axis for more than 25 km south of the latitude of Point Sal. This evidence and a co-linear belt of folded upper Pliocene and Quaternary strata (PG&E, 1990, Response to Question GSG-1, seismic reflection lines GSI-115 and GSI-118) document the current activity of these structures.

A similar linear trend defined by thinned post-Wisconsin sediment and exposed older rock (PG&E, 1988, plate 4) follows the Hosgri fault zone north of Point Sal, but is less evident north of Point San Luis, where wave-cut platforms border the fault zone on the northeast. The distribution and thickness of post-Wisconsin sediment thus defines three of the most active members of the Hosgri fault system--the Purisima and Lompoc structures south of Point Sal and the Hosgri fault zone to the north--and shows that compression and uplift along this trend has persisted during the latest Quaternary.

Earthquake activity: Historic seismicity provides several touchstones for evaluating the nature and degree of earthquake hazard along the Hosgri fault zone. The largest earthquake, and surely the most difficult to locate precisely (figure 3), is the Lompoc earthquake of 4 November 1927. Some early locations for this earthquake predated modern knowledge of crustal velocity structure (Byerly, 1930; ISS, 1931) and are clearly too far west. Jeffreys and Bullen (1935), however, developed crustal velocity data from global earthquake records and in doing so they located the earthquake close to shore near Point Sal (lat 34.9° N, long 120.7° W).

Gawthrop (1978) reported two locations: one, based on 80 world-wide stations, at lat

34.95° N, long 120.7° W; the other, based on 37 selected "good" stations, at lat 34.88° N, long 120.7° W. Gawthrop's and Jeffreys and Bullen's locations group together near the Hosgri fault, but Gawthrop's 95% confidence ellipse for his preferred solution includes all 3 locations as well as the Purisima and Lompoc structures.

Hanks employed aftershock data from regional observatories to locate the mainshock at lat 34.6° N, long 120.9° W, about 40 km south-southwest of the Gawthrop locations. Hanks (1979, p. 460) notes, however, that uncertainties in his location overlap with Gawthrop's error ellipse. Both the Hanks and Gawthrop analyses are compatible with intermediate locations near the Purisima or Lompoc structures, or on the southern part of the Hosgri fault as mapped by PG&E.

PG&E relocated the 1927 earthquake for the LTSP, using records from observatories at De Bilt, Netherlands, and Santa Barbara and Pasadena in California. Their initial (PG&E, 1988) location at lat 34.5° N, long 120.9° W was revised later (PG&E, 1990, Response to Question GSG 8) to lat 34.35° N, long 120.9° W. The revised location is 40 km west-southwest of Point Conception, 25 km south of the Hanks location, and 60 km south of the Gawthrop and Jeffreys and Bullen locations. A location (figure 3) for the sea-floor tsunami source, based on wave analysis (PG&E, 1990, Response to Question GSG 5), is at lat 34.2° N, long 120.75° W, 40 km southwest of Point Conception.

The PG&E locations are so far south of the Hosgri fault system that, if they are correct, the 1927 earthquake becomes much less relevant to earthquake assessment of the Diablo Canyon plant. These locations, however, are difficult to reconcile with observed damage and shaking effects--the seismic intensity--of the earthquake. These effects, well documented throughout south central California (Byerly, 1930; Toppozada and Parke, 1982), show that the highest intensities (Rossi-Forel VIII to IX or Modified Mercalli VII; see Table 1) struck a narrow coastal strip (figure 3) from north of Point Conception to northern San Luis Obispo Bay. Evernden and others (1981, p.27-36) have shown that this pattern and that of other, lower, intensity bands requires a fault break near Gawthrop's location and closer to the Hosgri fault than the PG&E locations.

Intensity patterns for the 17 October, 1989, Loma Prieta earthquake (Plafker and Galloway, 1989, figure 16; Stover and others, 1990, figures 1 and 2) provide an independent test of the different locations proposed for the 1927 earthquake. Loma Prieta and the 1927 earthquake were of similar magnitude and both occurred in crustal rocks of coastal California. When the intensity map and well-located epicenter of the Loma Prieta earthquake are compared with the 1927 intensity map and alternative 1927 locations, only more northerly locations, near those of Gawthrop, Hanks, and Jeffreys and Bullen, yield

Modified Mercalli intensities at the observed VII level along the coast.

Despite debate about its location, the 1927 earthquake is recognized as a major event (M_S between 7 and 7.5) that generated a tsunami and thus was almost surely a reverse or thrust fault. The reverse or thrust alternatives have been confirmed by PG&E (1988, figure 2-20) in seismologically derived focal mechanisms, which also indicate that the fault strikes N 20° W. This is also the strike of the Hosgri fault zone and the Purisima and Lompoc structures. Although the tsunami suggests an offshore deep water source, a point which favors the PG&E location, most of the other evidence favors a more northerly location within the Hosgri fault system. Despite the uncertainties, that part of the Hosgri fault system between Point Sal and Point Pedernales still appears to be the most likely location for this earthquake. The 1927 earthquake cannot be eliminated from the seismic hazard assessment.

A magnitude 5.4 earthquake and its aftershocks show that seismogenic slip on the San Simeon fault occurs on a northeastward-dipping (55°) failure surface and is oblique (Eaton, 1984; Dehlinger and Bolt, 1987). Epicenters of these earthquakes are a few kilometers northeast of the mapped surface trace of the fault, but their fault planes, projected to the surface from focal mechanism analyses, fall along the mapped trace of the San Simeon fault. Focal mechanisms for other earthquakes (Dehlinger and Bolt, 1987) along the San Simeon fault and other nearby parts of the Hosgri fault system show similar northwest-striking reverse, thrust, and oblique slip geometry. A few kilometers east and southeast of San Simeon Point the focal mechanisms of 3 smaller earthquakes on the San Simeon fault (PG&E, 1989, Response to Question 43x, figure 43x-23) also exhibit dominantly thrust or reverse slip. The earthquake focal mechanism data are consistent with the strike-slip observed by PG&E near San Simeon Point, but they also show a dominant or equal component of vertical slip at earthquake depths on this part of the Hosgri fault system.

Hosgri fault segmentation model: PG&E (1988, p. 2-97 to 2-98; 3-23 to 3-24) discusses earthquake potential on the Hosgri fault zone in terms of segmentation: dividing the zone into parts (segments) that will tend to fail individually, thereby repeatedly producing earthquakes of similar magnitude (characteristic earthquakes) on each segment. The credibility of this method for evaluating the Hosgri fault zone suffers from the lack of any record of past earthquake activity and from continuing questions about whether the fault slip is reverse, thrust, strike, or oblique. Many of the segmentation arguments spring from analogies with faults having known slip mechanisms, but in distant parts of the world and in other tectonic environments. The detailed segmentation model presented by PG&E tends to conceal our ignorance of the fault's seismic history behind a cloud of speculative theory and analogy.

Some fault segments, however, do appear to control the fault rupture process, and two areas along the Hosgri fault zone may define such boundaries. These are the change in fault trend off Estero Bay near the junction of the Los Osos fault with the Hosgri fault, and the change in trend and structural style near Point Sal, where deformation along the Hosgri fault zone shifts to the Purisima and Lompoc structures. Both of these possible segment boundaries combine the junction of major geologic structures with changes in strike of the Hosgri fault zone, but neither boundary has yet shown any evidence that it has stopped past fault ruptures.

An important point, somewhat obscured by the segmentation hypothesis, is that the earthquakes of concern to such critical facilities as dams or nuclear power plants are those that rupture through segment boundaries. We are less concerned with the low-magnitude characteristic earthquakes defined by postulated short segment boundaries than with the more damaging multi-segment breaks.

Slip rates and fault mechanism: PG&E estimated horizontal slip rates on the order of 1 to 3 mm/yr from geologic relations along the San Simeon fault, 2 km north of San Simeon Point. These rates are well documented and presumed to be accurate for the fault breaks examined, but evidence for a significant component of vertical slip, down to the southwest, comes from mapped and subsurface geologic units (Hall, 1976, PG&E, 1988, plate 14) near San Simeon Point. There, rocks of the Point Sal Formation (lower Miocene), Monterey Formation (upper and middle Miocene), and Careaga Sandstone (upper Pliocene) southwest of the fault are juxtaposed against Franciscan rocks northeast of the fault, indicating apparent Quaternary (post-Careaga) uplift of the Franciscan rocks. If these rock units were juxtaposed solely by strike slip, the Point Sal-Monterey-Careaga section should reappear, horizontally displaced to the southeast and on the opposite side of the fault. In fact, Franciscan basement adjoins that side of the San Simeon fault for at least 37 km southeast of San Simeon Point. The mapped relations, however, are simply explained if slip along the San Simeon fault possesses a strong vertical component similar to that indicated by earthquake focal mechanisms and discussed in the section on Earthquake activity.

Similarities in the strike and structural setting of the San Simeon and Hosgri faults make it likely that some or all of the strike slip measured near San Simeon Point is transferred to the northern part of the Hosgri fault zone, where the amount of slip has not been measured directly. PG&E has therefore applied displacement and slip data from the San Simeon fault to its evaluation of the Hosgri fault. Given the present state of knowledge, this is a reasonable procedure and it provides a basis for estimating the strike-slip component of movement on the Hosgri fault. It does not provide an appropriate

measure of other components of faulting, which from some lines of evidence appear to be at least equally important.

Reviewer's questions regarding other slip components on the Hosgri fault caused PG&E to evaluate this issue; they concluded (PG&E, 1990, Response to Questions GSG 3 and GSG 4) that vertical slip rates could not exceed a few tenths of a millimeter per year. This estimate is of doubtful value because the methods used do not satisfy the usual test for vertical offset: a distinctive stratigraphic marker that is well dated and whose displacement can be measured at nearby localities on opposite sides of the fault zone.

An unconformity, used as such a marker by PG&E, is identified on many seismic reflection records by the termination of bedding reflections at the unconformable surface. Strata in the first layer beneath the unconformity typically yield seismic velocities of 2,230 m/s; strata above the unconformity and below the seafloor yield velocities of 1,770 m/s. This break in the sedimentary record is designated the middle Pliocene unconformity, by PG&E, but age control for the strata above it appears to be based mainly (PG&E, 1990, Response to Question GSG Q1-A, p.22) on evidence from the Point Arguello oil field, 80 km south of the Diablo Canyon site. The relationship of oil field structure and stratigraphy to the Hosgri fault zone is unstated. Moreover, the strata above this unconformity contain no distinctive features indicative of their age except for their low seismic velocity and the known Holocene age of their uppermost layers, which are still being deposited at the seafloor. Basal parts of the 1,770 m/s seismic velocity unit may actually be much younger than the 2.8- to 3.0-Ma minimum age assigned to the unconformity by PG&E, because no independent criteria (fossil control, dated unique lithologic markers, or radiometric ages) establish the age of any internal part of the unit.

This lack of internal stratigraphic control prevents quantitative analysis where strata with a seismic velocity of 1,770 m/s are found, displaced, on opposite sides of a fault. The similar seismic velocities establish neither strict contemporaneity nor lithologic equivalence. Also unreliable are attempted correlations between undated, velocity-defined, packets of offshore strata and distant onshore stratigraphic sequences. And where correlation is attempted across a fault with kilometers of horizontal strike-slip, as well as vertical displacement, success is possible only with very strong, well-matched, and redundant stratigraphic controls on both sides of the fault.

The stratigraphic data presented by PG&E lack the age control needed to constrain the vertical component of slip, which may be many times greater than the amounts cited. Other evidence from geology, geophysics, and seismology points toward greater components of both vertical and compressional slip; an oblique slip fault seems most consistent with these

data. For PG&E's estimated 1 to 3 mm/yr. of strike slip, this implies a somewhat greater net slip, which will vary with the dip of the fault and with the ratio of horizontal to vertical slip.

If it is not listric and rooted in a near-horizontal detachment fault, the Hosgri fault zone at seismogenic depths probably dips within the range of 50 to 70°. For these dips and the most likely combinations of horizontal- and vertical-slip, net slip will exceed PG&E's strike-slip estimates by less than 60 percent. This difference is much less than the uncertainty in the estimates of strike slip on the Hosgri fault, and it does not significantly change earthquake magnitude or recurrence intervals. Vertical slip components, however, may affect estimates of earthquake ground motions.

Summary, Hosgri fault zone: This fault zone is part of a broader, more complex fault system than was generally recognized prior to the LTSP. Surface faulting along the zone, the fault and fold belt adjoining it to the southwest, and the regional structural high adjoining it to the northeast appear to form elements of a major active structure. The Hosgri fault system is most likely a belt of compressional reverse- and thrust-faults with a right-lateral strike-slip component, which dips northeastward beneath the structural high along the coast. The right-reverse, oblique-slip, character of the faulting may be dominated by thrusting and folding south of Point Sal.

Strike-slip rates of 1 to 3 mm/yr (PG&E, 1988, 2-119 to 2-120) derived from surface geologic evidence almost certainly represent only part of the seismogenic slip that can be expected at depth. The amount of structural relief (>1 to 2 km), the width of the deformed zone, the strong contrast in the structural style of rocks on opposite sides of the fault, and oblique slip or thrust earthquakes can be considered strong evidence for greater net slip on a single, simpler failure surface at depth. Although some of these interpretations differ from those by PG&E (1988, 1989, 1990), the earthquake magnitude assumed by PG&E for the Hosgri fault, M_S=7.2, is a reasonable value, given present knowledge of the fault zone.

Several sets of data support the interpretation that at earthquake depths the Hosgri fault zone dips 50 to 70° northeast. Evidence for this direction of dip is consistent and compelling. Evidence for the amount of dip is strong, but not so conclusive, because the only real control at seismogenic depths comes from earthquake focal mechanisms along the San Simeon fault. Conceivably, the fault could be steeper, as PG&E suggests, or it could flatten, become listric, and join a detachment surface at depths of a few kilometers, as others have argued. Currently, the evidence favors the intermediate, 50 to 70°, dip; new data may modify this and other structural interpretations.

The potential impact of new data extends well beyond estimates of fault dip. Our knowledge of the Hosgri fault zone and its related structures has been greatly expanded by the LTSP, but that knowledge is still incomplete and, in some respects, ambiguous. More earth-science discoveries are likely during the operating life of the Diablo Canyon power plant, and some of these may require us to re-evaluate the seismic potential of nearby faults and folds.

Los Osos fault

The Los Osos fault on the northeast side of the Pismo syncline, and an opposing zone of faults (Olson, San Luis Bay, Wilmar Avenue) on the southwest side, have been shown to be active by PG&E. Balanced structure sections across the Pismo syncline (PG&E, 1990, Response to Question GSG 11) illustrate the structural complexity of the region between the two fault trends and display two of many possible structural interpretations. The faults are considered (PG&E, 1988) to steepen with depth and to bound a crustal block that is currently undergoing vertical uplift. Under this interpretation, crustal shortening across the Pismo syncline, which formerly folded the Miocene and Pliocene rocks, now deforms the syncline and nearby crust northeast of the Hosgri fault by rigid block uplift or subsidence along northwest-trending reverse faults.

Other interpretations may require a less drastic change in the deformational style. For example, faults bounding the Pismo syncline may be thrusts produced by the same compressional forces that formed the syncline. Both active fault zones dip toward the synclinal axis, both exhibit low-angle thrusting near the surface, and the USL-Heller well near the synclinal axis and 7.5 km northeast of the Diablo Canyon plant encountered a repeated section, indicative of thrusting, below 5,546 ft. (1,690 m). Compression-induced northeastward thrusting along the Los Osos fault satisfies the observed geologic relations and requires no major change in tectonics since the episode of synclinal folding.

The Los Osos fault possesses higher earthquake potential than the faults on the south side of the syncline: it can be mapped as a continuous structure over a greater distance, it exhibits much more structural relief in upper Quaternary and Holocene deposits, and its topographic expression is stronger. Historic small earthquakes (M=4±) in 1913 and 1916, felt at points near the Pismo syncline (Toppozada and others, 1978, p. 16, 18), may have been located on either fault trend or on some other nearby structure. Focal mechanisms calculated for 2 recent small earthquakes near the Los Osos fault (PG&E, 1990, Response to Question Q43x, p. 31, 34) yield thrust solutions that match the strike of that fault.

Net slip rates for the Los Osos fault, estimated by PG&E (1988, p. 2-135) from

surface and subsurface geologic data, are as much as 0.5 mm/yr, a reasonable value for the data available. No deterministic magnitude is given, but a mean-value maximum magnitude of 6.8, derived from the logic-tree probability distribution (PG&E, 1988, figure 3-11, figure 3-14), is consistent with the data. This magnitude implies that the Los Osos fault is presumed capable of producing an earthquake at least as large as the San Fernando, California, earthquake of February, 1971.

Los Osos down-dip geometry: Questions, however, may be raised about the dip of the Los Osos fault at depth. The surface dip was measured at about 20° SW in trench exposures. Confirming evidence of a very low surface dip is the arcuate, concave-to-the-southwest, mapped trace of the fault on the north side of the Pismo syncline (PG&E, 1988, plate 16). This map pattern combined with topography defines a nearly horizontal surface. Projected subsurface dips of 20 and 35° are shown in an interpretive section (PG&E, 1988, figure 2-51), but in the logic tree PG&E prefers a dip of 60° (70 percent probability; PG&E, 1988, figure 3-6). Balanced structure sections (PG&E, 1988, Response to Question GSG 11) depict the fault with a surface dip of 52° (section AA') or essentially dismiss it (section BB') as a controlling structural element. The inconsistency of PG&E's preferred working model with observed fault dips reveals deficiencies of the model and a need for more subsurface data.

Los Osos segmentation model: The proposed segmented structure of the Los Osos fault is also difficult to accept as a tested, valid working hypothesis. Because no historic earthquakes are known to be located on this fault, much of the skepticism regarding postulated segments on the Hosgri fault also apply here. Moreover, segments proposed for the Los Osos fault are based chiefly on differences in summit elevations in the hills to the southwest of the fault. These elevation differences are attributed to different uplift rates, which supposedly define individual fault blocks. At best, this concept seriously oversimplifies the origin of relatively modest terrain features, which have been formed by multiple geologic processes acting on rocks with diverse properties. At worst, it implies such complete knowledge of the Los Osos fault that we can confidently specify rupture lengths and probable earthquake magnitudes for precisely defined segments. The concept may be plausible, but the evidence supporting it is weak and subject to other, more probable, interpretations.

The questions raised above may not significantly alter the magnitude estimate nor greatly alter earthquake recurrence times. They do affect probabilistic estimates of hazard, because they demonstrate the feasibility of tectonic models other than those chosen by PG&E. Questions regarding the amount of dip on the Los Osos fault may also be relevant to ground motion estimates.

Olson, San Luis Bay, and Wilmar Avenue faults

These 3 west-trending, north-dipping, reverse and thrust faults form a right-stepping fault zone along the southwest side of the Pismo syncline. Each of these faults is active, as shown by offset marine wave-cut platforms and terrace deposits of late Quaternary age. Each also either terminates near or converges with a linear structural trend that is defined by: the San Miguelito fault, minor folds that may or may not be faulted, and the Pismo fault. The San Miguelito and Pismo faults are considered inactive; the former was shown to exhibit no evidence of late Quaternary surface faulting by PG&E field investigations during the LTSP.

The slip rate on each of these faults is much lower than that on the Los Osos fault. Except possibly for the Wilmar Avenue fault, none have been mapped for distances greater than about 5 km. Although each offsets Quaternary deposits, their displacement of older rocks can be demonstrated chiefly in outcrops rather than on scales depicted by geologic maps.

The low slip rates, the short length of individual faults, and the geographic separation between them would generally be considered evidence of small structures, incapable of generating large, damaging earthquakes. They may, however, possess more hazard potential than is obvious. First, because their extent offshore is unclear, one or more of them may extend seaward for several more kilometers, significantly increasing their earthquake potential. Of perhaps greater concern is their possible relationship to the San Miguelito-Pismo fault trend.

Both the San Luis Bay and Wilmar Avenue faults converge with the San Miguelito-Pismo fault trend (PG&E, 1990, Response to Question GSG 16, plate 16A); the Olson fault has been mapped to within 3 km of it. If, as PG&E (1988, p. 2-38) proposes, these west-trending faults bound the 'San Luis-Pismo structural block' (a structural subdivision proposed by PG&E) they must somehow merge into a northwest-trending structure, because geologic mapping (Hall, 1973; Hall and others, 1979) demonstrates structural and stratigraphic continuity in the rocks northeast of the San Miguelito-Pismo trend. The most likely candidate for such a merger is clearly the San Miguelito-Pismo trend itself; it does not cut Quaternary deposits or features but could be active at depths below its junction with the Olson, San Luis Bay, and Wilmar Avenue faults. An active, subsurface fault along this trend could extend 20 km and possibly farther if it continued beyond the mapped northern end of the San Miguelito fault.

The threat from an earthquake on such a fault, or from one on the individual west-

trending surface faults, probably is much less than that from either the Los Osos fault or the Hosgri fault. The geologic evidence for a clearly-defined southwestern boundary to the 'San Luis-Pismo structural block' is not overwhelming, and if the block uplift concept is doubtful, the need for merging west-trending faults into a northwest-trending block boundary diminishes. Possibly the Olson, San Luis Bay, and Wilmar Avenue faults are local structures caused by compression and folding near the basement contact along the south limb of the Pismo syncline. If so, they may be relatively shallow failures with small rupture areas and with little capacity for generating large earthquakes.

LOGIC TREES

The purpose and content of logic trees (PG&E, 1988, chapter 3) were discussed in the section of this review titled LTSP Findings and in more detail in the PG&E Final Report. Although this review is concerned chiefly with the Geology/Seismology/Geophysics phase of the LTSP, many of the findings from those investigations are employed in logic trees to characterize earthquake magnitudes for the Hosgri, Los Osos, and San Luis Bay faults. Seismic hazard analyses, based on much the same data, are also employed for probabilistic risk assessments (PG&E, 1988, Chapter 6).

The logic tree probability distributions yield reasonable estimates of the mean magnitudes, given the ranges in uncertainty about the means. Individual components of the logic trees, however, may inaccurately reflect the data or its interpretation and may bias results when they are used elsewhere. Most of these points are discussed in preceding parts of this review and are noted here only as they relate to specific nodes or branches of the designated logic tree:

- Hosgri sense of slip: Strike slip is assigned a probability (P) of 0.65, which may approximate the prevailing view before LTSP. The evidence gathered during this investigation, and data published by others, strongly supports oblique slip and thrust models. The entire thrust branch of the logic tree is accorded a probability of 0.05. So low a weight is difficult to reconcile with PG&E's own interpretations of offshore seismic data and it surely understates published geologic work that interprets the Hosgri fault and other nearby structures as becoming listric at depths of 2-5 km. This weight also discounts the evidence from earthquake focal mechanisms on the San Simeon fault and from published studies of the November, 1927, Lompoc earthquake.

- Hosgri dip: Assigned probability values for the dip of a strike slip fault are: 90°, P=0.60 and 70°, P=0.40; for oblique slip: 90°, P=0.30; 60°, P=0.60; and 45°,

P=0.10. These values cannot easily be reconciled with the geologic and seismologic data for dips at, or approaching, earthquake depths. Seismic reflection lines and earthquake focal mechanisms indicate lower dips at depths below 2 or 3 km. The assignment of different weights for the same dip value shows that decisions are driven by a model, not by the data.

- Hosgri total length: The total length of a fault is determined by geologic criteria that test for continuity of similar dislocations along a linear trend. It is not a variable function of sense of slip (PG&E, 1988, p. 3-22). The 4 different total lengths entered here introduce spurious branches and unrealistically multiply the number of final outcomes in the probability distribution. Some geologists may disagree about the total length of the Hosgri fault, but neither this model-driven analysis nor the set of total lengths accurately represents the underlying geologic reasons for that disagreement.

- Hosgri rupture lengths: The set of rupture lengths for thrust-and oblique-slip branches appears to be heavily biased toward short (20 km) breaks. If the intent of the logic tree is to examine the set of maximum magnitude earthquakes (as opposed to the universe of all earthquakes), the heavy weighting of 20-km breaks seems unrealistic for two reasons. First, these shorter lengths depend on a segmentation point at the junction of the Pecho fault with the Hosgri fault; the evidence for a major structural break at that junction is unconvincing. Second, logic dictates that the earthquakes of most concern are those that will rupture through one or more segmentation points, not those that are constrained to a single segment. The heavy weight accorded to 20-km breaks unrealistically loads the low end of the probability distribution, especially for the oblique-slip and thrust models.

- Hosgri average displacement: Branches for the strike-slip model display 1-, 2-, and 3-m values, based on geologic evidence from the San Simeon Point area. 'No data' are indicated for the thrust and oblique-slip models. The values given for strike slip are data for an oblique-slip model, for they describe the horizontal component of net slip. Omitting horizontal slip data from the oblique-slip model unrealistically reduces the number of outcomes for that model.

- Los Osos dip: Measured surface dips and mapped fault contacts indicate that the dip on this fault is about 20° or less. The preferred thrust solution in the logic tree exhibits two branches: one at 60°, P=0.70; another at 30°, P=0.30. The logic tree values and weights conflict with field data, and appear to be model driven.

- Los Osos total length: Total length values are the same for both the thrust and

oblique-slip models and are based on geologic evidence; this data-driven analysis is more logical than its counterpart given in the Hosgri fault logic tree.

- Los Osos rupture length: As discussed for these branches of the Hosgri fault tree, the earthquakes of most concern for seismic hazard analysis are those that break through segment boundaries. Such earthquakes are given low weight (P=0.30) here, unrealistically loading the low end of the probability distribution for magnitude.

- Los Osos maximum displacement: The rationale for assuming a 2.1-m maximum earthquake displacement as given (PG&E, 1988, p. 3-29) in the text is not convincing. The probability that any trench, however favorably sited, would disclose a maximum magnitude slip is very small. Although 2.1 m is an impressive amount of slip for this fault, it is difficult to believe that it is the maximum.

These issues chiefly affect the relative importance of the 3 basic fault mechanism models--strike-, oblique-, and reverse- or thrust-slip--and the probability distribution functions generated by the logic tree for the Hosgri fault. Several of the points raised above would increase the weight for oblique slip and thrust, and decrease the weight for strike slip. Some points would also change the number of outcomes in the same sense, producing more thrust and oblique-slip outcomes. [PG&E's (1988, p. 3-21) logic tree yields nearly 4,000 outcomes, 59 percent of them strike slip, 33 percent oblique slip, and 8 percent thrust mechanisms.] These and other points may tend to raise the mean value for maximum magnitude derived from the probability distribution, or to alter that distribution in such a way as to change its standard deviation.

The same points generally apply to the seismic hazard logic tree for the Hosgri fault and its probability distribution. Most of these issues may prove to be of more importance to estimates of ground motion than to estimates of maximum magnitude. This is in part because PG&E has adopted a deterministic magnitude of M_S=7.2 for the Hosgri fault zone, a value that if not 'very conservative' (PG&E, 1988, p.10), is at least reasonable in terms of current knowledge. But estimates of the severity of ground motion for earthquakes greater than M_S=7 at distances less than 5 km are derived from a very small body of observational data, some of which suggests that geologic and seismologic variables other than magnitude may control the severity of ground motion.

REFERENCES CITED

Byerly, Perry, 1930, The California earthquake of November 4, 1927: Bulletin of the Seismological Society of America, v. 20, no. 2, p. 53-66.

Crain, W. E., Mero, W. E., and Patterson, Don, 1985, Geology of the Point Arguello discovery: American Association of Petroleum Geologists Bulletin, v. 69, no. 4, p. 537-545.

Crouch, J. K., Bachman, S. B., and Shay, J. T., 1984, Post-Miocene compressional tectonics along the central California margin, *in* Crouch, J. K., and Bachman, S. B., eds., Tectonics and sedimentation along the California margin: Society of Economic Paleontologists and Mineralogists, Pacific Section, v. 38, p. 37-54.

Dehlinger, Peter, and Bolt, Bruce, 1987, Earthquakes and associated tectonics in a part of coastal central California: Bulletin of the Seismological Society of America, v. 77, no. 6, p. 2056-2073.

Eaton, J. E., 1984, Focal mechanisms of near-shore earthquakes between Santa Barbara and Monterey, California: U.S. Geological Survey Open-File Report 84-447, 9 p.

Evernden, J. F., Kohler, W. M., and Clow, G. D., 1981, Seismic intensities of earthquakes of conterminous United States--their prediction and interpretation: U.S. Geological Survey Professional Paper 1223, 56 p.

Gawthrop, William, 1978, The 1927 Lompoc, California earthquake: Bulletin of the Seismological Society of America, v. 68, no. 6, p. 1705-1716.

Hall, Clarence, 1973, Geology of the Arroyo Grande Quadrangle, California: California Division of Mines and Geology Map Sheet 24, scale 1:48,000.

_____, 1976, Geologic map of the San Simeon-Piedras Blancas region, San Luis Obispo County, California: U.S. Geological Survey Miscellaneous Field Studies Map MF-784, scale 1:24,000.

Hall, Clarence, and Corbató, Charles, 1967, Stratigraphy and structure of Mesozoic and Cenozoic rocks, Nipomo Quadrangle, Southern Coast Ranges, California: Geological Society of America Bulletin, v. 78, p. 559-582.

Hall, C. A., Jr., Ernst, W. G., Prior, S. W., and Wiese, J. W., 1979, Geologic map of the San Luis Obispo-San Simeon region, California: U.S. Geological Survey Miscellaneous Investigations Series, Map I-1097, scale 1:48,000

Hamilton, D. H., 1984, The tectonic boundary of coastal central California: Stanford, California, Stanford University Ph.D. dissertation, 290 p.

Hanks, Thomas, 1979, The Lompoc, California, earthquake (November 4, 1927; *M*=7.3) and its aftershocks: Bulletin of the Seismological Society of America, v. 69, no. 2, p. 451-462.

ISS, 1931, International seismological summary for 1927, October, November, December: University Observatory, Oxford.

Jeffreys, H., and Bullen, K. E., 1935, Time of transmission of earthquake waves: International Geodetic and Geophysical Union, Section of Seismology, Series A, Travaux Scientifiques, No. 11.

Jennings, C. W., compiler, 1958, Geologic map of California, San Luis Obispo sheet: California Division of Mines, scale 1:250,000.

Jennings, C. W., compiler, 1959, Geologic map of California, Santa Maria sheet: California Division of Mines, scale 1:250,000.

McCulloch, David, 1989, Evolution of the offshore central California margin, *in* Winterer, E. L., Hussong, D. M., and Decker, R. W., eds., The Eastern Pacific Ocean and Hawaii: Boulder, Colorado, Geological Society of America, The Geology of North America, v. N, p. 439-470.

Niemi, Tina, Branch, Charles, Hall, N. T., and Shiller, G. I., 1987, GSA Poster presentation sheets, *in* PG&E, 1989, Response to Question 43 *l.*

Pacific Gas and Electric Co., 1988, Final Report of the Diablo Canyon Long Term Seismic Program--July 1988: San Francisco, 650 p.

Pacific Gas and Electric Co., 1989, Response to Questions--January and February, 1989

Pacific Gas and Electric Co., 1990, Response to Questions--March, 1990.

Plafker, George, and Galloway, John, eds., 1989, Lessons learned from the Loma Prieta, California, earthquake of October 17, 1989: U.S. Geological Survey Circular 1045, 48 p.

Stover, C. W., Reagor, B. G., Baldwin, F. W., and Brewer, L. R., 1990, Preliminary isoseismal map for the Santa Cruz (Loma Prieta), California, earthquake of October 18, 1989 UTC: U.S. Geological Survey Open-File Report 90-18, 24 p.

Toppozada, Tousson, Parke, D. L., and Higgins, C. T., 1978, Seismicity of California, 1900-1931: California Division of Mines and Geology Special Report 135, 39 p.

Toppozada, Tousson, and Parke, D. L., 1982, Areas damaged by California earthquakes, 1900-1949, annual technical report to U.S. Geological Survey: California Division of Mines and Geology Open File Report 82-17 SAC, 65 p.

Table 1

Modified Mercalli Scale of Wood and Newman (1931) as further modified by Toppozada and Parke (1982) and edited for this report.
(**bold type** indicates upper range of intensities for 1927 earthquake, see figure 3)

I Not felt--or rarely felt under especially favorable circumstances.
Under certain conditions at and outside the boundary of the area in which a great shock is felt: some birds or animals appear uneasy or disturbed; some people experience dizziness or nausea ; some trees, structures, liquids, or bodies of water sway; doors may swing very slowly.

II Felt indoors by few, especially on upper floors, or by sensitive or nervous persons.
Also, as in intensity I, but more noticeably: some hanging objects swing, especially when delicately suspended; some trees, structures, liquids or bodies of water sway; doors may swing very slowly; some birds or animals appear uneasy or disturbed; some people experience dizziness or nausea.

III Felt indoors by some, motion usually rapid vibration.
Sometimes not immediately recognized as an earthquake. Vibration like that of passing light, or lightly-loaded, trucks; or of heavy trucks at a distance. Hanging objects may swing slightly. Movements may be appreciable on upper levels of tall structures. Standing motor cars rock slightly.

IV Felt indoors by many, outdoors by few.
Awakens few, especially light sleepers. Vibration like that due to passing of heavy or heavily-loaded trucks. Sensation like that of heavy body striking building or of heavy objects falling inside. Dishes, windows, and doors rattle; glassware and crockery clink and clash. Walls and frame creak, especially in the upper range of this intensity grade. Many hanging objects swing. Liquids in open vessels disturbed slightly. Standing motor cars rock noticeably.

V Felt indoors by practically all, outdoors by many or most: outdoors direction estimated.
Awakens many or most. Frightens many; slight excitement, a few run outdoors. Buildings tremble throughout. Some dishes and glassware break. Some windows crack (but not most). Small or unstable objects and vases are overturned and a few of them fall. Many hanging objects and doors swing. Pictures knock against

wall or swing out of place. Doors and shutters open or close abruptly. Pendulum clocks start, stop, or run fast or slow. Small objects or furnishings move; the latter only slightly. Small amounts of liquid spill from filled open containers. Trees and bushes shake. Minor cracking of plaster. Felt by most at an hour when most would be asleep. Small bells, such as doorbells, ring.

VI Frightens most or all, excitement general, some alarm, many or all run outdoors.
Persons move unsteadily. Liquid set in strong motion. Small bells (church, chapel, school) ring. Damage slight in poorly built buildings. Fall of small amounts of plaster. Some chimneys cracked. Much breakage of dishes and glassware; some windows break. Knick-knacks, books, and pictures fall. Much furniture overturned; some moderately heavy furnishings moved.
Some brick walls cracked slightly. A few loose bricks knocked from walls. Many plaster walls cracked. Some people can stand only with difficulty.

VII Noticed by drivers of automobiles or horse-drawn carriages. Rings large church bells.
Suspended objects quiver. Damage negligible in buildings of good design and construction, slight to moderate in well-built ordinary buildings, considerable in poorly-built or badly designed buildings, adobe houses, old walls (especially where laid up with mortar), spires, etc. Many chimneys cracked; some walls. Moderate to large amounts of fallen plaster. Many broken windows; some broken furniture. Loosened brickwork and tiles fall; weak chimneys break at roof-line, some of them causing roof damage. Cornices fall from towers and buildings. Bricks and stones are dislodged. Heavy furniture overturns with damage from breaking. Some fire walls fall.

VIII Disturbs drivers of automobiles. Branches and trunks of trees broken; especially palms. Damage slight in structures (brick) built especially to withstand earthquakes; considerable in ordinary substantial buildings, partial collapse; wooden houses on stilts racked or tumbled down; panel walls in frame structures thrown out, decayed piling broken off. Walls fall; solid stone walls seriously cracked or broken. Most or all chimneys, columns, monuments, factory stacks,

and towers twist or fall. Very heavy furniture moves conspicuously or overturns. Frame structures move on their foundations. Some weak adobe buildings collapse.

IX Damage considerable in (masonry) structures built especially to withstand earthquakes. Some wood-frame houses built especially to withstand earthquakes thrown out of plumb. Damage great in substantial (masonry) buildings; some collapse (partial collapse of a number of buildings, a few buildings largely collapsed, or both), or frame buildings shifted off foundations; racked frames.

X Severe damage to well-built wooden structures and bridges; some destroyed. Dangerous cracks in excellent brick walls. Masonry and frame structures of good construction destroyed; foundations of such structures also damaged.

XI Severe damage to wood-frame structures. Damage great to dams, dikes, and embankments--many at great distances. Few, if any, well-constructed (masonry) structures remain standing. Large well-built bridges destroyed by wrecking of supporting piers and pillars. Less damage to more elastic wooden bridges.

XII Damage total--practically all works of construction damaged greatly or destroyed.

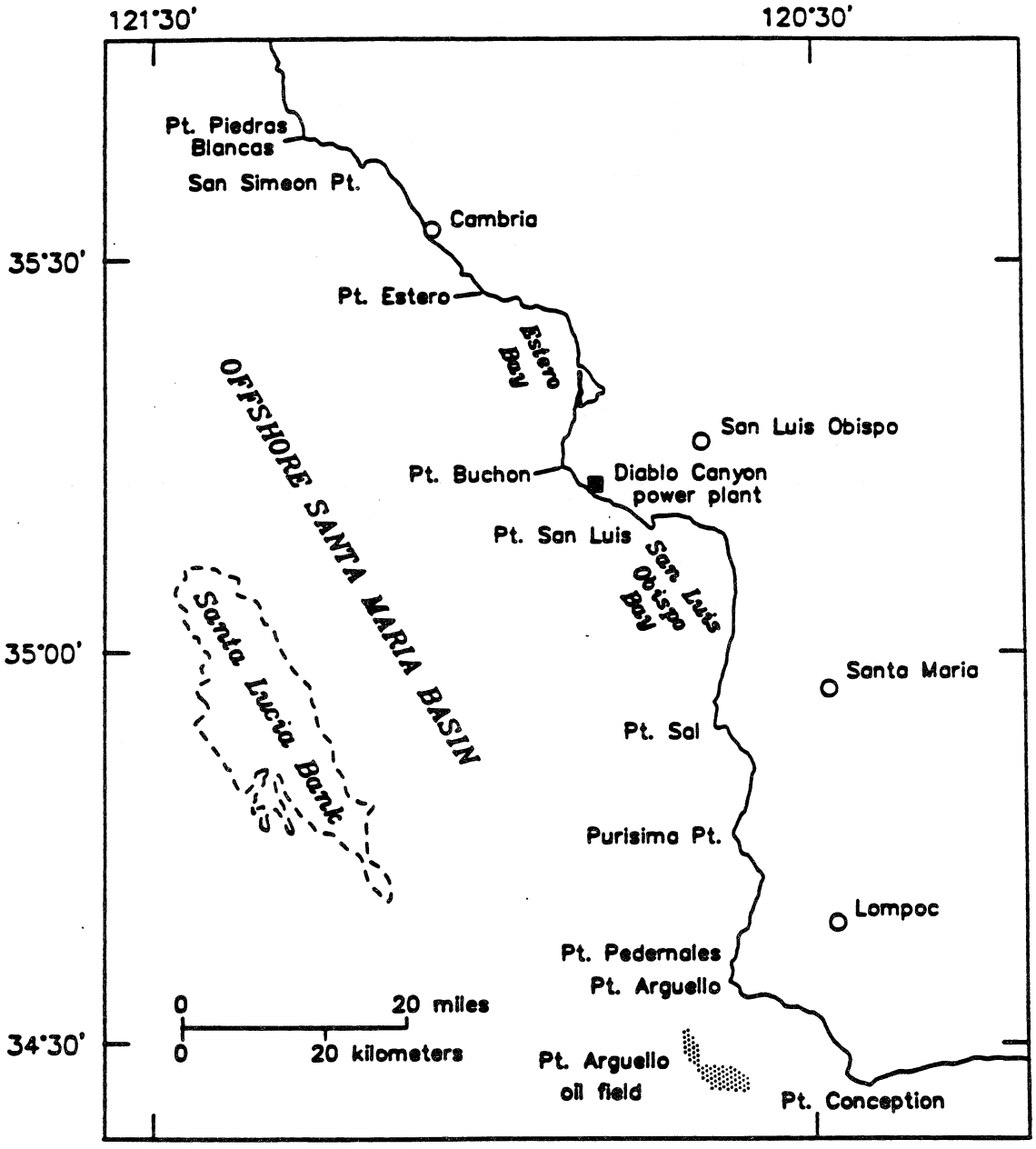


Figure 1 Location map of the region near Diablo Canyon power plant. Santa Lucia Bank is outlined by the -500 m bathymetric contour. Location of Point Arguello oil field from Crain and others (1985, fig. 12)

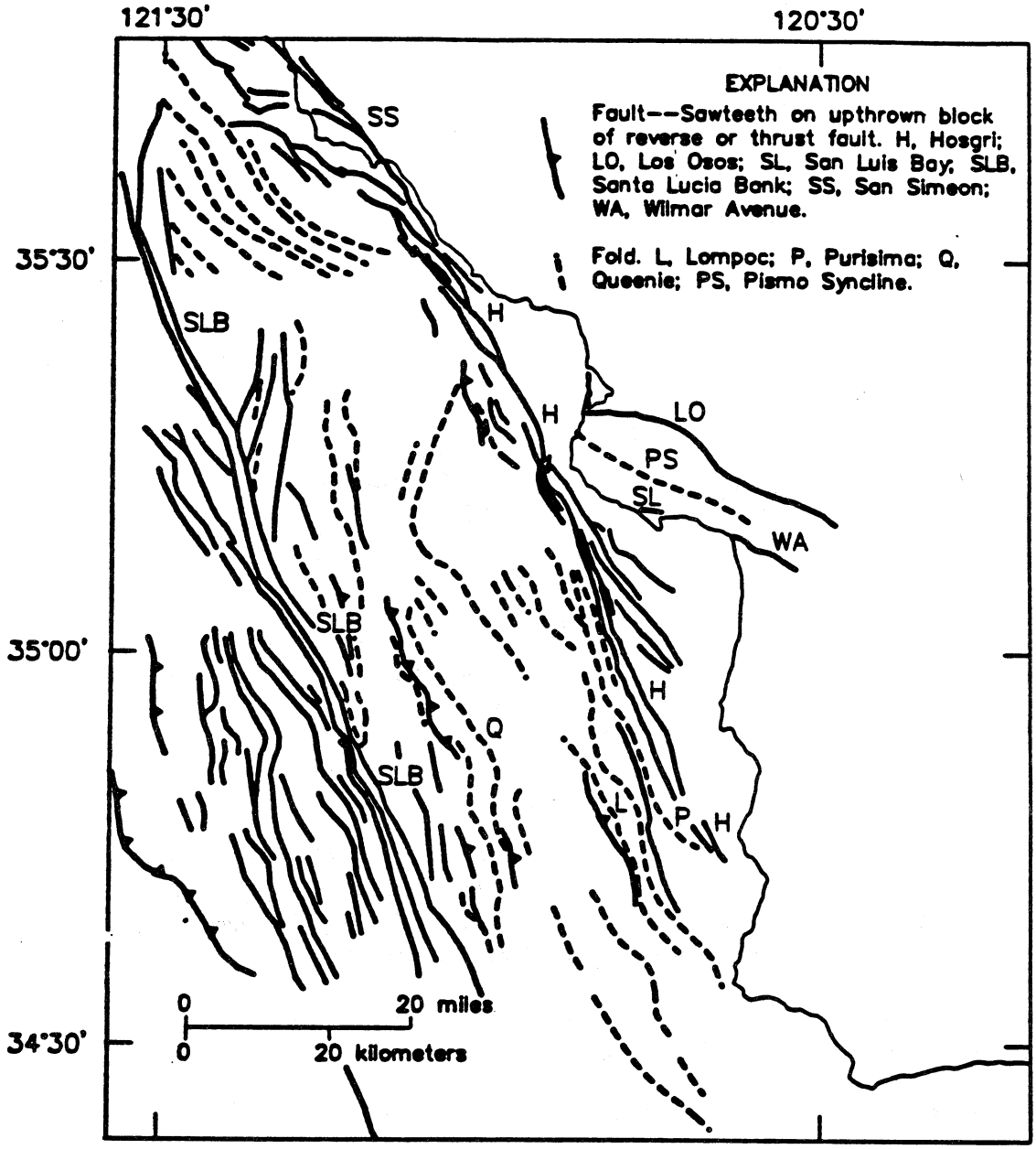
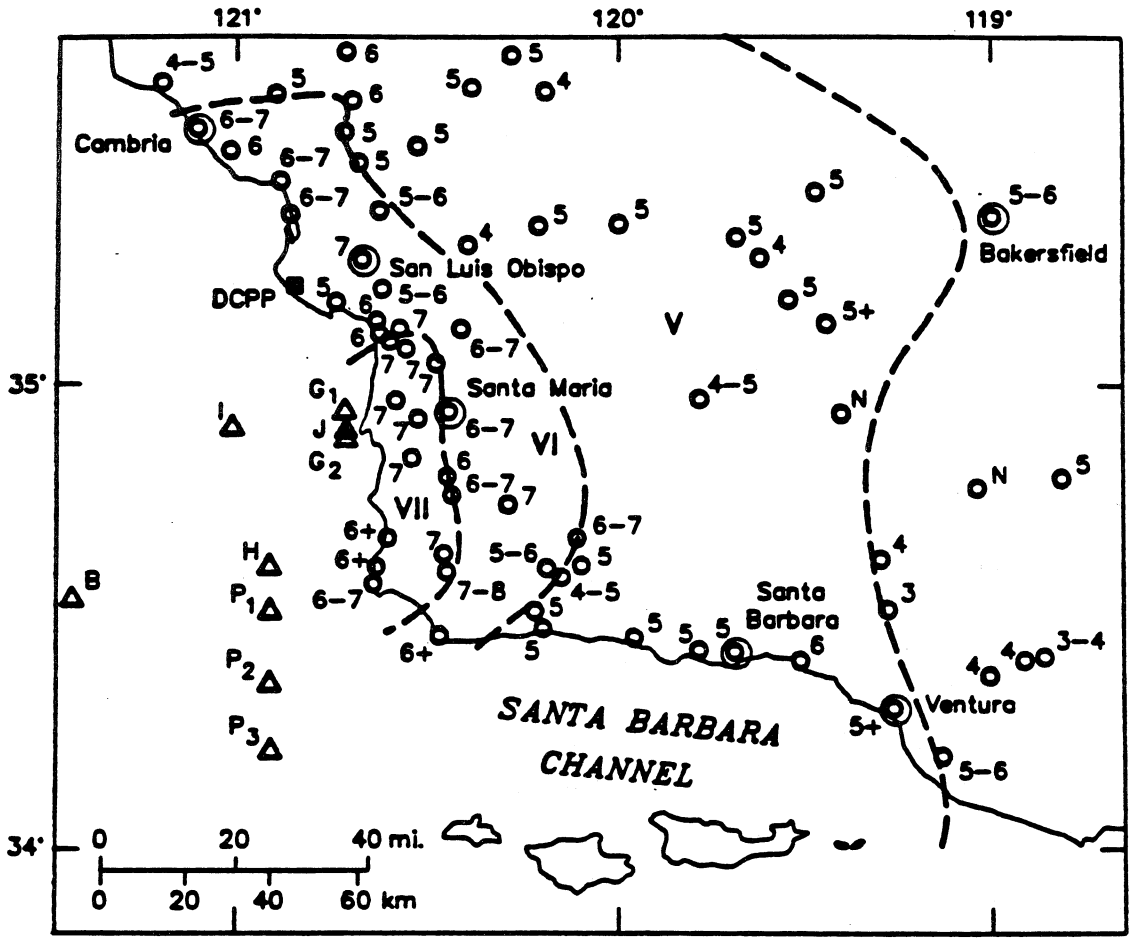


Figure 2 Sketch map of selected geologic structures in the offshore Santa Maria Basin near the Diablo Canyon power plant. Offshore geologic structures are generalized from McCulloch (1989); onshore structures near Diablo Canyon from PG&E (1988).



EXPLANATION

△ Epicenter of 1927 earthquake from: B, Byerly, (1930); G_1 and G_2, Gawthrop, (1978); H, Hanks, (1979); I, ISS, (1931); J, Jeffreys and Bullen, (1935); P_1, PG&E, (1988); P_2, PG&E, (1990, Response to Question 8); P_3, PG&E, (1990, Response to Question 5).

o^6 Observed Modified Mercalli intensity of 1927 earthquake from Toppozada and Parke (1982); N, not felt.

VI Modified Mercalli intensity bands from Toppozada and Parke (1982).

Figure 3 Intensity data, isoseismals, and proposed epicentral locations for the 4 November 1927, Lompoc, earthquake. For explanation of intensity values, see Table 1.

APPENDIX D

TECHNICAL EVALUATION REPORT

UNIVERSITY OF NEVADA-RENO

INDEPENDENT ASSESSMENT OF THE EARTHQUAKE POTENTIAL AT THE DIABLO CANYON POWER PLANT, SAN LUIS OBISPO COUNTY, CA

David B. Slemmons

and

Douglas G. Clark

Center for Neotectonic Studies,
Mackay School of Mines,
University of Nevada,
Reno, NV 89557

April 10, 1991

TABLE OF CONTENTS

		Page
1.0	INTRODUCTION	1
1.1	Purpose of Study	1
1.2	Scope of UNR Work	2
2.0	SEISMOTECTONIC SETTING	5
2.1	Regional Tectonic Setting	5
2.2	Regional Seismicity	20
3.0	DETERMINATION OF MAXIMUM CREDIBLE EARTHQUAKE (MCE)	25
3.1	Introduction	25
3.2	Empirical Relations	26
3.3	Moment Magnitude Regressions	26
3.4	Fault Segmentation	26
3.5	Logic Trees	27
3.6	Maximum Credible Earthquake (MCE)	27
4.0	SOURCE CHARACTERIZATION OF CAPABLE FAULTS SIGNIFICANT TO DCNPP	28
4.1	Introduction	28
4.2	Hosgri Fault	30
4.3	Los Osos Fault	37
4.4	Faults Within the San Luis/Pismo Block	41
4.5	Southwest Boundary Zone	41
5.0	SEISMIC SOURCE CHARACTERIZATION: ASSESSMENT OF MAXIMUM CREDIBLE EARTHQUAKES	50
5.1	Introduction	50
5.2	Hosgri fault	50
5.3	Los Osos fault	54
5.4	Southwest Boundary Zone	54
6.0	Conclusions and Recommendations	55
7.0	References	56

LIST OF FIGURES

Figure	Caption	Page
2-1	Generalized fault and seismotectonic domain map of central coastal California .	7
2-2	Structural blocks and faults	11
2-3	Northwest-trending structural blocks	14
2-4	Paleo fluvial terraces across the San Luis/Pismo block	15
2-5	Subblocks and generalized topographic contours of the San Luis/Pismo block ..	16
2-6	Historical earthquakes of magnitude 5 and larger, 1812-1988	21
2-7	Seismicity data of earthquakes from January 1, 1980 through May 31, 1988	23
2-8	Focal mechanisms of earthquakes of magnitude 3 and greater	24
4-1	Depth-corrected seismic reflection record across the Hosgri fault zone	31
4-2	Segmentation model of PG&E for the Hosgri fault zone	34
4-3	Structural elements of the San Luis/Pismo block.....	38
4-4	Rupture lengths considered by PG&E for Los Osos and San Luis Bay fault zones .	40
4-5	Marine shoreline angle elevations between the Los Osos Fault and Point San Luis .	43

LIST OF TABLES

Table	Caption	Page
3-1	Earthquake magnitude (M_S) for an assumed 50 km rupture length.....	29

1.0 Introduction

1.1 Purpose of Study

The purpose of this study is to provide an independent geological evaluation to the U. S. Nuclear Regulatory Commission (NRC) for their review of Pacific Gas and Electric's (PG&E) Long Term Seismic Program (LTSP) for the Diablo Canyon Nuclear Power Plant (DCNPP). The contract between NRC and the University of Nevada, Reno (UNR) began in July 1985 and included the following objectives:

> "The objective of this contract is to investigate the earthquake capability and earthquake potential of faults in the Diablo Canyon site area, particularly the Hosgri fault zone. To accomplish this, all available data on the geological, geophysical, and seismological character of the regional and local faults and folds will be integrated and evaluated to establish the seismogenic and neotectonic potential at the site. The site assessment will specifically investigate the probabilities of future surface faulting and strong ground motion. Worldwide data on earthquake size and associated fault and fold parameters will be compared with seismogenic geologic structures near the site to assess the Maximum Credible Earthquake.

The following ten areas of study were specified in the contract:

(1) Review, as specified, the licensee's revalidation program.

(2) Advise and assist NRC in developing its parallel geologic and seismic program.

(3) Collect, review, and evaluate existing geological, geophysical and seismologic data to determine the neotectonic setting of the site.

(4) Acquire and interpret existing aerial photographs and imagery, conduct aerial observations and obtain and analyze low-sun angle aerial photographs.

(5) Review the results of the licensee's geological and seismological investigations to revalidate the seismic design bases for the DCNPP site.

(6) Attend meetings, as required, to accomplish the subtasks and coordinate activities with NRC, USGS, and licensee.

(7) In coordination with NRC geoscientists, USGS, and PG&E and their contractors, synthesize all data to determine the character of seismogenic faulting and folding, calibrate earthquake size with worldwide data, determine fault parameters, evaluate earthquake potential and determine the magnitude of the Maximum Credible Earthquake (MCE).

(8) Prepare, based on the subtasks described above, reports, theses, and draft evaluations.

(9) Provide a final evaluation report to be included in the NRC Supplemental Safety Evaluation Report.

(10) Prepare written testimony and appear as an expert witness at ACRS Subcommittee and ACRS Full Committee meetings, and ASLB hearings, as necessary.

In brief, this report responds to NRC's request to review geological, geophysical, and seismological data needed to characterize potential seismic sources that could affect the site for estimation of the Maximum Credible Earthquake (MCE).

1.2 Scope of UNR Work

1.2.1 Participation in Meetings

D. B. Slemmons with appropriate UNR staff participated in all major NRC/PG&E geological and geophysical meetings and data audits since 1985.

1.2.2 Master's Theses and Ph. D. Study

Four UNR Master's theses and one Ph.D. dissertation were undertaken on topics related to these project goals. The main purpose of the thesis work was to provide a familiarity with major issues related to the seismic hazard at the site, to search for undetected capable faults or active tectonic structures that needed to be investigated, to provide information needed for the assessment of known faults, and to provide regional constraints on styles and rates of active tectonic deformation and associated earthquake processes in the coastal central California region. The five projects are:

(1) Steve Nitchman (1988): "Tectonic geomorphology and neotectonics of the San Luis Range, San Luis Obispo County, California"

Steve Nitchman's investigations included discovery of the activity and capability of the Wilmar Avenue fault along parts of the southwestern margin of the San Luis/Pismo structural block, and characterization of the Los Osos fault. He also studied tectonic and stratigraphic interrelationships on the northeast margin of the block and Quaternary folding processes in the onshore Santa Maria basin.

(2) Katheryn Killeen (1988): "Timing of folding and uplift of the Pismo Synclinorium, San Luis Obispo County, California"

Katheryn Killeen investigated marine and fluvial terraces on the margins and within the San Luis/Pismo block to help characterize capable faults at or near the

site. The study demonstrated neotectonic activity associated with the Los Osos fault zone and faults of the southwestern boundary zone of the San Luis/Pismo block. In addition, the study documented the lack of middle and late Quaternary folding of the Pismo syncline, and the inactivity of faults within the San Luis Range, including the San Miguelito and Edna faults.

(3) Barbara Matz (1989): "Remote sensing and geomorphic studies for seismotectonic analysis, Santa Maria basin, California"

Her study included an analysis of detailed 1:12,000 scale low-sun angle aerial photographs flown for UNR of capable and suspected capable faults near the site, and evaluation of pseudo-radar, synthetic aperture radar, Thematic Mapper imagery, and large and small scale aerial photography. Two of her thesis figures (Figs. 19 and 20) suggest that, at least locally, fault zones truncate folded beds.

(4) Doug Clark (1991): "Quaternary tectonic deformation in the Casmalia Range"

Doug Clark completed his thesis on neotectonic relations in the Casmalia Range in early 1991. The main finding of his study is that the Casmalia Range is being uplifted along capable, block-bounding faults at a rate of 0.14 to 0.17 mm/yr in the late Quaternary, slightly less than that of the San Luis/Pismo structural block. Marine and fluvial terraces on the margins and within the range indicate uniform, block-style uplift, with significant localized folding (blind thrusting) on the Orcutt Frontal fault (or Casmalia fault) and minor reverse movements on the Lions Head fault. Quaternary data can be interpreted in two ways: (1) ongoing fault-propagation folding of the range, a style of deformation which contrasts with the purely brittle type of deformation in the San Luis Range; and (2) localized drag folding with some surface faulting along the Orcutt Frontal fault.

(5) Xiaoyi Zhang (unfinished Ph. D. dissertation) worked on studies of worldwide relationships between earthquake size and fault rupture and/or folding parameters. Although his thesis was not completed, the data indicate very small differences in earthquake magnitude for different fault types (strike-slip, oblique-slip, thrust/reverse-slip) for given source dimensions, and that linear regressions using moment magnitude improve the statistical relationships, with smaller standard deviations than earlier regressions using surface magnitude (Zhang and others, 1989; Wells and others, 1989; and Slemmons and others, 1989).

1.2.3 Other Investigations

Other investigations that were part of the project include:

(1) Etiziano Vittori (Vittori, 1987; Vittori and others, 1991) studied regional faults, folds, and joints to determine the present orientations of principal stress axes in

the San Luis Range vicinity. Vittori's work supports the results of Zoback and others (1987) and Mount and Suppe (1987), by showing from fault, joint and bedding plane orientations that the regional maximum horizontal stress direction for the Central Coast region is about N32°E.

(2) Craig dePolo and others (1989, 1991) investigated the application of fault segmentation models for the Basin and Range province in the western United States. This study of normal and associated strike-slip faults indicates that within an extensional tectonic setting about half of the fault rupture terminations are not at readily recognized segmentation points and more than one segment may rupture during larger events of $M > 7$.

(3) Craig dePolo and D. Burton Slemmons (1990) paper "Estimation of Earthquake Size for Seismic Hazard" was published in Reviews in Engineering Geology of the Geological Society of America. This article summarizes many of the methods and approaches in current use.

1.2.4 Publications

In addition to the studies listed above, more than 19 papers and abstracts were published or are in press or preparation. These include the work of Steve Nitchman (Nitchman and Slemmons, 1987 and 1991); Katheryn Killeen (Killeen and others, 1987), Barbara Matz (Matz and Slemmons, 1987), Doug Clark (Clark, 1990 and 1991; Clark and Slemmons, 1990; Clark and others, 1991; Kennedy and others, 1990); Xiaoyi Zhang (Zhang and others, 1989; Wells and others, 1989), and D. Burton Slemmons (Slemmons, 1987; Slemmons and others, 1989; dePolo and Slemmons, 1990).

1.2.5 Other Comments

The scope of the studies included extensive review of the geologic literature and study of PG&E responses to all questions dealing with geologic and seismotectonic issues, including NRC Questions 3, 40-47, GSG 1-16, SSC 1-6, and LP 7-13 (as referenced in Table A1-1 of the PG&E Addendum, 1991).

This report was prepared by D. Burton Slemmons and Douglas Clark as part of a University of Nevada, Reno (UNR) research contract with the U. S. Nuclear Regulatory Commission (NRC). The study will be referred to throughout this report as the UNR study. The conclusions and assessments of this report are the result of investigations by project staff; UNR is not responsible for technical decisions. The authors are grateful for the many editorial suggestions from Ruth M. Slemmons and David R. Slemmons.

2.0 SEISMOTECTONIC SETTING

2.1 Regional Tectonic Setting

2.1.1 Late Cenozoic Evolution of Coastal Central California

The coastal region between Big Sur and Point Conception is in part of the North American-Pacific plate boundary system, a broad, complex zone of translational and compressional deformation extending across coastal California and contiguous areas. The region's present seismotectonic character is largely the result of influence from the development of the San Andreas transform fault system. Mesozoic and Tertiary subduction along the North American plate margin in central California was gradually replaced in the Miocene by a broad zone of right-lateral shear between the Pacific and North American plates (Atwater, 1970). The evolving San Andreas fault system greatly affected nearly the entire California coastal region, contributing to the prominent northwest-oriented structural grain, right-lateral strike-slip fault systems, en echelon folds, and pull-apart basins (Blake and others, 1978; Page, 1981).

Major Late Cenozoic right-lateral translations on the San Andreas fault, and to a lesser extent on the Rinconada and San Gregorio-Hosgri fault zones, increased the region's structural and seismotectonic complexity by juxtaposing crustal blocks with dissimilar rock types and geologic histories (Hill and Dibblee, 1953; Dibblee, 1976; Graham and Dickinson, 1978). Neogene right-lateral shear may also be responsible for the clockwise rotation of the Transverse Ranges (Luyendyk and others, 1980; Hornafius, 1985).

Regional transtension (strike-slip and extensional deformation) with accompanying basin formation and extensive marine deposition began to give way to a more transpressive (strike-slip and contractional deformation) tectonic regime in the Pliocene (Jahns, 1973; Blake and others, 1978). The change in regional stress orientation appears to be related to a clockwise rotation of the direction of the Pacific plate's relative movement between 3.4 to 3.9 Ma and the present (Page and Engebretsen, 1984; Cox and Engebretson, 1985; Harbert and Cox, 1989). This change resulted in a component of convergence between the Pacific and North American plates. Post-Miocene contraction initiated a phase of intense folding, reverse faulting, and range uplift that culminated in the late Pliocene and Quaternary Coast Range orogeny (Reed, 1933; Taliaferro, 1943; Page, 1966, 1981). Numerous folds and reverse faults originated or were accentuated during the transpressive regime, concomitant with continued right-slip on faults of the San Andreas system.

2.1.2 San Andreas Fault System

The San Andreas fault continues to be the locus of most of the differential motion between the Pacific and North American plates. However, a significant component of the present day plate motion is taken up by dextral strike-slip displacements in a broad region both east and west of the San Andreas fault, and by contraction in the Transverse Ranges and southern Coast Ranges (Minster and Jordan, 1984; Weldon and Humphreys, 1986). Minster and Jordan (1978, 1984,

1987) found that the slip vector derived from global plate motion models (revised to 48 mm/yr, N35°W by DeMets and others, 1987) was inconsistent with geodetic and geologic data from along the San Andreas fault (34±3 mm/yr, at a latitude of N41°±2°; Savage and Burford, 1973; Sieh and Jahns, 1984). Much of the discrepancy, 5 mm/yr of right-lateral slip parallel to the San Andreas fault and 7 mm/yr of fault-normal shortening (DeMets and others, 1987), was attributed to deformation west of the San Andreas fault. New results from very long baseline interferometry (VLBL) substantially, but not conclusively, reduce the component of the "San Andreas Discrepancy" west of the San Andreas fault in central California; Ward (1990) concludes "a few millimeters per year of right-lateral slip on offshore faults cannot be rejected."

The plate margin in coastal central California is not a simple rigid boundary, but is instead a broad, complex zone of transform and contractional deformation that extends across the coastal region. Seismotectonic responses to interplate stresses are highly variable along this portion of the plate margin: present-day transpressive plate motion is distributed over a system of active strike-slip faults, subparallel reverse and reverse-oblique faults, and related folds and detachments.

The San Andreas fault system (see Wallace, R. E., editor. 1991), rather than being expressed as a single rupture, includes several major, active branches in the Coast Ranges, both to the northeast and southwest. Branches to the north include the Calaveras-Paicines-Sunol-Concord-Green Valley system, the Hayward-Rogers Creek-Healdsburg-Maacama system, and, faults and folds extending northward of Davis, California. The main fault branch to the southwest is the San Gregorio/Hosgri system.

Slemmons (1987) and Clark and others (1991) present a generalized seismotectonic framework for coastal central California using data from geologic, geomorphic, and seismologic investigations. These data suggest that coastal central California is divided into five structurally and physiographically distinct seismotectonic "domains", regions characterized by distinctive patterns of Quaternary and/or late Quaternary tectonic deformation and seismicity (Fig. 2-1). The domains recognized in this study are: (1) the Transverse Ranges; (2) Santa Maria basin-San Luis Range (includes the DCNPP site); (3) coastal Franciscan; (4) Salinian; and (5) western San Joaquin Valley domains. The domains are in most cases bounded by major, principally Quaternary faults (e.g., San Andreas fault, San Gregorio-Hosgri fault), which accommodate much of the regional strain release. Internally, domains are defined by consistent styles and orientations of active faulting, seismicity patterns, geomorphic expression, and basement rock characteristics. A progressive change in seismotectonic character occurs across this region, from left-lateral reverse-oblique deformation in the Transverse Ranges, to nearly pure compression in the onshore Santa Maria basin and San Luis Range, to reverse and right-lateral reverse-oblique displacements in the coastal Franciscan domain, to nearly pure right-lateral strike-slip faulting in the Salinian block (Eaton, 1984, 1985a and 1985b; Clark and others, 1991). The western margin of the San Joaquin Valley is subject to principally contractional deformation.

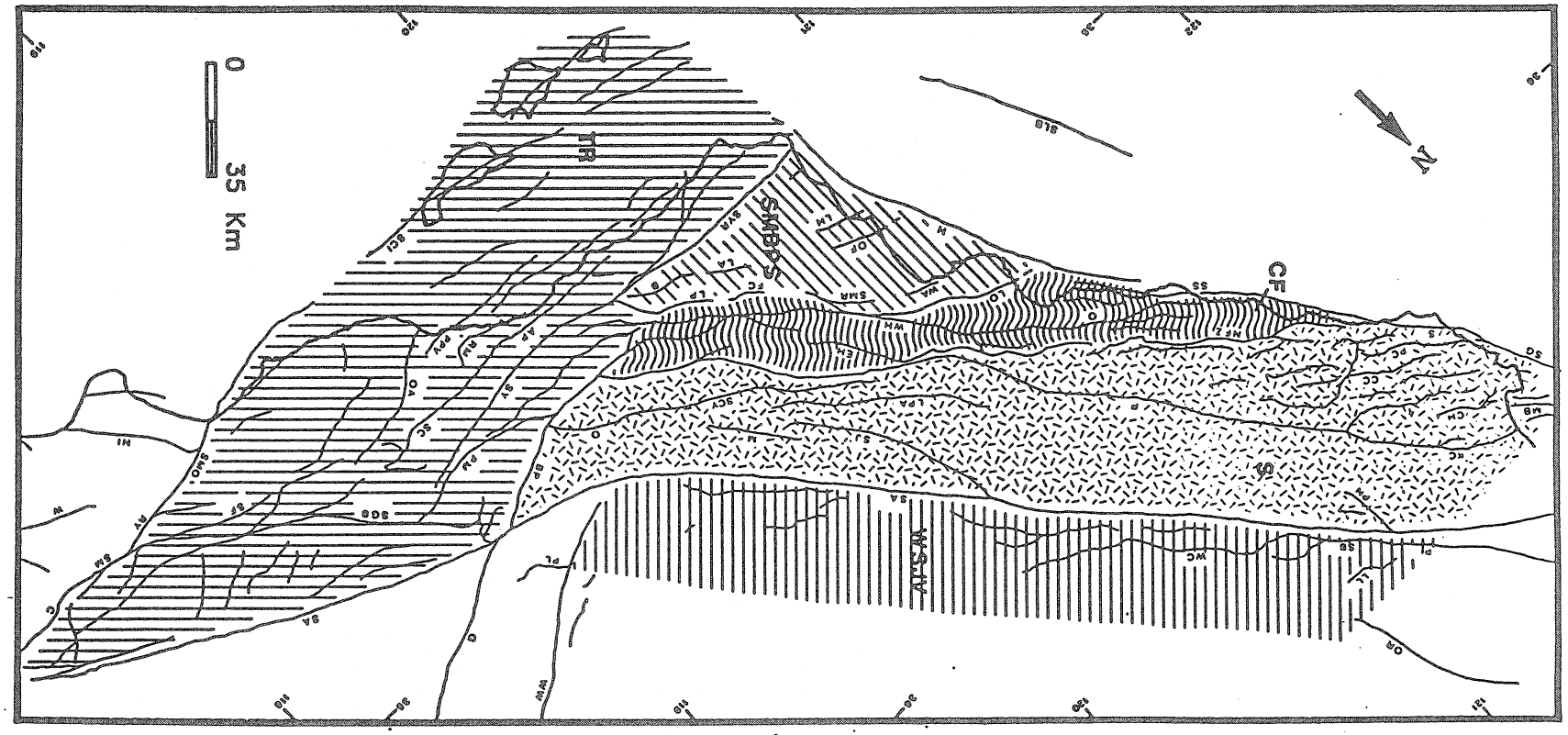


Figure 2-1. Generalized fault and seismotectonic domain map of central coastal California.

Seismotectonic domains: CF = Coastal Franciscan; S = Salinian; SMBPS = Santa Maria Basin-Pismo Syncline; TR = Transverse Ranges; WSJV = Western San Joaquin Valley. Faults and fault zones: AR = Arroyo Parida; B= Baseline; BP = Big Pine; C = Cucamonga; CC = Church Creek; CH = Chupines; EH = East Huasna = FC = Foxen Canyon; G = Garlock; H = Hosgri; KC = King City; LA = Los Alamos; LH = Lions Head; LL = Llanda; LO = Los Osos; LP = Little Pine; LPA = La Panza; M = Morales; MB = Monterey Bay; NFZ Nacimiento; NI = Newport Inglewood; O = Oceanic; OA = Oakridge; OF = Orcutt Frontal (and subparallel Casmalia and Pezzoni faults); OR = Ortigalita; O = Ozena; P = Paicines; PC = Palo Colorado; PL = Pleito; PM = Pine Mountain; N = Pinnacles; PPV = Pitas Point-Ventura; R = Rinconada; RM = Red Mountain; RY = Raymond; S = Sur; SA = San Andreas; SB = San Benito; SC San Cayetano; SCI Santa Cruz Island; SCY = South Cuyama; SF = San Fernando; SG = San Gregorio; SGB = San Gabriel; SJ = San Juan; SLB = Santa Lucia Bank; SM = Sierra Madre; SMO = Santa Monica; SMR = Santa Maria River; SS = San Simeon; SY Santa Ynez; SYR Santa Ynez River; W = Whittier; WA = Wilmar Avenue; WC = Waltham Canyon; WH = West Huasna; WW = White Wolf (modified from Jennings, 1975).

2.1.3 Stress Data

Contemporary stress orientations are inferred from recent geologic data, earthquake focal mechanisms, and in situ stress measurements (Zoback and Zoback, 1980). These data indicate a slight clockwise rotation of the maximum horizontal contraction direction from north-northeast in the Transverse Ranges, to a relatively uniform northeast orientation in the southern Coast Ranges, nearly perpendicular to the N40°W strike of the San Andreas fault (Zoback and others, 1987; Mount and Suppe, 1987; Vittori and others, 1991) and at a high angle to the N28°W strike of the San Gregorio-Hosgri fault zone.

The most recent study of the Santa Maria basin by Feigl and others (1990) showed that east of the Hosgri fault, across the Santa Maria basin (Nitchman, 1988), the integrated geodetic rate of deformation is 7 ± 1 mm/yr orientated N03°E$\pm$13°. This vector can be decomposed into 6 ± 2 mm/yr of crustal shortening on the general structural trend of N30°E and 3 ± 1 mm/yr of right-lateral shear.

2.1.4 Active Contraction in Coastal Central California

Many workers emphasize the contractional nature of Pliocene and Quaternary tectonism in the California coastal region (Reed, 1933; Taliaferro, 1943; Page, 1966, 1981; Gawthrop, 1978a; Crouch and others, 1984; Zoback and others, 1987; Namson and Davis, 1988a, 1988b, 1990). Contractional deformation is unequivocal in the Transverse Ranges. The current tectonic regime of the southern Coast Ranges and adjacent offshore region, where both strike-slip and reverse faulting appear to be developing simultaneously, is the subject of considerable recent debate. The southern Coast Ranges have commonly been interpreted as being under a shear tectonic regime related to right-lateral movements on the San Andreas and associated faults. While there is strong evidence for recent horizontal displacements on sections of several faults which are subparallel to the San Andreas fault (e.g., the Rinconada fault and sections of the San Gregorio-Hosgri fault), the nature of recent movements on other northwest-trending structures is less certain.

Geologic data, stress measurements, and earthquake focal mechanisms indicate significant contractional deformation oriented roughly normal to the strike of the San Andreas fault (Zoback and others, 1987). Fault-normal contraction accounts for only a small percentage of the total relative motion between the North American and Pacific plate. However, its effects on earthquake processes in regions away from the San Andreas fault itself may be substantial. Reverse and reverse-oblique faulting and related folding are a significant deformation process in many parts of coastal central California.

The ultimate causes of contraction perpendicular to the San Andreas fault are not well understood. Past studies attribute contractional deformation in the southern Coast Ranges to wrench movements on the San Andreas and related faults. Contraction in the Transverse Ranges is commonly attributed to the restraining geometry of the "Big Bend" in the San Andreas fault. Several recent workers (Page, 1981; Crouch and others, 1984; Zoback and others, 1987;

Namson and Davis, 1988a) note the parallelism of reverse faults and folds to the San Andreas fault and argue that these structures do not have the proper orientation for wrench structures. They state that the reverse faults and folds that parallel the San Andreas fault may instead be related to a misalignment of the San Andreas fault relative to the direction of North American-Pacific plate motion (Minster and Jordan, 1978; Page and Engebretsen, 1984), producing a component of convergence across the plate margin. Convergence may also be related in part to extension in the Basin and Range province (Wright, 1976).

Zoback and others (1987) and Mount and Suppe (1987) propose that the San Andreas fault is a nearly frictionless or "weak" fault, and that convergent deformation normal to the plate margin is largely decoupled from the San Andreas fault. A form of strain partitioning involving separation of strike-slip and reverse-slip deformation in the upper crust may also be occurring on the Hosgri fault and other faults in the region (PG&E, 1988 and docket amendments). The implications of fault-normal contractional strain for seismic hazard assessments is currently being debated.

2.1.5 Seismically Active Folds

The recognition of active folding as a sudden, coseismic process is a recent development that applies to at least some parts of California. Yeats (1986), Davis and McIntosh (1987), Namson and Davis (1988a, 1988b, 1990), Nitchman (1988), and Stein and Yeats (1989) suggest that many of the seismogenic faults in coastal central California do not produce surface rupture, but instead accommodate coseismic deformation at the surface by folding. The Coalinga anticline, for example, is a young fold in the upper plate of a system of buried active thrust faults (Namson and Davis, 1988a; Wentworth and Zoback, 1989) that was seismically active in 1983 (M_S=6.5). Similarly, the 1973 Point Mugu earthquake (M_L=5.9), the 1979 Malibu earthquake (M_L=5.0), and the 1987 Whittier Narrows earthquake (M_L=5.9) are believed to have occurred on a west-trending blind thrust fault system located at the southern margin of the Transverse Ranges (Hauksson and others, 1988).

While relatively little work has been done to assess the timing and style of folding outside of the Transverse Ranges and the west margin of the San Joaquin Valley, fold deformation in coastal central California is widespread and often intense. Namson and Davis (1988a) and Stein and Yeats (1989) discuss some of the difficulties in applying traditional seismic hazard evaluation techniques in areas of active folding. Deformation commonly occurs without accompanying surface faulting, and fault-fold geometry can be obscure and extremely complex. Seismic hazard assessments must consider the recency of activity, rates of deformation, and potential segmentation of surface folds and underlying blind thrust and reverse faults.

PG&E (1988 and docket amendments) and several researchers (Nitchman, 1988; Namson and Davis, 1990) propose that there is a possibility of active folding in the onshore Santa Maria basin. Quaternary data do not support major folding within the San Luis/Pismo structural block (PG&E, 1988; 1990, GSG-10; Killeen, 1988; Nitchman, 1988). Active folding appears to be

localized along the Hosgri fault and also with parts of the Piedras Blancas Anticlinorium and southern offshore Santa Maria basin regions. There is some evidence for neotectonic folding along several sections of the Hosgri fault. However, as noted by PG&E in the San Simeon area, reverse faulting and associated folding is subordinate to strike-slip faulting.

2.1.6 Detachment Surfaces

Various workers (Hadley and Kanamori, 1978; Yeats, 1981: Crouch and others, 1984; Eaton, 1985a; Namson and Davis, 1988a, 1988b, 1990) propose the existence of regional detachment faults, or decollements, along most of coastal central California. Seismic reflection data and limited earthquake focal mechanism data suggest that many thrust and reverse faults decrease in dip with depth and root into subhorizontal detachment surfaces near the base of the seismogenic zone (brittle-ductile transition). In order to be seismogenic, detachment surfaces would have to be present at a depth between 6 and 12 km depth. Currently, in the region north of the Santa Maria basin, and landward of the Hosgri fault zone, there is no conclusive geological, geomorphological, structural, or seismological evidence for active detachment faults of this type.

2.1.7 San Gregorio/Hosgri Fault System

The San Gregorio-Sur-San Simeon-Hosgri fault system (Fig. 2-2, and Fig. 2-38 in PG&E, 1988) is connected to the San Andreas fault near Bolinas, and is a major north-northwest-striking, predominantly right-lateral fault system that shows abundant evidence of late Pleistocene and Holocene activity (Coppersmith and Griggs, 1978; PG&E, 1988 and docket amendments). The San Gregorio-Hosgri fault forms a major structural boundary between northwest-oriented structures in the onshore Santa Maria, San Luis Range, and Santa Lucia Mountains, and north-northwest-oriented structural trends in the offshore Santa Maria and Sur basins (PG&E, 1988; McCulloch, 1989). The fault zone is linear and truncates anticlines and faults both north and south of the DCNPP. Previous studies document predominantly strike-slip deformation on the San Gregorio and San Simeon faults (Weber, 1979a, 1979b, and 1983).

The Hosgri fault extends southeastward from the San Simeon fault zone and is completely offshore. Accordingly, information on its current style of deformation depends on different methods of study, including the extensive use of seismic reflection analysis. PG&E (1988 and docket amendments) documented Holocene right-lateral displacements on the San Simeon fault, and proposed that horizontal slip is transferred to the Hosgri fault across a 5 km (cross-strike distance) stepover. Estimates of cumulative right-slip along the San Gregorio-Hosgri system range from 10-20 km (post-Miocene; Hamilton and Willingham, 1977) to as much as 115 km (Neogene and Quaternary; Graham and Dickinson, 1978). Crouch and others (1984), however, cite reverse faults and fault-parallel folds both onshore and offshore as evidence for mainly thrust and reverse faulting on the Hosgri fault in post-Miocene time. Both strike-slip and reverse-slip types of faulting and deformation may be currently active, with oblique-slip strain partitioned in the upper crust into strike-slip and reverse and thrust components (e.g., note the partitioning

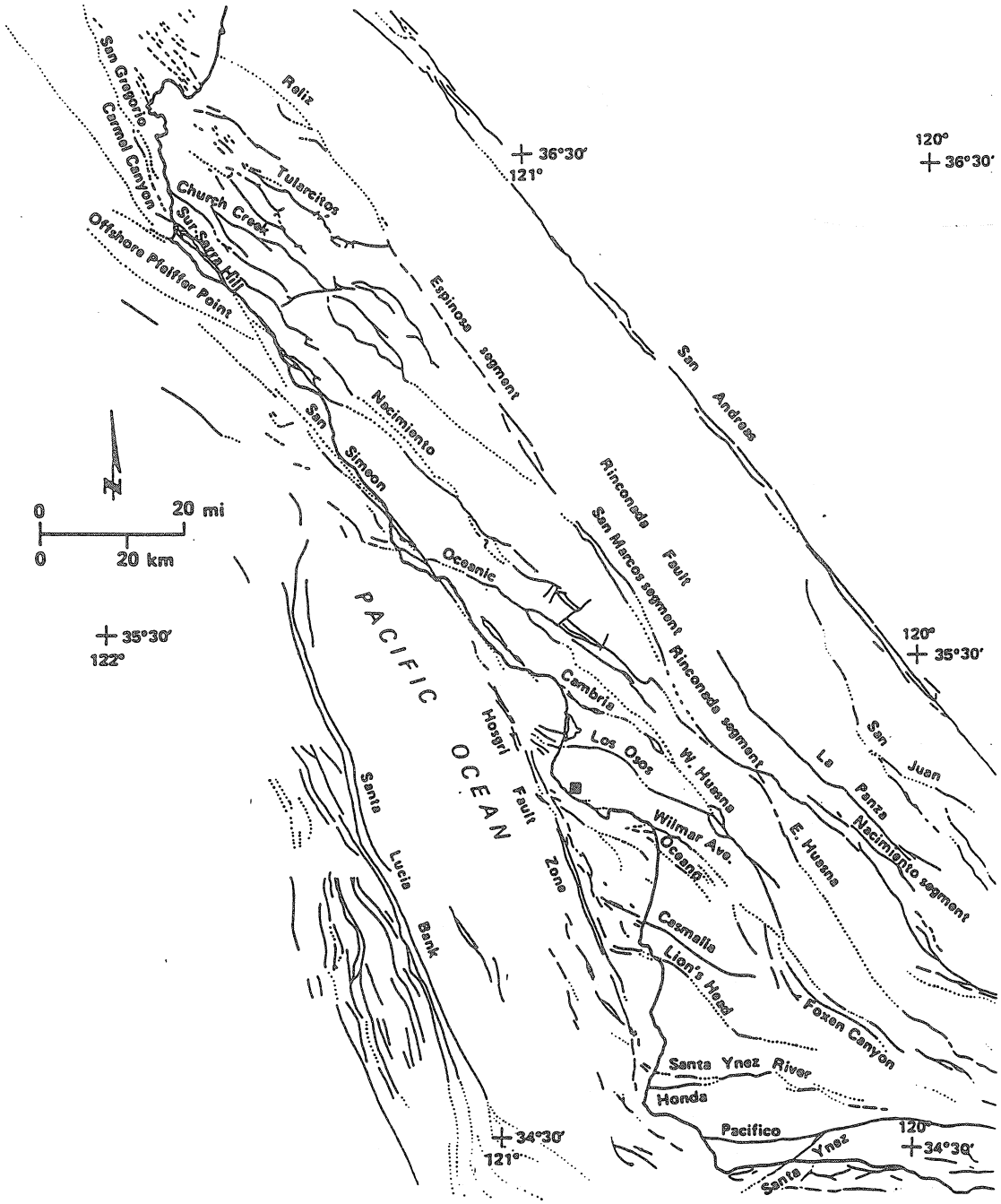


Figure 2-2. Structural blocks and faults (from Fig. 2-7 of the PG&E Final Report (1988).

Map of structural blocks and faults in the south-central California coastal region illustrating the regional geologic setting of the south-central California Coast. SAL = Salinian block, SLR = Santa Lucia Range block, PBA = Piedras Blancas Anticlinorium, CAM = Cambrian block, SLP = San Luis/Pismo block, OFSMB = Offshore Santa Maria Basin block, SMV = Santa Maria Valley block, CAS = Casmalia block, VSY = Vandenberg/Santa Ynez Valley block, PH = Purisma Hills block, SH = Solomon Hills block.

model presented by PG&E at the May 1990 meeting in San Francisco, and Lettis and Hanson, 1991, in press).

2.1.8 San Luis Range/Santa Maria Basin

Although the San Luis Range and the Santa Maria basin are considered together as one region by Slemmons (1987) and Clark and others (1991), there are some differences in late Quaternary deformation styles, suggesting that they could be classified as separate regions or subdomains. The San Luis Range, site of the DCNPP, is a west-northwest-trending, fault-bounded coastal mountain range in San Luis Obispo County, California. Figure 2-2 shows the location of the San Luis Range block (SLR) and its relation to the Santa Maria basin (shown in hachured pattern), the offshore Santa Maria basin (OFSMB). The San Luis Range/Santa Maria basin is at a structural and geomorphic transition between the predominantly northwest-trending Santa Lucia and San Rafael Mountains of the southern Coast Ranges and the west-oriented Santa Ynez Mountains of the western Transverse Ranges (Fig. 2-1). N50°W to N80°W-oriented structural trends in the San Luis Range/Santa Maria basin are abruptly truncated in the offshore by the north-northwest-striking Hosgri fault.

The San Luis Range and onshore Santa Maria basin are currently undergoing north-northeast-directed convergence and crustal shortening, as indicated by active west- to northwest-striking thrust and reverse faults (Nitchman, 1988; PG&E, 1988; Clark and others, 1991), other structural data (Vittori, 1991), uplifted late Pleistocene marine and fluvial terraces, reverse and left-lateral reverse-oblique earthquake focal mechanisms (Eaton, 1984, 1985a), in situ stress measurements (Zoback and others, 1987), and geodetic data (Feigl and others, 1990). Seismic activity and rates of faulting and coastal uplift are significantly lower in the San Luis Range/Santa Maria basin than in the adjacent Transverse Ranges, and appear to be somewhat lower than in the more active portions of the southern Coast Ranges. Geomorphic expression of active faulting and folding is likewise more subdued than in the more active portions of the Transverse Ranges and southern Coast Ranges. Quaternary fault-related folds may continue to be active in the onshore Santa Maria basin.

Two types of tectonic models have been proposed for the recent development of the San Luis Range, Santa Maria basin, and adjoining areas. Crouch and others (1984), Nitchman (1988), and Namson and Davis (1990) describe parts or all of this region as an active fold-and-thrust belt, with fault-propagation and fault-bend folds developed above buried thrust faults which root into a regional low-angle detachment surface at depth. Crouch and others (1984) and Namson and Davis (1990) interpret high angle faults mapped at the surface as secondary structures related to deformation in the hanging walls of major folds. In tectonic models of the type used by Crouch, ranges such as the San Luis Range and Casmalia Range are genetically related to, and underlain by major blind thrust faults.

In contrast, PG&E (1988 and docket amendments) states that late Quaternary tectonic deformation is dominated by movements on west- to northwest-striking, high-angle reverse faults, and the emergence and subsidence of rigid structural blocks, with only minor, localized

folding. This type of model was used by Nitchman (1988), who considered that the San Luis/Pismo block responds differently than the onshore Santa Maria basin. Deformation of the San Luis/Pismo block may have changed from folding during the Pliocene (Pismo syncline) to brittle failure during the Quaternary. In contrast, within the Santa Maria basin proper, fold and thrust belt-style deformation may have continued into the late Quaternary.

2.1.8.1 San Luis/Pismo Structural Block

The Pismo syncline of late Tertiary age forms the core of the northwest-trending San Luis Range. The Pismo syncline is no longer actively folding (Killeen and others, 1987; Killeen, 1988; PG&E, 1988 and docket amendments), but instead is being uplifted as a rigid structural block along N60°-70°W-trending reverse faults which bound the San Luis Range (Fig. 2-3). Killeen (1988) found from the elevation of fluvial terraces across the Pismo/San Luis block at San Luis Obispo Creek, between the Irish Hills and Edna subblocks, that there is no tilting across the block (Fig. 2-4), an observation that agrees with the marine terrace mapping and profiles along the coastline at the western edge of the Irish Hills subblock (PG&E, 1988 and docket amendments). The southwest-dipping Los Osos reverse or thrust fault forms the northeastern structural margin of the San Luis/Pismo block and is segmented by major cross structures of the block. The four subblocks (PG&E, 1988 and docket amendments) are from west to east: the Estero Bay, Irish Hills, Edna, and Newsom Ridge (Fig. 2-5). The Irish Hills segment shows multiple Holocene or late Pleistocene reverse or thrust fault displacements and has an estimated late Quaternary vertical slip rate of 0.2 to 0.4. mm/yr (PG&E, 1988). Down-dip slickensides on fault surfaces indicate nearly pure thrust or reverse displacements. The onshore segments show progressively less geomorphic evidence for activity from the Irish Hills segment to the Newsom Ridge segment.

The southwestern structural margin of the San Luis/Pismo block is more diffuse than the Los Osos fault zone. It consists of several west-northwest-striking, northeast-dipping reverse or thrust faults, including the San Luis Bay, Olson, Wilmar Avenue, Pecho, and Oceano faults. The absence of tilting or folding of the San Luis/Pismo block suggests that collectively the southwestern boundary zone faults have a rate of vertical separation that is subequal to that of the Los Osos fault zone. The zone trends eastward toward the Santa Maria River-Foxen Canyon-Little Pine faults. The geomorphic character of the southwestern boundary zone suggests that it may be segmented by the same San Luis/Pismo sublocks and cross structures that divide the Los Osos fault, and the rate of activity appears to decrease southeastward away from the Hosgri fault.

Capability, according to the 10 CRF 100 definition is expressed by the Olson and San Luis Bay faults at the Irish Hills subblock, and the Wilmar Avenue fault at the Edna subblock. Capability of the Wilmar Avenue and other faults at the Newsom Ridge subblock has not been conclusively resolved.

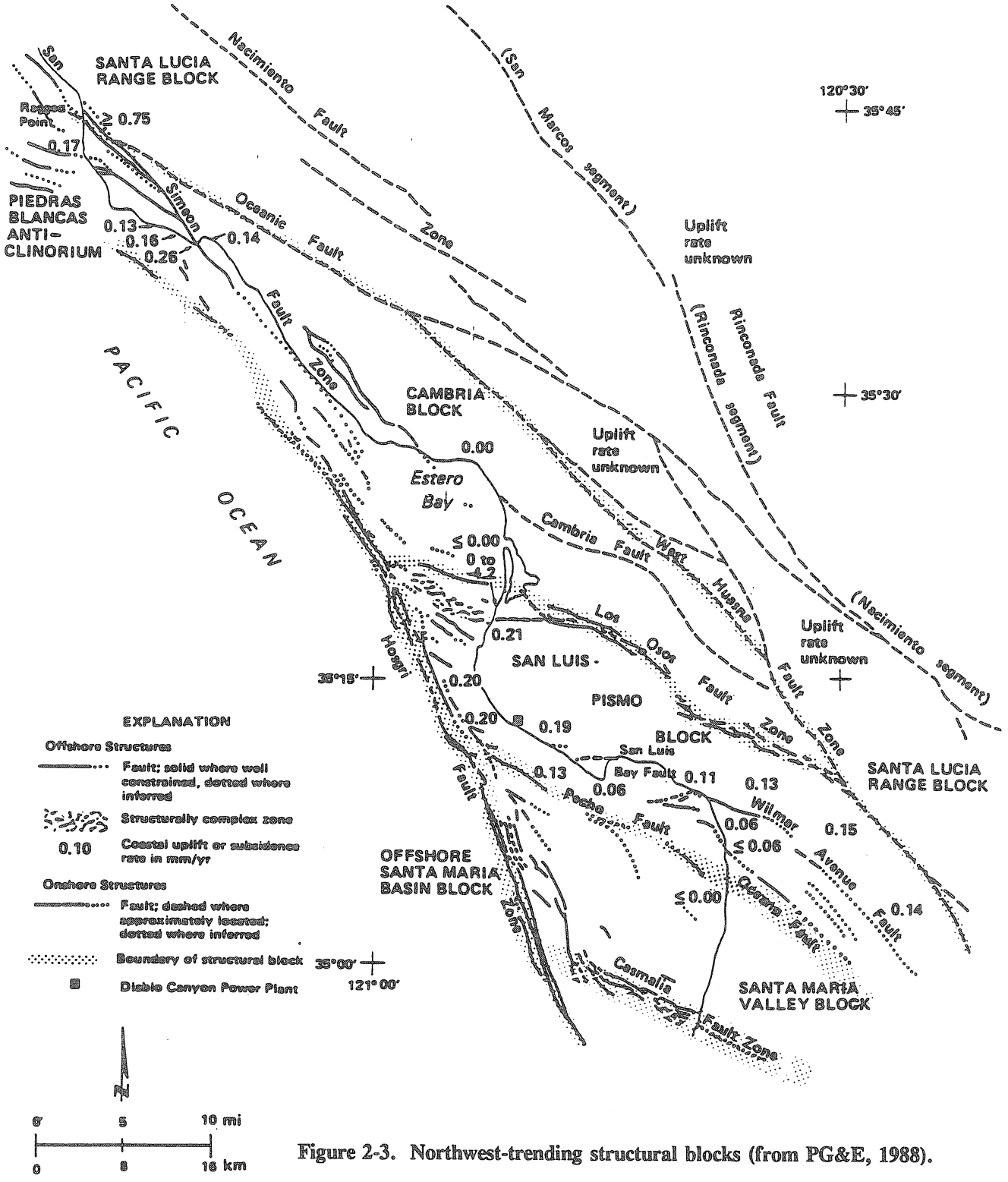


Figure 2-3. Northwest-trending structural blocks (from PG&E, 1988).

Map illustrating distribution of northwest-trending structural blocks and general location of faults in south-central coastal California. Uplift rates are derived from marine terrace shoreline angle elevations and are used, in part, to define the regional structural blocks.

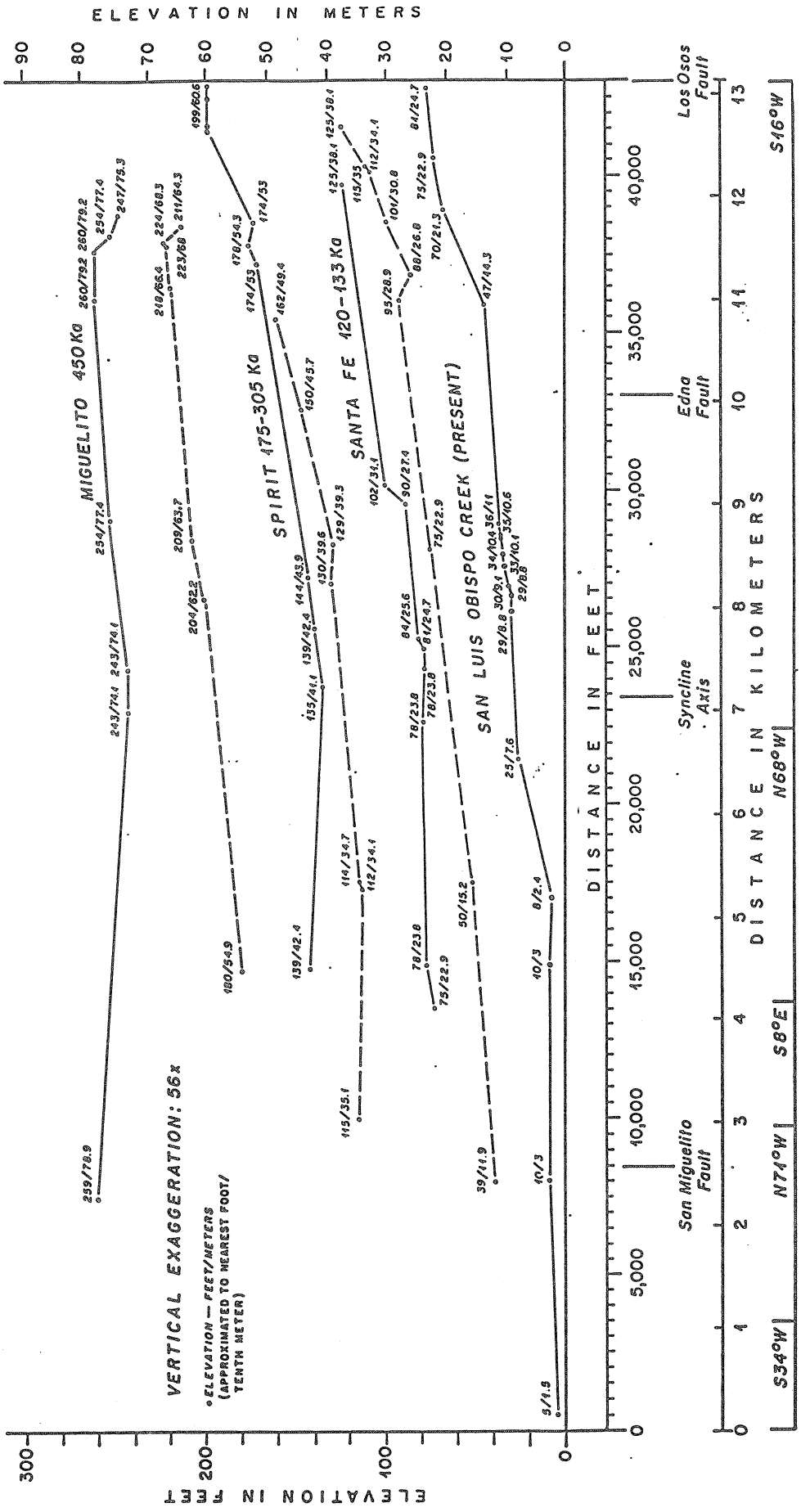


Figure 2-4. Paleo fluvial terraces across the San Luis/Pismo block, San Luis Obispo Creek (after Killeen, 1988).

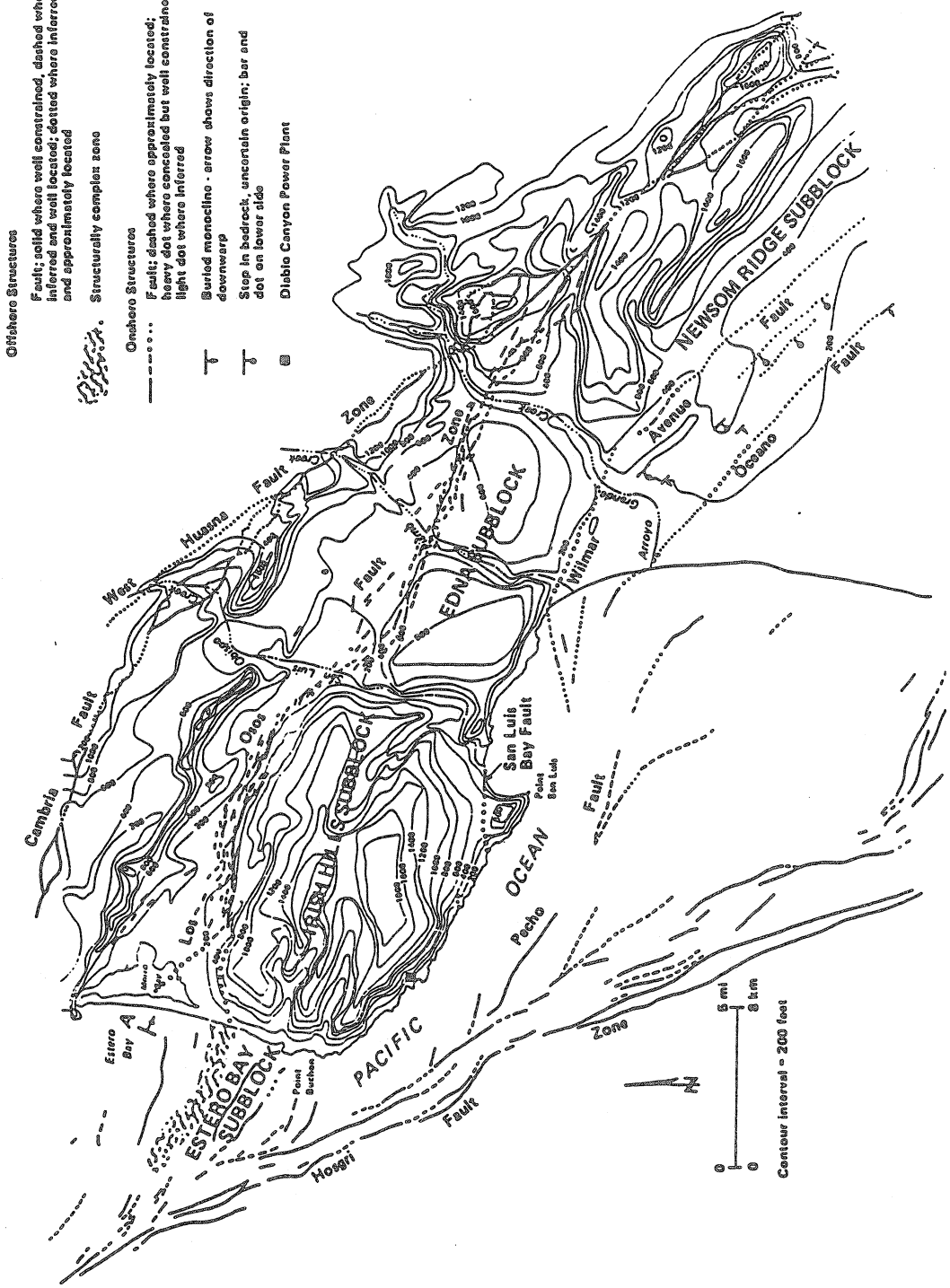


Figure 2-5. Generalized topographic contour map of the San Luis/Pismo block (from PG&E, 1988).

Generalized topographic contour map illustrating subblocks of the San Luis/Pismo structural block. Contours generalized from parts of the Morro Bay South, San Luis Obispo, Port San Luis, Pismo Beach, Arroyo Grande NE, Oceano, Tar Springs, Nipomo, Santa Maria, Huasna, Guadalupe, and Twitchell Dam U. S. Geological Survey 7.5-minute topographic quadrangles.

2.1.8.2 Santa Maria River-Foxen Canyon-Little Pine Faults

The Santa Maria River, Foxen Canyon, and Little Pine faults (Fig. 2-1) are interpreted by Hall (1978, 1981) as being part of a single fault system. These faults are located at the base of the San Rafael Mountains and strike northwest, discordant to the west-northwest-trending structural grain of the Santa Maria basin and San Luis Range. Faults within this system dip to the northeast, with progressively steeper dips towards the northwest (Dibblee, 1966; Hall, 1981). The Little Pine fault has a shallow to moderate dip and places Franciscan basement over Plio-Pleistocene age Paso Robles Formation (Dibblee, 1966). These faults have Tertiary strike-slip histories (Hall, 1981), but may accommodate reverse or reverse-oblique movements in the current contractional regime. Late Quaternary surface displacements and/or active folding have not been documented; however, the Paso Robles Formation is strongly folded along this trend (Dibblee, 1966; Hall, 1981; R.A. Schweickert, oral communication).

The available data do not show any suggestive geomorphic or Quaternary evidence for capability of the Santa Maria River fault, although fluvial erosion could have destroyed evidence for surface activity. Along this zone, PG&E (1988 and docket amendments) indicates evidence that there may be disruptions of Quaternary marine terraces along the southeastward projection of the Wilmar Avenue fault and the Oceano fault. Further southeast, the pronounced deformation of the Paso Robles Formation suggests that the Foxen Canyon and Little Pine faults may be capable, but this zone could connect with the Orcutt and Casmalia structures described by Clark (1991).

2.1.8.3 Casmalia-Orcutt Zone

The Casmalia Range is a fault-bounded anticlinal range in the northwestern part of the Santa Maria basin (Figs. 2-1 and 2-2). The west-northwest-trending Casmalia Range and its continuation to the east, the Solomon Hills, are underlain by a series of en echelon anticlines which together define the Casmalia-Orcutt anticlinal trend. The Orcutt Frontal fault, also referred to as the Casmalia fault, is interpreted by Clark (1991) as a seismically active blind thrust or reverse fault. The fault underlies the northeast margin of the Casmalia Range and Solomon Hills and separates these ranges from the adjacent Santa Maria Valley syncline. The Lions Head fault is a 70° northeast-dipping to vertical fault on the southwest margin of the Casmalia Range which accommodates minor reverse displacement in the present contractional regime. The Orcutt Frontal and Lions Head faults are capable faults (Clark and Slemmons, 1990).

As noted in the previous section, field and aerial reconnaissance observations suggest that this trend and possible extensions eastward to the Foxen Canyon fault show evidence of mid- to late-Quaternary neotectonic folding and faulting. This suggests that the activity of this zone extends eastward from the Hosgri fault to the eastern part of the onshore Santa Maria basin.

The thesis studies by Clark (1991) of Quaternary marine and fluvial terraces in the Casmalia Range indicate the following:

(1) Shoreline angle data from a flight of emergent marine terraces between the Lions Head fault and Point Sal indicate that the Casmalia Range has been uplifted at a late Quaternary rate of 0.14 to 0.17 mm/yr (similar to the 0.19 to 0.21 mm/yr uplift rate of the San Luis Range).

(2) The Lions Head fault is a steep, northeast-dipping reverse fault with an earlier history of strike-slip movement. A normal fault in the hanging wall of the Lions Head fault offsets the 5e (120 ka) marine terrace by 1.4 m vertically. Overall vertical displacement of middle and late Quaternary marine terraces across the Lions Head fault is no more than 0.012 to 0.017 mm/yr.

(3) The Orcutt Frontal fault (or the Casmalia fault) is a blind thrust or reverse fault along the range front and may have associated minor surface faulting. Late Quaternary alluvial deposits are disrupted by folding and minor surface faulting along this trend.

(4) Uplifted and deformed marine and fluvial terraces within and on the margins of the range indicate that the predominant style of late Quaternary, and probably middle Quaternary surface deformation is uniform, block-style range uplift, with significant localized folding occurring along the Orcutt Frontal fault. This pattern of uplift can be interpreted in two ways: (1) uplift of a rigid structural block along high angle reverse faults, with localized drag folding at the surface on the Orcutt Frontal fault; or (2) fault-propagation folding of the Casmalia Range above a listric blind thrust or reverse fault.

(5) Based on the uplift rate of marine terraces and assuming 30^0 and 60^0 fault dips, the Orcutt Frontal fault has an estimated minimum late Quaternary dip slip rate of 0.16 to 0.34 mm/yr.

2.1.9 Offshore Santa Maria Basin

The offshore Santa Maria basin is bounded by the Hosgri fault on the east and the Santa Lucia Bank fault on the west (Fig. 2-2). It is characterized by north-northwest-striking thrust and reverse faults and related folds which are subparallel to the Hosgri fault (PG&E, 1988; McCulloch, 1989). The offshore Santa Maria basin appears to be comprised of three general tectonic domains (PG&E, 1988, Fig. 2-10):

(1) The Piedras Blancas anticlinorium, with folds and faults that are somewhat oblique to and abut against the Hosgri fault. Quaternary tectonic activity and historical seismicity suggest that this is a moderately active region.

(2) The zone between the Piedras Blancas anticlinorium and the distributed folds south of Point Sal. This zone appears to be characterized by only minor

Quaternary deformation, as suggested by seismic reflection data and historical earthquake activity.

(3) The zone of distributed folds and thrust faults, with possible listric faulting, between Point Sal and Point Pedernales. These structures developed during the Tertiary, but at least some appear to show Quaternary activity and distributed historical seismicity (Fig. 2-6). Historically, this region has had infrequent moderate and large earthquakes and may be the source of the 1927 Lompoc earthquake of M_S=7.0. The epicentral location appears to be near or at the western boundary of the Offshore Santa Maria basin and the Santa Lucia Bank fault .

2.1.10 Oceanic-West Huasna faults

The Oceanic-West Huasna fault (Fig. 2-3) is believed to locally offset late Pleistocene deposits (Weber, 1979; Buchanan-Banks and others, 1978; Hart and others, 1986). A strong alignment of earthquake epicenters along the Oceanic-West Huasna fault trend (Fig. 2-6) suggests that this is a tectonically active zone of reverse and reverse-oblique-slip faulting. The Oceanic fault's geomorphic position near the base of the steep Santa Lucia Mountain range front, marked by many landslides, suggest recent vertical fault movements. This zone appears to be a seismically active 30 km "left-step" in activity between the San Gregorio/Hosgri activity in the San Simeon area to the Rinconada fault. The possible capability of the step-over zone received special field, aerial reconnaissance, and aerial photographic investigations by UNR for active surface faults, but none were identified. The Oceanic fault is difficult to assess, as it is extensively covered by landslide deposits and few Quaternary deposits are present along its trace. In addition, after repeated examinations, what appeared to be faceted spurs along the steep escarpment where the Oceanic-West Huasna fault is crossed by U. S. Highway 101 were determined to be of lithologic rather than structural origin. In the area northeast of San Luis Obispo, the main fault shows no geomorphic evidence of recent lateral or vertical separation.

2.1.11 Nacimiento fault zone

The Nacimiento fault zone, together with the southern portion of the Rinconada fault (Figs. 2-1 and 2-2), comprise the complex tectonic boundary between Franciscan basement and granitic and crystalline metamorphic basement of the Salinian block (Page, 1970). The Nacimiento fault zone consists of numerous mainly northwest-striking faults with long, complex histories of reverse, strike-slip and normal displacements (Page, 1970, 1981; Hart, 1976; Dickinson, 1983). Quaternary fault movements have not been recognized. However, low to moderate seismic activity along the trend of the Nacimiento fault zone (Richter, 1969; Poley and others, 1987) suggests that some strain is currently being released along or near the fault. The lack of geomorphic features that are characteristic of faults with late Quaternary movements suggests a very low rate of activity.

2.1.12 Rinconada fault

The Rinconada fault, and its northern extensions, the Reliz and King City faults, are important elements of the San Andreas fault system (Fig. 2-2). The Rinconada fault is believed to have accommodated about 60 km of Neogene right-lateral displacement and 18 km of post-Miocene offset (Dibblee, 1976). Major truncations and offsets of the Plio-Pleistocene Paso Robles Formation along the Rinconada and Reliz faults indicate movements well into the Pleistocene (Dibblee, 1976; Hart, 1976).

Moderately well developed geomorphic expressions of active faulting and apparent offsets of older alluvium along portions of the Rinconada fault further suggest late Quaternary and possibly Holocene activity (Hart, 1976). Field and low-sun-angle aerial reconnaissance by UNR in the vicinity of Atascadero show apparent late Quaternary right-lateral offset of small-scale ridges and drainage lines along the fault and confirmed the conclusions of Hart (1976) for the activity of this section of the fault. No evidence for late Quaternary activity was noted north of Atascadero.

The King City and Reliz faults' geomorphic positions at the base of the steep Sierra de Salinas range front indicate significant vertical Quaternary displacements. However, careful examination of outcrops along Arroyo Seco Creek which crosses the Reliz fault showed a conspicuous right-reverse-oblique fault that does not offset late Quaternary terrace gravels.

2.1.13 Transverse Ranges

The Transverse Ranges are characterized by moderate to high rates of active tectonism. Extensive north-south contraction is accommodated by west-trending reverse and left-lateral reverse-oblique faulting and associated folding. A relatively high frequency of damaging earthquakes with moderate and large magnitudes (M=5.0 to 7.2) have occurred in historical time, including both surface faulting and blind thrust events. Earthquakes in this region typically have north-northeast-oriented P-axes and reverse and reverse-oblique focal mechanisms.

2.2 Regional Seismicity

2.2.1 Maximum Historical Earthquakes

Coastal central California is an active plate margin setting with a history of damaging earthquakes, most notably along the San Andreas fault and in the Transverse Ranges. Historical earthquakes with $M \geq 5.0$ are shown in Figure 2-6. The locations of pre-instrumental events are poorly constrained and instrumental events earlier than about 1970 are only approximately located (within 10 or 20 km) due to incomplete seismograph network coverage.

The largest historical earthquake in the coastal central California region is the 1927 Lompoc Earthquake of M_s=7.0. The location of the epicenter has been controversial (Gawthrop, 1978b; Evernden and others, 1981; and Hanks, 1979). PG&E attribute the 1927 earthquake to the Santa

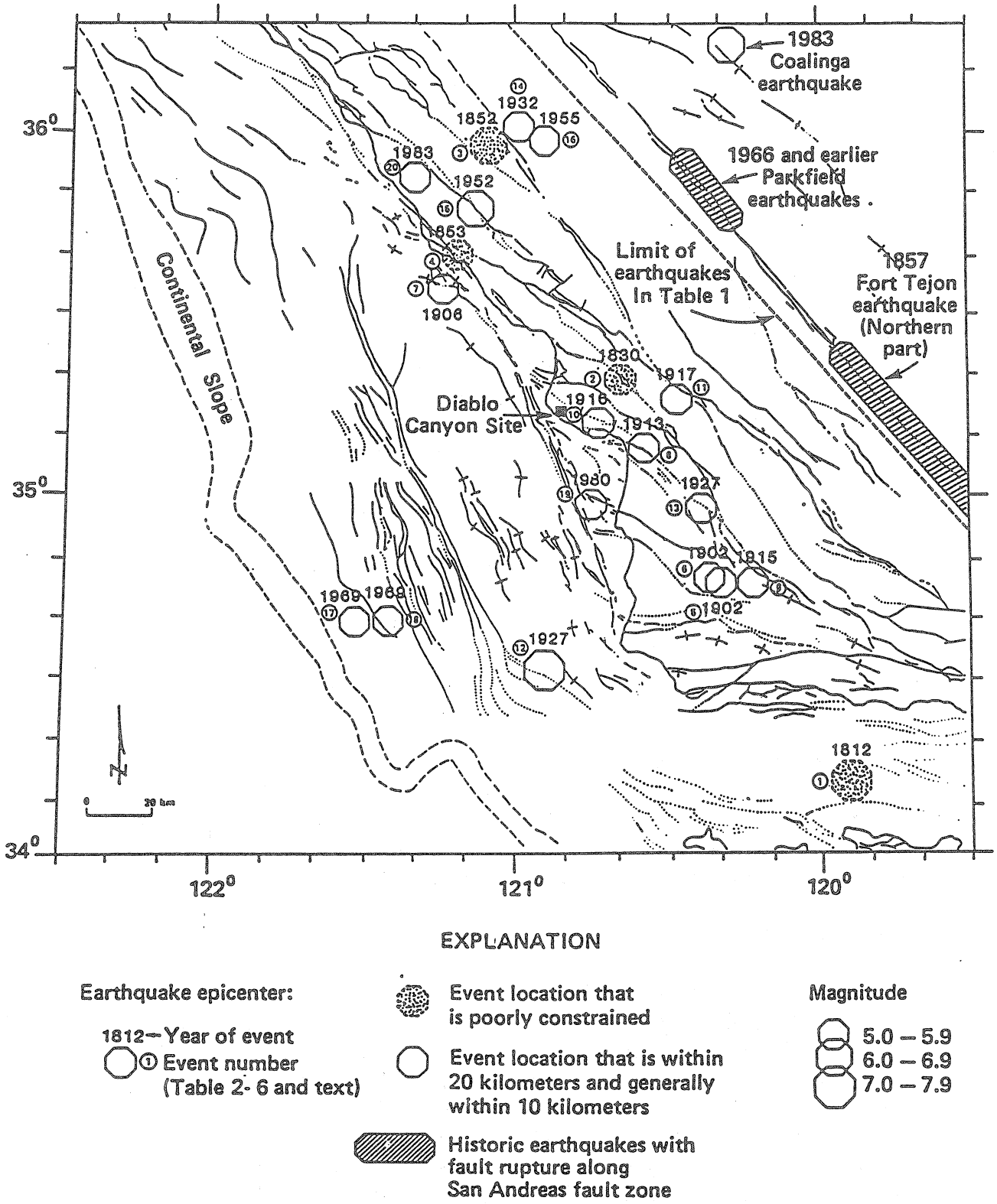


Figure 2-6. Historical earthquakes of magnitude 5 and larger, 1812-1988, in south-central coastal California (from PG&E, 1988).

Lucia Bank fault. Other prominent historical earthquakes in the region include the Los Alamos earthquakes of 1902 and 1915 (M= 5.4 and 5.8, respectively), the 1952 Bryson earthquake (M_L=6.2), the 1969 Santa Lucia Bank earthquakes (M_L=5.4 and M_L=5.6), the 1980 Point Sal earthquake (M_L=5.1), and the 1983 San Simeon earthquake (M_L=5.2). No historical earthquakes with M>5.0 have been assigned unequivocally to the Hosgri fault, Los Osos fault, or the southwestern boundary zone of faults.

2.2.2 Instrumental Seismicity Patterns

Seismic activity during the period from 1980 to 1988 is shown in Figure 2-7. Figure 2-7 indicates a distributed pattern of contemporary plate margin deformation. Earthquake epicenters are prominently aligned along the creeping segment of the San Andreas fault and scattered in areas west of the fault. Epicenter clusters exist along sections of the San Gregorio-Hosgri fault, the Nacimiento fault, and in a broad belt from Monterey to Cholame (Poley and others, 1987). There is an especially conspicuous broad alignment of seismicity that crosses from beneath the Santa Lucia Range along the Nacimiento and Oceanic-West Huasna faults to the Rinconada fault segment (Areas D and E on Figure 2-7). There is also a zone of activity at or near the Piedras Blancas Anticlinorium, that may connect with the northern end of the Santa Lucia Bank fault.

Epicenter trends along the San Gregorio-Hosgri fault, while generally linear, do not define clearly vertical or inclined hypocenter alignments (Savage and McLaren, 1987). The diffuse activity, such as the cluster of epicenters northeast of San Simeon, reflects broad, internal deformation of weak basement rocks, and/or fault slip on inclined reverse or reverse-oblique fault planes and associated folds (Eaton, 1985a). Relatively dense epicenter concentrations also occur in the Transverse Ranges.

Background seismicity in the San Luis Range/Santa Maria basin occurs at a lower level than in the adjacent Transverse Ranges and the more active portions of the southern Coast Ranges. Seismicity during the period from 1980 to 1988 showed widely scattered activity, with clusters of seismicity occurring on the Los Alamos-Orcutt Frontal fault trend and along the Los Osos fault near its intersection with the Hosgri fault (PG&E, 1988).

2.2.3 Earthquake Focal Mechanisms

Compilations of earthquake focal mechanisms in coastal central California by Eaton (1984, 1985a and 1985b), Dehlinger and Bolt (1987), and PG&E (1988) indicate earthquakes with right-slip focal mechanisms, and north-oriented P-axes along the San Andreas fault (Fig. 2-8). These are flanked by broad zones of contractional, oblique-slip, and strike-slip faulting, with predominantly northeast-oriented P-axes. Eaton's (1984) fault-plane solution for the 29 August 1983 San Simeon earthquake (M_L=5.2) suggests right-reverse-oblique displacement on a N39°W-striking, 55°NE-dipping fault plane, possibly one of the faults of the San Simeon-Hosgri system. Focal plane solutions for the 29 May 1980 Point Sal earthquake and the 23 September 1982 Santa Maria earthquake (M_L=4.0) indicate reverse and left-reverse-oblique slip, respectively, on west-northwest-trending fault planes (Eaton, 1984). Focal plane solutions for

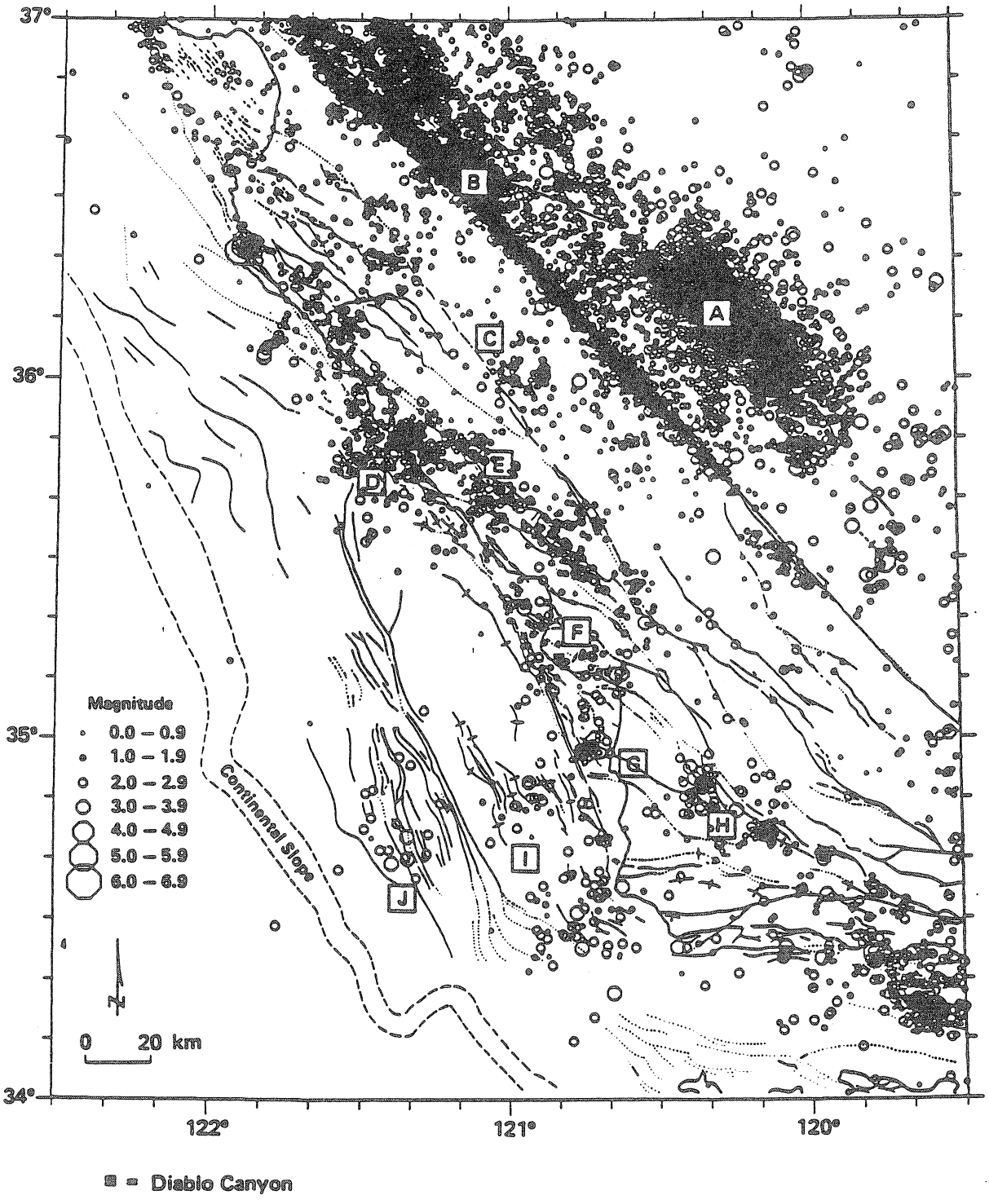


Figure 2-7. Map of seismicity data from the U. S. Geological Survey and California Institute of Technology, January 1, 1980, through May 31, 1988 (from PG&E, 1988).

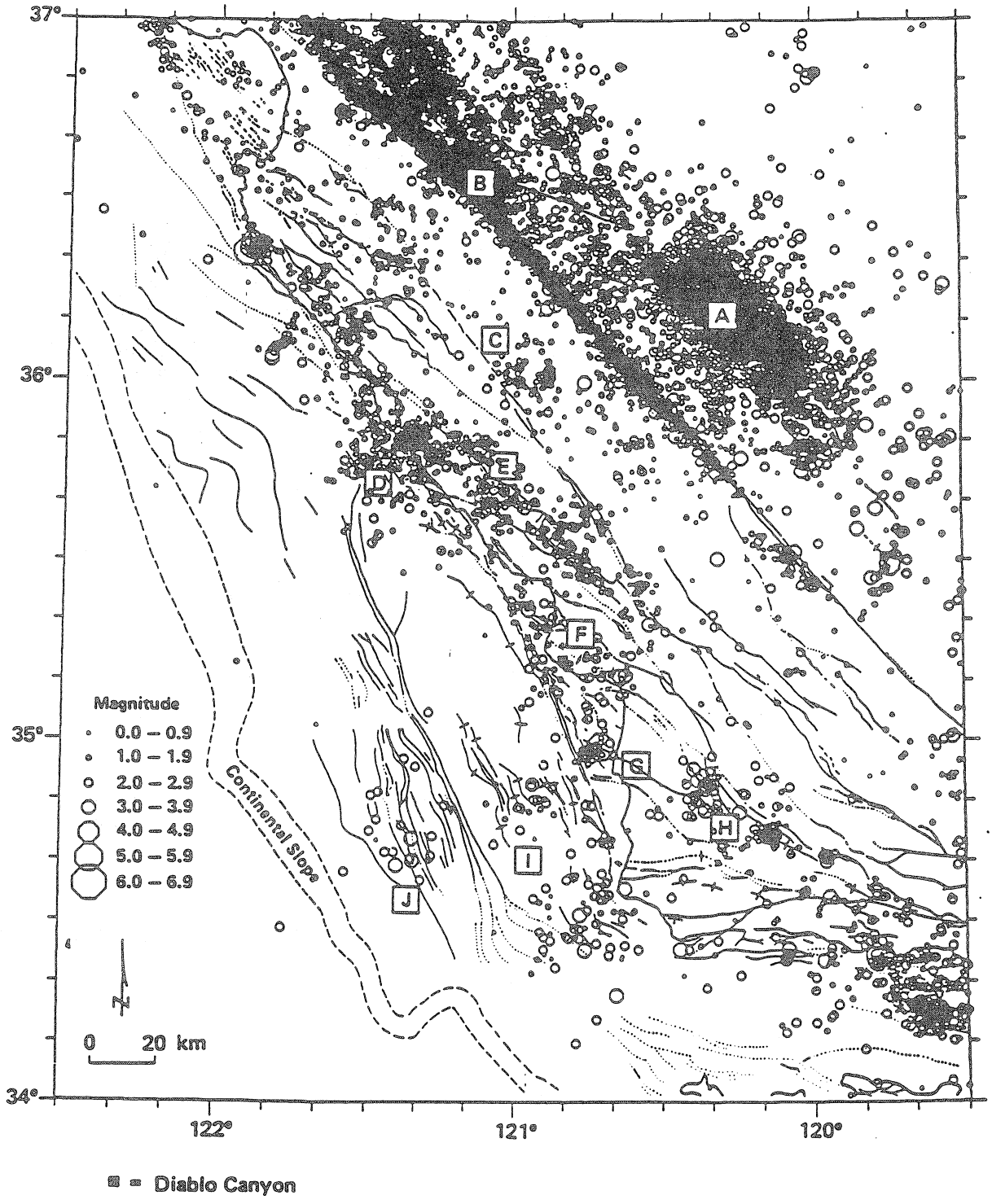


Figure 2-8. Compilation of focal mechanisms for earthquakes of magnitude 3 and greater in the south-central coastal California region (from PG&E, 1988).

events on the Hosgri fault zone vary from right-lateral, strike-slip to reverse-oblique-slip (PG&E, 1988, Figs. 2-30 and 2-36).

2.2.4 1927 Lompoc Earthquake

The 1927 Lompoc earthquake was reviewed by UNR staff. The magnitude was approximately M_S=7.0 (PG&E, 1988 and docket amendments) and the epicenter was in or near the edge of the offshore Santa Maria Basin (Fig. 2-8). Although the exact location of the epicenter is uncertain, the seismological data and the small tsunami that was generated indicate that the epicenter was west of the Hosgri fault and was accompanied by uplift of part of the continental shelf, possibly with thrust faulting and/or folding. The epicenter either appears to be along the Santa Lucia Bank fault or an unidentified structure in the southwestern part of the offshore Santa Maria Basin. The event may provide a lower bound MCE for earthquakes within or along the edge of the province.

2.2.5 Earthquake Limitations of the Historical Earthquake Record

The historical earthquake record in California, while useful for characterizing styles of contemporary deformation, spans less than 200 years and provides only a partial indication of seismic hazard. The absence of earthquakes on many recognized active faults and fault-related folds in California reflects recurrence intervals greater than the historical record, rather than lack of potential for future damaging earthquakes.

3.0 DETERMINATION OF MAXIMUM CREDIBLE EARTHQUAKE (MCE)

3.1 Introduction

Estimations of the potential sizes of future earthquakes are essential for providing input data for the determination of the Maximum Credible Earthquake (MCE) for seismic source determinations and for probabilistic studies. Earthquake size estimations commonly include a variety of approaches using several methods, including among others: maximum historical earthquake method, paleoseismic approach, and seismic source characterization (Slemmons and dePolo, 1986; Schwartz and Coppersmith, 1986, Schwartz, 1988; dePolo and Slemmons, 1990).

PG&E utilized an integrated, multi-factor approach for assessing MCE values for the site. Their methodology is conservatively selected, clearly presented, and the results are technically sound. The use of multiple techniques leads to a more reliable estimate of MCE than use of any single method. This method was evaluated by NRC for previous studies, such as for the San Onofre Nuclear Generation Plant in southern California.

The Diablo Canyon LTSP has a more extensive geological, geophysical, and seismological data base for characterizing potential seismic sources than has been previously available for other nuclear power plants. The investigation led to identification and characterization of previously unrecognized capable faults, greatly reduced geologic uncertainties, and used all possible types of geophysical and seismological studies to supplement the geologic record.

3.2 Empirical Relations

The basic concept relating the size or magnitude of an earthquake to fault parameters such as rupture length and surface displacement evolved from the initial analysis of Tocher (1958) to more sophisticated empirical relations between earthquake magnitude and total fault length, fault type, surface and subsurface rupture length, fault area, and average and maximum displacement per event. Empirical regressions include two earthquake size measures: surface magnitude (M_S) (Slemmons, 1982; Slemmons and Chung, 1982; Bonilla and others, 1984; Slemmons and others, 1989) and moment magnitude (M_W) (Kanamori, 1977; Hanks and Kanamori, 1979; Wyss, 1979; Wesnousky, 1986).

In order to use a multiple approach, PG&E uses a suite of regressions for their analyses (PG&E, 1988). The UNR analysis also uses a similar, but independent multiple factor approach (Table 3-1). The regressions of Slemmons and others (1989) are preferred for the UNR analysis because they include high quality, well documented, events for the data base. The analysis is based on the observation that the energy release for similar source parameters is comparable (with results that are within 0.1-0.2 magnitude units value) for strike-slip, normal-slip, and reverse-slip faults for both contractional and extensional tectonic settings. Thus, the inclusion of a much larger worldwide data base for all fault types is an improvement over the previously used data base that was divided into several individual fault types. The advantage of this regression analysis for the Diablo Canyon LTSP is that the conflicting models for the Hosgri fault, pure strike-slip, oblique-slip, and thrust/reverse-slip, all have similar magnitudes for a given rupture length. Thus the type of tectonic model for the Hosgri fault is not critical for the determination of the MCE at DCNPP. Table 3-1 shows the results from different widely used regressions using an arbitrary 50 km rupture length.

3.3 Moment Magnitude Regressions

Surface wave magnitude (M_S) and moment magnitude (M_W) values are similar for the range of magnitudes between 6 and 8, a relationship recognized by Kanamori (1983). Preliminary analyses by Wells and others (1989) and Zhang and others (1989) indicate that the use of moment magnitudes instead of surface magnitudes gives similar results, but has a somewhat better statistical basis than previously derived regressions, with improved coefficients of correlation and lower standard deviations. The M_W regressions presented by PG&E at Geology/ Geophysics Workshops have somewhat better statistical results for the MCE analysis. They are not used in this report, however, because the regressions are preliminary, have not received peer review and provide similar MCE magnitudes to the M_S magnitudes derived from previous regressions.

3.4 Fault Segmentation

Fault segmentation models were first proposed by Schwartz and Coppersmith (1984) for the Wasatch and San Andreas faults, and are now widely used for seismic hazard assessments (Schwartz, 1988; dePolo and others, 1989; Knuepfer, 1989). The fault segmentation method

is an attempt to quantify the length of a fault that may rupture during individual seismic events, using physical information about the fault or fault zone. The concept is based on the observation that many ruptures initiate or terminate at fault discontinuities or segmentation points along faults. Discontinuities fall into several categories: geometric, structural, behavioral, paleoseismic, geomorphic, geological, geophysical, and rheological (dePolo and others, 1989). It is generally regarded that segmentation points are best defined by behavioral characteristics, and by coincidence of several types of criteria for segmentation.

The fault segmentation method provides a relatively simple approach that dovetails with the idea of characteristic events (Schwartz and Coppersmith, 1984; 1986). Although segmentation and characteristic fault rupture models are becoming widely accepted and used, there are some problems in their application (dePolo and others, 1989; Knuepfer, 1989). Almost one-half of historical surface rupture endpoints are at points not coinciding with segmentation points that could have been identified prior to the rupture. Further, some discontinuities or segmentation points are ruptured through, and multiple segments may rupture during a single event. Despite uncertainties, however, the segmentation method should be included as one of the major methods of analysis. The use of segmentation models is much more valid than the arbitrarily assumed one-half or other fractional fault rupture lengths used in older earthquake hazard evaluations.

3.5 Logic Trees

Logic trees, described in detail by PG&E (1988, p. 3-2 to 3-8), enable uncertainties to be assigned at each stage of the earthquake estimation process. The logic tree's multiple branches allow incorporation of a full range of expert opinions into the estimate. This is particularly important for the Hosgri fault, where fault parameters such as fault geometry and fault style are interpreted differently by different workers.

Logic trees are used in the LTSP for probabilistic seismic hazard analyses, and for assessment of the Hosgri deterministic earthquake. PG&E relied on the professional judgments of specialists to assign weights to various source parameters. Most of the values are reasonable, complete, and consistent with available data bases. Because this is one of the most important parts of seismic hazard assessment, all of the PG&E logic tree assessments were reviewed and where the UNR preferred or alternative values for fault type, length, maximum displacement, and magnitude are substantially different, a discussion is included in sections 4 and 5.

The logic tree weightings used in this UNR report were first independently selected by the two authors. This was followed by discussion of the relative importance and uncertainties of the factors influencing the weighting values. Final values shown in this report were then determined. In all cases there was agreement on the final value.

3.6 Maximum Credible Earthquake (MCE)

The use of the various approaches for determination of the MCE is discussed by PG&E (1988) and dePolo and Slemmons (1990). dePolo and Slemmons (1990) use the following definition:

> The term "maximum credible earthquake" (MCE) means the largest or maximum earthquake that appears capable of occurring in an area or along a fault (California Division of Mines and Geology, 1975). The maximum credible earthquake is a time-independent earthquake...

At the present time, there is no universally accepted definition or approach for determining the MCE. Most analyses are based on judgement, or involve assumptions as to the seismic source, or have the addition of a fractional earthquake magnitude to allow for uncertainties in the historical record or in the assumption used. In most cases, use of the linear regression between fault rupture parameters and the earthquake magnitude values yields a best fit and lower magnitude value, rather than the MCE value. The estimation of the higher MCE value is commonly obtained by arbitrary selection of a higher magnitude, by assumption of the magnitude for given earthquake segments rupturing, or by a fractional fault length rupturing. The use of one full segment rupture may lead to a characteristic earthquake. However, many large earthquakes with magnitudes greater than about M=7 are accompanied by rupture of two or more segments (Knuepfer, 1989; dePolo and others, 1989). Examination of regression relations using a rupture of two segments commonly leads to results that are about 1/4 to 1/3rd unit of magnitude higher than for rupture of one segment.

PG&E uses for its MCE or deterministic earthquake magnitude for the Hosgri fault zone (PG&E, 1988, Table 3-1) a mean value obtained from a logic tree analysis distribution and arbitrarily adds 0.2 magnitude. The method used in the UNR analysis uses a similar logic tree approach based on estimated rupture lengths for the Hosgri fault, with a variable length for one, two and three fault segment lengths. The result is similar to that obtained by the simple assumption of rupture of two adjoining fault segments of the Hosgri fault, including the segment nearest the DCNPP site.

4.0 SOURCE CHARACTERIZATION OF CAPABLE FAULTS SIGNIFICANT TO DCNPP

4.1 Introduction

Discussions in this report are limited to faults and folds that are capable according to the definition in the Federal Code of Regulations, 10 CFR 100, Appendix A. There are several significant capable faults near the DCNPP. Specifically, these are the Hosgri fault zone, the Los Osos fault zone, and faults at the southwestern boundary of the San Luis/Pismo block, including the San Luis Bay, Olson (or Olson trace), Wilmar Avenue, and Pecho faults (Fig. 2-3). Other, more distant capable faults are excluded from this discussion, including the Rinconada fault zone and several faults in the onshore Santa Maria basin, such as the Orcutt Frontal (Casmalia), Lions Head, and Los Alamos faults.

Table 3-1. Earthquake Magnitude (M_S) for an Assumed 50 Km Rupture Length

REGRESSION	MAGNITUDE (M_S)
Strike-Slip Faults	
Slemmons (1982) $M_S = 1.40 + 1.17$ Log L	6.9
Bonilla and others (1984) $M_S = 6.23 + 0.61$ log L	7.3-
*Slemmons and others (1989) $M_S = 5.73 + 0.85$ Log L	7.2-
Reverse-Slip Faults	
Slemmons (1982) $M_S = 2.021 + 1.142 \log_{10}$(Rupture Length in m)	7.3-
Bonilla and others (1984) $M_S = 5.71 + 0.916 \log_{10}$ (Rupture Length in km)	7.4-
*Slemmons and others (1989) $M_S = 5.10 + 1.29$ Log L	7.3-
All Events, for All Fault Types and Both Contractional and Extensional Settings	
Wyss (1979) $M_S = 4.15 + \log_{10}$(Rupture Area in km^2)	6.9
Slemmons (1982) $M_S = 2.06 + 1.07$ Log L	7.1-
Bonilla and others (1984) $M_S = 6.04 + 0.71$ Log L	7.2+
Wesnousky (1985) $M_S = 5.13 + 1.15$ log L	7.1
*Slemmons and others (1989) $M_S = 5.39 + 1.03$ Log L	7.1+
Mean	7.2-

* This regression is preferred to Slemmons (1982), as it has a better data base.

4.2 Hosgri Fault

4.2.1 Fault Continuity

PG&E in the LTSP and related documents makes strong arguments, supported by extensive geological and geophysical data, that the Hosgri fault zone is a throughgoing, linear, steeply dipping, strike-slip fault. Previous studies of the Hosgri fault are summarized by PG&E (1988 and docket amendments). In this report the Hosgri fault zone is considered to be part of an integrated system that includes the San Gregorio, Sur, and San Simeon faults. The system splays southward from the San Andreas fault near Bolinas to at least Point Pedernales, opposite the western Transverse Ranges (Fig. 2-2). Faults and folds on the east side of the San Gregorio-Hosgri fault are generally truncated by the fault system, whereas most faults and folds in the Sur and offshore Santa Maria basins are parallel or subparallel to the system (PG&E, 1988; McCulloch, 1989).

PG&E (1988 and docket amendments) maps the northern termination of the Hosgri fault near the Cambria/Point Estero region, where the fault appears to die out and has an en echelon right-step relation with the San Simeon fault. There is no universal agreement as to the location of the southern termination of the fault. However, it has been suggested that there are several possible neotectonic splays or "horsetails" inland along fault and fault-related fold trends such as the Casmalia-Orcutt, Lions Head, and Santa Ynez River zones. This splaying or branching southeastward into the Transverse Ranges, rather than by simple right-slip fault splays, involves both a change in orientation and to reverse-slip faults or folds.

This report assigns a 100 percent probability for continuity and a 410 km length from Bolinas southward to Point Pedernales, but it is possible that the fault zone extends as far as the Santa Barbara Channel. The fault zone appears to die out, or has relatively low slip rates and poor structural expression in the region opposite Point Pedernales.

4.2.2 Fault Geometry

Figure 4-1 is a depth-corrected seismic reflection profile across the Hosgri fault near the DCNPP to illustrate some aspects of the fault's geometry. The Hosgri fault typically consists of two or three subparallel traces: (1) an eastern high angle trace, (2) a western high angle trace generally 1 or 2 km from the eastern trace, and (3) a low angle, less continuous trace which appears to merge with the western high angle trace at depths of 2-4 km on many seismic reflection profiles. The eastern trace commonly has vertical to steeply dipping faults in the upper 1 km decreasing to dips of 60°-70° at depths of 2-4 km (Fig. 4-1) and may be a few kilometers east of the easternmost surface trace at the base of the seismogenic zone. The traces are associated with reflector offsets, seafloor scarps, and disruptions of post-Wisconsinan age sediments along the entire length of the Hosgri. The eastern trace appears to be the main and most active trace, with many geomorphic and stratigraphic indications of Quaternary activity. The western trace commonly dips at moderate angles to the east or has associated folds in the uppermost sediments. This trace generally appears to be inactive or has a low rate of activity. Low angle

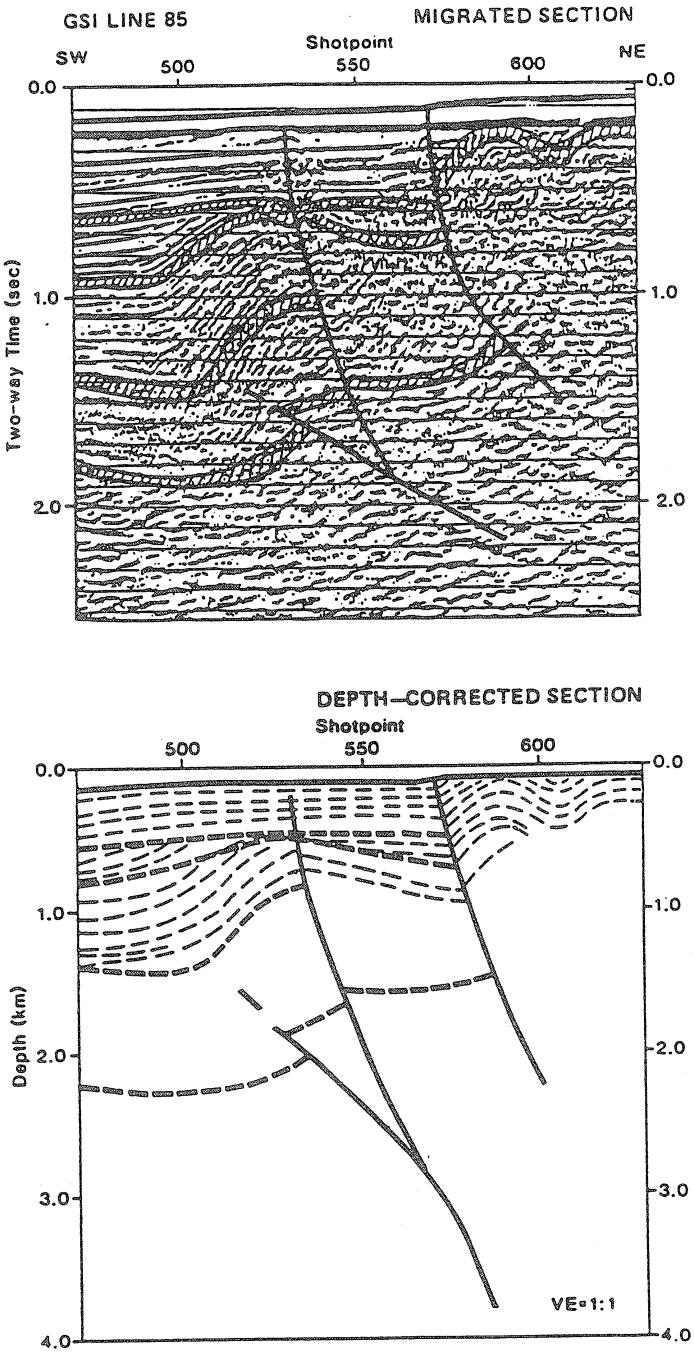


Figure 4-1. Depth corrected seismic reflection record across the Hosgri fault offshore from Point Buchon (from PG&E, 1988).

Depth-corrected section to illustrate true dip of fault plane. Note truncation of shotpoint 525 and tight folding east of fault zone.

faults dip northeastward and may be associated with upper plate fault-propagation-style folds (PG&E,1990, GSG-1). These two branches of the Hosgri fault may be strain partitioned with the strike-slip component distributed mainly on one trace, generally the eastern trace, with the contractional component on the other trace (PG&E docket amendments, and Lettis and Hanson, 1991).

The Hosgri fault dips northeastward at a moderate to high angle, as shown on most seismic reflection profiles. These dips are estimated from depth-corrected profiles, and in general, the high angle traces have dips between 60° and 80° in the upper 2-4 km (PG&E, 1988, Plate 6). Significantly lower Hosgri fault dips may be precluded by the hypocenter location of the 1980 Point Sal earthquake, which is attributed to the Orcutt Frontal or Casmalia fault east of the Hosgri fault. The USGS location constrains the Hosgri fault to a dip of >45°; PG&E's relocation of the Point Sal earthquake constrains the Hosgri fault to a dip of >70°.

The UNR review of the data on fault geometry at seismogenic depth led to the selection of a 0.80 probability for a 70° geometry and a 0.10 probability for 90° and 45° geometries.

4.2.3 Fault Type

PG&E (1988 and docket amendments) maintains that the active Hosgri fault is a linear, vertical to steeply northeast-dipping strike-slip fault. Low angle faults west of and parallel to the high angle traces of the Hosgri are interpreted as mainly inactive structures inherited from a previous contractional regime. Another alternative considered by PG&E is that oblique strain is partitioned at the surface into strike-slip faulting on high angle fault traces and thrust/reverse-slip and associated folding on low angle faults, with strike-slip deformation being the dominant style of deformation (PG&E, 1990, GSG-2). This interpretation is preferred in the UNR analysis, at least for parts of the fault zone. Other interpretations in the literature and discussed at NRC/PG&E meetings and data audits include both oblique and purely thrust fault types (e.g., Crouch and others, 1984).

The reviewed data strongly suggest that the Hosgri fault is connected to the San Gregorio-Sur-San Simeon faults. The San Gregorio-Hosgri system shows clear Holocene evidence of mainly strike-slip deformation where it trends onshore (Weber and Lajoie, 1979a, 1979b; Weber, 1983; PG&E, 1988), and has remarkable continuity and linearity between the San Andreas fault and its southern termination near Point Pedernales. On the other hand, blind thrust faults along the western trace of the Hosgri fault zone show some evidence of tilting or folding of upper Pliocene or Quaternary sediments along the entire length of the Hosgri fault (PG&E, 1988, Plate 6; PG&E, 1990, GSG-1) and elsewhere on the San Gregorio-Hosgri system (Greene and others, 1973; Weber and Lajoie, 1979b). This indicates that the system has a subordinate reverse-slip component. A right-reverse slip component is also indicated by earthquake focal mechanisms (Fig. 2-8). PG&E accommodates some of the uncertainty of fault type by defining strike-slip deformation as having a >2:1 ratio of strike-slip to vertical deformation, and by considering strike-slip, oblique-slip, and thrust cases in their probabilistic and deterministic analyses.

The UNR project staff believes that the late Quaternary behavior of the Hosgri fault is predominantly strike-slip, but with a significant thrust/reverse component. The UNR analysis generally agrees with the PG&E relative weightings for fault type: 0.65 for strike-slip, 0.3 for oblique-slip, and 0.05 for reverse-slip/thrust. However, the UNR analysis considers the Hosgri fault to dip at a high angle (~70°), rather than PG&E's preference for a 90° dipping fault. This value is similar to the 60-75° reported by Castillo and Ellsworth (1991) for the Maacama strike-slip fault.

4.2.4 Fault Length

The total length of the San Gregorio-Hosgri fault system from the San Andreas fault intersection near Bolinas Bay to Point Pedernales is ~410 km (PG&E, 1988). The Hosgri fault, as defined by PG&E (1988), is a section of the total fault system that extends ~110 km from the offshore region near Point Estero to near Point Pedernales. South of this point, the Hosgri fault may die out or merge with more westerly-trending structures of the Transverse Ranges or the Santa Barbara Channel. Steritz and Luyendyk (1991) map the Hosgri fault continuing to the Santa Barbara Channel, giving a total length of ~450 km for the system. If the Steritz and Luyendyk (1991) model is correct, then the fault length is greater than 410 km. The 410 km total length value is used for this analysis based on the currently unresolved character of seismic reflection profiles south of Point Pedernales and the geodetic work of Feigl and others (1990), which shows that a station near Point Arguello is moving with the Pacific plate.

4.2.5 Segmentation

The segmentation model of PG&E (1988) for the Hosgri fault is shown in Figure 4-2. The model defines several "segmentation points" along the fault, based mainly on geometric data (fault intersections, stepovers) and apparent behavioral changes (changes in vertical separation rates). The following comments apply to the PG&E segmentation points:

(1) Cambria stepover: The segmentation point at the north end of the Hosgri fault is placed by PG&E at the Cambria stepover (1988 and docket amendments). This segmentation point is well supported by the evidence compiled by PG&E. The UNR study suggests the alternative possibility that the point is at the intersection with the Piedras Blancas Anticlinorium trend. This would increase the length of the Northern Reach of the Hosgri fault by several kilometers.

(2) Los Osos fault intersection: Evidence for this segmentation point is supported by several independent lines of data: a 11° bend in the fault trace, a change in trace complexity to the north and south, and an offshore fold belt north of Los Osos. Consideration of a southwesterly dip of the Los Osos fault would move the segmentation point at seismogenic depth to a few kilometers southwest of the position shown by PG&E. This decreases the length of the San Luis/Pismo reach somewhat, but increases the length of the Northern reach.

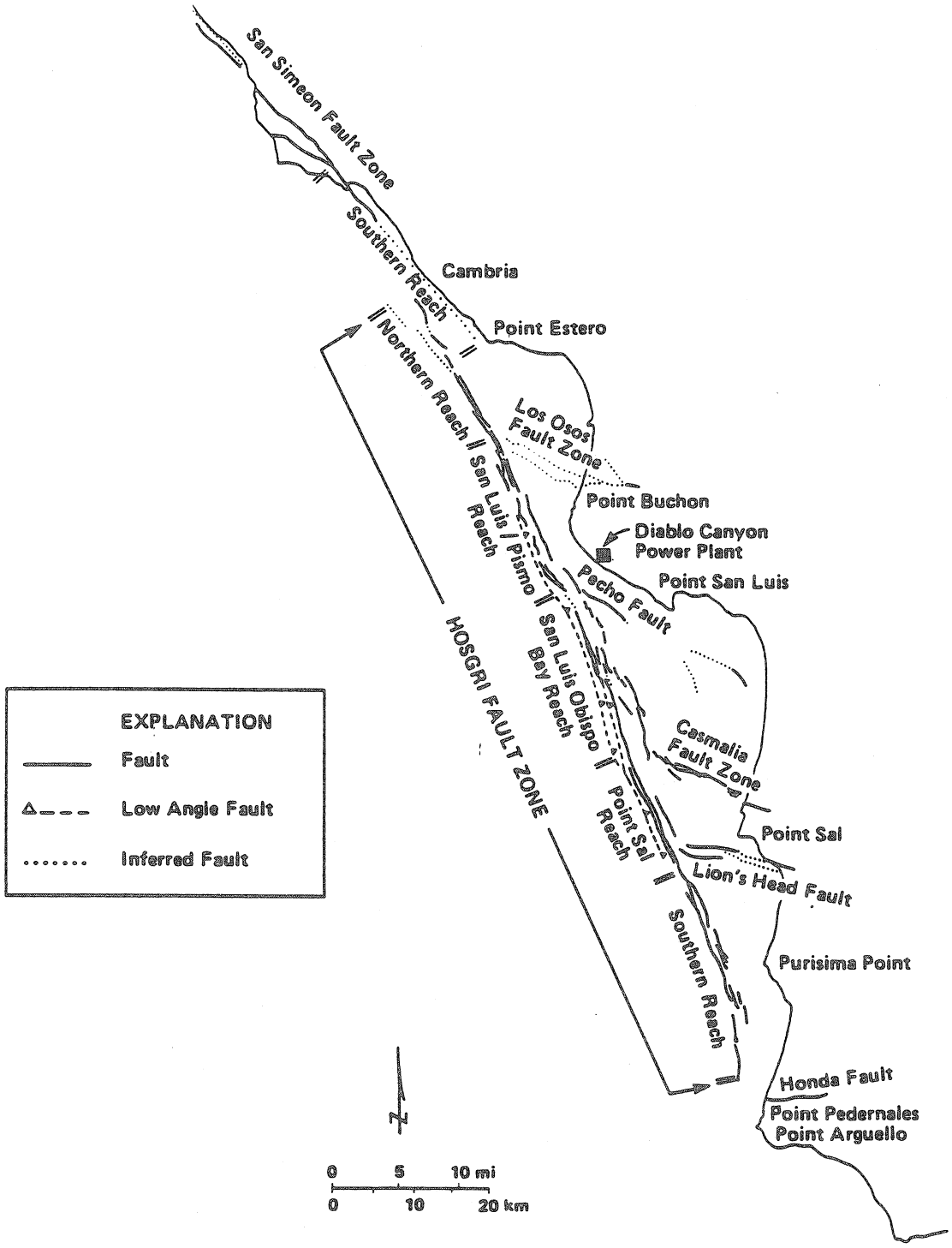


Figure 4-2. Segmentation points and intervening reaches along the Hosgri fault zone (PG&E, 1988).

(3) Pecho fault intersection: This segmentation point is not strongly supported by clear-cut seismic reflection evidence. The southwestern boundary zone is characterized by PG&E as a diffuse zone averaging 4 to 5 kilometers wide. PG&E selected the southern edge of this zone at the Pecho fault (with a low 0.01 to 0.02 mm/yr slip rate) as a segmentation point with the Hosgri fault system rather than at other faults that have higher rates of activity (e.g., the San Luis Bay/Olson faults with a post-substage 5e rate of 0.03-0.06 mm/yr at Avila Beach, 0.04 to 0.07 (UNR est. = 0.04) mm/yr the Rattlesnake trace, and 0.01 to 0.04 (UNR est. = 0.08) at the Olson fault. Selection of the segmentation point nearer the average, or main zone of deformation (the San Luis Bay fault) of the southwestern boundary zone, seems more appropriate. The northeasterly dip of the San Luis Bay fault also suggests that at seismogenic depth this point may even be several kilometers further northwest. Selection of these other segmentation points for this segmentation point instead of the Pecho-Hosgri fault intersection would decrease the length of the San Luis/Pismo reach, but would increase the length of the San Luis Obispo Bay reach by a few kilometers.

(4) Casmalia fault intersection: This point is well constrained, coinciding with an inferred change in the vertical component of the Hosgri fault and a change in the pattern of folds and thrust faults on the west side of the Hosgri fault.

(5) Lions Head fault intersection: The location of this point is well constrained. However, the amount of late Quaternary activity on the Lions Head fault is very low (<0.012-0.017 mm/yr; Clark and Slemmons, 1990). Accordingly, the Lions Head fault is not as well defined as the segmentation points listed above.

(6) Southern termination: This termination point is not clearly defined, but may be near the Honda fault intersection. If the Steritz and Luyendyk (1991) model for the southern Hosgri fault is correct, and the Hosgri fault extends into the Santa Barbara Channel, there may be additional fault segments south of Pt. Pedernales.

Although each of these segmentation points have some uncertainties, they are generally well expressed by onshore geomorphic features, coastal uplift patterns, and intersections with capable faults and fault-related folds. Two of the segmentation points, the Cambria and Casmalia points, are also well supported by structures of the block west of the Hosgri fault.

Based on the above segmentation scenario, which is modified from PG&E (1988), the following rupture lengths and logic tree weightings were selected by UNR to characterize the Hosgri fault: 22 km (0.1), 45 km (0.5), 70 km (0.35), and 110 km (0.05), or a weighted average of about 53 km, slightly more than the 50 km length shown on Table 3-1. These values are considered to be appropriate for either strike-slip or right-oblique-slip cases. UNR's preferred logic tree weightings for 45 and 70 km rupture lengths are higher than those of PG&E. These higher weightings are based on uncertainties regarding the number of fault segments that would rupture during a maximum Hosgri fault event, and on the common occurrence of multiple ruptures of

fault segments for earthquakes above magnitude 6.5 to 7.0 (dePolo and others, 1989). In particular, the importance and location of intersecting structures (e.g., the Los Osos and southwestern boundary zone fault intersections) as potential sites of earthquake initiation and/or termination are not thoroughly understood. The higher preference for rupturing of two or three segments is based on the observation that for earthquakes of magnitude greater than 7 there are many multiple historical segment ruptures.

4.2.6 Slip Rate

The slip rate cannot be directly measured for the offshore Hosgri fault. However, the San Simeon fault data is relatively well constrained, with many right-slip measurements of 1-3 mm/yr (PG&E, 1988, Table 2-12). Strike-slip deformation is believed to be transferred to the Hosgri fault via the stepover, and may be diminished incrementally to the south as a result of capable thrust or reverse fault intersections, such as the Los Osos, San Luis Bay-Wilmar Avenue, Casmalia, and Lions Head faults. Vertical separation on the Hosgri fault could be somewhat augmented by contractional deformation in the active Piedras Blancas anticlinorium.

PG&E (1988 and docket amendments) estimated the amount of vertical separation across the Hosgri fault (PG&E, 1990, GSG-3, GSG-4) to suggest that the strike-slip component of slip is much greater than the vertical component, particularly for the reach of the Hosgri adjacent to the DCNPP. This conclusion is consistent with other lines of data regarding fault type.

The UNR analysis leads to the following comments:

(1) The ages of strata used as piercing points to measure vertical separation across the Hosgri fault have significant uncertainties and in many cases wave erosion has removed equivalent units east of the fault.

(2) PG&E compared the vertical separation component to the strike-slip component, which, depending on dip angle, could underestimate the dip-slip faulting component for lower Hosgri dip scenarios.

(3) A Holocene slip rate value of about 2 to 3 mm/yr as measured on the San Simeon fault at Airport Creek is preferred for the UNR logic tree analysis. This value is within the preferred 1 to 3 mm/yr range determined by PG&E by other methods.

4.2.7 Displacement Per Event

No direct data is available for displacement per event along the Hosgri fault. The San Simeon studies of PG&E suggest that there is an average displacement of 1 or 2 m per event. The UNR analysis concurs with this estimate of the amount of offset that is likely to occur on the Hosgri fault.

4.2.8 Maximum Depth of Rupture

The inferred maximum depth of rupture is estimated as the maximum depth of observed seismicity. Earthquake depths in coastal California are generally confined to the upper 12 km of the crust (PG&E, 1988 and docket amendments; Sibson, 1982) and the 12 km depth value used by PG&E is also used for the UNR analysis.

4.2.9 Recurrence Interval and Fault-Slip Rate

As there is no direct evidence for recurrence interval, the recurrence interval value derived for the San Simeon fault has been used. This is estimated at $1,100 \pm 450$ yrs and is reasonable and well justified.

4.3 Los Osos Fault

The Los Osos fault is a northwest-striking, southwest-dipping zone of subparallel and en echelon faults up to 2 km in width. The fault zone defines the northeastern margin of the San Luis/Pismo structural block (Figs. 2-3 and 4-3). The fault is truncated by the Hosgri fault on the northwest and extends southeast to the West Huasna fault. The closest surface trace of the fault is 9.5 km from the DCNPP. The fault is capable and has evidence for multiple Holocene displacements. PG&E's (1988) characterization of the fault as a major, seismogenic, range-front thrust or reverse fault is supported by a wide range of data developed during the LTSP.

4.3.1 Fault Geometry

The primary, active faults within the Los Osos fault zone dip southwest from 9° to 29° in the shallow subsurface. High angle and northeast-dipping faults are interpreted as secondary structures in the hanging wall of the northernmost, main fault trace (PG&E, 1988; Fig. 2-51). The sparse well data and earthquake hypocenter trends are not adequate to constrain the fault dip at depth. PG&E considered several fault geometries for seismic source characterization.

The UNR studies lead to the same weightings that were used by PG&E, with a weighting of 0.7 for reverse-slip (60°) and 0.3 weighting for thrust (30°) geometries. It is possible or probable that at seismogenic depth the fault dip is even higher than 60°. The 60° dip is also suggested by many of the focal mechanisms from small earthquakes.

4.3.2 Fault Style

The style of faulting of the Los Osos fault is essentially pure dip-slip, based on the presence of the near vertical rake of slickensides on fault planes and the absence of laterally offset geomorphic features. This weighting is also consistent with the following:

(1) The principal horizontal stress direction of Zoback and others (1987) and Vittori and others (1991) at about N32°E.

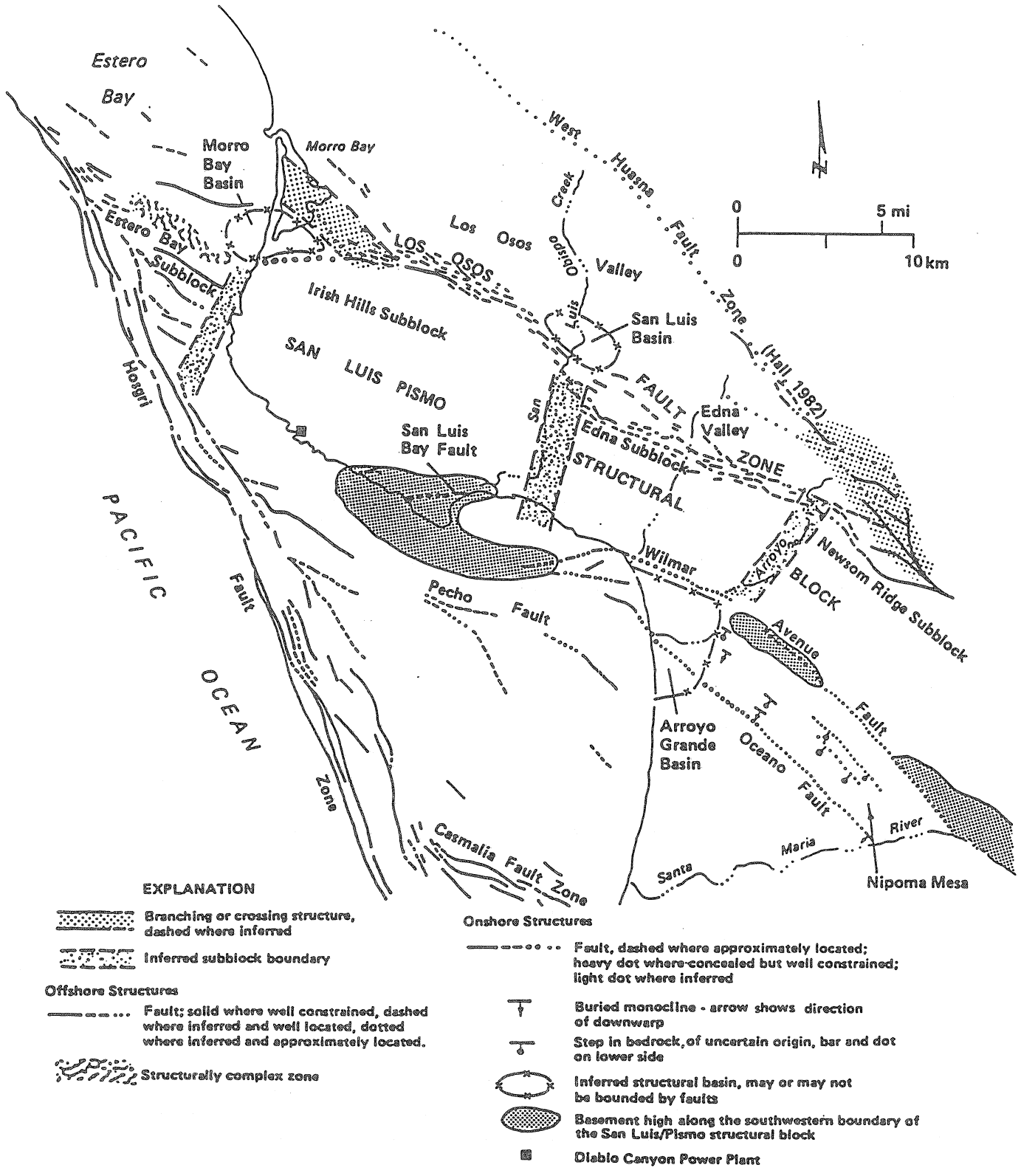


Figure 4-3. Structural elements associated with the San Luis/Pismo structural block (from PG&E, 1988). Approximate locations of the three cross-structures are indicated.

(2) The 1980 Point Sal earthquake (M_L=5.1), considered to have occurred on the Orcutt Frontal fault, which is subparallel to the Los Osos fault, had an essentially pure dip-slip focal mechanism (Eaton, 1984).

(3) Striae on other sub-parallel faults of the region, including the Los Alamos fault, show reverse fault style (Guptill and others, 1980).

4.3.3 Fault Length

The fault is mapped by PG&E from the Hosgri fault to the Lopez Reservoir, a distance of 49 km. The fault has a length of 57 km, if if activity extends to the West Huasna fault, but activity could connect to the Foxen Canyon fault (Fig.2-2) by the Wilmar Avenue fault at Nipomo, the Oceano fault, and other faults beneath the young sediments of Santa Maria Valley.

4.3.4 Segmentation

PG&E divided the Los Osos fault into four segments (Figs. 4-3 and 4-4), from northwest to southeast: (a) the Estero Bay segment (~13 km), (b) Irish Hills segment (~19 km), (c) Lopez Reservoir segment (~17 km), and (d) Newsom Ridge segment (~8 km). This segmentation scenario is well supported by geologic, geomorphic and topographic features which cross the entire San Luis/Pismo block (PG&E, 1988, Figs. 2-16, 2-17, 2-50).

The segmentation point between the Irish hills and Lopez Reservoir segments, in particular, is well supported by multiple lines of data. It is located at a 1-2 km right stepover in the fault and the range front, coinciding with topographic segmentation of the San Luis Range (Fig. 3-4) and with an inferred northeast-trending cross structure at San Luis Obispo Creek. It also occurs where the Los Osos fault appears to have an apparent major change in timing of faulting and/or slip rate. The Irish Hills segment is well expressed geomorphologically and is at the base of a steep, linear range front, and shows evidence of multiple Holocene or late Pleistocene events. The Lopez Reservoir segment has less definitive geomorphic expression (Nitchman, 1988), but low-sun angle aerial reconnaissance suggests that there is distributed late Quaternary faulting on this segment.

4.3.5 Slip Rate

The Ingley trench T-2 on the Irish Hills segment of the fault showed a 4.0-4.9 m cumulative net thrust displacement of a buried A soil horizon on four fault traces. Assuming a 15-30 ka age for the soil horizon based on relative soil development and using the low-angle fault dips exposed in the trench, a fault slip rate of 0.13-0.33 mm/yr is determined using a 9°- 23° dip of the fault plane. This estimate has fairly large uncertainties due to the poorly constrained age of the soil horizon and the possibility that not all recent deformation on the Los Osos fault is captured in Ingley trench T-2.

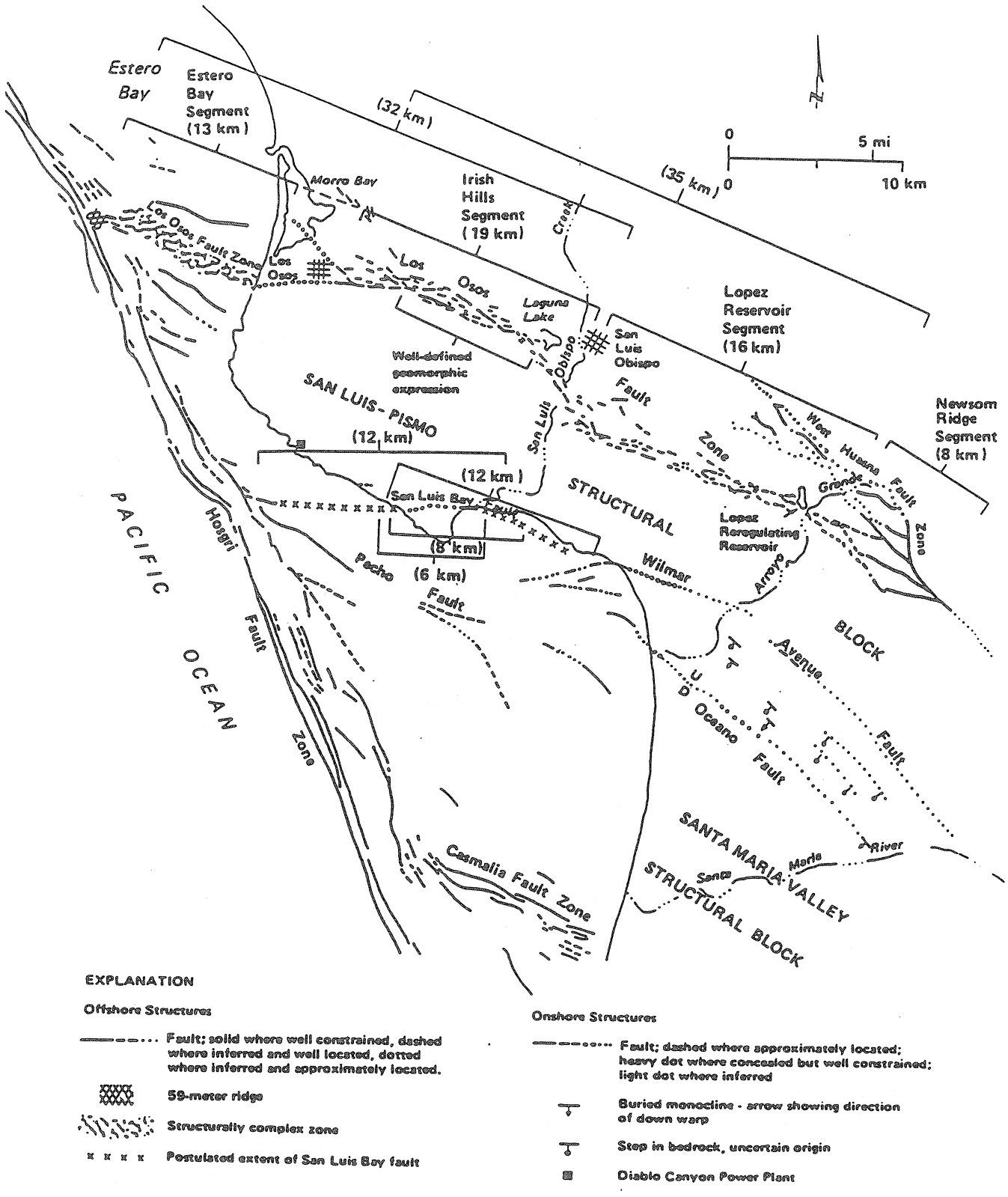


Figure 4-4. Rupture lengths considered by PG&E for Los Osos and San Bay Luis Bay fault zones (PG&E, 1988).

Marine terrace data provide better constrained slip rate estimates, as they are more accurately dated and span the entire fault zone. Slip rates derived from vertical displacements of marine terraces, however, are strongly dependent on inferred fault geometry. PG&E (1988 and docket amendments) estimated dip-slip rates of 0.25-0.8 mm/yr using marine terrace data and vertical component slip rates of >0.20 mm/yr.

4.3.6 Surface Displacement Per Event

Displacement per event is determined from one exploratory trench, Ingley trench T-2. Based on a 4.0-4.9 m cumulative net slip offset of a buried A soil horizon, PG&E estimated a 2.1 m maximum displacement and 0.5-1.5 m average displacement for the Los Osos fault. These values are not well constrained, as the dip at depth is not well established and surface gravity effects may exaggerate the apparent tectonic displacement. However, the PG&E estimate of maximum displacement of 2.1 m appears to be conservatively estimated and is consistent with an earthquake rupture of the entire Irish Hills segment. This is also compatible with surface faulting displacements of up to 2.5 meters during the 1971 San Fernando event (M=6.5) which ruptured a fault zone of 16 km length.

4.3.7 MCE for Los Osos Fault Zone

The MCE determined from Figure 3-11 of PG&E (1988) is 6.81 with a standard deviation of 0.28. Use of the regression for all types of earthquakes from Slemmons and others (1991) has a similar value of $M_S = 6.7$ for a 19 km length. Comparison with the San Fernando earthquake of 1971 with a $M_S = 6.5$ suggests that the geological effects from the most recent paleoseismic event for the Irish Hills segment of the Los Osos fault was similar or less than the San Fernando event.

4.4 Faults Within the San Luis/Pismo Block

Faults included within the block are the Edna, Crowbar, and San Miguelito faults. PG&E clearly demonstrated that the Edna and the San Miguelito faults are not capable faults. Although the Crowbar faults extend shoreward of PG&E's geophysical coverage, the absence of marine terrace displacements onshore, and the lack of geomorphic expression within the range, indicate lack of capability. Detailed marine (PG&E, 1988, and docket amendments) and fluvial terrace investigations (Killeen, 1988) preclude the existence of other significant capable faults onshore within the block.

4.5 Southwestern Boundary Zone

4.5.1 Introduction

The southwestern boundary zone of the San Luis/Pismo structural block is a diffuse zone of northeast-dipping thrust and/or reverse faults. These include the Pecho, San Luis Bay, Olson, Wilmar Avenue, and Oceano faults (Figs. 2-3 and 4-4). Collectively these faults truncate and

elevate the San Luis/Pismo block, separating it from the adjacent, subsiding Santa Maria Valley structural block.

Recent fault activity within the zone is recorded by late Quaternary marine terraces, which make ideal strain gauges for assessing rates and styles of deformation. The San Luis Bay fault, Olson fault (or Olson trace of the San Luis Bay fault), Wilmar Avenue fault, and probably the Oceano fault, disrupt marine terraces and are capable faults. The Pecho fault is entirely offshore, and is not as well characterized as onshore structures and the seismic reflection data do not show definitive evidence of capability. These faults and parallel structures account for the decrease in uplift rates of marine terrace shoreline angle elevations across the fault zone from ~0.2 mm/yr at Irish Hills at the San Luis/Pismo block to subsidence at a low rate of the offshore Santa Maria Valley block.

4.5.2 Pecho Fault

The Pecho fault (Fig 2-3) is considered by PG&E to be the southwesternmost fault of the boundary zone, and an inferred segmentation point for the Hosgri fault. PG&E maps the Pecho fault from the Hosgri fault to near the coastline, a distance of ~22 km (including a 4.5 km gap in the mapped trace of the fault). The fault splays into two branches south of Point San Luis.

Fault parameters for the Pecho fault are not well constrained. The fault is not well expressed by submarine geomorphic or bathymetric features. It is mapped on the basis of discontinuous, southwest-facing seafloor scarps and truncated seismic reflection horizons. PG&E interprets the Pecho fault to be a high-angle to vertical, northeast-dipping fault with northeast-side-up separation. Displaced sediments of probable lower Pleistocene age suggest 0.01-0.02 mm/yr vertical separation rate across the fault. The lack of strong topographic and stratigraphic expression, low slip rate, and high angle of fault dip suggest that opposite the Irish Hills subblock, the Pecho fault appears to be a minor or subordinate element of the southwestern boundary zone system. The distance from the Olson, San Luis Bay, and Wilmar Avenue faults suggest that it is a separate seismic source.

4.5.3 San Luis Bay and Olson Faults, and Possible Undetected Offshore Faults

The San Luis Bay and Olson faults are important structures of the southwestern boundary zone and are the nearest documented onshore capable faults, approximately 4 to 8 km southeast of DCNPP along the coastline (Fig. 4-5). These faults, although poorly exposed, consist of at least three documented localities with late Quaternary fault offset and warp or tilt 5e marine terraces (see detailed discussions in response to question GSG 16). The UNR vertical separation and vertical separation rate values are estimated from Figure 4-5. The UNR values are: (1) north trace of the Olson fault, >5 m, or 0.04 mm/yr rate (PG&E estimates 2 to 4 m), and >5 m, or 0.04 mm/yr rate (PG&E estimates 2.1 to 2.4 m) across the south trace for a total Olson deformation of 12 m or 0.10 mm/yr rate; (2) Rattlesnake trace of the San Luis Bay fault about 4 to 5 m or 0.04 mm/yr rate (PG&E estimates 1 to 4.6 m with a rate of 0.02 to 0.04 mm/yr. The total vertical separation of the entire zone is about 17 m, or a 0.14 mm/yr rate for faulting, tilting and warping across the zone; and (3) at Avila Beach, the only location where the fault is exposed a well constrained separation of 5 to 8.5 m and 0.04 to 0.07 mm/yr slip rate.

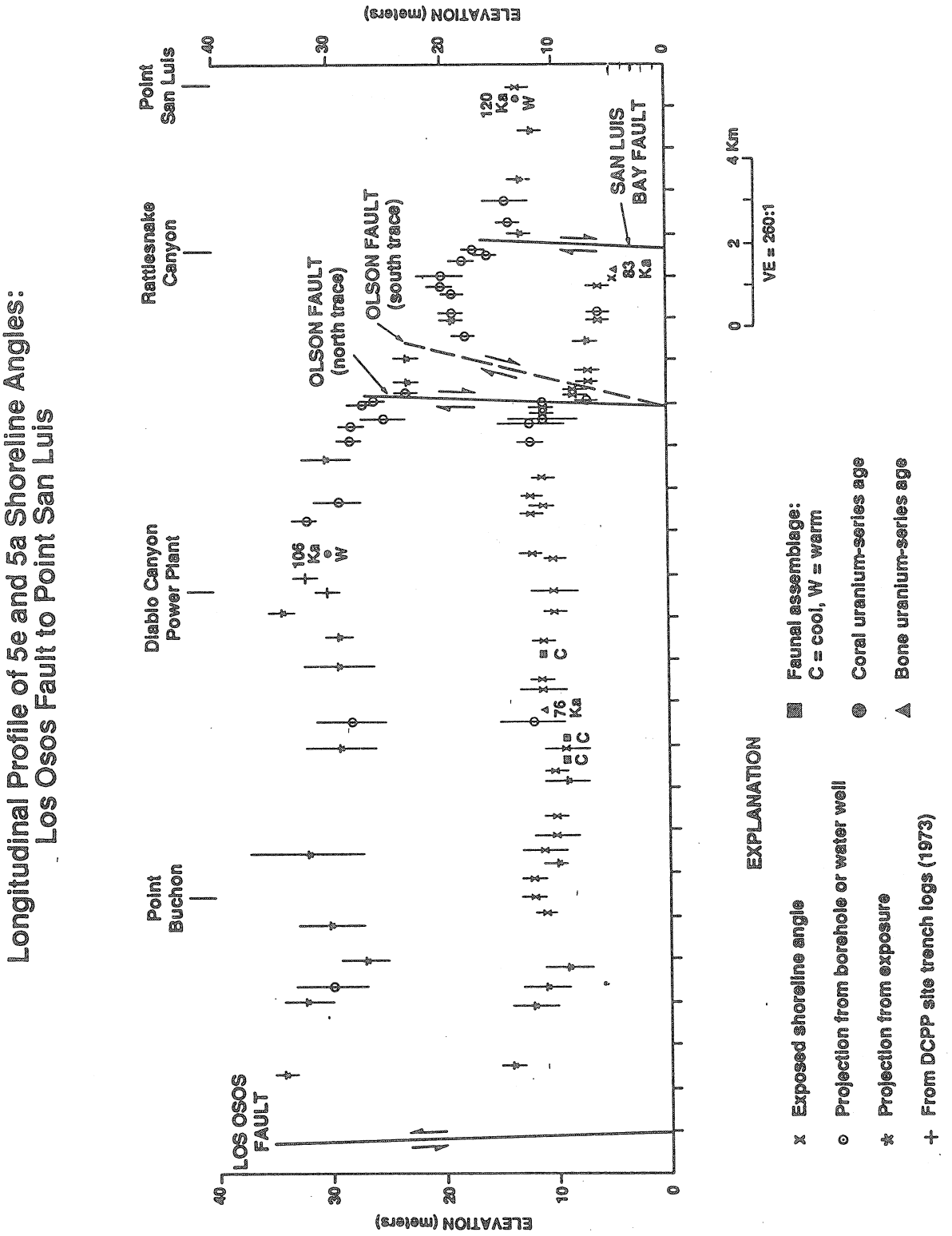


Figure 4-5. Marine terrace elevations of 5e and 5a shoreline angles between the Los Osos fault and Point San Luis to illustrate the lack of folding and faulting except for the zone including the Olson and San Luis Bay faults (PG&E docket).

PG&E (1988, and docket amendments) maps the San Luis Bay fault as an east-trending zone of "approximately located and inferred faults". Surface and subsurface continuity along this zone between the two main localities is inferred. The Rattlesnake trace and the Avila Beach exposure are considered to be connected through a topographic saddle between the Irish Hills and San Luis Hill. PG&E maps offshore continuations of the fault both east and west of the on land exposures, and the endpoints are poorly constrained.

The Olson fault is not conclusively demonstrated to be part of the San Luis Bay fault, but the UNR analysis infers a connection at depth based on the proximity of the faults, similar location within the subblock, en echelon relationship, and continuity of deformation of the 5a and 5e marine terraces between the Olson and Rattlesnake localities.

The relationship of the Olson fault to the San Luis Bay fault is not resolved. PG&E prefers to treat the Olson fault as a separate seismic source, whereas the UNR analysis considers the Olson fault to be an en echelon trace of the San Luis Bay fault. The 5e (120 ka) marine terrace appears to be faulted and/or tilted with a net uplift of about 18 m across the zone between the Olson and San Luis Bay faults (Fig. 4-5). The slope of the deformed terrace between the faults, the proximity of the faults, and their parallel strike suggest that the two faults are part of the same zone of deformation at depth. Accordingly, the San Luis Bay fault and the Olson fault are treated together in the UNR seismic characterization of capable faults. Other more distant faults such as the Pecho and Oceano faults are part of the southwestern boundary zone, but are considered as separate seismic sources. The marine terrace uplift data suggest that about 2/3 (17 m, or 0.14 mm/yr) of the main deformation (0.20 mm/yr) across the southwestern boundary zone at Irish Hills is on the Olson and San Luis Bay faults, and about 1/3 (0.06 mm/yr) is on the Pecho fault or other offshore faults.

4.5.3.1 Fault Geometry

Where the fault is exposed at Avila Beach, it dips 15°-46° to the northeast. PG&E interpret the fault as a high angle reverse fault based on progressively steepening fault dip with depth at the Avila Beach exposure, and from limited seismic reflection data. This report uses a 60° dip on a reverse fault zone at seismogenic depth.

4.5.3.2 Fault Style

Slickensides exposed at Avila Beach indicate essentially pure thrust or reverse displacement. This style of faulting is consistent with the fault's west-northwest trend and the north-northeast-oriented maximum horizontal stress direction in the region (Section 2.1.3).

4.5.3.3 Fault Length and Fault Rupture Lengths

Total fault length and potential earthquake rupture lengths are not well constrained. PG&E (1988) consider 6, 12 and 19 km total lengths (0.4, 0.4, and 0.2 logic tree weightings, respectively) and 6, 8, and 12 km potential rupture lengths (0.4, 0.4, and 0.2 logic tree

weightings respectively as noted in Fig. 3-8 of PG&E, 1988). This is based on their interpretations of studies of limited data that could be collected for the onshore and offshore areas and PG&E's characterization of the San Luis Bay fault as a relatively short, discontinuous fault.

We suggest an alternative interpretation that the fault has subsurface continuity of a broad zone that extends eastward from the Hosgri fault to the Wilmar Avenue fault along the Irish Hills subblock (Fig. 4-3). This leads to higher assigned probability for a longer total fault rupture length than is shown by PG&E's logic tree pathways. The total fault length for this model is approximately 13 km, somewhat more than the PG&E 12 km logic tree length. The UNR model is based on strong fault segmentation along each subblock of the San Luis/Pismo block, and does not require a direct connection of the San Luis Bay fault to the Wilmar Avenue fault. The length of this segment may be less than 13 km at seismogenic depth, depending on the dip angle of the Hosgri fault zone, and the exact location of the San Luis Obispo Creek cross structure.

4.5.3.4 Slip Rate

The estimated slip rate of the San Luis Bay fault based on displacements of marine terraces is 0.07 to 0.14 mm/yr, depending on inclusion of the Olson fault in an integrated model. This slip rate appears to be fairly well constrained.

4.5.3.5 Other Fault Parameters

Displacement per event and recurrence interval information are not available for faults of the southwestern boundary zone, and can only be estimated by analogy with the Los Osos fault zone.

4.5.4 Wilmar Avenue Fault

The Wilmar Avenue fault and the Oceano fault are the primary, active structures on the southwestern margin of the Edna and Newsom Ridge portions of the San Luis/Pismo structural block. The Wilmar Avenue fault is mapped by PG&E from the offshore near Pismo Beach east-southeast to the Santa Maria River (Fig. 4-3). It is a capable fault, offsetting late Quaternary marine terraces at the coast. Detailed mapping inland from the coast is complicated by the fault's inferred location beneath Highway 101 and other cultural features. Low-sun angle aerial photography and reconnaissance agrees with PG&E's analysis that the segment opposite Newsom Ridge is inactive, or has a very low rate of deformation.

4.5.4.1 Fault Geometry and Style

At its seacliff exposure at Pismo Beach, the Wilmar Avenue fault consists of fault planes that strike N64°W to E-W and dip 45°-60° northeast. Based on this geometry and the presence of down-dip slickensides, the fault is considered to be a reverse fault. The geometry at depth is not known, but is inferred to have a 60° dip.

4.5.4.2 Fault Length and Segmentation

The Wilmar Avenue fault as mapped by PG&E has a total length of ~30 km, but this includes parts of two topographic segments of the San Luis/Pismo block (Fig. 4-3). PG&E divides the fault into four segments, from northwest to southeast: (1) the Birdrock segment (5.2 km); (2) Pismo Beach segment (7 km); (3) Picacho segment (7.5 km); and (4) Nipomo segment (10 km). This segmentation scheme is not well constrained by behavioral or geometric data. The Birdrock and Pismo Beach segments are both within the Edna subblock of the San Luis/Pismo structural block (Fig. 4-3) and may belong to a single southwestern boundary zone segment. The Birdrock segment is entirely offshore and has a more westerly strike than the rest of the fault zone. The Pismo Beach and Picacho segments have similar late Quaternary slip rates, but are in different subblocks of the San Luis/Pismo structural block. Little data are available for the Nipomo segment.

The UNR staff analysis led to the belief that the topographic segmentation of the San Luis/Pismo block, used as segmentation points for the Los Osos fault, could be used for the southwestern boundary zone as well. Because of the sparse data base, this report uses a segmentation model that is based on subblock topography (Fig. 4-3), general uplift rates (Fig. 2-3) and geologic expression. This suggests that there is a single, approximately 12 km long fault segment at the Edna subblock, and a segment of length >17 km at the Newsom Ridge subblock.

4.5.4.3 Slip Rate

The 5e marine terrace is disrupted with 4 to 6.4 m of north-side-up displacement by the Wilmar Avenue fault at its seacliff exposure and at the Farmboy Quarry. Assuming 45^0-60^0 fault dips, this yields a 0.04 to 0.07 mm/yr slip rate. While there is no direct evidence of multiple displacements, the large offsets suggest multiple faulting events.

4.5.5 Oceano fault

The Oceano fault is a reverse fault and/or monocline with a N45°-50°W strike at the north edge of the Santa Maria Valley. The fault is buried by eolian sand and alluvial deposits and is not exposed at the surface, however, its location is constrained by borehole and seismic reflection data. The fault terminates in San Luis Obispo Bay, ~ 3 km from the coast. To the southeast, the fault may be continuous with the Santa Maria Valley fault shown by Hall (1982). No surface data are present to indicate capability. The Oceano fault's position near the base of a flight of marine terraces suggests that it is probably a capable structure.

4.5.6 Inferred Coast-Parallel Fault

The possible existence of an unidentified active thrust or reverse fault in the near offshore zone between Point Buchon and Point San Luis was discussed at NRC/PG&E meetings. This inferred fault is suggested by the steep and linear coastline, and by a late Quaternary slip deficit of 0.06 mm/yr (less about 0.01-0.02 mm/yr along the Pecho fault) on the southwest margin of the Irish

Hills subblock. It is also suggested by the steep, linear range front along the Point Buchon to Point San Luis part of the coastline. Other arguments for a coast-parallel offshore fault are summarized by Nitchman (1988).

Although the coastline linearity and slip deficit is consistent with a tectonic structure, the PG&E offshore investigations by a diver geologist (Plates GSG Q 16-1A, 16-2 and 16-5) indicate that major geologic units and structures, including the Olson and San Luis Bay faults are oblique to the coastline and appear to preclude the existence of a coast-parallel fault. Accordingly, the UNR model does not assume a coast-parallel surface fault for the southwestern boundary zone, although another somewhat similar southwestern boundary zone model is used.

4.5.7 Difficulty in Determining Subsurface Continuity for the Southwestern Boundary Zone

In past NRC/PG&E meetings and correspondence with NRC, the UNR staff discussed the possibility of a narrower, more continuous, and integrated seismogenic structure on the southwestern boundary zone than is used in the PG&E (1988; and response to Question SSC-5) analysis. Although it is very unlikely that all of the capable faults of the southwestern boundary zone coalesce into a single fault, many features of this zone suggest the possibility of subsurface fault continuity for the main zone of deformation. The lack of surface continuity may result from several factors, including:

(1) Low fault slip rates and the associated difficulty in mapping active faults.

(2) Limited geologic exposures on land due to cultural development, extensive Quaternary deposits, and the shallow marine environment of the offshore area.

(3) Difficulty in detecting and obtaining evidence of style, continuity, and activity rates of offshore faults.

(4) Limited geophysical data available for the nearshore zone.

The UNR project staff concurs with PG&E's observation that the southwestern boundary zone is diffuse at the surface. We propose an alternative model to the PG&E's separate source model in which opposite the Irish Hills subblock, the San Luis Bay and Olson faults may be structurally interconnected at depth. Several factors influence this judgment, although none of the individual factors are definitive. They are:

(1) The length of more than 50 km from the Hosgri fault to beyond Newsom Ridge, and the general continuity of the San Luis/Pismo block suggests that both the northwest and southwest border zones are sub-equivalent structures.

(2) The uplift, without tilting, within each of the subblocks of the Pismo/San Luis block, as shown by generalized topographic contours (Fig. 2-5), marine terraces

at the northwestern end of the structure (PG&E Plate A2-4), and fluvial terraces (Fig. 2-4). This indicates that the Los Osos fault zone of the northeastern border of the range has an equivalent counterpart uplift on faults on the southwestern side.

For the southwestern boundary zne, the UNR analysis uses a shorter fault rupture length for the Irish Hills subblock than for the Los Osos fault, due to the oblique intersection and truncation by the Hosgri fault zone. This, and the eastward dip of the Hosgri fault zone, limits the length of the earthquake source dimension to approximately 13 km, and leads to lower earthquake magnitudes for the southwestern boundary of the Irish Hills subblock than for the Irish Hills segment of the Los Osos fault zone.

The highest rate of activity along this zone appears to be concentrated along the Irish Hills and Edna subblocks of the San Luis Range, with a low rate of activity opposite the Newsom Ridge section as shown by low-sun angle aerial reconnaissance and aerial photography. Here the southwestern boundary zone is between the San Luis/Pismo block that is uplifted, without tilting, from 0.12 to ~0.2 mm/yr and the subsiding and southwestward tilted Santa Maria Valley block (Figs. 2-3 and 4-3).

4.5.8 Cross-Structures in the San Luis/Pismo Block

Three major non-active structural features trending N05°E cross the San Luis/Pismo block (Figure 4-3). These features appear to coincide with strong segmentation points along the Los Osos and southwestern boundary zone faults. They are, from west to east:

(1) The coastline zone separates a stable or subsiding offshore block from the San Luis/Pismo block that is uplifted about 0.2 mm/yr and marked by a flight of terraces of up to at least 0.5 my age.

(2) The San Luis Obispo Creek zone is near the structure that separates the Irish Hills and Edna subblocks of the San Luis/Pismo block. The river terrace studies on either side of San Luis Obispo Creek do not show any vertical offsets, even of the Santa Fe (120-133 ka), Spirit (175-305 ka) or Miguelito (450 ka) ages (Killeen, 1988). This suggests that there has been no surface deformation on this cross-structure during the past 450 ka. The zone is near the western edge of the zone shown in Figure 4-3 and is located near Mallagh Landing, about 2 miles east of Avila and does not offset the 5e (120,000 bp) marine terrace.

(3) The Arroyo Grande zone separates the Edna and Newsom Ridge subblocks of the San Luis/Pismo block.

None of the three cross structures of the San Luis/Pismo block show evidence for Quaternary fault activity. They are regarded as aseismic, deeply rooted segmentation structures that affect

the boundary faults of the block and are expressed in the geologic and topographic character of each of the four subblocks of the San Luis/Pismo block.

4.5.9 Criteria Suggestive of Continuity of the Southwestern Boundary Zone

The following features suggest an alternative integrated fault model to those of PG&E:

(1) The length of the southwestern boundary zone is at least equivalent to the Los Osos fault.

(2) The lack of tilting within each segment of the San Luis/Pismo block as demonstrated by the marine terraces along the Irish Hills subblock (PG&E, 1988 and docket amendments), generalized topographic contours (Fig. 2-5), and the fluvial terraces (Fig. 2-4) along San Luis Obispo Creek (Killeen, 1988).

(3) It is more difficult to have individual, or isolated, nearby seismic sources that together have slip-rates that are generally balanced with an integrated fault zone on the opposite side of the block.

(4) The 18 meters of Q2 terrace deformation along the San Luis Bay/Olson fault zone indicates substantial deformation in the past 120,000 years, and appears to be more compatible with an integrated fault zone than with smaller isolated sources.

(5) The general belt of seismicity along and near the San Luis/Pismo block, particularly at the Irish Hills subblock, suggests that the zone is integrated or continuous, although there is a decrease in rate of activity southeast of the Irish Hills subblock.

Evidence favoring a separate source model include apparent differences in surface faulting at the different sources, and subdued geomorphic expression that contrasts with the Los Osos fault zone.

4.5.10 Weightings For Fault Models

Four models are considered for the UNR analysis. Available data do not conclusively eliminate any of these models from consideration. The following provides our estimate of their weightings:

Integrated Fault Model: This model considers the main trace of the southwestern boundary zone to include the San Luis Bay, Olson, and Wilmar Avenue faults and is assigned a weighting of 0.5. Integration, probably below the base of the seismogenic zone, could include the Pecho fault, but unless connected by a detachment surface of low dip, needs to be considered as a separate seismic source.

Separate Seismic Sources: This is the main model presented by PG&E and is assigned a weighting of 0.5. The characterization of the length, location, and potential earthquake magnitudes in the PG&E analysis are reasonable and carefully documented.

Model A, Shallow Postulated Thrust Ramp Model: This model, discussed in PG&E response to Question GSG 11, is based on a retrodeformable cross section analysis. It places a blind thrust at 5 km, a depth that would not be significantly seismogenic. We assign a weighting of 0.0.

Model B, Deeper Postulated Thrust Ramp Model: This model, discussed in PG&E response to Question GSG 11, is based on a retrodeformable cross section analysis. It places a blind thrust at 6 to 9 km and could produce earthquakes of above magnitude 6. The model requires low angle detachments that are not consistent with the dip of Franciscan basement rocks. We agree with PG&E that this model does not have significant implications for the probabilistic or deterministic ground motions. This model is assigned a weighting of 0.0.

4.5.11 Magnitude for an Integrated Southwestern Boundary Zone

The main trace of the southwestern boundary zone appears to be about 2 or 3 km southwest of DCNPP in the zone that includes the San Luis Bay and Olson faults. The total zone of possible rupturing of about 13 km length is shorter than for the Los Osos segment at Irish Hills, as it is partly truncated by the Hosgri fault system. Use of appropriate regression formulas of Table 3-1 and by PG&E in their response to Question GSG 11 (in Figure GSG Q11-8) lead to magnitude values from about M = 6 to 6.5. The main energy release would be from the seismogenic zone, below 5 to 7 km depth (see PG&E response to Question GSG-2 for the Hosgri fault). For a rupture of the entire 13 km segment with an integrated model along the zone bounding the Irish Hills subblock, the regression relations for earthquake magnitudes of Slemmons and others (1989) lead to $M_s = 5.39 + 1.03 \log 13 = 6.54$ (all fault types) and $M_s = 5.10 + 1.29 \log 13 = 6.6$ (reverse-slip faults).

5.0 SEISMIC SOURCE CHARACTERIZATION: ASSESSMENT OF MAXIMUM CREDIBLE EARTHQUAKES

5.1 Introduction

5.1.1 Style of Deformation

The analysis used in this report considers several types of deformation in the DCNPP region. The styles are:

San Gregorio/Hosgri fault system: The San Gregorio/Hosgri fault system at seismogenic depth is considered to be mainly a strike-slip fault with a right-slip rate of about 3 mm/yr, and a subordinate reverse-slip component on an eastward dipping fault zone of about 70°-80°. The system appears to be strain partitioned in places, with a combination of near vertical, subparallel and anastomosing right-lateral faults, and associated thrust faults and folds, mostly located just

west of the main trace of the Hosgri fault zone. The adjoining blocks are more stable, but the distributed tectonic activity is contractional with reverse faults and folding.

San Luis/Pismo block zone: Deformation of this area is mainly by brittle upper crustal deformation (above 10 - 12 km), and within this zone seismogenic faults appear to be rooted. The proposed fold-and-thrust models (Namson and Davis, 1990) do not fit the pattern of neotectonic structures and this model is not used in the UNR analysis.

Southern Onshore Santa Maria basin: Faults and folds of the onshore Santa Maria basin appear to show a different style of Quaternary deformation than the adjacent San Luis/Pismo structural block. There is clear evidence in the Casmalia Range, Solomon Hills, and Purisima Hills of early and middle Quaternary fold and thrust belt-style deformation, and evidence for at least local late Quaternary folding . The focal mechanism of the 1980 Point Sal earthquake (Fig. 2-6) suggests that present day deformation is occurring on major reverse faults that extend to seismogenic depth. Resolution of the style of deformation is not considered to be critical to our analysis, as this is the same segmentation point suggested for either the PG&E or UNR model along the southern Hosgri fault.

5.1.2 Capable Faults

The UNR analysis agrees with that of PG&E (1988 and docket amendments) that the capable faults of the Diablo Canyon area include the Hosgri, Los Osos, Olson, San Luis Bay and Wilmar Avenue faults. The UNR analysis also agrees that the San Miguelito, Edna, and Pismo faults are not capable faults. The analysis differs from PG&E's by using an alternate model that the southwestern boundary zone of the San Luis/Pismo block is an integrated capable fault zone, rather than several separate capable faults. The boundary zone is considered to be distinctly divided by segmentation points that cross the San Luis Range, to separate both the Los Osos fault zone and the southwestern boundary zone into segments opposite the Irish Hills, Edna and Newsom Ridge subblocks.

5.1.3 Potential for Significant Unknown Faults

The PG&E study included intensive field and offshore geophysical investigations. The UNR search for active faults was independently conducted and included remote sensing studies of the site area. The study included special low-sun angle aerial photography along all zones of suspected activity or capability. These studies included extensive use of the Fairchild aerial photographs with moderately low-sun angle conditions and before most of the cultural development of the San Luis Obispo/Santa Maria Basin region. The extensive development of marine (PG&E, 1988) and fluvial terraces (Killeen, 1988) along the western and southern part of the block and across the block provide data that preclude major, unrecognized faults or continued folding in the western part of the San Luis/Pismo block. These studies and investigations of Nitchman (1988) and Clark (1991) support the conclusion of PG&E (1988), that all significant capable faults have been identified in the onshore area, and that there is little

potential for significant seismogenic blind thrusts and fold-and-thrust structures along or within the Pismo/San Luis block near DCNPP.

5.2 Hosgri Fault Zone

PG&E determined a M = 7.2 MCE or Maximum Credible Earthquake magnitude for the Hosgri fault using a source characterization and a logic tree analysis approach and multiple methods. Although the UNR analysis differs somewhat in weightings, segmentation lengths, and number of segments to rupture during an event, the results are generally consistent with that of PG&E and leads to a similar magnitude value of M = 7.2.

5.2.1 Sense of Slip

The PG&E analysis led to:

> "a "fairly strong" preference (0.65) for strike-slip faulting. Oblique-slip faulting is given a moderate but significant weight (0.3) to account for the evidence of a dip-slip component along the zone. Evidence for thrust or reverse faulting is judged to be relatively weak" (about 0.05).

Many lines of evidence indicate that the Hosgri fault accommodates some convergence. The UNR analysis leads to strong and convincing evidence supporting a major strike-slip component, but there is also data that supports a subordinate oblique-slip component on a steeply dipping reverse fault. For example, observations indicate evidence for an oblique-reverse component in many places along the San Gregorio-Hosgri fault system. These include Ano Nuevo (Weber and Lajoie, 1979b), Monterey Bay (Greene and others, 1973), and the Big Sur area. Also the Lopez Point earthquake of March 1, 1991 had a reverse-slip focal mechanism.

Crouch and others (1984) expressed concern that the Hosgri fault is dominantly a thrust or reverse fault (Section 2.1.7 of this report). They also postulate that the Hosgri fault consists of separate, unconnected structures. Most of the geophysical data, onshore geological data, earthquake epicenter distributions, and earthquake focal mechanisms support a subordinate, or at most equal, amount of contraction across the dominantly strike-slip Hosgri fault. In particular, strike-slip and oblique slip focal mechanisms (Fig. 2-6, and PG&E, 1988 and docket amendments) near and along the trend of the Hosgri fault indicate a strong or dominant component of strike-slip faulting. In addition, our regression analyses (Slemmons and others, 1989) indicate that the magnitude from either reverse-slip or strike-slip earthquakes is similar for a given rupture length.

5.2.2 Dip

The data are sparse to indicate the dip below the resolution of seismic reflection profiles and at seismogenic depths. Based on the analysis presented earlier in this report, the UNR analysis

uses a 70° dip on an east-dipping strike-slip fault that has a subordinate reverse-slip component.

5.2.3 Depth of Faulting

The analysis provided by PG&E is adequately justified and leads to a seismogenic base for capable, rooted faults in the site region at approximately 12 km.

5.2.4 Rupture Length

The PG&E analysis that leads to rupture lengths of 20, 45, 70, and 110 km, and their weightings (0.25, 0.4, 0.25, and 0.1, respectably) are reasonable. The UNR independent analysis uses somewhat different lengths for rupture segments. These are from north to south, 26 (Northern reach), 22 km (Pismo reach), and 26 km (San Luis Obispo Bay reach). These lengths are somewhat uncertain due to uncertainties in the location of the segmentation points, questions of the dip and location of the Los Osos fault zone, southwestern border zone (San Luis Bay or Pecho), and the Casmalia faults at seismogenic depth. It is difficult to assign likely rupture segments further south, where the fault zone has a greater number of intersection structures. For example, the Lions Head fault may not represent a good segmentation point for the subdivision of the Point Sal and Southern reaches, as it has a very low late Quaternary fault slip rate.

The UNR analysis assigns a low weighting (0.20) for the <22 km length at the Pismo/San Luis block, prefers (0.55) a length of >45 km (50 km), assigns a somewhat lower (0.20) weighting for the 70 km rupture length, and a somewhat lower (0.05) weighting for the 110 km rupture length. This analysis places the highest probability of a two segment rupture scenario (~ 50 km long rupture length) for an event of about $M_s = 7.2$. The basis for this judgement is the commonplace rupture of multiple segments during events of above magnitude 7 (dePolo and others, 1989), at least for the extensional regions of western United States.

5.2.5 Average Displacement Per Event

The weightings for average displacements of 1 m (0.4), and 2 m (0.5) are reasonable values. The 3 m (0.1) value appears to be too high. Our review of worldwide data indicates that the average displacement is about 0.5 times the maximum displacement (with a range from about 0.25 to 0.75) that would suggest maximum values of 2 to 4 m for the 1 or 2 m average value, but leads to an improbably high 6 m maximum offset for a 3 m average. The weightings assigned in the UNR study for 1 and 2 m average displacements are weightings of (0.5) and (0.5).

5.2.6 Magnitude Values

The UNR staff prefers a rupture length for the Hosgri fault (weighted average of assigned logic tree weightings) of 53 km yields estimated earthquake magnitudes of 7.2 and 7.3, respectively,

using strike-slip fault-type regressions by Slemmons and others (1989) and Bonilla and others (1984). The use of multi-methods of analysis, shown in Table 3-1, supports the estimation of MCE at about M = 7.2

5.3 Los Osos Fault

The UNR analysis concurs with the very conservatively selected PG&E weightings. This included a reverse-slip model (assigned a weight of 0.9) and a higher weighting for a high angle fault. UNR concurs with the PG&E selection of 12 km depth as the preferred depth value. The total length of 57 km is well justified, but is very unlikely to rupture during a single event. The 19 km rupture length is reasonable for the Irish Hills segment, and there is a slight chance of a longer rupture on two segments of 36 km length. The maximum displacement per event is estimated from exploratory trench work to be about 2 m; this is a conservatively selected value. The PG&E maximum magnitude event, according to its probability distribution, is 6.8. Our analysis used a similar single, full segment rupture of 18 km ($M = 5.10+1.29 \log 19 = 6.7$). This value may be high when compared with the size of other comparable historical rupture zones. For example, the 1971 San Fernando earthquake is considered to be a comparable event with M = 6.5, total surface rupture length of 16 km, and maximum net left-oblique slip of 2.1 to 2.5 m. UNR concludes that the MCE for the Los Osos fault zone is approximately 6.5 to 6.8.

5.4 Southwestern Boundary Zone

The evaluation of this zone is very difficult because of the low fault slip rates for the capable faults, the distributed rupture pattern, and poor and incomplete surface expression of the faults. Sporadic exposures of active faults are recognized but it is not possible to resolve with certainty the character of possible interconnections.

The UNR staff shares the concern expressed by Ziony and Yerkes (1985) for characterization of the potential rupture lengths in the nearby Transverse Ranges and the Los Angeles area. They stated:

> "Many of the faults of the region are overlapping echelon segments of longer zones, and knowledge of their configuration and possible linkage at depth is insufficient to define with reasonable certainty their effective lengths for possible earthquake generation".

One approach is to identify each locality where active faults have been identified within the zone of a few km width, and make calculations for relatively frequent, but lower magnitude events, and to use all possible techniques to infer or determine the connections expressed in a few localities. This type of analysis led to PG&E's fault rupture lengths for the San Luis Bay fault along the southwestern boundary zone of 6, 8, and 12 km rupture lengths, with 0.4, 0.4, and 0.2 logic tree weightings, and corresponding magnitudes determined from regressions on Table 3-1 of PG&E (1988). The PG&E analysis determined the estimated earthquake magnitude to be M= 6.15, the mean of the logic tree magnitudes based on the above lengths.

The UNR analysis proposes an alternate model with some of the individual active faults of the southwestern boundary zone integrated at seismogenic depth and rupturing in well-defined segments. This relationship, although not strictly a mirror image relationship to the Los Osos fault zone, leads to a capable, moderately to steeply dipping reverse fault opposite the Irish Hills segment. The length of this segment would be shorter than the Irish Hills segment of the Los Osos fault zone because of the oblique truncation of the San Luis/Pismo block by the Hosgri fault system.

The UNR study prefers use of a 13 km rupture length, a fault dip of ~60°, and a depth of ~12 km for the San Luis Bay fault. This preferred rupture length assumes single segment rupture (consistent with topographic segmentation of the San Luis/Pismo block) and Hosgri fault dips of 70°-90°. This suggests a magnitude of 6.5 using the regression of Slemmons and others (1989) for all types of earthquakes. Use of the regression in the 1990 PG&E response to Question GSG 11 leads to an estimated magnitude of 6.0. This rupture appears to us to be consistent with geomorphic data in the San Luis/Pismo block and provides a conservative approach for incorporating the uncertainties. If some of the individual faults within and along the southwestern boundary zone are structurally interconnected at depth, this could cause a significantly larger seismic event than the maximum earthquake M = 6.15 determined for the San Luis Bay fault (PG&E, 1988).

The fault parameters determined, or estimated by PG&E (1988 and docket amendments) are reasonable and consistent with their model. The UNR model proposed in this report leads to a much higher recurrence rate (about 10,000 years) and could result in simultaneous rupturing of two or more branch or secondary faults of the boundary zone. The recurrence rate is estimated from the similar rates for the Los Osos fault zone, or by inferring about 12 deformation events of about 2 meters each during the 120,000 yr period of uplift of the 5e terrace.

6.0 CONCLUSIONS AND RECOMMENDATIONS

6.1 Hosgri Fault Zone

The characterization of essential parameters and earthquake potential of the Hosgri fault zone is similar to that of PG&E (1988, and docket amendments), but uses somewhat different weightings and segment boundaries. The fault is primarily a strike-slip fault although it may have a subordinate oblique-slip component, with weightings of 0.65 for strike-slip, 0.3 for oblique-slip and 0.05 for thrust. The fault zone appears to be partitioned, at least in places along its length. The fault extends to a depth of 12 km. The fault zone is well segmented with segment lengths and weightings of <22 km (0.20), 50 km (0.55), 70 km (0.20) and 110 km (0.05), or a weighted average of <53 km. The average displacement to be expected is 1 (0.5) or 2 (0.5) m. The slip rate preferred in our analysis is within the PG&E range of 1-3 mm/yr, at 2-3 mm/yr. The recurrence rate is 300 to 2,000 yrs, with a preferred rate of about 1,000 yrs. The MCE is 7.2.

6.2 Los Osos Fault Zone

The characterization of essential parameters and earthquake potential for the Los Osos fault zone is similar to that of PG&E (1988, and docket amendments), although our estimate of maximum credible earthquakes is slightly lower than that of PG&E. The fault is part of a zone of about 2 or 3 km width and is strongly partitioned opposite the San Luis/Pismo subblocks. The activity rate may decrease to the east. A reverse-slip fault (0.9) style is preferred to oblique slip (0.1) and a moderately high dip of 60° (0.70) to a lower dip of 30° (0.30). A full segment rupture length 18 km is preferred. The average displacement is about 2.1 to 2.5 m. A magnitude of 6.5 to 6.8 is estimated for the MCE. The vertical component of the fault slip rate is 0.2 mm/yr.

6.3 Southwestern Border Zone

An alternate characterization to the PG&E (1988, and docket amendments) model is suggested. Although the PG&E model of separate seismic sources fits available data for the southwestern boundary zone and their analysis is consistent with field observations, we also believe that the alternative model for the San Luis Bay and Olson fault zone also fits the field, seismologic and structural relationships. Active faults are considered to be distributed over a 4 km width opposite the Irish Hills subblock and the zone is strongly segmented for length. Similar weightings as used in the PG&E analysis for reverse-slip faulting for the Los Osos fault are used in our analysis. A fault rupture length of the Irish Hills subblock segment is approximately 13 km. The vertical component of slip rate for the zone is 0.20 mm/yr with about 70 percent of the deformation occurring on/or across the Olson fault-San Luis Bay fault zones, and about 30 percent offshore on the Pecho and possible unidentified structures. The integrated boundary zone model yields a MCE magnitude of 6.5 with a seismogenic depth of at least 5 to 7 km.

7.0 REFERENCES

Atwater, T., 1970, Implications of plate tectonics for the Cenozoic tectonic evolution of western North America: Geological Society of America Bulletin, v. 81, p. 3513-3536.

Blake, M.C., Jr., Campbell, R.H., Dibblee, T.W., Jr., Howell, D.G., Nilsen, T.H., Normark, W.R., Vedder, J.C., and Silver, E.A., 1978, Neogene basin formation in relation to plate tectonic evolution of the San Andreas fault system, California: American Association of Petroleum Geologists Bulletin, v. 62, p. 344-372.

Bonilla, M.G., Mark, R.K., and Lienkaemper, J.J., 1984, Statistical relations among earthquake magnitude, surface rupture length, and surface fault displacement: Seismological Society of America Bulletin, v. 74, p. 2379-2411.

Buchanan-Banks, J.M., Pampeyan, E.H., Wagner, H.C., and McCulloch, D.S., 1978, Preliminary map showing recency of faulting in coastal south-central California: U.S. Geological Survey Map MF-910, 3 sheets, scale 1:250,000.

Castillo, D.A., 1991, The seismotectonics of the San Andreas fault system north of Point Arena along the Coast Ranges of Northern California: Geological Society of America Abstracts with Programs, v. 23, no. 2, p. 12.

Clark, D.G., 1990, Late Quaternary tectonic deformation in the Casmalia Range, coastal south-central California: in Lettis, W.R., ed., Neotectonics of south-central coastal California, 1990 Friends of the Pleistocene Pacific Cell Field Trip Guidebook, p. 349-383.

Clark, D.G., 1991, Quaternary Tectonic Deformation and Seismic Hazard in the Casmalia Range, Coastal South-Central California [M.S. thesis]: University of Nevada, Reno, 123 p. (preliminary draft).

Clark, D.G., and Slemmons, D.B., 1990, Late Pleistocene deformation in the Casmalia Hills region, coastal central California: Geological Society of America Abstracts with Programs, v. 22, p. 14.

Clark, D.G., Slemmons, D.B., Caskey, J.S., and dePolo, D., 1991, Seismotectonic domains in coastal central California, in Alterman, I.B., ed., Seismotectonics of Central and Coastal California: Geological Society of America Special Paper, in press.

Code of Federal Regulations, 1978, Title 10, Energy, Part 100 [10 CFR 100], Reactor site criteria: Appendix A, Seismic and geologic siting criteria for nuclear power plants: Washington, D.C., U. S. Nuclear Regulatory Commission.

Coppersmith, K.J., Griggs, G.B., 1978, Morphology, recent activity, and seismicity of the San Gregorio fault zone, in Silver, E.A., and Normark, W.R., eds., San Gregorio-Hosgri Fault Zone, California: California Division of Mines and Geology Special Report 137, p. 33-43.

Cox, A., and Engebretsen, D., 1985, Change in motion of Pacific plate at 5 Myr BP: Nature, v. 313, p. 472-474.

Crouch, J.K., Bachman, S.B, and Shay, J.T., 1984, Post-Miocene compressional tectonics along the central California margin,in Crouch, J.K., and Bachman, S.B., eds., Tectonics and Sedimentation Along the California Margin: Pacific Section of Society of Economic Paleontologists and Mineralogists, v. 38, p. 37-54.

Davis, T.L., and McIntosh, K.D., 1987, A retrodeformable structural solution across the southern Coast Ranges and implications for seismically active structures: Geological Society of America Abstracts with Programs, v. 19, p. 370.

Dehlinger, P., and Bolt, B.A., 1987, Earthquakes and associated tectonics in a part of coastal central California: Seismological Society of America Bulletin, v. 77, p. 2056-2073.

DeMets, C., Gordon, R.G., Stein, S., and Argus, D.F., 1987, A revised estimate of Pacific-North American motion and implications for western North American plate boundary zone tectonics: Geophysical Research Letters, v. 14, p. 911-914.

dePolo, C.M., Clark, D.G., Slemmons, D.B., and Aymard, W.H., 1989, Historical basin and range province surface faulting and fault segmentation, in Schwartz, D. P., and Sibson, R.H., eds., Fault Segmentation and Controls of Rupture Initiation and Termination: U.S. Geological Survey Open-File Report 89-315, p. 131-162.

dePolo, C.M., and Slemmons, D.B., 1990, Estimation of earthquake size for seismic hazards: Geological Society of America Reviews in Engineering Geology, in Krinitzsky, E.L., and Slemmons, D.B. eds, v. xviii, p. 1-28.

dePolo, C.M., Clark, D.G, and Slemmons, D.B., 1991, Historical surface faulting in the Basin and Range province, western North America: Implications for fault segmentation: Journal of Journal of Structural Geology, v. 13, no. 2, p. 123-136

Dibblee, T.W., Jr., 1966, Geology of the central Santa Ynez mountains, Santa Barbara County, California: California Division of Mines and Geology Bulletin 186, 99 p.

Dibblee, T.W., Jr., 1976, The Rinconada and related faults in the southern Coast Ranges, California, and their tectonic significance: U.S.Geological Survey Professional Paper 981, 55 p.

Dickinson, W.R., 1983, Cretaceous sinistral strike slip along the Nacimiento fault in coastal California: American Association of Petroleum Geologists Bulletin, v. 67, no. 4, p. 624-645.

Eaton, J.P., 1984, Focal mechanisms of near-shore earthquakes between Santa Barbara and Monterey, California: U.S. Geological Survey Open-File Report 84-477, 10 p.

Eaton, J.P., 1985a, Regional seismic background of the May 2, 1983 Coalinga earthquake, in Rymer, M.J., and Ellsworth, W.L., eds., Mechanics of the May 2, 1983 Coalinga Earthquake: U.S. Geological Survey Open-File Report 85-44, p. 44-60.

Eaton, J.P., 1985b, The May 2, 1983 Coalinga earthquake and its aftershocks-A detailed study of the hypocenter distribution and focal mechanisms of the larger aftershocks, in Rymer, M.J., and Ellsworth, W.L., eds., Mechanics of the May 2, 1983 Coalinga Earthquake: U.S. Geological Survey Open-File Report 85-44, p. 132-202.

Evernden, J.F., Kohler, W.M., and Clow, G.D., 1981, Seismic intensities of earthquakes of conterminous United States--their prediction and interpretation: U.S. Geological Survey Professional Paper 1223, 56 p.

Feigl, K.L, King, R.W., and Jordan, T.H., 1990, Geodetic measurement of tectonic deformation in the Santa Maria fold and thrust belt, California: Journal of Geophysical Research, v. 95, p. 2679-2699.

Gawthrop, W.H., 1978a, Seismicity and tectonics of the central California coastal region, in Silver, E.A., and Normark, W.R., eds., San Gregorio-Hosgri Fault Zone, California: California Division of Mines and Geology Special Report 137, p. 45-56.

Gawthrop, W.H., 1978b, The 1927 Lompoc, California earthquake: Seismological Society of America Bulletin, v. 68, p. 1705-1716.

Graham, S.A., and Dickinson, W.R., 1978, Apparent offsets of on-land geologic features across the San Gregorio-Hosgri fault trend, in Silver, E.A., and Normark, W.R., eds., San Gregorio-Hosgri Fault Zone, California: California Division of Mines and Geology Special Report 137, p. 13-23.

Greene, H.G., Lee, W.H., McCulloch, D.S., and Brabb, E.E., 1973, Faults and earthquakes in the Monterey Bay Region, California: U. S. Geological Survey Map MF-518.

Guptill, P.D., Heath, E.G., and Brogan, G.E., 1980, Surface fault traces and historical earthquake effects near Los Alamos Valley, Santa Barbara County, California: Menlo Park, California, Technical Report for U.S. Geological Survey, Contract No. 14-08-0001-18255, 125 p.

Hadley, D., and Kanamori, H., 1978, Recent seismicity in the San Fernando region and tectonics in the west-central Transverse Ranges, California: Seismological Society of America Bulletin, v. 68, p. 1449-1457.

Hall, C.A., Jr., 1978, Origin and development of the Lompoc-Santa Maria pull-apart basin and its relation to the San Simeon-Hosgri strike-slip fault, western California, in Silver, E.A., and Normark, W.R., eds., San Gregorio-Hosgri Fault Zone, California: California Division of Mines and Geology Special Report 137, p. 25-31.

Hall, C.A., Jr., 1981, San Luis Obispo transform fault and middle Miocene rotation of the western Transverse Ranges, California: Journal of Geophysical Research, v. 86, no. B2, p. 1015-1031.

Hall, C.A., Jr., 1982, Pre-Monterey subcrop and structure contour maps, south-central California: U.S. Geological Survey Map MF-384, 6 sheets, scale 1:62,500.

Hamilton, D.H., and Willingham, C.R., 1977, Hosgri fault zone: Structure, amount of displacement, and relationship to structures of the western Transverse Ranges: Geological Society of America Abstracts with Programs, v. 9, p. 429.

Hanks, T.C., 1979, The Lompoc, California, earthquake (November 4, 1927; M= 7.3) and its aftershocks: Seismological Society of America Bulletin, v. 69, p. 451-462.

Hanks, T.C., and Kanamori, H., 1979, A moment magnitude scale: Journal of Geophysical Research, v. 84, no. 4, p. 582-600.

Harbert, W., and Cox, A., 1989, Late Neogene motion of the Pacific Plate: Journal of Geophysical Research, v. 94, p. 3052-3064.

Hart, E.W., 1976, Basic Geology of the Santa Margarita area, San Luis Obispo County, California: California Division of Mines and Geology Bulletin 199, 45 p.

Hart, E.W., Bryant, W.A., Manson, M.W., and Kahle, J.E., 1986, Summary Report: Fault Evaluation Program, 1984-1985 area (southern Coast Ranges region and other areas): California Division of Mines and Geology Open-File Report 86-3 SF, 8 p., 1 table, 1 plate.

Hauksson, E., Jones, L.M., Davis, T.L., Hutton, K., Brady, A.G., Reasenberg, P.A., Michael, A.L., Yerkes, R.F., Williams, P., Reagor, G., Stover, C.W., Bent, A.L., Shakal, A.K., Etheredge,E., Porcella, R.L., Bufe, C.G., Johnston, M.J.S., and Cranswick,E., 1988, The 1987 Whittier Narrows earthquake in the Los Angeles Metropolitan area, California: Science, v. 239, p. 1409-1412.

Hill, M.L., and Dibblee, T.W., Jr., 1953, San Andreas, Garlock, and Big Pine faults, California--A study of the character, history, and tectonic significance of their displacements: Geological Society of America Bulletin, v. 64, p. 443-458.

Hornafius, J.S., 1985, Neogene tectonic rotation of the Santa Ynez Range, western Transverse Ranges, California, suggested by paleomagnetic investigation of the Monterey Formation: Journal of Geophysical Research, v. 90, no. B14, p. 12,503-12,522.

Jahns, R.H., 1973, Tectonic evolution of the Transverse Ranges province as related to the San Andreas fault system: Stanford University Publications in Geological Sciences, v. 13, p. 149-170.

Jennings, C.W., 1975, Fault map of California with locations of volcanoes, thermal springs and thermal wells: California Division of Mines and Geology, 1 map, scale 1: 750,000.

Kanamori, H., 1977, The energy release in great earthquakes: Journal of Geophysical Research, v. 82, p. 2981-1987.

Kanamori, H., 1983, Magnitude scale and quantification of earthquakes: Tectonophysics, v. 93, p. 185-199.

Kennedy, G.L., Clark, D.G., and Wehmiller, J.F., 1990, The southern Oregonian province in the late Pleistocene: changing paleoclimates and sea level history based on integrated faunal and aminostratigraphic studies, Casmalia Hills, coastal California: Geological Society of America Abstracts with Programs.

Killeen, K.M., 1988, Timing of Folding and Uplift of the Pismo Syncline, San Luis Obispo County, California [M.S. Thesis]: University of Nevada, Reno, 75 p.

Killeen, K.M., Slemmons, D.B., and Swanson, K.E., 1987, Timing of folding and uplift of the Pismo syncline, San Luis Obispo County, California: Geological Society of America Abstracts with Programs, v. 19, p. 394.

Kneupfer, P.L., 1989, Implications of the characteristics of endpoints of historical surface fault ruptures for the nature of fault segmentation, in Schwartz, D.P., and Sibson, R.H., eds., Fault Segmentation and Controls of Rupture Initiation and Termination: U. S. Geological Survey Open-File Report 89-315, p. 193-228.

Leinkaemper, J.J., 1984, Comparison of two surfacewave magnitude scales: M of Gutenberg and Richter (1954) and M_S of "Preliminary Determination of Epicenters": Seismological Society of America Bulletin, V. 74, p. 2357-2378.

Lettis, W.R., and Hanson, K.L., 1991, Crustal strain partitioning: Implications for seismic hazard assessment in western California: Geology, in press.

Luyendyk, B.P, Kamerling, M.J., and Terres, R., 1980, Geometric model for Neogene crustal rotations in southern California: Geological Society of America Bulletin, v. 91, p. 211-217.

Matz, B., 1989, Remote sensing and geomorphic studies for seismotectonic analysis, Santa Maria basin, California [M. S. thesis]: University of Nevada, Reno, 90 p.

Matz, B., and Slemmons, D.B., 1987, Remote sensing study of Pismo syncline and Santa Maria basin, central coastal California: Geological Society of America Abstracts with Programs, v. 19, p. 429.

McCulloch, D.S., 1989, Evolution of the offshore central California margin, in Winterer, E.L, Hussong, D.M., and Decker, R.W., eds., The Eastern Pacific Ocean and Hawaii: Geological Society of America, The Geology of North America, v. N., p. 439-470.

Minster, J.B., and Jordon, T.H., 1978, Present-day plate motions: Journal of Geophysical Research, v. 83, no. B11, p. 5331-5354.

Minster, J.B., and Jordan, T., 1984, Vector constraints on Quaternary deformation of the western United States east and west of the San Andreas fault, in Crouch, J.K., and Bachman, S.B., eds., Tectonics and Sedimentation Along the California Margin: Los Angeles, Society of Economic Paleontologists and Mineralogists, Pacific Section, v. 38, p. 1-16.

Minster, J. B., and Jordan, T.H., 1987, Vector constraints on western United States deformation from space geodesy, neotectonics and plate motions: Journal of Geophysical Research, v. 92, no. B6, p. 4798-4804.

Mount, V.S., and Suppe, J., 1987, State of stress near the San Andreas fault: Implications for wrench tectonics: Geology, v. 15, p. 1143-1146.

Namson, J.S., and Davis, T.L., 1988a, Seismically active fold and thrust belt in the San Joaquin Valley, central California: Geological Society of America Bulletin, v. 100, p. 257-273.

Namson, J.S., and Davis, T.L., 1988b, Structural transect of the western Transverse Ranges, California--Implications for lithospheric kinematics and seismic risk evaluation: Geology, v. 16, p. 675-679.

Namson, J.S. and Davis, T.L., 1990, Subsurface study of the late Cenozoic structural geology of the Santa Maria Basin, western Transverse Ranges and southern Coast Ranges, California: American Association of Petroleum Geologists Bulletin, v. 74, p. 467-492.

Nitchman, S.P, 1988, Tectonic geomorphology and neotectonics of the San Luis Range, San Luis Obispo County, California [M.S. thesis]: Reno, University of Nevada, 120 p.

Nitchman, S.P., and Slemmons, D.B., 1987, Pleistocene flexural slip faulting possibly triggered by crustal unloading, Pismo Beach, central coast California: Geological Society of America Abstracts with Programs, v. 19, p. 437.

Nitchman, S.P, and Slemmons, D.B., 1991, The Wilmar Avenue fault, an active fault near Pismo Beach: Geological Society of America Special Paper, in press.

Pacific Gas and Electric Company, 1988, Final Report of the Diablo Canyon Long Term Seismic Program: U.S. Nuclear Regulatory Commission Docket Nos. 50-275 and 50-23.

Pacific Gas and Electric Company, 1991, Addendum to the Final Report of the Diablo Canyon Long Term Seismic Program Docket Nos. 50-275 and 50-323.

Page, B.M., 1966, Geology of the Coast Ranges of California, in Bailey, E.H., ed., Geology of Northern California: California Division of Mines and Geology Bulletin 190, p. 255-276.

Page, B.M., 1970, Sur-Nacimiento fault zone of California: Continental margin tectonics: Geological Society of America Bulletin, v. 81, p. 667-690.

Page, B.M., 1981, The southern Coast Ranges, in Ernst, W.G., ed., The Geotectonic Development of California: Englewood Cliffs, New Jersey, Prentice-Hall, Inc., p. 329-417.

Page, B.M., and Engebretsen, D.C., 1984, Correlation between the geologic record and computed plate motions for central California: Tectonics, v. 3, p. 133-155.

Poley, C.M., Eaton, J.P., and Lindh, A.G., 1987, Recent seismicity of the central California region from San Francisco to the Transverse Ranges: Geological Society of America Abstracts with Programs, v. 19, p. 440.

Reed, R.D., 1933, Geology of California: Tulsa, Oklahoma, American Association of Petroleum, 355 p.

Richter, C.F., 1969, Possible seismicity of the Nacimiento fault, California: Geological Society of America Bulletin, v. 80, p. 1363-1366.

Savage, J.C., and Burford, R.O., 1973, Geodetic determination of relative plate motion in central California: Journal of Geophysical Research, v. 78, no. 5, p. 832-845.

Savage, W.U., and McLaren, M.K., 1987, Recent seismicity of south-central California: Geological Society of America Abstracts with Programs, v. 19, p. 446-447.

Schwartz, D.P., and Coppersmith, 1984, Fault behavior and characteristic earthquakes: Examples from the Wasatch and San Andreas faults: Journal of Geophysical Research, v. 89, p. 5681-5698.

Schwartz, D.P, 1988, Geological characterization of seismic sources; moving into the 1990's, in Von Thun, J.L., ed., Proceedings; Earthquake Engineering and Soil Dynamics II, Recent Advances in Ground-Motion Evaluation: Geotechnical Special Publication, v. 20, p. 1-42.

Schwartz, D.P., and Coppersmith, K.J., 1986, Seismic hazards: New trends in analysis using geologic data: in Active Tectonics, ed. National Academy Press, Washington, D.C., p. 215-230.

Sibson, R.H., 1982, Fault zone models, heat flow, and the depth distribution of earthquakes in the continental crust of the United Sates: Seismological Society of America Bulletin, v. 72, p. 151-163.

Slemmons, D.B., 1982, Determination of design earthquake magnitudes for microzonation: Proceedings Third International Earthquake Microzonation Conference, v. 1, p. 119-130.

Slemmons, D.B., 1987, Capable faults and tectonically active folds of the California Central Coast Ranges [abst.]: Geological Society of America Abstracts with Programs, v. 19, no. 6, p. 452.

Slemmons, D.B., and Chung, D.H., 1982, Maximum credible earthquake magnitudes for the Calaveras and Hayward fault zones, California: Proceedings of the Conference on Earthquake Hazards in the Eastern San Francisco Bay Area; California Division of Mines and Geology Special Paper 62, p. 115-124.

Slemmons, D.B., and dePolo, C.M., 1986, Evaluation of Active Faulting and Associated Hazards: in Active Tectonics, Wallace, R.E., editor, Geophysics Study Committee, National Academy Press, Washington, D.C., p. 45-62.

Slemmons, D.B., Bodin, P., and Zhang, X., 1989, Determination of earthquake size from Surface faulting events: Proceedings Third Seminar on Seismic Zonation, Guangzhou, China, p. 157-169.

Stein, R.S., and Yeats, R.S., 1989, Hidden earthquakes: Scientific American, v. 260, p. 48-57.

Steritz, J. W., and Luyendyk, B.P., 1991, Hosgri fault zone, offshore Santa Maria Basin, California: Geological Society of America Special Paper, in press.

Taliaferro, N.L., 1943, Geologic history and structure of the central Coast Ranges of California: California Division of Mines and Geology Bulletin 118, p. 119-163.

Tocher, D., 1958, Earthquake energy and ground breakage: Seismological Society of America Bulletin, v. 48, p. 147-153.

Vittori, E., 1987, Structural analysis of late Cenozoic deformation, Southern California Coast Ranges, Central California: Geological Society of America Abstracts with Programs, v. 19, no. 6, p. 460.

Vittori, E., Nitchman, S., and Slemmons, D.B., 1991, Structural analysis of the late Pliocene and Quaternary deformation in coastal central California: in Alterman, I.B., and others, eds., in press.

Wallace, R.E., ed., 1991, The San Andreas fault system, California: U. S. Geological Survey Professional Paper 1515, 283 p.

Ward, S.N., 1990, Pacific-North America Plate Motions: New Results from Very Long Baseline Interferometry: Journal of Geophysical Research, v. 95, No. B13, p. 21,965-21,981

Weber, G.E., 1979, Geologic investigation of the marine terraces of the San Simeon region and Pleistocene activity on the San Simeon fault zone, San Luis Obispo County, California: Menlo Park, California, Technical Report to U.S. Geological Survey, Contract No. 14-08-001-18230, 66 p.

Weber, G.E., 1983, Geologic investigation of the marine terraces of the San Simeon region and Pleistocene activity on the San Simeon fault zone, San Luis Obispo County, California: Menlo Park, California, Technical Report to U. S. Geological Survey, Contract No. 14-08-001-18230, 66 p.

Weber, G.E., and Lajoie, K.R., 1979a, Late Pleistocene rates of movement along the San Gregorio fault zone, determined from offset of marine terrace shoreline angles, in Weber, G.E., Lajoie, K.R., and Griggs, G.B., eds., Coastal Tectonics and Coastal Geologic Hazards in Santa Cruz and San Mateo Counties, California: Geological Society of America, Cordilleran Section 75th Annual Meeting, Field Guide.

Weber, G.E., and Lajoie, K.R., 1979b, Evidence for Holocene movement on the Frijoles fault near Point Ano Nuevo, San Mateo County, California: in Weber, G.E., Lajoie, K.R., and Griggs, G.B., eds., Coastal Tectonics and Coastal Geologic Hazards in Santa Cruz and San Mateo Counties, California: Field Trip Guide for Cordilleran Section of the Geological Society of America, 75th Annual Meeting, p. 92-100.

Weldon, R., and Humphreys, E., 1986, A kinematic model of southern California: Tectonics, v. 5, p. 33-48.

Wells, D., Coppersmith , K., Zhang, X., and Slemmons, D.B., 1989, New earthquake magnitude and fault rupture parameters: Part II. Maximum and average relationships [abstr.]: Seismological Society of America, Seismological Research letters, v. 60, n. 1.

Wentworth, C.M., and Zoback, M.D., 1989, The style of Late Cenozoic deformation at the eastern front of the California Coast Ranges: Tectonics, v. 8, p. 237-246.

Wesnousky, S.G., 1986, Earthquakes, Quaternary faults, and seismic hazard in California: Journal of Geophysical Research, v. 91, no. B12, p. 12,587-12,631.

Wright, L., 1976, Late Cenozoic fault patterns and stress fields in the Great Basin and westward displacement of the Sierra Nevada block: Geology, v. 4, p. 489-494.

Wyss, M., 1979, Estimating maximum expectable magnitude of earthquakes from fault dimensions: Geology, v. 7, p. 336-340.

Yeats, R.S., 1981, Quaternary flake tectonics of the California Transverse Ranges: Geology, v. 9, p. 16-20.

Yeats, R.S., 1986, Active faults related to folding: in Active Tectonics, Wallace, R.E., editor, National Academy Press, Washington, D.C., p. 63-79.

Zhang, X., Slemmons, D.B., Wells, D., and Coppersmith, K., 1989, New earthquake magnitude and fault rupture parameters: Part I. Surface rupture length and rupture area relationships [abstr.]: Seismological Society of America, Seismological Research Letters, v. 60, n. 1.

Ziony, J.I., and Yerkes, R.F., 1985, Evaluating earthquake and surface-faulting potential, in Ziony, J.I., ed., Evaluating Earthquake Hazards in the Los Angeles Region--An Earth-Science Perspective: U.S. Geological Survey Professional Paper 1360, p. 43-91.

APPENDIX E

GLOSSARY OF ABBREVIATIONS AND TECHNICAL TERMS

ac - alternating current

accelerogram - a record or chart of acceleration versus time

accelerometer - An instrument used to measure acceleration of ground motion

accident sequence - the combination of an initiating event and the resulting systems failures and successes, resulting in a definable outcome, generally core damage; each branch of an event tree may be considered to be the end-point of a separate accident sequence

ACI - American Concrete Institute

ACRS - NRC's Advisory Committee on Reactor Safeguards

AE - an architect/engineering organization

AEC - Atomic Energy Commission, predecessor agency to the NRC

aftershock - an earthquake that follows a larger earthquake and originates at or near the hypocenter of the larger earthquake

AFW - auxiliary feedwater

airgun - an energy source used in marine seismic surveys; air under high pressure is explosively released to generate a shock wave

AISC - American Institute of Steel Construction

alluvium - sedimentary deposits made by streams on river beds or flood plains

anticline - a fold, generally convex upward, whose core contains stratigraphically older rocks

anticlinorium - a composite anticlinal structure of regional extent composed of lesser folds

aseismic - not seismically active

ASLAB - NRC's Atomic Safety and Licensing Appeal Board

ASLB - NRC's Atomic Safety and Licensing Board

ASME - American Society of Mechanical Engineers

ASW - auxiliary saltwater

ATWT - anticipated transient without trip; also referred to as ATWS, anticipated transient without scram

AW - loss of AFW system; a top event

backwasted - the progressive retreat of an escarpment or mountain front from its original position, as a result of erosion

basemat - the foundation slab of a large structure or building, usually constructed of thick, reinforced concrete

basement - the rocks, commonly igneous and metamorphic rocks, that underlie the sedimentary deposits that usually make up the top layers of the earth's crust

Basin and Range - a physiographic province in the southwestern United States that is characterized by a series of tilted fault blocks forming ridges and mountains and broad, intervening basins

bathymetry - the bed of the ocean or other body of water

Bechtel - Bechtel Power Corporation, an AE firm

Birnbaum importance - the Birnbaum importance of a component with respect to a given risk measure is the risk measure with the component assumed to be failed less the risk measure with the component assumed to be working

binning - assigning to bins

BNL - Brookhaven National Laboratory

BOP - balance of plant; not associated with the NSSS

borehole - a circular hole made by boring; a deep hole of small diameter, such as an oil or water well

capable - when applied to a fault, capable means a fault that is capable of movement in the near future; in general, a fault on which there has been movement within the last 35,000 years (see 10 CFR Part 100, Appendix A)

CCW - component cooling water

CDF - core damage frequency

CDFM - conservative deterministic failure margin

Cenozoic - the most recent of the four eras into which geologic time is divided; it extends from about 65 mybp to the present

CFR - Code of Federal Regulations

CLASSI - Continuum Linear Analysis for Soil-Structure Interaction - a computer program used for SSI analysis

colluvial deposits - loose and incoherent deposits, usually at the foot of a slope or cliff and brought there by gravity

convolve - a mathematical procedure by which a hazard function is integrated with a conditional fragility curve to determine an unconditional probability of failure

CP - construction permit

Cretaceous - the final period of the Mesozoic era, extending from about 140 to 65 mybp

CRFIRE - control room and/or cable spreading room fire

cross-tie - an intertie or interconnection between two systems, trains, units

crustal block - a block in the earth's crust that acts as a single unit when acted upon by tectonic forces

CSF - top event conditional split fraction

dc - direct current

DCPRA - Diablo Canyon probabilistic risk assessment

DDE - double design earthquake

decollement - detachment structure of strata due to deformation, resulting in independent styles of deformation in the rocks above and below

de minimis - so small as to be insignificant

DG - diesel generator

dip of a fault - the angle the fault makes with the horizontal

dip-slip fault - a fault on which the movement is parallel to the dip of the fault

DPD - discrete probability distribution

DSM - dominant sequence model

DSP - dedicated shutdown panel

EBT - energy balance technique

ECCS - emergency core cooling system

ELOCA - excessive LOCA; an internal initiating event; any LOCA more severe than the design-basis LOCA

end branch - The end of one of the branches of an event tree, usually a single consequence or class of consequences.

en-echelon - said of geologic features that are in an overlapping or staggered arrangement; each is relatively short but collectively they form a linear zone, in which the strike of the individual features is oblique to that of the zone as a whole

Eocene - an epoch of the early Tertiary period from about 37 to 58 mybp, after the Paleocene and before the Oligocene

epicenter - the point on the earth's surface directly above the hypocenter (the point within the earth that is the center of energy release of an earthquake)

EPRI - Electric Power Research Institute

escarpment - a long, more or less continuous cliff, separating two level or gently sloping surfaces, and produced by erosion or faulting; a scarp

ESD - event sequence diagram

event tree - a description of all the possible consequences (depending upon plant system and operator responses) that may result from a specific initiating event, ordered in a branching, tree-like diagram

EXFW - excessive feedwater; an internal initiating event

external initiating event - an initiating event that originates outside the plant systems; fire, flood, earthquakes

FA - fragility analysis

fault - a fracture along which there has been displacement of the sides relative to one another parallel to the fracture

fault-bend fold - a fold that occurs above a change in dip of an upward-ramping thrust fault; for example, a flattening of dip caused by the intersection of, and continued propagation along a bedding plane

fault-propagation fold - a fold that occurs when a propagating thrust fault loses slip and terminates upsection by transferring its shortening to a fold developing at its tip

fault segmentation point - a point on a fault where the fault bends or otherwise changes character

fault system - a wider band of faulting and deformation than a fault zone; two or more interconnecting groups of faults that are parallel or nearly so and that are related to a particular deformational episode.

fault tree analysis - an analytical technique, whereby an undesired state of a system is specified (usually a state that is critical from a safety standpoint), and the system is then analyzed in the context of its environment and operation to find all credible ways in which the undesired event can occur; a primary method used in PRA

fault zone - a zone expressed as numerous small fractures that may be hundreds of meters wide

F_{gmi} - spatial incoherence factor

FHB - fuel handling building

firewater - water supply used for extinguishing fires

fluvial - produced by the action of a stream or river

FMEA - failure modes and effects analysis; an analytical method that considers the ways in which system components can fail and what the effects of those failures are in terms of system operability; a supplementary method used in PRA

focal mechanism - a procedure for determining type of fault slip from observations of body waves recorded at the earth's surface

footplate - a metal plate upon which a component rests and to which it is attached; a base plate

footwall of a fault - the side of a fault that lies beneath the fault; the opposite of the hanging wall of the fault

fragility - the conditional probability of failure of a structure, system, or component for a given value of a ground-motion parameter, for example, spectral acceleration

frontline - a system used directly to perform a safety-related function; a mainline system; to be distinguished from support systems, which support frontline systems

FS_i - seismic margin scale factor

FSAR - final safety analysis report

F_{ss} - Spectral shape factor

Fussel-Vesely importance - the Fussel-Vesely importance of a component is the fractional reduction in the risk measure if the component were perfectly reliable

geodetic - pertaining to the position of geographic points

geomorphic - pertaining to the form of the earth or of its surface features

geomorphology - the science that studies the general configuration of the earth's surface; specifically, the study of the classification, description, nature, origin, and development of landforms and their relationship to underlying structures, and the history of geologic changes as recorded by these surface features

geoscience - geology, or earth science

GERS - generic equipment ruggedness spectrum

graben - an enlongate, relatively depressed crustal unit or block that is bounded by faults on both of its long sides

GSG - geology, seismology, and geophysics

halfgraben - an enlongate, relatively depressed crustal unit or block that is bounded by a fault on one of its long sides

halfspace - half of the three-dimensional expanse

hanging wall of a fault - the side of a fault that lies above the fault; the opposite of the footwall of the fault

hazard curve - a curve showing the probability of exceeding each of a number of seismic acceleration values; the curve usually shows annual frequency of exceedance versus spectral acceleration or peak ground acceleration

HBFT - heat balance fault tree

HCLPF - high confidence of low probability of failure

HCR - human cognitive reliability

Holocene - an epoch of the Quaternary period, from the end of the Pleistocene, approximately 10,000 years ago, to the present time

HPI - high-pressure injection

HRA - human reliability analysis; an analytical technique, whereby the ways in which human actions initiate, propagate, or terminate fault and accident sequences are identified and quantified

HSDP - hot shutdown panel

HTGR - high-temperature gas-cooled reactor

hypocenter - the center of the energy release of an earthquake

hysteretic - pertaining to the lag in the return of an elastically deformed body to its original shape after the load has been removed

hysteretic damping - energy loss during a cycle of loading and unloading resulting from interparticle friction in soils; internal damping

Hz - hertz, a unit of frequency equal to one cycle per second

IDVP - independent design verification program

IEA - inelastic energy absorption

igneous - pertaining to rock that solidified from molten or partly molten material; one of the three main classes into which rocks are divided, the others being metamorphic and sedimentary

IMSIV - closure of all MSIVs; an internal initiating event

initiating event - an event (usually undesirable) that results in a change in plant state

internal initiating event - an event initiating an event tree that originates within the plant, such as system or component failures, or human actions

intertie - a crosstie or interconnection between two systems, trains, or units

ISI - inadvertent safety injection; an internal initiating event

isopach - a line drawn on a map through points of equal thickness of a stratigraphic unit or group of stratigraphic units

Jurassic - the second period of the Mesozoic era (after the Triassic and before the Cretaceous), thought to have covered the span of time between 205 and 140 million years ago

kinematic model - a mechanical model which treats pure motion, without reference to mass or cause

kip - one thousand pounds force

L1DC - loss of one dc bus; an internal initiating event

LCV - loss of condenser vacuum; an internal initiating event

lineament - a linear topographic feature of regional extent that is believed to reflect crustal structure

liquefaction - the process of transforming a sediment to a state in which it behaves like a liquid; liquefaction can be induced by earthquake ground motions

listric fault - a fault whose dip angle decreases (becomes more horizontal) with depth, often merging at depth with a horizontal detachment surface (a decollement)

LLOCA - large LOCA, resulting from a break in a pipe greater than 6 inches in diameter; an internal initiating event

LOCA - loss-of-coolant accident

LOCC - loss of CCW; an internal initiating event; usually referred to as LPCC

LOCV - loss of control room ventilation; an internal initiating event

LOOP - loss of offsite power; an internal initiating event

LOPF - loss of primary flow; an internal initiating event

LOSW - loss of ASW; an internal initiating event

LOSWV - loss of switchgear ventilation; an internal initiating event

LP - Loma Prieta

LPCC - loss of CCW; an internal initiating event; sometimes referred to as LOCC

LPI - low-pressure injection

LT - long-term cooling frontline system module

LTSP - long-term seismic program

marine terrace - a wave-cut platform that has been exposed by uplift along a seacoast or by lowering of sea level; an elevated marine-cut bench

melange - a mappable body of rock that includes fragments and blocks of all sizes embedded in a fragmented and generally sheared matrix

Mesozoic - an era of geologic time, from the end of the Paleozoic to the beginning of the Cenozoic, or from about 250 to about 65 million years ago

metamorphic - pertaining to rock that is formed from pre-existing rock as a result of physical and chemical conditions imposed at depth that differ from the conditions under which the rocks originated; one of the three main classes into which rocks are divided, the others being igneous and sedimentary

MFW - main feedwater

microearthquake - a small earthquake, less than about magnitude 3

Miocene - an epoch of the early Tertiary period (5-23 mybp), after the Oligocene and before the Pliocene

MLD - master logic diagram

MLOCA - medium LOCA resulting from a break in a pipe between 2 inches and 6 inches in diameter; an internal initiating event

MME - maximum magnitude earthquake

MSIV - main steam isolation valve

MWe - megawatts electric

mybp - millions of years before the present

Neogene - an interval of time incorporating the Miocene, Pliocene, and Pleistocene epochs (1.6-23 mybp)

noncapable - a fault that is not capable of movement in the near future; in general, a fault on which there has not been movement within the last 35,000 years (see Appendix A to 10 CFR 100)

nonisolable - not capable of being isolated

normal fault - a fault which is experiencing vertical motion due to tensile forces; the hanging wall appears to have moved downward relative to the footwall

North American plate - the crustal plate underlying the North American continent

NRC - Nuclear Regulatory Commission

NSSS - nuclear steam supply system

OBE - operating-basis earthquake

oblique slip fault - a fault on which the slip is oblique (some combination of vertical and horizontal motion) to the dip of the fault

off shore - pertaining to a direction seaward from the land

OL - operating license

onlap - an overlap characterized by the regular and progressive pinching out, toward the margins or shores of a depositional basin, of the sedimentary units within a conformable sequence of rocks, in which the boundary of each unit is transgressed by the next overlying unit and each unit in turn terminates farther from the point of reference

on shore - pertaining to a direction landward from the sea

ophiolite - an assemblage of basic igneous rocks associated with geosynclinal sediments formed during an early phase of the development of a geosyncline (trough or basin)

orogeny - the process of formation of mountains

outlier - an item whose value lies outside the general range of values of comparable items

Pacific plate - the crustal plate underlying the Pacific Ocean and the part of California lying to the west of the San Andreas fault system

paleoseismic - the study of prehistoric seismic activity

PGA - peak ground acceleration

plate - a thin part of the earth's lithosphere (crust and upper mantle or about 100 km thick) which moves horizontally and adjoins other plates along zones of seismic activity

Pleistocene - an epoch of the Quaternary period, after the Pliocene and before the Holocene; it began 1.6 million years ago and ended about 10,000 years ago

PLG - Pickard, Lowe and Garrick, an engineering consulting firm

Pliocene - an epoch of the Tertiary period (1.6-5 mybp), after the Miocene and before the Pleistocene

PLMFW - partial loss of MFW; an internal initiating event

Poisson's ratio - the ratio of lateral to longitudinal strain

PORV - power (or pilot) operated relief valve

power block - the major plant structure grouped together around the containment building, including the auxiliary building and the turbine building

PRA - probabilistic risk assessment; a technique for integrating diverse aspects of the design and operation of a nuclear power plant in order to analyze all scenarios leading to reactor core damage, estimate the probability of such scenarios occurring, and assess the consequences of each scenario to obtain an estimate of overall risk; fault tree analysis and event tree analysis are the primary analytical tools used in PRA

PSF - performance shaping factor

PTS - pressurized thermal shock

pull-apart basin - a geologic depression created as a result of the moving apart of the zones on either side of the basin

PWR - pressurized-water reactor

Quaternary - the second period of the Cenozoic era, following the Tertiary; it began 1.6 million years ago and extends to the present; it consists of two epochs: the Pleistocene, up to about 10,000 years ago, and the Holocene since that time

RCP - reactor coolant pump

RCS - reactor coolant system

reach of a fault - a segment of a fault

rebar - steel bar used to reinforce concrete structures

reliability block diagram - a method of analytically modeling a system, in which each block represents a component or group of components, and for which a reliability estimate is made; a supplementary method used in PRA; by appropriate combination of component reliabilities, an overall reliability estimate for the system is obtained

retrodeformable analysis - an analysis in which the existing strata of the earth are deformed to project their relative position at times in the past

reverse fault - a fault which is experiencing vertical motion due to compressive forces, in which the hanging wall has been raised relative to the footwall

RHR - residual heat removal

right lateral - displacement on a fault such that the side of the fault opposite the observer appears displaced to the right

rightstep - apparent displacement to the right

risk - the likelihood of a specific set of undesirable consequences, typically, core damage

RISKMAN - family of computer codes; includes SQLINK

RPS - reactor protection system

RRP - risk reduction potential

RRS - required response spectrum

RT - reactor trip; an internal initiating event

RWST - refueling water storage tank

sag pond - a small body of water occupying an enclosed depression or sag formed where active or recent fault movement has impounded drainage

Sandia - the Sandia National Laboratory

SASSI - System for Analysis of Soil-Structure Interaction - a computer program that performs SSI analysis

SBO - station blackout

scarp - a line of cliffs produced by faulting or erosion; an escarpment

SE - RCP seal LOCA; a top event

sea stack - an isolated, pillar-like rocky island, detached from a headland by wave erosion

sedimentary - pertaining to rock that resulted from the consolidation of sediment; one of the three main classes into which rocks are divided, the others being igneous and metamorphic

seismic - pertaining to an earthquake or earth vibration, including those that are artificially induced

seismic gap - an area along a fault which, in contrast to other areas on the same fault, has not been seismically active in the recent past

seismicity - the degree of earthquake activity; i.e., the number and magnitude of earthquakes in an area

seismic reflection line - a line on a map describing the path over which a seismic reflection profile has been taken

seismic reflection profile - a chart of the earth's interior obtained from the reflection of sonic waves

seismogenic - capable of generating earthquakes

seismogenic crust - seismogenic zone

seismogenic zone - that part of the earth's crust within which earthquakes are generated; the seismogenic zone in California extends to a depth of about 12 km

seismogram - a record of earthquake vibration made by a seismograph

seismograph - an instrument used to detect vibratory earth motion

sense of slip - the type of motion on a fault, e.g., strike-slip, reverse-slip, thrust; the style of faulting

SER - safety evaluation report

SGH - San Gregorio-Hosgri, a major fault system that passes near Diablo Canyon

SGTR - steam generator tube rupture

SH wave - a horizontally polarized shear wave (see also SV wave)

shear wave - a seismic wave in the earth, propagated by a shearing motion that involves oscillation perpendicular to the direction of propagation

SLBI - steamline break inside containment; an internal initiating event

SLBO - steamline break outside containment; an internal initiating event

slickensides - a polished and striated rock surface that results from friction along a fault plane

SLIM - success likelihood index method

slip rate - the rate of slip, or differential motion, across a fault

SLOCI - small LOCA, isolable, resulting from a break in a pipe less than 2 inches in diameter; an internal initiating event

SLOCN - small LOCA, nonisolable, resulting from a break in a pipe less than 2 inches in diameter; an internal initiating event

SME - seismic margin earthquake

SNL - the Sandia National Laboratory

SQLINK - computer code; part of the RISKMAN family of codes

SRP - Standard Review Plan, NUREG-0800

SRSS - square root of the sum of the squares

SRV - safety relief valve

SSC - seismic source characterization; also structures, systems, and components

SSE - safe shutdown earthquake

SSER - supplemental safety evaluation report

SSI - soil-structure interaction

SSPS - solid-state protection system

SSRS - site-specific response spectrum

stepover - an area within a zone of faulting in which a specific fault trace ends and, at a distance laterally, another fault trace begins

stillstand - a period of time when mean sea level did not change with respect to the elevation of a land area such as a continent or island

stochastic - a process in which the dependant variable is random and described by a probability distribution

strand of a fault - a single fault plane, frequently one of many parallel or subparallel strands in a zone of faulting

strain partitioning - the partitioning of strain into horizontal and vertical components

stratigraphic - pertaining to the arrangement of the sequence of rock strata

strike of a fault - the direction taken by a structural surface (e.g., the plane of a fault) as it intersects the horizontal

structural block - a crustal block that acts as a single unit when acted upon by tectonic forces

style of faulting - the type of motion on a fault, e.g., strike-slip, reverse-slip, thrust; the sense of slip of the fault

subduction - the process of one lithospheric plate descending beneath another

subparallel - nearly parallel

subhorizontal - nearly horizontal

subsidence - sinking or downward settlement of the earth's surface

SV wave - a vertically polarized shear wave (see also SH wave)

switchgear - an enclosed assembly of power circuit switching devices and the associated electrical busses

syncline - a fold in the earth, generally concave upward, the core of which contains stratigraphically younger rocks

synclinorium - a composite synclinal structure of regional extent composed of lesser folds

synform - a fold whose limbs close downward in strata for which the stratigraphic sequence is unknown

tau effect - a parameter that accounts for the combined effects of SSI, structure embedment, and ground motion incoherence

tectonics - a branch of geology dealing with the broad architecture of the outer part of the earth, i.e., the major structural or deformational features and their relations, origin, and historical evolution

teleseismic - pertaining to earthquakes recorded at a distance greater than about 2000 km

Tertiary - the first period of the Cenozoic era; between 65 and 1.6 million years ago

thrust fault - a reverse fault with a dip of 45° or less, on which the hanging wall appears to have moved upward relative to the footwall

TLMFW - total loss of MFW; an internal initiating event

tonal lineament - a linear topographic feature of regional extent that is made visible by a difference in color or tone across the lineament

top event - an explicit, specific statement which describes the undesired state of the system or undesired event for a system of interest

transcurrent fault - a large-scale strike-slip fault in which the fault surface is steeply inclined

transcurrent displacement - strike-slip displacement on a transcurrent fault

transcurrent stress regime - the crustal stress field that gives rise to a transcurrent fault

transgression - the spread of the sea over land areas

transpression - a crustal stress regime that is predominantly transcurrent, but with a compressional component

transtension - a crustal stress regime that is predominantly transcurrent, but with a tensile component

trend of a fault - the direction or strike of the fault

triaxial - pertaining to all three perpendicular geometric axes (e.g., north-south, east-west and up-down)

TRS - test response spectrum

tsunami - a great sea wave produced by a submarine earthquake or volcanic eruption

TT - turbine trip; an internal initiating event

tuff - a general term for all consolidated, pyroclastic rocks, i.e., rocks that have been consolidated from material explosively or aerially ejected from a volcanic vent

unconformity - the surface between two groups of sedimentary rocks that are not in their normal sequence of deposition

UNR - University of Nevada, Reno

upthrown - vertically displaced upward

USGS - United States Geologic Survey

VDI - interfacing systems LOCA; an internal initiating event resulting from a pipe break on the discharge side of the RHR pump

vergent - trending or inclining toward

volcanics - finely crystalline or glassy igneous rock resulting from volcanic action at or near the earth's surface, either explosively ejected or extruded as lava

VSI - interfacing systems LOCA; an internal initiating event resulting from a pipe break on the suction side of the RHR pump

walkdown - to physically walk along the entire extent of a system to observe its characteristics, components, connections with other systems, and so forth

wave-cut bench - a level to gently sloping narrow surface produced by wave erosion, extending outward from a cliff that was produced by wave erosion

wave-cut platform - a gently sloping surface produced by wave erosion, extending far into the sea from the base of a cliff that was produced by wave erosion

Wisconsinan - pertaining to the classical fourth glacial state of the Pleistocene epoch, following the Sangamon interglacial stage and preceding the Holocene epoch

WOG - Westinghouse owner's group

WQ - workshop question

ybp - years before the present

NRC FORM 335 (2-89) NRCM 1102, 3201, 3202

U.S. NUCLEAR REGULATORY COMMISSION

BIBLIOGRAPHIC DATA SHEET

(See instructions on the reverse)

1. REPORT NUMBER (Assigned by NRC. Add Vol., Supp., Rev., and Addendum Numbers, if any.)
NUREG-0675
Supplement No. 34

2. TITLE AND SUBTITLE
Safety Evaluation Report related to the operation of Diablo Canyon Nuclear Power Plant, Units 1 and 2

3. DATE REPORT PUBLISHED
MONTH: June
YEAR: 1991

4. FIN OR GRANT NUMBER
N/A

5. AUTHOR(S)
H. Rood, N. Chokshi, R. McMullen, R. Pichumani, P. Sobel

6. TYPE OF REPORT
Final

7. PERIOD COVERED *(Inclusive Dates)*
7/31/88 - 6/6/91

8. PERFORMING ORGANIZATION – NAME AND ADDRESS *(If NRC, provide Division, Office or Region, U.S. Nuclear Regulatory Commission, and mailing address; if contractor, provide name and mailing address.)*
Division of Reactor Projects III/IV/V
Office of Nuclear Reactor Regulation
U.S. Nuclear Regulatory Commission
Washington, D.C. 20555

9. SPONSORING ORGANIZATION – NAME AND ADDRESS *(If NRC, type "Same as above"; if contractor, provide NRC Division, Office or Region, U.S. Nuclear Regulatory Commission, and mailing address.)*
Same as above

10. SUPPLEMENTARY NOTES

11. ABSTRACT *(200 words or less)*
Supplement 34 to the Safety Evaluation Report for the application by Pacific Gas and Electric Company (PG&E) for licenses to operate Diablo Canyon Nuclear Power Plant, Unit Nos. 1 and 2 (Docket Nos. 50-275 and 50-323, respectively) has been prepared by the Office of Nuclear Reactor Regulation of the U.S. Nuclear Regulatory Commission. This supplement documents the NRC staff review of the Long-Term Seismic Program conducted by PG&E in response to License Condition 2.C.(7) of Facility Operating License DPR-80, the Diablo Canyon Unit 1 operating license.

12. KEY WORDS/DESCRIPTORS *(List words or phrases that will assist researchers in locating the report.)*
Long-Term Seismic Program
LTSP
PRA
Seismic
Seismic Reevaluation
Seismology
Geology

13. AVAILABILITY STATEMENT
Unlimited

14. SECURITY CLASSIFICATION
(This Page) Unclassified
(This Report) Unclassified

15. NUMBER OF PAGES

16. PRICE

THIS DOCUMENT WAS PRINTED USING RECYCLED PAPER

UNITED STATES
NUCLEAR REGULATORY COMMISSION
WASHINGTON, D.C. 20555

OFFICIAL BUSINESS
PENALTY FOR PRIVATE USE, $300

FIRST CLASS MAIL
POSTAGE & FEES PAID
USNRC

PERMIT No. G-67